

UNIVERSITY OF DERBY

The Pathogenesis of Human Papillomavirus (HPV)  
in Cancer of the Oropharynx

Rebecca Mallender

A submission in partial fulfilment of the requirements of the University of  
Derby for the award of the degree of Doctor of Philosophy

College of Science and Engineering

## TABLE OF CONTENTS

<b>LIST OF FIGURES</b> .....	<b>8</b>
<b>LIST OF TABLES</b> .....	<b>11</b>
<b>GLOSSARY OF NOMENCLATURE</b> .....	<b>14</b>
<b>DECLARATION</b> .....	<b>20</b>
<b>ACKNOWLEDGEMENTS</b> .....	<b>21</b>
<b>ABSTRACT</b> .....	<b>23</b>
<b>CHAPTER 1: INTRODUCTION</b> .....	<b>25</b>
<b>1.1 Head and neck squamous cell carcinoma</b> .....	<b>25</b>
<b>1.2 Oropharyngeal squamous cell carcinoma</b> .....	<b>25</b>
1.2.1 Anatomy of the palatine tonsils .....	25
1.2.2 Epidemiology and risk factors of OPSCC .....	30
1.2.2.1 Human papillomavirus.....	30
1.2.2.2 Tobacco, alcohol, and other carcinogens.....	31
1.2.2.3 Trends of disease.....	32
<b>1.3 HPV virology</b> .....	<b>33</b>
1.3.1 HPV classification .....	33
1.3.2 HPV genome .....	34
1.3.2.1 Early region .....	37
1.3.2.1.1 E1.....	37
1.3.2.1.2 E2.....	37
1.3.2.1.3 E8^E2C.....	38
1.3.2.1.4 E4 and E1^E4 .....	39
1.3.2.1.5 E5.....	39
1.3.2.1.6 E6.....	40
1.3.2.1.7 E7.....	41
1.3.2.1.8 The synergistic relationship of E6 and E7 .....	42
1.3.2.2 Late region .....	42
1.3.2.2.1 L1 .....	42
1.3.2.2.2 L2.....	43
<b>1.4 Biology of infection</b> .....	<b>43</b>
1.4.1 HPV viral entry.....	43
1.4.2 HPV viral lifecycle .....	44

1.4.3	HPV-mediated carcinogenesis.....	45
<b>1.5</b>	<b>Clinical management of OPSCC .....</b>	<b>49</b>
1.5.1	Clinical presentation, examination, and diagnosis .....	49
1.5.2	Histopathology .....	49
1.5.2.1	Keratinising squamous cell carcinomas .....	50
1.5.2.2	Non-keratinising squamous cell carcinomas .....	51
1.5.3	HPV testing.....	54
1.5.3.1	p16 immunohistochemistry.....	54
1.5.3.2	HPV DNA <i>in-situ</i> hybridisation.....	55
1.5.3.3	Discordance of p16 and HPV DNA or RNA status in OPSCCs .....	55
<b>1.6</b>	<b>Aptamers.....</b>	<b>56</b>
1.6.1	History of aptamers.....	56
1.6.2	RNA and DNA aptamers.....	57
1.6.3	Systematic evolution of ligands by exponential enrichment.....	57
1.6.4	Aptamers in diagnostic and therapeutic applications .....	60
<b>1.7</b>	<b>Aims and objectives.....</b>	<b>61</b>
<b>CHAPTER 2: MATERIALS AND METHODS .....</b>		<b>62</b>
<b>2.1</b>	<b>Human tissue and ethical approval .....</b>	<b>62</b>
<b>2.2</b>	<b>Histopathology .....</b>	<b>64</b>
2.2.1	Tissue sectioning.....	64
2.2.2	Haematoxylin and eosin staining .....	64
<b>2.3</b>	<b>Automated immunostaining.....</b>	<b>65</b>
2.3.1	Chromogenic immunohistochemistry .....	65
2.3.2	Multiplex immunofluorescence.....	69
2.3.2.1	First primary antibody and Alexa Fluor™ 555 tyramide.....	70
2.3.2.2	Second primary antibody and Alexa Fluor™ 488 tyramide .....	70
2.3.2.3	Third primary antibody, Alexa Fluor™ 647 tyramide, and DAPI .....	71
2.3.2.4	Slide mounting and scanning .....	71
<b>2.4</b>	<b>Molecular pathology .....</b>	<b>71</b>
2.4.1	HPV DNA <i>in-situ</i> hybridisation .....	71
2.4.2	DNA FFPE extraction.....	71
2.4.3	Real-time polymerase chain reaction.....	73
<b>2.5</b>	<b>Systematic evolution of ligands by exponential enrichment .....</b>	<b>73</b>
2.5.1	Preparing the protein for targeting .....	73

2.5.2	First round of positive selection .....	74
2.5.3	First round of negative selection .....	75
2.5.4	Purification procedure .....	75
2.5.5	Polymerase chain reaction.....	76
2.5.6	Subsequent rounds of selection.....	76
<b>2.6</b>	<b>Gel electrophoresis.....</b>	<b>78</b>
<b>2.7</b>	<b>Aptamer development.....</b>	<b>78</b>
2.7.1	Next generation sequencing .....	78
2.7.2	Sequence extraction .....	80
2.7.3	Thermodynamic stability and secondary DNA structure prediction .....	80
2.7.4	Tertiary structure prediction and structural correction .....	80
2.7.5	Fixed docking experiments .....	81
2.7.6	Computational modelling .....	83
<b>2.8</b>	<b>Fluorescent-based binding assay .....</b>	<b>84</b>
2.8.1	Antibody binding assay .....	85
2.8.2	Aptamer binding assay .....	86
2.8.3	Statistical analysis.....	86
<b>2.9</b>	<b>Cell culture.....</b>	<b>88</b>
2.9.1	General growth .....	88
<b>2.10</b>	<b>Cell immunofluorescence.....</b>	<b>88</b>
2.10.1	Fixation .....	88
2.10.2	Antibody immunofluorescence.....	90
2.10.3	Aptamer immunofluorescence .....	90
2.10.4	Cell immunofluorescence imaging .....	90
<b>CHAPTER 3: HISTOLOGICAL CHARACTERISATION OF NORMAL PALATINE TONSILS AND OROPHARYNGEAL SQUAMOUS CELL CARCINOMAS.....</b>		<b>91</b>
<b>3.1</b>	<b>Introduction .....</b>	<b>91</b>
<b>3.2</b>	<b>Results .....</b>	<b>93</b>
3.2.1	Histological characterisation of the normal cervix and CCs .....	93
3.2.2	Histological characterisation of the normal palatine tonsil.....	95
3.2.3	Biomarker optimisation within the normal palatine tonsil.....	98
3.2.4	Histological characterisation of OPSCCs.....	101
3.2.5	Morphological type alone does not reliably inform of HPV status in OPSCC.....	106

3.2.6	HPV positivity correlates with p16 overexpression, but not CK7 expression .....	108
3.2.7	HPV-negative OPSCCs with non-keratinising morphology exhibit higher expression of CD8 .....	111
<b>3.3</b>	<b>Conclusion.....</b>	<b>116</b>
<b>CHAPTER 4: IMMUNOHISTOCHEMICAL EVALUATION OF COMMERCIALY-AVAILABLE HPV ANTIBODIES .....</b>		<b>120</b>
<b>4.1</b>	<b>Introduction .....</b>	<b>120</b>
<b>4.2</b>	<b>Results.....</b>	<b>121</b>
4.2.1	Commercially-available HPV antibodies tested demonstrated positive staining within CCs .....	121
4.2.2	Commercially-available HPV-16 E6 + HPV-18 E6 antibody demonstrated unexpected staining in HPV-positive and HPV-negative OPSCCs.....	124
4.2.3	Further commercially-available HPV antibodies demonstrated unexpected staining results .....	130
4.2.4	Molecular screening of tissues for HPV .....	142
<b>4.3</b>	<b>Conclusion.....</b>	<b>145</b>
<b>CHAPTER 5: APTAMER DEVELOPMENT OF HPV PROTEINS .....</b>		<b>147</b>
<b>5.1</b>	<b>Introduction .....</b>	<b>147</b>
<b>5.2</b>	<b>Results.....</b>	<b>148</b>
5.2.1	DNA aptamers against selected HPV target proteins underwent successful selection.....	148
5.2.2	<i>In silico</i> secondary and tertiary aptamer structure prediction .....	150
5.2.3	Fixed docking data and computational modelling .....	154
5.2.4	Identification of HPV aptamer candidates based upon nature of the observed interactions.....	158
5.2.4.1	HPV-16 E2 .....	158
5.2.4.2	HPV-16 E6 and HPV-16 E7-E6.....	159
5.2.4.3	HPV-18 E6 .....	160
5.2.4.4	HPV-18 E7 .....	161
5.2.5	Alexa Fluor™ 488 fluorophore integration into HPV aptamers .....	162
5.2.6	Binding assays of HPV antibodies and aptamers .....	162
5.2.7	Cell immunofluorescence using HPV antibodies and aptamers.....	167

<b>5.3 Conclusion.....</b>	<b>172</b>
<b>CHAPTER 6: DISCUSSION .....</b>	<b>176</b>
<b>6.1 HPV testing within OPSCC .....</b>	<b>176</b>
6.1.1 The utilisation of p16 for determining HPV status .....	176
6.1.2 Discordance of p16 and HPV status .....	178
6.1.3 Sensitivity and specificity of p16 .....	180
6.1.4 Sensitivity and specificity of HPV DNA ISH .....	181
6.1.5 Patient impact.....	184
<b>6.2 Other biomarkers associated with HPV-positive OPSCC .....</b>	<b>185</b>
6.2.1 Immune biomarker expression in OPSCC .....	185
6.2.2 Prognostic biomarkers of OPSCC .....	187
6.2.3 Cytokeratin 7 expression does not correlate with HPV status in OPSCC.....	188
<b>6.3 Biomarkers against HPV proteins .....</b>	<b>189</b>
6.3.1 HPV antibodies were unsuccessful in IHC.....	189
6.3.2 Novel approach for targeting HPV proteins.....	191
<b>6.4 Future work.....</b>	<b>194</b>
<b>CHAPTER 7: CONCLUSION.....</b>	<b>195</b>
<b>REFERENCES.....</b>	<b>196</b>
<b>APPENDICES .....</b>	<b>I</b>
Appendix 1: Ethical approval ETH2021-3493.....	I
Appendix 2: Ethical approval ETH2021-3493.....	X
Appendix 3: Ethical application ETH2223-0341 .....	XI
Appendix 4: Ethical approval ETH2223-0341.....	XXI
Appendix 5: HBRC approval letter with amendment 21-374A1-HBRC.....	XXII
Appendix 6: BOND™ RX IHC protocol F-standard .....	XXIII
Appendix 7: BOND™ RX IHC protocol F 30 min primary antibody incubation ....	XXVII
Appendix 8: BOND™ RX IHC protocol F 60 min primary antibody incubation .....	XXXI
Appendix 9: VENTANA DISCOVERY ULTRA RUO universal protocol: mouse and mouse first and second primary antibodies .....	XXXV
Appendix 10: VENTANA DISCOVERY ULTRA RUO universal protocol: rabbit and rabbit first and second primary antibodies.....	XLII
Appendix 11: VENTANA DISCOVERY ULTRA RUO universal protocol: mouse and rabbit first and second primary antibodies.....	XLIX

Appendix 12: VENTANA DISCOVERY ULTRA RUO universal protocol: rabbit third primary antibody and DAPI .....	LV
Appendix 13: VENTANA DISCOVERY ULTRA RUO universal protocol: mouse third primary antibody and DAPI .....	LIX
Appendix 14: Non-specific staining retesting and discontinuation emails.....	LXIII
Appendix 15: mFold secondary structures for other aptamer candidate sequences for each HPV protein target.....	LXIV
Appendix 16: ZDOCK scores and polar contacts between HPV-16 E2 and the control ligand 4TS2, natural ligand BRD4, and HPV-16 E2 aptamer candidates .....	LXVIII
Appendix 17: ZDOCK scores and polar contacts between HPV-16 E6 and the control ligand 4TS2, natural ligand p53, and HPV-16 E7-E6 aptamer candidates .....	LXXIV
Appendix 18: ZDOCK outputs and polar contacts between HPV-18 E6 and the control ligand 4TS2, natural ligand p53, and HPV-18 E6 aptamer candidates.....	LXXXIII
Appendix 19: ZDOCK outputs and polar contacts between HPV-18 E7 and the control ligand 4TS2, natural ligand pRb, and HPV-18 E7 aptamer candidates .....	XC
Appendix 20: Final HPV aptamer candidates and observed polar contacts .....	XCVI

## LIST OF FIGURES

<b>Figure 1: Anatomical sites of HNSCCs and OPSCCs.....</b>	<b>27</b>
<b>Figure 2: Histology of the normal palatine tonsil. ....</b>	<b>28</b>
<b>Figure 3: Histology of the lymphoid follicle, surface epithelium, and reticulated epithelium of the normal palatine tonsil.....</b>	<b>29</b>
<b>Figure 4: HPV genome organisation.....</b>	<b>35</b>
<b>Figure 5: HPV-mediated progression to CC.....</b>	<b>47</b>
<b>Figure 6: HPV-mediated carcinogenesis within the tonsillar crypt.....</b>	<b>48</b>
<b>Figure 7: Histology of keratinising squamous cell carcinoma.....</b>	<b>52</b>
<b>Figure 8: Histology of non-keratinising squamous cell carcinoma.....</b>	<b>53</b>
<b>Figure 9: Overview of SELEX process. ....</b>	<b>59</b>
<b>Figure 10: Summary of aptamer development procedure. ....</b>	<b>79</b>
<b>Figure 12: H&amp;E and p16 of three CC tissues. ....</b>	<b>94</b>
<b>Figure 11: H&amp;E and p16 of the squamocolumnar junction of the cervix.....</b>	<b>94</b>
<b>Figure 13: H&amp;E of the normal palatine tonsil.....</b>	<b>96</b>
<b>Figure 14: H&amp;Es of the lymphoid follicle, surface epithelium, and reticulated epithelium of the normal palatine tonsil.....</b>	<b>97</b>
<b>Figure 15: p16, PD-1, PD-L1, CD8, and Ki67 expression in normal palatine tonsil. ....</b>	<b>99</b>
<b>Figure 16: ER<math>\alpha</math>, CK7, AE1/AE3, and EGFR expression in normal palatine tonsil. ....</b>	<b>100</b>
<b>Figure 17: H&amp;E of OPSCC 1 with keratinising morphology.....</b>	<b>103</b>
<b>Figure 18: H&amp;E of OPSCC 2 with non-keratinising morphology.....</b>	<b>103</b>
<b>Figure 19: H&amp;E of OPSCC 3 with non-keratinising morphology.....</b>	<b>104</b>
<b>Figure 20: H&amp;E of OPSCC 4 with keratinising morphology.....</b>	<b>104</b>
<b>Figure 21: H&amp;E of OPSCC 5 with keratinising morphology.....</b>	<b>105</b>
<b>Figure 22: HPV DNA ISH of OPSCCs determined that not all NKSCC are HPV-associated.....</b>	<b>107</b>
<b>Figure 23: HPV positivity correlates with p16 overexpression, but not CK7 expression. ....</b>	<b>110</b>
<b>Figure 24: CK7/p16/ER<math>\alpha</math> expression within five OPSCCs.....</b>	<b>112</b>
<b>Figure 25: PD-1/PD-L1/CD8 expression within five OPSCCs.....</b>	<b>113</b>
<b>Figure 26: EGFR/p16/PD-L1 expression within five OPSCCs.....</b>	<b>114</b>



<b>Figure 27: Ki67 expression within five OPSCCs.....</b>	<b>115</b>
<b>Figure 28: HPV-16 E2, HPV-16 E6 + HPV-18 E6, HPV-16 E6/HPV-18 E6, and HPV-16 E7 staining in three CC tissues.....</b>	<b>123</b>
<b>Figure 29: Positive staining of HPV-16 E6 + HPV-18 E6 is found across different cell types in OPSCC 1.....</b>	<b>126</b>
<b>Figure 30: Positive staining of HPV-16 E6 + HPV-18 E6 is found within the tumour of OPSCC 2.....</b>	<b>127</b>
<b>Figure 31: Positive staining of HPV-16 E6 + HPV-18 E6 is found in ductal epithelium in OPSCC 3.....</b>	<b>127</b>
<b>Figure 32: Positive staining of HPV-16 E6 + HPV-18 E6 is shown across different cell types in OPSCC 4.....</b>	<b>128</b>
<b>Figure 33: Positive staining of HPV-16 E6 + HPV-18 E6 is shown across different cell types in OPSCC 5.....</b>	<b>129</b>
<b>Figure 34: Buffer negative staining in multiple tissue types.....</b>	<b>131</b>
<b>Figure 35: Positive staining of HPV-16 E2 is found across multiple tissue types.....</b>	<b>132</b>
<b>Figure 36: Positive staining of HPV-16 E6 + HPV-18 E6 is found across multiple tissue types.....</b>	<b>133</b>
<b>Figure 37: Positive staining of HPV-16 E6/HPV-18 E6 is found across multiple tissue types.....</b>	<b>134</b>
<b>Figure 38: Positive staining of HPV-16 E7 is found across multiple tissue types.....</b>	<b>135</b>
<b>Figure 39: Positive staining of HPV-16 E6 is found across multiple tissue types.....</b>	<b>138</b>
<b>Figure 40: Positive staining of HPV-16 E7 is found across multiple tissue types.....</b>	<b>139</b>
<b>Figure 41: Positive staining of HPV-18 E6 is found across multiple tissue types.....</b>	<b>140</b>
<b>Figure 42: Positive staining of HPV-18 E7 is found across multiple tissue types.....</b>	<b>141</b>
<b>Figure 43: Screening for HPV positivity in first batch of multiple tissue types.....</b>	<b>143</b>
<b>Figure 44: Screening for HPV positivity in second batch of multiple tissue types.....</b>	<b>144</b>

<b>Figure 45: Confirmation agarose gel of HPV aptamers amplified with extended primers.</b>	149
<b>Figure 46: Secondary DNA structures of three aptamer candidates chosen from the top ten sequence candidates based on <math>\Delta G</math> predicted by mFold for each HPV protein target.</b>	153
<b>Figure 47: Computational modelling of HPV proteins with natural ligands, the control ligand 4TS2, and their corresponding HPV aptamer candidates.</b>	157
<b>Figure 48: Confirmation agarose gels of HPV-16 E2, HPV-16 E7-E6, HPV-18 E6, and HPV-18 E7 aptamers with integrated Alexa Fluor™ 488.</b>	163
<b>Figure 49: Binding affinities of positive HPV-16 E2 and HPV-16 E7-E6 antibody and aptamer plates.</b>	164
<b>Figure 50: Binding affinities of the positive HPV-18 E6 and HPV-18 E7 antibody and aptamer plates.</b>	165
<b>Figure 51: Binding affinities of negative antibody and aptamer plates.</b>	166
<b>Figure 52: MCF7, SiHa, and SCC-040T cell lines stained with HPV-16 E6, HPV16-E7, and secondary-only antibodies.</b>	168
<b>Figure 53: MCF7 and HeLa cell lines stained with HPV-18 E6, HPV-18 E7, and secondary-only antibodies.</b>	169
<b>Figure 54: MCF7, SiHa, SCC-040T, and SCC-147T cell lines stained with positive HPV-16 E7-E6, and negative HPV-16 E7-E6 aptamers.</b>	170
<b>Figure 55: MCF7, SiHa, and HeLa cell lines stained with positive HPV-18 E6, HPV-18 E7, and negative HPV-18 E6 and HPV-18 E7 aptamers.</b>	171
<b>Figure 56: Secondary DNA structures of seven aptamer candidates chosen from the top ten sequence candidates based on <math>\Delta G</math> predicted by mFold for HPV-16 E2.</b>	LXIV
<b>Figure 57: Secondary DNA structures of seven aptamer candidates chosen from the top ten sequence candidates based on <math>\Delta G</math> predicted by mFold for HPV-16 E7-E6.</b>	LXV
<b>Figure 58: Secondary DNA structures of seven aptamer candidates chosen from the top ten sequence candidates based on <math>\Delta G</math> predicted by mFold for HPV-18 E6.</b>	LXVI
<b>Figure 59: Secondary DNA structures of seven aptamer candidates chosen from the top ten sequence candidates based on <math>\Delta G</math> predicted by mFold for HPV-18 E7.</b>	LXVII

## LIST OF TABLES

<b>Table 1: Molecular sizes and functions of the proteins in HPV genome.....</b>	<b>36</b>
<b>Table 2: FFPE tissue types sourced from Tissue Solutions with associated pathologies used for antibody optimisation and control staining.....</b>	<b>63</b>
<b>Table 3: Primary antibodies used for automated chromogenic immunohistochemistry on BOND™ RX Fully Automated Research Stainer and multiplex immunofluorescence on VENTANA DISCOVERY ULTRA Research Staining System .....</b>	<b>67</b>
<b>Table 4: Primary antibody dilutions, antigen retrieval solutions, incubation times and staining patterns used for automated chromogenic immunohistochemistry on BOND™ RX Fully Automated Research Stainer and multiplex immunofluorescence on VENTANA DISCOVERY ULTRA Research Staining System .....</b>	<b>68</b>
<b>Table 5: Positive and negative SELEX rounds and selection pressures introduced for each HPV aptamer pool.....</b>	<b>77</b>
<b>Table 6: RCSB PDB files and modifications used for fixed docking experiments .....</b>	<b>82</b>
<b>Table 7: Positive and negative HPV antibodies and aptamers and their working concentrations for fluorescent-based binding assays and cell immunofluorescence .....</b>	<b>87</b>
<b>Table 8: Cell lines grown for cell immunofluorescence.....</b>	<b>89</b>
<b>Table 9: HPV aptamer candidate sequences selected through lowest <math>\Delta G</math> value .....</b>	<b>152</b>
<b>Table 10: Final HPV aptamer candidates selected based on ZDOCK Score and number and length of polar contacts .....</b>	<b>156</b>
<b>Table 11: Final HPV aptamer candidates and their sequences chosen based on computational modelling observations.....</b>	<b>156</b>
<b>Table 12: ZDOCK score, and polar contacts between HPV-16 E2 protein and the control ligand 4TS2.....</b>	<b>LXVIII</b>
<b>Table 13: ZDOCK score, and polar contacts between HPV-16 E2 protein and the natural ligand Brd4.....</b>	<b>LXVIII</b>

<b>Table 14: ZDOCK scores, and polar contacts between HPV-16 E2 protein and HPV-16 E2 sequence 4995 aptamer candidate-experiment one.....</b>	<b>LXIX</b>
<b>Table 15: ZDOCK scores, and polar contacts between HPV-16 E2 protein and HPV-16 E2 sequence 4995 aptamer candidate-experiment two.....</b>	<b>LXIX</b>
<b>Table 16: ZDOCK scores, and polar contacts between HPV-16 E2 protein and HPV-16 E2 sequence 324 aptamer candidate-experiment one.....</b>	<b>LXX</b>
<b>Table 17: ZDOCK scores, and polar contacts between HPV-16 E2 protein and HPV-16 E2 sequence 324 aptamer candidate-experiment two.....</b>	<b>LXXI</b>
<b>Table 18: ZDOCK scores, and polar contacts between HPV-16 E2 protein and HPV-16 E2 sequence 5709 aptamer candidate-experiment one.....</b>	<b>LXXII</b>
<b>Table 19: ZDOCK scores, and polar contacts between HPV-16 E2 protein and HPV-16 E2 sequence 5709 aptamer candidate-experiment two.....</b>	<b>LXXIII</b>
<b>Table 20: ZDOCK score, and polar contacts between HPV-16 E6 protein and the control ligand 4TS2.....</b>	<b>LXXIV</b>
<b>Table 21: ZDOCK score, and polar contacts between HPV-16 E6 protein and the natural ligand p53.....</b>	<b>LXXV</b>
<b>Table 22: ZDOCK scores, and polar contacts between HPV-16 E6 protein and HPV-16 E7-E6 sequence 6045 aptamer candidate-experiment one.....</b>	<b>LXXVI</b>
<b>Table 23: ZDOCK scores, and polar contacts between HPV-16 E6 protein and HPV-16 E7-E6 sequence 6045 aptamer candidate-experiment two.....</b>	<b>LXXVII</b>
<b>Table 24: ZDOCK scores, and polar contacts between HPV-16 E6 protein and HPV-16 E7-E6 sequence 6362 aptamer candidate-experiment one.....</b>	<b>LXXVIII</b>
<b>Table 25: ZDOCK scores, and polar contacts between HPV-16 E6 protein and HPV-16 E7-E6 sequence 6362 aptamer candidate-experiment two.....</b>	<b>LXXIX</b>
<b>Table 26: ZDOCK scores, and polar contacts between HPV-16 E6 protein and HPV-16 E7-E6 sequence 3271 aptamer candidate-experiment one.....</b>	<b>LXXX</b>
<b>Table 27: ZDOCK scores, and polar contacts between HPV-16 E6 protein and HPV-16 E7-E6 sequence 3271 aptamer candidate-experiment two.....</b>	<b>LXXXII</b>
<b>Table 28: ZDOCK score, and polar contacts between HPV-18 E6 protein and the control ligand 4TS2.....</b>	<b>LXXXIII</b>
<b>Table 29: ZDOCK score, and polar contacts between HPV-18 E6 protein and the natural ligand p53.....</b>	<b>LXXXIII</b>
<b>Table 30: ZDOCK scores, and polar contacts between HPV-18 E6 protein and HPV-18 E6 sequence 12797 aptamer candidate-experiment one.....</b>	<b>LXXXIV</b>

<b>Table 31: ZDOCK scores, and polar contacts between HPV-18 E6 protein and HPV-18 E6 sequence 12797 aptamer candidate-experiment two .....</b>	<b>LXXXV</b>
<b>Table 32: ZDOCK scores, and polar contacts between HPV-18 E6 protein and HPV-18 E6 sequence 2720 aptamer candidate-experiment one.....</b>	<b>LXXXVI</b>
<b>Table 33: ZDOCK scores, and polar contacts between HPV-18 E6 protein and HPV-18 E6 sequence 2720 aptamer candidate-experiment two.....</b>	<b>LXXXVII</b>
<b>Table 34: ZDOCK scores, and polar contacts between HPV-18 E6 protein and HPV-18 E6 sequence 10017 aptamer candidate-experiment one.....</b>	<b>LXXXVIII</b>
<b>Table 35: ZDOCK scores, and polar contacts between HPV-18 E6 protein and HPV-18 E6 sequence 10017 aptamer candidate-experiment two .....</b>	<b>LXXXIX</b>
<b>Table 36: ZDOCK score, and polar contacts between HPV-18 E7 protein and the control ligand 4TS2.....</b>	<b>XC</b>
<b>Table 37: ZDOCK score, and polar contacts between HPV-18 E7 protein and the natural ligand pRb.....</b>	<b>XC</b>
<b>Table 38: ZDOCK scores, and polar contacts between HPV-18 E7 protein and HPV-18 E7 sequence 820 aptamer candidate-experiment one.....</b>	<b>XCI</b>
<b>Table 39: ZDOCK scores, and polar contacts between HPV-18 E7 protein and HPV-18 E7 sequence 820 aptamer candidate-experiment two.....</b>	<b>XCI</b>
<b>Table 40: ZDOCK scores, and polar contacts between HPV-18 E7 protein and HPV-18 E7 sequence 392 aptamer candidate-experiment one.....</b>	<b>XCII</b>
<b>Table 41: ZDOCK scores, and polar contacts between HPV-18 E7 protein and HPV-18 E7 sequence 392 aptamer candidate-experiment two.....</b>	<b>XCIII</b>
<b>Table 42: ZDOCK scores, and polar contacts between HPV-18 E7 protein and HPV-18 E7 sequence 5772 aptamer candidate-experiment one.....</b>	<b>XCIV</b>
<b>Table 43: ZDOCK scores, and polar contacts between HPV-18 E7 protein and HPV-18 E7 sequence 5772 aptamer candidate-experiment two.....</b>	<b>XCV</b>
<b>Table 44: ZDOCK scores, and observed polar contacts between HPV-16 E2 protein and HPV-16 E2 sequence 324 aptamer candidate.....</b>	<b>XCVI</b>
<b>Table 45: ZDOCK scores, and observed polar contacts between HPV-16 E6 protein and HPV-16 E7-E6 sequence 3271 aptamer candidate .....</b>	<b>XCVIII</b>
<b>Table 46: ZDOCK scores, and observed polar contacts between HPV-18 E6 protein and HPV-18 E6 sequence 2720 aptamer candidate.....</b>	<b>CII</b>
<b>Table 47: ZDOCK scores, and observed polar contacts between HPV-18 E7 protein and HPV-18 E7 sequence 5772 aptamer candidate.....</b>	<b>CV</b>

## GLOSSARY OF NOMENCLATURE

<b>A</b>	Adenine
<b>Å</b>	Angstroms
<b>AA</b>	Amino acid
<b>AJCC</b>	American Joint Committee on Cancer
<b>Ala</b>	Alanine
<b>Arg</b>	Arginine
<b>Asn</b>	Asparagine
<b>ASR</b>	Age-standardised incidence rate
<b>ATP</b>	Adenosine triphosphate
<b>ATPase</b>	Adenosine 5'-triphosphatase
<b>bp</b>	Base pairs
<b>Brd4</b>	Bromodomain protein 4
<b>BSA</b>	Bovine serum albumin
<b>bZIP</b>	Basic domain-containing leucine-zipper
<b>C</b>	Cytosine
<b>CAP</b>	College of American Pathologists
<b>CBP</b>	CREB-binding protein
<b>CC</b>	Cervical carcinoma
<b>CC2</b>	Cell Conditioning 2
<b>CDK</b>	Cyclin-dependent kinase
<b>CIN</b>	Cervical intraepithelial neoplasia
<b>CIS</b>	Carcinoma <i>in-situ</i>
<b>CK7</b>	Cytokeratin 7
<b>CR1</b>	Conserved region 1
<b>CR2</b>	Conserved region 2
<b>CR3</b>	Conserved region 3
<b>CT</b>	Computed tomography
<b>CUP</b>	Cancer of unknown primary

<b>CyP</b>	Cyclophilin
<b>DAB</b>	3,3'-diaminobenzidine
<b>DAPI</b>	4',6-diamidino-2-phenylindole
<b>DBD</b>	DNA-binding domain
<b>DMEM</b>	Dulbecco's modified eagle medium
<b>DNA</b>	Deoxyribonucleic acid
<b>DNase</b>	Deoxyribonuclease
<b>dNTP</b>	Deoxynucleoside triphosphate
<b>dsDNA</b>	Double-stranded deoxyribonucleic acid
<b>dsRNA</b>	Double-stranded ribonucleic acid
<b>E</b>	Early
<b>E2BSs</b>	E2-binding sites
<b>E6AP</b>	E6-associated protein
<b>ECM</b>	Extracellular matrix
<b>EDTA</b>	Ethylenediaminetetraacetic acid
<b>EGFR</b>	Epidermal growth factor receptor
<b>ENT</b>	Ear, nose, and throat
<b>ER1</b>	Epitope Retrieval 1
<b>ER2</b>	Epitope Retrieval 2
<b>ER<math>\alpha</math></b>	Estrogen receptor alpha
<b>ESCRT</b>	Endosomal sorting complex required for transport
<b>FBS</b>	Foetal bovine serum
<b>FDA</b>	Food and Drug Administration
<b>FFPE</b>	Formalin-fixed, paraffin-embedded
<b>FISH</b>	Fluorescent <i>in-situ</i> hybridisation
<b>FNA</b>	Fine needle aspiration
<b>G</b>	Guanine
<b>GCP</b>	Good Clinical Practice
<b>GFP</b>	Green fluorescent protein
<b>Gln</b>	Glutamine

<b>GLP</b>	Good Laboratory Practice
<b>Glu</b>	Glutamate
<b>Gly</b>	Glycine
<b>H&amp;E</b>	Haematoxylin and eosin
<b>HBRC</b>	Human Biomaterials Resource Centre
<b>HEPES</b>	N-2-hydroxyethylpiperazine-N-2-ethane sulphonic acid
<b>HIER</b>	Heat-induced epitope retrieval
<b>HNSCC</b>	Head and neck squamous cell carcinoma
<b>HPV</b>	Human papillomavirus
<b>HR-HPV</b>	High-risk human papillomavirus
<b>HRP</b>	Horseradish peroxidase
<b>HSPGs</b>	Heparin sulphate proteoglycans
<b>HTA</b>	Human Tissue Authority
<b>HTECs</b>	Human tonsillar epithelial cells
<b>hTERT</b>	Human telomerase reverse transcriptase
<b>IARC</b>	International Agency for Research on Cancer
<b>ICCR</b>	International Collaboration on Cancer Reporting
<b>ICD</b>	International Classification of Diseases
<b>IDA</b>	Industrial denatured alcohol
<b>IHC</b>	Immunohistochemistry
<b>IMS</b>	Industrial methylated spirit
<b>ISH</b>	<i>In-situ</i> hybridisation
<b>ISO</b>	International Organisation for Standardisation
<b>IVD</b>	In vitro diagnostics
<b>KSCC</b>	Keratinising squamous cell carcinoma
<b>L</b>	Late
<b>LC</b>	Laryngeal carcinoma
<b>LCR</b>	Long-control region
<b>LCS</b>	Liquid Coverslip
<b>Leu</b>	Leucine



<b>LR-HPV</b>	Low-risk human papillomavirus
<b>Lys</b>	Lysine
<b>MALT</b>	Mucosal-associated lymphoid tissue
<b>MgCl<sub>2</sub></b>	Magnesium chloride
<b>mIF</b>	Multiplex immunofluorescence
<b>MRI</b>	Magnetic resonance imaging
<b>mRNA</b>	Messenger ribonucleic acid
<b>NCCN</b>	National Comprehensive Cancer Network
<b>NCR</b>	Non-coding region
<b>ND10</b>	Nuclear domain 10
<b>NDS</b>	Normal donkey serum
<b>NEAA</b>	Non-essential amino acids
<b>NES</b>	Nuclear export signal
<b>NGS</b>	Next generation sequencing
<b>NICE</b>	National Institute of Health and Care Excellence
<b>NKSCC</b>	Non-keratinising squamous cell carcinoma
<b>NLS</b>	Nuclear localisation signal
<b>nt</b>	Nucleotide
<b>NTC</b>	Non-template control
<b>OC</b>	Oral carcinoma
<b>OPSCC</b>	Oropharyngeal squamous cell carcinoma
<b>ORF</b>	Open-reading frame
<b><i>ori</i></b>	Origin of replication
<b>p16INK4A</b>	p16
<b>pA<sub>E</sub></b>	Early polyadenylation
<b>pA<sub>L</sub></b>	Late polyadenylation
<b>PBM</b>	PSD95/Discs Large/ZO-1-binding motif
<b>PBS</b>	Phosphate buffered saline
<b>PCR</b>	Polymerase chain reaction
<b>PD-1</b>	Programmed cell death protein-1

<b>PDB</b>	Protein Data Bank
<b>PD-L1</b>	Programmed cell death-ligand 1
<b>PDZ</b>	PSD95/Discs Large/ZO-1
<b>P<sub>E</sub></b>	Early promoter
<b>P<sub>L</sub></b>	Late promoter
<b>PML</b>	Promyelocytic leukaemia
<b>pRb</b>	Retinoblastoma protein
<b>Pro</b>	Proline
<b>RCPATH</b>	The Royal College of Pathologists
<b>Real-Time PCR</b>	Real-time polymerase chain reaction
<b>RNA</b>	Ribonucleic acid
<b>RNase</b>	Ribonuclease
<b>ROI</b>	Regions of interest
<b>RT-PCR</b>	Reverse transcription polymerase chain reaction
<b>RTU</b>	Ready-to-use
<b>RUO</b>	Research use only
<b>SCBT</b>	Santa Cruz Biotechnology
<b>SCC</b>	Squamous cell carcinoma
<b>SCJ</b>	Squamocolumnar junction
<b>SDS</b>	Sodium lauryl sulphate
<b>SDG</b>	Sustainability development goals
<b>SELEX</b>	Systematic evolution of ligands by exponential enrichment
<b>Ser</b>	Serine
<b>SQL</b>	Structured Query Language
<b>ssDNA</b>	Single-stranded deoxyribonucleic acid
<b>ssRNA</b>	Single-stranded ribonucleic acid
<b>STI</b>	Sexually transmitted infection
<b>T</b>	Thymine
<b>TAD</b>	Transactivation domain
<b>TBE</b>	Tris-borate-ethylenediaminetetraacetic acid

<b>TGN</b>	<i>Trans</i> -Golgi network
<b>Thr</b>	Threonine
<b>TILs</b>	Tumour-infiltrating lymphocytes
<b>TMD</b>	Transmembrane domain
<b>TME</b>	Tumour microenvironment
<b>TNM</b>	Tumour, node and metastasis
<b>tRNA</b>	Transfer ribonucleic acid
<b>Trp</b>	Tryptophan
<b>Tyr</b>	Tyrosine
<b>TZ</b>	Transformation zone
<b>U</b>	Uracil
<b>UICC</b>	Union for International Cancer Control
<b>UK NSC</b>	UK National Screening Committee
<b>UN</b>	United Nations
<b>URR</b>	Upstream regulatory region
<b>Val</b>	Valine
<b>VEGF</b>	Vascular endothelial growth factor
<b>VLP</b>	Virus-like particle
<b>WHO</b>	World Health Organisation
<b><math>\Delta G</math></b>	Gibbs free energy

## **DECLARATION**

I declare that all writing in this thesis is my own and that all the references cited have been consulted by me, unless otherwise stated. This work has not been submitted for consideration for any other higher degree or qualification at this or any other University. I confirm that my research has been ethically approved (ETH2021-3493 and ETH2223-0341, Appendices 1-4).

## ACKNOWLEDGEMENTS

During the past few years, I have been very fortunate to come across some wonderful people without whom this body of work would not have been possible.

Firstly, never-ending thanks to my supervisors Elizabeth Marsh, Thomas Illingworth, and Laurice Fretwell. Elizabeth, I am eternally grateful to you for believing in me and telling me to apply for that MPhil back in 2020. It has changed my life for the better and I cannot thank you enough for this opportunity. Tom, thank you for introducing me to aptamers. It has given me a new set of skills and opened doors for me that I never thought would be possible. And Laurice, thank you for your support and feedback along the way; it has not gone unnoticed. Thank you all for the supportive chats, hugs, curries, and cups of coffee that we have shared. Without you, this PhD would not have been possible.

I would also like to thank Mary-Anne Freckleton for all the enjoyable chats, laughs, and chocolate. It has been great experiencing this journey with you, and I really value our friendship. To all the other PhD students: Marie, Jake, Asha, Priya, Jaya, and Agnieszka; you have made this journey more enjoyable. Thank you for all the chats, laughs, and snacks long the way.

To everyone at HistologiX, thank you for being such a wonderful, welcoming group of people. Most of all, thank you for giving me the opportunity to do my PhD. Without your support and help along the way, this would not have been possible without you. I will miss all the great chats, cake, and laughs we have shared. Also, thank you to Amandeep Mann for taking the time to sit with me and look at the slides together. Your help was very insightful and much appreciated. And I would like to thank my examiners Mohammed Aleskandarany and Nathaniel Milton for taking the time to read through my thesis and provide feedback on my work during my viva. Despite the grilling, I enjoyed my viva more than I had anticipated.

Lastly, to my wonderful family. Mum and Dad, thank you for being so supportive over the years and believing in me. You have helped to shape me as the person that I am today. I know that I have made you proud. And to the rest of my family and friends,

thank you for always being there. The days out, the meals, the laughs, and the silent discos have made this journey worthwhile. Long may they continue. Finally, I would like to thank my wonderful husband, Martin. The long and tiring days were all worth it as you and Winston were always there for me at the end of the day. Without your unwavering support, kindness, and love, this PhD journey would not have been possible.

## ABSTRACT

**BACKGROUND:** Human papillomavirus (HPV) has become increasingly associated with head and neck squamous cell carcinomas (HNSCC), particularly oropharyngeal squamous cell carcinomas (OPSCC). Currently, the number of HPV-positive OPSCCs has now surpassed cervical carcinoma (CC), and is expected to increase for the next 30 years, with one of the most prevalent subtypes, HPV-16, accounting for 87-96% of cases. Unfortunately, there are currently no screening programmes for OPSCC, the reticulated crypts of the palatine tonsils. Current NHS guidelines for determining HPV status in OPSCC is p16INK4A (p16) immunohistochemistry (IHC), which has become the widely accepted method of detection. However, despite its high sensitivity, the use of p16 as a standalone marker for OPSCC has drawn criticism due to its lack of specificity.

**AIMS:** To characterise HPV-positive and HPV-negative OPSCC tissues using potential biomarkers believed to be indicators of HPV-mediated OPSCC development, as well as develop multiplex immunofluorescent (mIF) assays and aptamers against various HPV proteins.

**METHODS:** The study employed histological techniques including haematoxylin and eosin (H&E) staining, IHC, and mIF techniques for characterisation of five OPSCC tissues obtained from the Human Biomaterials Resource Centre (HBRC) at the University of Birmingham. These OPSCC samples also underwent p16 and HPV DNA *in-situ* hybridisation (ISH) as per NHS clinical guidelines for determination of HPV status. Commercially-available HPV antibodies were tested in various tissue types, with molecular screening for HPV confirmation performed by real-time polymerase chain reaction (real-time PCR). Aptamers isolated against HPV proteins (HPV-16 E2, HPV-16 E7-E6, HPV-18 E6, and HPV-18 E7) were developed using systematic evolution of ligands by exponential enrichment (SELEX), and post-SELEX experiments, including comparison against commercially-available HPV antibodies.

**RESULTS:** Within our sample, both HPV-positive and HPV-negative OPSCCs deviated from the typical tumour profiles. Three OPSCCs were determined to be HPV-

negative, despite two of these exhibiting non-keratinising morphology which is typically associated with p16/HPV DNA ISH positivity. The remaining two OPSCCs were determined to be HPV-positive (p16-/HPV DNA ISH-positive), despite exhibiting keratinising morphology which is commonly associated with HPV-negative OPSCCs. Furthermore, staining with prognostic biomarkers using IHC and mIF mostly deviated from the typical staining expected, with higher PD-L1 and CD8 expression observed in HPV-negative OPSCCs, in comparison to HPV-positive OPSCCs. Commercially-available HPV antibodies were unsuccessful, with non-specific staining observed in normal tissues that were confirmed molecularly to be HPV-negative. Aptamers isolated against HPV-16 E2, HPV-16 E7-E6, HPV-18 E6, and HPV-18 E7 proteins underwent successful selection by SELEX, and subsequent molecular docking and computational modelling. This demonstrated that the interactions observed between each HPV aptamer, and their corresponding HPV protein, have been observed in nature, and are suggestive of real interactions. Cell immunofluorescence with HPV aptamers demonstrated minimal background staining, and nuclear and endosomal staining consistent with nuclear and endosomal localisation of E6 and E7 proteins.

**CONCLUSIONS:** The use of p16 as a surrogate biomarker within HPV-mediated OPSCCs is unsuitable. Using HPV proteins directly could pose as better biomarkers for HPV-positive OPSCC; therefore, we propose aptamers as a novel method for HPV subtype detection.



## CHAPTER 1: INTRODUCTION

### 1.1 Head and neck squamous cell carcinoma

Head and neck squamous cell carcinoma (HNSCC) is a heterogeneous disease of the oral cavity, nasopharynx, oropharynx, hypopharynx, and larynx (Figure 1) (Gillison *et al.*, 2000). Biologically, HNSCCs within these subsites are diverse, varying in invasiveness, growth, and metastatic capabilities, due to the different clinical, epidemiological, and molecular differences between these diseases, including tumour origin and environmental factors such as tobacco and alcohol consumption (Tamás *et al.*, 2011, Gillison *et al.*, 2012).

HNSCC is the sixth most common malignancy worldwide, with a 2022 reported global incidence of over 940,000 new cases and over 480,000 deaths (Ferlay *et al.*, 2024). Approximately 75% of HNSCCs correlate with tobacco and alcohol consumption, whilst 25% are caused by human papillomavirus (HPV) (Hashibe *et al.*, 2009, Ndiaye *et al.*, 2014, Whiteman and Wilson, 2016, Chang *et al.*, 2017, de Martel *et al.*, 2017). HPV is mostly known to cause cervical carcinomas (CC), however, it has now become increasingly associated with HNSCCs, particularly oropharyngeal squamous cell carcinomas (OPSCC) (Ndiaye *et al.*, 2014, de Martel *et al.*, 2017).

### 1.2 Oropharyngeal squamous cell carcinoma

#### 1.2.1 Anatomy of the palatine tonsils

OPSCC, a subset of HNSCC occurring within the oropharynx, includes the soft palate, uvula, palatine tonsils, base of tongue, lingual tonsils, and posterior pharyngeal wall (Figure 1) (Tham *et al.*, 2020, Lorenzoni *et al.*, 2022). It is located posterior to the oral cavity, extending from the soft palate to the hyoid bone, with most cancers occurring within the palatine tonsils and base of tongue (Ndiaye *et al.*, 2014, Fossum *et al.*, 2017, Tham *et al.*, 2020).

The palatine tonsils are paired secondary lymphoid organs that are involved in initiating immune responses against any foreign antigen that enters the oropharynx (Nave *et al.*, 2001). They are located between the palatoglossal and palatopharyngeal arches (right and left sides) within the circular mucosal-associated lymphoid tissue (MALT), known as the Waldeyer's ring (Waldeyer, 1884, Fossum *et al.*, 2017).

Histologically, the outer surface of the palatine tonsil is covered by non-keratinising stratified squamous epithelium, which invaginates into the lamina propria, forming 10-30 tonsillar crypts (300 cm<sup>2</sup> surface area) (Figures 2 and 3A) (Howie, 1980, Dudás, 2023). These crypts have blind ends that branch out and are lined by reticulated epithelium, which, unlike the surface epithelium, has a discontinuous basement membrane that is densely infiltrated with lymphocytes (Figure 3B) (Stöhr, 1882, Olah, 1978, Nave *et al.*, 2001). This lymphoepithelium, where epithelial cells and lymphocytes coexist, is known as lymphoepithelial symbiosis (Schmincke, 1921, Fioretti, 1957). The reasoning for the abundance of lymphocytes may be due to the depth of the crypts making them susceptible to bacteria and foreign antigens, thus representing an immune-privileged site (Lyford-Pike *et al.*, 2013). Beneath the palatine tonsillar surface epithelium are lymphoid follicles surrounded by connective tissue within the parenchyma (Figure 3C), which is supported by skeletal muscle (Fossum *et al.*, 2017, Dudás, 2023). Lymphoid follicles are spherical or oval in shape, containing germinal centres composed of three zones: dark, light, and mantle where T and B lymphocytes reside (Nave *et al.*, 2001, Fossum *et al.*, 2017).

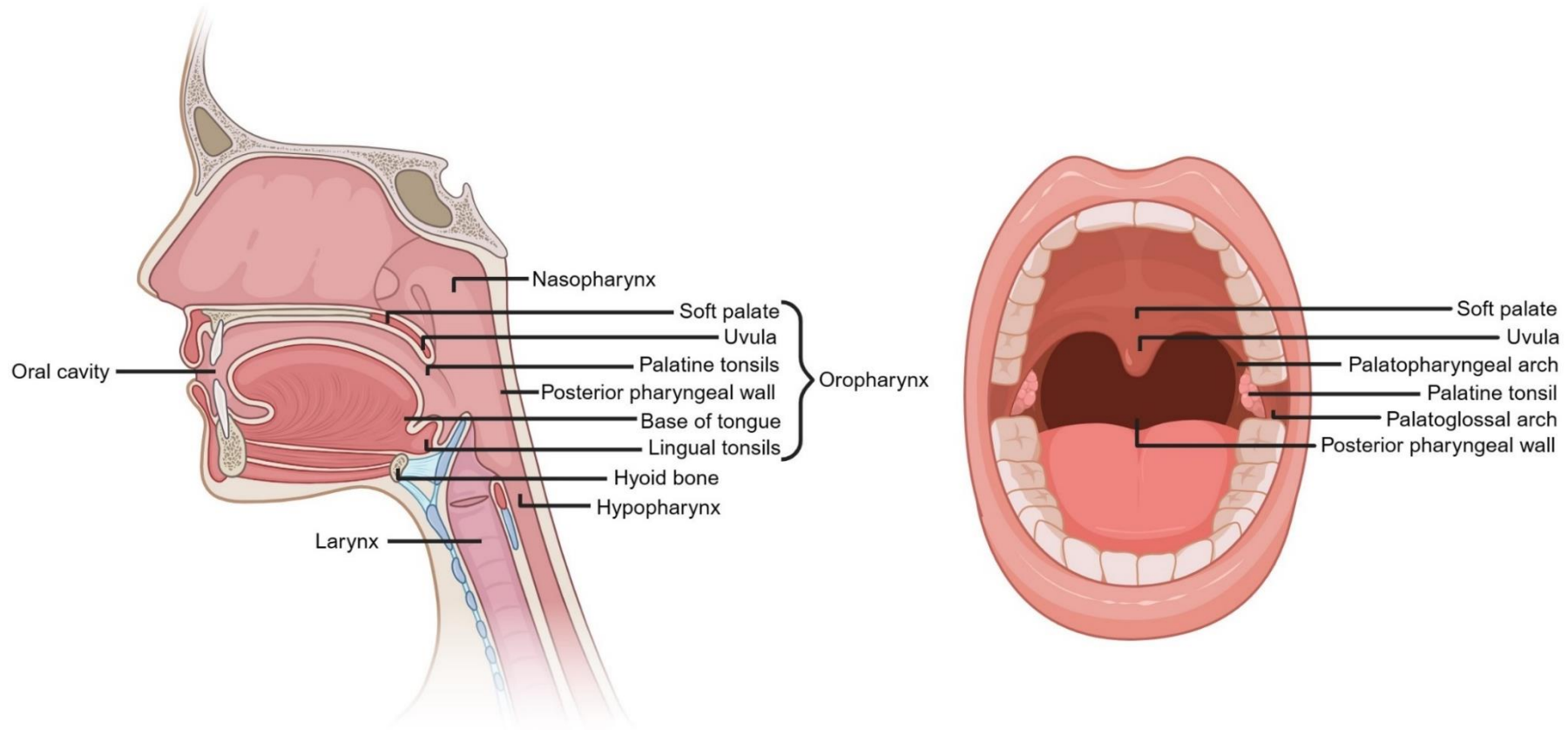


**Figure 1: Anatomical sites of HNSCCs and OPSCCs.**

HNSCCs arise from the mucosal epithelium of the oral cavity, nasopharynx, oropharynx (soft palate, uvula, palatine tonsils, base of tongue, lingual tonsils, and posterior pharyngeal wall), hypopharynx, and larynx. The oropharynx is located posterior to the oral cavity, extending from the soft palate to the hyoid bone, with most OPSCCs occurring within the palatine tonsils and base of tongue. Created with BioRender.com, 18/05/2024.

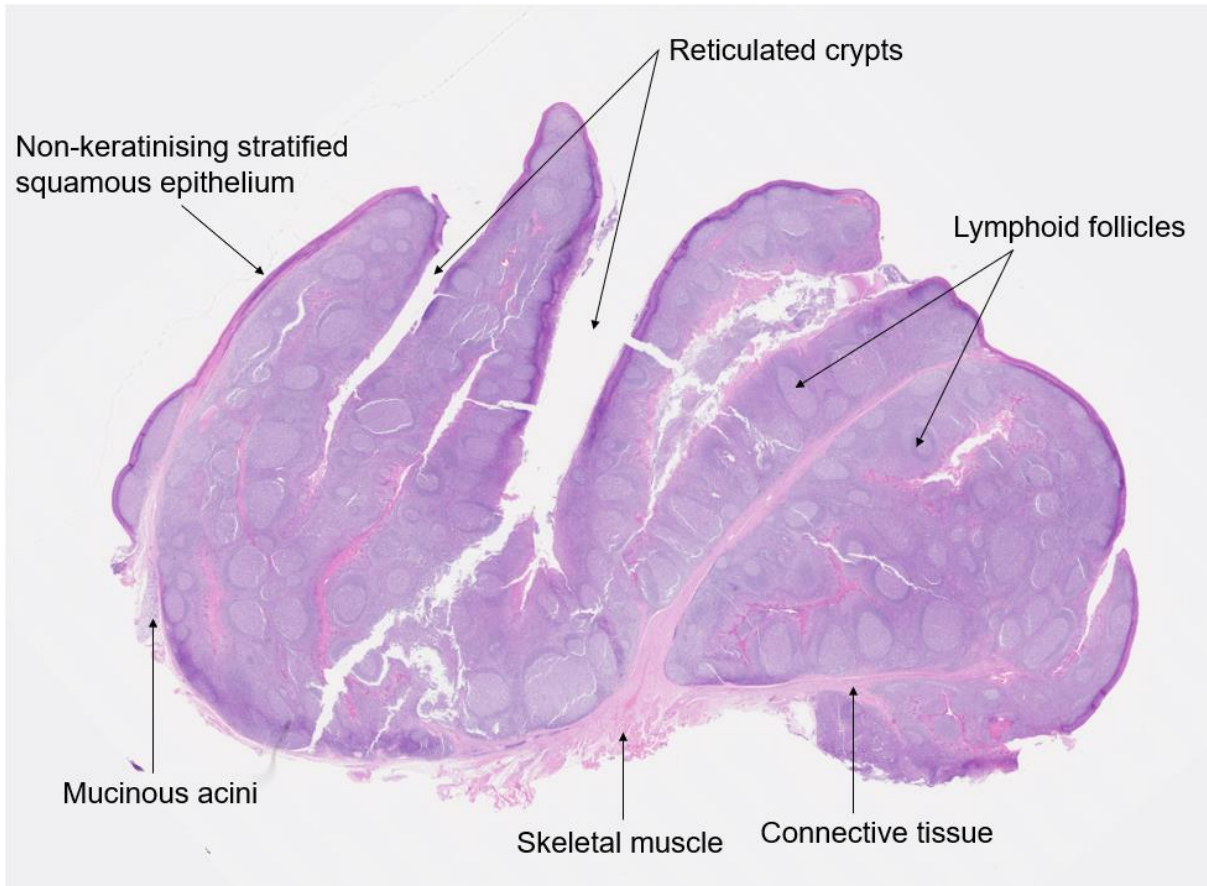


**Figure 2: Histology of the normal palatine tonsil.**

The outer surface of the normal palatine tonsil is covered by non-keratinising stratified squamous epithelium, which invaginates into the underlying tissue forming reticulated crypts. Within the parenchyma reside lymphoid follicles which are spherical or ovoid in shape and contain B and T lymphocytes. Image captured on NDP.view2 software at 0.44x magnification.

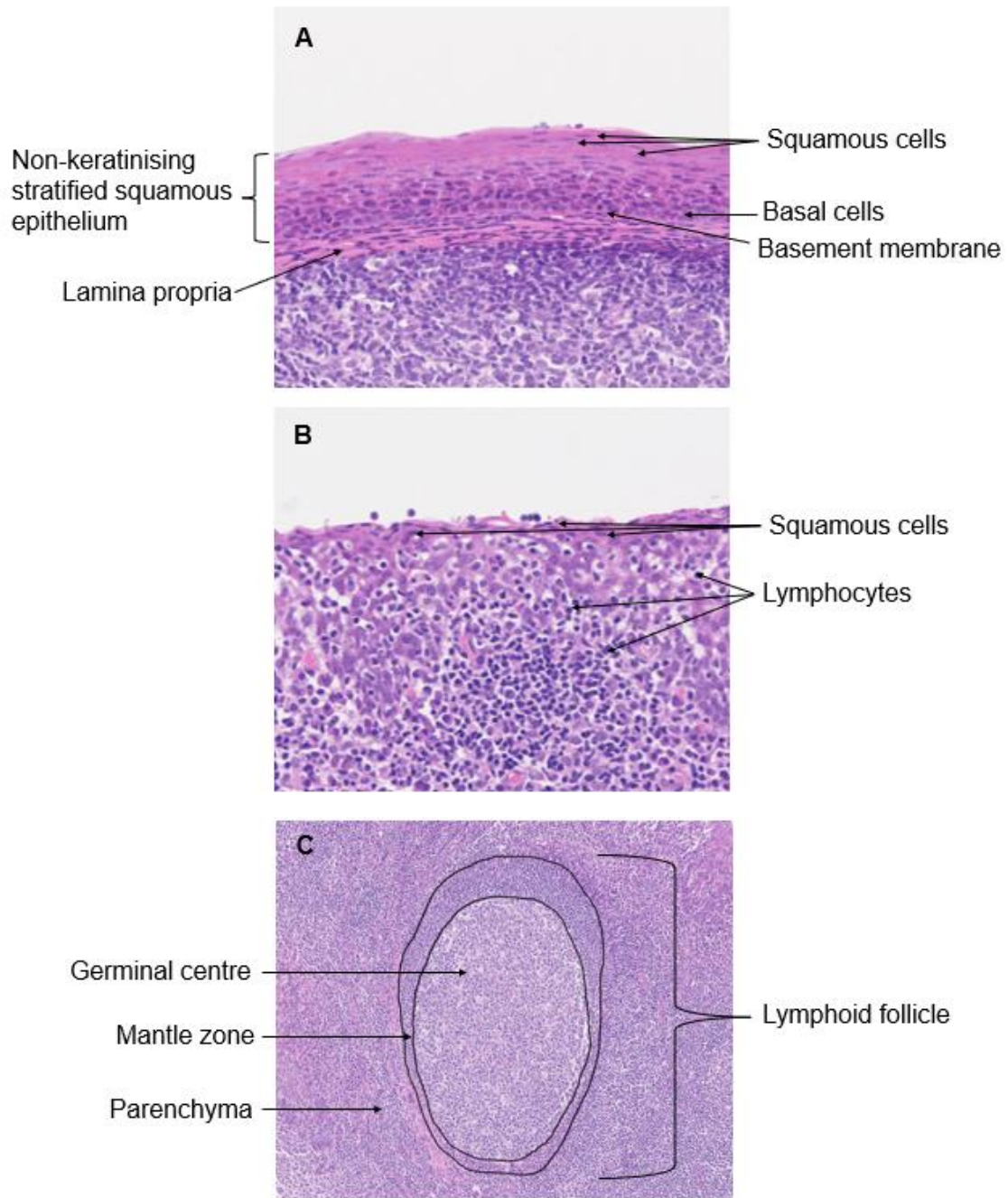


**Figure 3: Histology of the lymphoid follicle, surface epithelium, and reticulated epithelium of the normal palatine tonsil.**

A lymphoid follicle within the tonsil parenchyma, consisting of a germinal centre (light) in the centre and the mantle zone (dark) surrounding it (A). The surface epithelium is non-stratified squamous epithelium, with squamous cells present on the upmost surface, and basal cells towards the bottom resting on the intact basement membrane. The lamina propria consists of connective tissue, which is located below the basement membrane (B). The reticulated epithelium consists of an indistinct basement membrane, which is obscured by the dense infiltration of lymphocytes admixed with squamous cells (C). Images captured on NDP.view2 software at 40x (A and B), and 10x (C) magnification.

## **1.2.2 Epidemiology and risk factors of OPSCC**

The aetiology associated with OPSCC is multifactorial, with epidemiological studies conducted by the International Agency for Research on Cancer (IARC) of the World Health Organisation (WHO) publicising numerous risk factors including tobacco and alcohol, alongside HPV as predominant risk factors (International Agency for Research on Cancer, 2023).

### **1.2.2.1 Human papillomavirus**

HPV was first described in CC tissue by zur Hausen *et al.*, in 1983 (zur Hausen *et al.*, 1983). Globally, CC is both the fourth most commonly diagnosed cancer and the fourth leading cause of cancer-related deaths in women, accounting for 662,301 new cases and 348,874 deaths in 2022 (Ferlay *et al.*, 2024). These statistics were highest in the Asian and African populations with 397,082 new cases and 199,795 deaths and 125,699 new cases and 80,614 deaths respectively, compared to 3,235 new cases and 1,154 deaths within the UK (Ferlay *et al.*, 2024). This disparity between geographical regions could be attributable to smoking, genetics, and ethnicity as well as the absence or limited uptake of vaccination and screening programmes in some parts of the world (Hull *et al.*, 2020, Bruni *et al.*, 2021, Bruni *et al.*, 2022).

In 1983, Syrjänen *et al.*, reported a link between HPV and oral carcinoma (OC), with Gillison *et al.*, establishing a link between HPV and OPSCC in 2000 (Syrjänen *et al.*, 1983, Gillison *et al.*, 2000). It is hypothesised that HPV infection may establish within the reticulated crypts of the palatine tonsil (Kim *et al.*, 2007). In 2018, the estimated number of new global cases of cancers of the oropharynx was 136,000, with 42,100 attributable to HPV infection (de Martel *et al.*, 2020). Unlike CC, there are currently no effective screening programmes for OPSCC (D'Souza *et al.*, 2024) Explanations for this include the inability to adequately sample the tonsillar crypts; precursor lesions not yet being identified within the tonsils; and the justification for a cancer screening programme (Fakhry *et al.*, 2012, Palmer *et al.*, 2014, Quabius *et al.*, 2021, World Health Organisation, 2022). Within the UK, for a cancer screening programme to be implemented, it has to be appraised by the UK National Screening Committee (UK NSC) (UK National Screening Committee, 2022). The criteria dictate that the condition should be an important health problem and that all cost-effective primary prevention interventions have been implemented as far as practicable. Additionally, the screening

test should be safe, simple, precise, and validated, with the distribution of test values and results acceptable to the target population. The screening programme should also be effective in reducing mortality or morbidity, balance the benefits versus harm regarding overdiagnosis and false positives; and be cost effective (UK National Screening Committee, 2022, World Health Organisation, 2022). As no OPSCC precursor lesions have been identified at present, this makes population screening difficult (Timbang *et al.*, 2019). Therefore, emphasis should be placed on raising public awareness around HPV including risk factors, behavioural changes, and widespread usage of the HPV vaccine in order to address the HPV-positive OPSCC epidemic (Timbang *et al.*, 2019). Indeed, HPV accounts for almost 5% of human cancers globally; however, it is important to note that approximately 80% of oncogenic HPV infections are transient, and do not progress to malignancy (Cuschieri *et al.*, 2005, Wood *et al.*, 2017, Bray *et al.*, 2018).

#### **1.2.2.2 Tobacco, alcohol, and other carcinogens**

Historically, OPSCC was associated with chewing and smoking tobacco, and alcohol consumption (Goodman *et al.*, 2015). Among never drinkers, smoking tobacco (ten or more cigarettes per day) for ten years or more is associated with increased risk of OPSCC. However, among never smokers of tobacco, alcohol consumption is only associated with an increased risk of OPSCC when consumed at a high frequency (more than 3 alcoholic drinks daily (Hashibe *et al.*, 2007, Hashibe *et al.*, 2009). Together, tobacco and alcohol consumption (more than 3 alcoholic drinks daily) are associated with HPV-negative OPSCC, with both increasing the risk over 35-fold (Blot *et al.*, 1988, Freedman *et al.*, 2007, Hashibe *et al.*, 2009, Gillison *et al.*, 2012). However, studies have shown that tobacco and alcohol can also increase the risk of HPV-positive OPSCC (Smith *et al.*, 2010, Auguste *et al.*, 2020, Chen *et al.*, 2020, Lai *et al.*, 2022). They can cause cellular alterations, deoxyribonucleic acid (DNA) damage and breaks, HPV oncoprotein overexpression, and greater viral loads, thus promoting HPV infection and persistence (Nakayama *et al.*, 1985, Moore *et al.*, 2001, Giuliano *et al.*, 2002, Torre *et al.*, 2005, D'Souza *et al.*, 2009, Wei *et al.*, 2009, Xi *et al.*, 2009).

Due to public health interventions and reduced tobacco smoking, HPV-negative OPSCCs have declined by approximately 50% in high-income countries (Chaturvedi *et al.*, 2011, Schache *et al.*, 2016). In comparison, tobacco smoking has increased in

the Middle East and several low-income countries, with smokeless tobacco (for example areca nut) highest in South-East Asia (Lee *et al.*, 2018, Zhang *et al.*, 2018, World Health Organisation, 2021). Additionally, the adverse effects of electronic cigarettes upon tumourigenesis remains currently unknown, and will only become evident in years to come (Wilson *et al.*, 2022).

### **1.2.2.3 Trends of disease**

OPSCC is rapidly increasing worldwide in high-income countries including the USA and UK (Chaturvedi *et al.*, 2011, Louie *et al.*, 2015, Mehanna *et al.*, 2016b). Between 1988 and 2004 in the USA, the number of OPSCC cases increased by 225% (Chaturvedi *et al.*, 2011). It was projected that OPSCC incidence would increase by 239% in England between 2011 and 2025; however, this has not yet been realised (Louie *et al.*, 2015). Today, the number of OPSCCs in the USA and UK has now surpassed CC within women, with this epidemic expected to increase for the next 30 years before the efficacy of the HPV vaccine becomes apparent (Lechner *et al.*, 2022, Ferlay *et al.*, 2024).

The incidence of OPSCC is typically higher in men than women (Chaturvedi *et al.*, 2013). In England between 1995 and 2017, the age-standardised incidence rate (ASR) of carcinomas of the oropharynx (palatine tonsils only) increased from 1.0/100,000 to 4.8/100,000 in men and 0.4/100,000 to 1.5/100,000 in women (Office for National Statistics, 2019). Previously, HPV-positive OPSCC was typically seen in middle-aged men with a median age of 53 years, versus a median age of 60 years in HPV-negative OPSCC (Windon *et al.*, 2018, Mahal *et al.*, 2019). However, recent studies have reported that the median age for HPV-positive OPSCC is increasing, with men born after 1935-1940 affected (Chaturvedi *et al.*, 2008, Gillison *et al.*, 2015, Zumsteg *et al.*, 2016, Windon *et al.*, 2018, Tota *et al.*, 2019). This increase is likely related to changes in sexual habits, including early sexual debut, number of oral and vaginal sexual partners, casual sex, and infrequent use of condoms, as well as men generally having more sexual partners (Gillison *et al.*, 2008, D'Souza *et al.*, 2009, Chaturvedi *et al.*, 2015). HPV is a sexually transmitted infection (STI), and it is estimated globally that 31% of men have a genital HPV infection at any one time, supporting the theory that men are reservoirs of HPV infection (Reiter *et al.*, 2010, de Martel *et al.*, 2017, Bruni *et al.*, 2023). Additionally, it is suggested that women are more likely to seroconvert



after a genital HPV-16 infection than men, reducing the risk against any subsequent oral HPV infection by approximately 50%, thus maintaining their lower OPSCC prevalence (Ho *et al.*, 2002, Safaeian *et al.*, 2010, Wilson *et al.*, 2014, Windon *et al.*, 2019).

In 2024, it was reported that the global incidence of HPV-positive OPSCC was 42%; however, the prevalence of HPV in OPSCC varies depending on the geographical region, with 10% and 85% reported in Spain and Lesotho, in comparison to 71% and 51.8% reported in the USA and UK respectively (Schache *et al.*, 2016, Faraji *et al.*, 2019, Maroun *et al.*, 2020, Mena *et al.*, 2020, Fonsêca *et al.*, 2024). This burden corresponds with the higher incidence of HPV-positive OPSCC in White ethnicities, in comparison to Black or Asian/Pacific Islander ethnicities, who are more associated with HPV-negative OPSCC (Chaturvedi *et al.*, 2008, Chaturvedi *et al.*, 2011, Mahal *et al.*, 2019). Low prevalence of HPV-positive OPSCC has been reported in several African countries, despite high incidences of CC, including Mozambique and Cameroon, which may be explained by minimal oral sex behaviours, in comparison to high-income countries (Ndiaye *et al.*, 2013, Blumberg *et al.*, 2015, Oga *et al.*, 2016, Kofi *et al.*, 2019, Rettig *et al.*, 2019). Although oral sex behavioural differences can partially explain the epidemiological differences between different ethnicities; genetic and epigenetic HPV variants may have a role in this, with Black ethnicities with OPSCC having a lower HPV-16 versus higher HPV-18 incidence than White ethnicities (Ragin *et al.*, 2016).

### **1.3 HPV virology**

#### **1.3.1 HPV classification**

HPV is a member of the *Papillomaviridae* family which have an epitheliotropism within various anatomic sites including the skin, genital regions, and oropharynx in both men and women (de Villiers *et al.*, 2004, Schiffman *et al.*, 2016). Over 220 HPV types have been classified, based on the L1 nucleotide sequence, into five genera: alpha, which infect both mucosal and cutaneous epithelium, and beta, gamma, mu, and nu, which infects cutaneous epithelium (Bernard *et al.*, 2010, Van Doorslaer *et al.*, 2016). It is estimated that 54 HPV types are associated with genital infections, versus 19 HPV types associated with HNSCC (de Sanjosé *et al.*, 2010, Gillison *et al.*, 2015, de Martel *et al.*, 2017).

Mucosal *Alphapapillomaviruses* are classified into two types: low-risk HPVs (LR-HPV) and high-risk HPVs (HR-HPV), based on their malignant potential (Bernard *et al.*, 2010, Doorbar *et al.*, 2016). LR-HPVs for example, include HPV-6 and -11 infections that can vary from genital warts to papillomas; however, whilst causing a wide range of pathologies, LR-HPVs do not typically lead to cancer (Middleton *et al.*, 2003, Major *et al.*, 2005).

Currently, the WHO has classified 14 HR-HPV subtypes: HPV-16, -18, -31, -33, -35, -39, -45, -51, -52, -56, -58, -59, -66 and -68 (Kreimer *et al.*, 2005). The most common subtypes are HPV-16 and -18, which cause 70% (50% and 20%, respectively) of cervical squamous cell carcinomas (SCC), and collectively 35% of cervical adenocarcinomas, which are more strongly associated with HPV-18 (Muñoz *et al.*, 2003, Smith *et al.*, 2007, Li *et al.*, 2011). Comparatively, HPV-16 causes 87-96% of OPSCCs, versus HPV-18 causing 1.5-3% (Kreimer *et al.*, 2005, Schache *et al.*, 2016).

### **1.3.2 HPV genome**

HPVs are small double-stranded DNA (dsDNA) viruses with a circular genome of approximately 8,000 base pairs (bp) (de Villiers *et al.*, 2004, Rautava and Syrjänen, 2012). The virion consists of a lipoprotein-free membrane, a core, and a non-enveloped icosahedral protein capsid with a diameter of 55 nm, and a molecular weight of  $5 \times 10^6$  Daltons (Syrjänen, 2018, Dong *et al.*, 2021). Within the genome only one DNA strand is used for transcription, which contains three genomic regions: an early (E) region and a late (L) region which are separated by early ( $pA_E$ ) and late ( $pA_L$ ) polyadenylation sites (essential for early and late viral protein expression). These consist of approximately ten open reading frames (ORFs), that are expressed from polycistronic messenger ribonucleic acids (mRNAs) (Zheng and Baker, 2006, Harden and Munger, 2017). The third region is the upstream regulatory region (URR) (also known as the long control region (LCR) or non-coding region (NCR)), 500-1000 bp long, containing the origin of replication (*ori*). It also contains the early promoter ( $P_E$ ) and regulatory sequences involved in viral transcription (Engel *et al.*, 1983, Harden and Munger, 2017) (Figure 4). Together, the virus encodes six early proteins and two late proteins, with some reports of additional viral proteins of unknown function (E3, E8) in some viral types (Table 1).

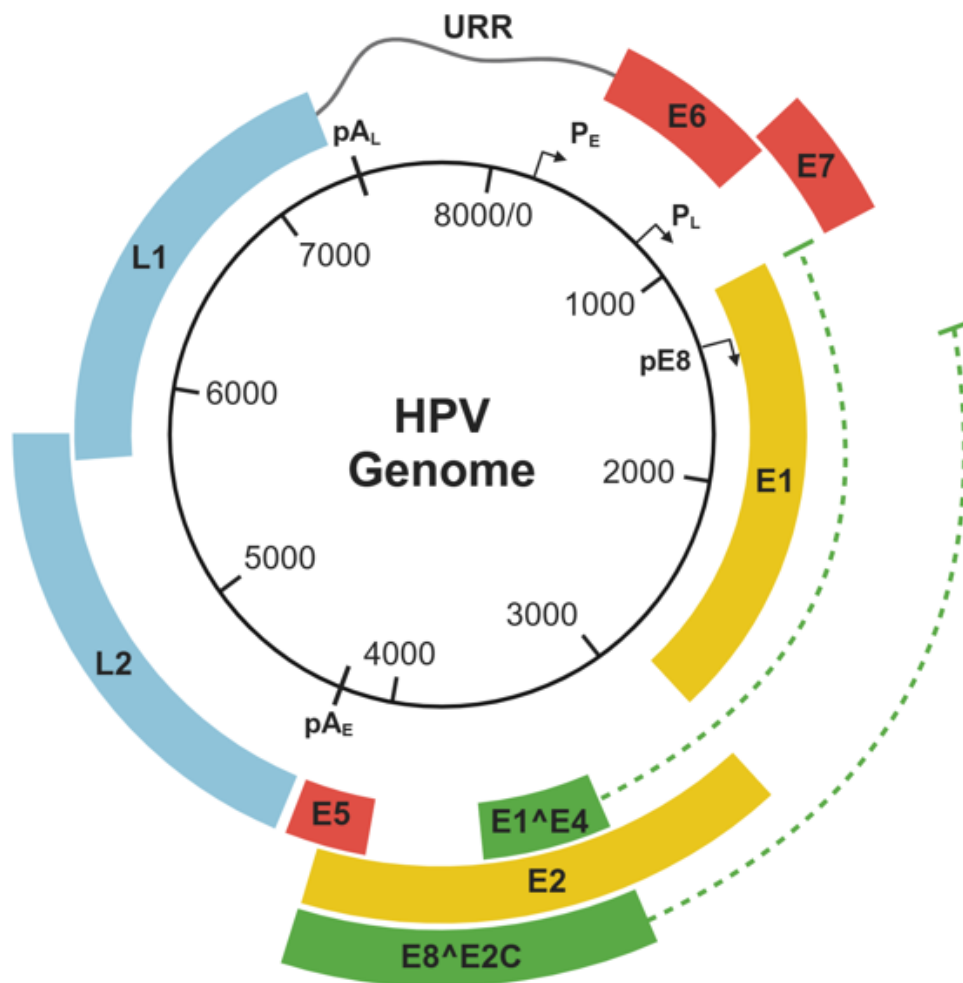


**Figure 4: HPV genome organisation.**

Five early ORFs E1, E2 (in yellow), E5, E6, and E7 (in red) are expressed from the early promoter (p97) at different stages of the HPV viral life cycle. The spliced early transcript E8<sup>E2C</sup> (in green) is expressed from the pE8 within the E1 ORF. E1<sup>E4</sup> (in green) and two late ORFs (L1 and L2; in blue) are expressed from the late promoter (p670) in the upper epithelial layers. The pA<sub>E</sub> and pA<sub>L</sub> are essential for early and late viral protein expression. The URR contains the *ori* and regulatory sequences involved in viral replication and transcription. Created with BioRender.com, 31/07/2024.

**Table 1: Molecular sizes and functions of the proteins in HPV genome**

	<b>Viral protein</b>	<b>Length</b>	<b>Cell localisation</b>	<b>Function</b>	<b>References</b>
<b>Early region</b>	E1	649 AA	Nucleus and cytoplasm	ATPase-dependent DNA helicase with unique enzymatic activity involved in viral replication	(Castro-Muñoz <i>et al.</i> , 2019, The UniProt Consortium, 2022)
	E2	365 AA	Nucleus and cytoplasm	DNA-binding protein involved in viral transcription and replication. Recruits E1 to initiate replication	(Mohr <i>et al.</i> , 1990, Chiang <i>et al.</i> , 1992, Bouvard <i>et al.</i> , 1994b, Davy <i>et al.</i> , 2009, The UniProt Consortium, 2022)
	E3	Unknown	Unknown	Unknown function; present in only a few HPV types	(Rautava and Syrjänen, 2012)
	E1 <sup>^</sup> E4	92 AA	Cytoplasm	Assemble into amyloid fibrils disrupting cellular keratin networks contributing to virion release	(Doorbar <i>et al.</i> , 1991, Wang <i>et al.</i> , 2004, McIntosh <i>et al.</i> , 2008, Davy <i>et al.</i> , 2009, The UniProt Consortium, 2022)
	E5	83 AA	Cytoplasm and membrane	Believed to induce EGFR signalling and lesser oncoprotein possibly associated with enhancement of E6 and E7	(Bouvard <i>et al.</i> , 1994a, Valle and Banks, 1995, Fehrmann <i>et al.</i> , 2003, Maufort <i>et al.</i> , 2010, Wasson <i>et al.</i> , 2017, The UniProt Consortium, 2022)
	E6	158 AA	Nuclear and cytoplasm	Oncoprotein that degrades p53 tumour suppressor protein	(Scheffner <i>et al.</i> , 1990, Lee <i>et al.</i> , 2007, The UniProt Consortium, 2022)
	E7	98 AA	Nuclear and cytoplasm	Oncoprotein that degrades pRb tumour suppressor protein	(Dyson <i>et al.</i> , 1989, Patrick <i>et al.</i> , 1994, Knapp <i>et al.</i> , 2009, The UniProt Consortium, 2022)
	E8	Unknown	Unknown	Unknown function; present in only a few HPV types	(Rautava and Syrjänen, 2012)
	E8 <sup>^</sup> E2C	177 AA	Nuclear	Transcriptional repressor of viral replication	(Hubert <i>et al.</i> , 1988, Straub <i>et al.</i> , 2015, The UniProt Consortium, 2022)
<b>Late region</b>	L1	505 AA	Cytoplasm	Major capsid protein	(Kirnbauer <i>et al.</i> , 1992, Day <i>et al.</i> , 2013, The UniProt Consortium, 2022)
	L2	473 AA	Nuclear and cytoplasm	Minor capsid protein	(Kirnbauer <i>et al.</i> , 1992, Day <i>et al.</i> , 2004, The UniProt Consortium, 2022)

### 1.3.2.1 Early region

The early region encodes the proteins E1, E2, E4, E5, E6, and E7, an approximately 4,000 bp region transcribed from a P<sub>E</sub> (p97 in HPV-16 and p105 in HPV-18), which lies upstream from the E6 ORF (Engel *et al.*, 1983, Schneider-Gädicke and Schwarz, 1986, Smotkin and Wettstein, 1986, Thierry *et al.*, 1987, Romanczuk *et al.*, 1990, Grassmann *et al.*, 1996). The P<sub>E</sub> is responsible for almost all early protein expression, and is tightly controlled within the URR (Smotkin and Wettstein, 1986, Zheng and Baker, 2006). E1 and E2 are well-conserved ORFs and are necessary for viral replication and transcription; E4 is believed to contribute to virion release and transmission from the upper epithelial layers; and E5, E6, and E7 are oncoproteins that are involved in malignant transformation (Mohr *et al.*, 1990, Patrick *et al.*, 1994, de Villiers *et al.*, 2004, Wang *et al.*, 2004, Lee *et al.*, 2007, Maufort *et al.*, 2010, Egawa *et al.*, 2012).

#### 1.3.2.1.1 E1

E1 is a protein that possesses unique enzymatic activity and plays a vital role in viral replication (Egawa *et al.*, 2012, Castro-Muñoz *et al.*, 2019). It localises within the nucleus and cytoplasm of host cells and consists of 3 domains. The N-terminus contains a nuclear localisation signal (NLS) and a nuclear export signal (NES); the central portion contains a DNA-binding domain (DBD) and interacts with the *ori* in the URR; and the C-terminus, which contains an adenosine 5'-triphosphatase (ATPase)-dependant helicase (Castro-Muñoz *et al.*, 2019). E1 recruits replication factors and with E2, binds to E1- and E2-binding sites (E2BSs), within the *ori* of the URR (Egawa *et al.*, 2012, Nakahara *et al.*, 2015). This interaction results in the formation of a hexameric DNA helicase, which together with adenosine triphosphate (ATP), hydrolyses and unwinds viral DNA (Castro-Muñoz *et al.*, 2019).

#### 1.3.2.1.2 E2

E2 is a protein essential for viral genome replication with E1 protein as well as transcriptional activation of E6 and E7 (Bernard *et al.*, 1989, Mohr *et al.*, 1990, Chiang *et al.*, 1992, Bouvard *et al.*, 1994b). It consists of two domains which are connected by a flexible linker sequence or “hinge”: an N-terminus which encodes a transactivation domain (TAD) and a C-terminus, which encodes a DBD (Giri and Yaniv, 1988, McBride *et al.*, 1988, McBride *et al.*, 1989). E2 proteins bind to four consensus palindromic

E2BSs, three of which flank the E1 binding site within the *ori* of the URR and recruit E1 (Mohr *et al.*, 1990, Yasugi *et al.*, 1997, Sánchez *et al.*, 2008). The fourth E2BS induces transcription from the P<sub>E</sub>, leading to the production of the early viral proteins (Sánchez *et al.*, 2008).

The E2 DBD binds to E2BSs within the viral genome, whereas the TAD interacts with cellular chromatin which tethers to the viral episomes during cell division, which is essential for viral genome persistence and productive HPV infection (Androphy *et al.*, 1987, Skiadopoulou and McBride, 1998, Ilves *et al.*, 1999, Bastien and McBride, 2000, Abroi *et al.*, 2004, Feeney and Parish, 2009). Bromodomain protein 4 (Brd4) is involved in viral genome tethering to mitotic chromosomes in some papillomavirus types, however this is not the case in *Alphapapillomavirus*, where they can interact with mitotic chromosomes independently (You *et al.*, 2004, McPhillips *et al.*, 2006). Nevertheless, Brd4 is still required for E2-mediated transactivation for all papillomaviruses, and replication in HPV-16 (McPhillips *et al.*, 2006, Wang *et al.*, 2013). E2 is expressed in the early stages of the HPV viral lifecycle within the host nucleus and cytoplasm (Xue *et al.*, 2010). It suppresses cellular growth by repressing the P<sub>E</sub>, resulting in inhibition of E6 and E7 expression (Bernard *et al.*, 1989, Romanczuk *et al.*, 1990, Thierry and Howley, 1991, Dowhanick *et al.*, 1995). E2 is also frequently disrupted during viral integration, resulting in uncontrollable overexpression of E6 and E7 oncoproteins during malignant transformation (Davy *et al.*, 2009, Xue *et al.*, 2010).

#### **1.3.2.1.3 E8<sup>Δ</sup>E2C**

A nuclear spliced transcript, E8<sup>Δ</sup>E2, can also exist in some papillomavirus types, which is formed from the E1 ORF (pE8) spliced into the E2 3' exon containing the DBD (Hubert *et al.*, 1988, Wang *et al.*, 2011). Because of this, it is unable to bind to E1 protein and transcriptional regulators that are bound to the full-length of E2 (Kurg *et al.*, 2010). Consequently, E8<sup>Δ</sup>E2 is a strong replicational and transcriptional repressor by competing with and excluding E1 from the *ori* and preventing E2 activation (Straub *et al.*, 2015).

#### **1.3.2.1.4 E4 and E1<sup>E4</sup>**

E4 is encoded with the E2 ORF, but lacks an AUG initiation codon. Therefore, it is translated from a spliced mRNA consisting of the first five amino acid (AA) residues (including initiation codon) of E1 (Longworth and Laimins, 2004, Doorbar, 2013). This cytoplasmic E1<sup>E4</sup> fusion protein, is the most abundantly expressed protein within the productive stages of the viral lifecycle (Doorbar *et al.*, 1986, McIntosh *et al.*, 2008, Davy *et al.*, 2009). It is considered a late protein, as its transcript is initiated from the P<sub>L</sub>, before it is polyadenylated at the pA<sub>E</sub> site to encode the protein (Yu *et al.*, 2022). E1<sup>E4</sup> protein is believed to assemble into amyloid fibrils, disrupting cellular keratin networks and inducing abnormalities of the cornified cell envelope, thus contributing to virion release and transmission from the upper epithelial layers (Doorbar *et al.*, 1991, Wang *et al.*, 2004, Brown *et al.*, 2006, McIntosh *et al.*, 2008).

#### **1.3.2.1.5 E5**

E5 is a small, hydrophobic transmembrane protein that localises to the Golgi, endoplasmic reticulum, nuclear membrane, and to a lesser extent plasma membranes (Fehrmann *et al.*, 2003, Genter *et al.*, 2003). It consists of three α-helical structures known as transmembrane domains (TMD), with short regions at the N- and C-termini (Barbaresi *et al.*, 2010, Krawczyk *et al.*, 2011). The functions of E5 are not well understood, with studies suggesting that E5 proteins from different HPV types are believed to have different functions during the productive phase of the viral lifecycle. HPV-16, -18, and -31 models demonstrated that E5 proteins possess no apparent role in viral genome maintenance or proliferation (Fehrmann *et al.*, 2003, Genter *et al.*, 2003, Wasson *et al.*, 2017). However, it was demonstrated within the HPV-18 raft model that E5-induced epidermal growth factor receptor (EGFR) signalling contributed to cell cycle progression and unscheduled DNA synthesis in differentiating suprabasal cells, but not genome amplification or late viral protein expression (Wasson *et al.*, 2017). Nevertheless, it is considered as an oncoprotein, lesser so than E6 and E7, as expression of E5 is not detected within HPV-positive tumours, suggesting that it may enhance rather than initiate carcinogenesis (Bouvard *et al.*, 1994a, Valle and Banks, 1995, Maufort *et al.*, 2010).

### 1.3.2.1.6 E6

E6 is an oncoprotein that is localised to both the nucleus and cytoplasm of the host cell (Lee *et al.*, 2007). It consists of N-terminal (E6N) and C-terminal (E6C) zinc-binding domains, each consisting of two CXXC zinc-binding motifs (Barbosa *et al.*, 1989, Zanier *et al.*, 2012, Zanier *et al.*, 2013). Each domain is homologous and formed from three  $\alpha$ -helices and three  $\beta$ -sheets, except for the N-terminal regions of E6N and E6C, which possess a flexible loop and an additional  $\beta$ -sheet respectively (Zanier *et al.*, 2012). These domains are connected by a linker  $\alpha$ -helix which forms a hydrophobic binding pocket, allowing it to recruit the E3 ubiquitin ligase E6-associated protein (E6AP) by binding to its LXXLL motif (Huibregtse *et al.*, 1991, Huibregtse *et al.*, 1993, Scheffner *et al.*, 1993, Chen *et al.*, 1998, Zanier *et al.*, 2013). The association between E6 and E6AP forms a tertiary complex with the tumour suppressor protein, p53, a cell cycle and DNA repair regulator, which is then ubiquitinated and degraded in HR-HPV types, resulting in uncontrolled cell proliferation and tumourigenesis (Scheffner *et al.*, 1990, Huibregtse *et al.*, 1993). This does not occur in LR-HPV types as they are unable to degrade p53 (Mietz *et al.*, 1992). Despite both LR- and HR-HPV E6 can bind to the p53 C-terminus; however, only HR-HPV E6 is capable of binding to the core region of p53 (Crook *et al.*, 1991, Li and Coffino, 1996). Additionally, p53 degradation can also occur by targeting its coactivator p300/CREB-binding protein (CBP) via the formation of the p53-E6-p300-CBP complex (Patel *et al.*, 1999, Zimmerman *et al.*, 1999).

Host-cell immortalisation is also driven by E6 protein, which upregulates human telomerase reverse transcriptase (hTERT), a catalytic subunit of telomerase. This interaction promotes increased hTERT activity resulting in subsequent lengthening of telomeres and ultimately chromosomal instability and cellular immortalisation (Klingelutz *et al.*, 1996, Veldman *et al.*, 2001). Again, this is only achieved with HR-HPV types, as LR-HPV E6 proteins do not activate telomerase (Van Doorslaer and Burk, 2012). Lastly, E6 proteins also contain PSD95/Discs Large/ZO-1 (PDZ)-binding motifs (PBM) within the C-terminus that binds to and degrades PDZ domains, which are involved in cell polarity and adhesion, as well as mitotic control (Zhang *et al.*, 2007, Charbonnier *et al.*, 2011, Zanier *et al.*, 2013, Marsh *et al.*, 2017). These PDZ domains are only targeted by HR-HPV E6 proteins; however, as LR-HPV E6 proteins lack the PBM, which is required for episomal maintenance and genome amplification, suggests



their importance within the viral lifecycle (Lee and Laimins, 2004, Thomas *et al.*, 2008, Nicolaidis *et al.*, 2011, Delury *et al.*, 2013).

#### **1.3.2.1.7 E7**

E7 is a multifunctional oncoprotein, like E6, which consists of three conserved regions: CR1 and CR2 both within the N-terminus, and CR3 within the C-terminus (Patrick *et al.*, 1994). It also contains both NLS and NES, suggesting that it can traffic to and have functions in both the nucleus and cytoplasm (Knapp *et al.*, 2009). CR2 contains a LXCXE motif which mediates high affinity binding with retinoblastoma protein (pRb), as well as pocket proteins p107 and p130. CR3 however, is a homologous structure containing two  $\alpha$ -helices and two  $\beta$ -sheets located within the C-terminus, as well as a zinc-binding domain (two CXXC motifs), which also interacts with pRb via its C-terminus (Barbosa *et al.*, 1989, Dyson *et al.*, 1989, Munger *et al.*, 1989b, Dyson *et al.*, 1992, Patrick *et al.*, 1994, Dahiya *et al.*, 2000, Liu *et al.*, 2006).

E7 proteins within HR-HPV types have a greater transformation potential than LR-HPV, which is attributable to their ability to bind with high affinity to pRb (Scheffner *et al.*, 1992). This is because the amino acid preceding the LXCXE motif is different in both LR- (glycine) and HR-HPV (aspartic acid) E7 proteins (Heck *et al.*, 1992, Zhang *et al.*, 2006). pRb is a tumour suppressor protein that is an important regulator of the cell cycle (Dyson *et al.*, 1989). In normal cells, hypophosphorylated pRb binds to the transcription factor E2F preventing S phase entry (Chellappan *et al.*, 1991). However, when pRb becomes hyperphosphorylated by the cyclin D/cyclin-dependent kinase (CDK) 4-6 complex, E2F is released allowing for S phase re-entry (Ewen *et al.*, 1993, Flemington *et al.*, 1993, Helin *et al.*, 1993, Kato *et al.*, 1994). This is tightly controlled by the CDK inhibitor p16INK4A (CDKN2A or p16), which regulates cell cycle progression via a negative feedback loop by binding to CDK 4-6, and preventing cyclin D/CDK 4-6 complex formation (Serrano *et al.*, 1993, Serrano, 1997). pRb remains hypophosphorylated and binds to E2F ultimately leading to cell cycle arrest through the G1 phase (Chellappan *et al.*, 1991, Serrano, 1997). During infection, binding of E7 to pRb results in its degradation, dysregulation of E2F, and promotes G1/S phase transition, thus resulting in cell cycle progression and increased cell proliferation (Dyson *et al.*, 1989, Munger *et al.*, 1989b, Dyson *et al.*, 1992). Phosphorylation of pRb also causes overexpression of p16 which inhibits the cyclin D/CDK 4-6 complex, and

prevents G1/S phase transition (Serrano *et al.*, 1993, Kamb *et al.*, 1994, Li *et al.*, 1994, Nobori *et al.*, 1994, Fåhræus *et al.*, 1996). This ultimately induces uncontrolled proliferation and subsequent transformation to malignancy.

#### **1.3.2.1.8 The synergistic relationship of E6 and E7**

Both E6 and E7 proteins are encoded by a single bicistronic transcript, with splicing allowing for oncoprotein expression. They work together synergistically which is necessary for malignancy, as absence of either protein directly affects the other proteins' actions (Butz *et al.*, 2003, Zheng *et al.*, 2004, Downham *et al.*, 2024). Therefore, they have evolved numerous mechanisms to prevent this, with only a handful discussed above. Dysregulation of pRb by E7 results in overexpression of p53, and is counteracted by E6 interacting with E6AP, resulting in ubiquitination of p53, which are the main targets for transformation (Scheffner *et al.*, 1993). Additionally, both E6 and E7 are required to induce keratinocyte immortalisation and resistance to terminal differentiation, as well as target host-signalling pathways and mediate immune evasion (Münger *et al.*, 1989a, Scarth *et al.*, 2021). Together, the cooperative activities of E6 and E7 oncoproteins are necessary for persistent infection and subsequent malignant transformation.

#### **1.3.2.2 Late region**

The late region encodes the proteins L1 and L2, an approximately 3,000 bp region transcribed from a P<sub>L</sub> (p670 in HPV-16 and p811 in HPV-18) which is responsible for all late protein expression, and lies within the E7 ORF (Engel *et al.*, 1983, Grassmann *et al.*, 1996, Wang *et al.*, 2011). L1 and L2 are well-conserved ORFs and structural capsid proteins that are involved in assembly and trafficking of the virion (de Villiers *et al.*, 2004, Day *et al.*, 2013, Van Doorslaer *et al.*, 2016).

##### **1.3.2.2.1 L1**

L1 is a major capsid protein that is arranged into 72 pentameric capsomeres, totalling 360 L1 molecules within a virion (Kirnbauer *et al.*, 1992, Chen *et al.*, 2000). Each of these pentamers contains an eight stranded  $\beta$ -jellyroll core, which is supported by the extended "invading arms" of the N- and C-termini (Chen *et al.*, 2000, Modis *et al.*, 2002, Wolf *et al.*, 2010). The C-terminus of L1 interacts with other capsomeres by extending out and linking via calcium ions and disulphide bonds, stabilising the

structure (Wolf *et al.*, 2010). L1 is also involved in trafficking of the virion to the endosomes, but is retained within the cytoplasm (Day *et al.*, 2013). In all papillomaviruses, the L1 protein is the most conserved protein, with sequence differences of at least 10% between each genotype (Bernard *et al.*, 2010). As the primary structural protein, L1 can self-assemble into virus-like particles (VLPs), upon which current prophylactic vaccines are based (Chen *et al.*, 2000, Paavonen *et al.*, 2007).

#### **1.3.2.2.2 L2**

L2 is a minor capsid protein with up to 72 proteins in one single capsid (Kirnbauer *et al.*, 1992, Buck *et al.*, 2008). A sequence close to the N-terminus is exposed on the virion surface during a conformational change, whilst the remaining L2 sequence is hidden within the viral capsid (Liu *et al.*, 1997, Richards *et al.*, 2006). The N-terminus of L2 interacts with L1 via a disulphide hairpin loop (Buck *et al.*, 2008, Campos and Ozbun, 2009, Gambhira *et al.*, 2009). Additionally, the C-terminus contains a peptide which helps facilitate its exit from the late endosome (Kämper *et al.*, 2006). L2 is also involved in encapsidation and trafficking of the viral genome to the *trans*-Golgi network (TGN) prior to entering the host nucleus (Buck *et al.*, 2008, Day *et al.*, 2013).

### **1.4 Biology of infection**

#### **1.4.1 HPV viral entry**

HPV virions enter the epithelium via micro-abrasions or a discrete cell population and bind to either the basement membrane or extracellular matrix (ECM) (Culp *et al.*, 2006, Roberts *et al.*, 2007, Herfs *et al.*, 2012, Cerqueira *et al.*, 2016). *In vivo* and *in vitro* models suggest that HPV uses retrograde filopodia transport to reach and bind to heparin sulphate proteoglycans (HSPGs) on basal cells, via its L1 protein (Joyce *et al.*, 1999, Girolou *et al.*, 2001, Roberts *et al.*, 2007, Schelhaas *et al.*, 2008, Smith *et al.*, 2008b). Following attachment, cyclophilin (CyP) B facilitates conformational changes in the capsid, exposing the L2 N-terminus which is subsequently cleaved by furin (Richards *et al.*, 2006, Bienkowska-Haba *et al.*, 2012). This causes decreased binding affinity of the capsid for HSPGs (Kines *et al.*, 2009). Internalisation of the virus occurs via endocytosis, with various studies detailing different endocytic pathways with regards to HPV-16 including clathrin- and caveolin-mediated, and -independent endocytosis (Spoden *et al.*, 2008, Laniosz *et al.*, 2009, Schelhaas *et al.*, 2012).

Trafficking of the viral genome into the nucleus is a critical step in HPV infection (Aksoy *et al.*, 2017). The virion localises to early endosomes, before transportation to late endosomes/lysosomes via the cellular endosomal sorting complex required for transport (ESCRT), whose interaction with L2 protein has been shown to be necessary for viral infection (Spoden *et al.*, 2008, Laniosz *et al.*, 2009, Broniarczyk *et al.*, 2014). The use of an L1 antibody has been used to assess the dissociation of L1 from the L2/DNA complex, which is facilitated by pH reduction as well as CyPs (Chen *et al.*, 2000, Bienkowska-Haba *et al.*, 2012, DiGiuseppe *et al.*, 2014). Leaving the majority of L1 retained within the endosome, the L2/DNA complex traffics to the TGN, Golgi, and endoplasmic reticulum, mediated by the retromer complex, before entering the nucleus (Laniosz *et al.*, 2009, Day *et al.*, 2013, Lipovsky *et al.*, 2013, DiGiuseppe *et al.*, 2014). The cell cycle must progress into mitosis to allow trafficking of the L2/DNA complex into the host-cell nucleus, causing nuclear envelope disruption and L2-mediated binding of viral DNA to mitotic chromosomes (Pyeon *et al.*, 2009, Aydin *et al.*, 2014, Aydin *et al.*, 2017). Following nuclear entry, the L2/DNA complex is delivered to nuclear regions known as nuclear domain 10 (ND10) or promyelocytic leukaemia (PML) bodies, a critical step for establishing infection and initiating viral transcription (Day *et al.*, 2004).

#### **1.4.2 HPV viral lifecycle**

Following delivery of the L2/DNA complex into the nucleus, the viral genome is amplified to 50-100 copies per cell (Maglennon *et al.*, 2011). This is achieved by E2 DBD binding to E2BSs within the *ori* of the URR which recruits E1 protein and DNA replication machinery (Mohr *et al.*, 1990, Yasugi *et al.*, 1997, Ilves *et al.*, 1999, Sánchez *et al.*, 2008, McKinney *et al.*, 2016). E2 both induces and represses transcription by targeting the P<sub>E</sub> alongside Brd4, which results in subsequent maintenance of low episomal copy number within the basal cells (Romanczuk *et al.*, 1990, Ozbun, 2002, McKinney *et al.*, 2016). Brd4 also interacts with the E2 TAD in most papillomavirus types and together with cellular chromatin, tethers to the viral episomes, which is essential for viral genome persistence and productive HPV infection (Androphy *et al.*, 1987, Skiadopoulou and McBride, 1998, Bastien and McBride, 2000, Abroi *et al.*, 2004, You *et al.*, 2004, McPhillips *et al.*, 2006, Feeney and Parish, 2009). However, this is not the case with HPV-16, as it can interact with mitotic chromosomes independently, with the ATP-dependent DNA helicase ChIR1,

regulating chromatin attachment and maintaining episomal HPV-16 E2 (McPhillips *et al.*, 2006, Parish *et al.*, 2006a, Parish *et al.*, 2006b, Harris *et al.*, 2017). As a result, E1 converts to a DNA helicase and displaces E2 from the URR, whilst both E6 and E7 oncoproteins are expressed at relatively low levels (Sanders and Stenlund, 1998, Thomas *et al.*, 1999, Oh *et al.*, 2004).

During HPV infection, uninfected daughter cells undergo normal cell division and become detached from the basement membrane, removing themselves from the cell cycle (Doorbar *et al.*, 1997, Li and Kirschner, 2014). However, infected daughter cells containing episomal DNA partition evenly, either remaining within the basal layer or migrating to the suprabasal layer and remaining active within the cell cycle, entering into S phase whilst undergoing differentiation (Cheng *et al.*, 1995, Doorbar *et al.*, 1997, Feeney and Parish, 2009). As mentioned above, both E6 and E7 oncoproteins are expressed at relatively low levels; however, they are still able to bind to the cell cycle regulators p53 and pRb, which ensures continuation to S phase (Dyson *et al.*, 1989, Scheffner *et al.*, 1990, Thomas *et al.*, 1999, Oh *et al.*, 2004). The P<sub>L</sub> becomes activated, which leads to increased production of E1 and E2, and E4 and E5, which ensures both viral and productive replication (Hummel *et al.*, 1992, Fehrman *et al.*, 2003). The lifecycle terminates when the L1 and L2 capsid proteins are expressed and encapsidate the viral genomes, before E4 facilitates progeny virion release from the uppermost epithelial layers (Hummel *et al.*, 1992, Florin *et al.*, 2002, Wang *et al.*, 2004). Virion release may then help recapitulate a new HPV infection locally, or within other individuals.

### **1.4.3 HPV-mediated carcinogenesis**

Within the cervix, HPV infection occurs within the transformation zone (TZ) of the squamocolumnar junction (SCJ), which consists of non-keratinising stratified squamous epithelium (ectocervix) transitioning to simple columnar epithelium (endocervix) (Figure 5) (Herfs *et al.*, 2012, Dudás, 2023). Within the head and neck, it is hypothesised that HPV infection may establish within the reticulated crypts of the palatine tonsil (Kim *et al.*, 2007). HPV pathogenesis within the oropharynx remains poorly understood in comparison to the cervix; however possible explanations include possession of transitional epithelium similar to the cervix; a discontinuous basement membrane, which provides greater susceptibility to foreign antigens; the deep crypts

possibly functioning as a reservoir for HPV; and the abundance of lymphocytes and programmed cell death-ligand 1 (PD-L1) expression, representing an immune-privileged site (Figure 6) (Lyford-Pike *et al.*, 2013, Elrefaey *et al.*, 2014, Chi *et al.*, 2015).

Most cervical and oral HPV infections are transient and clear within two years, but failure to clear a persistent HR-HPV infection may result in malignant transformation (Plummer *et al.*, 2007, Kreimer *et al.*, 2013, D'Souza *et al.*, 2020, Bettampadi *et al.*, 2021). However, latency has been observed experimentally in rabbit models and the cervix, suggesting that it may increase the likelihood of persistent HPV infection (Maglennon *et al.*, 2011, Hammer *et al.*, 2019). Persistent infection can occur when HPV is either episomal or integrated within the host genome; integration is often related to uncontrollable overexpression of E6 and E7 oncoproteins, caused by E2 becoming continually disrupted during viral integration (Vinokurova *et al.*, 2008, Xue *et al.*, 2010, Parfenov *et al.*, 2014). This increases viral load amplification to more than 1000 copies per cell (Reinson *et al.*, 2015).

Persistent HR-HPV infection within the cervix can lead to the development of the precursor lesions known as cervical intraepithelial neoplasia's (CINs), which can progress to CC (Herfs *et al.*, 2012, Lee *et al.*, 2017). However, it is currently unknown whether any precursor lesions exist within the palatine tonsils. This may be related to OPSCCs possessing a rapid growth rate, making such lesions difficult to detect (Tamás *et al.*, 2011, Palmer *et al.*, 2014, Quabius *et al.*, 2021). HPV-16 appears to persist longer than other HR-HPV types, and may contribute to higher cancer risk, which is reflected in the high percentages of HPV-16-associated CC and OPSCC (Muñoz *et al.*, 2003, Koshiol *et al.*, 2006, Schiffman *et al.*, 2010, Schache *et al.*, 2016). Additionally, HPV-16 E6 seropositivity could be detected 20-30 years before OPSCC presentation; therefore, detection of E6 and E7 oncoproteins in serum/plasma samples could be useful for identifying pre-cancerous lesions (Kreimer *et al.*, 2019).

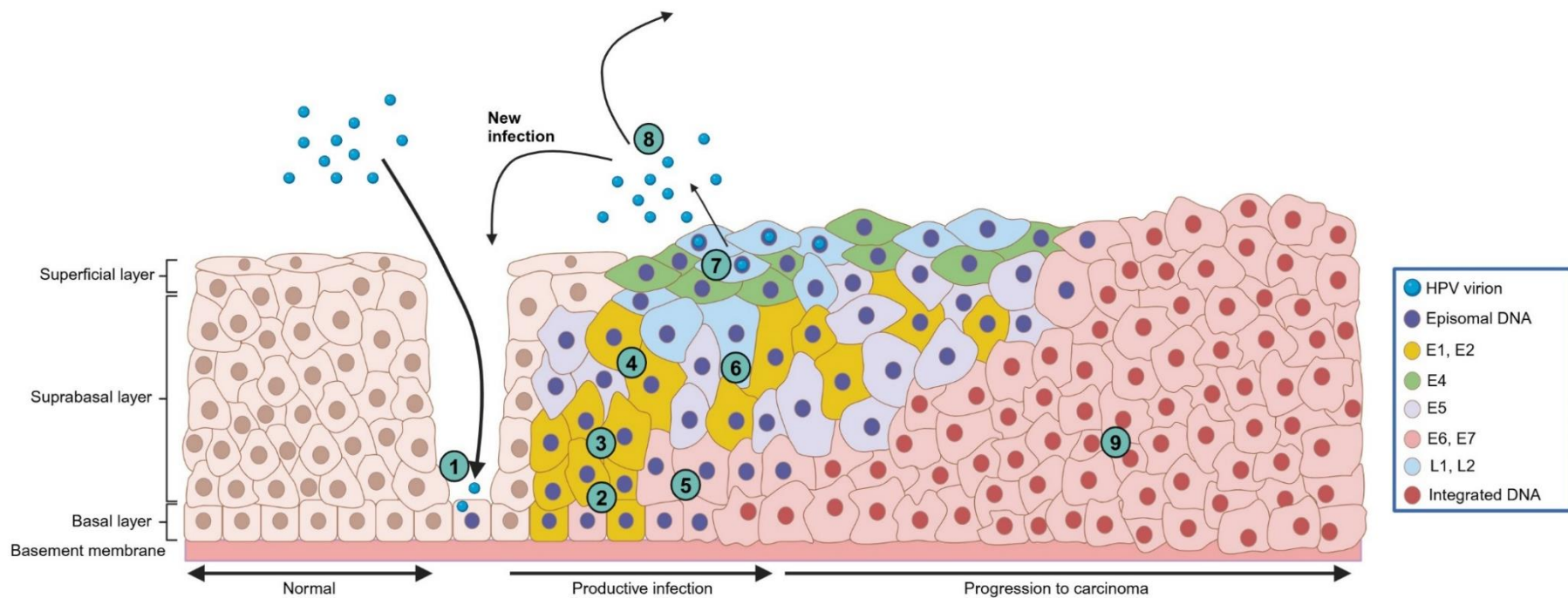


**Figure 5: HPV-mediated progression to CC.**

HPV virion infects basal cells resting on the basement membrane through micro-abrasions in the cervical epithelium (1). Following infection, E1 and E2 are expressed, whilst E6 and E7 are expressed at relatively low levels (2). Basal cells containing episomal DNA replicate and migrate into the suprabasal layer (3). In the suprabasal layer, the viral genome is replicated further and the late proteins L1 and L2 are expressed (4). E6 and E7 are still expressed at relatively low levels (5). There is increased production of E1, E2, E4, and E5, ensuring viral and productive replication (6). L1 and L2 are expressed and encapsidate the viral genome to form progeny virions within the nucleus. E4 is also expressed, which facilitates progeny virion release from the upper epithelial layer (superficial layer) (7). The virus can then initiate a new infection (8). Untreated high-risk HPV infections can progress to invasive carcinoma, which is associated with viral genome integration and subsequent uncontrollable overexpression of E6 and E7 oncoproteins (9). Created with BioRender.com, 23/05/2024.

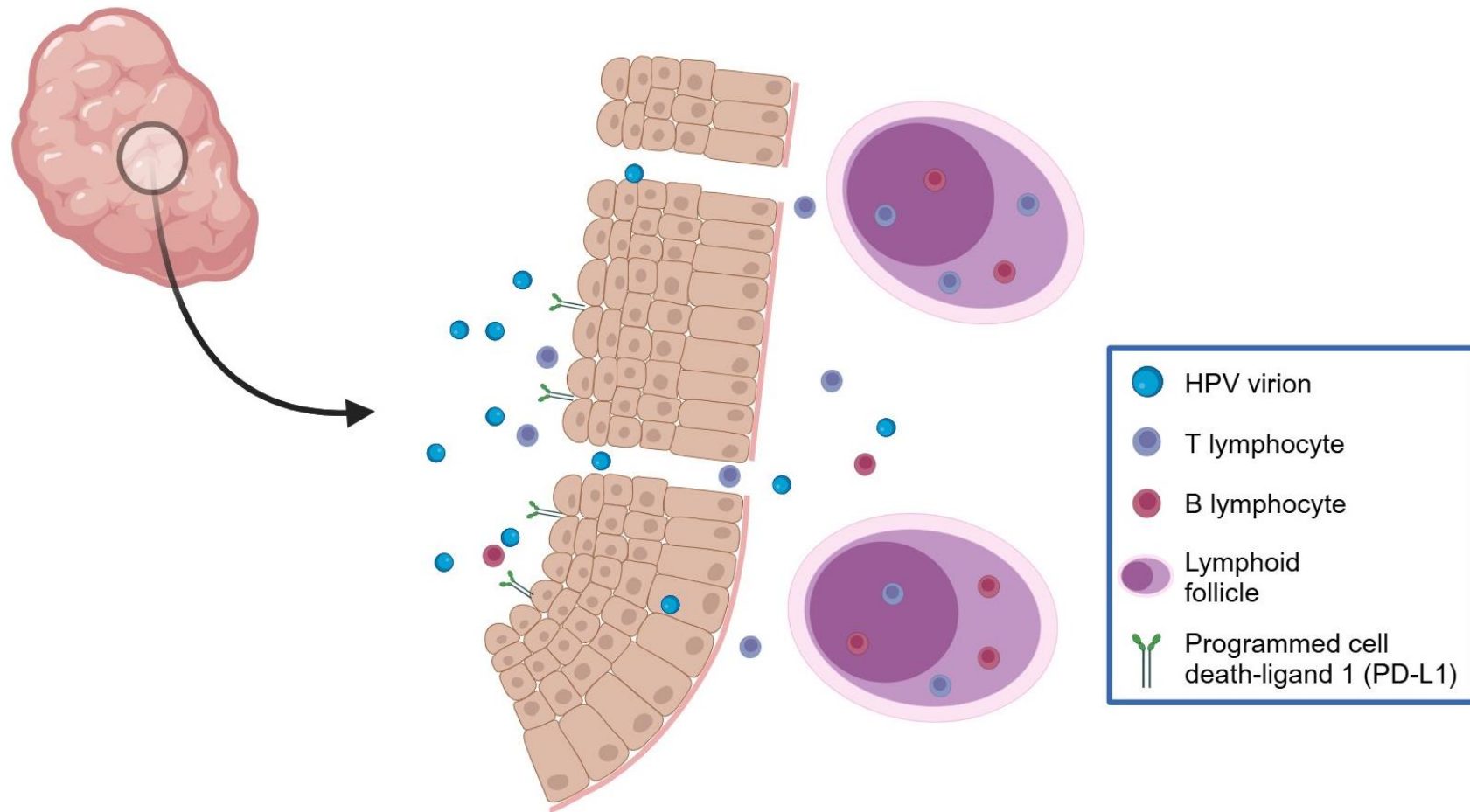


**Figure 6: HPV-mediated carcinogenesis within the tonsillar crypt.**

Tonsillar crypt believed to be the site for HPV infection within the oropharynx. The reticulated epithelium, discontinuous basement membrane, deep crypt, and lymphocyte and PD-L1 abundance are factors that may help HPV infection establish. Created with BioRender.com, 23/05/2024.



## **1.5 Clinical management of OPSCC**

### **1.5.1 Clinical presentation, examination, and diagnosis**

Both HPV-positive and HPV-negative OPSCC patients typically present with symptoms including a neck mass, globus sensation (lump in throat), bleeding, weight loss, otalgia (ear pain), change in voice/muffled voice/“hot potato voice”/dysphonia/dysarthria, dysphagia (difficulty swallowing), and odynophagia (painful swallowing). The presence of a neck mass and otalgia are more common in HPV-positive OPSCCs, with dysphagia and odynophagia more commonly observed in HPV-negative OPSCCs (McIlwain *et al.*, 2014). In HPV-positive OPSCC, as the primary tumour is small and believed to originate within the reticulated crypts, this makes diagnosis difficult as it may be missed during clinical examination and imaging (Cianchetti *et al.*, 2009).

As per the Head and Neck Cancer: UK National Multidisciplinary Guidelines (2024), patients who present with suspected OPSCC should be seen within a dedicated ear, nose, and throat (ENT), oral and maxillofacial surgery, or neck lump specialist clinic within two weeks. A thorough head and neck examination is performed, alongside fibre-optic nasopharyngolaryngoscopy, skin inspection (for enlarged lymph nodes), ultrasound, and ultrasound-guided tissue sampling either by fine needle aspiration (FNA) or core biopsy. Other imaging modalities are also performed including computed tomography (CT) and magnetic resonance imaging (MRI) alongside ultrasound imaging, which are essential for primary tumour staging, bone invasion, and lymph node involvement (Homer and Winter, 2024).

### **1.5.2 Histopathology**

Prior to 2022, the WHO International Classification of Diseases (ICD) 10<sup>th</sup> revision, classified cancers of the tonsil and oropharynx by their ICD codes; C09 Malignant neoplasm of tonsil, and C10 Malignant neoplasm of oropharynx (World Health Organisation, 2004). Now, in the ICD 11<sup>th</sup> revision, the codes have completely changed, including separate codes for specific anatomy, histopathology, and malignant neoplasm severity. Their ICD codes are now 2B69 Malignant neoplasms of tonsil and 2B6A Malignant neoplasms of oropharynx, with both including codes for SCCs (World Health Organisation, 2019/2021).

Tissue biopsies and surgical resections of primary OPSCCs are reported according to The Royal College of Pathologists (RCPATH) guidelines (2021) for histopathological reporting of carcinomas of the oropharynx and nasopharynx (Hunter *et al.*, 2021). Conventional OPSCCs are categorised into three subtypes based on their morphological features: keratinising (KSCC) which are most-commonly associated with HPV-negative OPSCC; non-keratinising (NKSCC) and non-keratinising with maturation (partially keratinising/hybrid variant), which are most-commonly associated with HPV-positive OPSCC (El-Mofty and Lu, 2003, El-Mofty and Patil, 2006, El-Mofty *et al.*, 2008). Other less common SCC variants include adenosquamous carcinoma, basaloid SCC, lymphoepithelial carcinoma, papillary SCC, spindle cell (sarcomatoid) carcinoma, and verrucous carcinoma (El-Mofty, 2014, Bishop, 2015). HPV-positive OPSCCs typically demonstrate non-keratinising morphology; however they may be any histological variant (Helliwell and Giles, 2016).

#### **1.5.2.1 Keratinising squamous cell carcinomas**

Typically, KSCCs arise within the surface stratified squamous epithelium which can demonstrate various severities of dysplasia and/or carcinoma *in-situ* (CIS) (Bishop, 2015). Dysplasia is graded 1-3 depending on the atypia of the surface epithelium: grade 1 (lower one-third)-mild dysplasia; grade 2 (lower two-thirds)-moderate dysplasia; and grade 3 (full thickness)-severe dysplasia/CIS (Pai and Westra, 2009). KSCC can also be graded as well, moderately, and poorly differentiated (Bishop, 2015).

Well differentiated tumours have epithelium resembling that of the surface epithelium, which invades through the basement membrane and infiltrates as nests and cords, inducing a stromal desmoplasia (Figure 7). They contain polygonal cells with distinct cell borders and eosinophilic cytoplasm. Diffuse squamous differentiation is present, with cells arranging into layers with irregular keratinisation known as keratin pearls, and intercellular bridges (El-Mofty and Lu, 2003, El-Mofty and Patil, 2006, Bishop, 2015). Poorly differentiated tumours have immature cells demonstrating nuclear pleomorphism, atypical mitoses, and little-to-no keratinisation (Bishop, 2015).

### **1.5.2.2 Non-keratinising squamous cell carcinomas**

Tumours infiltrate as sheets, nests, and trabeculae with sharply defined, smooth borders, eliciting little stromal desmoplasia (Figure 8). They have basaloid morphology, including monomorphic and ovoid to spindle shaped cells, with indistinct borders, hyperchromatic nuclei, and prominent mitoses. There is also a high nuclear-to-cytoplasmic ratio as well as apoptosis and comedonecrosis observed (El-Mofty and Lu, 2003, El-Mofty and Patil, 2006, El-Mofty, 2014, Bishop, 2015). HPV-positive OPSCC can also show involvement of the surface epithelium, which are classed as an abrupt extension of the tumour (Kim *et al.*, 2007, Bishop, 2015). Occasionally, some tumours can exhibit morphological features that are seen in both KSCCs and NKSCCs, such as focal squamous maturation and focal and partial keratinisation, with these tumours referred to as either non-keratinising with maturation SCCs or hybrid variant (El-Mofty *et al.*, 2008).

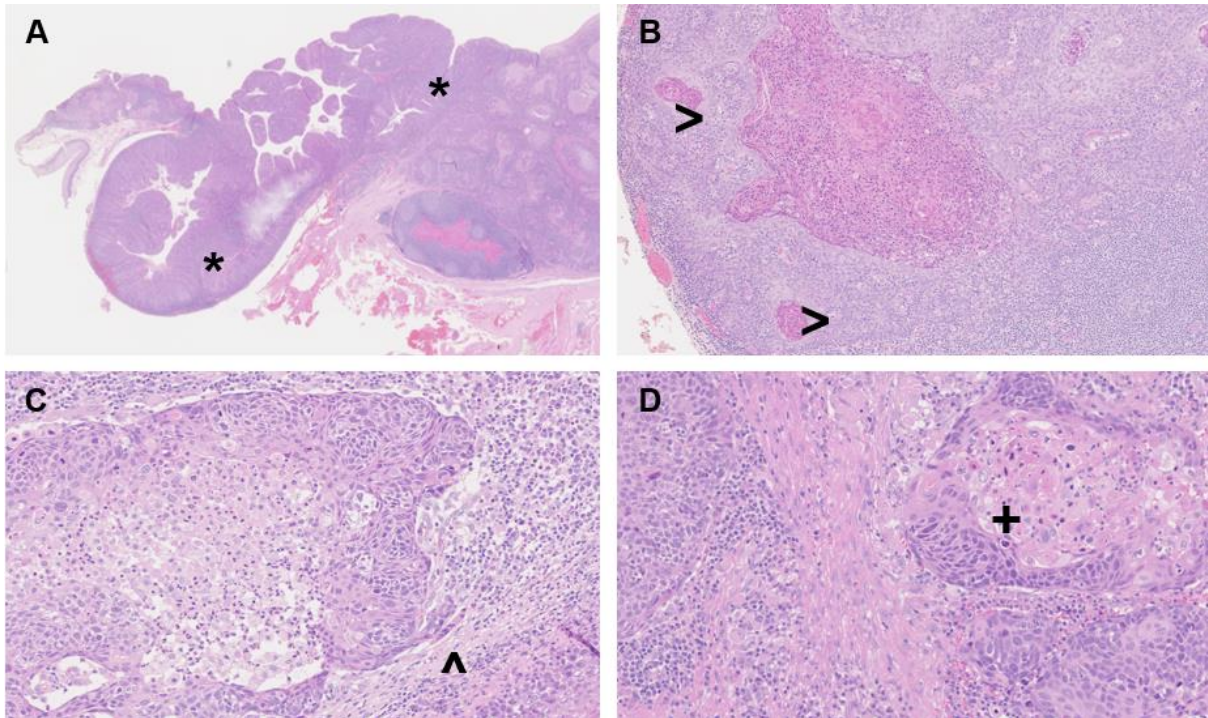


**Figure 7: Histology of keratinising squamous cell carcinoma.**

Infiltrative nests (\*) of tumour cells within the surface epithelium have infiltrated into the underlying tissue, as well as an extension of the tumour (A). Tumour nests contain polygonal cells with distinct cell borders and keratin pearls (>) (B). Stromal desmoplasia (^) is also present (C and D), as well as demonstration of a poorly differentiated tumour (C) and intercellular bridges (+) (D). Images captured on NDP.view2 software at 1.25x (A), 10x (B), and 20x (C and D) magnification.

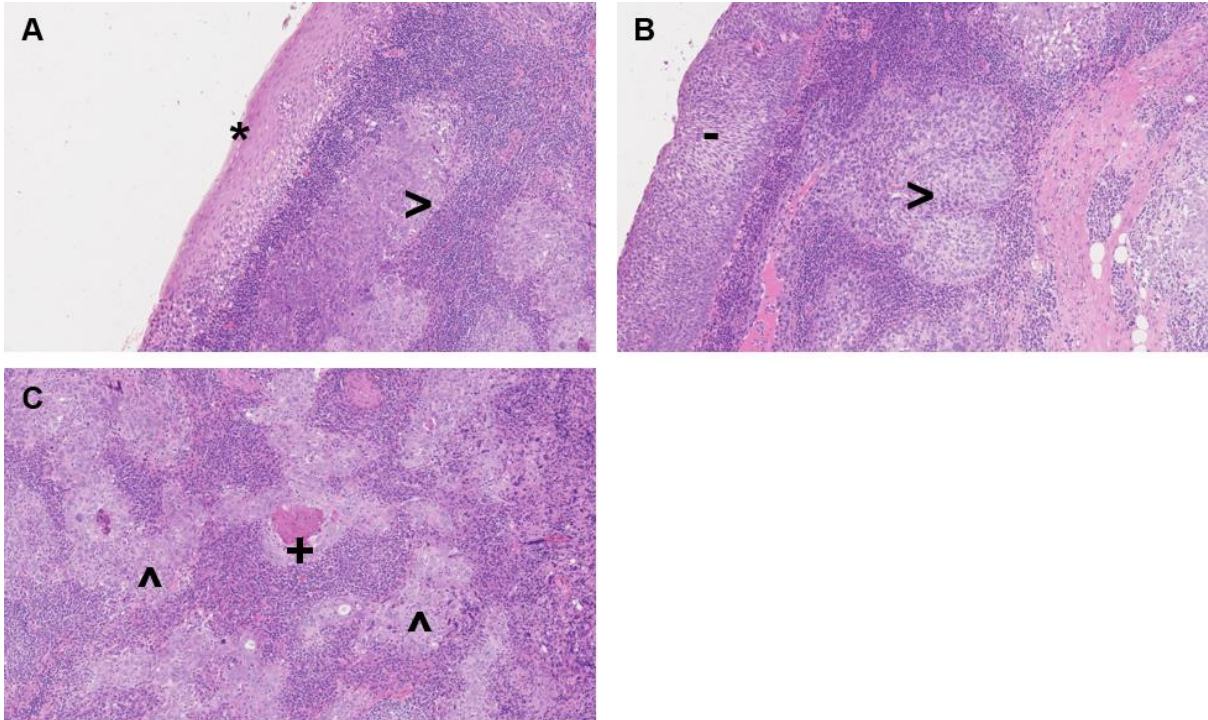


**Figure 8: Histology of non-keratinising squamous cell carcinoma.**

There is an area of moderate dysplasia (\*) seen within the surface epithelium, with infiltrative nests of tumour cells (>) within the underlying tissue (A and B). It appears the tumour has infiltrated into the surface epithelium (-), giving this region a crypt-like phenotype. Tumour nests also contain poorly differentiated cells and irregular borders (^), as well as comedonecrosis (+) (C). Morphology is consistent with reticulated epithelium. Images captured on NDP.view2 software at 10x (A-C) magnification.

### 1.5.3 HPV testing

#### 1.5.3.1 p16 immunohistochemistry

The National Institute of Health and Care Excellence (NICE) (2016), Union for International Cancer Control (UICC) 8<sup>th</sup> edition (2016), American Joint Committee on Cancer (AJCC) 8<sup>th</sup> edition (2017), College of American Pathologists (CAP) (2018), International Collaboration on Cancer Reporting (ICCR) (2018), National Comprehensive Cancer Network (NCCN) (2020), RCPATH (2021) and the WHO Classification of Tumours; Head and Neck Tumours 5<sup>th</sup> edition, volume 9 (2024), have advised that p16INK4A (p16) immunohistochemistry (IHC) be performed as part of HPV testing on all OPSCC (Brierly *et al.*, 2016, National Institute for Health and Care Excellence (NICE), 2016, Amin *et al.*, 2017, Lewis *et al.*, 2018a, Lewis *et al.*, 2018b, National Comprehensive Cancer Network, 2020, Hunter *et al.*, 2021, World Health Organisation, 2024). HPV testing should be carried out using validated methods and appropriate tissue controls within a diagnostic laboratory service which is accredited and quality assured by an organisation such as International Organisation for Standardisation (ISO) (ISO15189:2022) (Mehanna *et al.*, 2016a, Homer and Winter, 2024).

Since 2003, p16 IHC has been used as the validated surrogate marker for HPV status within OPSCC (Klussman *et al.*, 2003, Sedghizadeh *et al.*, 2016, Lewis *et al.*, 2018b, Hunter *et al.*, 2021). Criterion for p16-positive IHC is based on the current guidelines for moderate to intense nuclear and cytoplasmic staining in 70% or more of the tumour cells (Lewis *et al.*, 2018b, Hunter *et al.*, 2021). It has become the widely accepted method, largely due to low cost, simplicity and feasibility, as well as being considered a sensitive technique for transcriptionally-active HR-HPV (El-Naggar and Westra, 2012, Lewis *et al.*, 2018b). However, the use of p16 as a standalone marker within OPSCC has drawn criticism given its specificity, which ranges from 76-100% (Schlecht *et al.*, 2012, Shelton *et al.*, 2017, Arsa *et al.*, 2021).

In 2017, major updates were made in the AJCC 8<sup>th</sup> edition (2017) regarding staging of OPSCCs (Amin *et al.*, 2017). It includes important changes for OPSCC, separating it into two entities: HPV-positive and HPV-negative, based on p16 positivity using the tumour, node, and metastasis (TNM) system (Brierly *et al.*, 2016, Amin *et al.*, 2017, Lydiatt *et al.*, 2017). These necessary changes have resulted in positive outcomes,

with both the clinical and pathological staging system of the AJCC 8<sup>th</sup> edition (2017) performing better than the 7<sup>th</sup> edition (2010) with predicting 5-year overall survival (Gupta *et al.*, 2018).

Both the CAP (2018) and RCPATH (2021) guidelines recommend that additional HR-HPV-specific testing be performed on OPSCCs that have been determined as p16-positive (Lewis *et al.*, 2018b, Hunter *et al.*, 2021).

### **1.5.3.2 HPV DNA *in-situ* hybridisation**

Within the UK, HPV DNA *in-situ* hybridisation (ISH) is the current HR-HPV-specific testing of choice; however, this is not widely available (Henley-Smith *et al.*, 2020). UK studies have recommended routine performance of HR-HPV-specific testing for p16-positive IHC confirmation, as well as for cases where p16 IHC is equivocal; for example, overexpression in KSCCs, negative in NKSCCs, or only nuclear or cytoplasmic staining patterns (Thavaraj *et al.*, 2011, Craig *et al.*, 2019, Craig *et al.*, 2020, Shinn *et al.*, 2021).

HPV DNA ISH detects the presence of the HPV viral genome and is identifiable as blue dots within the host cell nucleus (Lewis *et al.*, 2010, Schlecht *et al.*, 2012). The staining patterns can be identified as either episomal, which appears as large, homogeneous and globular blue precipitate, or integrated, appearing as small, stippled blue precipitate within the nuclei (Witt *et al.*, 2014). This technique has a high specificity, allowing for distinction between episomal and integrated DNA; however, it has reduced sensitivity particularly with low viral loads, as well as it being technically difficult to interpret (Lewis *et al.*, 2012, Mirghani *et al.*, 2015, Suresh *et al.*, 2021).

### **1.5.3.3 Discordance of p16 and HPV DNA or RNA status in OPSCCs**

Despite p16 being used as a surrogate marker for HPV in clinical practice, there are issues surrounding its lack of specificity and false positives. Numerous studies have reported that p16 staining within OPSCC formalin-fixed, paraffin-embedded (FFPE) tissues were found to be discordant with HPV DNA and RNA testing including polymerase chain reaction (PCR) and ISH, reporting overall sensitivities between 69-100% and specificities between 76-100% (Schache *et al.*, 2011, Jordan *et al.*, 2012, Pannone *et al.*, 2012, Schlecht *et al.*, 2012, Holzinger *et al.*, 2013, Mirghani *et al.*,

2015, Shelton *et al.*, 2017, Arsa *et al.*, 2021). It is suggested that inconsistencies in the performance of different detection techniques may account for these discordant p16/HPV results (Guzmán-Arocho and Nishino, 2022), with numerous studies reporting 4-30% of cases showing discordance between p16 and HPV DNA or RNA status (Smith *et al.*, 2008a, Rischin *et al.*, 2010, Ukpo *et al.*, 2011, Bishop *et al.*, 2012, Holzinger *et al.*, 2012, Rietbergen *et al.*, 2013, Ndiaye *et al.*, 2014, Rietbergen *et al.*, 2014, Kerr *et al.*, 2015, Mirghani *et al.*, 2016, Augustin *et al.*, 2018, Randén-Brady *et al.*, 2019). This is problematic as 4-30% of discordant cases could be inaccurately staged, including its insufficiency for determining suitable treatment de-escalation that is suitable in the instance of HPV-mediated disease (Henley-Smith *et al.*, 2020, Wagner *et al.*, 2021).

In 2023, a multicentre, multinational meta-analysis looked at the discordance and prognostic implications between p16 and HPV DNA and RNA status (Mehanna *et al.*, 2023). OPSCC patients with discordant p16-positive/HPV-negative or p16-negative/HPV-positive status had a worse prognosis than double-positive patients and a better prognosis than double-negative patients. Discordant p16-negative/HPV-positive patients displayed poorer prognosis, survival, and recurrence rates than double-positive patients; however, they had slightly better prognosis, survival and rate of recurrence than double-negative patients. However, they should not be treated the same as double-negative patients, as they would need to undergo an appropriate de-intensified treatment regimen. This meta-analysis suggests that p16 alone for de-escalation trial risk stratification may introduce bias, and harm ever smoker patients who have p16-positive/HPV-negative tumours. Therefore, they propose that p16 IHC alone is not sufficient in routine clinical practice for predicting patient prognosis and determining an appropriate treatment regimen (Mehanna *et al.*, 2023).

## **1.6 Aptamers**

### **1.6.1 History of aptamers**

Aptamers are single-stranded (ss) RNA or DNA oligonucleotides, that were first discovered independently by three research groups (Ellington and Szostak, 1990, Robertson and Joyce, 1990, Tuerk and Gold, 1990). RNA aptamers were first discussed in early 1990, where they were described using *in vitro* selection to modify a group I ribozyme (RNA enzyme) to cleave DNA instead of ssRNA (Robertson and



Joyce, 1990). That same year, one group discussed the selection of RNA molecules to the bacteriophage T4 DNA polymerase, naming this process systematic evolution of ligands by exponential enrichment (SELEX), and another group, in quick succession, reported on RNA molecules binding to an organic dye, naming them aptamers (aptus (to fit) and meros (part)) (Ellington and Szostak, 1990, Tuerk and Gold, 1990). Aptamers are capable of binding with high-affinity to specific targets based on their three-dimensional structures (Ellington and Szostak, 1990, Robertson and Joyce, 1990, Tuerk and Gold, 1990, Bock *et al.*, 1992). Their three-dimensional structures are characterised by loops, stems, bulges, triplexes, and quadruplexes, allowing aptamers to bind via van der Waals forces, hydrogen bonds, and electrostatic interactions to a large variety of targets (Hermann and Patel, 2000).

### **1.6.2 RNA and DNA aptamers**

Prior to the isolation of DNA aptamers, RNA aptamers were considered the most favourable option, as they were believed to fold into more varied three-dimensional structures due to the absence of Watson-Crick base pairing and the presence of a 2'-hydroxyl group (Wang *et al.*, 2019b). This theory was quashed when the first DNA aptamers were first isolated in 1992, demonstrating that it had similar binding properties to RNA aptamers (Bock *et al.*, 1992, Ellington and Szostak, 1992). In fact, DNA aptamers are capable of forming more complicated structures, as the libraries they are selected from contain longer randomised sequences (Zhu *et al.*, 2015). They are also simpler and cheaper to synthesise, in addition to being more stable than RNA aptamers, as they lack a 2'-hydroxyl group present on the deoxyribose sugar (Savory *et al.*, 2010, Zhu *et al.*, 2012). Furthermore, the RNA SELEX process requires reverse transcription polymerase chain reaction (RT-PCR) for every selection round compared to PCR in DNA SELEX, as well as initial transcription for conversion from a DNA library (Tuerk and Gold, 1990, Bock *et al.*, 1992).

### **1.6.3 Systematic evolution of ligands by exponential enrichment**

Aptamers can be isolated using the *in vitro* process known as SELEX, which is considered the gold-standard methodology for aptamer development. SELEX involves the target molecule or protein pool undergoing alternate, multiple rounds of ligand selection and amplification, to exponentially enrich the target and obtain the highest affinity product (Tuerk and Gold., 1990).

The SELEX process begins with obtaining a random ssDNA or ssRNA library and incubating it with the target molecule on an immobilised surface (Figure 9) (Röthlisberger and Hollenstein, 2018, DeRosa *et al.*, 2023). Aptamer libraries contain a random or wobble (N) region typically 15-70 nucleotides (nt) long, which is flanked by constant primer regions for PCR amplification (Zhu *et al.*, 2015). These libraries can contain as many as  $10^{14}$ - $10^{16}$  random sequences (Zhang *et al.*, 2019). The length of the wobble region is important, as longer random sequences, for instance  $\geq 30$  nt, allows for screening of more diverse libraries, thus better aptamer library development. However, if a shorter wobble region is used, for example 15 nt, the copy number would be in the thousands, even within a small input volume. Therefore, they cover a more restricted sequence, contributing highly to primers during formation of the aptamer structure (Blind and Blank., 2015). However, this is up for debate as it has been regarded that libraries with random sequences longer than 25 nt contain the same number of sequence variants as shorter libraries and identical aptamer structures (Kulbachinskiy, 2007).

Next, unbound sequences are separated, and aptamers bound to the target are retained, followed by determining the quantity of DNA or RNA, to measure the progress of the selection before undergoing amplification with PCR (DNA) or RT-PCR (RNA) (Stoltenburg *et al.*, 2007, Blind and Blank, 2015, Röthlisberger and Hollenstein, 2018). The resulting dsDNA or dsRNA sequences after amplification are reverted back to ssDNA or ssRNA sequences, with the new enriched pool then used for the subsequent round of selection (Stoltenburg *et al.*, 2007, Röthlisberger and Hollenstein, 2018). Through iterative rounds of SELEX, the bound target molecule is exposed to different selection pressures with increased stringencies per round. The conditions are chosen based on the nature of the target and the intended end-use of the aptamer, for example temperature, pH and salinity (including binding and washing conditions) (Stoltenburg *et al.*, 2007, DeRosa *et al.*, 2023). A negative selection step is also included to minimise enrichment of unspecific sequences that have bound to the target molecule (Stoltenburg *et al.*, 2007, Röthlisberger and Hollenstein, 2018). The SELEX process can be repeated for 8-16 rounds until no further DNA or RNA is detectable, with the final SELEX round sequenced (for example next generation sequencing (NGS)) to identify suitable candidates for post-SELEX experiments (Blind and Blank, 2015, Röthlisberger and Hollenstein, 2018, Komarova and Kuznetsov, 2019).

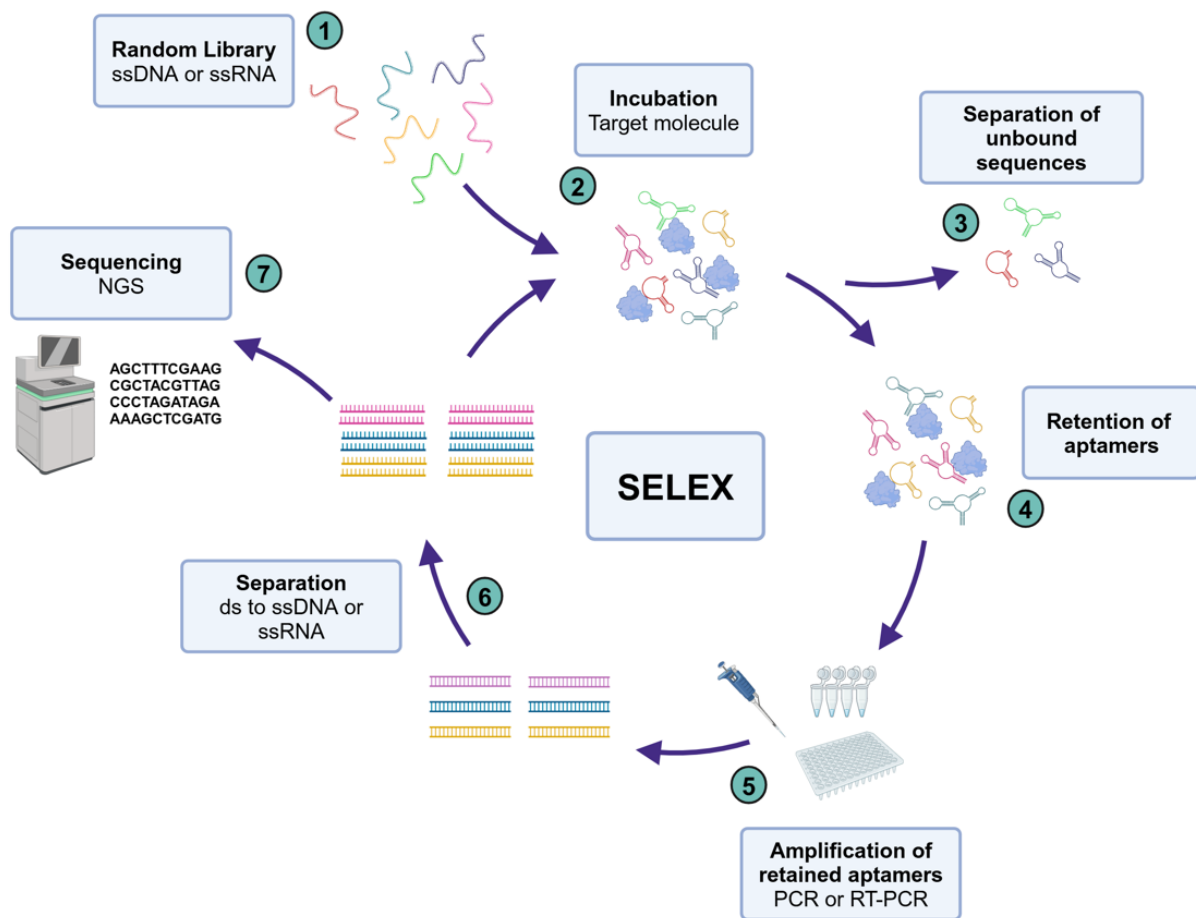


**Figure 9: Overview of SELEX process.**

The process begins with random ssDNA or ssRNA libraries which are flanked by constant primer regions required for amplification (1). The library is incubated with the target molecule on a immobilised surface (2), before unbound sequences are separated (3). Aptamers bound to the target are retained (4) and undergo amplification by PCR (DNA) or RT-PCR (RNA) (5). The resulting dsDNA or dsRNA sequences are reverted back to ssDNA or ssRNA (6), with the new enriched pool used for the subsequent cycle of selection. This selection cycle can be repeated 8-16 times (2-6), to enrich the sequence pool which is sequenced (NGS) (7) to identify suitable aptamer candidates. Created with BioRender.com, 31/07/2024.

#### 1.6.4 Aptamers in diagnostic and therapeutic applications

Aptamers are also known as 'chemical antibodies', as they bind specifically to target molecules via an induced fit mechanism and have a similar binding-affinity compared to monoclonal antibodies (Zhu *et al.*, 2015, Bauer *et al.*, 2019). Additionally, aptamers are also capable of recognising a distinct epitope present on the target molecule (Jenison *et al.*, 1994). Aptamers have clinical and industrial advantages over antibodies including non-immunogenicity, high penetration, unlimited targets, less batch variation, short production times, and cost-effectiveness (Sun and Zu, 2015). It has been previously calculated that it costs 0.002 USD per assay for an aptamer versus 2 USD per assay for an antibody against CD4 (Zhang *et al.*, 2010). This could be useful in pathological techniques including histochemistry and fluorescent staining, with aptamer-based histochemistry (apthistochemistry) assays useful for biomarker detection in clinical FFPE samples by making the process more cost-effective (Zeng *et al.*, 2010, Zamay *et al.*, 2017).

Aptamers have been isolated against a varying range of targets including bacteria, viruses, metal ions, antibiotics, proteins, cells, and tissue (Li *et al.*, 2019, Wang *et al.*, 2019a, Wang *et al.*, 2019b, Raducanu *et al.*, 2020, Su *et al.*, 2020, Zhang *et al.*, 2020, Gruenke *et al.*, 2022). This also includes aptamer development against HPV proteins, including RNA and DNA aptamers against HPV-16 L1, E6, and E7 proteins (Toscano-Garibay *et al.*, 2011, Gourronc *et al.*, 2013, Leija-Montoya *et al.*, 2014, Cesur *et al.*, 2015, Toscano-Garibay *et al.*, 2015, Trausch *et al.*, 2017, Valencia-Reséndiz *et al.*, 2018, Yang *et al.*, 2024). Additionally, aptamers have also been tested for various applications including bioanalysis, bioimaging, drug delivery and molecular diagnostics (Liu *et al.*, 2018, Yamada *et al.*, 2019, Zhang *et al.*, 2021, Hassiban *et al.*, 2024).

To date, only one aptamer has been developed for therapeutic use within the clinic. In 2004, the U.S. Food and Drug Administration (FDA) approved the therapeutic use of pegaptanib sodium within the USA and Europe, marketed as Macugen® by Pfizer and Eyetech (Gragoudas *et al.*, 2004, VEGF Inhibition Study in Ocular Neovascularization (V.I.S.I.O.N.) Clinical Trial Group, 2006). Pegaptanib was an RNA aptamer developed against extracellular vascular endothelial growth factor (VEGF), which prevented VEGF from binding with VEGFR1, VEGFR2, and all isoforms of VEGFA except

VEGF121 (Ruckman *et al.*, 1998, Gragoudas *et al.*, 2004, Keefe *et al.*, 2010). It was proven to be an effective therapeutic treatment for neovascular age-related macular degeneration and sold well after regulatory approval. However, after ranibizumab (Lucentis®; Genentech), an antibody fragment which binds to all isoforms of VEGFA came to market, Pegaptanib lost revenue and was discontinued in 2011 (Gragoudas *et al.*, 2004, Keefe *et al.*, 2010, European Medicines Agency, 2011, U.S. Food and Drugs Administration, 2011). Since the expiration of the original SELEX patents in the early 2010s, there has been an increased academic and commercial interest in aptamers (DeRosa *et al.*, 2023). In March 2024, the aptamers market was estimated at 1.48 billion USD, which is projected to reach 2.77 billion USD by the year 2030 (Research and Markets, 2024).

### **1.7 Aims and objectives**

The aim of this study was to understand the pathogenesis of HPV within cancers of the oropharynx, given this is poorly understood within the literature. To achieve this, the objectives were as follows:

- Full histological characterisation of normal palatine tonsil and OPSCC tissues
- Confirm HPV positivity in OPSCC tissues using HPV DNA ISH
- Examine the expression of biomarkers believed to be prognostic indicators for the development of HPV-mediated disease within normal palatine tonsil and HPV-positive and HPV-negative OPSCC tissues using IHC
- Develop multiplex immunofluorescence (mIF) assays using prognostic biomarkers on HPV-positive and HPV-negative OPSCC tissues
- Confirm HPV protein detection in tissues by IHC, and use to determine the HPV subtype of HPV-positive OPSCCs
- Design and develop aptamers against chosen HPV proteins and validate against commercially-available HPV antibodies

## CHAPTER 2: MATERIALS AND METHODS

### 2.1 Human tissue and ethical approval

All histopathology, automated histochemistry (chromogenic immunohistochemistry (IHC) and multiplex immunofluorescence (mIF)), slide scanning, and visualisations were performed at HistologiX Ltd (Nottingham, UK); a Human Tissue Authority (HTA) licensed and Good Laboratory Practice/Good Clinical Practice (GLP/GCP) compliant ethically-approved laboratory.

Formalin-fixed, paraffin-embedded (FFPE) tissue blocks were provided by Tissue Solutions (Glasgow, UK); a biobank who provide ethically sourced and fully consented human tissue samples, which comply with HTA guidelines for use at HistologiX Ltd (Table 2). These tissue samples were used for the optimisation stages to determine a final working assay, as well as controls.

Pre-cut FFPE OPSCC tissue sections were obtained from the Human Biomaterials Resource Centre (HBRC, University of Birmingham); an HTA-licensed ethically-approved Research Tissue Bank that is authorised to release samples, and associated data, to Chief Investigators whose research falls under the remit of that ethical approval; for Dr Elizabeth Marsh's study this work was granted approval from the centre (21-374A1-HBRC) (Appendix 5).

**Table 2: FFPE tissue types sourced from Tissue Solutions with associated pathologies used for antibody optimisation and control staining**

<b>Tissue type</b>	<b>Gender</b>	<b>Age (years)</b>	<b>Pathology</b>
Normal tonsil 1	Female	Not provided	Normal
Normal tonsil 2	Female	Not provided	Normal
Normal tonsil 3	Female	Not provided	Normal
Normal tonsil 4	Male	Not provided	Normal
CC <sup>1</sup> 1	Female	56	Diseased
CC 2	Female	54	Diseased
CC 3	Female	Not provided	Diseased
Normal cervix 1	Female	46	Normal
CC 4	Female	Not provided	Diseased
LC <sup>2</sup> 1	Male	52	Diseased
LC 2	Male	55	Diseased
Normal spinal cord 1	Female	41	Normal
Prostate carcinoma 1	Male	Not provided	Diseased
Prostate carcinoma 2	Male	67	Diseased
Normal liver 1	Male	44	Normal
Normal liver 2	Male	61	Normal
Normal placenta 1	Female	21	Normal

<sup>1</sup>Cervical carcinoma, <sup>2</sup>Laryngeal carcinoma

## **2.2 Histopathology**

### **2.2.1 Tissue sectioning**

FFPE blocks were sectioned at 4 µm on a HistoCore BIOCUT manual rotary microtome (Leica Biosystems, Leica Microsystems (UK) Ltd, Milton Keynes, UK), and collected from a HistoCore water bath (Leica Biosystems, Leica Microsystems (UK) Ltd, Milton Keynes, UK). Slides were dried on a hotplate at 37-40°C for 5 minutes (cat. no: JAY-0100-00A-CellPath Ltd, Wales, UK), and stored in an incubator at 30-40°C until fully dry.

### **2.2.2 Haematoxylin and eosin staining**

Routine diagnostic haematoxylin and eosin (H&E) staining was performed on the Leica ST4040 Linear Staining System (Leica Biosystems, Leica Microsystems (UK) Ltd, Milton Keynes, UK), using sections placed on White Snowcoat slides (cat. no: 3808100GE-Leica Biosystems, Leica Microsystems (UK) Ltd, Milton Keynes, UK). Each immersion step was 40 seconds.

Slides were deparaffinised in xylene (cat. no: XYL050-Genta Medical, Genta Environmental Ltd, York, UK) four times, before rehydration in 99% industrial denatured alcohol (IDA) (cat. no: I99050-Genta Medical, Genta Environmental Ltd, York, UK) twice, and then 95% IDA. Next, slides were immersed in Harris's haematoxylin (cat. no: PRC/R/51-Pioneer Research Chemicals Ltd, Essex, UK) five times, before immersion in deionised water, and then 0.5% acid alcohol (2895 ml deionised water, 50 ml hydrochloric acid (cat. no: 10053023-Fisher Chemical, Fisher Scientific UK Ltd, Loughborough, UK) and 6965 ml 99% IDA). Subsequently, slides were immersed in deionised water, followed by Scott's tap water (cat. no: 3802901E-Leica Biosystems, Leica Microsystems (UK) Ltd, Milton Keynes, UK), and then deionised water again. Slides were then immersed and counterstained in 0.5% aqueous eosin, followed by immersion in 1% aqueous eosin (cat. no: 3801590BBE-Leica Biosystems, Leica Microsystems (UK) Ltd, Milton Keynes, UK) twice. Finally, slides were immersed in deionised water, before dehydrating in 95% IDA, followed by 99% IDA twice, and cleared in xylene twice before mounting.

Slides were mounted using a Dako™ Coverslipper (Dako™, Agilent Technologies LDA UK Ltd, Cheshire, UK), DPX (phthalate free) mounting medium (cat. no: SEA-



1300-00A-CellPath Ltd, Wales, UK), and Menzel™ microscope coverslips (cat. no: 11778691-Epredia™, Fisher Scientific UK Ltd, Loughborough, UK). All visualisations were performed with an Olympus BX51 Microscope (Olympus UK & Ireland, Southend-on-Sea, UK), before using a NanoZoomer S360 Digital Slide Scanner and NZAcquire Software to scan slides, and viewing in NDP.view2 Software (all Hamamatsu Photonics UK Ltd, Hertfordshire, UK).

## **2.3 Automated immunostaining**

### **2.3.1 Chromogenic immunohistochemistry**

Chromogenic immunohistochemistry (IHC) was performed on the BOND™ RX Fully Automated Research Stainer, using the BOND™ Polymer Refine Detection Kit (cat. no: DS9800) (both Leica Biosystems, Leica Microsystems (UK) Ltd, Milton Keynes, UK), which contained Peroxide Block, Post Primary, Polymer, 3,3'-diaminobenzidine (DAB) Part 1, 2, and 3 (Mixed DAB Refine), and Haematoxylin reagents. Bulk reagents used included BOND™ Dewax Solution (cat. no: AR9222), BOND™ Epitope Retrieval 1 (ER1) and 2 (ER2) Solutions (cat. no: AR9961 and AR9640), BOND™ Primary Antibody Diluent (cat. no: AR9352), and BOND™ Wash 10x Solution (diluted to 1x for use) (cat. no: AR9590) (all Leica Biosystems, Leica Microsystems (UK) Ltd, Milton Keynes, UK).

Sections were mounted on Superfrost Plus slides, to prevent them falling off the slide due to high temperature exposure. Slide labels were generated using the BOND™ RX Software, labelling slides appropriately, before loading onto trays with a covertile placed on top before insertion into the platform. All reagents were dispensed at 150 µl. Each antibody used the standard Leica Biosystems IHC Protocol F, with changes made only to the primary antibody incubation times. These steps are fully detailed in Appendices 6-8. Each step except deparaffinisation, and antigen retrieval, were performed at ambient temperature. Antigen retrieval, antibodies, dilutions, and incubation times are detailed in Tables 3 and 4.

Slides were deparaffinised in BOND™ Dewax solution, and incubated at 72°C for 30 minutes, before immersion in 99% IDA. Slides were rinsed with BOND™ Wash Solution, prior to heat-induced epitope retrieval (HIER) at 100°C for the appropriate incubation time. Slides were rinsed again with BOND™ Wash Solution, before

incubating in Peroxide Block for 5 minutes. Slides were rinsed in BOND™ Wash Solution three times, and then incubated with primary antibody for the appropriate incubation time. Slides were rinsed again in BOND™ Wash Solution three times, then incubated in Post Primary for 8 minutes, before an extra rinse in BOND™ Wash Solution for 6 minutes. Next, slides were immersed in Polymer for 8 minutes, and rinsed in BOND™ Wash solution for 4 minutes. Slides were then rinsed in deionised water, and incubated in Mixed DAB Refine for 10 minutes, before rinsing in deionised water, and incubating further in Haematoxylin for 5 minutes. Slides were then finally rinsed in deionised water, BOND™ Wash Solution, and deionised water, respectively. Appropriate positive and negative tissue controls were used for each antibody.

Slides were dehydrated in 99% IDA followed by clearing in xylene, and hand mounting. All visualisations were performed with an Olympus BX51 Microscope before using a NanoZoomer S360 Digital Slide Scanner and NZAcquire Software to scan slides, and viewing in NDP.view2 Software.

**Table 3: Primary antibodies used for automated chromogenic immunohistochemistry on BOND™ RX Fully Automated Research Stainer and multiplex immunofluorescence on VENTANA DISCOVERY ULTRA Research Staining System**

Primary antibody	Regulatory status	Host species	Clone	Class	Isotype	Supplier	Product code
p16	IVD <sup>6</sup>	Mouse	6H12	Monoclonal	IgG2b	BOND™, Leica Biosystems, Leica Microsystems (UK) Ltd, Milton Keynes, UK	PA0016
PD-1 <sup>1</sup>	IVD	Rabbit	CAL20	Monoclonal	IgG1	BOND™, Leica Biosystems, Leica Microsystems (UK) Ltd, Milton Keynes, UK	PA0216
PD-L1 <sup>2</sup>	IVD	Rabbit	73-10	Monoclonal	IgG	BOND™, Leica Biosystems, Leica Microsystems (UK) Ltd, Milton Keynes, UK	PA0832
CK7 <sup>3</sup>	IVD	Mouse	RN7	Monoclonal	IgG1	Novocastra™, Leica Biosystems, Leica Microsystems (UK) Ltd, Milton Keynes, UK	NCL-L-CK7-560
EGFR <sup>4</sup>	IVD	Mouse	EGFR 113	Monoclonal	IgG2a	Novocastra™, Leica Biosystems, Leica Microsystems (UK) Ltd, Milton Keynes, UK	NCL-L-EGFR
CD8	IVD	Mouse	C8/144B	Monoclonal	IgG1k	Dako™, Agilent Technologies LDA UK Ltd, Cheshire, UK	M710301-2
AE1/AE3	IVD	Mouse	AE1/AE3	Monoclonal	IgG1k	Dako™, Agilent Technologies LDA UK Ltd, Cheshire, UK	M351501-2
ERα <sup>5</sup>	RUO <sup>7</sup>	Rabbit	D6R2W	Monoclonal	IgG	Cell Signalling Technology, London, UK	13258S
Ki67	RUO	Rabbit	SP6	Monoclonal	IgG	Abcam PLC, Cambridge, UK	ab16667
HPV-16 E2	RUO	Mouse	TVG-261	Monoclonal	IgG1	Abcam PLC, Cambridge, UK	ab17185
HPV-16 E6	RUO	Mouse	HPV-13E2	Monoclonal	IgG1	Neo Biotech, Nanterre, France	NB-22-52681-100
HPV-16 E6 + HPV-18 E6	RUO	Mouse	C1P5	Monoclonal	IgG1	Abcam PLC, Cambridge, UK	ab70
HPV-16 E6/HPV-18 E6	RUO	Mouse	C1P5	Monoclonal	IgG1	Santa Cruz Biotechnology, Texas, USA	sc-460
HPV-16 E7	RUO	Mouse	ED17	Monoclonal	IgG1	Santa Cruz Biotechnology, Texas, USA	sc-6981
HPV-16 E7	RUO	Mouse	TVG 701Y	Monoclonal	IgG2a	Invitrogen™, Thermo Fisher Scientific, Fisher Scientific UK Ltd, Loughborough, UK	MA5-14132
HPV-18 E6	RUO	Mouse	HPV-4G3	Monoclonal	IgG1	Neo Biotech, Nanterre, France	NB-22-52683-100
HPV-18 E7	RUO	Mouse	8E2	Monoclonal	IgG1	Abcam PLC, Cambridge, UK	ab100953

<sup>1</sup>Programmed cell death protein-1, <sup>2</sup>Programmed cell death-ligand 1, <sup>3</sup>Cytokeratin 7, <sup>4</sup>Epidermal growth factor receptor, <sup>5</sup>Estrogen receptor alpha, <sup>6</sup>In vitro diagnostics, <sup>7</sup>Research use only

**Table 4: Primary antibody dilutions, antigen retrieval solutions, incubation times and staining patterns used for automated chromogenic immunohistochemistry on BOND™ RX Fully Automated Research Stainer and multiplex immunofluorescence on VENTANA DISCOVERY ULTRA Research Staining System**

Primary antibody	Dilution	BOND™ RX		VENTANA DISCOVERY ULTRA		Staining pattern
		Primary incubation	Antigen retrieval and incubation	Primary incubation	Antigen retrieval and incubation	
p16	RTU <sup>6</sup>	15 mins	ER2 <sup>7</sup> 20 mins	60 mins	CC2 <sup>9</sup> 92 mins	Nuclear and cytoplasmic
PD-1 <sup>1</sup>	RTU	15 mins	ER2 20 mins	60 mins	CC2 92 mins	Cytoplasmic and membranous
PD-L1 <sup>2</sup>	RTU	15 mins	ER1 <sup>8</sup> 20 mins	60 mins	CC2 92 mins	Membranous
CK7 <sup>3</sup>	1:100	30 mins	ER2 20 mins	60 mins	CC2 92 mins	Cytoplasmic and membranous
EGFR <sup>4</sup>	1:20	30 mins	ER2 20 mins	60 mins	CC2 92 mins	Membranous
CD8	1:200	30 mins	ER2 20 mins	60 mins	CC2 92 mins	Membranous
AE1/AE3	1:200	30 mins	ER2 20 mins	60 mins	CC2 92 mins	Cytoplasmic
ERα <sup>5</sup>	1:100	60 mins	ER2 40 mins	60 mins	CC2 92 mins	Nuclear
Ki67	1:400	60 mins	ER2 92 mins	60 mins	CC2 92 mins	Nuclear
HPV-16 E2	1:50	60 mins	ER2 92 mins	N/A	N/A	N/A
HPV-16 E6	1:100	60 mins	ER2 92 mins	N/A	N/A	N/A
HPV-16 E6 + HPV-18 E6	1:100	60 mins	ER2 92 mins	60 mins	CC2 92 mins	N/A
HPV-16 E6/HPV-18 E6	1:50	60 mins	ER2 92 mins	N/A	N/A	N/A
HPV-16 E7	1:50	60 mins	ER2 92 mins	N/A	N/A	N/A
HPV-16 E7	1:100	60 mins	ER2 92 mins	N/A	N/A	N/A
HPV-18 E6	1:50	60 mins	ER2 92 mins	N/A	N/A	N/A
HPV-18 E7	1:100	60 mins	ER2 92 mins	N/A	N/A	N/A

<sup>1</sup>Programmed cell death protein-1, <sup>2</sup>Programmed cell death-ligand 1, <sup>3</sup>Cytokeratin 7, <sup>4</sup>Epidermal growth factor receptor, <sup>5</sup> Estrogen receptor alpha, <sup>6</sup>Ready-to-use, <sup>7</sup>Epitope Retrieval 2 (pH 9-EDTA based), <sup>8</sup>Epitope Retrieval 1 (pH 6-citrate based), <sup>9</sup>Cell Conditioning 2 (pH 6-citrate based)

### 2.3.2 Multiplex immunofluorescence

Multiplex immunofluorescence (mIF) was performed on the VENTANA DISCOVERY ULTRA Research Staining System (Roche Diagnostics Ltd, West Sussex, UK). Bulk reagents used included DISCOVERY Wash, (cat. no: 950-510), ULTRA Cell Conditioning 2 (CC2) (cat. no: 950-223), Reaction Buffer 10x Concentrate (cat. no: 950-300), ULTRA Liquid Coverslip (LCS) (cat. no: 650-210), DISCOVERY Antibody Diluent (cat. no: 760-108), and EZ Prep 10x Concentrate (cat. no: 950-102) (all Roche Diagnostics Ltd, West Sussex, UK). Concentrates were diluted to 1x in bulk containers, before adding to the platform. Sections were mounted on Superfrost Plus slides to prevent sections falling off the slide due to high temperature exposure. Slide labels were generated using the VENTANA Software, slides labelled appropriately, and loaded onto heat plates in their own individual drawers on the platform.

Alexa Fluor™ 488 (rabbit) and 555 (mouse) Tyramide SuperBoost™ Kits (cat. no: B40922 and B40913) (both Invitrogen™ Thermo Fisher Scientific, Fisher Scientific UK Ltd, Loughborough, UK) were used according to the manufacturer's protocol. The kits contained 3% Hydrogen Peroxide, 1x Blocking buffer (10% Goat Serum), 20x Reaction buffer, Reaction Stop Reagent, 1x Poly-horseradish peroxidase (HRP)-conjugated secondary antibody (mouse and rabbit) and Alexa Fluor™ 444 and 555 tyramide reagents. Alexa Fluor™ 647 tyramide reagent (cat. no: B40958) and 4', 6-diamidino-2-phenylindole (DAPI) (cat. no: D3571) (both Invitrogen™, Thermo Fisher Scientific, Fisher Scientific UK Ltd, Loughborough, UK) were purchased separately. As the manufacturer protocol is designed for bench application, changes were made to incubation times, temperatures and rinsing steps, to be appropriate for automated application, which are detailed below.

Protocols were designed and optimised for use, with each mIF having two separate protocols due to the vast number of steps within each protocol. The first protocol was for the first two primary antibodies, with the second protocol following on from the first for the third antibody and DAPI application. A dispenser and antibody number were allocated to 3% Hydrogen Peroxide, 1x Blocking buffer, rabbit and mouse Poly-HRP-conjugated secondary antibodies, and DAPI, with these becoming automated steps within the protocol. The only differences with each automated step of the protocol was the Poly-HRP-conjugated secondary antibody that was dispensed, as this is specific

to the primary antibody species. Primary antibody, tyramide reagent working solutions and Reaction Stop Reagent working solutions were manually applied. All reagents were dispensed/manually applied at 100 µl.

Denaturation steps were introduced in between each sequential primary antibody (except after the third antibody) to deactivate Poly-HRP-conjugated secondary antibody, and allow visualisation of multiple antibodies of the same or different species with different fluorophores at varying wavelengths. Rinsing of slides with Reaction Buffer, EZ Prep and LCS were not controllable as they are built into the standard research use only (RUO) DISCOVERY Universal protocol. These steps are fully detailed in Appendices 9-13.

#### **2.3.2.1 First primary antibody and Alexa Fluor™ 555 tyramide**

Slides underwent extended deparaffinisation in DISCOVERY Wash solution at 72°C for 16 minutes, before antigen retrieval with CC2 at 93°C for 92 minutes. Slide heaters were disabled and slides incubated in 3% Hydrogen Peroxide for 16 minutes. Next, slide heaters were disabled again, and slides incubated in 1x Blocking buffer for 28 minutes, before primary antibody manual application (Tables 3 and 4) and incubation at 37°C for 60 minutes. Slide heaters were disabled and slides incubated in rabbit or mouse 1x Poly-HRP-conjugated secondary antibody for 32 minutes. Slide heaters were disabled again, before Alexa Fluor™ 555 tyramide stock solution manual application and incubation for 8 minutes, before disabling slide heaters again, manual application of Reaction Stop Reagent working solution and incubation for 8 minutes. Lastly, slides underwent denaturation at 60°C for 32 minutes.

#### **2.3.2.2 Second primary antibody and Alexa Fluor™ 488 tyramide**

The above process was repeated again (except deparaffinisation and antigen retrieval), following the antigen retrieval step. The primary antibody and Alexa Fluor™ 488 tyramide working solution were applied as appropriate. After the second denaturation step, the protocol finished, and slides were removed and relabelled with a different protocol for the final antibody application. The protocol resumed following the denaturation step.

### **2.3.2.3 Third primary antibody, Alexa Fluor™ 647 tyramide, and DAPI**

Again, the above process was repeated again (except deparaffinisation and antigen retrieval), following the denaturation step. The primary antibody and Alexa Fluor™ 647 tyramide working solution were applied as appropriate. After the last Reaction Stop Reagent working solution step application, DAPI was applied, and the slides incubated at 37°C for 32 minutes. This was the last step of the protocol.

### **2.3.2.4 Slide mounting and scanning**

Once the final protocol was completed, slides were rinsed in EZ Prep twice for 5 minutes each before rinsing in water twice for 5 minutes each. Slides were then mounted using ProLong™ Gold Antifade Mountant (cat. no: P36934-Invitrogen™, Thermo Fisher Scientific, Fisher Scientific UK Ltd, Loughborough, UK) and Menzel™ Microscope Coverslips and stored in the dark at 4°C until required. All visualisations were performed using an Olympus BX51 Microscope, before using a ZEISS Axio Scan.Z1, with ZEN pro Microscopy Software to scan and view slides. Scans were also viewable using ZEN lite Microscopy Software (all Carl Zeiss Ltd-Meditec, Microscopy and Consumer Optics, Cambridge, UK).

## **2.4 Molecular pathology**

### **2.4.1 HPV DNA *in-situ* hybridisation**

HPV DNA *in-situ* hybridisation (ISH) was performed on the VENTANA BenchMark ULTRA Advanced Staining System, using the VENTANA INFORM HPV III Family 16 Probe (B) (cat. no 780-4295), in conjunction with the VENTANA ISH MIEW Blue Plus Detection Kit (cat. no: 760-097) and other accessory reagents (all Roche Diagnostics Ltd, West Sussex, UK). The probe contains a cocktail of labelled HPV genomic probes against the following genotypes: HPV-16, -18, -31, -33, -35, -45, -52, -56, -58 and -66. The staining was undertaken at NovoPath, Cellular Pathology, Royal Victoria Infirmary, Newcastle upon Tyne. All visualisations were performed with an Olympus BX51 Microscope, before using a NanoZoomer S360 Digital Slide Scanner and NZAcquire Software to scan slides, and viewing in NDP.view2 Software.

### **2.4.2 DNA FFPE extraction**

For each FFPE block in Section 2.1 Table 2, up to 3.5 mm<sup>3</sup> was taken, through multiple sections at 5 µm depending on surface area according to the QIAamp DNA FFPE

Advanced Kit (cat. no: 56604-Qiagen Ltd, Manchester, UK) manufacturer's protocol. No more than 4 mm<sup>3</sup> was to be taken for each block as too much starting material could have led to insufficiency. Sections from each block were transferred to a 2 ml ribonuclease (RNase)-free microfuge tube (cat. no: AM12425-Invitrogen™, Thermo Fisher Scientific, Loughborough, UK), using a different part of, or a new, low profile microtome blade (cat. no: 14035843497-Leica Biosystems, Leica Microsystems (UK) Ltd, Milton Keynes, UK), with clean stainless-steel forceps between each block to prevent cross-contamination.

DNA was extracted using the QIAamp DNA FFPE Advanced Kit, according to the manufacturer's protocol. Briefly, Deparaffinisation Solution was added to the sections, before vortexing for 10 seconds, and briefly centrifuging. Tubes were incubated at 56°C for 3 minutes, and cooled to room temperature. Buffer FTB, RNase-free water and Proteinase K were added, and vortexed, before incubation at 56°C for 60 minutes. Tubes were briefly vortexed at 15-minute intervals. DNA extractions were then incubated at 90°C for a further 60 minutes. To the lower aqueous lysate, RNase-free water and RNase A were added, and vortexed, before incubation at room temperature for 2 minutes. Next, Proteinase K was added, samples vortexed, and incubated at 65°C for 15 minutes. Buffer AL and 96-100% Industrial Methylated Spirit (IMS) (cat. no: 10552904-Fisher Chemical, Fisher Scientific UK Ltd, Loughborough, UK) were added, and samples vortexed. Lysate was transferred into a QIAamp UCP MinElute column (in a 2 ml collection tube), and centrifuged at 15000 x *g* for 30 seconds. Residual lysate was then transferred to the same column, and centrifuged at 15000 x *g* for 1 minute. Buffer AW1 was added to each column, and centrifuged at 15000 x *g* for 30 seconds, before repeating with Buffer AW2. IMS (96-100%) was added, and centrifuged at 15000 x *g* for 30 seconds. Each column was placed into a new 2 ml collection tube, and centrifuged at 16000 x *g* for 3 minutes to remove any residual liquid, before placing into a clean 1.5 ml microcentrifuge tube. Buffer ATE was applied to the centre of the membrane of each column, before incubation at room temperature for 1 minute, and centrifugation at 16000 x *g* for 1 minute. This process was repeated to increase DNA yield. DNA samples were stored at -20°C until required.



### **2.4.3 Real-time polymerase chain reaction**

Extracted DNA was quantified using a NanoDrop™ 2000 Spectrophotometer, and NanoDrop™ 2000/2000c Software (both Thermo Scientific™, Thermo Fisher Scientific, Fisher Scientific UK Ltd, Loughborough, UK) to check DNA concentration. HPV-18 DNA plasmid (gift from Dr S Roberts, University of Birmingham), SiHa DNA (extracted from the cell pellet of cat. no: HTB-35-ATCC, Virginia, USA), and molecular-grade water (cat. no: J71786.AE-Thermo Scientific Chemicals, Thermo Fisher Scientific, Fisher Scientific UK Ltd, Loughborough, UK) were analysed in triplicate. 25 ng/μl of DNA was added to each well alongside 2x PowerTrack™ SYBR Green Master Mix (cat. no: A46109-Applied Biosystems™, Thermo Fisher Scientific, Fisher Scientific UK Ltd, Loughborough, UK), 10 μM GP5+/6+ primers (both synthesised by Eurofins Genomics GmbH, Germany) (de Roda Husman *et al.*, 1995) and molecular-grade-water (to a final volume of 20 μl).

The polymerase chain reaction (PCR) plate (cat. no: 72.1981-Sarstedt AGA & Co. KG, Germany) was centrifuged on a Grant-bio LMC-3000 (Grant Instruments (Cambridge) Ltd, Cambridgeshire, UK) at 140 x g for 2 minutes, and thermocycled on the StepOnePlus™ Real-Time PCR System (Applied Biosystems™, Thermo Fisher Scientific, Fisher Scientific UK Ltd, Loughborough, UK) with the following cycling conditions: 95°C for 3 minutes, followed by 95°C for 20 seconds, 52°C for 30 seconds, and 72°C for 10 seconds, in 40 cycles, followed by a melt curve. Data were analysed using StepOnePlus™ Software (Applied Biosystems™, Thermo Fisher Scientific, Fisher Scientific UK Ltd, Loughborough, UK).

## **2.5 Systematic evolution of ligands by exponential enrichment**

### **2.5.1 Preparing the protein for targeting**

The methodology for preparing the protein for targeting was adapted from 'the physical and functional behaviour of capture antibodies adsorbed on polystyrene' (Butler *et al.*, 1992). This procedure involved preparing a separate positive and negative plate for each recombinant protein. 1 μg/ml protein solution containing HPV-16 E2 (cat. no: CSB-EP365852HML-Cusabio, Texas, USA), HPV-16 E7-E6 (cat. no: TP780004-OriGene Technologies GmbH, Germany), HPV-18 E6 (cat. no: MBS157269-MyBioSource, Inc., California, USA) or HPV-18 E7 (cat.no: CSB-EP361948HMN-Cusabio, Texas, USA) recombinant protein was prepared in 0.1 M carbonate-

bicarbonate buffer (cat. no: S2127-500G and S8875-500G) (both Sigma Aldrich®, Merck Life Science UK Limited, Dorset, UK). 100 µl 1 µg/ml protein solution was added to each well of a 96-well plate (cat. no: 83-3924.005-Sarstedt AGA & Co. KG, Germany) and incubated at 37°C for 24 hours.

After incubation, the protein solution was removed and blocking buffer (0.1% w/v instant dried skimmed milk in 1x Oxoid™ phosphate buffered saline (PBS)) (cat. no: BR0014G-Thermo Scientific™, Thermo Fisher Scientific, Fisher Scientific UK Ltd, Loughborough, UK) was added to each well and incubated at 37°C for 24 hours. The blocking solution was removed, and the plate dried with nitrogen gas, and stored at 4°C until required. The same process was repeated for the four negative selection plates, except that the recombinant protein was replaced with 1 µg/ml bovine serum albumin (BSA) (cat. no: A7906-10G-Sigma Aldrich®, Merck Life Science UK Limited, Dorset, UK) in 0.1 M carbonate-bicarbonate buffer. Each selection described is based on one column of a 96-well plate at one time, undergoing different selection pressures during each selection round of systematic evolution of ligands by exponential enrichment (SELEX).

### 2.5.2 First round of positive selection

A DNA library pool containing 10 nM DNA random aptamer library

*Content removed for copyright purposes*

in binding buffer, pH 7.28 (25 mM Glucose (cat. no: G8270-100G), 4 µM transfer RNA (tRNA) (cat. no: R8759-500UN), 15.15 µM BSA, 0.5 M magnesium chloride (MgCl<sub>2</sub>) (cat. no: M8266-100G) (all Sigma Aldrich®, Merck Life Science UK limited, Dorset, UK) in 1x PBS), was combined in a 1.5 ml tube, vortexed, and heated to 95°C for 5 minutes, and snap cooled on ice. 40 µl of this DNA library pool was added to each well of the first column of the 96 well plate, and incubated at 4°C for 24 hours.

After incubation, the DNA library pool was removed, and retained in separate tubes for each well of the first column. This step is only performed once throughout the whole of the SELEX process. Next, each well was washed with 50 µl washing buffer (25 mM glucose and 1 M MgCl<sub>2</sub> in 1x PBS) three times, with washings retained, and added to the same tubes as mentioned above. These were labelled as the negative positive

selection control and stored at -20°C until required for use as the negative control aptamers for binding assays and cell immunofluorescence (Sections 2.8 and 2.10).

In the positive selections, using a clean pipette tip, the protein was scraped from the well surface and pipetted into a 1.5 ml tube (cat. no: 0030123328-Eppendorf UK Ltd, Stevenage, UK). Using the same tip, 100 µl Nuclease-Free water (cat. no: 129115-Qiagen Ltd, Manchester, UK) was added to the well, and aspirated off and collected in the same tube. This was repeated for each well of the first column, and each tube labelled appropriately. Each tube was then heated to 95°C for 10 minutes, and suspended DNA recovered by centrifugation at 13,000 x *g* for 5 minutes. Supernatant was discarded, and the pellet retained. Positive selection samples were stored at -20°C in IMS for 2-3 hours, to allow DNA precipitation.

### **2.5.3 First round of negative selection**

A DNA library pool containing 10 nM DNA random aptamer library in binding buffer, pH 7.28 was combined in a 1.5 ml tube, vortexed, and heated to 95°C for 5 minutes, and snap cooled on ice. 40 µl of this DNA library pool was added to each well of the first column of the 96 well plate and incubated at 4°C for 24 hours. After incubation, the DNA library pool was removed and retained in one tube for each well of the first column. This was labelled as 1<sup>st</sup> negative selection and stored at -20°C until required for PCR.

### **2.5.4 Purification procedure**

This process was carried out after each positive selection using the MinElute PCR Purification Kit (cat. no: 28006-Qiagen Ltd, Manchester, UK), according to the manufacturer's protocol. IMS was removed and the sample resuspended in 100 µl deoxyribonuclease (DNase)/RNase free water. Each sample was quantified using a NanoDrop™ 2000 Spectrophotometer and NanoDrop™ 2000/2000c Software. 10 µl was removed from each tube as detailed in Section 2.5.2 and consolidated into one tube (80 µl in total).

Briefly, 1 volume of sample was added to 5 volumes of Buffer PB and vortexed. The sample was applied to a MinElute column in a 2 ml collection tube, and centrifuged at 11,000 x *g* for 1 minute, before discarding flowthrough. Buffer PE was added to the

MinElute column, and centrifuged at 11000 x *g* for 1 minute, before discarding flowthrough. The MinElute column was centrifuged again to remove any residual Buffer PE at 11000 x *g* for 1 minute, before placing the column in a new 1.5 ml tube. Buffer EB was added to the centre of the column membrane, and left for 1 minute, before centrifugation at 11000 x *g* for 1 minute. Samples were quantified using a NanoDrop™ 2000 Spectrophotometer and NanoDrop™ 2000/2000c Software to check DNA concentration before proceeding to either PCR or next selection.

### 2.5.5 Polymerase chain reaction

100 µM of DNA was added to each PCR tube (cat .no: TA531-Appleton Woods Limited, Birmingham, UK), alongside 10x PCR buffer, 25 mM MgCl<sub>2</sub>, 5 U/µl *Taq* DNA polymerase (cat. no: M0320L-New England BioLabs, Hertfordshire, UK), 10 µM

*Content removed for copyright purposes*

synthesised by Eurofins Genomics Germany GmbH, Germany), 10 mM deoxynucleoside triphosphate (dNTP) mix (cat. no: 201900-Qiagen Ltd, Manchester, UK) and Nuclease-Free water to a final volume of 25 µl.

Samples were thermocycled on the Techne™ Flexigene PCR Thermal Cycler (Techne™, Fisher Scientific UK Ltd, Loughborough, UK) with the following cycling conditions: 95°C for 5 minutes followed by 25-33 cycles of 95°C for 30 seconds, 50°C for 30 seconds and 72°C for 30 seconds, then 72°C for 5 minutes. Samples were purified after each PCR reaction as per Section 2.5.4. 10 nM DNA library from each purified PCR reaction was then used for the next round of selection.

### 2.5.6 Subsequent rounds of selection

For each subsequent round of positive and negative selection, Sections 2.5.2-2.5.5 are repeated moving along each column of the 96-well plate. Positive selections had one selection pressure changed each subsequent SELEX round. Negative selections only had to be performed every other positive selection therefore, some had one or two selection pressures during each SELEX round. This is done as we are looking to remove non-specific binding from the aptamers. Selection pressures involved overnight incubation temperature, binding buffer pH, and MgCl<sub>2</sub> concentration which are detailed in Table 5.

**Table 5: Positive and negative SELEX rounds and selection pressures introduced for each HPV aptamer pool**

	SELEX round	Selection pressures		
		Incubation temperature (°C)	Binding buffer pH	MgCl <sub>2</sub> concentration (M)
Positive selections	1	4	7.28	1.00
	2	10	7.28	1.00
	3	24	7.28	1.00
	4	37	7.28	1.00
	5	37	7.00	1.00
	6	37	6.75	1.00
	7	37	7.28 (6.5)	0.75
	8	37	7.28 (6.25)	0.50
	9	37	7.28	0.25 (0.75)
	10	37	7.28	0.10 (0.50)
	11 <sup>1</sup>	37	7.28	0.25
	12 <sup>1</sup>	37	7.28	0.10
Negative selections	1	37	7.28 (7.26)	1.00
	2	24	7.28 (7.26)	1.00
	3	10	7.24 (7.26)	1.00
	4	4	7.20 (7.24)	1.00
	5	37	7.28	0.75
	6	37	7.28	0.50
	7	37	7.28	0.25
	8	37	7.28	0.10

<sup>1</sup>Selections for HPV-16 E2 only

Numbers in brackets represent the selection pressures for HPV-16 E2 only

## 2.6 Gel electrophoresis

This was performed at intervals throughout the SELEX process, to ensure that DNA was retained between selections. 3 µl of each PCR product was electrophoresed through 3% w/v agarose (cat. no: BIO-41025-Meridian Bioscience, London, UK) in 1x UltraPure™ tris-borate-ethylenediaminetetraacetic acid (EDTA) (TBE) buffer, pH 8 (cat. no: 15581-044-Invitrogen™, Thermo Fisher Scientific, Fisher Scientific UK Ltd, Loughborough, UK) alongside a Low Molecular Weight DNA Ladder (cat. no: N3233S-New England Biolabs, Hertfordshire, UK).

Gels were run at 80V and 120mA for 70 minutes and post-stained with GelRed® (cat. no: 41003-Biotium, Inc., California, USA) (eliminates smearing of ladder bands) for 30 minutes, before visualisation using the ChemiDoc™ XRS+ Molecular Imager® and Image Lab™ Software (both Bio-Rad Laboratories Ltd, Hertfordshire, UK).

## 2.7 Aptamer development

### 2.7.1 Next generation sequencing

Next generation sequencing (NGS) was performed on the 10<sup>th</sup> positive selections of HPV-16 E7-E6, HPV-18 E6 and HPV-18 E7, and the 12<sup>th</sup> positive selection of HPV-16 E2 pools as these were the last selections performed, where no DNA was recovered after the selection. Each prospective NGS sample underwent PCR with extended

*Content removed for copyright purposes*

primers (both synthesised by Eurofins Genomics Germany GmbH, Germany) to extend the length of the sequences, which were electrophoresed through a 3% gel as per Section 2.6. NGS involves Adapter Ligation Technology that generates libraries for sequencing, by utilising an enzyme to attach adaptors to both ends of the DNA fragments, generating at least 5 million read pairs. This work was undertaken using an Illumina NovaSeq (Illumina, Inc., California, USA) at Eurofins Genomics Europe Sequencing GmbH, Germany.

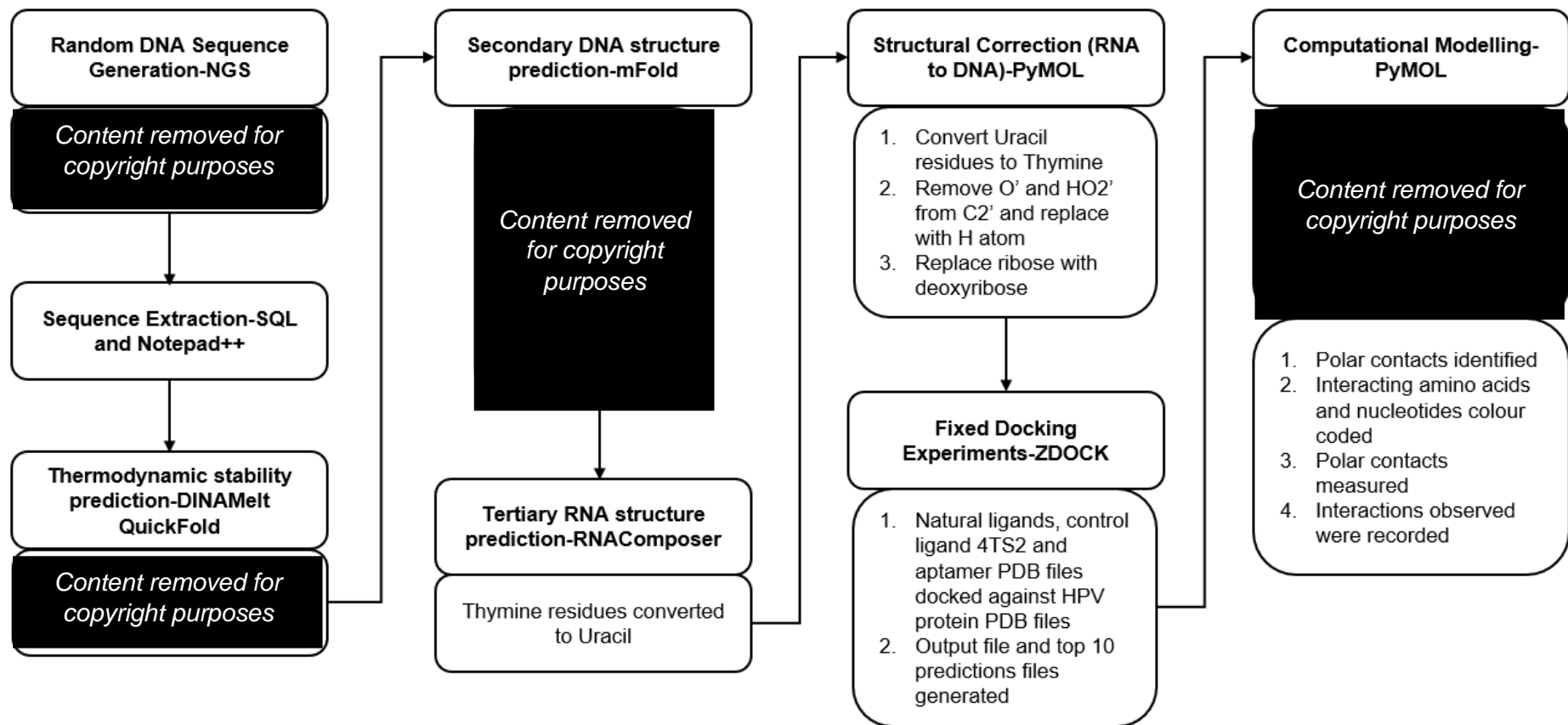


**Figure 10: Summary of aptamer development procedure.**

Samples sent for NGS generated thousands of DNA reads, which were searched for the forward and reverse primer sequences and a length of 70 characters. Extracted sequences underwent thermodynamic stability prediction, which was used to select sequences with Gibbs free energy ( $\Delta G$ ) values below -20 kcal/mol. The top 10 sequences selected underwent secondary DNA structure prediction and tertiary structure prediction. Here Thymine (T) residues were converted to Uracil (U), before structural correction converting U residues back to T, and removing atoms to replace ribose with deoxyribose. Natural ligands, control ligand 4TS2 and aptamer candidates were docked against their respective HPV protein, generating both output and prediction files. Amino acids and nucleotides were colour coded appropriately and measurements and interactions recorded during computational modelling.

### 2.7.2 Sequence extraction

NGS data for each HPV aptamer pool was received as FASTQ files. Each FASTQ file was loaded into Notepad++ (<https://notepad-plus-plus.org/>) and searched for all lines containing string A (known forward primer sequence). The results generated for that search were searched again for all lines containing string B (opposite and reverse of the known reverse primer sequence) and saved as a new text file. A new database was created in Microsoft SQL Server (<https://www.microsoft.com/en-GB/sql-server/sql-server-downloads>) and a table added for each results file. The contents of each new text file was loaded into the database table using a SQL bulk insert. Using structured query language (SQL), each database table for all rows containing a text value was searched for sequences starting with string A, ending with string B and being 70 characters long (70 nt long); comprising 21 nt for known forward primer, 19 nt for known reverse primer, and 30 nt for aptamer library wobble region. The values generated were returned as query results, and copied into a new text file.

### 2.7.3 Thermodynamic stability and secondary DNA structure prediction

Each of the sequences generated at 70 nt long were inputted into DINAMelt server-QuickFold web server (<http://www.unafold.org/Dinamelt/applications/quickfold.php>) which predicted thermodynamic stability (Markham and Zuker, 2005). Sequences were required to have negative Gibbs free energy ( $\Delta G$ ) values, using the following folding parameters: Energy rules: DNA at 4°C, [Na<sup>+</sup>] = 1 M, [Mg<sup>++</sup>] = 0 M; Sequence type: Linear; Structures: 5% at suboptimal, maximum of 1 folding; Maximum distance between paired bases: no limit. Generation of secondary DNA structure prediction for the top ten structures of each aptamer, based on their negative  $\Delta G$  value, was performed using mFold (<http://www.unafold.org/mfold/applications/dna-folding-form.php>) using the same parameters that were used for QuickFold (Zuker, 2003).

### 2.7.4 Tertiary structure prediction and structural correction

The top ten aptamer candidate sequences for each HPV protein target were inputted into RNAComposer (<http://rnacomposer.ibch.poznan.pl/>) to generate predicted tertiary structures, with all Thymine (T) residues converted to Uracil (U) for folding purposes (Popenda *et al.*, 2012). Protein Data Bank (PDB) files generated were then modified in PyMOL (<https://pymol.org/2/>) using the mutagenesis wizard to convert the U residues to T, and commands inputted into the PyMOL command line to remove the



ribose groups and replace them with deoxyribose groups (Schrödinger LLC, 2015). Commands used were to remove the O' and HO2' atoms from each C2' atom present in each residue and add a hydrogen atom in their place. Structures generated were saved as PDB files for fixed docking experiments.

### **2.7.5 Fixed docking experiments**

PDB files generated for the top ten aptamer candidate sequences for each HPV protein target were compared to see which three aptamer candidates per HPV protein target were the most similar based on thermodynamic stability and the nature of free hydrogen bonds (Liang *et al.*, 2006). Fixed docking experiments using ZDOCK server (<https://zdock.umassmed.edu/>) were used to determine predicted interactions, where both the protein and ligand bond angles and atomic positioning were fixed (Nabuurs *et al.*, 2007, Pierce *et al.*, 2014). PDB files of each of the respective HPV proteins (HPV-16 E2, HPV-16 E6, HPV-18 E6 and HPV-18 E7), their natural ligands (Brd4, p53 and pRb) and the control ligand 4TS2 structures were downloaded from RCSB PDB (<https://www.rcsb.org/>) with PDB file names and modifications made described in Table 6 (Berman *et al.*, 2000). 4TS2, a spinach RNA aptamer was chosen as a control to dock against each target protein as it is a non-species target to HPV.

Each HPV protein underwent one docking experiment against 4TS2 (first experiment only), and two docking experiments against their natural ligand and the three aptamer candidate sequences per respective HPV protein target (36 in total). The first experiment involved free-binding of the natural ligand, the control ligand 4TS2, and each of the three aptamer candidate sequences per respective HPV protein target to their respective HPV protein. The second experiment was performed two ways. For the natural ligands, they were instructed to dock to the amino acid (AA) residues, that were interacted with on their respective HPV protein within their PDB models. However, for the three aptamer candidate sequences per respective HPV protein target, they were instructed to dock to the AA residues that were interacted with on their respective HPV protein within their first docking experiment with their natural ligand. Each fixed docking experiment generated an output file and top ten predictions files. In the output file, an average was taken for all the ZDOCK scores (last column) as well as an average for the top three predictions (aptamer candidates only).

**Table 6: RCSB PDB files and modifications used for fixed docking experiments**

	<b>PDB file name</b>	<b>Modifications made to PDB file</b>	<b>Reference</b>
<b>HPV proteins</b>	1BY9 (crystal structure of the E2 DNA-binding domain from human papillomavirus type-16: implications for its DNA binding-site selection mechanism)	Water ions removed 1BY9 docked with 2NNU	(Hegde and Androphy, 1998)
	4XR8 (crystal structure of the HPV-16 E6/E6AP/p53 ternary complex at 2.25 Å resolution)	Chain A-maltose-binding periplasmic protein and E6AP, Chain B-maltose-binding periplasmic protein, Chain C-p53, Chain E-HPV-16 E6, Chains G and H-alpha-D-glucopyranose-(1,4)-alpha-D-glucopyranose, Chains I, J, M and Q-di(hydroxyethyl)ether, Chains K, L, N, O and R-zinc ions, Chain P-1,2-ethanediol and water ions removed Chain B containing E6AP sequence retained Interactions recorded between p53 and E6 protein and p53 removed 4XR8 docked with 8F2I	(Martinez-Zapien <i>et al.</i> , 2016)
	6SJV (structure of HPV-18 E6 oncoprotein in complex with mutant E6AP LXXLL motif)	Chain A-maltodextrin-binding protein, Chain B-alpha-D-glucopyranose-(1,4)-alpha-D-glucopyranose, Chains C and D-zinc ions, and water ions removed E6AP LXXLL motif removed, saved as a separate PDB file and docked to bind to HPV-18 E6	(Suarez <i>et al.</i> , Unpublished)
	6IWD (the PTP domain of human PTPN14 in a complex with the CR3 domain of HPV-18 E7)	Chain A tyrosine-protein phosphatase non-receptor type 14, Chain C chloride ions, Chains D and E phosphate ions, Chain F zinc ions and water ions removed 6IWD docked with 3POM	(Yun <i>et al.</i> , 2019)
<b>Natural ligands</b>	2NNU (crystal structure of the papillomavirus DNA tethering complex E2:Brd4)	Chain A HPV-16 E2 and water ions removed Brd4 sequence retained 2NNU docked with 1BY9	(Abbate <i>et al.</i> , 2006)
	8F2I (p53 monomer structure)	No modifications made 8F2I docked with residues that were interacted with between HPV-16 E6 and p53 in 4XR8	(Solares <i>et al.</i> , 2022)
	3POM (crystal structure of the unliganded retinoblastoma protein pocket domain)	Chain B pRb and water ions removed 3POM docked with 6IWD	(Balog <i>et al.</i> , 2011)
<b>Control ligand</b>	4TS2 (crystal structure of the Spinach RNA aptamer in complex with DFHBI, magnesium ions)	Magnesium, potassium and water ions removed	(Warner <i>et al.</i> , 2014)

### 2.7.6 Computational modelling

Every top ten prediction file for each natural ligand, the control ligand 4TS2, and each of the three aptamer candidates per respective HPV protein target that were docked, were extracted twice to generate ten PDB files. The top prediction for each natural ligand and the control ligand 4TS2, and the top three predictions of the three aptamer candidates per respective HPV protein target were opened in PyMOL. Using the external GUI window, the display tab was selected, followed by the sequence tab, which displayed the sequences in the PyMOL viewer window for each of the structures present. Next, the display tab was selected again, followed by the sequence mode tab and the residue names tab, which displayed the abbreviated AA names, instead of their symbols. Within the PyMOL viewer window, each of the sequences was highlighted individually, and the following steps performed. Using the object control panel on the right-hand side of the screen, the action (A) and colour (C) command buttons were selected to rename and change the colour of each sequence respectively, which were shown in the drop-down menu. Next, the show (S) command button was selected, followed by the sticks tab in the drop-down menu, which displayed the sequence in stick view. Lastly, the hide (H) command button was selected, followed by the cartoon tab in the drop-down menu, which removed the cartoon view.

Next, within the PyMOL viewer window, the aptamer sequence was selected. Using the object control panel, the action (A) command button was selected, then within each subsequent drop-down menu, the following tabs were selected: find, polar contacts, and to other atoms in object. This displayed any polar contacts occurring between atoms. For the protein sequence, any AAs that had polar contacts with a DNA residue were highlighted, with any bound DNA residue highlighted as appropriate (as shown in Section 5.2.3, Figure 47). Once all the polar contacts had been identified, using the object control panel, the hide (H) command button was selected, followed by selecting the everything tab in the drop-down menu for each sequence. This hid the 3D model within the PyMOL viewer window. Next, in the PyMOL viewer window, each of the residues that had been highlighted a different colour from the original were selected, and using the show (S) command button, the sticks tab was selected in the drop down. Using the measurement wizard, each of the polar contacts was measured by selecting one atom, followed by selecting the second interacting atom to give a measurement

in Angstroms (Å). Lastly, the label (L) command button in the object control panel was selected, and using the drop-down menu, the atom name tab was selected. This labelled all the atoms present in both the DNA nt and AAs. Each file was saved as session files in pse format.

For each natural ligand, the control ligand 4TS2, and top three predictions for the three aptamer candidates per HPV protein target, the DNA residue and AA that interacted were noted down, as well as Å measurement, output for the corresponding complex, and a description of what was happening in each interaction. The Å measurements were only considered if they were in the range of 2.2-4.0 Å, as there is a minimum distance in between atoms due to intermolecular forces (Jeffrey, 1997). A candidate for each aptamer was chosen based on ZDOCK score, interactions between protein and aptamer, nature of the interactions, distances, structure and how the structure was interacting with the protein.

## 2.8 Fluorescent-based binding assay

This methodology was adapted from AFBI assay-aptamer fluorescence binding and internalisation assay for cultured adherent cells (Thiel and Giangrande, 2016). 96-well plates were prepared as per Section 2.5.1 for the positive and negative plates, except they were all blocked with 0.1% BSA in PBS.

Synthesised HPV-16 E2, HPV-16 E7-E6, HPV-18 E6 and HPV-18 E7 aptamers and HPV-16 E2, HPV-16 E7-E6, HPV-18 E6 and HPV-18 E7 negative control aptamers (negative positive selection controls) from Section 2.5.2 underwent PCR as per Section 2.5.5, using a 5' Alexa Fluor™ 488 forward primer [REDACTED]

[REDACTED] (synthesised by Eurofins Genomics Germany GmbH, Germany), for fluorescent labelling. These were then electrophoresed through a 3% gel as per Section 2.5.5, to ensure integration of fluorophore into the aptamer. A gel loading buffer (0.1 M EDTA, pH 8.0 (cat. no: E9884-100G-Sigma Aldrich®, Merck Life Science UK Limited, Dorset, UK), 40% (w/v) sucrose (cat. no: 10634932-Fisher Chemical, Fisher Scientific UK Ltd, Loughborough, UK), and 0.5% (w/v) sodium lauryl sulphate (SDS) (cat. no: 10593335-Fisher BioReagents, Fisher Scientific UK Ltd, Loughborough, UK), was made and used to run with the fluorescently-labelled aptamers. As the original loading dye fluoresces,

we wanted to run the aptamers without a visible dye front to show integration of the 5' Alexa Fluor™ 488 fluorophore.

Aptamers and antibodies were prepared as per working concentrations detailed in Table 7, in filter sterilised 1x binding buffer, pH 7.4 (1.5 M sodium chloride (cat. no: 10112640-Fisher Chemical, Fisher Scientific UK Ltd, Loughborough, UK), 20 mM calcium chloride (cat. no: C1016-100G) and 200 mM N-2-hydroxyethylpiperazine-N-2-ethane sulphonic acid (HEPES) (cat. no: H4034-100G) (both Sigma Aldrich®, Merck Life Science UK Limited, Dorset, UK) and chilled on ice. Aptamer and antibody concentration range was wide enough to cover both ends of a binding curve, with a 10-fold serial dilution carried out across the plate.

### **2.8.1 Antibody binding assay**

Wells were washed with 200 µl washing 1x binding buffer twice, and decanted between washes. Wells were then blocked with 100 µl 1x binding buffer containing 10% normal donkey serum (NDS) (cat. no: ab7475-Abcam PLC, Cambridge, UK), to decrease non-specific binding, for 10-20 minutes at 4°C. The wells were then incubated with 25 µl of antibody or secondary antibody (negative control), which allowed for equilibrium binding to be established.

A 10-fold serial dilution of antibody or secondary antibody (negative control) was generated across the plate. Plates were incubated overnight at 4°C. Antibodies were decanted from the plates, and wells washed twice with 200 µl washing 1x binding buffer. Plates were incubated with 25 µl donkey anti-mouse Alexa Fluor® 488 secondary antibody (cat. no: ab150105-Abcam PLC, Cambridge, UK) for 60 minutes at room temperature. Secondary antibody was decanted, and wells washed twice with 200 µl washing 1x binding buffer. After the final wash, plates were tilted for 30 seconds, and decanted again to fully dry the wells. Fluorescence was measured using the green fluorescent protein (GFP) protocol for fluorescence intensity with endpoint mode on a FLUOstar Omega microplate reader using Omega Software to run fluorescence measurement and Mars Software for data analysis (all BMG Labtech, Germany).

### **2.8.2 Aptamer binding assay**

Wells were washed twice with 200  $\mu$ l washing 1x binding buffer, and decanted between washes. Wells were then blocked with 100  $\mu$ l 1x binding buffer containing 1  $\mu$ g/ml BSA, to decrease non-specific binding, for 10-20 minutes at 4°C. The wells were then incubated with 25  $\mu$ l of aptamer, or negative aptamer, which allowed for equilibrium binding to be established.

Aptamer starting concentrations were based on the concentration used in IHC, with a 10-fold serial dilution generated across the plate. Plates were incubated overnight at 4°C. Aptamers and antibodies were decanted from the plates, and wells washed twice with 200  $\mu$ l washing 1x binding buffer. Aptamer plates did not require further incubation or washes after this step. Fluorescence was measured using the GFP protocol for fluorescence intensity with endpoint mode on a FLUOstar Omega microplate reader using Omega Software to run fluorescence measurement and Mars Software for data analysis (all BMG Labtech, Germany).

### **2.8.3 Statistical analysis**

Binding assays were tested for statistical significance by Two-Way ANOVA (Geisser-Greenhouse correction, matched values spread across a row; Bonferroni's multiple comparisons test, with individual variances computed for each comparison) using Prism 10 (GraphPad Software Inc) <https://www.graphpad.com/>. P-values <0.05 were taken to be significant.

**Table 7: Positive and negative HPV antibodies and aptamers and their working concentrations for fluorescent-based binding assays and cell immunofluorescence**

	<b>HPV target protein</b>	<b>Stock concentration (µg/ml)</b>	<b>Working concentration (µg/ml)</b>
<b>Antibody</b>	HPV-16 E2	1000	20
	HPV-16 E6	100	1
	HPV-16 E7	200	2
	HPV-18 E6	100	2
	HPV-18 E7	1000	10
<b>Secondary antibody</b>	Donkey anti-mouse Alexa Fluor™ 488	2000	4
<b>Aptamer</b>	HPV-16 E2	449.3	2
	HPV-16 E7-E6	337.8	1
	HPV-18 E6	412.2	2
	HPV-18 E7	303.9	1
<b>Negative aptamer</b>	HPV-16 E2	345.0	4
	HPV-16 E7-E6	439.0	4
	HPV-18 E6	395.2	4
	HPV-18 E7	347.7	4

## **2.9 Cell culture**

### **2.9.1 General growth**

All cell culture experiments were carried out in a Class II Laminar flow cabinet. MCF7, SiHa, HeLa, VU-SCC-040T and VU-SCC-147T cell lines (Table 8) were grown in Dulbecco's modified eagle medium (DMEM) (cat. no: 10-013-CV-Corning, Scientific Laboratory Supplies Ltd, Nottingham, UK) supplemented with 10% foetal bovine serum (FBS) (cat. no: A4766801-Gibco™, Thermo Fisher Scientific, Fisher Scientific UK Ltd, Loughborough, UK), 1% penicillin-streptomycin (cat. no: P4333-100ML) and 1% non-essential AA (NEAA) (cat. no: M7145-100ML) (both Sigma Aldrich®, Merck Life Science UK Limited, Dorset, UK) (VU-SCC-040T and VU-SCC-147T only) in T75 flasks. These were all grown at 37°C in 5% CO<sub>2</sub>. Cell lines were passaged around twice a week at 80% confluency.

## **2.10 Cell immunofluorescence**

### **2.10.1 Fixation**

19 x 19 mm coverslips (cat. no: 12323138-Fisherbrand™, Fisher Scientific UK Ltd, Loughborough, UK), were sterilised in 70% IMS, dried and one coverslip placed in each well of a 12-well plate (cat. no: 83.3921-Sarstedt AGA & Co. KG, Germany) (in duplicate for each cell type). 1 ml of poly-D-lysine (cat. no: A38904-01-Gibco™, Thermo Fisher Scientific, Fisher Scientific UK Ltd, Loughborough, UK) was added to each coverslip for 20 minutes then removed.  $4.8 \times 10^5$  cells in complete media were added to each well and incubated overnight at 37°C in 5% CO<sub>2</sub>.

After overnight incubation, plates were washed twice with 1x PBS, and then incubated in 0.1 M glycine (cat. no: G8898-1KG-Sigma Aldrich® Merck Life Science UK Limited, Dorset, UK) for 30 minutes. Glycine was removed and ice-cold acetone (cat. no: 10131560-Fisher Chemical, Fisher Scientific UK Ltd, Loughborough, UK), added, and incubated for 10 minutes. Wells were washed three times with 1x PBS, then 900 µl 1x PBS and 100 µl penicillin-streptomycin added to each well to prevent drying out and fungal growth. Each plate was sealed with parafilm and stored in a cold room until required.



**Table 8: Cell lines grown for cell immunofluorescence**

Cell line	Growth properties	Doubling time	Gender	Age (years)	Primary tumour	Cell type	Disease	HPV status and type	Source
MCF7	Adherent	29 hours	Female	69	Breast: Mammary gland	Epithelial	Adenocarcinoma	Negative	HTB-22 ATCC <sup>1</sup> , Virginia, USA
SiHa	Adherent	2.6 days	Female	55	Uterus; Cervix	Epithelial	Squamous cell carcinoma	HPV-16 Positive	HTB-35 ATCC, Virginia, USA
HeLa	Adherent	1.3 days	Female	31	Uterus: Cervix	Epithelial	Adenocarcinoma	HPV-18 Positive	CCL-2 ATCC, Virginia, USA
VU-SCC-040T	Adherent	27 ± 3 hours	Female	65	Tongue	Epithelial	Squamous cell carcinoma	Negative	Gift from Professor H Joenje, VU Medical Centre, Amsterdam (via Dr S Roberts, University of Birmingham)
VU-SCC-147T	Adherent	2.2 days	Male	58	Floor of mouth	Epithelial	Squamous cell carcinoma	HPV-16 Positive	Gift from Professor H Joenje, VU Medical Centre, Amsterdam (via Dr S Roberts, University of Birmingham)

<sup>1</sup>American Type Culture Collection

### **2.10.2 Antibody immunofluorescence**

Cells were permeabilised with 1x PBS with 0.1% Triton X-100 (cat. no: X100-100ML- Sigma Aldrich®, Merck Life Science UK Limited, Dorset, UK) and incubated for 10 minutes. Coverslips were washed three times with 1x PBS and blocked with 10% NDS in 1x PBS for 30 minutes. After incubation, primary antibodies were added in blocking solution at dilutions provided in Table 7 and incubated at 4°C for 48 hours. Coverslips were washed three times with 1x ice cold PBS, before adding secondary antibody in 10% NDS at room temperature for 60 minutes. Coverslips were dried and mounted with Fluoroshield™ with DAPI mounting medium (cat. no: F6057-20ML- Sigma Aldrich®, Merck Life Science UK Limited, Dorset, UK), and sealed with clear nail varnish.

### **2.10.3 Aptamer immunofluorescence**

Cells were washed three times with 1x PBS and blocked with 1% BSA for 30 minutes. After incubation, aptamers were added in blocking solution (1% BSA in 1x PBS), at dilutions provided in Table 7 and incubated at 4°C for 48 hours. Cells were washed three times with 1x ice cold PBS. Coverslips were dried and mounted with Fluoroshield™ with DAPI mounting medium, and sealed with clear nail varnish. As aptamers were amplified by PCR using a 5' Alexa Fluor™ 488 forward primer, they did not require secondary antibody application.

### **2.10.4 Cell immunofluorescence imaging**

Slides were visualised and imaged on the Nikon Eclipse Ti inverted microscope and NIS-Elements AR imaging software (both Nikon Instruments Inc., New York, USA) using the GFP channel at the University of Sheffield. Images were taken using a 60x oil immersion lens, and saved in nd2 format. All images were viewed in ImageJ software (<https://imagej.net/ij/download.html>) (Schneider *et al.*, 2012).

## CHAPTER 3: HISTOLOGICAL CHARACTERISATION OF NORMAL PALATINE TONSILS AND OROPHARYNGEAL SQUAMOUS CELL CARCINOMAS

### 3.1 Introduction

In cervical carcinoma (CC), high-risk (HR)-HPV infect the basal cells of the basement membrane through traumatised epithelium within the transformation zone (TZ) of the squamocolumnar junction (SCJ). The TZ consists of non-keratinising stratified squamous epithelium (ectocervix) which transitions to simple columnar epithelium (endocervix) (Herfs *et al.*, 2012, Dudás, 2023). Persistent infection with HR-HPV can lead to the development of precursor lesions known as cervical intraepithelial neoplasia's (CIN), which can progress to CC (Herfs *et al.*, 2012, Lee *et al.*, 2017). The TZ is a site pre-disposed to HPV-mediated disease that stains positive for cytokeratin 7, a ductal, glandular, and transitional epithelial marker which is also present within the reticulated crypt of the normal palatine tonsil (Lee *et al.*, 2017, Woods *et al.*, 2017, Woods *et al.*, 2022). In HPV-positive OPSCC, it is hypothesised that HPV infection may establish within these reticulated crypts (Kim *et al.*, 2007).

The surface epithelium of the normal palatine tonsil is covered by non-keratinising stratified squamous epithelium, which invaginates into the lamina propria, forming 10-30 tonsillar crypts (up to 300 cm<sup>2</sup> total surface area) (Howie, 1980, Dudás, 2023). These crypts have branching blind ends that are lined by reticulated epithelium, which, unlike the surface epithelium, has a discontinuous basement membrane that is densely infiltrated with lymphocytes (Stöhr, 1882, Olah, 1978, Nave *et al.*, 2001). This lymphoepithelium, where epithelial cells and lymphocytes coexist, is known as lymphoepithelial symbiosis (Schmincke, 1921, Fioretti, 1957). The depth of the crypts makes them susceptible to bacteria and foreign antigens, with the abundance of lymphocytes and programmed cell death-ligand 1 (PD-L1) expression within the crypts representing an immune-privileged site (Lyford-Pike *et al.*, 2013).

PD-L1 (transmembrane glycoprotein expressed on T and B lymphocytes, macrophages, and dendritic cells as well as cancer cells) is capable of binding to programmed cell death protein-1 (PD-1) (transmembrane protein receptor that is expressed on activated T lymphocytes, B lymphocytes, and macrophages) (Dong *et al.*, 1999, de Vincente *et al.*, 2019). Within the tumour microenvironment (TME), they

bind and approach the tumour-infiltrating lymphocytes (TILs) which are positive for CD8, a transmembrane glycoprotein also present on cytotoxic T lymphocytes which increases antitumour immune responses (Lyford-Pike *et al.*, 2013, de Vincente *et al.*, 2019, Atipas *et al.*, 2023). Together, PD-L1 and PD-1 act as part of the immune checkpoint pathway, and are cancer immunotherapy targets (for the monoclonals Nivolumab and Pembrolizumab) to treat metastatic and recurrent HNSCC (Lyu *et al.*, 2019, Oliva *et al.*, 2019). Epidermal growth factor receptor (EGFR) is a transmembrane receptor tyrosine kinase that is also an approved targeted treatment for HNSCC whose expression is most commonly-associated with HPV-negative OPSCCs (Taberna *et al.*, 2018, Deuss *et al.*, 2020). The EGFR-targeting monoclonal Cetuximab has low response rates (10-15%) compared to Pembrolizumab and is associated with poor prognosis (Vermorken *et al.*, 2008, Bonner *et al.*, 2010, Harrington *et al.*, 2017, Cohen *et al.*, 2019).

Unlike in the cervix, it is currently unknown whether any precursor lesions exist within the tonsils prior to cancer (Palmer *et al.*, 2014, Quabius *et al.*, 2021). In diagnosing disease, p16INK4A immunohistochemistry (IHC) is a validated prognostic marker used for testing HPV status within OPSCC within the UK (Klussman *et al.*, 2003, Sedghizadeh *et al.*, 2016, Lewis *et al.*, 2018b, Hunter *et al.*, 2021). p16 is a surrogate marker for HPV, which is overexpressed when the tumour suppressor protein and cell cycle regulator, retinoblastoma protein (pRb), is degraded (Dyson *et al.*, 1989, Li *et al.*, 1994, Klussman *et al.*, 2003). Additional HR-HPV-specific tests are also available including HPV DNA *in-situ* hybridisation (ISH); however there is no consensus on the best methodology for HPV testing within the oropharynx (Hunter *et al.*, 2021).

Cancers of the oropharynx particularly OPSCCs can be identified using the pancytokeratin AE1/AE3, which identifies cytokeratins of simple and stratified epithelial origin (Tseng *et al.*, 1982, Woodcock-Mitchell *et al.*, 1982, Sun *et al.*, 1984, Giotakis *et al.*, 2023). CK7 can also be used to determine tumour origin, particularly tumours of reticulated crypt origin (Woods *et al.*, 2017). Other prognostic markers that have also been associated with both HPV-positive and HPV-negative OPSCC include Ki67, a proliferation marker, and ER $\alpha$ , a prognostic biomarker and therapeutic target (Chatzkel *et al.*, 2017, Kwon *et al.*, 2020).

This chapter therefore examines and characterises the histology of normal and cancerous tonsil, in comparison with normal and cancerous cervix, using a variety of biomarkers believed to be involved in the development of HPV-mediated disease.

## **3.2 Results**

### **3.2.1 Histological characterisation of the normal cervix and CCs**

HPV infection within the cervix has been well characterised. Unfortunately, normal cervical tissue with the SCJ could not be sought for the study; therefore, an image was sourced from the literature. The haematoxylin and eosin (H&E) showed normal cervix (Figure 11A), with a discernible basement membrane, where non-keratinising stratified squamous epithelium transitioned to simple columnar epithelium. These two epithelial types formed the TZ within the SCJ. To characterise the normal cervix further, we would have stained it with p16, as this is a biomarker of HPV status also identified in CC and cervical precancerous lesions. Again, an example of p16 stained in normal cervix was sourced from the literature. Staining of p16 was negative within the normal cervical epithelium (Figure 11B).

Three CC tissues were also stained with H&E and p16 (Figure 12). The pathology showed invasive squamous cell carcinoma (SCC) for all three CCs; the tumours resembled neoplastic squamous epithelium that infiltrated into the cervical stroma as irregular nests and sheets. Additionally, they were tumour-positive for p16 staining, which suggested that these were HPV-positive CCs. There was no glandular appearance in any of the tumour nests confirming non-keratinising SCC (NKSCC) origin rather than adenocarcinoma, therefore representing an excellent comparator for OPSCC tissue characterisation.

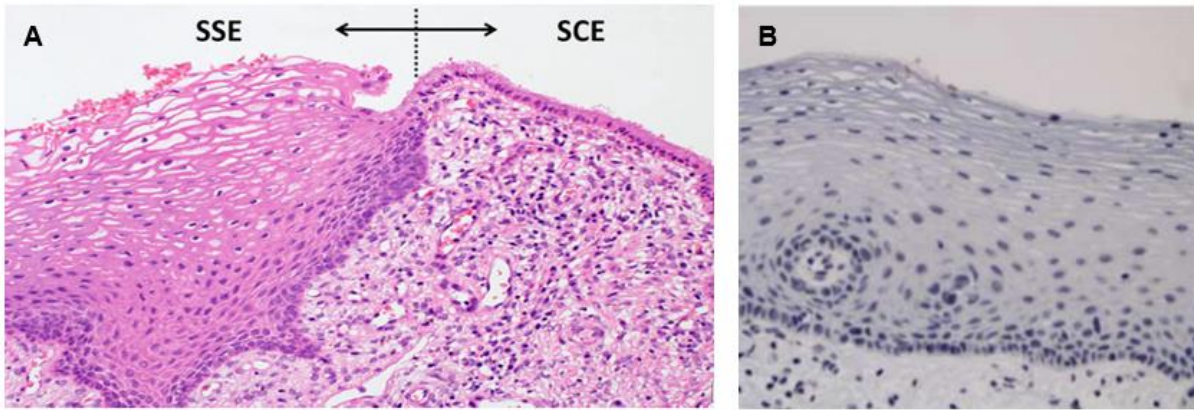


**Figure 12: H&E and p16 of the squamocolumnar junction of the cervix.**

The cervical squamocolumnar junction consisted of non-keratinising stratified squamous epithelium (SSE) and simple columnar epithelium (SCE), where there is a clearly defined change between the two epithelial cell types (A). Unlike the normal palatine tonsil, there is a discernible basement membrane. p16 expression was negative within the normal cervical epithelium and underlying tissue (B). Images sourced from (Kurita *et al.*, 2019) (A) and (Feng *et al.*, 2007) (B) at unknown magnifications.

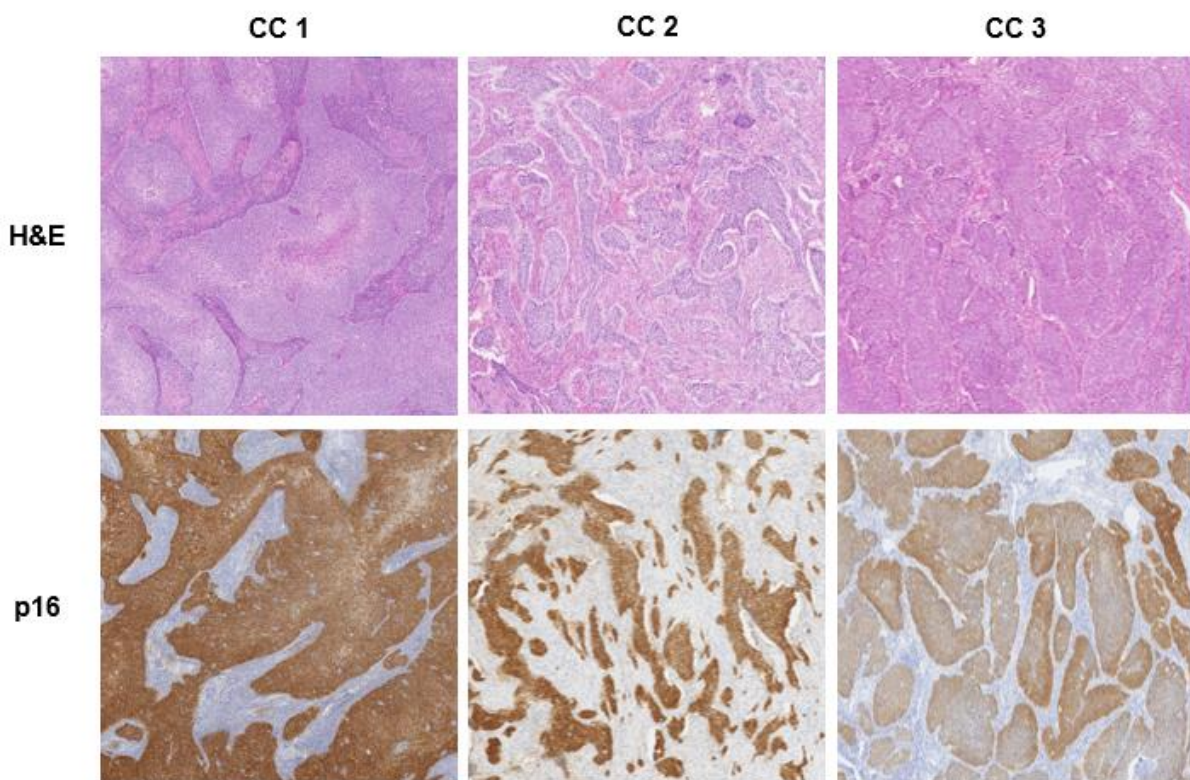


**Figure 11: H&E and p16 of three CC tissues.**

Invasive CCs demonstrating NKSCC morphology. The tumours infiltrated as nests and sheets throughout. No glandular morphology was present, therefore excluding the tumours as adenocarcinomas. Invasive CCs exhibiting tumour-positive staining for p16. Images captured on NDP.view2 software at 5x magnification.

### **3.2.2 Histological characterisation of the normal palatine tonsil**

Unlike in the normal cervix, HPV infection within the normal palatine tonsil has not been well characterised. Firstly, H&E sections of normal palatine tonsil were observed and described, in order to characterise the normal tissue.

The H&E showed two halves of the same tonsil, which appeared unremarkable and morphologically normal (Figure 13). The surface epithelium showed invagination into two crypts, with two further crypts apparent within the parenchyma. Also, within the parenchyma, were numerous lymphoid follicles that were spheroid in shape, each containing a germinal centre (light), surrounded by a mantle zone (dark) (Figure 14A). The tonsil surface was covered in non-keratinising stratified squamous epithelium, which had an intact basement membrane with basal cells resting on it, and the underlying lamina propria below it (Figure 14B). Each crypt was lined with reticulated epithelium consisting of squamous cells and lymphocytes coexisting together, with an indistinct basement membrane present (Figure 14C). This demonstrated the discontinuity that is seen between the surface and reticulated epithelium, with this example showing an indistinct basement membrane, which could make this particular tonsillar crypt an easier target for foreign antigens including HPV. As there is transitional epithelium present in both tissue types, the normal cervix represents an excellent comparator for further tissue characterisation of the normal palatine tonsil.

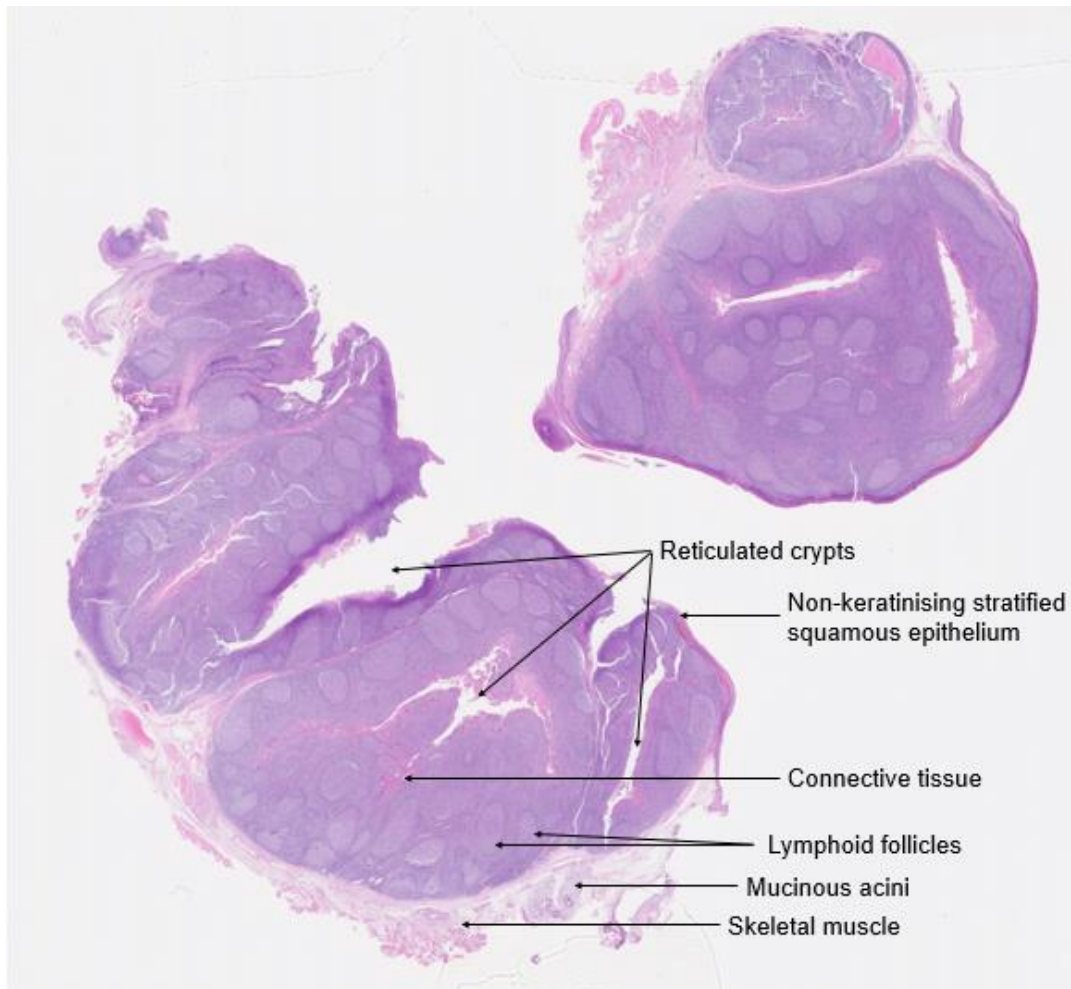


**Figure 13: H&E of the normal palatine tonsil.**

Image was captured on NDP.view2 software at 0.42x magnification.



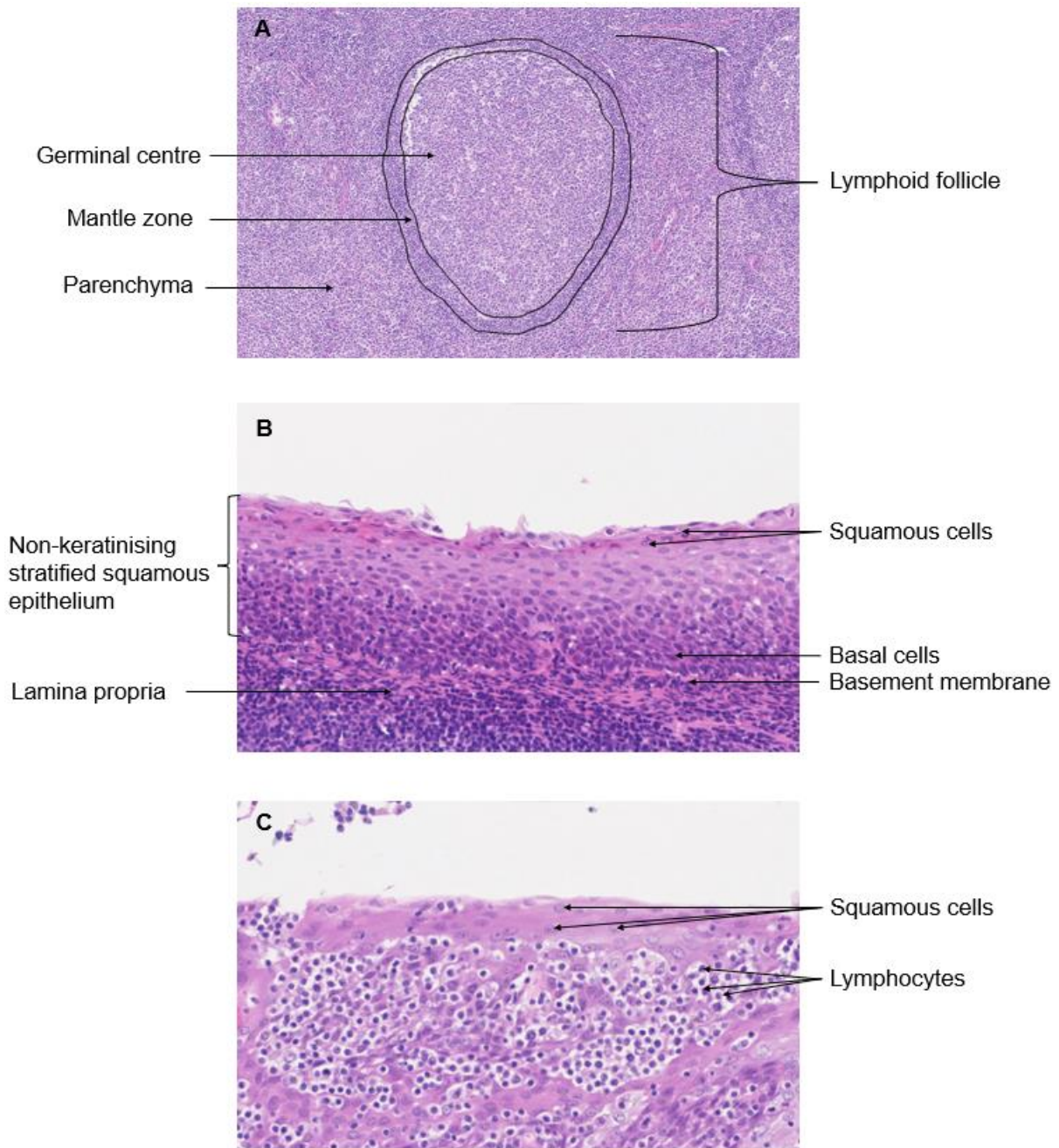


**Figure 14: H&Es of the lymphoid follicle, surface epithelium, and reticulated epithelium of the normal palatine tonsil.**

A lymphoid follicle within the tonsil parenchyma, consisting of a germinal centre (light) in the centre and the mantle zone (dark) surrounding it (**A**). The surface epithelium was non-stratified squamous epithelium, with squamous cells present on the upmost surface, and basal cells towards the bottom, which rested on the intact basement membrane. The lamina propria consisted of connective tissue, which was located below the basement membrane (**B**). The reticulated epithelium consisted of an indistinct basement membrane, which was obscured by the dense infiltration of lymphocytes admixed with squamous cells (**C**). Images were captured on NDP.view2 software at 10x (**A**), and 40x (**B and C**) magnification.

### 3.2.3 Biomarker optimisation within the normal palatine tonsil

To characterise the normal palatine tonsil further, nine biomarkers were selected from the literature, that were identified as prognostic biomarkers for OPSCC: p16, the surrogate HPV marker; PD-1, a checkpoint receptor and its ligand, PD-L1; CD8, a cytotoxic T lymphocyte marker; Ki67, a proliferation marker; ER $\alpha$ , a prognostic biomarker and therapeutic target; CK7, a reticulated epithelial marker; AE1/AE3, a pancytokeratin epithelial marker; and EGFR, a transmembrane receptor associated with poor prognosis (Klussman *et al.*, 2003, Lyford-Pike *et al.*, 2013, Chatzkel *et al.*, 2017, Woods *et al.*, 2017, Koenigs *et al.*, 2019, Deuss *et al.*, 2020, Atipas *et al.*, 2023, Giotakis *et al.*, 2023).

Staining for all nine biomarkers was optimised within the same normal palatine tonsil (Figures 15 and 16). Expression within the reticulated epithelium was observed with staining of p16, PD-L1, CD8, Ki67, CK7, AE1/AE3, and EGFR. p16 (nuclear and cytoplasmic), PD-L1 (membranous), and CK7 (cytoplasmic and membranous) demonstrated similar distribution of staining in the uppermost layers of the reticulated epithelium, compared to stronger and more abundant staining of AE1/AE3 (cytoplasmic), which stains for numerous cytokeratins. Within the germinal centres, staining of lymphocytes was observed with PD-L1, PD-1 (cytoplasmic and membranous), CD8 (membranous), and Ki67 (nuclear). Lastly, expression of CD8, Ki67, ER $\alpha$  (nuclear), and EGFR (membranous), was observed alongside AE1/AE3 within the surface epithelium. AE1/AE3 and EGFR are found within the surface epithelium, with Ki67, ER $\alpha$ , and CD8 seen within the basal cells above the basement membrane, where proliferating cells are found. With the normal palatine tonsil histology and expression of the biomarkers characterised, we then turned our attention to characterising OPSCCs.

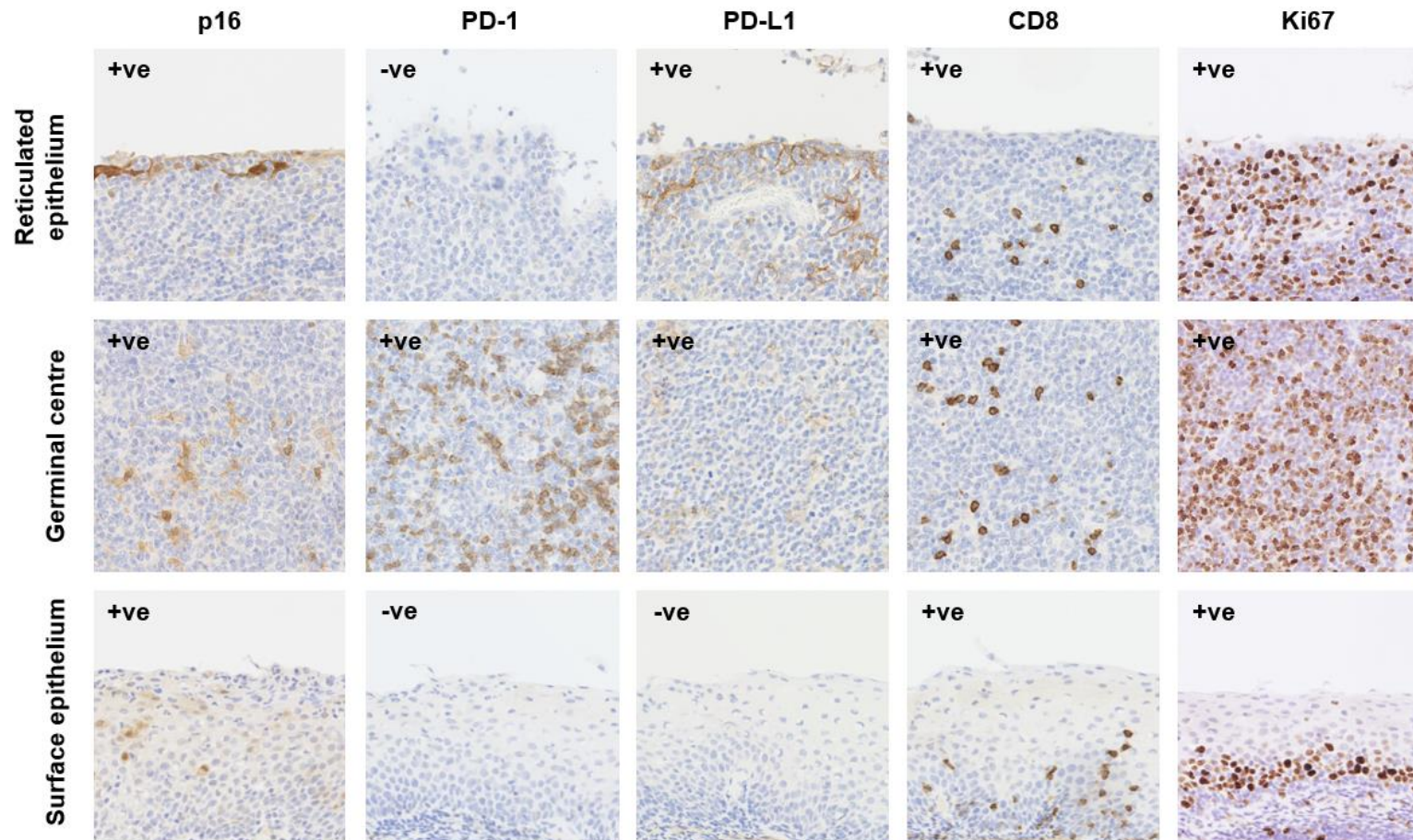


**Figure 15: p16, PD-1, PD-L1, CD8, and Ki67 expression in normal palatine tonsil.**

p16 and PD-L1 expression was observed mostly within the reticulated epithelium; however, PD-1 was negative. Some cells were positive for p16 within the surface epithelium. All three were positive within the germinal centres. Some CD8 expression was observed close to the reticulated epithelium and within the surface epithelium, but was mostly observed the germinal centres. Ki67 expression was observed in a scattered distribution within the reticulated epithelium, and mostly within the germinal centres and basal cells of the surface epithelium. Images were captured on NDP.view2 software at 40x magnification.

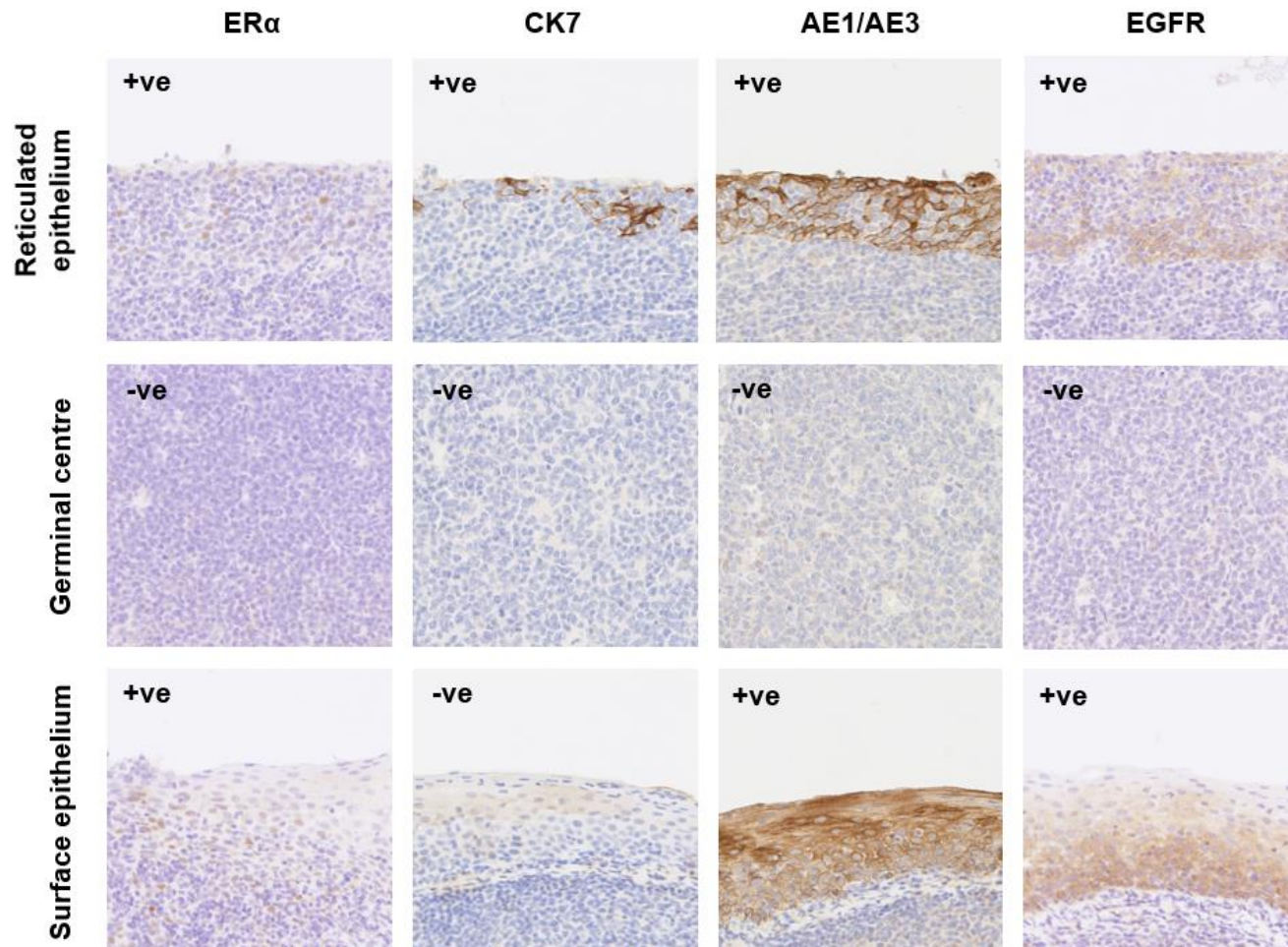


**Figure 16: ER $\alpha$ , CK7, AE1/AE3, and EGFR expression in normal palatine tonsil.**

Weak ER $\alpha$  expression was observed in a scattered distribution within the reticulated epithelium and surface epithelium. CK7 expression was observed only within the reticulated epithelium, with no staining observed within the surface epithelium. AE1/AE3 expression was observed within the reticulated epithelium and surface epithelium. Weak EGFR expression was observed within the reticulated epithelium, with moderate expression observed within the surface epithelium. All four were negative within the germinal centres. Images were captured on NDP.view2 software at 40x magnification.

### **3.2.4 Histological characterisation of OPSCCs**

Five OPSCCs were obtained as unstained sections. An H&E was performed on each OPSCC to allow for histological characterisation. The histopathological type for each OPSCC was determined in consultation with Dr Amandeep Mann, Consultant histopathologist, University Hospitals of Derby and Burton (UHDB).

OPSCC 1 was a conventional invasive keratinising squamous cell carcinoma (KSCC), that showed surface epithelium involvement, where the tumour had invaded through the basement membrane into the stroma (Figure 17). The tumour infiltrated as nests and cords that were angulated, containing polygonal cells with eosinophilic cytoplasm, distinct cell borders, and intercellular bridges. Keratin formation was also present alongside stromal desmoplasia. This tumour was well differentiated, as it resembled the surface epithelium.

OPSCC 2 and OPSCC 3 were NKSCC which infiltrated as sheets, nests, and trabeculae into the stroma, eliciting very little stromal response (Figures 18 and 19). The cell borders were indistinct and contained ovoid to spindle, hyperchromatic cells lacking remarkable nucleoli. Frequent mitoses and comedonecrosis was also seen. In OPSCC 2 some moderate dysplasia was seen which did not breach the basement membrane of the surface epithelium. However, further along the surface epithelium, it appeared that the tumour had infiltrated into the underlying tissue, giving this region a crypt-like phenotype. OPSCC 3 showed extension of the tumour, extending beyond the surface epithelium. Both OPSCC 2 and 3 were poorly differentiated, as they were characterised by high nuclear pleomorphism and frequent atypical mitoses, as well as minimum keratinisation and structural organisation.

Finally, OPSCC 4 and OPSCC 5 were conventional KSCCs (Figures 20 and 21). The tumours infiltrated as nests and cords that were angulated, containing polygonal cells with eosinophilic cytoplasm, distinct cell borders and intercellular bridges. Keratin formation was also present alongside stromal desmoplasia. OPSCC 4 was moderately differentiated, compared to OPSCC 5 which was poorly differentiated. Additionally, OPSCC 5 showed the involvement of surface epithelium, where the tumour had invaded through the basement membrane into the stroma, as well as extension of the tumour, involving the surface epithelium.

We made predictions based upon the morphology of the five OPSCCs as to HPV status. Firstly, OPSCCs 1, 4, and 5 exhibited morphology that was consistent with KSCC, which is predominantly linked with HPV-negative OPSCC, therefore, these were predicted to be HPV-negative OPSCCs. Comparatively, OPSCCs 2 and 3 exhibited morphology that were consistent with NKSCC, which is predominantly linked with HPV-positive OPSCCs, therefore, these were predicted to be HPV-positive OPSCCs. To test these assumptions, we performed further immunohistochemical investigations to determine which, if any, of these OPSCCs were HPV-positive and HPV-negative disease.

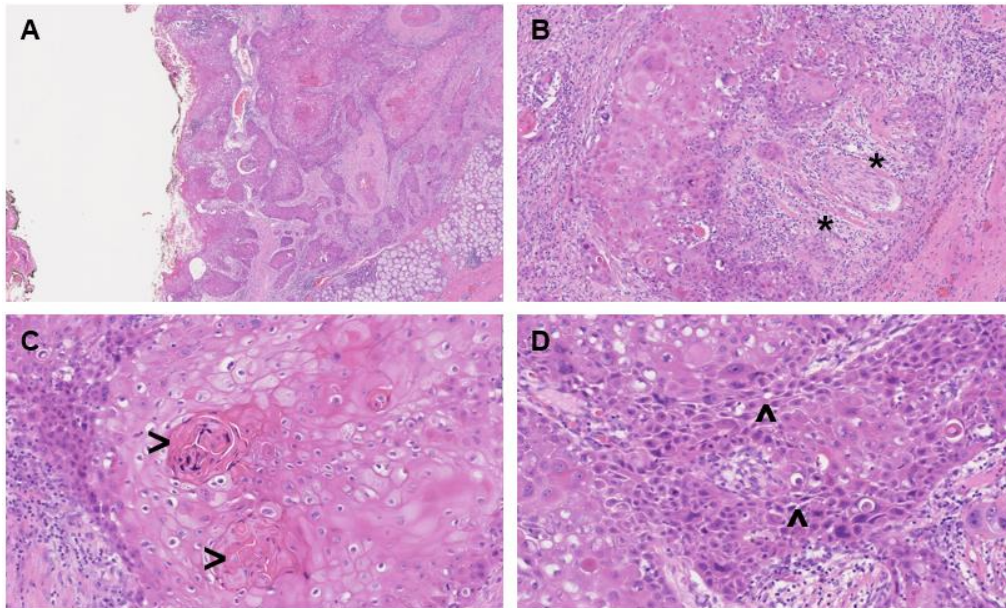


**Figure 17: H&E of OPSCC 1 with keratinising morphology.**

There were infiltrative nests of tumour cells within the surface epithelium infiltrating into the underlying tissue (A), with stromal desmoplasia (\*) (B). Tumour nests contained polygonal cells with distinct cell borders, with keratin pearls (>) (C) and intercellular bridges (^) present (D). Images were captured on NDP.view2 software at 2.5x (A), 10x (B), and 20x (C and D) magnification.

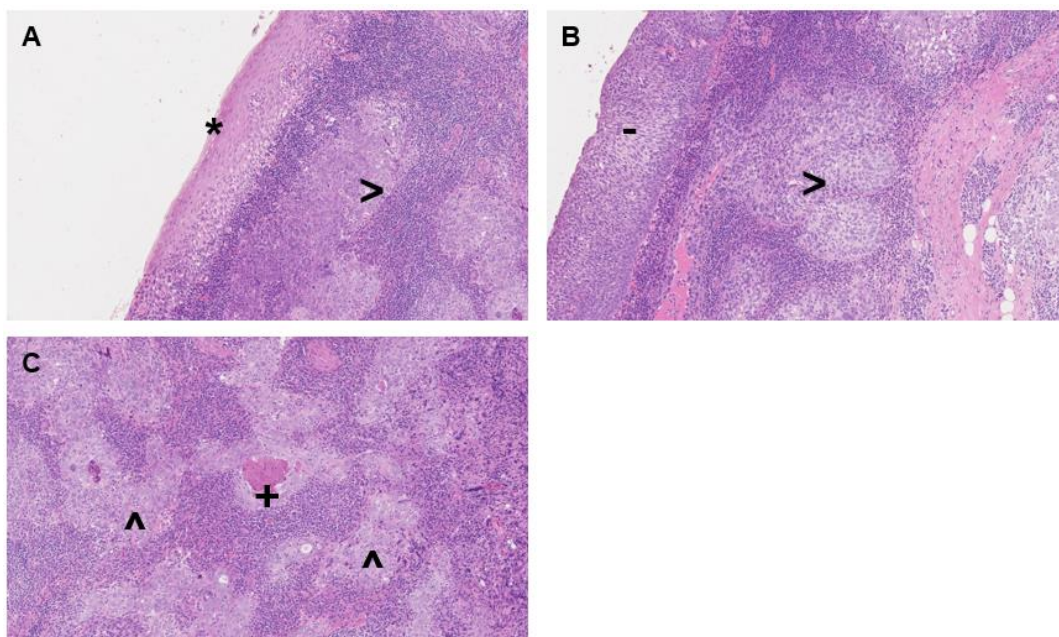


**Figure 18: H&E of OPSCC 2 with non-keratinising morphology.**

There was an area of moderate dysplasia (\*) seen within the surface epithelium, with infiltrative nests of tumour cells (>) within the underlying tissue (A and B). It appeared the tumour had infiltrated into the underlying tissue (-), giving this region a crypt-like phenotype. Tumour nests also contained poorly differentiated cells and irregular borders (^), as well as comedonecrosis (+) (C). Morphology was consistent with reticulated epithelium. Images were captured on NDP.view2 software at 10x (A-C) magnification.

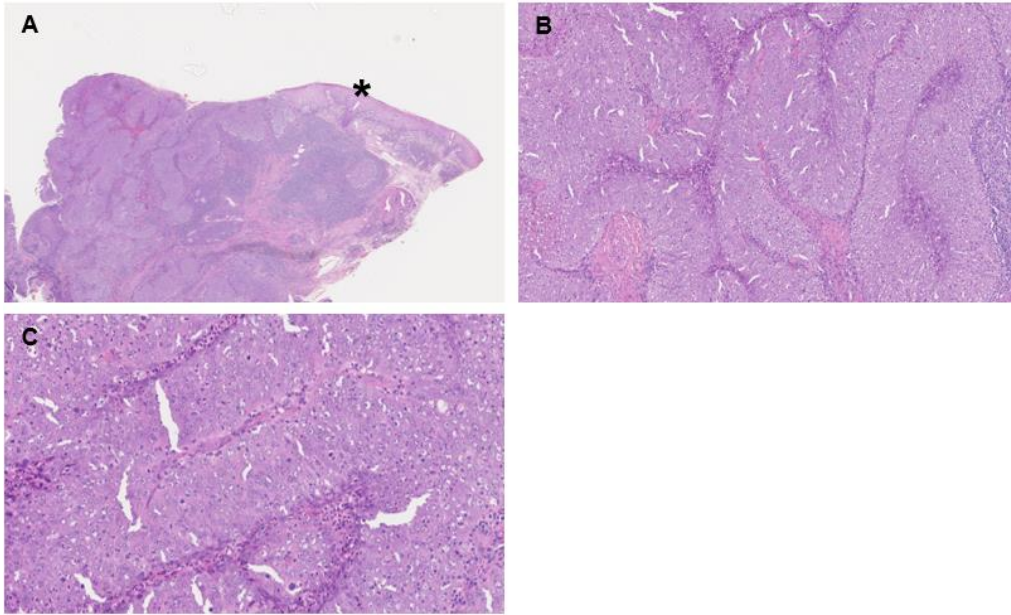


**Figure 19: H&E of OPSCC 3 with non-keratinising morphology.**

There was extension (\*) of the tumour as the underlying tissue met and extended beyond the surface epithelium (A). The tumour infiltrated as sheets and nests with indistinct borders; however, most of the normal architecture was distorted and poorly differentiated (B and C). Images were captured on NDP.view2 software at 2.5x (A), 10x (B), and 20x (C) magnification.

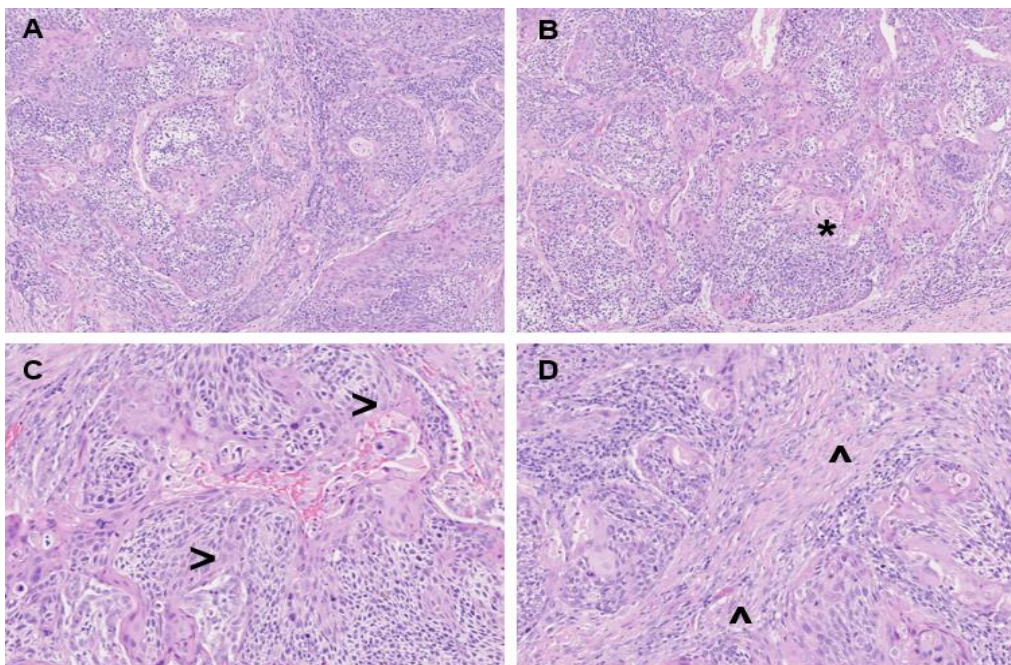


**Figure 20: H&E of OPSCC 4 with keratinising morphology.**

There were infiltrative nests of tumour cells within the underlying tissue, with some keratinising morphology (A), and keratin pearls present (\*) with the tumour being moderately differentiated (B). Intercellular bridges (>) were also present (C) as well as stromal desmoplasia (^) (D). Images were captured on NDP.view2 software at 10x (A and B), and 20x (C and D) magnification.



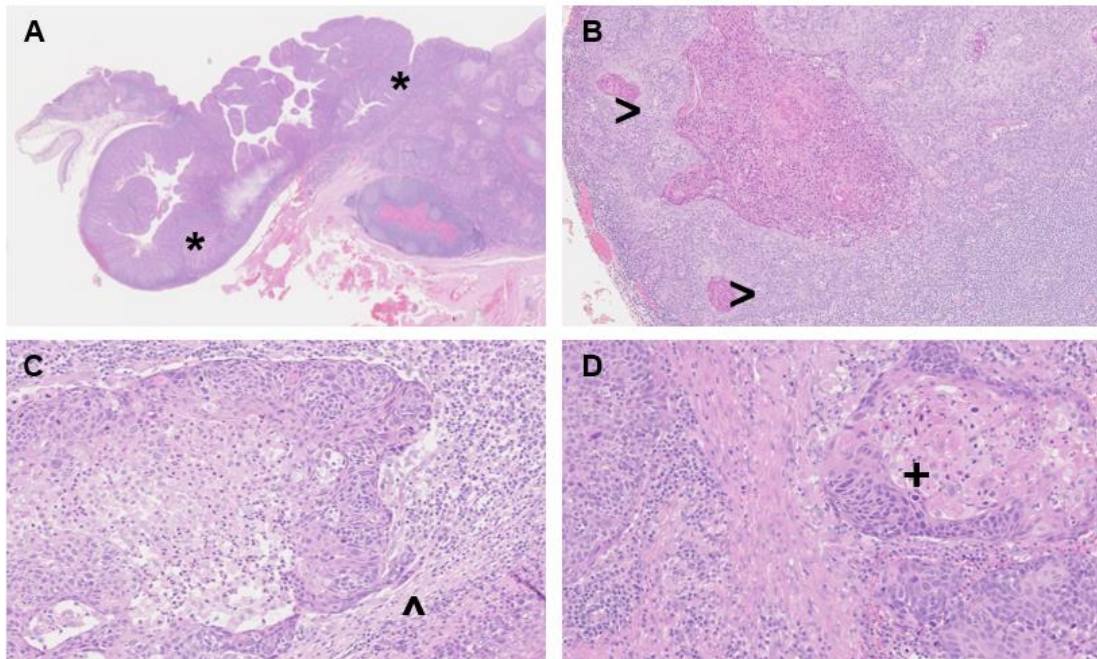


**Figure 21: H&E of OPSCC 5 with keratinising morphology.**

Infiltrative nests (\*) of tumour cells within the surface epithelium infiltrated into the underlying tissue, as well as extension of the tumour (A). Tumour nests contained polygonal cells with distinct cell borders and keratin pearls (>) (B). Stromal desmoplasia (^) was also present (C and D), as well as demonstration of a poorly differentiated tumour (C) and intercellular bridges (+) (D). Images were captured on NDP.view2 software at 1.25x (A), 10x (B), and 20x (C and D) magnification.

### **3.2.5 Morphological type alone does not reliably inform of HPV status in OPSCC**

To confirm our observations and predictions of HPV status, we outsourced one section of each OPSCC for HPV DNA ISH, which was performed by NovoPath, Cellular Pathology, Royal Victoria Infirmary, Newcastle upon Tyne. Criteria for positive HPV DNA ISH staining was identified as blue nuclear dots (Lewis *et al.*, 2010).

Surprisingly, the results were not as we had predicted (Figure 22). We proposed that OPSCC 1, 4, and 5 were HPV-negative based on their KSCC morphology, and that OPSCC 2 and 3 were HPV-positive based on their NKSCC morphology via H&E staining. Whilst OPSCC 1 was tumour-negative for HPV DNA ISH, which correlated with the morphology and prediction we had made, incorrect predictions were made for the rest of the OPSCCs. OPSCC 2 and 3 were also tumour-negative for HPV DNA ISH, despite their NKSCC morphology. In contrast, OPSCC 4 and 5 were tumour-positive for HPV DNA ISH, despite their KSCC morphology. OPSCC 4 demonstrated focal staining, with positive cells spread out across the entirety of the tumour. In comparison, OPSCC 5 mostly demonstrated fairly strong and diffuse positive staining across the entire tumour. Therefore, in this small sample, this demonstrates that diagnosis by H&E alone is poorly predictive of HPV status. We continued to characterise the OPSCCs further, staining them with other biomarkers.

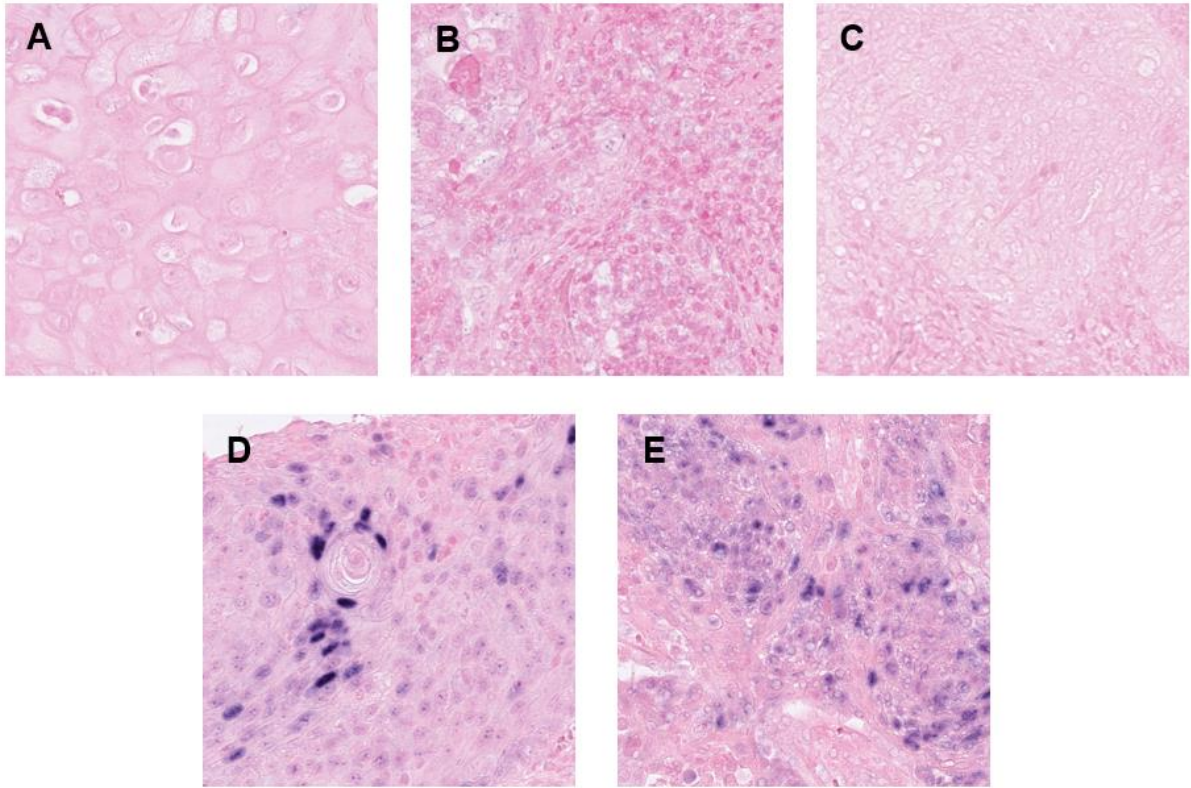


**Figure 22: HPV DNA ISH of OPSCCs determined that not all NKSCC are HPV-associated.**

OPSCC 1 was tumour-negative for HPV DNA ISH, which correlated with the KSCC morphology (**A**). However, OPSCC 2 and 3 were tumour-negative for HPV DNA ISH, despite their NKSCC morphology (**B and C**). Surprisingly, OPSCC 4 and 5 were tumour-positive for HPV DNA ISH, regardless of their KSCC morphology (**D and E**). Images were captured on NDP.view2 software at 40x magnification.

### **3.2.6 HPV positivity correlates with p16 overexpression, but not CK7 expression**

As H&E staining alone is not reliable for determining HPV status, we decided to characterise the OPSCCs further. We first stained the sections chromogenically with p16, the surrogate HPV marker; AE1/AE3, a pancytokeratin epithelial marker; and CK7, a reticulated epithelial marker. Criterion for p16-positive IHC was based on the current guidelines for moderate to intense nuclear and cytoplasmic staining in 70% or more of the tumour cells (Lewis *et al.*, 2018b, Hunter *et al.*, 2021). Normal staining observed with these biomarkers across the remainder of the tissue section acted as internal positive controls. Across all five sections, normal expression of p16 was exhibited in the reticulated epithelium and germinal centres; AE1/AE3 was exhibited in the surface, reticulated, and ductal epithelia, and mucinous acini; and CK7 was exhibited within the reticulated and ductal epithelium, and mucinous acini (Figure 23). Moreover, all five OPSCCs were tumour-positive for AE1/AE3, which in conjunction with the morphology of each of the OPSCCs, demonstrated that they were all of epithelial origin.

OPSCC 1 was tumour-negative for p16 and CK7 (Figure 23), and had been determined as KSCC via H&E staining. Together with the tumour-negative staining of HPV DNA ISH, p16, and CK7, this was consistent with HPV-negative OPSCC. OPSCC 2 was tumour-negative for p16 (Figure 23), though surprisingly, there was a small dysplastic area within the surface epithelium that was p16-positive. Additionally, OPSCC 2 was tumour-positive for the tonsillar reticulated epithelial marker CK7, with some positivity seen within the surface epithelium, which was unusual. However, as was observed in the H&E, this confirmed that the tumour had infiltrated the underlying tissue, giving this region a crypt-like phenotype. OPSCC 2 was determined as NKSCC via H&E staining, and together with the tumour-negative staining of HPV DNA ISH, p16, and CK7, this was not consistent with HPV-negative OPSCC.

OPSCC 3 was tumour-negative for p16 and CK7 (Figure 23). Like OPSCC 2, there was surprisingly some small areas of p16 staining within the surface epithelium. OPSCC 3 was determined as NKSCC via H&E staining, and together with the tumour-negative staining of HPV DNA ISH, p16, and CK7, this was consistent with HPV-negative OPSCC. Conversely, OPSCC 4 and 5 were tumour-positive for p16, with

strong, diffuse staining indicative of p16 overexpression within the tumour (Figure 23). The p16 positivity would also suggest that the tumours were HPV-positive, despite their keratinising morphology; indeed, this was confirmed by HPV DNA ISH (Figure 22).

However, despite being positive for p16 and HPV DNA ISH, both OPSCC 4 and 5 were tumour-negative for CK7, which could suggest that they are not associated with the reticulated epithelium (Figure 23). CK7 is expressed within the SCJ of the cervix, which is the site pre-disposed to HPV-mediated disease (Woods *et al.*, 2017). However, CK7 expression is also observed within the reticulated epithelium of the palatine tonsil, which is believed to be where HPV infection establishes, and was a useful marker for determining whether HPV-positive OPSCCs arose within the reticulated crypts (Kim *et al.*, 2007, Woods *et al.*, 2022). Therefore, in this small sample, HPV positivity is shown to correlate with p16 overexpression, but not with CK7 expression.

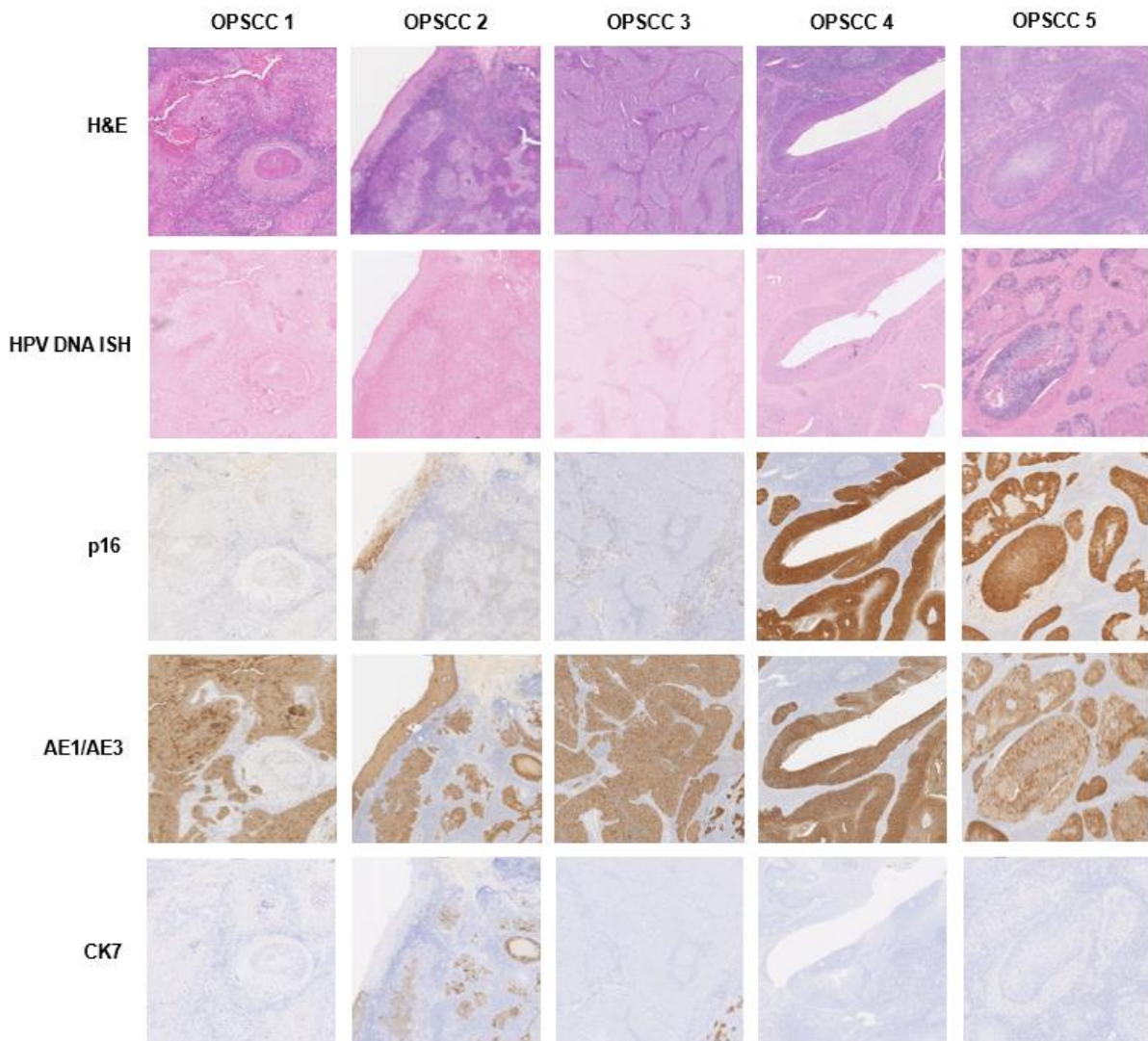


**Figure 23: HPV positivity correlates with p16 overexpression, but not CK7 expression.**

OPSCC 1 was tumour-negative for HPV DNA ISH, p16, and CK7. OPSCC 2 was tumour-negative for HPV DNA ISH and p16, but tumour-positive for CK7. This could be as the tumour has breached into the surface epithelium, giving it a crypt-like phenotype. OPSCC 3 are tumour-negative for HPV DNA ISH, p16, and CK7. OPSCC 4 and 5 were tumour-positive for HPV DNA ISH and p16, but tumour-negative, which was surprising. All five OPSCCs were tumour-positive for AE1/AE3, suggesting that all are tumours of epithelial origin. Images captured on NDP.view2 software at 5x magnification.

### 3.2.7 HPV-negative OPSCCs with non-keratinising morphology exhibit higher expression of CD8

To characterise the tumours further, and permit comparisons to be made between HPV-positive and HPV-negative disease, we used immunofluorescence and multiplex immunofluorescence (mIF) techniques to examine the expression of eight disease-relevant biomarkers selected from the literature, which we had characterised in normal palatine tonsil tissue (Figures 15 and 16).

Firstly, CK7 expression was only positive in the tumour of OPSCC 2, a NKSCC, with p16 tumour-positive in OPSCCs 4 and 5, both KSCCs (Figure 24), which was anticipated, as these results are consistent with the IHC performed earlier (Figure 23). Surprisingly, all five OPSCCs were tumour-negative for the prognostic biomarker and therapeutic target, ER $\alpha$  (Figure 24); with weaker expression of the checkpoint receptor, PD-1, in all five OPSCCs (Figure 25), particularly in OPSCC 4 and 5, as overexpression of both biomarkers are related to HPV-positive OPSCCs (Lyford-Pike *et al.*, 2013, Koenigs *et al.*, 2019). Contrastingly expression of the PD-1 ligand, PD-L1, was mostly seen within the tumour periphery in OPSCCs 1, a KSCC; OPSCC 3, a NKSCC; and OPSCCs 4 and 5, with the strongest expression seen within OPSCC 3, compared to weaker expression observed in OPSCC 2 (Figure 25). The most surprising observation was that we observed overexpression of CD8, a cytotoxic T lymphocyte marker, within the tumours of OPSCCs 2 and 3, in comparison to OPSCCs 1, 4, and 5 (Figure 25); both PD-L1 and CD8 overexpression are associated with HPV, therefore, these observations were not predicted within HPV-negative disease. Additionally, overexpression of EGFR, a transmembrane receptor associated with poor prognosis, was only observed in OPSCC 3, and did not correlate with PD-L1 and p16 expression (Figure 26), as it is commonly seen in HPV-negative OPSCCs (Deuss *et al.*, 2020). Finally, overexpression of the proliferation marker Ki67 was observed in OPSCCs 2, 3, 4, and 5, with weaker expression seen in OPSCC 1, which is associated with rapid growth rate of OPSCC within the palatine tonsils (Figure 27). Therefore, in this small sample, these data demonstrate that the expression of these biomarkers has somewhat deviated from the typical profiles seen with HPV-positive and HPV-negative OPSCCs within the literature.

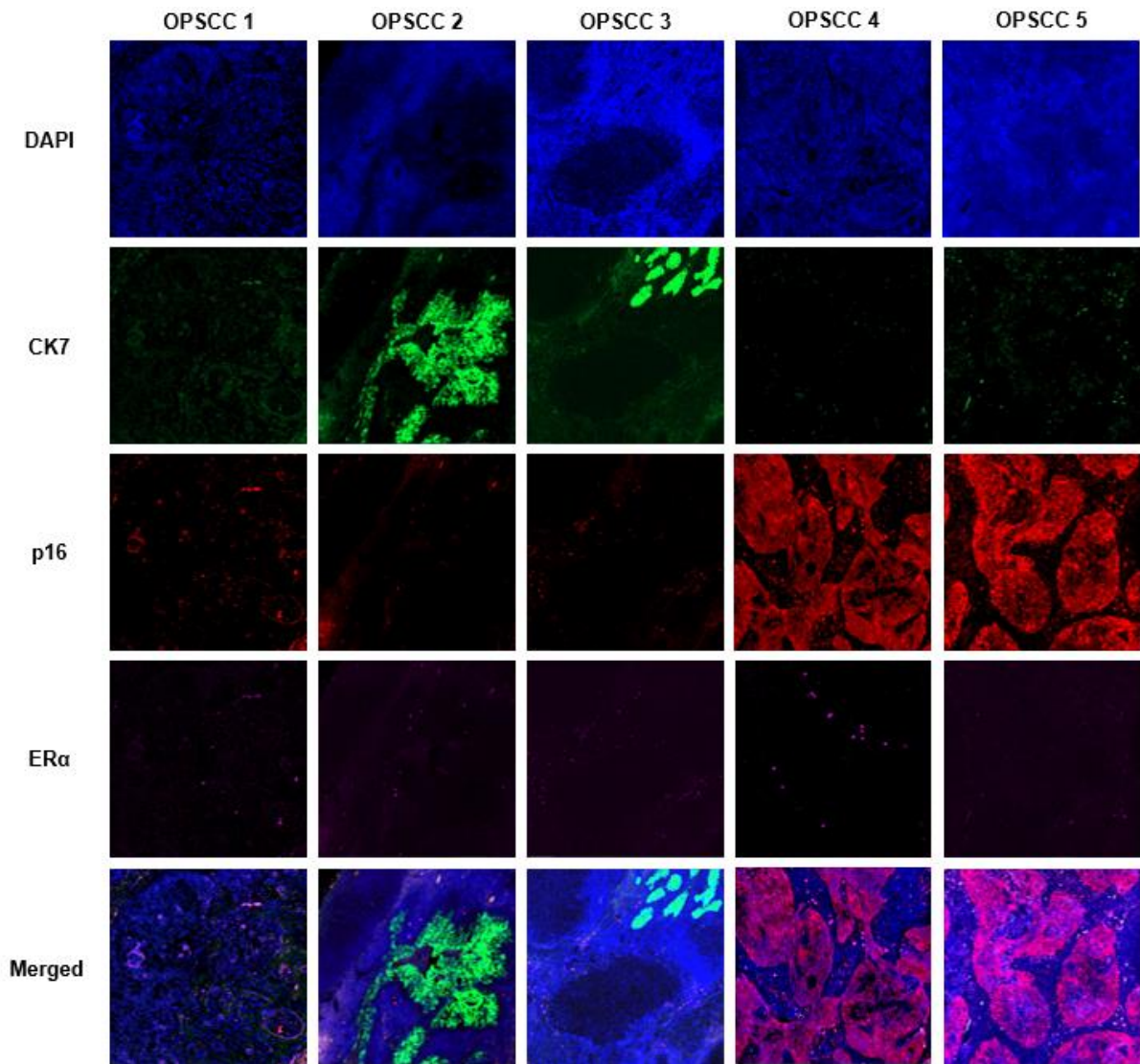


**Figure 24: CK7/p16/ERα expression within five OPSCCs.**

OPSCC 1 was tumour-negative for CK7, and p16. OPSCC 2 was tumour-positive for CK7, however, it was tumour-negative for p16. OPSCC 3 was tumour-negative for CK7 and p16, with normal CK7 expression observed within the ductal epithelium. OPSCC 4 and 5 were tumour-negative for CK7, but exhibited p16 overexpression within the tumours. All five OPSCCs were negative for ERα. Images were captured on Zen Pro Microscopy software at 10x magnification, using the 488, 555, and 647 filters on the ZEISS Axio Scan.Z1.



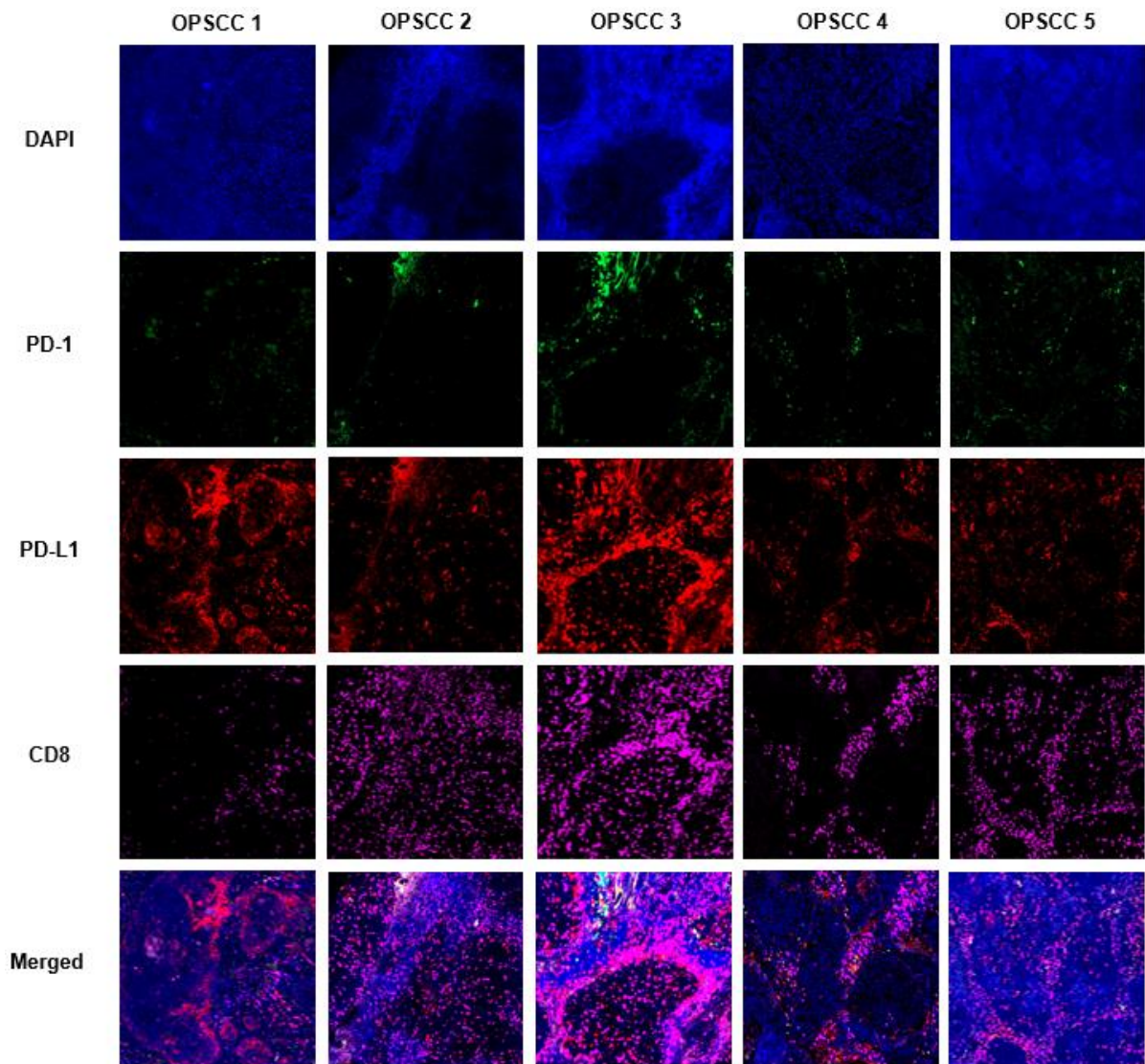


**Figure 25: PD-1/PD-L1/CD8 expression within five OPSCCs.**

OPSCC 1 demonstrated weak PD-1 expression, in comparison to moderate PD-L1 expression and weak CD8 expression within the tumour periphery. OPSCC 2 demonstrated weak PD-1 expression, in comparison to moderate PD-L1 expression within the tumour periphery and stroma and strong CD8 expression within the tumour and stroma. OPSCC 3 demonstrated weak PD-1 expression, with strong PD-L1 and CD8 expression within the tumour periphery, tumour, and stroma. OPSCC 4 and 5 exhibited weak PD-1 expression, with moderate PD-L1 and CD8 expression within the tumour periphery and stroma, with weak expression within the tumours. Images were captured on Zen Pro Microscopy software at 10x magnification. Using the 488, 555, and 647 filters on the ZEISS Axio Scan.Z1.

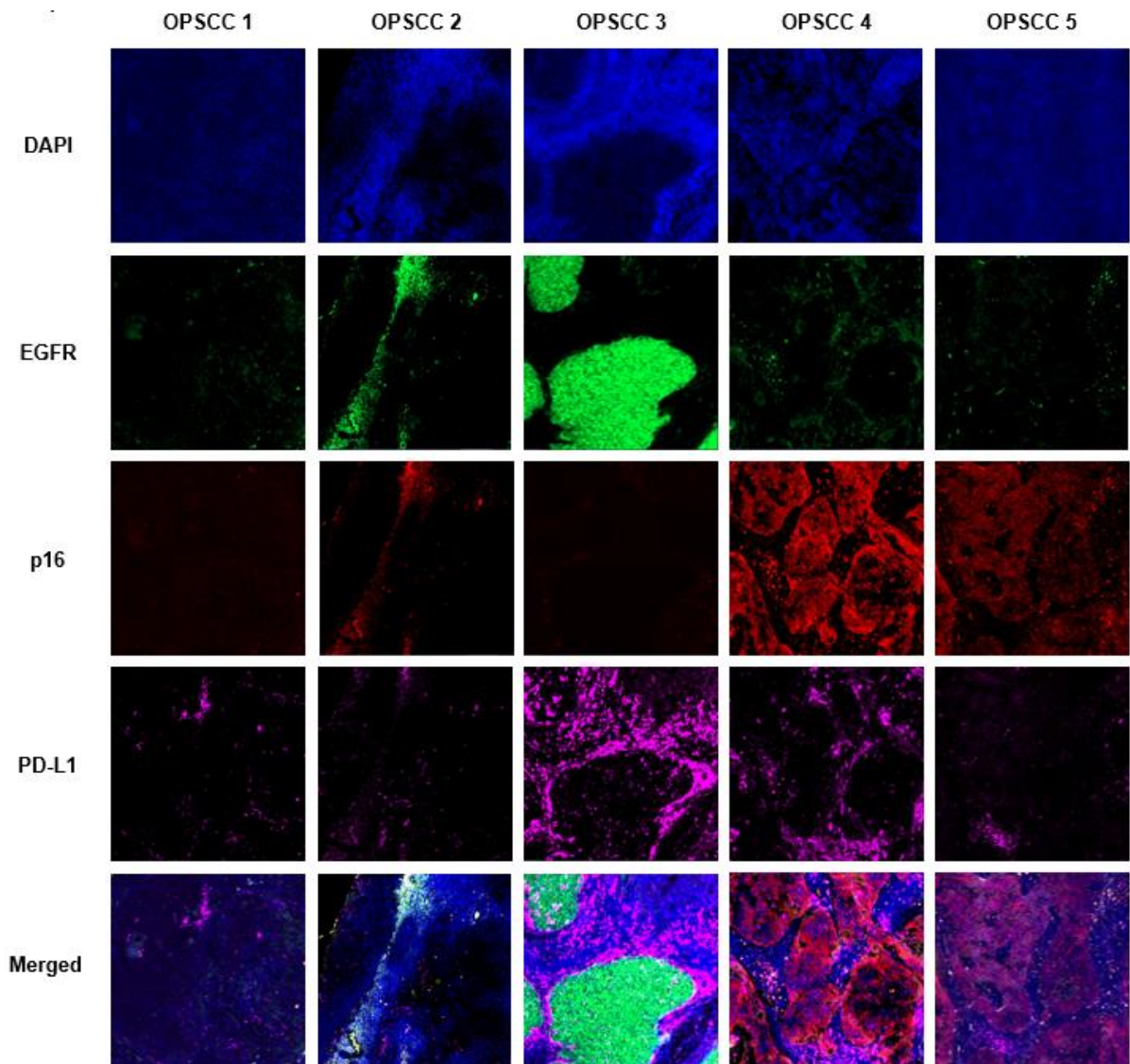


**Figure 26: EGFR/p16/PD-L1 expression within five OPSCCs.**

OPSCC 1 was tumour-negative for EGFR and p16; however, demonstrated some PD-L1 tumour periphery staining. OPSCC 2 was tumour-negative for EGFR and p16 (staining observed here is autofluorescence). Weak PD-L1 expression was also observed within the tumour periphery. OPSCC 3 overexpressed EGFR, but was tumour-negative for p16. Strong PD-L1 expression levels were observed within the tumour periphery and stroma. OPSCC 4 and 5 were tumour-negative for EGFR, but overexpressed p16. Both demonstrated moderate PD-L1 expression within the tumour periphery and stroma. Images were captured on Zen Pro Microscopy software at 10x magnification, using the 488, 555, and 647 filters on the ZEISS Axio Scan.Z1.

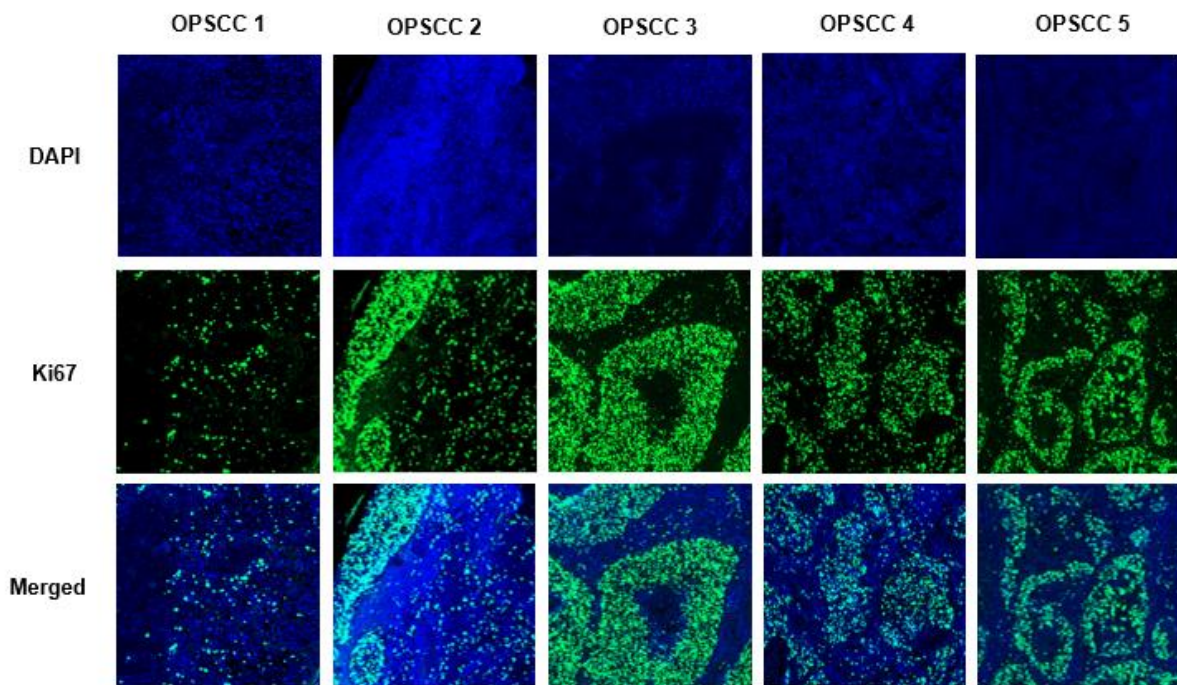


**Figure 27: Ki67 expression within five OPSCCs.**

All five OPSCCs demonstrated Ki67 expression, with overexpression exhibited within OPSCCs 2, 3, 4 and 5. Weak Ki67 expression was exhibited in OPSCC 1. Images were captured on Zen Pro Microscopy software at 10x magnification, using the 488 filter on the ZEISS Axio Scan.Z1.

### 3.3 Conclusion

The OPSCCs were characterised morphologically, but this does not reliably inform HPV status. Indeed, based on H&E examination alone, the Consultant Histopathologist predicted OPSCC 3, a NKSCC, to be p16-positive, and therefore HPV-positive, whereas it is both p16- and HPV DNA ISH-negative. It is thought that the majority of HPV-positive OPSCCs have non-keratinising morphology; however, it is possible for HPV-positive OPSCCs to have keratinising morphology (in the region of 20-35%) (El-Mofty and Lu, 2003, El-Mofty and Patil, 2006, Chernock *et al.*, 2009, Gondim *et al.*, 2016, Lewis *et al.*, 2021, Shinn *et al.*, 2021), and as seen in this study for HPV-positive OPSCCs 4 and 5.

The surrogate marker p16 is a reliable marker for HPV-positivity in cervical pre-neoplastic and neoplastic lesions associated with HR-HPV infections, although cervical screening protocol now determines HPV status molecularly (Ganesan *et al.*, 2021, Reed *et al.*, 2021). Therefore, today, p16 IHC is only required for cases that are not detected during screening (Ganesan *et al.*, 2021). In comparison, during diagnosis, OPSCCs undergo p16 IHC as part of the World Health Organisation (WHO) classification, with overexpression in 70% or more of the tumour cells suggestive of HPV positivity (World Health Organisation, 2024). HPV-positive OPSCCs with non-keratinising morphology have previously demonstrated 70-100% sensitivity of p16-positivity (Chernock *et al.*, 2009, Gondim *et al.*, 2016, Lewis *et al.*, 2021, Shinn *et al.*, 2021). Due to this high sensitivity observed within such tumours, it has been suggested that the morphology by H&E examination alone, being NKSCC, is enough of an indicator for p16-positivity, removing the need for IHC at all (Chernock *et al.*, 2009, Lewis *et al.*, 2010); these data dispute this.

Indeed OPSCC 4 and 5 in this study, both KSCC, would have been missed as HPV-positive disease should this have been the diagnostic process. Furthermore, despite the strong correlation with p16 and HPV DNA ISH positivity within this study, the sample is limited to just two HPV-positive OPSCCs; other studies suggest that p16 is not a reliable marker of HPV positivity within the head and neck. In some cases, p16 has been found to be discordant with HPV DNA and RNA testing including polymerase chain reaction (PCR) and ISH, with meta-analyses reporting variations in specificity of 54-100% (Suresh *et al.*, 2021) and a pooled specificity of 83% based on 23 studies

(Prigge *et al.*, 2017). Additionally, a multicentre study reported that of the 7654 patient samples tested; 415 out of 3805 (10.9%) were p16-positive/HPV-negative and 289 out of 3849 (7.5%) were p16-negative/HPV-positive (Mehanna *et al.*, 2023), which questions its validity as a surrogate marker. There are also caveats with other HPV testing including the insufficient sensitivity of HPV DNA ISH which could produce false-negatives, as well as excessive sensitivity of PCR, which may detect clinically insignificant HPV types (Doxtader and Katzenstein, 2012). With the number of tests available, and this emerging data, it is not surprising that there is not yet a consensus for determining HPV status within OPSCC (Mena *et al.*, 2022).

CK7 is a marker of the reticulated epithelium, and can be used to suggest the origin of tumours. It is expressed within the SCJ of the cervix, which is the site pre-disposed to HPV-mediated disease, as well as the reticulated crypt of the normal palatine tonsil (Woods *et al.*, 2017, Woods *et al.*, 2022). Indeed, OPSCC 2 in this study, a HPV-negative OPSCC, strongly expressed CK7 suggesting this tumour originated within the reticulated crypt. HPV is believed to have a predilection for reticulated epithelium, with possible explanations including: possessing transitional epithelium similar to the cervix; a discontinuous basement membrane, which provides greater susceptibility to foreign antigens such as HPV; the deep crypts possibly functioning as a reservoir for HPV; and the abundance of lymphocytes, which represents an immune-privileged site (Lyford-Pike *et al.*, 2013, Elrefaey *et al.*, 2014, Chi *et al.*, 2015). Surprisingly, CK7 expression was not observed within the HPV-positive tumours (OPSCC 4 and 5) used within this study, which could imply that these tumours did not originate from HPV infections that had established within tonsillar crypts. However, CK7 expression may be absent within HPV-positive OPSCCs for a number of reasons.

One explanation is that HPV-positive OPSCC may originate within the crypts, but that CK7 expression may be lost as cells differentiate, where the tumour consists of differentiated and undifferentiated components and possess a CK7-negative phenotype (Pitiyage *et al.*, 2015). Another explanation could be that CK7 expression may be associated with viral DNA and not transcriptionally-active HR-HPV, which is associated with E6 and E7 expression (Mehrad *et al.*, 2018). Additionally, it may be that it is related to episomal HPV DNA; not integrated, within both the cervix and oropharynx (Lee *et al.*, 2017, Mehrad *et al.*, 2018, Roberts *et al.*, 2019). It is also

plausible that CK7 may only be expressed in NKSCCs, as they are typically p16- and HPV DNA ISH-positive; based on clinicopathologic data it appeared that CK7 positivity was more likely to be associated with non-keratinising morphology than keratinising in OPSCC (Mehrad *et al.*, 2018). However, the data also showed that non-keratinising OPSCCs were just as likely to be CK7-negative than keratinising OPSCC. A study reported that 87% of cervical SCCs vs 27% of HNSCCs were positive for CK7 expression, which may indicate that CK7 may not be as significant within HPV-positive head and neck SCCs as it is in CC (Chu *et al.*, 2000). As such, the clinical significance of CK7 to HPV-positive OPSCC remains unknown.

With characterisation of the OPSCC tumours, it was surprising to observe that all OPSCCs, particularly OPSCC 4 and 5 in this study, were negative for ER $\alpha$ , as it can be overexpressed in HPV-positive OPSCCs (Bristol *et al.*, 2020, Kwon *et al.*, 2020). However, it appears that it is just as likely to be negative in HPV-positive OPSCCs, with HPV-negative OPSCCs even less likely to be ER $\alpha$ -positive (Kwon *et al.*, 2020). This suggests that ER status is not a reliable marker of either CC or OPSCC. Another observation we did not anticipate was weak PD-1 expression within any of the OPSCCs, particularly OPSCC 4 and 5, as stronger PD-1 expression was observed within HPV-positive OPSCCs due to the presence of tumour-infiltrating lymphocytes (TILs) (Badoual *et al.*, 2013, Concha-Benavente *et al.*, 2016, Gameiro *et al.*, 2018). In support of this, others have observed no difference in PD-1 expression between HPV-positive and HPV-negative OPSCCs (Oguejiofor *et al.*, 2017). In this study, stronger expression of PD-L1 and CD8 was observed within OPSCCs 2 and 3, HPV-negative OPSCCs in comparison to OPSCCs 4 and 5, which are HPV-positive OPSCCs. This observation was surprising, as these are expression patterns from the literature that are mostly seen in HPV-positive OPSCCs (Lyford-Pike *et al.*, 2013, Gameiro *et al.*, 2018, Pokrývková *et al.*, 2022). However, CD8-positive TILs are still observed within HPV-negative OPSCC (Pokrývková *et al.*, 2022, Atipas *et al.*, 2023). Contrastingly, EGFR overexpression was observed in OPSCC 3, which is consistent with its p16-negative status (Deuss *et al.*, 2020). Finally, Ki67 overexpression was observed in OPSCCs 2, 3, 4, and 5, which is consistent with their morphology as Ki67 expression is significantly stronger in poorly differentiated OPSCCs, such as OPSCC 2, 3, and 5 compared to well differentiated OPSCCs such as OPSCC 1 (Yadav *et al.*, 2019).

Therefore, within our sample, both HPV-positive and HPV-negative OPSCCs deviated from the typical tumour profiles described in the literature through both histological characterisation and biomarker expression. Despite a limited sample number, together this work highlights the complexity of HPV pathogenesis within OPSCC.

## CHAPTER 4: IMMUNOHISTOCHEMICAL EVALUATION OF COMMERCIALY-AVAILABLE HPV ANTIBODIES

### 4.1 Introduction

The links between HPV and cervical carcinoma (CC) and OPSCC were first described in 1983 and 2000 respectively (zur Hausen *et al.*, 1983, Gillison *et al.*, 2000). Consequently, HPV-negative OPSCCs have declined due to public health interventions and smoking cessation in high income countries, in comparison to HPV-positive OPSCCs which have increased rapidly, likely as a result of changes in sexual habits (Gillison *et al.*, 2008, D'Souza *et al.*, 2009, Chaturvedi *et al.*, 2011, Chaturvedi *et al.*, 2015, Louie *et al.*, 2015, Schache *et al.*, 2016). Unfortunately, the number of HPV-positive OPSCCs has now surpassed CC, and is expected to increase for the next 30 years (Lechner *et al.*, 2022, Ferlay *et al.*, 2024). In CC, HR-HPV-16 and -18 cause 70% of cervical squamous cell carcinomas (SCC), in comparison to 87-96% and 1.5-3% of OPSCC respectively (Muñoz *et al.*, 2003, Kreimer *et al.*, 2005, Smith *et al.*, 2007, Schache *et al.*, 2016).

The 8,000 base pair (bp) HPV viral genome expresses six early proteins during its life cycle (Rautava and Syrjänen, 2012). E2 is expressed in the early stages of the HPV viral life cycle, and is frequently disrupted during viral integration into host genome, which results in uncontrollable overexpression of E6 and E7 oncoproteins during malignant transformation (Xue *et al.*, 2010). Expression of both E6 and E7 is necessary for malignancy as they work synergistically, with absence of either protein directly affecting the other proteins' actions (Butz *et al.*, 2003, Downham *et al.*, 2024). E2 expression is generally lost during viral integration, and is often not expressed in cancerous tissues (Xue *et al.*, 2010).

There are numerous antibodies targeting HPV proteins that are commercially-available. However, they are for research use only (RUO) and not for in vitro diagnostic (IVD) use in clinical settings. We wanted to test a number of HPV antibodies from different suppliers in positive control tissue, ahead of optimisation in OPSCCs using immunohistochemistry (IHC) to determine whether the expression of HPV proteins is possible within tissue, and its relation to the pathogenesis of HPV within OPSCC.



This chapter examines IHC in multiple tissue types using commercially-available HPV antibodies from multiple suppliers, as well as multiplex immunofluorescence (mIF). The antibodies chosen targeted HPV-16 and HPV-18 specifically, with E2, E6, and E7 being the proteins of interest. The various tissue types tested were also tested molecularly by real-time polymerase chain reaction (real-time PCR) to verify HPV status. The results of this chapter will determine if HPV proteins can be detected in tissues by IHC, and potentially be used to determine the HPV subtype of HPV-positive OPSCCs.

## **4.2 Results**

### **4.2.1 Commercially-available HPV antibodies tested demonstrated positive staining within CCs**

Commercially-available HPV antibodies were purchased, targeting HPV-16 E2, HPV-16 E6 and E7, and HPV-18 E6 oncoproteins: HPV-16 E2 (TVG-261) (Abcam), HPV-16 E6 + HPV-18 E6 (C1P5) (Abcam), HPV-16 E6/HPV-18 E6 (C1P5) and HPV-16 E7 (ED17) (both Santa Cruz Biotechnology (SCBT)). These were optimised using three CC tissue specimens, as these would be expected to demonstrate some staining, except for HPV-16 E2; which was expected to be negative. However, staining with these antibodies in CCs 1-3 gave somewhat anticipated results (Figure 28); there was weak cytoplasmic staining of HPV-16 E2 within the tumours of CCs 1 and 3; with cytoplasmic staining observed in CC 2, which would not express E2, as it is lost during viral integration (Xue *et al.*, 2010). The staining of HPV-16 E6 + HPV-18 E6 (Abcam) exhibited cytoplasmic and membranous staining within the tumour of CC 1, with a weaker intensity seen with the staining of HPV-16 E6/HPV-18 E6 (SCBT) and HPV-16 E7. CC 2 was tumour-negative, showing cytoplasmic staining within the stroma with all three antibodies. Finally, CC 3 exhibited weak cytoplasmic staining within the tumour with HPV-16 E6 + HPV-18 E6 (Abcam); however, it was tumour-negative for HPV-16 E6/HPV-18 E6 (SCBT) and HPV-16 E7.

Unexpectedly, the staining did not correlate between antibodies; however, nothing seemed unusual about the staining observed, except for HPV-16 E2, which showed staining in all three CC tissue specimens and will be discussed later on in Section 4.2.3. The other antibodies tested were only against two of the 14 HR-HPV subtypes, therefore negative staining observed could be because the cervical tumours were

caused by a different HPV type. Secondly, the antibodies are from two different suppliers, therefore the antibody quality and staining was presumed to differ between samples, which was observed between HPV-16 E6 + HPV-18 E6 (Abcam), where staining was stronger in comparison to weaker staining in HPV-16 E6/HPV-18 E6 (SCBT), despite them being the same C1P5 clone. Thirdly, E6 and E7 work synergistically, and would be expressed together, which was seen in CC 1 and 3, despite weak staining observed with HPV-16 E6/HPV-18 E6 (SCBT) and HPV-16 E7 in comparison to HPV-16 E6 + HPV-18 E6 (Abcam). Therefore, the observed staining for the E6 and E7 oncoproteins was determined as real at this point.

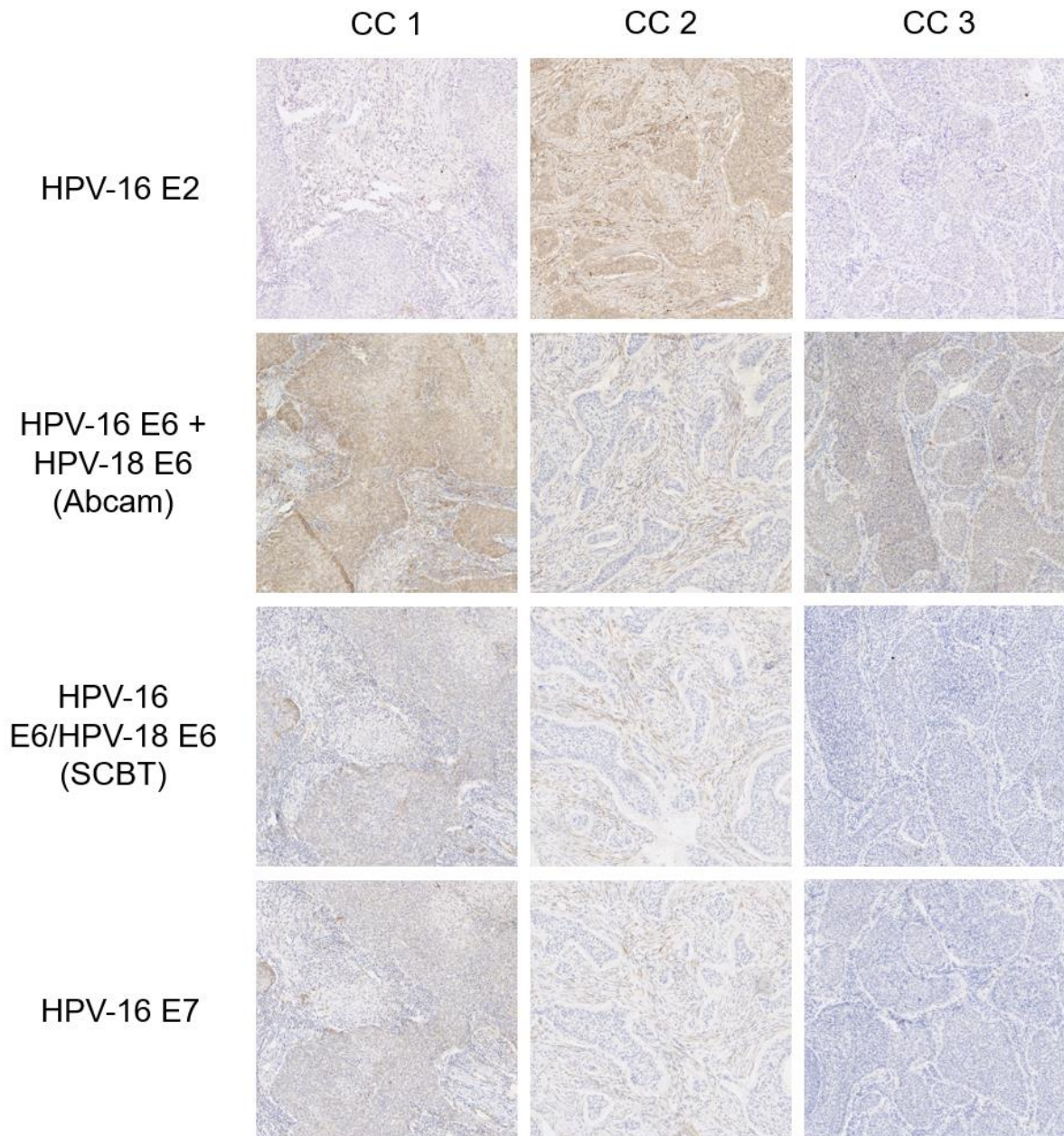


**Figure 28: HPV-16 E2, HPV-16 E6 + HPV-18 E6, HPV-16 E6/HPV-18 E6, and HPV-16 E7 staining in three CC tissues.**

There was cytoplasmic and membranous staining observed within the tumour and stroma with HPV-16 E6 + HPV-18 E6 (Abcam), with weak cytoplasmic staining with HPV-16 E2 (Abcam), HPV-16 E6/HPV-18 E6 (SCBT) and HPV-16 E7 (SCBT) within parts of the tumour and stroma of CC 1. Cytoplasmic staining was observed within the tumour and stroma with HPV-16 E2, with negative staining within the tumour but cytoplasmic staining within the stroma with HPV-16 E6 + HPV-18 E6, HPV-16 E6/HPV-18 E6 and HPV-16 E7 in CC 2. Weak cytoplasmic staining was observed within the tumour and stroma with HPV-16 E2 and HPV-16 E6 + HPV-18 E6 with negative staining within the tumour with HPV-16 E6/HPV-18 E6 and HPV-16 E7 in CC 3. Images captured on NDP.view2 software at 10x magnification.

#### **4.2.2 Commercially-available HPV-16 E6 + HPV-18 E6 antibody demonstrated unexpected staining in HPV-positive and HPV-negative OPSCCs**

As the staining with the afore-mentioned HPV antibodies was determined as real and optimised in CC tissue, HPV-16 E6 + HPV-18 E6 (Abcam) was chosen to stain OPSCC samples fluorescently. Unfortunately, HPV-16 E6/HPV-18 E6 (SCBT) and HPV-16 E7 were not tested fluorescently, as the staining was already weak via IHC despite using a low dilution, and when adding antibodies to the slides on the VENTANA DISCOVERY, they were diluted even further. Therefore, it was deemed not worthwhile testing any further.

Triplex staining using the biomarkers CK7 (a ductal, glandular, and transitional epithelial marker that is expressed within the palatine tonsillar reticulated crypts), p16 (the surrogate marker for HPV status) and HPV-16 E6/HPV-18 E6, were performed on five OPSCC specimens. Each of the five OPSCCs were positive for CK7 expression, with normal staining exhibited within the reticulated epithelium of OPSCCs 1, 4, and 5 (Figures 29, 32, and 33); ductal epithelium of OPSCCs 1 and 3 (Figures 29 and 31), and the tumour of OPSCC 2 (Figure 30). Additionally, p16 expression was exhibited within the reticulated crypts of OPSCCs 1, 4, and 5 (Figures 29, 32, and 33), and tumours of OPSCCs 4 and 5 (Figures 32 and 33). This fluorescent staining of CK7 and p16 was consistent with the IHC results for these tumours (Section 3.2.6).

Surprisingly, HPV-16 E6 + HPV-18 E6 expression was observed within all five OPSCCs (Figures 29-33), whose expression appeared to co-localise with CK7 most of the time. This was not anticipated, as the CK7 staining was consistent with the IHC data, so we believed the staining was real. However, no expression of CK7 was exhibited within the germinal centres, unlike HPV-16 E6 + HPV-18 E6. This staining was compared to the CK7/p16/ER $\alpha$ , PD-1/PD-L1/CD8, and EGFR/p16/PD-L1 mIF staining in Section 3.2.7, which did not show any co-localisation issues. This further supported that there were no co-localisation issues, and at this point, we believed that each OPSCC was HPV-positive.

Overexpression of p16 was observed in OPSCCs 4 and 5 which was associated with HPV, as determined by HPV DNA *in-situ* hybridisation (ISH) (Section 3.2.5). However, HPV-16 E6 + HPV-18 E6 expression was not observed within these HPV-positive

tumours and did not co-stain with p16. Surprisingly, HPV-16 E6 + HPV-18 E6 was expressed within the tumour of OPSCC 2, which had already been identified as HPV-negative, as well as being found in other structures within OPSCC 1 and 3. These observations were questionable, given all the other data collected; therefore, further commercially-available HPV antibodies were ordered from different suppliers to be tested in these OPSCCs alongside a range of other tissue types.

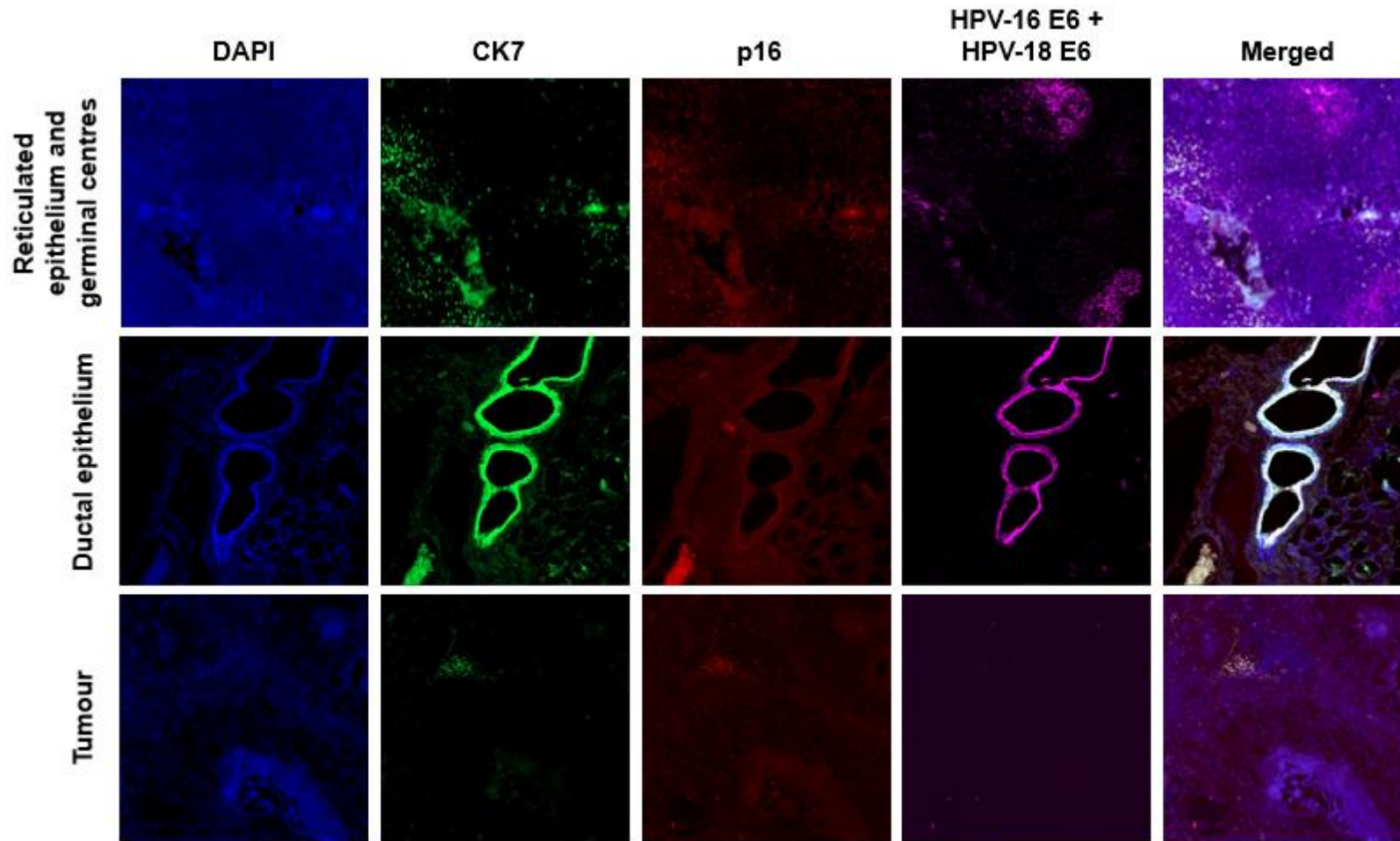


**Figure 29: Positive staining of HPV-16 E6 + HPV-18 E6 is found across different cell types in OPSCC 1.**

Weak CK7 expression was observed within the reticulated epithelium, with strong expression observed within the ductal epithelium and acini. No CK7 expression was observed within the tumour. Weak p16 expression was observed in the reticulated epithelium, however it was negative within the ducts and tumour. Surprisingly, HPV-16 E6 + HPV-18 E6 expression was observed within the germinal centres, and ductal epithelium; however, no expression was observed within the tumour. Images captured on Zen Pro Microscopy Software at 10x magnification.

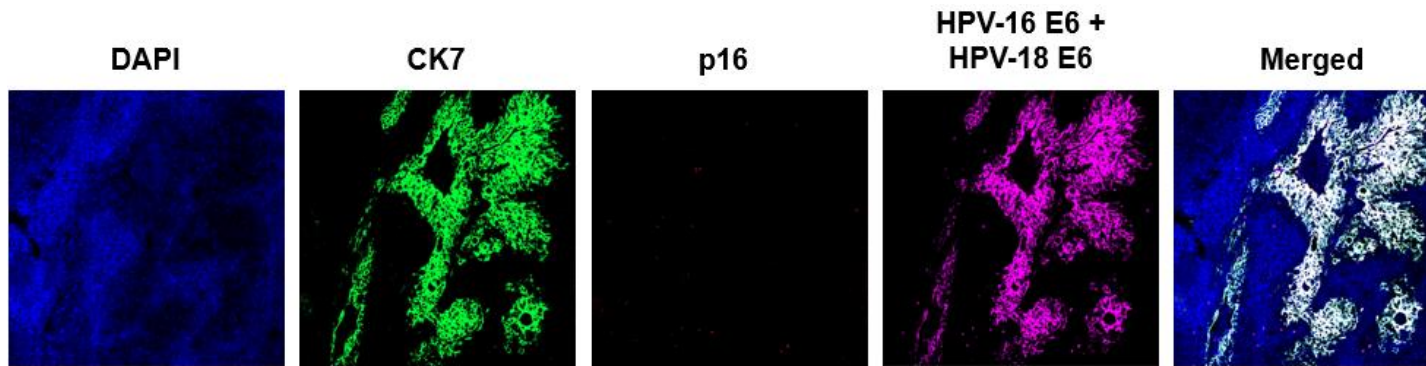


**Figure 30: Positive staining of HPV-16 E6 + HPV-18 E6 is found within the tumour of OPSCC 2.**

Strong CK7 expression was observed within the tumour. No p16 expression was exhibited. Surprisingly, HPV-16 E6 + HPV-18 E6 expression was observed within the tumour. Images captured on Zen Pro Microscopy Software at 10x magnification.

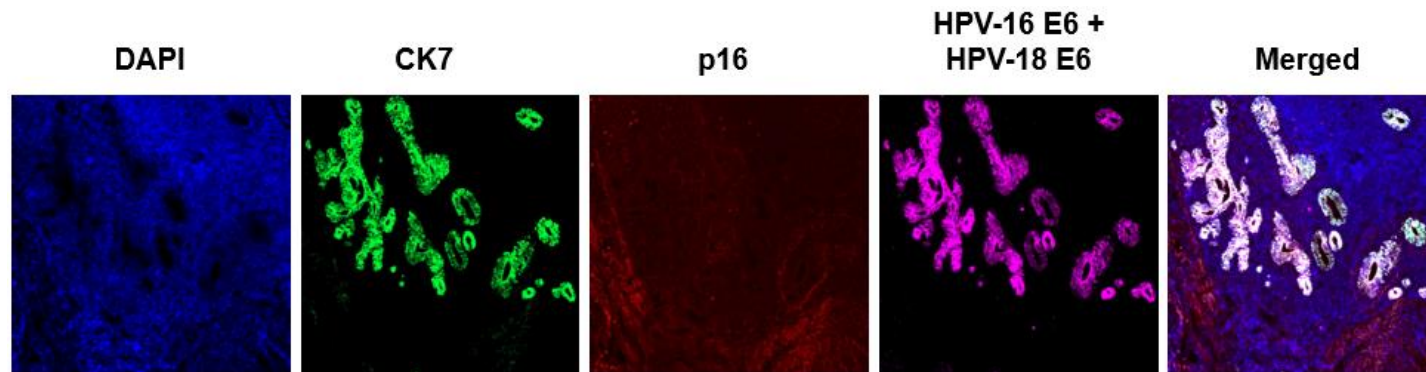


**Figure 31: Positive staining of HPV-16 E6 + HPV-18 E6 is found in ductal epithelium in OPSCC 3.**

Strong CK7 expression was observed within the ductal epithelium, with no expression exhibited within the tumour. No p16 expression was observed. Surprisingly, HPV-16 E6 + HPV-18 E6 expression was observed within the ductal epithelium; however, no expression was observed within the tumour. Images captured on Zen Pro Microscopy Software 10x magnification.

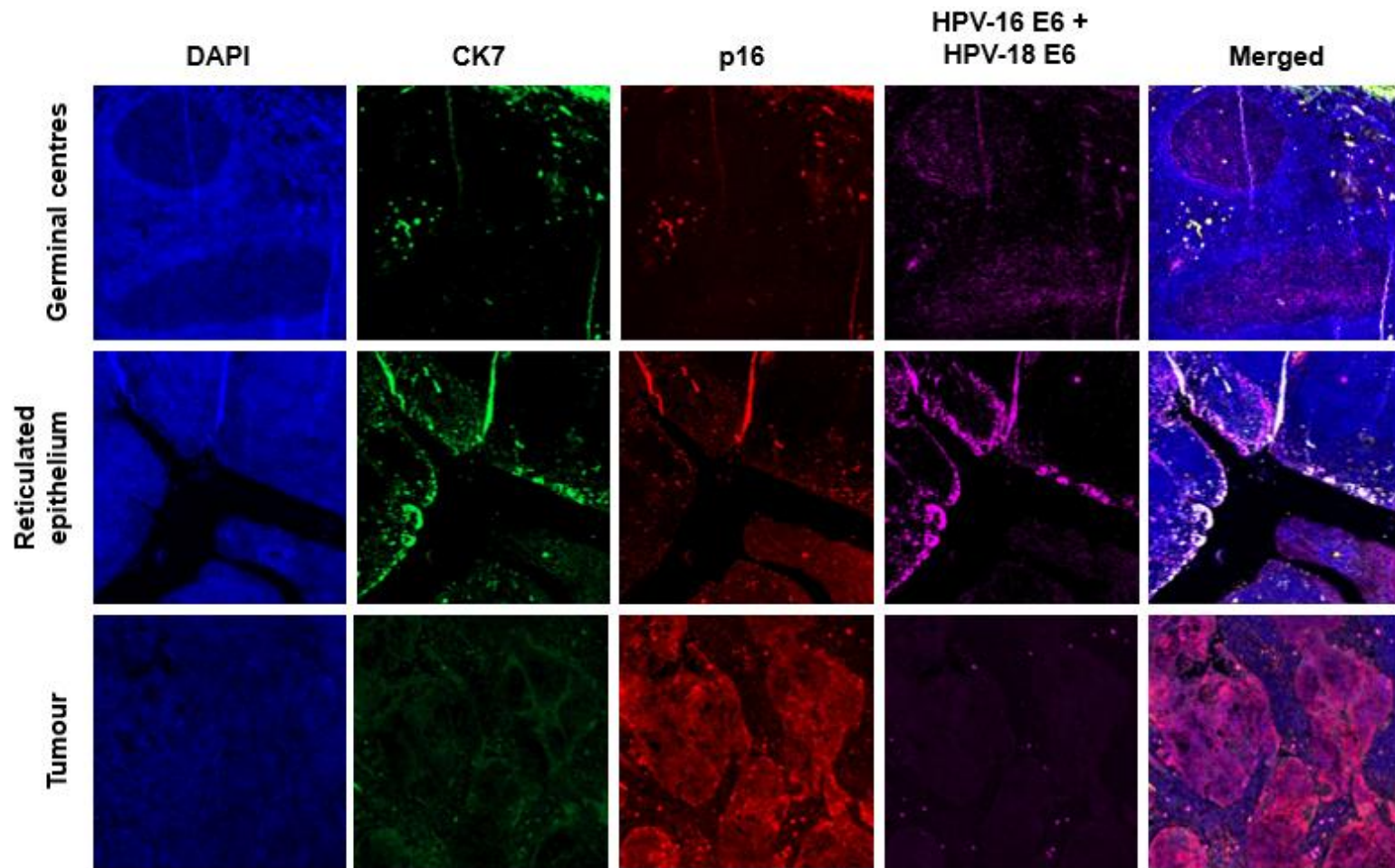


**Figure 32: Positive staining of HPV-16 E6 + HPV-18 E6 is shown across different cell types in OPSCC 4.**

CK7 expression was observed within the reticulated epithelium, with no expression observed within the germinal centres and tumour. Strong p16 expression was observed in the reticulated epithelium and tumour, however it was negative within the germinal centres. Surprisingly, HPV-16 E6 + HPV-18 E6 expression was observed within the germinal centres, and reticulated epithelium; however, no expression was observed within the tumour. Images captured on Zen Pro Microscopy Software at 10x magnification.



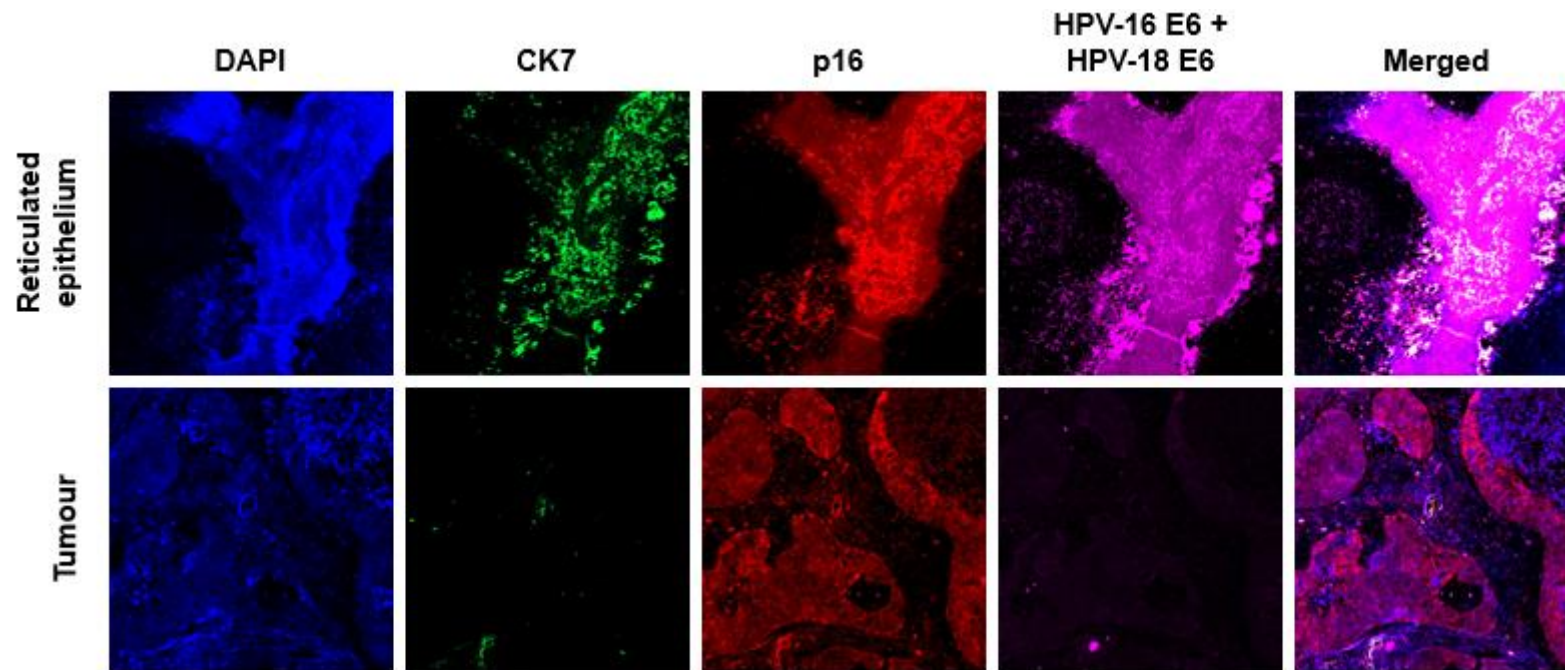


**Figure 33: Positive staining of HPV-16 E6 + HPV-18 E6 is shown across different cell types in OPSCC 5.**

CK7 expression was observed within the reticulated epithelium, with no expression observed within the tumour. Strong p16 expression was observed in the reticulated epithelium and tumour. Surprisingly, HPV-16 E6 + HPV-18 E6 expression was observed within the reticulated epithelium, and reticulated epithelium same as CK7 and p16; however, no expression was observed within the tumour. Images captured on Zen Pro Microscopy Software at 10x magnification.

### **4.2.3 Further commercially-available HPV antibodies demonstrated unexpected staining results**

Given the unexpected mIF staining observed above, we decided to test the HPV-16 E2 (TVG-261) (Abcam), HPV-16 E6 + HPV-18 E6 (C1P5) (Abcam), HPV-16 E6/HPV-18 E6 (C1P5), and HPV-16 E7 (ED17) (both Santa Cruz Biotechnology (SCBT)) antibodies again through IHC in a range of other tissue types that were pathologically normal (tonsil, cervix, spinal cord, liver, and placenta) or cancerous (CC, laryngeal carcinoma (LC), and prostate carcinoma) (Section 2.1 Table 2). Varying degrees of staining intensity were observed in all tissue types, with each of the HPV antibodies.

A negative buffer control was run for each tissue type (Figure 34). Each tissue type had the primary antibody substituted for antibody diluent, which demonstrated haematoxylin staining as the counterstain, with some observed background 3,3'-diaminobenzidine (DAB) staining in a few tissue types, which appeared as precipitate on the tissue section. This was important, as this allowed us to distinguish what was precipitate on the section from the DAB, and what was real staining within the tissue.

Unexpectedly, staining with HPV-16 E2 (TVG-261) (Abcam), HPV-16 E6 + HPV-18 E6 (C1P5) (Abcam), HPV-16 E6/HPV-18 E6 (C1P5), and HPV-16 E7 (ED17) (both SCBT) was observed within normal tonsils 1-4 and normal cervix 1 (Figures 35-38); however, E2, E6, and E7 expression would not be present in normal tissue as they are only expressed in precancerous and cancerous tissues (Dymalla *et al.*, 2009, Xue *et al.*, 2010). CC 4 exhibited negative staining for three antibodies (except HPV-16 E6 + HPV-18 E6) (Abcam), which was possible, as it could be caused by an alternate HPV type (Figure 35, 37 and 38). Both LC 1 and 2 exhibited some staining, which was surprising, although some LCs can be caused by HPV; however, again, expression of E2 would likely be lost during viral integration (Figure 35-38) (Castellsagué *et al.*, 2016). Staining was also observed in normal spinal cord 1, prostate carcinoma 1, normal liver 1, and normal placenta 1 tissues, which should not be HPV-positive (Figures 35-38).

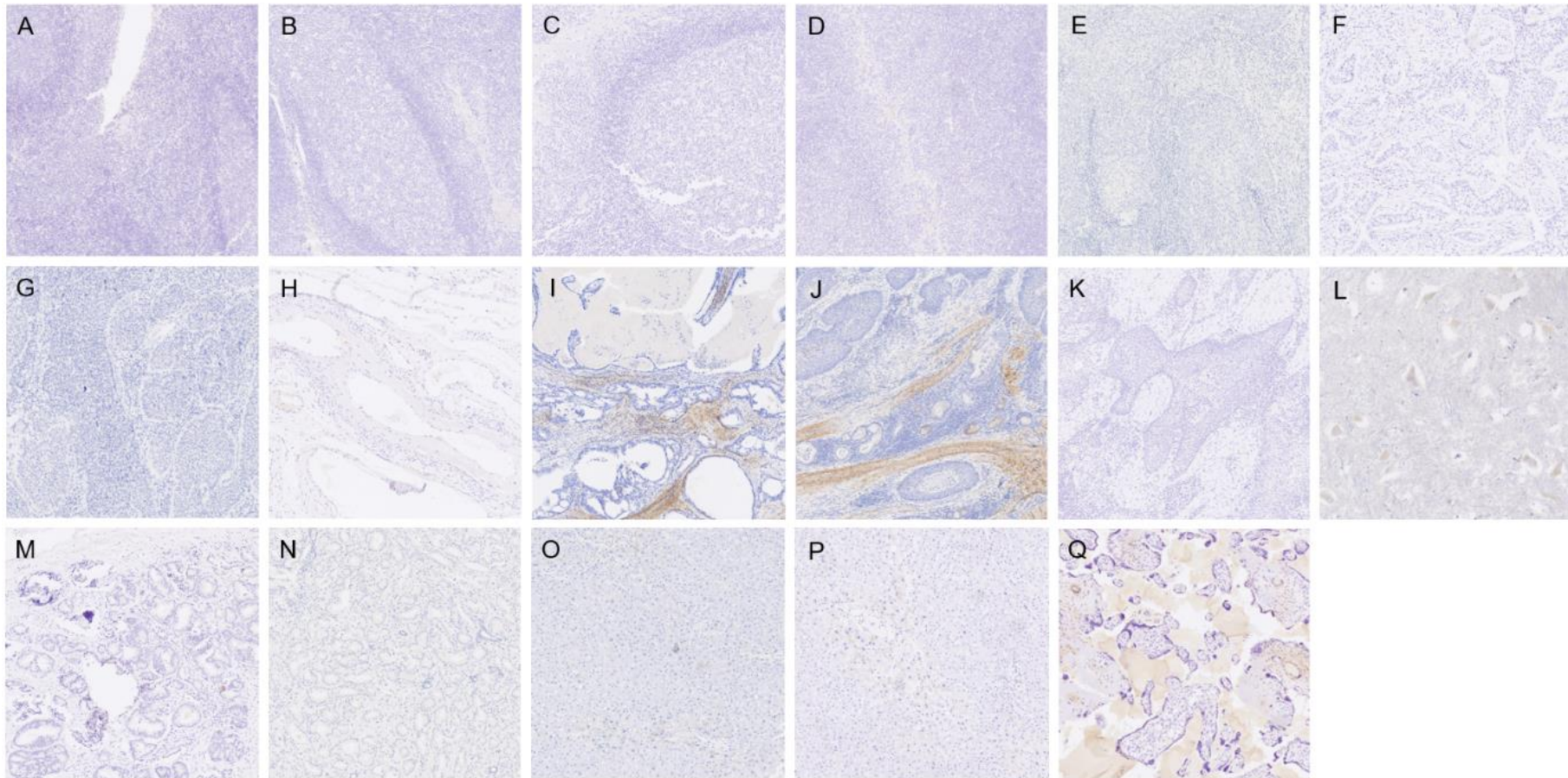


**Figure 34: Buffer negative staining in multiple tissue types.**

Tissue sections (n=17) were stained without primary antibody. Normal tonsils 1-4 (**A-D**), CC 1-3 (**E-G**), normal cervix 1 (**H**), CC 4 (**I**), LCs 1 and 2 (**J and K**), normal spinal cord 1 (**L**), prostate carcinomas 1 and 2 (**M and N**), normal livers 1 and 2 (**O and P**), and normal placenta 1 (**Q**). Images captured on NDP.view2 software at 10x magnification.

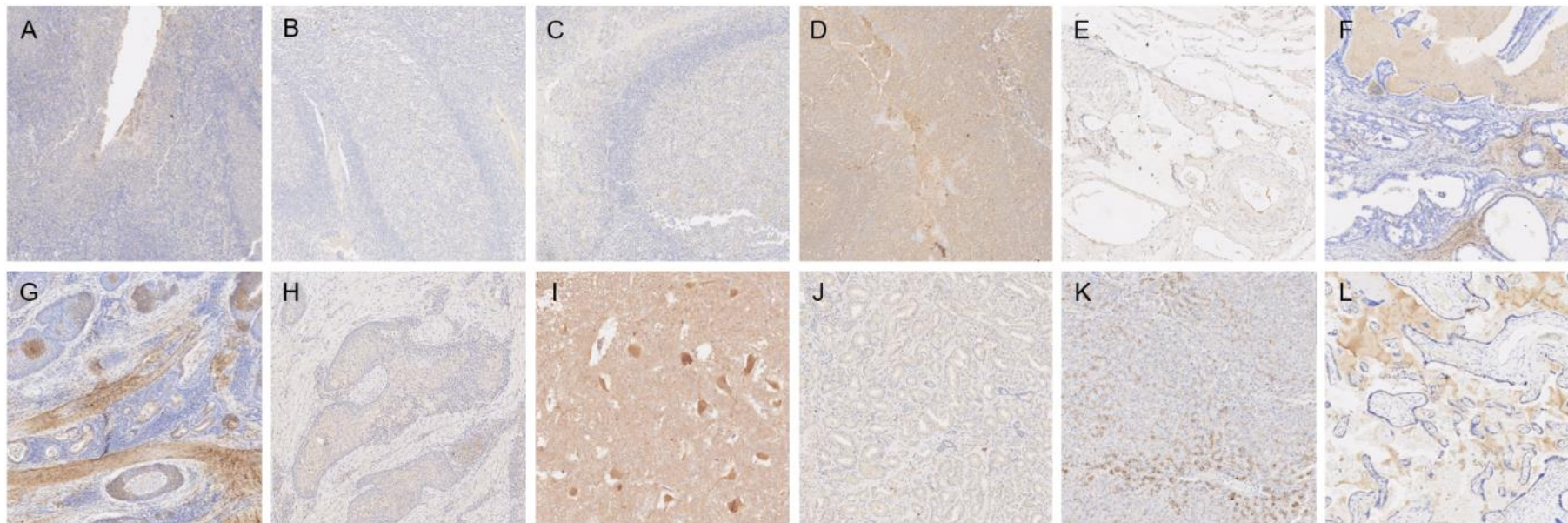


**Figure 35: Positive staining of HPV-16 E2 is found across multiple tissue types.**

Tissue sections (n=12) were stained with HPV-16 E2 (TVG-261) (Abcam) antibody. Very weak background staining within the tonsil parenchyma and germinal centres of normal tonsils 1-3 (**A-C**), with staining also in the stroma. Strong background staining within the tonsil parenchyma and germinal centres and some staining in the stroma of normal tonsil 4 (**D**). Weak staining within the stroma of normal cervix 1 (**E**); however, CC 5 was tumour-negative (**F**). Weak cytoplasmic staining within the tumour and stroma of LCs 1 and 2 (**G and H**). Positive cytoplasmic staining within the nerve fibres in the white matter and neuronal cells in the grey matter of normal spinal cord 1 (**I**). Cytoplasmic staining within the tumour and stroma of prostate carcinoma 1 (**J**). Weak cytoplasmic staining within the hepatocytes of normal liver 1, with strong staining within the haemosiderin (**K**). Membranous and cytoplasmic staining in villi of normal placenta 1 (**L**). Images captured on NDP.view2 software at 10x magnification.

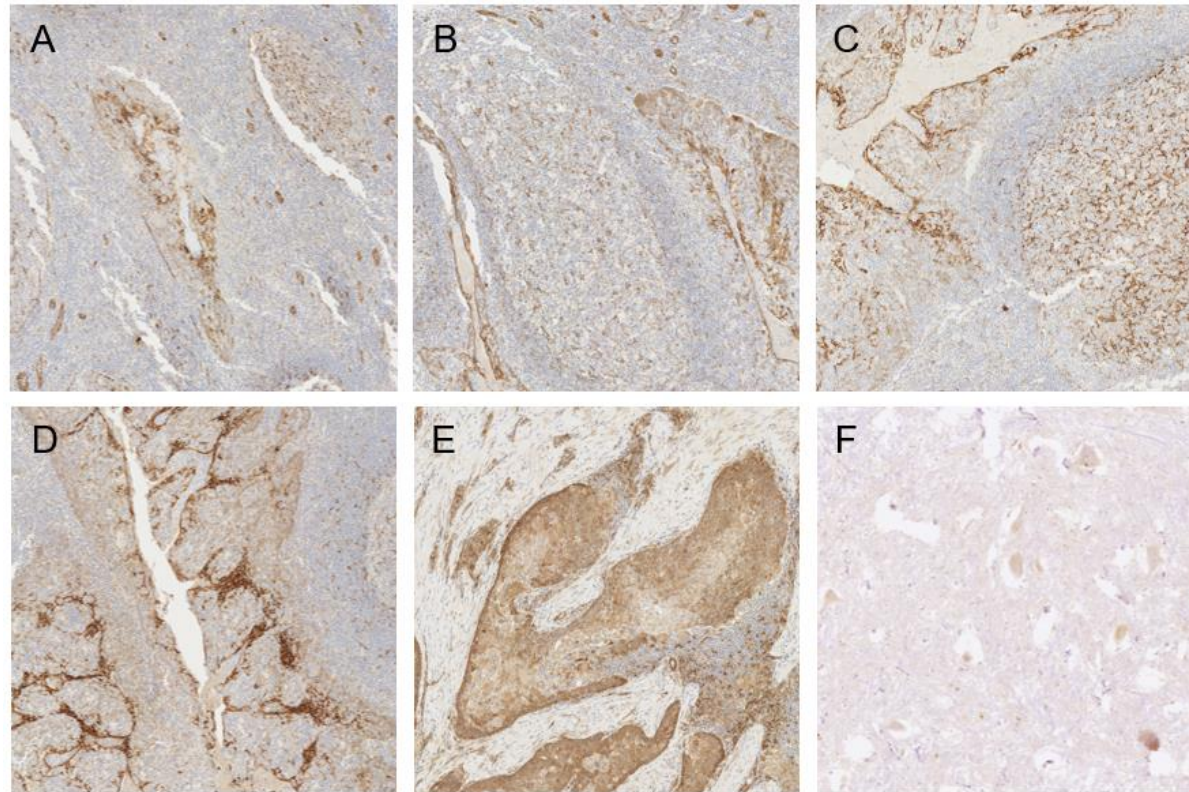


**Figure 36: Positive staining of HPV-16 E6 + HPV-18 E6 is found across multiple tissue types.**

Tissue sections (n=6) were stained with HPV-16 E6 + HPV-18 E6 (C1P5) (Abcam) antibody. Strong cytoplasmic and membranous staining within tonsil parenchyma, germinal centres, reticulated crypt epithelium and endothelium of normal tonsils 1-4 (**A-D**), with some staining in the stroma. Strong cytoplasmic and membranous staining within tumour and stroma of LC 2 (**E**). Cytoplasmic staining within the nerve fibres within in white matter and neuronal cells within in grey matter of normal spinal cord 1 (**F**). Images captured on NDP.view2 software at 10x magnification.

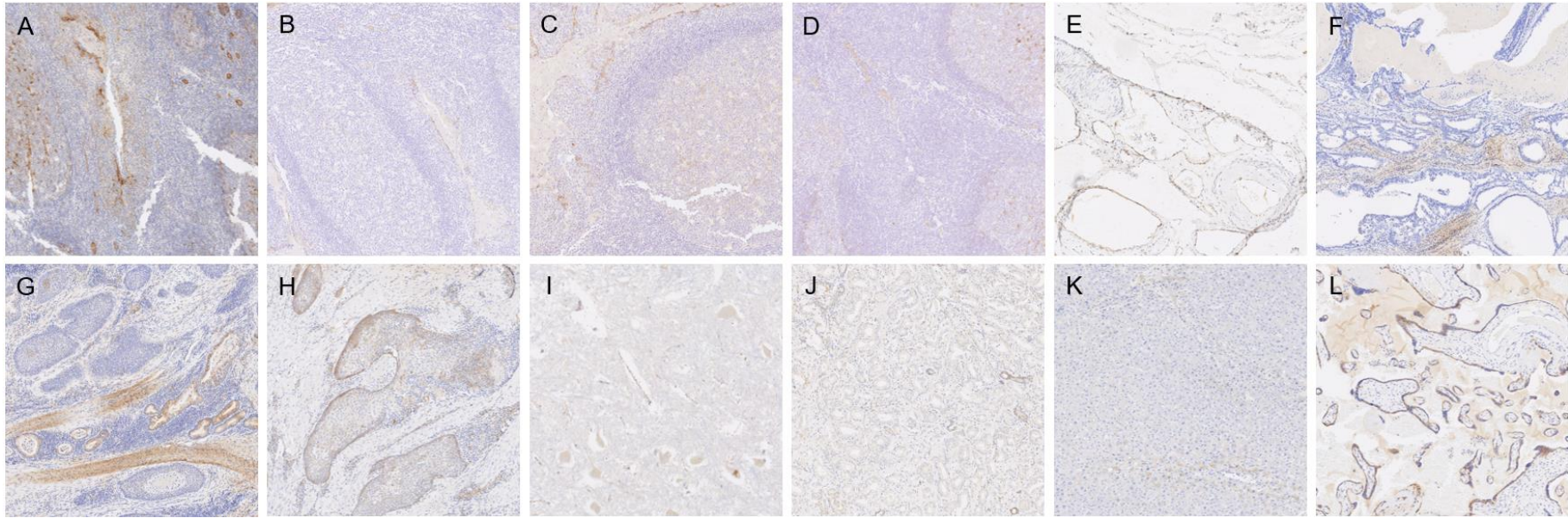


**Figure 37: Positive staining of HPV-16 E6/HPV-18 E6 is found across multiple tissue types.**

Tissue sections (n=12) were stained with HPV-16 E6/HPV-18 E6 (C1P5) (Santa Cruz Biotechnology) antibody. Strong membranous staining within tonsil parenchyma, germinal centres, reticulated crypt epithelium and endothelium of normal tonsil 1 (**A**). Membranous staining within tonsil parenchyma, germinal centres, reticulated crypt epithelium and endothelium of normal tonsils 2-4 (**B-D**). Weak membranous staining within the endothelium of normal cervix 1, with no staining within the stroma (**E**), however, CC 4 is tumour-negative (**F**). Cytoplasmic staining within the tumour and stroma of LCs 1 and 2 (**G and H**). Weak cytoplasmic staining within the nerve fibres within the white matter and neuronal cells within the grey matter of normal spinal cord 1 (**I**). Cytoplasmic staining within the tumour and stroma of prostate carcinoma 1 (**J**). Normal liver 1 was negative, except for staining of haemosiderin (**K**). Membranous and cytoplasmic staining within the villi and decidua of normal placenta 1 (**L**). Images captured on NDP.view2 software at 10x magnification.

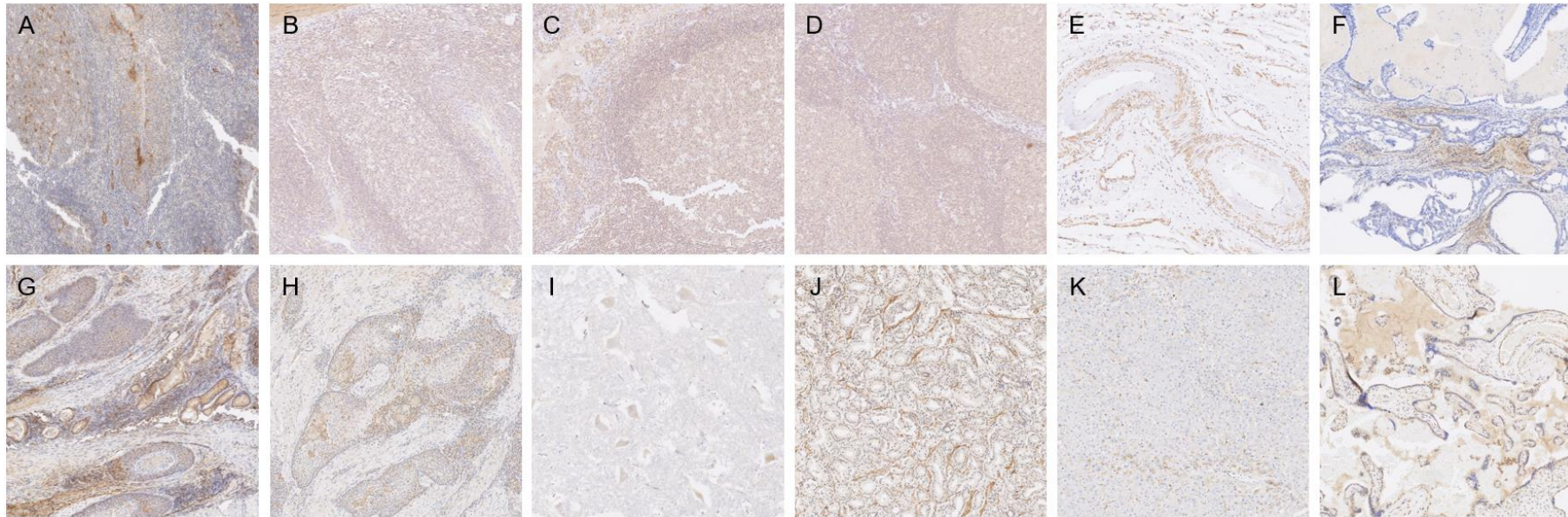


**Figure 38: Positive staining of HPV-16 E7 is found across multiple tissue types.**

Tissue sections (n=12) were stained with HPV-16 E7 (ED17) (Santa Cruz Biotechnology) antibody. Cytoplasmic and membranous staining within tonsil parenchyma, germinal centres and reticulated crypt epithelium, as well as some staining within the stroma of normal tonsils 1-4 (**A-D**). Membranous staining within the endothelium and stroma of normal cervix 1 (**E**), however, CC 5 is tumour-negative (**F**). Nuclear, cytoplasmic and membranous staining within the tumour and stroma of LCs 1 and 2 (**G and H**). Weak cytoplasmic staining within the nerve fibres within the white matter and neuronal cells within the grey matter of normal spinal cord 1 (**I**). Cytoplasmic staining within the tumour and stroma of prostate carcinoma 1 (**J**). Cytoplasmic staining within smooth muscle, endothelium, Kupffer cells and haemosiderin of normal liver 1 (**K**). Cytoplasmic and membranous staining within the villi of normal placenta 1 (**L**). Images captured on NDP.view2 software at 10x magnification.

Given these unexpected staining patterns, we purchased new commercially-available antibodies from different suppliers: HPV-16 E6 (HPV-13E2) (Neo Biotech), HPV-16 E7 (TVG 701Y) (Thermo Fisher Scientific), HPV-18 E6 (HPV-4G3) (Neo Biotech), and HPV-18 E7 (8E2) (Abcam). An alternative commercially-available antibody for HPV-16 E2 was not purchased; we had not been able to find an antibody that was validated for IHC use. These were also tested through IHC, using the same range of tissue types as mentioned above as well as the three CC tissues tested previously; however, some of the tested tissue types were not tested for with these new HPV antibodies (detailed in each of the figure legends). This was because the tissue used had been cut through the block and therefore there was no more tissue left. However, an alternative block was found with the same pathology. Again, varying degrees of staining intensity were observed in all tissue types, with each of the HPV antibodies.

Surprisingly, staining with HPV-16 E6 (HPV-13E2) (Neo Biotech), HPV-16 E7 (TVG 701Y) (Thermo Fisher Scientific), HPV-18 E6 (HPV-4G3) (Neo Biotech), and HPV-18 E7 (8E2) (Abcam), was also observed within normal tonsils 1-4 and normal cervix 1 (except HPV-18 E6) (Figures 39-42); however, E6 and E7 expression would not be present in normal tissue as they are only expressed in precancerous and cancerous tissues (Dymalla *et al.*, 2009). Staining for HPV-16 E6 and HPV-16 E7 was exhibited in CCs 1-4 (Figures 39 and 40). This was plausible if they are HPV-16-associated cancers as they would express both E6 and E7 oncoproteins. However, there were unexpected staining results for HPV-18 E6 and HPV-18 E7. CC 1 exhibited staining for HPV-18 E7, with HPV-18 E6 staining observed in CC 4 (Figures 41 and 42). As these had both already shown staining for HPV-16 E6 and HPV-16 E7, it is unlikely that it is positive for two HR-HPV types. Again, this was the same for CCs 2 and 3, which both exhibited staining for HPV-18 E6 and HPV-18 E7 (Figures 41 and 42). However, HPV-18 E6 and E7 does cause CC (Muñoz *et al.*, 2003, Smith *et al.*, 2007). Both LCs 1 and 2 exhibited some staining for all four antibodies. Again, some LCs can be caused by HPV; however, it is unlikely that it would be positive for two HR-HPV types. Finally, staining was also observed in normal spinal cord 1, prostate carcinoma 2, normal liver 2, and normal placenta 1; tissues, which should not be HPV-positive (Figures 39-42), suggesting together that the staining was not real at all.



We note that some of the tissue types, both normal and cancerous, were positive for antibody staining for E6 and E7 in both HPV-16 and -18 viral types. This seemed highly unlikely, as one HR-HPV type would be the likely cause of the oncogenic infection. Additionally, some tissue types were positive for either E6 or E7 of one viral type, which again should not be possible as both E6 and E7 work synergistically in establishing an infection, and should therefore be present together. Together, all these HPV antibodies have been rigorously tested, with the data shown suggesting that the antibodies are staining non-specifically throughout the various tissue types tested.

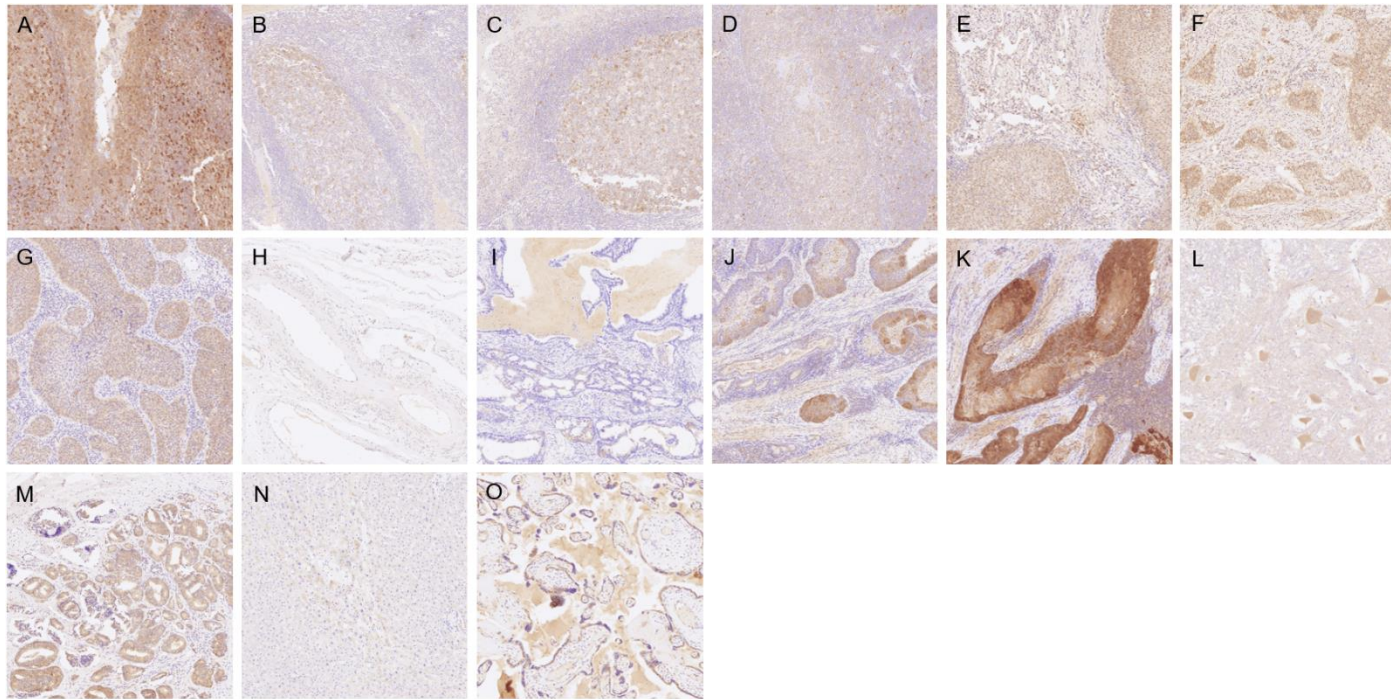


**Figure 39: Positive staining of HPV-16 E6 is found across multiple tissue types.**

Tissue sections (n=15) were stained with HPV-16 E6 (HPV-13E2) (Neo Biotech) antibody. Strong cytoplasmic and membranous staining within the tonsil parenchyma, germinal centres and reticulated crypt epithelium of normal tonsil 1 (**A**), with some staining in the stroma. Cytoplasmic and membranous staining within the tonsil parenchyma, germinal centres and reticulated crypt epithelium of normal tonsils 2-4 (**B-D**). Nuclear and cytoplasmic staining within the tumour and stroma of CCs 1 and 2 (**E and F**), with cytoplasmic staining within the tumour of CC 3 (**G**). Weak membranous staining within the endothelium of normal cervix 1 (**H**), with CC 4 (**I**) demonstrating occasional weak cytoplasmic staining within the tumour. Nuclear and membranous staining within the tumour and stroma of LC 1 (**J**). Weak nuclear, membranous, and cytoplasmic staining within the tumour of LC 2 (**K**). Weak cytoplasmic staining within the nerve fibres in the white matter and neuronal cells in the grey matter of normal spinal cord 1 (**L**). Strong cytoplasmic and membranous staining within the tumour of prostate carcinoma 2 (**M**). Weak cytoplasmic staining within the hepatocytes of normal liver 2, with weak staining within the haemosiderin (**N**). Cytoplasmic staining in villi and decidua of normal placenta 1 (**O**). Images captured on NDP.view2 software at 10x magnification.

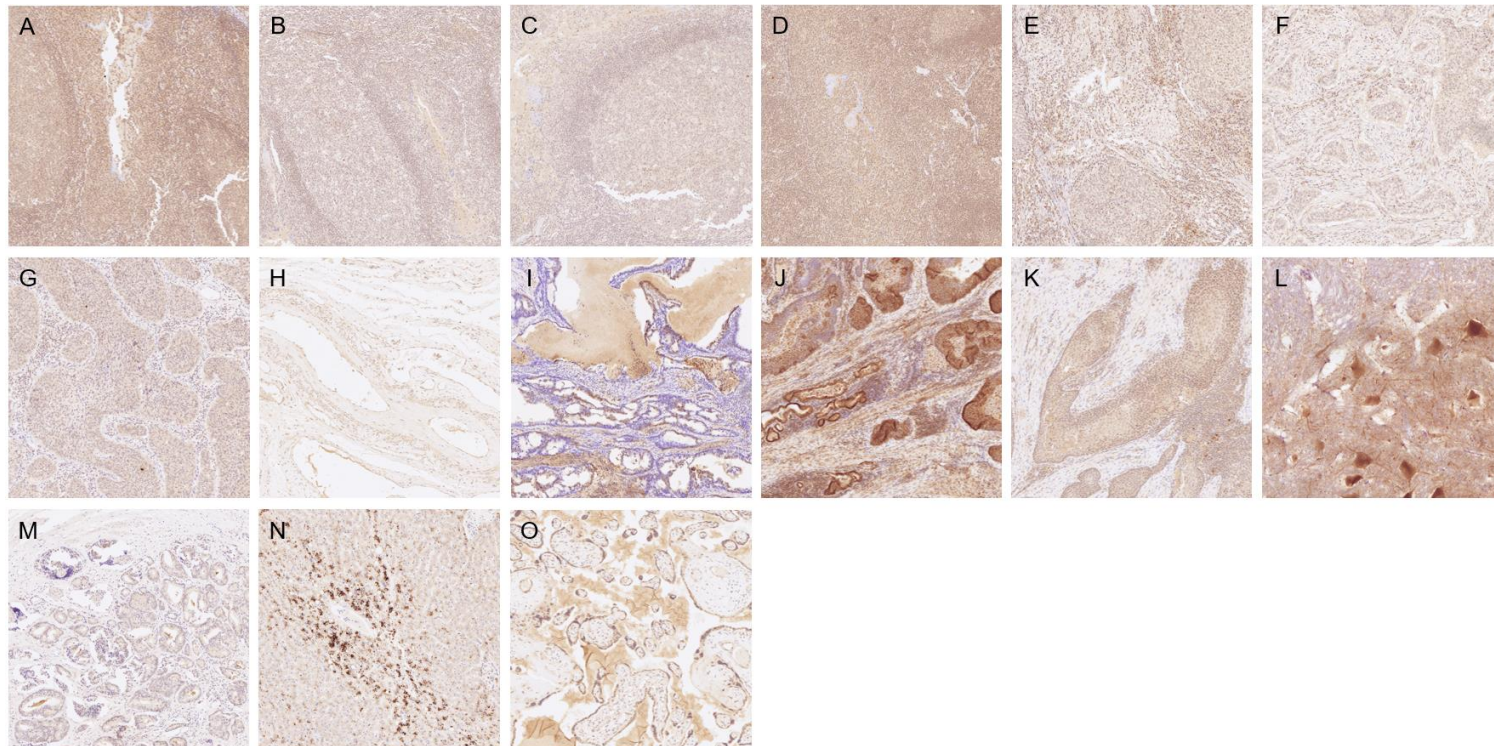


**Figure 40: Positive staining of HPV-16 E7 is found across multiple tissue types.**

Tissue sections (n=15) were stained with HPV-16 E7 (TVG 701Y) (Thermo Fisher Scientific). Nuclear and cytoplasmic staining within the tonsil parenchyma, germinal centres and reticulated crypt epithelium of normal tonsils 1-3 (**A-C**). Strong nuclear and cytoplasmic staining within the tonsil parenchyma, germinal centres and reticulated crypt epithelium of normal tonsil 4 (**D**). Nuclear, cytoplasmic and membranous staining within the tumour and stroma of CCs 1-3 (**E-G**). Weak membranous staining within the endothelium and stroma of normal cervix 1 (**H**), with CC 5 (**I**) demonstrating nuclear and cytoplasmic staining within the tumour. Nuclear, cytoplasmic and membranous staining within the tumour, surface epithelium and stroma of LCs 1 and 2 (**J and K**). Strong cytoplasmic staining within the nerve fibres in the white matter and neuronal cells in the grey matter of normal spinal cord 1 (**L**). Weak cytoplasmic and membranous staining within the tumour and stroma of prostate carcinoma 2 (**M**). Cytoplasmic staining within the hepatocytes of normal liver 2, with strong staining within the haemosiderin (**N**). Cytoplasmic and membranous staining in the villi and decidua of normal placenta 1 (**O**). Images captured on NDP.view2 software at 10x magnification.

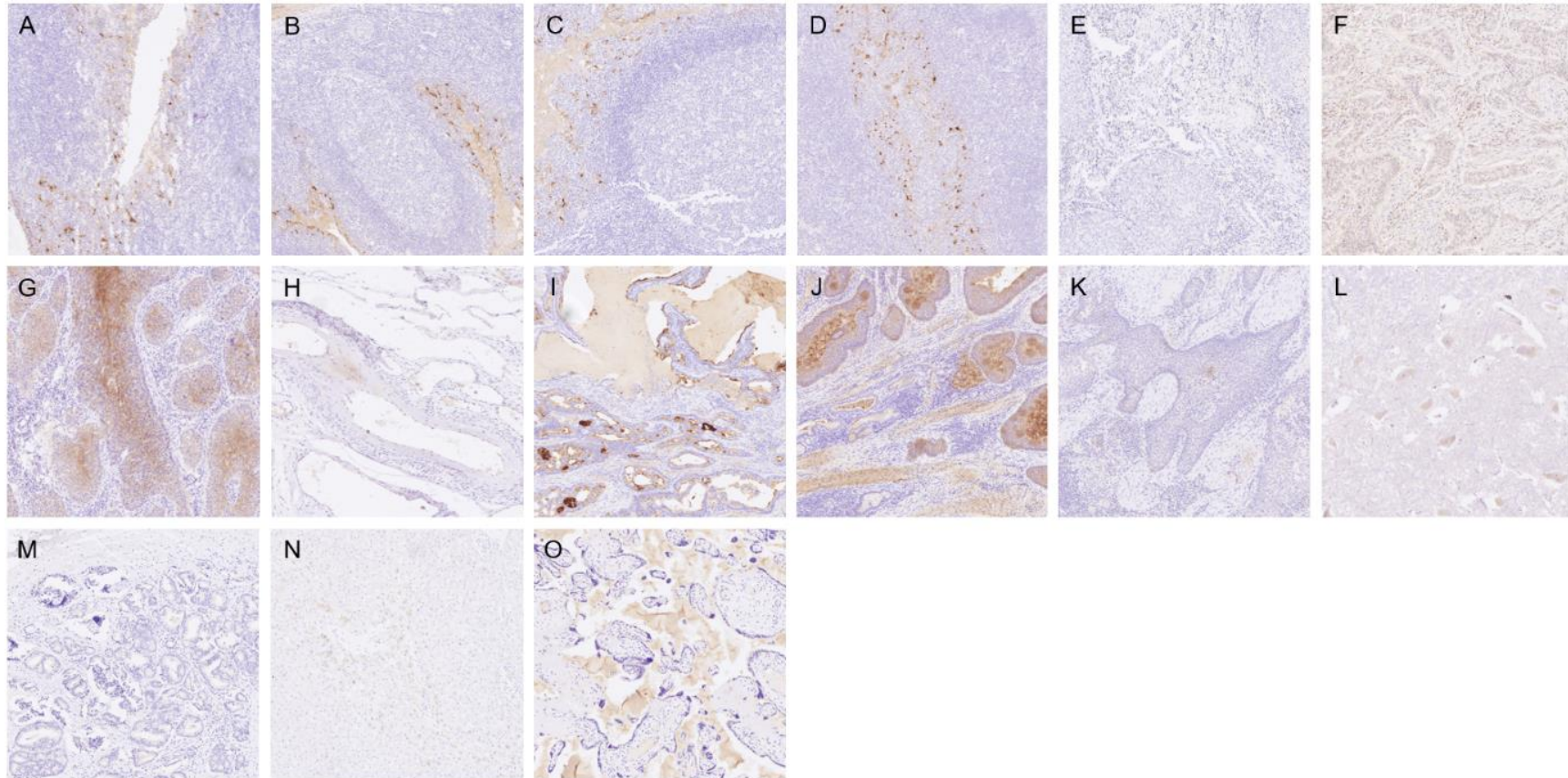


**Figure 41: Positive staining of HPV-18 E6 is found across multiple tissue types.**

Tissue sections (n=15) were stained with HPV-18 E6 (HPV-4G3) (Neo Biotech) antibody. Membranous staining within the reticulated crypt epithelium of normal tonsils 1-4 (**A-D**). CC 1 was negative (**E**). Cytoplasmic staining within the tumour and stroma of CC 2 (**F**). Cytoplasmic and membranous staining within the tumour and stroma of CC 3 (**G**). Normal cervix 1 was negative (**H**), with cytoplasmic staining within the tumour of CC 5 (**I**). Cytoplasmic and membranous staining within the tumour and stroma of LCs 1 and 2 (**J and K**). Weak cytoplasmic staining within the neuronal cells in the grey matter of normal spinal cord 1 (**L**). Prostate carcinoma 2, normal liver 2, and normal placenta 1 were negative (**M-O**). Images captured on NDP.view2 software at 10x magnification.

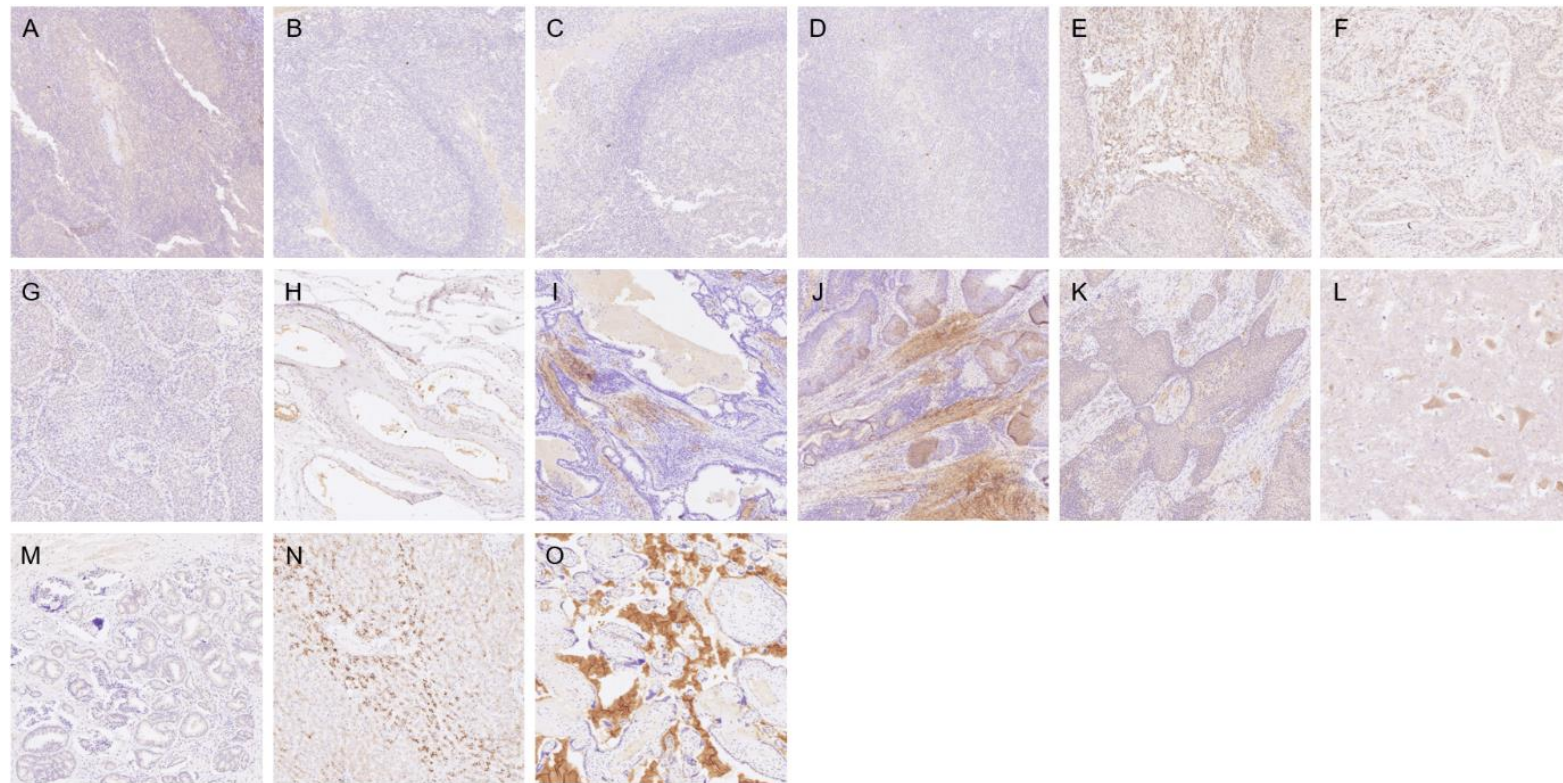


**Figure 42: Positive staining of HPV-18 E7 is found across multiple tissue types.**

Tissue sections (n=15) were stained with HPV-18 E7 (8E2) (Abcam) antibody. Very weak background staining within the tonsil parenchyma and germinal centres of normal tonsils 1-4 (**A-D**). Cytoplasmic and membranous staining within the tumour and stroma of CC 1 (**E**), with weak cytoplasmic staining within the tumour and stroma of CC 2 (**F**). Weak membranous staining within the tumour and stroma of CC 3 (**G**). Weak membranous staining within the endothelium and stroma of normal cervix 1 (**H**); however, CC 4 was negative (**I**). Cytoplasmic staining within the tumour and stroma of LC 1 (**J**). Weak nuclear and cytoplasmic staining within the tumour and stroma of LC 2 (**K**). Cytoplasmic and punctate staining within the nerve fibres in the white matter and neuronal cells in the grey matter of Spinal Cord 1 (**L**). Prostate carcinoma 2 was negative (**M**). Cytoplasmic staining within the hepatocytes of normal liver 2, with strong staining within the haemosiderin (**N**). Very weak cytoplasmic and membranous staining within the villi of normal placenta 1 (**O**). Images captured on NDP.view2 software at 10x magnification.

#### 4.2.4 Molecular screening of tissues for HPV

Given the unexpected staining phenotypes described above we investigated the HPV status of each of the tissues. This was examined molecularly on DNA extracted from formalin-fixed, paraffin-embedded (FFPE) tissue using a real-time PCR method with GP5+/6+ primers that recognise the L1 gene of over 20 mucosal types of HPV, developed by our group (de Roda Husman *et al.*, 1995, Whitton *et al.*, 2024).

The first tissue types tested were normal tonsils 1-4 and CCs 1-3, and their melt curves evaluated for HPV DNA (Figure 43, courtesy of M.A. Freckleton). It was anticipated that Cervix 1-3 would be positive, as more than 99.7% of CCs are caused by HR-HPV (Walboomers *et al.*, 1999), whereas normal tonsils 1-4 were presumed to be negative as there was no abnormal pathology present. Indeed, normal tonsils 1-4 peaks did not align with either the SiHa or HPV-18 controls, and were determined as negative, with the product peaks showing non-specific amplification. CCs 1-3 however did align with the SiHa control, indicating that they were HPV-16-positive. The peak for CC 3 however is lower than those of CC 1 and 2, but this could be indicative of poor-quality DNA or amount of DNA within the sample.

The second tissue types tested were normal cervix 1, CC 4, LCs 1 and 2, normal spinal cord 1, prostate carcinoma 2, normal liver 2, and normal placenta 1, and their melt curves evaluated for HPV DNA (Figure 44, courtesy of M.A. Freckleton). Based on the antibody staining, it was anticipated that CC 4 would be positive, with the possibility of LCs 1 and 2 also being positive, whereas the rest were anticipated to be negative. Indeed, peaks for normal cervix 1, LCs 1 and 2, normal spinal cord 1, prostate carcinoma 2, normal liver 2, and normal placenta 1 did not align with either the SiHa or HPV-18 controls, and were all determined to be negative, with the product peaks showing non-specific amplification. Only CC 4 aligned with the HPV-18 plasmid control, indicating that it was HPV-18-positive.

This molecular data casts further doubt on the specificity of the commercially-available HPV antibody staining. Together, the data suggest that they are inadequate.

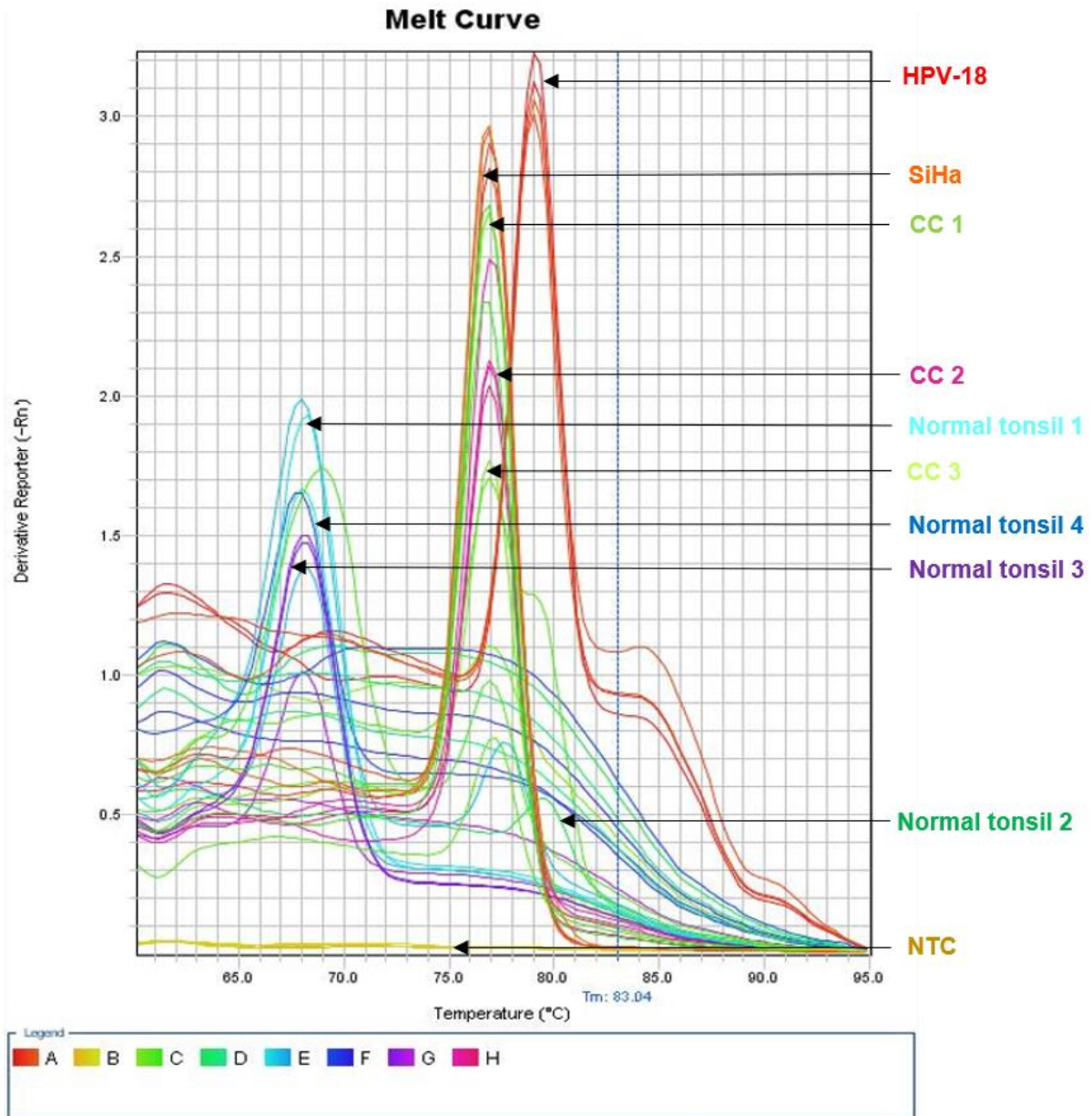


**Figure 43: Screening for HPV positivity in first batch of multiple tissue types.**

Melt curve analysis of real-time PCR products generated with GP5+/6+ consensus primers, designed to amplify a region of HPV L1, a late protein. Peaks from DNA isolated from FFPE sections of normal tonsils 1-4 did not align with either the SiHa or HPV-18 plasmid control, whereas CCs 1-3 did align with SiHa at 77°C. NTC-non-template control. Data courtesy of my colleague, M. A. Freckleton.

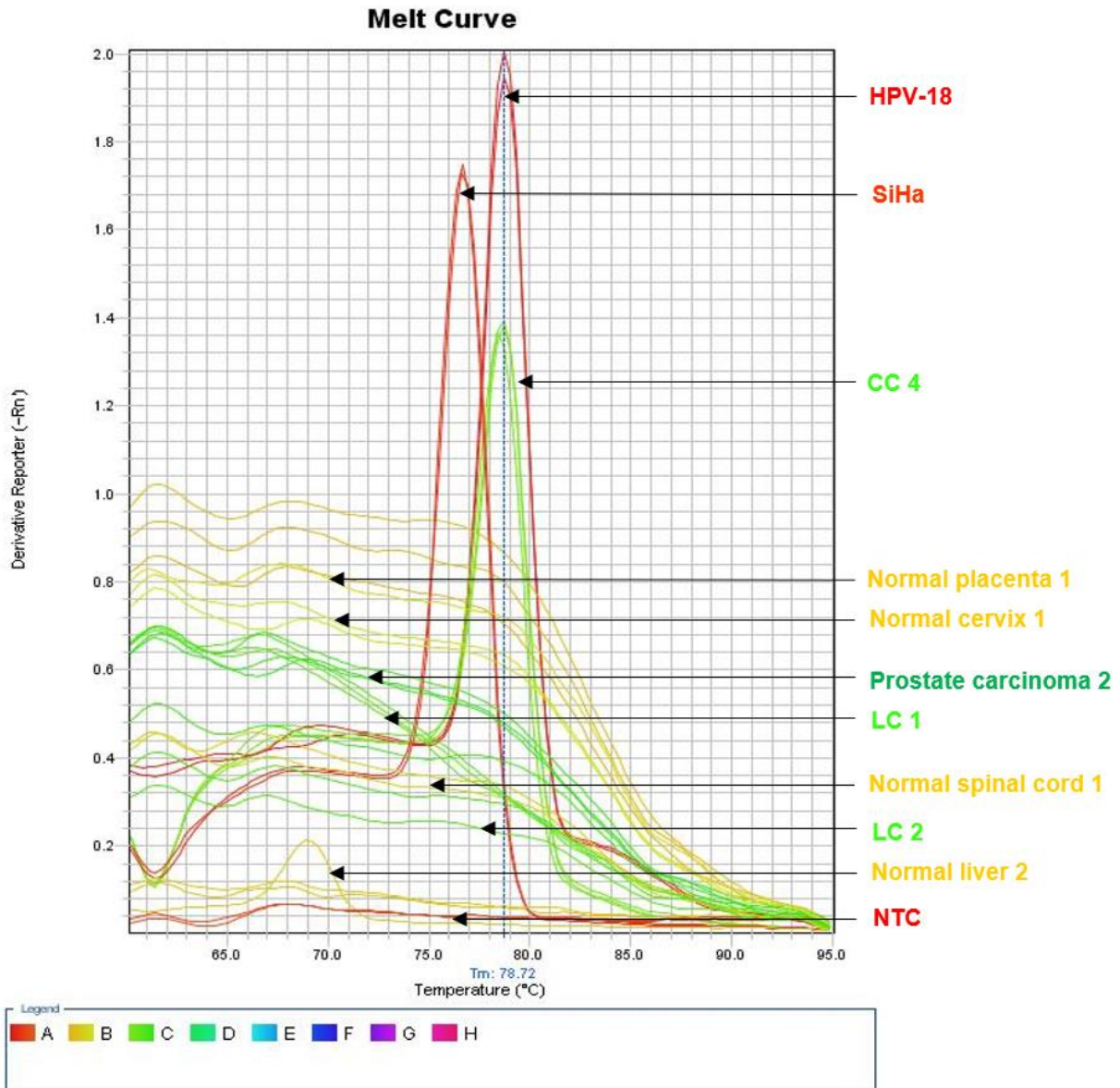


**Figure 44: Screening for HPV positivity in second batch of multiple tissue types.**

Melt curve analysis of real-time PCR products generated with GP5+/6+ consensus primers, designed to amplify a region of HPV L1, a late protein. Peaks from DNA isolated from FFPE sections of normal cervix 1, LCs 1 and 2, normal spinal cord 1, prostate carcinoma 2, normal liver 2, and normal placenta 1 did not align with either the SiHa or HPV-18 plasmid control, whereas CC 4 did align with HPV-18 plasmid at 79°C. NTC-non-template control. Data courtesy of my colleague, M.A. Freckleton.



### 4.3 Conclusion

To scrutinise the pathogenesis of HPV within the oropharynx further, a number of HPV antibodies from different suppliers were tested in multiple tissue types, ahead of use in OPSCCs. Unfortunately, they all showed non-specific staining to varying degrees across the vastly different cell types that we confirmed to be HPV-negative through molecular screening.

We were interested in the expression of E2, E6, and E7 proteins, particularly in HPV-16 and HPV-18, as these are two of the most prevalent types in OPSCC (Kreimer *et al.*, 2005, Schache *et al.*, 2016). E2 expression in the early stages of the HPV viral life cycle, can become disrupted during viral integration, resulting in uncontrollable overexpression of E6 and E7 oncoproteins (Xue *et al.*, 2010). As such, we would only expect E2 to be expressed in pre-cancerous tissue, and to be absent within HPV-positive cancerous tissues such as CC, due to the integration event, and normal tissue. However, staining was observed in both normal and cancerous tissues, which is likely indicative of a poor antibody, rather than evidence to refute this activity of E2 in our samples. It is worth noting that we have not been able to find a commercially-available HPV-16 E2 antibody that is validated for IHC use, despite extensive searching and enquiries; this may account for the non-specific IHC staining observed here. Additionally, both normal and cancerous tissues demonstrated E6 or E7 of either HPV-16 or -18, with expression of both E6 and E7 oncoproteins required for malignant transformation (Butz *et al.*, 2003). As we did not observe this co-expression, the staining cannot be considered as true positivity shown through HPV antibody staining.

This is supported by molecular data that shows these aforementioned normal tissue types are HPV-negative. Together, these data suggest that the commercially-available HPV antibodies do not stain the specific target protein within these tissues. Interestingly, we returned to the supplier for HPV-16 E6 + HPV-18 E6 (Abcam) with our observations, supported by our molecular analysis. The supplier retested the antibody in their own lab and contacted us later with their results. Their investigation demonstrated that they also found positive signals in non-specific and negative control samples, as well as their Western blot demonstrating multiple bands even in negative controls, validating our own findings. Subsequently the antibody was removed from their catalogue, with the product discontinued 7 months later (Appendix 14).

Unfortunately, this calls into question the data shown by (Lawson *et al.*, 2009, Stiasny *et al.*, 2016, He *et al.*, 2022, Zhang *et al.*, 2022a, Zhang *et al.*, 2022b, Huang *et al.*, 2023, Kumarasamy *et al.*, 2023), who have used this antibody for IHC purposes, staining in CC tissue, as well as head and neck, urothelial, and breast carcinomas. Additionally, Stiasny *et al.*, 2016, stated the possibility of using it for IHC evaluation in routine pathology, which raises significant questions for diagnosis on the basis of the data shown here.

As such, we were unable to progress our histological investigations into the pathogenesis of HPV further. We therefore suggest that HPV markers need to be re-evaluated for use in tissues to improve what is already present within the literature.

## CHAPTER 5: APTAMER DEVELOPMENT OF HPV PROTEINS

### 5.1 Introduction

In Chapter 4 we established that commercially-available HPV antibodies stain non-specifically, and instead stain tissue that we know to be molecularly HPV-16 and -18 negative, as well as also staining tissue types that are not anticipated to be HPV-positive. Although these antibodies are not for in vitro diagnostic (IVD) use, they are still being used for research use only (RUO).

In the UK, p16INK4A (p16) immunohistochemistry (IHC) is a validated prognostic marker used for testing HPV status within OPSCC (Klussman *et al.*, 2003, Sedghizadeh *et al.*, 2016, Lewis *et al.*, 2018b, Hunter *et al.*, 2021). However, using p16 IHC to detect HPV-positivity demonstrates limited sensitivity and specificity in the oropharynx, and can result in false positives in OPSCC (Schache *et al.*, 2011, El-Naggar and Westra, 2012, Suresh *et al.*, 2021, Mehanna *et al.*, 2023). With the low specificity of p16, and the non-specific and unexpected staining observed with HPV antibodies, we aimed to develop novel, alternate HPV markers.

Aptamers are single-stranded (ss) DNA or RNA oligonucleotides which are able to form unique three-dimensional structures, capable of binding with a high affinity to specific target molecules (Navien *et al.*, 2021). In 1990, three separate groups discovered aptamers, which are generated using the *in vitro* process known as systematic evolution of ligands by exponential enrichment (SELEX) (Ellington and Szostak, 1990, Robertson and Joyce, 1990, Tuerk and Gold, 1990). The target molecule is incubated on a suitable surface with a random ssDNA or ssRNA library and exposed to a selection pressure before amplification by polymerase chain reaction (PCR) or reverse transcription PCR (RT-PCR). This process is repeated as many as 8-16 times, exposing the target molecule to numerous selection pressures in order to increase its specificity and affinity (Mayer, 2009, Blind and Blank, 2015).

This chapter examines the designing and development of DNA aptamers as alternate HPV markers against the target proteins; HPV-16 E2, HPV-16 E7-E6, HPV-18 E6, and HPV-18 E7.

## 5.2 Results

### 5.2.1 DNA aptamers against selected HPV target proteins underwent successful selection

HPV target protein SELEX process finished after the 10<sup>th</sup> positive selections for HPV-16 E7-E6, HPV-18 E6, and HPV-18 E7, and the 12<sup>th</sup> positive selection for HPV-16 E2 pools. The difference between the number of positive selections was due to no DNA being recovered after the selection, indicating that further selections were not possible. HPV aptamers generated were 70 nucleotides (nt) in length, composed of a 30 nt wobble region flanked by the forward (21 nt) and reverse (19 nt) primer sequences on each end from the PCR amplification steps used within the SELEX process, with extended forward (37 nt) and reverse primers (35 nt), increasing the total sequence length to 102 nt, to assist with next generation sequencing (NGS). Agarose gel analysis demonstrated that each HPV aptamer pool had undergone successful selection, and subsequent extension of sequence length (Figure 45). The observed smearing of each HPV aptamer pool represents misfolding of the sequences during separation through the gel. Whilst the sequences were the same length in terms of nt, resolution in the gel was based on shape as well as size.

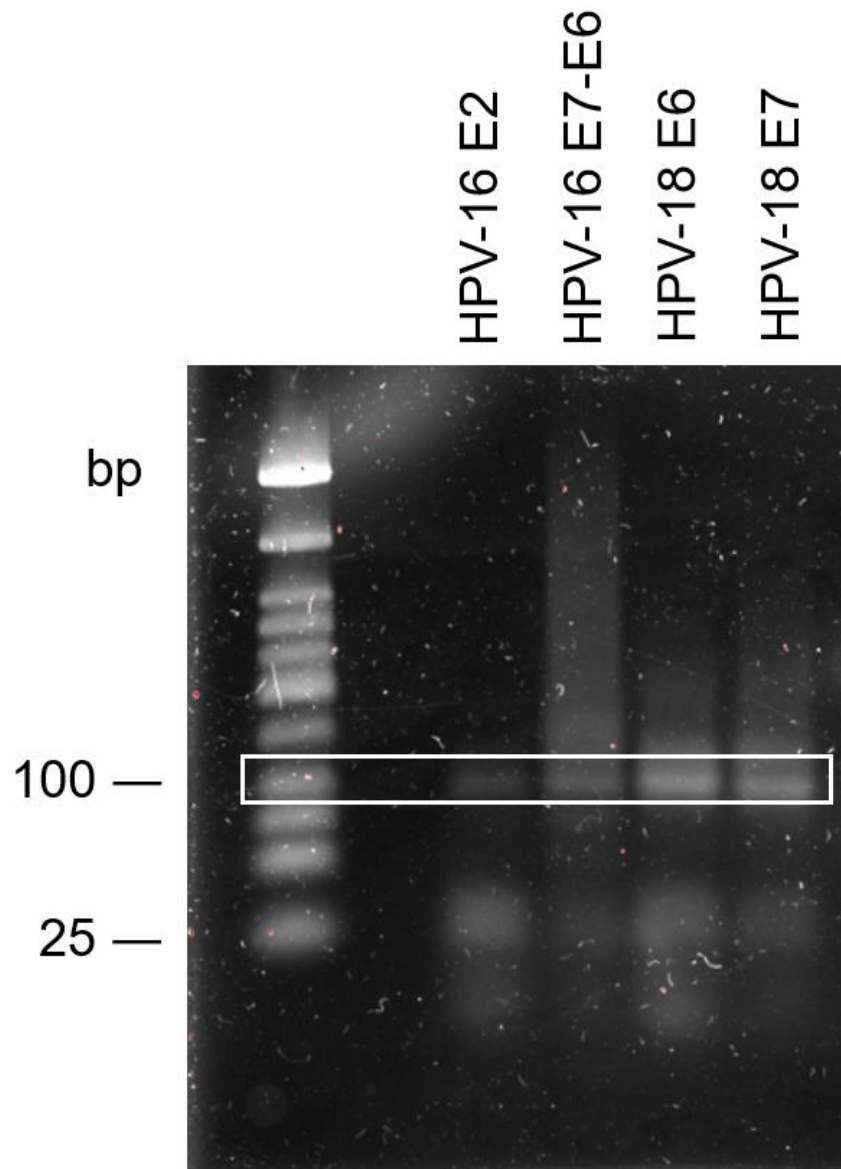


**Figure 45: Confirmation agarose gel of HPV aptamers amplified with extended primers.**

HPV-16 E2, HPV-16 E7-E6, HPV-18 E6, and HPV-18 E7 aptamers underwent PCR amplification with extended primers to increase sequence length. Distinct bands were visible at 100 bp, which indicated successful sequence length extension. Smearing present for each HPV aptamer indicated misfolding during the separation process. Bands at 25 bp and below were indicative of primer dimers. Image captured on Image Lab™ Software.

### 5.2.2 *In silico* secondary and tertiary aptamer structure prediction

After NGS, data was extracted from the generated FASTQ files for each HPV aptamer pool, and loaded into Notepad ++ (<https://notepad-plus-plus.org/>), searching for the known forward (21nt) primer sequence, with the results generated searched again for the known reverse (19nt) primer sequence. The results generated from this step were loaded into a Microsoft SQL server database (<https://www.microsoft.com/en-GB/sql-server/sql-server-downloads>), and using structured query language (SQL), searched through all the text-containing rows for sequences 70 characters long beginning and ending with the known forward and reverse primer sequences. A common approach to select sequences for further characterisation is to predict thermodynamic stability to generate Gibbs free energy ( $\Delta G$ ) values of both folded DNA and secondary DNA structure, and use these to screen potential HPV aptamer candidates (Sabri *et al.*, 2018, Navien *et al.*, 2021). Therefore, for each HPV aptamer sequence,  $\Delta G$  values were predicted by the DINAMelt server-QuickFold web server (<http://www.unafold.org/Dinamelt/applications/quickfold.php>) and vetted, with anything above  $\Delta G = -20$  kcal/mol omitted (Markham and Zuker, 2005). The top ten lowest  $\Delta G$  values were chosen as candidates for further scrutiny (Table 9), as these were predicted to be the most thermodynamically stable structures, with the observed variation in  $\Delta G$  due to the differences in GC content as well as presence of Watson-Crick base-pairing (Navien *et al.*, 2021).

Subsequently, the top ten aptamer candidate sequences for each HPV protein target were inputted into mFold (<http://www.unafold.org/mfold/applications/dna-folding-form.php>), to predict secondary DNA structure, followed by RNAComposer (<http://rnacomposer.ibch.poznan.pl/>), to predict their tertiary structures (Zuker, 2003, Popena *et al.*, 2012). There are few tertiary DNA structure prediction models compared to those available for RNA (Navien *et al.*, 2021); RNAComposer can also be used to predict tertiary DNA structure by generating a tertiary RNA structure and transforming it back to a tertiary DNA structure using programmes such as PyMOL (<https://pymol.org/2/>) (Schrödinger LLC, 2015, Sabri *et al.*, 2019, Wang *et al.*, 2019b, Yarizadeh *et al.*, 2019). It has been demonstrated previously that the folding of RNA and DNA is very similar, validating the use of RNA modelling servers for DNA purposes, with experiments performed *in silico* demonstrating that structural conversion between RNA and DNA resulted in virtually identical hairpin structures

(Zuker, 2003, Wang and Brown, 2006, Jeddi and Saiz, 2017). This is the approach that we took.

The structures generated by RNAComposer were saved as Protein Data Bank (PDB) files and underwent mutagenesis in PyMOL, whereby Uracil (U) residues were converted to Thymine (T) residues, and the ribose sugar backbone was converted to a deoxyribose sugar backbone. The methodology for changing backbone components is comprehensively detailed in Section 2.7.4. The top ten aptamer candidate sequences for each HPV protein target (40 structures in total), were saved as PDB files for docking experiments. After structure correction, three aptamer candidates were chosen for each HPV protein target (Figure 46), which were used for subsequent fixed docking experiments and computational modelling, with the methodologies used detailed in Sections 2.7.5 and 2.7.6. Across the three sequence candidates of each HPV protein target, we observed similar binding motifs, including hairpin, bulge, and internal loops. The presence of loops may provide flexibility to the structure, allowing it to interact in a variety of ways with the target protein (Hayashi *et al.*, 2014, Musafia *et al.*, 2014). The other seven secondary DNA structures for each HPV protein target are detailed in Appendix 15.

Table 9: HPV aptamer candidate sequences selected through lowest  $\Delta G$  value

*Content removed for copyright purposes*



*Content removed for copyright purposes*

**Figure 46: Secondary DNA structures of three aptamer candidates chosen from the top ten sequence candidates based on  $\Delta G$  predicted by mFold for each HPV protein target.**

Energy rules: DNA sequence: linear; folding temp; 4°C; ionic conditions:  $[\text{Na}^+] = 1 \text{ M}$ ,  $[\text{Mg}^{++}] = 0 \text{ M}$ ; Percent suboptimality: 5; Foldings: 1; Maximum distance between paired bases: no limit.

### 5.2.3 Fixed docking data and computational modelling

Fixed docking experiments using ZDOCK server (<https://zdock.umassmed.edu/>) were further used to determine predicted polar contacts, such as hydrogen bonds, electrostatic interactions, and Van der Waals forces, as well as the physicochemical properties of amino acid (AA) residues and DNA nt, where both the protein and ligand bond angles and atomic positioning were fixed (Nabuurs *et al.*, 2007, Meng *et al.*, 2011, Pierce *et al.*, 2014). The criteria for selection for the docking experiments was based on the thermodynamic stability and the nature of free hydrogen bonds formed, which would determine how the ssDNA would fold in on itself, as well as the presence of any binding motifs (SantaLucia and Hicks, 2004, Liang *et al.*, 2006). The ZDOCK score generated from fixed docking is based on a combination of these factors as well as the conditions that were specified during the experiment (Nguyen *et al.*, 2013).

PDB files of each of the respective HPV proteins (HPV-16 E2, HPV-16 E6, HPV-18 E6, and HPV-18 E7), their natural ligands (Bromodomain protein 4 (Brd4), p53, and retinoblastoma protein (pRb)), and the control ligand 4TS2 structures, were downloaded from (<https://www.rcsb.org/>) with PDB file names and modifications made described in Section 2.7.5 Table 6 (Berman *et al.*, 2000). The methodologies for fixed docking and computational modelling are comprehensively detailed in Sections 2.7.5 and 2.7.6. Briefly, the top prediction for each natural ligand and the control ligand 4TS2, and the top three predictions of the three aptamer candidates per respective HPV protein target were opened in PyMOL. In total, 80 predictions underwent computational modelling; each sequence/object as well as any interactions were colour coded for interactions between each HPV protein, their natural ligands, the control ligand 4TS2, and their three aptamer candidates per respective HPV protein target.

For each docking experiment, the ZDOCK score, polar contacts observed, number and length of polar contacts, and how it interacted with the corresponding HPV protein were recorded. For each HPV protein and their natural ligand, the ZDOCK score, and polar contacts generated for both the first and second fixed docking experiments were identical; therefore, these data for the second experiment are not included in Appendices 16-19. Similarly, the first and second fixed docking experiments yielded similar ZDOCK scores and polar contacts for the docking of the HPV proteins with

each of the three aptamer candidates per respective HPV protein target. A summary of the ZDOCK Score and nature and length of polar contacts for the natural ligands, the control ligand 4TS2, and the final candidate sequence for each HPV aptamer are provided in Table 10. The final (selected) HPV aptamer candidates are HPV-16 E2 Sequence 324, HPV-16 E7-E6 Sequence 3271, HPV-18 E6 Sequence 2720, and HPV-18 E7 5772 (Table 11 and Figure 47). The observed polar contacts and how the aptamer interacted with the corresponding HPV protein for complex one for each of the final (selected) HPV aptamer candidates are fully detailed below in Section 5.2.4. However, details of each interaction for the other two aptamer complexes examined can be found in Appendix 20.

**Table 10: Final HPV aptamer candidates selected based on ZDOCK Score and number and length of polar contacts**



*Content removed for copyright purposes*

**Figure 47: Computational modelling of HPV proteins with natural ligands, the control ligand 4TS2, and their corresponding HPV aptamer candidates.**

HPV proteins docked with their natural ligands to determine binding sites, which were used for aptamer docking. 4TS2 was also docked with each HPV protein, demonstrating binding that did not correspond to natural ligand binding. HPV proteins-deep teal; E6AP-hot pink; ligand (natural, 4TS2 and HPV aptamers)-orange; Adenine-red; Guanine-Blue; Thymine/Uracil-cyan; Cytosine-forest green; AA-nucleotide interaction-magenta; AA-AA interaction via polar bond (HPV protein and natural ligand only)-chartreuse; AA-AA interaction via peptide bond-white; nucleotide-nucleotide interaction via phosphodiester bond (excluding nucleotides that have other interactions)-light blue; polar contact-warm pink. Images captured using PyMOL.

#### **5.2.4 Identification of HPV aptamer candidates based upon nature of the observed interactions**

The final (selected) candidate sequence for each HPV aptamer was chosen from the ZDOCK Score, polar contacts observed, nature and length of polar contacts, and how the aptamer interacted with the corresponding HPV protein (Table 10). The observed polar contacts for complex one of the final (selected) HPV aptamer candidate are fully detailed below. However, details of each interaction for complex 2 and 3 for each HPV aptamer examined can be found in Appendix 20. Please note that, the AA residues for HPV-16 E2 (UniPROT ID P03120), HPV-16 E6 (UniPROT ID P03126) and HPV-18 E6 (UniPROT ID P06463) proteins have two numbers; the first corresponds to the AA residue number denoted within the sequence in PyMOL, and the second (in brackets) corresponds to the AA residue number denoted within their sequence in UniPROT (<https://www.uniprot.org/>) (The UniProt Consortium, 2022).

##### **5.2.4.1 HPV-16 E2**

Brd4 predicted two polar contacts at AA residues lysine (Lys) 290 (292) and tryptophan (Trp) 319 (321) of the HPV-16 E2 protein only. In contrast, docking predicted eight polar contacts between the HPV-16 E2 aptamer sequence 324 and HPV-16 E2 protein in complex one. Predictions were predominantly observed between the side chains of polar AA residues of HPV-16 E2 protein, including tyrosine (Tyr) 301 (303), Tyr310 (312), serine (Ser) 314 (316), threonine (Thr) 332 (334) and Thr334 (336). Interactions predicted included the hydroxyl group of Tyr301 (303) (interacted twice), and Tyr310 (312) (Tyr OH), Ser314 (316) (Ser OG) and Thr332 (334) and Thr334 (336) (Thr OG1) side chains, forming polar contacts with an oxygen atom (O4', O3', or OP1) within the phosphate backbone of the aptamer. Other predicted interactions included the non-polar AA residue amine group of Trp317 (319) (Trp NE1) side chain, forming a polar contact with an oxygen atom (O3') in the phosphate backbone of the aptamer, whereas with the polar AA residues; hydroxyl group of Tyr301 (303) (Tyr OH) side chain and oxygen atom (O) within the protein backbone of Ser362 (364), each formed a polar contact with a nitrogen atom (N3 or N2), within the nucleotide base of the aptamer.

Brd4 is only 22 AA residues, therefore it would be anticipated that Brd4 would have few interactions with HPV-16 E2 protein. The control ligand 4TS2, formed six polar

contacts with HPV-16 E2 protein, with two AA residues (Thr332 and Ser362) the same AA residues that HPV-16 E2 aptamer 324 interacted with in HPV-16 E2 protein. As only two interactions are the same, this shows that the control ligand 4TS2 does have some specificity for HPV-16 E2 protein.

#### **5.2.4.2 HPV-16 E6 and HPV-16 E7-E6**

The natural ligand p53 was docked and formation of five polar contacts at AA residues Ser82 (89), glutamine (Gln) 91 (98), Tyr92 (99), glycine (Gly) 130 (137) and glutamate (Glu) 148 (155) with HPV-16 E6 protein were predicted. Docking of HPV-16 E7-E6 aptamer sequence 3271 with HPV-16 E6 protein complex one predicted 14 polar contacts. All polar contacts except one involved the side chain of each AA residue of HPV-16 E6. Two recurrent predicted interactions occurred, involving the hydroxyl groups and amine groups of side chains in polar AA residues. The hydroxyl group of Ser80 (87) (Ser OG), and Tyr81 (88) (Tyr OH) side chains each formed a polar contacts with an oxygen atom (O2) or nitrogen atom (N1 or N3), within the nucleotide base of the aptamer. The hydroxyl group of AA residue Tyr84 (91) (Tyr OH) side chain formed two polar contacts with an oxygen atom (OP2 or O5') within the nucleotide base of the aptamer. Gln6 (13) (Gln NE2) (interacted twice) and asparagine (Asn) 127 (134) (Asn ND2) side chains, as well as the basic AA residue arginine (Arg) 124 (131) (Arg NH2) side chain formed polar contacts with an oxygen atom (O2 or O6) or nitrogen atom (N3) within the nucleotide base of the aptamer. The amine group of Asn93 (100) (Asn ND2) side chain also formed an polar contact with an oxygen atom (O3'), within the nucleotide base of the aptamer. Other interactions observed included basic AA residues, where the ammonium ion of Lys94 (101) (NZ) side chain and nitrogen atom (N) of protein backbone of Arg124 (131) each formed a polar contact with an oxygen atom (O3' or OP2) of the phosphate backbone of the aptamer. The acidic AA residue, Glu148 (135) formed three polar contacts, twice with its oxygen atoms (Glu OE1) and once with its oxygen ion (Glu OE2) that are present within the side chain, with a nitrogen atom (N1 or N6) within the nucleotide base of the aptamer.

HPV-16 E6 aptamer sequence 3271 has a similar binding motif to that predicted between HPV-16 E6 protein and p53, with polar contacts observed at Try92 (99) and Glu148 (155), suggesting that these AA residues are important for binding. The control ligand 4TS2, formed 21 polar contacts with HPV-16 E7-E6 protein. Five AA HPV16 E6

residues (Ser80, Tyr81 twice, Tyr92, Lys94, Asn127) formed polar contacts with 4TS2; these same AA residues are seen in HPV-16 E6, when interacting with HPV-16 E7-E6 aptamer sequence 3721. This suggests that these AA residues within HPV-16 E6 are important for binding, as well as showing that the control ligand 4TS2, does have some specificity for HPV-16 E6 protein.

#### **5.2.4.3 HPV-18 E6**

For HPV-18 E6 aptamer sequence 2720, the natural ligand p53 was predicted to form six polar contacts with HPV-18 E6 protein, at the AA residues proline (Pro) 1007 (x2), Tyr1012, Lys1092, leucine (Leu) 1098 and Gly1132 of HPV-18 E6 protein. HPV-18 E6 aptamer sequence 2720 and HPV-18 E6 protein complex one predicted eight polar contacts. All polar contacts, except Leu1102 (102), involved the side chain of each AA residue of HPV-18 E6, with hydroxyl groups and polar AA residues featuring heavily. The hydroxyl group of polar AA residues Tyr1012 (12) and Tyr1134 (134) (Tyr OH), Ser1082 (82) (Ser OG), and Thr1096 (96) (Thr OG1) (interacted twice) side chains formed an polar contacts with an oxygen atom (O3', OP1, or OP2) within the phosphate backbone of the aptamer. Additionally, the oxygen atom of Asn1100 (100) (Asn OD1) and ammonium ion of Lys1110 (110) (Lys NZ) polar side chains, formed a polar contact with a nitrogen atom (N2) within the nucleotide base or an oxygen atom (OP1) within the phosphate backbone of the aptamer. Polar interactions were also predicted through non-polar AA residue Leu1102 (102) nitrogen atom (N) within the protein backbone of HPV-18 E6, which interacted with an oxygen atom (O4') within the phosphate backbone of the aptamer. This demonstrated that HPV18 E6 aptamer 2730 has a similar binding motif to that predicted between HPV-18 E6 protein and p53.

Ten polar contacts were predicted between the control ligand 4TS2, and HPV-18 E6 protein, with two interactions observed in one AA residue (Asn1100), which was also observed in HPV-18 E6 protein, when interacting with HPV-18 E6 aptamer sequence 2730. This suggests that these AA residues with HPV-16 E6 are important for binding, as well as showing that the control ligand 4TS2, does have some specificity for HPV-18 E6 protein.



#### 5.2.4.4 HPV-18 E7

The natural ligand pRb was predicted to form three polar contacts with HPV-18 E7 protein at AA residues Ser95, Trp100 and Ser103. Docking of HPV-18 E7 sequence 5772 with HPV-18 E7 protein complex one predicted 15 polar contacts, predominantly between the side chains of polar AA residues. The hydroxyl group of polar AA residues Thr93 (Thr OG1) side chain, which formed a polar contacts with an oxygen atom (OP1) within the phosphate backbone of the aptamer, and Ser95 and Ser103 (Ser OG) (both interacted twice) side chains, which formed polar contacts, with an oxygen atom (O4) or nitrogen atom (N4, N6, or N7) within the nucleotide base of the aptamer. Polar contacts were also predicted through the ammonium ion and nitrenium ion of basic AA residues, Lys67 (Lys NZ) and Arg71 (Arg NH1) side chains respectively, formed a polar contact with an oxygen atom (O5' or O3') within the phosphate backbone of the aptamer. The amine group of the non-polar AA residue Trp100 (Trp NH) side chain predicted a polar contact with an oxygen atom (O5') within the phosphate backbone of the aptamer. Polar contacts were predicted with the oxygen atom (O) of polar AA residues Thr93 and Ser95 (predicted twice) within their protein backbones interacting with a nitrogen atom (N4) within the nucleotide base of the aptamer. Lastly, the nitrogen atom (N) of acidic AA residue Glu69 and non-polar AA residues valine (Val) 97 and Trp100 within their protein backbones formed polar contacts with oxygen atoms (OP2 or O4) within the nucleotide base and phosphate backbone of the aptamer, whereas the oxygen atom (O) of alanine (Ala) 102 protein backbone, formed a polar contact with a nitrogen atom (N4) within the nucleotide base of the aptamer. This demonstrated that HPV-18 E7 aptamer 5772 has a similar binding motif to that predicted for pRb.

Six polar contacts were formed between the control ligand 4TS2, and HPV-18 E7 protein, with four AA residues (Lys67, Thr93, Ser95 and Val97) the same as those involved in HPV-18 E7 protein, when interacting with HPV-18 E7 aptamer sequence 5772. This suggests that these AA residues within HPV-18 E7 are important for binding purposes, as well as showing that the control ligand 4TS2, does have some specificity for HPV-18 E7 protein.

Common themes were observed between each of the HPV proteins and the respective HPV aptamer candidates with both polar AA residues and hydroxyl groups within AA

residue side chains of the HPV proteins forming polar contacts with a nt within the HPV aptamer candidates. However, while there were similarities regarding the position of the two molecules in all the complexes, the specific interacting residues varies between complexes.

### **5.2.5 Alexa Fluor™ 488 fluorophore integration into HPV aptamers**

Selected aptamer candidates (summarised in Table 11) were fluorescently labelled via the use of a 5' Alexa Fluor™ 488 fluorophore conjugated on to the original forward primer sequence (Shigdar *et al.*, 2016). Successful integration of the fluorophore was shown by gel electrophoresis (Figure 48).

### **5.2.6 Binding assays of HPV antibodies and aptamers**

Binding assays were performed to determine the binding affinity of both HPV aptamers and HPV antibodies by measuring fluorescence intensity. Each of the plates were prepared as detailed in Section 2.5.1.

No significant differences in absorbance were seen between all HPV aptamers and their respective antibody counterparts (Figures 49 and 50), suggesting the aptamers are comparable with respect to affinity to the commercially-available antibodies. However, while there was no significant difference between the binding of either the HPV-16 E2 antibody or the aptamer, there was a decrease in absorbance. No significant difference in affinity was observed concerning the negative antibody and aptamers (Figure 51). Conversely, the binding affinities for the negative aptamers and negative antibody to the HPV target protein were not significantly different from each other as the concentration decreased across the positive plates (Figures 49 and 50). P-value >0.05 determined by Two-Way ANOVA. Again, the average absorbance (fluorescence) did not decrease across the plate as would be expected due to the serial dilution, suggesting that the initial starting concentration was too high. However, low binding affinities would be expected as they are negative controls, suggesting that there is non-specific binding present.

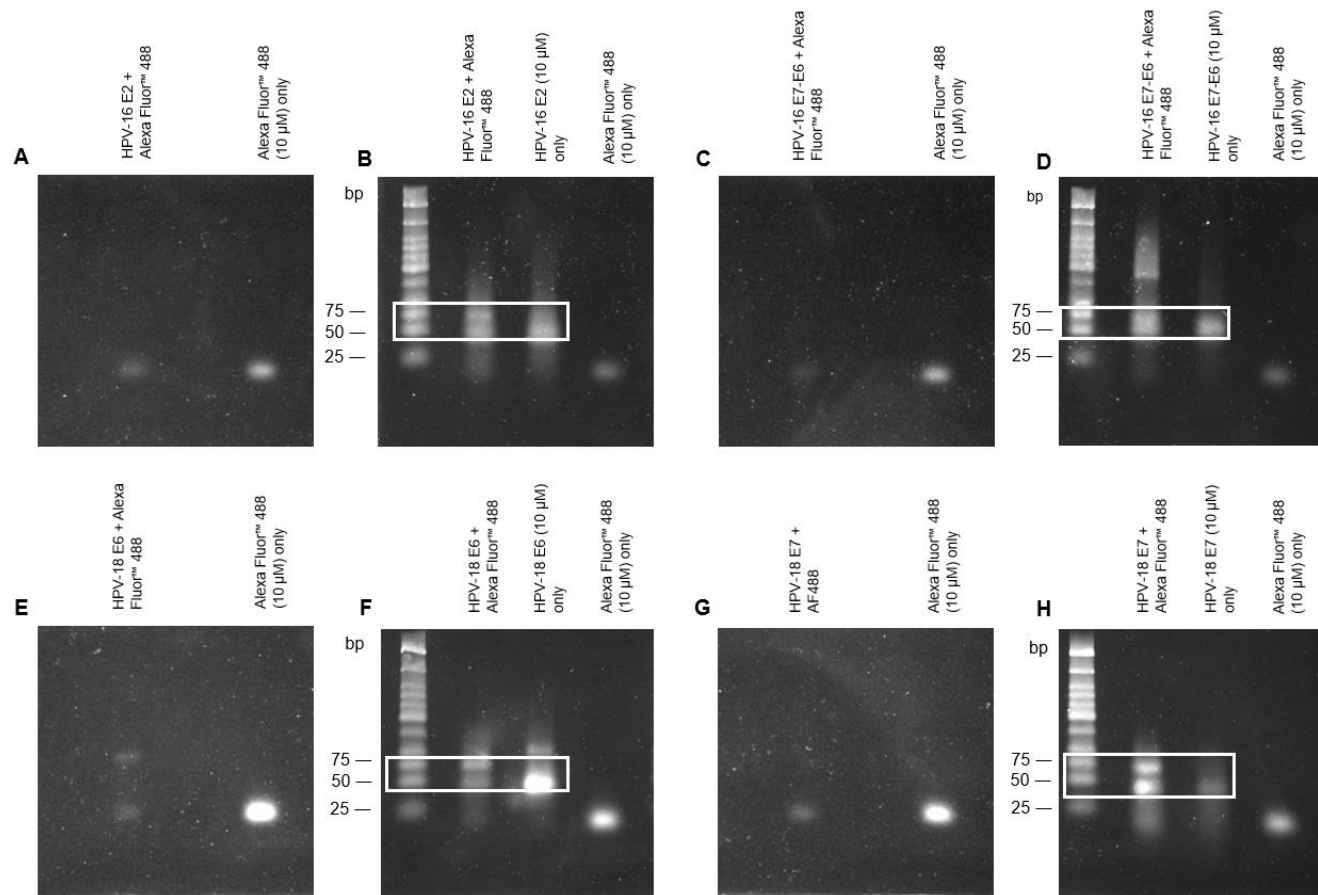


**Figure 48: Confirmation agarose gels of HPV-16 E2, HPV-16 E7-E6, HPV-18 E6, and HPV-18 E7 aptamers with integrated Alexa Fluor™ 488.**

All aptamer with integrated Alexa Fluor™ 488 and Alexa Fluor™ 488 only were visualised under the Alexa Fluor™ 488 filter of the ChemiDoc™ XRS+ Molecular Imager®, which showed that integration was successful and no autofluorescence was present (**A, C, E and G**). The same gels were post-stained in GelRed® for 30 minutes before visualising under the GelRed filter. The molecular ladder became visible, as did all the aptamers only (**B, D, F and H**). Bands at 70 bp and 50 bp were observed for all aptamers with Alexa Fluor™ 488 and all of the aptamers only, with smearing due to misfolding during separation. Bands at 25 bp and below were indicative of primer dimers. Images captured on Image Lab™ Software.

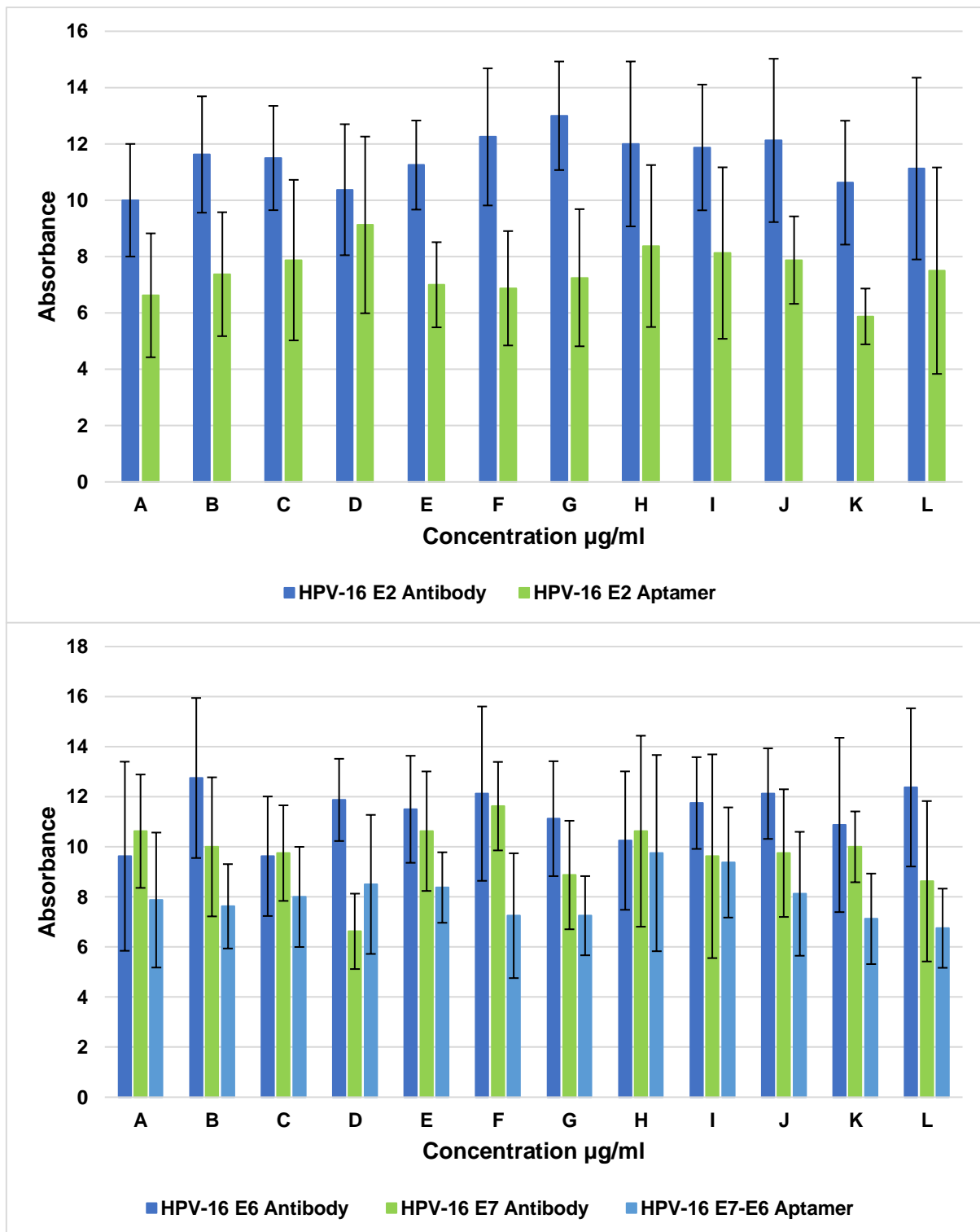


**Figure 49: Binding affinities of positive HPV-16 E2 and HPV-16 E7-E6 antibody and aptamer plates.**

Variable absorbances were observed across the positive HPV-16 E2 and HPV-16 E7-E6 antibody and aptamer plates. There was no significant difference between the binding of the antibody or aptamers,  $P > 0.05$ , determined by two-way ANOVA; however, it appeared that the results were comparable between the antibodies and aptamer for both HPV-16 E6, HPV-16 E7 and HPV16 E7-E6. Data shown are mean  $\pm$  standard deviation.

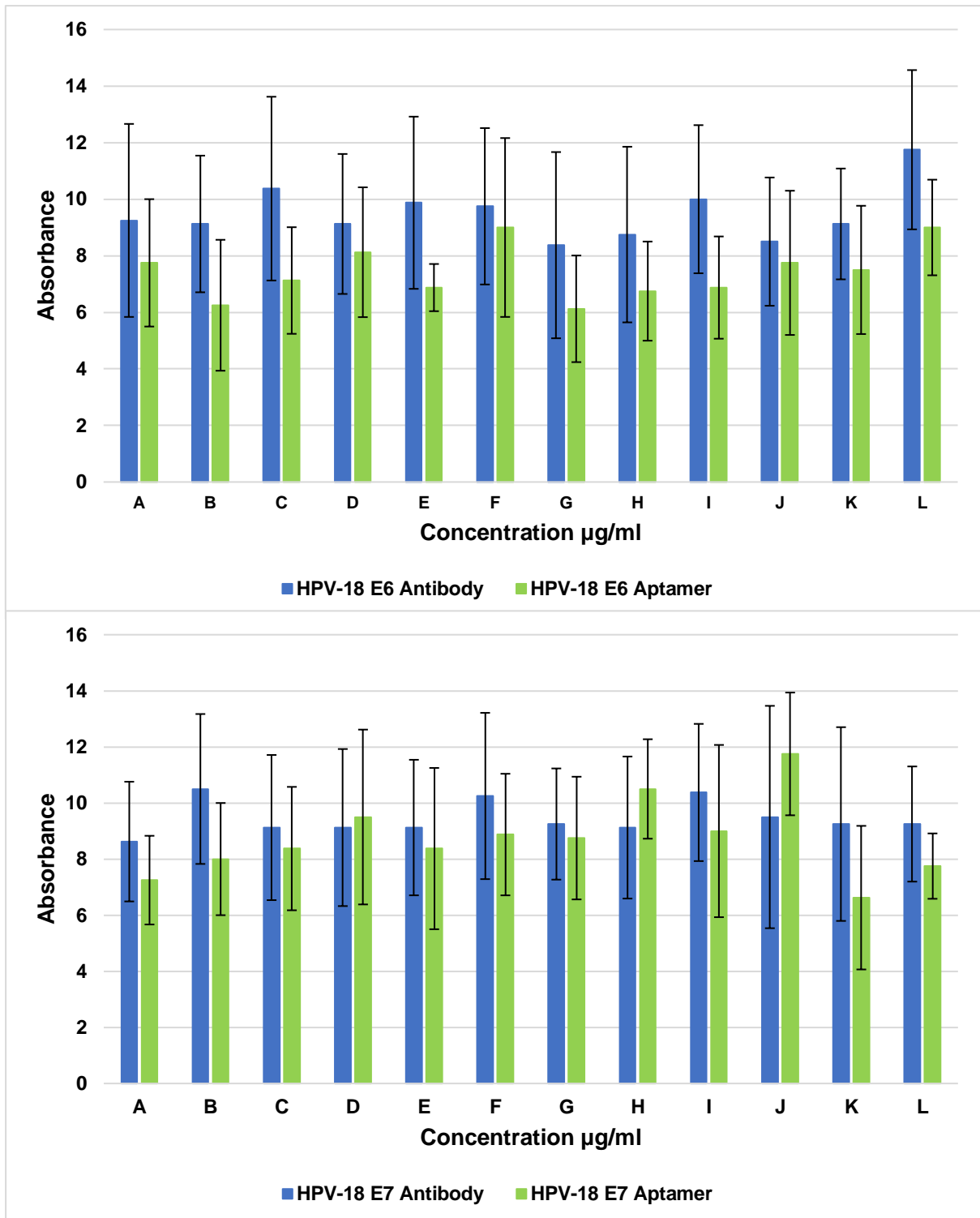


**Figure 50: Binding affinities of the positive HPV-18 E6 and HPV-18 E7 antibody and aptamer plates.**

Variable absorbances were observed across the positive HPV-18 E6 and HPV-18 E7 antibody and aptamer plates. There was no significant difference between the binding of the antibody or aptamers,  $P > 0.05$ , determined by two-way ANOVA; however, it appeared that the results were comparable between the antibody and aptamer for both HPV-18 E6 and HPV-18 E7. Data shown are mean  $\pm$  standard deviation.

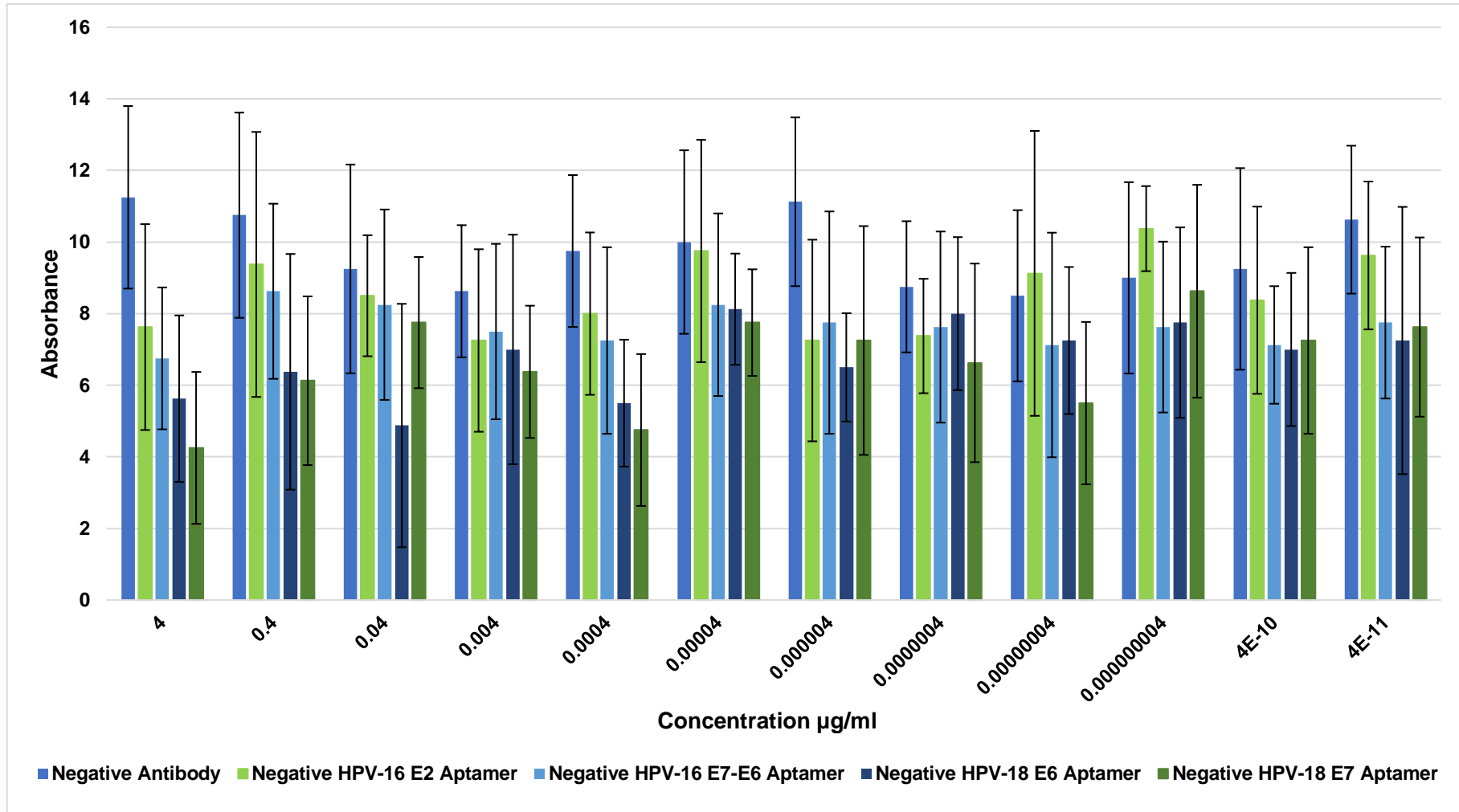


**Figure 51: Binding affinities of negative antibody and aptamer plates.**

Variable absorbances were observed across the negative plates. There was no significant difference between the binding of the antibody or aptamers,  $P > 0.05$ , determined by two-way ANOVA; however, it appeared that the results were comparable between the negative antibody and aptamers. Data shown are mean  $\pm$  standard deviation.

### 5.2.7 Cell immunofluorescence using HPV antibodies and aptamers

Relevant cell lines were stained with HPV antibodies and HPV aptamers to examine whether the aptamer bound with its target protein *in vitro*. The HPV-16-positive cell lines SiHa (CC) and SCC-147T (OPSCC) were stained with the HPV-16 antibodies and aptamers, whereas the HPV-18-positive HeLa (CC) cell line was used for the HPV-18 antibodies and aptamer. The breast carcinoma cell line MCF7 and OPSCC line SCC-040T are HPV-negative and used as controls.

The HPV antibodies showed a lot of background staining around the cells (Figures 52 and 53), indicating non-specific staining. The secondary-only antibody also exhibited significant levels background staining (Figures 52 and 53). Similarly, intracellular positive staining of the antibodies largely appeared to be endosomal and cytoplasmic, and not nuclear, despite the nuclear localisation of HPV E6 and E7 proteins (Lee *et al.*, 2007, Knapp *et al.*, 2009, Singh *et al.*, 2021). The only HPV antibody that looked somewhat promising was HPV-16 E6 within the SiHa cells. Surprisingly, we did not find a positive signal for HPV-18 E7 within HeLa cells, despite the suggestion of some HPV-18 E6 staining in the same cells. Together, this corroborates our earlier data that the commercially-available HPV antibodies are not suitable for IF within tissues, and now cells, and supports our proposal for alternative markers.

All positive HPV aptamers were negative within the HPV-negative MCF7 cell line, suggesting minimal non-specific binding (Figures 54 and 55). Nuclear body and endosomal staining was observed with HPV-16 E7-E6 within the SiHa and SCC-147T cells lines, and with HPV-18 E6 and HPV-18 E7 within the HeLa cell line, with some staining of nuclear bodies and endosomes observed within the HPV-negative SCC-040T cells. Negative HPV aptamers appeared to show positive staining within in each cell line (Figures 54 and 55); however, as these represent the non-bound aptamer library sequences from the selection process, each will contain a pool of sequences that has the potential to bind to anything within the cell.

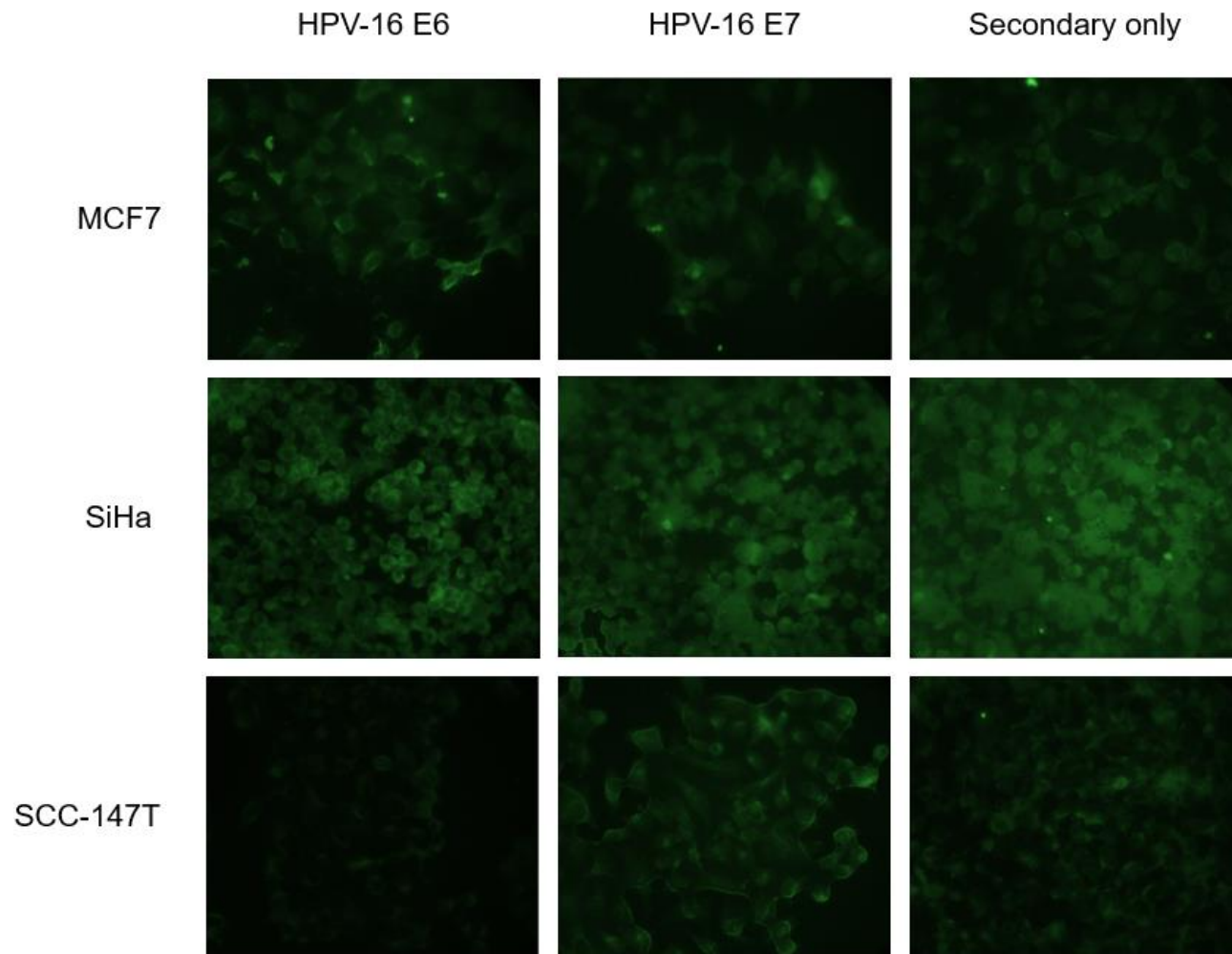


**Figure 52: MCF7, SiHa, and SCC-040T cell lines stained with HPV-16 E6, HPV16-E7, and secondary-only antibodies.**

Considerable non-specific staining was present with each of the HPV-16 antibodies and secondary-only antibody in each of the cell lines. Additionally, positive staining observed was endosomal and cytoplasmic. Images captured on NIS-Elements AR imaging software at 60x magnification.



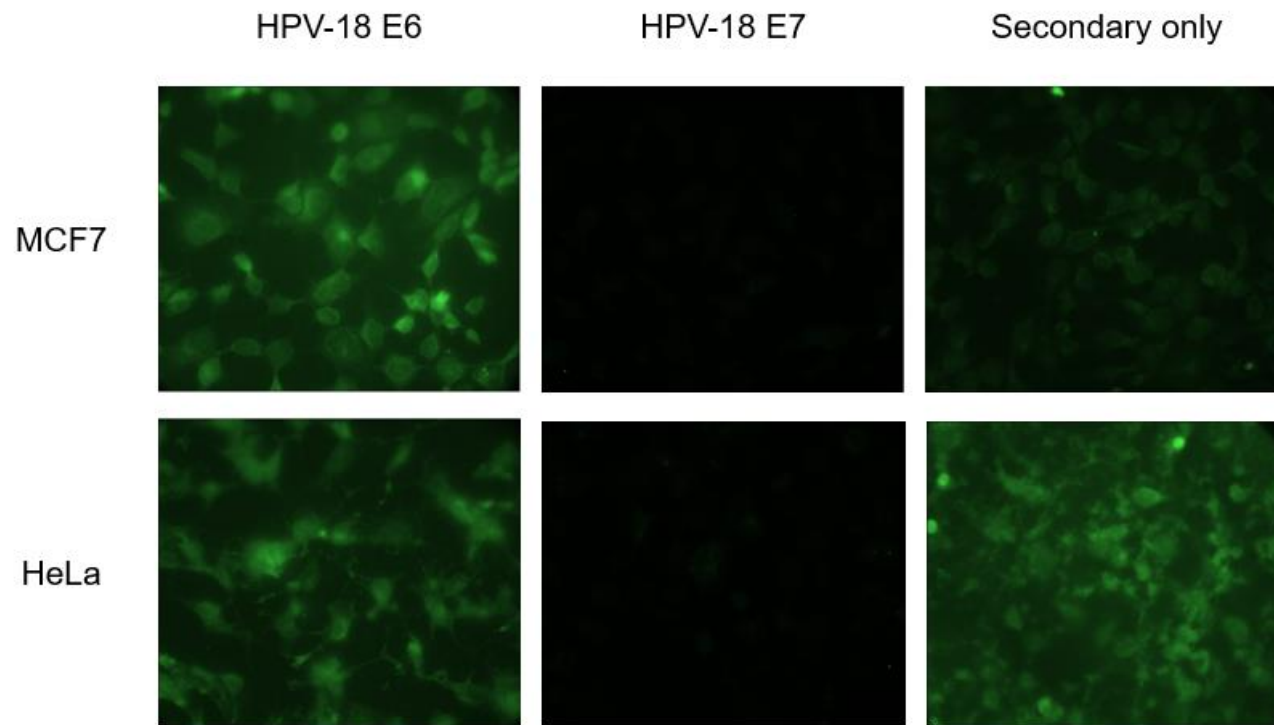


**Figure 53: MCF7 and HeLa cell lines stained with HPV-18 E6, HPV-18 E7, and secondary-only antibodies.**

Considerable non-specific staining was present with each of the HPV-18 antibodies and secondary-only antibody in each of the cell lines. Additionally, positive staining was endosomal and cytoplasmic. Images captured on NIS-Elements AR imaging software at 60x magnification.

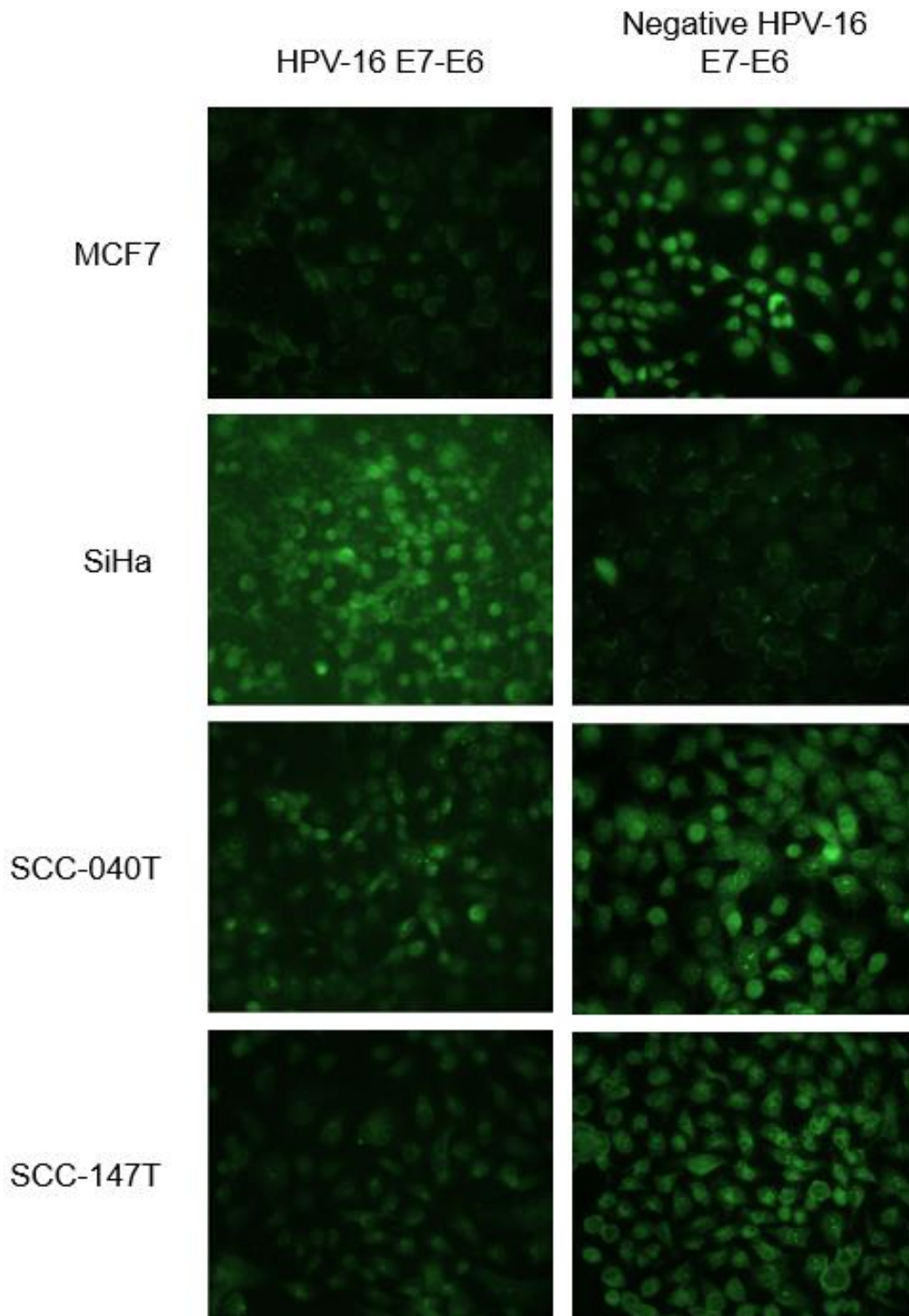


**Figure 54: MCF7, SiHa, SCC-040T, and SCC-147T cell lines stained with positive HPV-16 E7-E6, and negative HPV-16 E7-E6 aptamers.**

HPV-16 E7-E6 aptamer was negative within the MCF7 cells, with some nuclear body and endosomal staining observed within the SiHa and SCC-147T cells. Additionally, it appears that there is some staining of nuclear bodies and endosomes within the HPV-negative SCC-040T cells. Positive staining was observed within the negative aptamer. Images captured on NIS-Elements AR imaging software at 60x magnification.

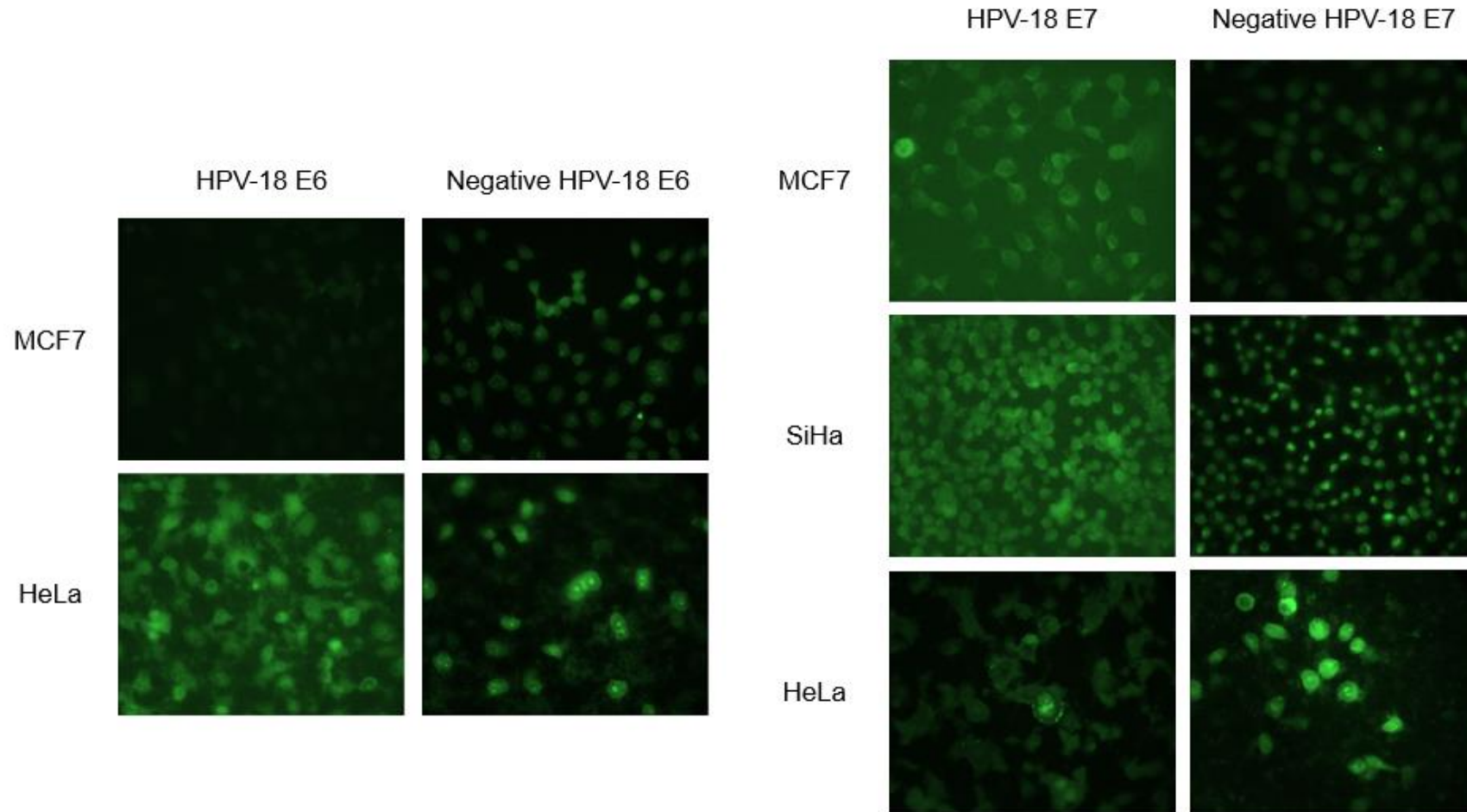


**Figure 55: MCF7, SiHa, and HeLa cell lines stained with positive HPV-18 E6, HPV-18 E7, and negative HPV-18 E6 and HPV-18 E7 aptamers.** HPV-18 E6 and E7 aptamer were negative within the MCF7 cells, with some positive nuclear body and endosomal staining observed within the HeLa cells. Additionally, SiHa cells were negative for HPV-18 E7 aptamer. Positive staining was observed with the negative aptamer in all cell types. Images captured on NIS-Elements AR imaging software at 60x magnification.

### 5.3 Conclusion

All four HPV aptamer pools underwent successful selection by SELEX and were subsequently sequenced. Candidate selection and validation through molecular docking, computational modelling, binding assays, and immunofluorescent microscopy are discussed below.

Molecular docking is based on predicting intermolecular forces such as Van der Waals forces, hydrogen bonds, and electrostatic interactions, as well as the physicochemical properties of AA residues and nt (Meng *et al.*, 2011). The ZDOCK score generated from molecular docking is based on a combination of these factors as well as the conditions that were specified during the experiment (Nguyen *et al.*, 2013). The interactions are predictions only; however, they can be argued based on known interactions between AA residues and nucleotides.

The polar contacts observed included the protein side-chains and protein backbone within the AA residues interacting with either the nucleotide base edge or phosphate backbone within the aptamers (Mandel-Gutfreund *et al.*, 1995). These were predominantly hydrogen bonds, where atoms acted as H-bond donors (O-H $\cdots$ X and N-H $\cdots$ X), with X being either an O or N atom, which acted as a H-bond acceptor (Kono and Sarai, 1999, Park *et al.*, 2014, Deepak and Sankararamakrishnan, 2016). Within all four final HPV aptamer candidate complexes, there were three AA residues that were consistently involved in some capacity; Thr, Ser and Tyr, which are tangible within the literature. Thr interacts predominantly with the phosphate backbone of the aptamers, which was observed within five out of the six polar contacts seen in all the HPV aptamers (Kono and Sarai, 1999, Luscombe *et al.*, 2001). As polar AA residues, Thr and Ser, make a large number of hydrogen bonds (Luscombe *et al.*, 2001). Highly conserved Ser residues were observed in DNA binding domains (DBD) of *Arabidopsis thaliana* basic domain-containing leucine-zipper (bZIP) transcription factors interacting with DNA, specifically through their side chains, which was also observed within our HPV aptamer structures in seven out of ten interactions (Kirchler *et al.*, 2010). Ser residues are also observed within 35% of DBDs of human bZIP transcription factors (Deppmann *et al.*, 2003). Additionally, highly conserved Tyr residues are also observed in the DBD of animal bZIP factors (Amoutzias *et al.*, 2006). Therefore,

suggesting that these are real interactions that have been demonstrated and observed within nature.

Interactions observed between the HPV proteins and respective HPV aptamers involved functional motifs/domains within the HPV protein structures. Within HPV-16 E2, interactions occurred at AA residues Tyr303, Tyr312, Ser316, Trp319, Thr334, Thr336, and Ser364. These are all located within 285-365 AA residues (UniPROT ID P03120) of the DNA-binding domain (DBD), which is essential for interacting with E1 protein (Hegde and Androphy, 1998, The UniProt Consortium, 2022). Additionally, interactions with HPV-16 E6 occurred at Arg131 and Asn134, which are within the 110-146 AA residues (UniPROT ID P03126) that make up the zinc-finger motif of HPV-16 E6, located near the C-terminus (Zanier *et al.*, 2012, The UniProt Consortium, 2022). Interestingly, interactions also occurred at AA residues Ser87, Tyr88, Tyr91, Tyr99, Asn100, and Lys101 located between the two zinc-finger motifs of HPV-16 E6, which together with the linker helix form a hydrophobic pocket. This motif is used to recruit E6-associated protein (E6AP), and subsequently, p53 (Zanier *et al.*, 2013, The UniProt Consortium, 2022). This is similar in HPV-18 E6, where interactions occurred at AA residues Lys110 and Tyr134, which are located within the C-terminus zinc-finger motif (105-141 AA) (UniPROT ID P06463), and Ser82, Thr96, Asn100, and Leu102, which are situated between two zinc-finger motifs of HPV-18 E6 (Zanier *et al.*, 2013, The UniProt Consortium, 2022). Again, this is a hydrophobic pocket that recruits E6AP, and subsequently, p53 (Zanier *et al.*, 2013). Lastly, interactions occurred at AA residues Lys67, Glu69, Arg71, Thr93, Ser95, Val97, and Trp100 of HPV-18 E7, which are within the zinc-finger motif (65-101 AA) located near the C-terminus (UniPROT ID P06788) (Liu *et al.*, 2006, The UniProt Consortium, 2022). The zinc-finger motif is within the CR3, a region which is necessary for interacting with the C-terminal of pRb (Patrick *et al.*, 1994, Liu *et al.*, 2006, Aarthy *et al.*, 2018). Observing these predictions within functional motifs/domains demonstrates that they have been observed in nature, suggesting that these interactions are real.

With each docked HPV protein, the most common observations between aptamer and natural ligand were that both polar AA residues and hydroxyl groups within AA residue side chains were the most likely to form polar contacts with a nucleotide within each HPV aptamer. Similarities in binding motifs between all three structures and their

corresponding natural ligands suggests these are important for binding in both scenarios. The presence of loops within the chosen structures for each HPV aptamer provide structural flexibility. This flexibility, combined with the smaller size allows binding to protein regions without causing conformational changes, something which larger structures such as antibodies cannot achieve (Gelinas *et al.*, 2016, Autiero *et al.*, 2018). This was demonstrated previously, with an RNA aptamer binding to S8 ribosomal proteins, where the aptamer was shown to change its structure but also improve its binding efficiency (Autiero *et al.*, 2018). The structural motifs not only provide flexibility to the aptamer, but they also have unique binding properties, allowing for aptamer-protein interactions.

In cell immunofluorescence, the HPV antibodies presented extensive non-specific staining, as well as a lot of background, as per our findings within tissues (Chapter 4). In comparison to the HPV antibodies, the HPV aptamers demonstrated minimal background staining. HPV-16 E7-E6, HPV-18 E6, and HPV-18 E7 aptamers demonstrated some staining of nuclear bodies and endosomes, which is consistent with the nuclear and endosomal localisation of HPV E6 and E7 proteins (Lee *et al.*, 2007, Knapp *et al.*, 2009, Cesur *et al.*, 2015, Ganti *et al.*, 2016, Singh *et al.*, 2021). HPV-16 E2 aptamer staining could not be shown within any of these cell lines; however, this was not surprising. E2 is an early protein whose expression is frequently lost in cancers due to integration to the host chromosome, and needs to be reviewed within cells with an early HPV-16 infection such as an S12 or W12 cell line (Lehman and Botchan, 1998, Bechtold *et al.*, 2003, Xue *et al.*, 2010), or artificially through transfection of HPV-16 E2 into a cell line such as HEK293.

The proposed next steps to take this work forward, would be to return to the final positive selection pool for each HPV aptamer and perform cell-SELEX. This would be run as a comparison on a non-specific cell line to help select out the non-HPV containing cell types. Additionally, if this work was successful, these would progress forward to be tested in tissues.

There has been advancement in aptamer development in recent years and through this work, we have managed to develop four potential HPV aptamer candidates, which have demonstrated similar binding affinity for the target molecules compared to their

respective HPV antibody proteins. Despite the molecular interactions described here being predictions only, the information gathered from molecular docking including the polar contacts observed, as well as the binding affinity, has been useful in determining the suitability of each of the sequences chosen for each HPV aptamer candidate. The data presented here, particularly when combined with the preliminary cellular immunofluorescence, is promising, suggesting a need for further development of the technology to refine the aptamer specificity, as the generated aptamers could be a viable alternative to antibody approaches moving forward.

## CHAPTER 6: DISCUSSION

The aims of this study were to characterise the histology of normal and cancerous palatine tonsil as HPV-mediated disease is not well understood within the oropharynx. We used normal and cancerous cervix as comparators, as HPV infection within the cervix has been well established. Additionally, prognostic biomarkers associated with OPSCC were characterised, including developing aptamers against various HPV proteins, which were to be tested and compared against commercially-available antibodies. OPSCCs were characterised morphologically using haematoxylin and eosin (H&E) staining and predictions made on HPV status based on H&E examination alone. Subsequently, HPV DNA *in-situ* hybridisation (ISH) was performed prior to staining with the NHS gold standard p16INK4A (p16) immunohistochemistry (IHC), to confirm our predictions. To characterise the tumours further, and permit comparisons to be made between HPV-positive and HPV-negative OPSCCs, we used IHC, immunofluorescence and developed multiplex immunofluorescence (mIF) techniques to examine the expression of eight disease-relevant biomarkers selected from the literature, which we had characterised in normal palatine tonsil tissue. Additionally, commercially-available HPV antibodies targeting E2, E6, and E7 proteins, were also tested to be used to determine the HPV subtype of HPV-positive OPSCCs. This work highlighted the complexity of HPV pathogenesis within the oropharynx; however, it also identified the inadequacy of HPV antibody staining within tissues. This presented the idea of using a novel approach for HPV protein detection by designing and developing aptamers, which if ultimately successful, could be used as an alternative to commercially-available antibodies in the future. The following chapter will discuss the current methodology used for OPSCC diagnosis, biomarkers associated with OPSCC, and aptamer development, and their potential impact with reference to the literature, limitations, and future work.

### 6.1 HPV testing within OPSCC

#### 6.1.1 The utilisation of p16 for determining HPV status

Determination of HPV status in OPSCC is important regarding staging of the disease. In 2017, major updates were made to the American Joint Committee on Cancer (AJCC) 8<sup>th</sup> edition (2017), which included separating OPSCC into two entities: HPV-



positive and HPV-negative, based on p16 positivity (Amin *et al.*, 2017). This has resulted in improved outcomes, with the new clinical and pathological staging systems demonstrating improved risk stratification and prognosis in patients with HPV-positive OPSCC (Gupta *et al.*, 2018). Since 2003, p16 IHC has been used as the surrogate marker for HPV status within cancers of the oropharynx (Klussman *et al.*, 2003). It is a validated prognostic marker used for testing HPV status within OPSCC (Klussman *et al.*, 2003, Sedghizadeh *et al.*, 2016, Lewis *et al.*, 2018b, Hunter *et al.*, 2021). Criterion for p16-positive IHC is based on the current College of American Pathologists (CAP) (2018) and The Royal College of Pathologists (RCPath) (2021) guidelines for moderate to intense nuclear and cytoplasmic staining in 70% or more of the tumour cells (Lewis *et al.*, 2018b, Hunter *et al.*, 2021). It has become the widely accepted diagnostic method, largely due to low cost, simplicity and feasibility (El-Naggar and Westra, 2012).

The World Health Organisation (WHO) Classification of Head and Neck Tumours 5<sup>th</sup> edition (2017) states that p16 alone is a suitable marker for HPV status, which is sensitive for transcriptionally-active high-risk (HR)-HPV (Lewis *et al.*, 2018b, World Health Organisation, 2024). In HR-HPV types, E7 proteins have a greater transformation potential than in low-risk (LR)-HPV. This is attributable to their ability to bind to retinoblastoma protein (pRb) with high affinity, ultimately resulting in its degradation and the subsequent overexpression of p16 (Scheffner *et al.*, 1992, Mooren *et al.*, 2014). However, this only seems to apply to HPV-positive non-keratinising squamous cell carcinomas (NKSCC) of the oropharynx as they are the most common morphological type of OPSCC (El-Mofty and Lu, 2003, El-Mofty and Patil, 2006, Chernock *et al.*, 2009, Gondim *et al.*, 2016). Indeed, HPV-positive OPSCCs with non-keratinising morphology have demonstrated 70-100% sensitivity of p16- and/or HPV-positivity (Chernock *et al.*, 2009, Gondim *et al.*, 2016, Lewis *et al.*, 2021, Shinn *et al.*, 2021). Due to this high sensitivity observed within such tumours, it has been further suggested that the morphology by H&E examination alone is enough of an indicator for p16-positivity, removing the need for IHC and offer a HPV status as part of the diagnosis (Chernock *et al.*, 2009, Lewis *et al.*, 2010). However, 12-26.2% of HPV-positive OPSCCs are keratinising SCC (KSCC) (Chernock *et al.*, 2009, Gondim *et al.*, 2016, Lewis, 2017, Lewis *et al.*, 2021, Shinn *et al.*, 2021), and would therefore be missed in such a diagnostic approach. Previously, it has been observed

that 20-35% of KSCC of the oropharynx are p16- and/or HPV-positive (Chernock *et al.*, 2009, Gondim *et al.*, 2016, Lewis *et al.*, 2021, Shinn *et al.*, 2021).

In Chapter Three, we showed that two OPSCCs used in this study overexpressed p16 via IHC despite demonstrating KSCC morphology, which is most-commonly associated with HPV-negative OPSCC (El-Mofty and Lu, 2003). Additionally, two other OPSCCs demonstrated NKSCC morphology; however, they were tumour-negative for p16, challenging the proposal from Chernock *et al.*, (2009), and Lewis *et al.*, (2021), that HPV status could be determined by morphology alone. Therefore, our observations raise concerns regarding determination of p16/HPV status based on morphology alone.

### **6.1.2 Discordance of p16 and HPV status**

One major caveat of p16 as a prognostic marker for HPV is that it does not fully correlate with HPV status, nor does it differentiate HPV subtype, unlike HR-HPV-specific tests (Singhi and Westra, 2010, Lewis *et al.*, 2012, Hong *et al.*, 2013). Overexpression of p16 may occur via HPV-independent mechanisms causing inactivation of pRb, such as gene deletion, mutation, or other mechanisms causing pRb pathway degradation (Smeets *et al.*, 2007, Rietbergen *et al.*, 2013, Sgaramella *et al.*, 2015). We showed that two OPSCCs had some small areas that were p16-positive within the surface epithelium, which appeared to be dysplastic. HPV-independent mechanisms that cause p16 overexpression may explain this positive staining observed as approximately 7.7% of p16-positive/HPV-negative OPSCCs have shown pRb loss (Holzinger *et al.*, 2013, Plath *et al.*, 2018). Surprisingly, p16 expression has also been observed in non-neoplastic palatine tonsils. A study performed p16 IHC on benign palatine tonsil tissue sections of 262 patients (Klingenberg *et al.*, 2010); overexpression of p16 was considered as moderate to strong nuclear and cytoplasmic staining in a small area of the normal palatine tonsil tissue. In the same study, DNA extracted from these tissues were also tested for HPV via polymerase chain reaction (PCR) analysis. Surprisingly, 28% of the patient tissues showed p16 overexpression, with staining observed within the reticulated crypt epithelium and germinal centres. However, HPV-16 and -18 were detected by PCR analysis in just 2/195 (1%) cases, which were negative with fluorescent ISH (FISH) for HPV DNA, and discordant with p16 IHC (Klingenberg *et al.*, 2010). Similar p16

expression was observed within the four normal palatine tonsils obtained as part of the current study (only one palatine tonsil shown in Section 3.2.3). However, these would not meet the requirement for the current CAP (2018) and RCPATH (2021) guidelines and criterion for p16 staining (moderate to intense nuclear and cytoplasmic staining in 70% or more cells) as this is solely based on staining observed within tumour cells (Lewis *et al.*, 2018b, Hunter *et al.*, 2021). These tissues also demonstrated negativity for HPV DNA via real-time PCR analysis (Chapter Four). p16 staining could be interpreted incorrectly and suggest evidence of an HPV-mediated precancer. One explanation for p16 overexpression in normal palatine tonsils could be related to cellular senescence which protects the cells from various forms of stress (Romagosa *et al.*, 2011). As the palatine tonsils are paired secondary lymphoid organs, they initiate immune responses against any foreign antigen (Nave *et al.*, 2001); therefore, prolonged activation of lymphocytes may contribute to this phenomena.

Within the UK, HPV DNA ISH is the current HR-HPV-specific testing of choice; however, this is not widely available (Henley-Smith *et al.*, 2020). It detects the presence of the HPV viral genome and is identifiable as blue dots within the host cell nucleus (Lewis *et al.*, 2010, Schlecht *et al.*, 2012). In Chapter Three, we demonstrated that two OPSCCs demonstrated positivity for HPV DNA ISH, which were consistent with p16 overexpression observed. However, despite the strong correlation with p16-positivity and HPV DNA ISH observed within this study, the sample is limited to just two HPV-positive OPSCCs.

It is recommended that additional HR-HPV-specific testing be performed on OPSCCs that have been determined as p16-positive (Lewis *et al.*, 2018b, Hunter *et al.*, 2021). Additional HR-HPV-specific testing is not common practice within the US and is only performed in limited circumstances where p16-positive samples should be followed by HR-HPV-specific testing; for example cancers of unknown primary (CUP) that are metastatic to cervical lymph nodes (Lewis *et al.*, 2018b, Guzmán-Arocho and Nishino, 2022). Comparatively, UK and USA studies and the RCPATH guidelines (2021) have recommended routine performance of HR-HPV-specific testing for p16-positive IHC confirmation, as well as for cases where p16 IHC is equivocal; for example, overexpression in KSCCs or negative in NKSCCs (Craig *et al.*, 2019, Craig *et al.*,

2020, Shinn *et al.*, 2021). The study performed by Shinn *et al.*, (2021) reported that discordance appeared to arise in patients that deviated from the typical tumour profiles, accounting for approximately 5% of test results. The explanation for this low discordance rate is that it is a USA-based cohort, which has a high HPV prevalence rate (Faraji *et al.*, 2019, Shinn *et al.*, 2021). This is further supported by Mehanna *et al.*, (2023), who reported that North America have a high HPV prevalence rate but a low rate of p16-positive/HPV-negative patients in comparison to Southern Europe, which has a low HPV prevalence rate and a high p16/HPV discordance rate. The biological reason for high p16/HPV discordance within the latter region is attributable to a higher population of smokers, which increases the probability of p16 inactivation by gene deletion, mutation, and promoter methylation (Ai *et al.*, 2003, The Cancer Genome Atlas Network, 2015, Mehanna *et al.*, 2023). Therefore, given that the discordance rate varies geographically, p16 IHC alone is not sufficient for risk stratification and prognostication of survival in patients.

### **6.1.3 Sensitivity and specificity of p16**

Approximately 4-30% of p16-positive OPSCCs that lack transcriptionally-active HR-HPV, are considered false-positives (Smith *et al.*, 2008a, Rischin *et al.*, 2010, Ukpo *et al.*, 2011, Bishop *et al.*, 2012, Holzinger *et al.*, 2012, Rietbergen *et al.*, 2013, Ndiaye *et al.*, 2014, Rietbergen *et al.*, 2014, Kerr *et al.*, 2015, Mirghani *et al.*, 2016, Augustin *et al.*, 2018, Randén-Brady *et al.*, 2019). It is suggested that inconsistencies in the performance of different detection techniques may account for false-positives, with numerous studies suggesting that discordant p16/HPV DNA ISH results are not reliable markers of HPV-positivity within the head and neck. The use of p16 as a standalone marker within the head and neck has drawn criticism given its specificity issues. Numerous studies have reported that p16 staining within OPSCC formalin-fixed, paraffin-embedded (FFPE) tissue were found to be discordant with HPV DNA and RNA testing including PCR and ISH. These studies collectively reported overall sensitivities between 69-100% and specificities between 76-100% for p16 IHC (Schache *et al.*, 2011, Jordan *et al.*, 2012, Pannone *et al.*, 2012, Schlecht *et al.*, 2012, Holzinger *et al.*, 2013, Mirghani *et al.*, 2015, Shelton *et al.*, 2017, Arsa *et al.*, 2021). Within these studies, various p16 clones, cut-offs, and scoring systems for p16 expression within positive cells were used, as well as manual or automated staining which are all factors that can contribute to the sensitivity and specificity of p16 staining

(Hong *et al.*, 2013, Deutsch *et al.*, 2022). The majority of OPSCCs are defined as positive or negative based on the current CAP (2018) and RCPATH (2021) guidelines for p16 staining (Lewis *et al.*, 2018b, Hunter *et al.*, 2021). However, in clinical practice equivocal staining patterns are occasionally observed in less than 5% of cases which can hinder interpretation (Thavaraj *et al.*, 2011). Some of these studies used cut-offs that deviated from the clinical guidelines for p16, introducing ambiguity regarding which samples are considered positive and negative based on both sides of cut-offs. The CAP (2018) guidelines detail that there is no gold standard p16 antibody, platform, or methodology for clinical practice in the head and neck (Lewis *et al.*, 2018b). This is due to the variability in HPV prevalence and implemented methodologies that has been observed worldwide, particularly in North America where there is low p16/HPV discordance and high oral HPV prevalence in comparison to Southern Europe where there is a high p16/HPV discordance and low oral HPV prevalence (Mehanna *et al.*, 2023).

Furthermore, seven of these eight studies used either DNA and/or RNA molecular techniques which can be highly sensitive, but are at risk of contamination and possible overestimation of HPV positivity (Schache *et al.*, 2011, Jordan *et al.*, 2012, Pannone *et al.*, 2012, Schlecht *et al.*, 2012, Holzinger *et al.*, 2013, Mirghani *et al.*, 2015, Arsa *et al.*, 2021). Therefore, the sensitivities and specificities that they have reported for p16 may not be accurate given the reference techniques they have used, highlighting the inaccuracy of p16 IHC as a surrogate for HPV oncogenic transformation.

#### **6.1.4 Sensitivity and specificity of HPV DNA ISH**

Besides p16, there are also issues with HPV DNA ISH. In comparison to p16 IHC, it has high specificity, allowing for distinction between episomal and integrated DNA; however, it has reduced sensitivity particularly with low copy number/viral load, as well as it being technically difficult to interpret (Lewis *et al.*, 2012, Mirghani *et al.*, 2015, Suresh *et al.*, 2021). It has been previously stated that staining assessments made at low magnification can result in false-negative results (Fatima *et al.*, 2013, Miller *et al.*, 2017). Given the issues surrounding p16 IHC and its specificity, additional testing with HPV DNA ISH is the HR-HPV-specific testing of choice despite its increased costs and turnaround times (Schache *et al.*, 2011, Thavaraj *et al.*, 2011, Robinson *et al.*, 2012, Henley-Smith *et al.*, 2020).

Numerous studies have reported that HPV DNA ISH in OPSCC FFPE tissue have been found to be discordant with p16 IHC and HPV DNA and RNA PCR testing. These studies collectively reported overall sensitivities between 38-88% and specificities between 27-100% for HPV DNA ISH (Schache *et al.*, 2011, Jordan *et al.*, 2012, Pannone *et al.*, 2012, Schlecht *et al.*, 2012, Mirghani *et al.*, 2015, Randén-Brady *et al.*, 2019, Craig *et al.*, 2020). Within these studies, three different HPV DNA ISH probes were tested; VENTANA INFORM HPV III Family 16 Probe (B) (Roche Diagnostics Ltd, West Sussex, UK), HPV-16-type specific DNA probe, and HPV-16/-18-type specific DNA probe (both Dako™, Agilent Technologies LDA UK Ltd, Cheshire, UK). Interestingly, Pannone *et al.*, (2012) reported low specificity for the VENTANA INFORM HPV III Family 16 Probe (B) in comparison to the HPV-16/-18-type specific DNA probe, which demonstrated 100% specificity. They also reported lower sensitivities for the HPV-16/-18-type specific DNA probe compared to the VENTANA INFORM HPV III Family 16 Probe (B). The reason for this may be due to interpretation, where the staining patterns stated for both probes were different. Positivity was described as specific nuclear localisation for the HPV-16/-18-type specific DNA probe, whereas positive, nuclear staining was required for the VENTANA INFORM HPV III Family 16 Probe (B). However, these were performed on tissue microarrays, which are not typically used within the clinical laboratory and may differ from FFPE tissue sections, therefore this may account for the stark difference in sensitivity and specificity observed in comparison to the other published research.

Both the VENTANA INFORM HPV III Family 16 Probe (B) and HPV-16/-18-type specific DNA probe are reported to detect copy numbers as low as 10-50 whereas the copy number detection limit of HPV-16-type specific DNA probe is a single-copy (Montag *et al.*, 2011, Jordan *et al.*, 2012, Roche Diagnostics, 2024). To account for their supposed low detectability, these probes use signal amplification techniques which is suggested to increase sensitivity; however, this is surprising given that HPV DNA ISH is known to have reduced sensitivity to low copy numbers which can account for false-positive results (Guo *et al.*, 2008, Montag *et al.*, 2011, Mirghani *et al.*, 2015, Suresh *et al.*, 2021). It has also been suggested that HPV DNA ISH may not detect transcriptionally-active HR-HPV. This is because viral DNA can be detected by HPV DNA ISH after viral integration, and once it has progressed to viral transcription, viral DNA is transcribed to RNA and subsequently mRNA which is detectable by HPV RNA

ISH (Bishop *et al.*, 2012, Suresh *et al.*, 2021). These two techniques are highly sensitive and specific and can be used to detect both integrated and transcriptionally-active HR-HPV (Bishop *et al.*, 2012, Randén-Brady *et al.*, 2019, Henley-Smith *et al.*, 2020, Suresh *et al.*, 2021). Therefore, the use of HPV RNA ISH could be a feasible alternative and replacement for HPV DNA ISH for clinical testing.

The combination of both p16 IHC and HPV DNA ISH together were compared by Schache *et al.*, (2011) and Jordan *et al.*, (2012), who reported sensitivities of 88% and 74%, and specificities of 88% and 90% respectively. Combining the two techniques together demonstrated some notable differences with Schache *et al.*, (2011) reporting worsened sensitivity of p16 by 6% but not HPV DNA ISH which remained the same, and improved specificity of both p16 and HPV DNA ISH which increased by 2-8%. Surprisingly, the opposite was seen by Jordan *et al.*, (2012), who stated that the sensitivity of both techniques decreased by 11% for p16 and 2% for HPV DNA ISH. They also observed increased specificity for both p16 and HPV DNA ISH to 97%. Again, it is difficult to make a comparison between the two studies given that they used different HPV DNA ISH probes; however, together with the data discussed above, this calls into question the validity of this as a technique for HPV detection within clinical samples.

In these studies discussed above, HPV DNA ISH probe, automated or manual application as well as methodologies, supplier and sample size, all need to be taken into consideration with regards to variations in discordance, as these are all factors that can contribute to the sensitivity and specificity of HPV detection techniques (Hong *et al.*, 2013, Deutsch *et al.*, 2022). Furthermore, the reference techniques observed within these studies are highly sensitive and useful, particularly E6/E7 mRNA PCR which is considered the gold standard for frozen tissue (Mirghani *et al.*, 2015). However, due to the expense, expertise, and requirement of frozen tissue, as well as issues with mRNA extraction from both FFPE and frozen tissue specimens, these techniques would not be viable within the clinical setting (Lewis *et al.*, 2010, Robinson *et al.*, 2012).

With the limitations of the work presented in this thesis due to the small sample size, together with the conclusions drawn from these studies, the validity of p16 as a

surrogate marker for HPV is questioned. With the small number of HR-HPV-specific tests available, and the data discussed above, it is not surprising that there is not yet a consensus for determining HPV status within OPSCC (Mena *et al.*, 2022).

### **6.1.5 Patient impact**

The lack of specificity and false-positives for p16 is problematic for the 5% of patients who are inaccurately staged (Henley-Smith *et al.*, 2020, Shinn *et al.*, 2021). Additionally, it is also insufficient for determining suitable treatment de-escalation that is suitable in instance of HPV-mediated disease (Wagner *et al.*, 2021). Discordant p16-negative/HPV-positive patients have worse recurrence rates than p16-positive/HPV-positive patients and have a poorer chance of survival. Despite this, they had slightly better prognosis, survival, and rate of recurrence than p16-negative/HPV-negative patients. However, they should not be treated the same, with patients needing to undergo an appropriate de-intensified treatment regimen (Mehanna *et al.*, 2023). However, despite HPV-positive OPSCCs having a better survival prognosis than their HPV-negative counterparts, the post-operative treatment guidelines are identical. This may be attributable to the critical clinical trials defining the standard adjuvant therapy, before HPV-positive and HPV-negative OPSCCs were defined as two separate entities (Bernier *et al.*, 2004, Cooper *et al.*, 2004, Ang *et al.*, 2010).

Based on our results, discordance was observed between p16 IHC and morphology, despite our small sample size. Given the distinctiveness of HPV-positive OPSCCs and their increasing incidence, the need for standardised HPV testing is urgent and compelling, highlighting the importance of reliable and accurate clinical biomarkers for appropriate staging and stratification of disease. To develop this study further, further testing using more specific and sensitive techniques could be performed, as well as including more OPSCC tissue samples would be performed, at cost. However, it would not be viable within a clinical pathology laboratory, if the prerequisites of developing a valid, reliable clinical test are not fulfilled. Therefore, it would be pertinent to develop a more suitable biomarker against HPV that could be used in a clinical NHS laboratory.

The requirements for this would be to first determine if a new biomarker can transition from research to clinical use. Pre- and post-analytical considerations need to be considered within the research laboratory, where it has to be identified if there is a



demand or unmet clinical need that needs to be addressed. This would also include determining its cost-effectiveness and ease of use as well as the sensitivity, specificity, and reproducibility of the assay. Once the biomarker has passed analytical testing within a research laboratory, the assay would need to be validated for use on control tissues and tested against other validated assays within the clinical laboratory. Assessment of the impact of the biomarker on patient outcome would also need to be performed, as well as pre-and post-analytical considerations to determine whether it is feasible and cost-effective within the clinical setting (Lazzari, 2009, Sturgeon *et al.*, 2010, Goldsmith *et al.*, 2024). Therefore, research to investigate new and improved biomarkers targeting HPV will hopefully help have a significant impact on patient treatment and outcome.

## **6.2 Other biomarkers associated with HPV-positive OPSCC**

In Chapter Three, we discussed biomarker expression in OPSCC using other prognostic biomarkers besides p16, that have been associated with both HPV-positive and HPV-negative OPSCCs.

### **6.2.1 Immune biomarker expression in OPSCC**

Within our study, expression of programmed cell death protein-1 (PD-1), programmed cell death-ligand 1 (PD-L1), and CD8 were investigated. Weak expression of PD-1, PD-L1, and CD8 were observed in the two OPSCCs identified as p16- and HPV DNA ISH-positive in comparison to two of the HPV-negative OPSCCs. These results were not expected as strong expression of PD-1, PD-L1, and CD8 are usually observed within HPV-positive OPSCCs suggesting that they are biologically relevant and play an important role in immune surveillance escape of HPV-mediated disease (Badoual *et al.*, 2013, Lyford-Pike *et al.*, 2013, Concha-Benavente *et al.*, 2016, Gameiro *et al.*, 2018, Pokrývková *et al.*, 2022, Atipas *et al.*, 2023). However, based on our results, despite our small sample size, it is possible that there is no correlation between p16 and HPV status and expression of these immune biomarkers.

There have been reports of no correlation between these immune biomarkers and p16 or HPV status (Badoual *et al.*, 2013, Kim *et al.*, 2016, Steuer *et al.*, 2018, Atipas *et al.*, 2023). However, the observations made by Kim *et al.*, (2016), and Atipas *et al.*, (2023) have limitations given that they were performed on Asian cohorts who typically have

low HPV prevalence and p16/HPV discordance, and would not therefore be comparable to a high HPV prevalent geographical region (Mehanna *et al.*, 2023). Surprisingly, it has also been demonstrated that high levels of PD-1 and PD-L1 expression have been observed in HPV-negative tumours, which are consistent with our results (Malm *et al.*, 2015). Despite this, the limitations of these studies include different interpretation criteria, antibodies, and ancillary reagents as well as methodology and scoring criteria.

Within the tumour microenvironment (TME) of OPSCC, CD8-positive T lymphocytes enhance antitumour immune responses and PD-L1-positive tumour cells bind to PD-1 present on activated T lymphocytes that are approaching the tumour (de Vincente *et al.*, 2019, Atipas *et al.*, 2023). Overexpression of these immune biomarkers would be expected in HPV-positive tumours as HPV foreign antigens would elicit an immune response; however, HPV can also avoid immune clearance (Lyford-Pike *et al.*, 2013). HPV infection is believed to establish within the reticulated crypts of the palatine tonsil which normally express PD-L1 and together with HPV E7 oncoprotein also driving PD-L1 overexpression, this may represent an viral-privileged site where viral-specific T lymphocytes are downregulated allowing HPV to establish and induce malignant transformation (Kim *et al.*, 2007, Lyford-Pike *et al.*, 2013, Liu *et al.*, 2017).

Despite this, CD8-positive TILs as well as PD-1 and PD-L1 expression are still observed within HPV-negative OPSCC (Lyford-Pike *et al.*, 2013, Malm *et al.*, 2015, Pokrývková *et al.*, 2022, Atipas *et al.*, 2023). Like HPV-positive OPSCCs, HPV-negative OPSCC have an immune-rich TME (Fialová *et al.*, 2020, Succaria *et al.*, 2021). This may be because the tonsils are secondary lymphoid organs that consist of lymphoid follicles composed of T and B lymphocytes as well as possessing reticulated crypt epithelium densely infiltrated with lymphocytes (Olah, 1978, Nave *et al.*, 2001, Fossum *et al.*, 2017). Therefore, you would still expect there to be expression of PD-1, PD-L1, and CD8. This is supported by others who have observed no difference in these biomarker expressions in HPV-positive and HPV-negative OPSCCs (Oguejiofor *et al.*, 2017, Succaria *et al.*, 2021). Our observations showed that these biomarkers were not in keeping with the literature and would be considered inadequate prognostic biomarkers given that HPV-positive OPSCCs have better prognosis and survival than HPV-negative OPSCCs. Therefore, based on the

observations we have made, and the literature discussed above, this highlights the complexity of both HPV-positive and HPV-negative OPSCCs.

### **6.2.2 Prognostic biomarkers of OPSCC**

In Chapter Three, we observed high expression levels of Ki67 in the majority of our OPSCC cohort, which was consistent with the literature. Ki67 overexpression is typically associated with poorly differentiated OPSCCs in comparison to well differentiated OPSCCs (Yadav *et al.*, 2019). This was observed within our HPV-positive OPSCCs, which are typically not histologically graded based on conventional grading schemes. Their appearance does appear poorly differentiated which is typically associated with poor prognosis and aggressive tumour growth; however, despite this HPV status is related to good prognosis (Bishop, 2015).

Currently, Ki67 is not used as a prognostic or predictive marker in head and neck squamous cell carcinoma (HNSCC), with some studies reporting inconclusive results (Kropveld *et al.*, 1998, Lavertu *et al.*, 2001, Couture *et al.*, 2002, Silva *et al.*, 2004, Chatzkel *et al.*, 2017). Numerous studies have reported varying conclusions regarding Ki67 expression and its relation to HPV. Studies have reported that Ki67 expression was highest in p16-positive cases, with a combination of Ki67 and HPV status possibly improving prognostic information with regards to patient survival (Liu *et al.*, 2015, de Perrot *et al.*, 2017, Sivakumar *et al.*, 2021). Contrarily, others observed that Ki67 expression was increased in HPV-negative cases, and that there was no prognostic difference between HPV-positive and HPV-negative tumours (Bu *et al.*, 2015, Tsuchida *et al.*, 2017). In the cervix, Ki67 and p16 together have demonstrated good performance as a triage test for HPV infection clearance in cytology samples (Rossi *et al.*, 2021). Therefore, Ki67 expression could be used to assess patients who have suspected oral HPV infections in the future. However, oral swabs and sampling of the tonsils requires further research.

Furthermore, patients with a high Ki67 proliferative index within tumours may benefit from more aggressive treatment, particularly those who are HPV-negative; however, this is yet to be validated (Gerdes *et al.*, 1984, Liu *et al.*, 2015, Yadav *et al.*, 2019). Currently, it is unknown if any precursor lesions exist within the tonsils, which may be related to OPSCCs possessing a rapid growth rate, making such lesions difficult to

detect (Tamás *et al.*, 2011, Palmer *et al.*, 2014, Quabius *et al.*, 2021). Overall, the use of Ki67 as a prognostic and predictive marker within OPSCC requires further investigation.

### **6.2.3 Cytokeratin 7 expression does not correlate with HPV status in OPSCC**

In our study, one OPSCC expressed CK7 within its tumour cells, whilst the rest were tumour-negative. It was determined as a NKSCC and HPV-negative OPSCC, which does not correlate with the literature. It has been previously observed that HPV-16 E7 protein directly interacts with CK7 (Kanduc, 2002). This is also supported by other studies that have investigated CK7 expression within OPSCC; of which there are very few. They reported that increased CK7 expression is associated with HPV-positive OPSCCs (Morbini *et al.*, 2015, Woods *et al.*, 2017, Woods *et al.*, 2022). It is also plausible that CK7 may only be expressed in NKSCCs, as they are typically p16- and HPV DNA ISH-positive; based on clinicopathologic data it appeared that CK7-positivity was more likely to be associated with non-keratinising morphology than keratinising in OPSCC (Morbini *et al.*, 2015, Mehrad *et al.*, 2018). However, they support the theory that HPV-positive OPSCCs arise within the tonsillar reticulated crypts.

However, Chu *et al.*, (2000), reported that 87% of cervical SCCs vs 27% of HNSCCs were positive for CK7 expression, which may indicate that CK7 may not be as significant within HPV-positive HNSCCs as it is in CC. Surprisingly, CK7 expression was not observed within the HPV-positive OPSCCs within this study, which could imply that these tumours did not originate from HPV infections that had established within tonsillar crypts. However, CK7 expression may be absent within HPV-positive OPSCCs for a number of reasons. One explanation is that HPV-positive OPSCC may originate within the crypts, but that CK7 expression may be lost as cells differentiate, where the tumour consists of differentiated and undifferentiated components and possesses a CK7-negative phenotype (Pitiyage *et al.*, 2015). The limitation with this is it appears to be the only case where this has been described within the literature to our knowledge.

Another explanation is that CK7 expression may be associated with viral DNA and not transcriptionally-active HR-HPV, which is associated with E6 and E7 expression (Mehrad *et al.*, 2018). However, it has been shown that HPV E7 interacts with CK7

and therefore this theory may not be plausible. Additionally, it may be that it is related to episomal HPV DNA; not integrated, within both the cervix and oropharynx (Lee *et al.*, 2017, Mehrad *et al.*, 2018, Roberts *et al.*, 2019). Our HPV DNA ISH data showed both episomal and integrated staining patterns within both p16-positive OPSCCs and would be expected based on the literature that there would be some CK7 positivity within the tumour. It has been postulated that there may be a viral-human hybrid episome that occurs within HPV-positive OPSCC; however, this is yet to be elucidated (Morgan *et al.*, 2017, Roberts *et al.*, 2019). It has also been observed that there is no significant difference between anatomical site and HPV status (Mehrad *et al.*, 2018). Therefore, this data and the observation of 27% of HNSCC being CK7-positive suggests that CK7 has no clinical significance within the head and neck in determining tumour origin, and currently still remains unknown.

Based on the findings of our work, it is possible that these tumours did not originate within the reticulated crypts as they have keratinising tumour morphology that is typical of HPV-negative OPSCC, and are CK7-negative; however, both KSCC and CK7 expression can be HPV-positive. Additionally, CK7 expression may only be associated with NKSCC; however, only one of our two non-keratinising OPSCCs was CK7-positive. Therefore, based on our results, despite limited sample size, it is difficult to determine the significance of CK7 in OPSCC.

The limitations with our study are largely associated with a limited sample size. Based on the uncertainty within the literature, our data clearly highlights the complexity of HPV pathogenesis within OPSCC, which is yet to be fully elucidated. Although further research is warranted to fully understand HPV-mediated disease within the oropharynx, to develop this study further it would be interesting to look at HPV proteins directly which could pose as better biomarkers for HPV-positive OPSCC.

### **6.3 Biomarkers against HPV proteins**

#### **6.3.1 HPV antibodies were unsuccessful in IHC**

Since 1941, the use of IHC to detect target antigens using antibodies has become a valuable tool for both diagnostic and research use (Coons *et al.*, 1941, Tan *et al.*, 2020). Today, IHC is commonly performed on automated systems within the clinical setting, as these are less labour-intensive than manual IHC (Tan *et al.*, 2020). This

includes the performance of p16 IHC on cancers of the oropharynx to determine whether they are HPV-positive or HPV-negative. However, there are numerous issues related to the use of p16 as a surrogate marker, discussed above. Alternatively, there are commercially-available HPV antibodies on the market, but these are for research use only (RUO), and cannot be used within clinical testing.

Rigorous testing of HPV antibodies performed as part of this study resulted in varying degrees of non-specific staining across the vastly different cell types that we confirmed to be HPV-negative through molecular screening. The automated staining that was performed had steps and reagents in place to reduce this staining from occurring. We used the BOND™ Polymer Refine Detection Kit (Leica Biosystems, Leica Microsystems (UK) Ltd, Milton Keynes, UK), which included a Peroxide Block reagent containing hydrogen peroxide which quenches endogenous peroxidase activity and avoids the use of streptavidin and biotin, eliminating non-specific staining related to endogenous biotin (Ramos-Vara, 2005, Leica Biosystems, 2024). Additionally, various epitope retrieval solutions, incubation times, and antibody dilutions were tested with the final parameters selected detailed in Section 2.3.1 Table 4. The antibody dilutions chosen were the lowest dilution that could be applied before no staining was visible, which was also observed when performing antigen retrieval for a shorter incubation time. However, despite having these in place we still achieved variable staining. Buffer negative controls were also performed for each tissue type with the same epitope retrieval solution and incubation time performed as for the HPV antibodies to achieve continuity, except for where the primary antibody was substituted for antibody diluent. In Section 4.2.3 Figure 34, there was some observed background 3,3'-diaminobenzidine (DAB) staining in a few tissue types, which appeared as precipitate on the tissue section. This allowed us to distinguish what was precipitate on the section from the DAB, and what was real staining within the tissue. As there was no comparison between the buffer negative controls and the HPV antibody staining, we knew that the non-specific staining we had observed was not due to the automated staining system, the BOND™ Polymer Refine Detection Kit or the tissue blocks used. This is supported by the staining observed using other primary antibodies as demonstrated in Chapter 3.

There are numerous issues with antibodies that can complicate IHC including batch-to-batch variation, the way antibodies are produced, and non-specificity. We primarily used monoclonal antibodies that are less likely to have these issues; however, they are still capable of them. With batch-to-batch variations, each new batch requires validation, and it is advised for projects to buy in bulk to prevent this. Additionally, the QC data generated years ago may be still published on the product sheet and the newer batches produced may not be able to generate the same data as they may have been immunised in a different animal species (Voskuil, 2014). Depending on the animal immunised, this can cause variations in antibody dilutions and batch-to-batch variation (Ramos-Vara, 2005). On the other hand, non-specific staining may occur if the antibody binds to unintended proteins. The affinity of an antibody is determined by the epitope's amino acid (AA) sequence and therefore, it is difficult to find antibodies that react with one protein only when there are other proteins with similar sequences. This could ultimately result in cross-reactivity (Voskuil, 2014), and may have been the case with our HPV staining results. However, this does not explain why we observed non-specific staining within HPV-negative tissues. Of the eight HPV antibodies tested, the epitope AA sequences were only available for three HPV antibodies: HPV-16 E2 (Abcam), HPV-16 E6 (Neo Biotech), and HPV-18 E7 (Abcam). Additionally, these antibodies may have only been optimised and validated for use in CC tissue or cell lines; therefore, they may not work in other tissue types that can be infected with HPV. The antibody's affinity would then be lower for the specific epitope and thus result in non-specific staining (Voskuil, 2014). This was also observed in the Western blot for HPV-16 E6 + HPV-18 E6 (Abcam) which showed positive staining in non-specific and negative controls (Appendix 14). Therefore, these data suggest that HPV markers need to be re-evaluated for use in tissues, and instead we propose a novel approach for targeting HPV proteins which could replace the current methodology.

### **6.3.2 Novel approach for targeting HPV proteins**

To address our observed issues of p16 and HPV DNA ISH discordance, coupled with the non-specific staining of HPV antibodies within tissue, we designed and developed DNA aptamers against HPV-16 E2, HPV-16 E7-E6, HPV-18 E6, and HPV-18 E7. This approach allows for identification of HPV subtypes that has not been achievable up until this point, as current HPV testing using p16 IHC and HPV DNA ISH cannot differentiate between HR-HPV subtypes.

Based on molecular docking and computational modelling, our HPV aptamers demonstrated interactions with their respective HPV proteins within functional motifs/domains which have been observed in nature. This suggested that these interactions were real. We also found that the presence of loops within the chosen structures for each HPV aptamer provided structural flexibility and combined with their smaller size allowed them to bind to protein regions without causing conformational changes, something which larger structures such as antibodies cannot achieve (Gelinas *et al.*, 2016, Autiero *et al.*, 2018). The angstrom (Å) measurements were only considered if they were in the range of 2.2-4.0 Å, as there is a minimum distance in between atoms due to intermolecular forces (Jeffrey, 1997). However, the limitation with this is that we do not know exactly what each intermolecular interaction is within our aptamer-protein complexes. Therefore, we would need to carry out further work to determine this such as X-ray crystallography, which generates crystal structures of the aptamer-protein complexes and can provide detailed information on the nature of the interactions (Ruigrok *et al.*, 2012).

There is limited HPV aptamer data within the literature as only a few groups have isolated aptamers against HPV proteins; HPV-16 E6 and E7 RNA aptamers (Toscano-Garibay *et al.*, 2011, Gourronc *et al.*, 2013, Nicol *et al.*, 2013, Cesur *et al.*, 2015), HPV-16 L1 RNA and DNA aptamers (Leija-Montoya *et al.*, 2014, Trausch *et al.*, 2017, Valencia-Reséndiz *et al.*, 2018), HPV L1 DNA aptamers targeting various HR-HPV subtypes (Yang *et al.*, 2024), and HPV-16 E6/E7 DNA aptamers (Graham and Zarbl, 2012). The majority of these were tested in CC cell lines or lysates including SiHa and HeLa, with Gourronc *et al.*, (2013) using HPV-16 E6/E7 transformed primary human tonsillar epithelial cells (HTECs). Aptamers isolated by Graham and Zarbl, (2012), Gourronc *et al.*, (2013), and Cesur *et al.*, (2015) were tested within the relevant cell lines and demonstrated positive staining by immunofluorescence. This was similar to our approach where HPV-16 E7-E6, HPV-18 E6, and HPV-18 E7 aptamers demonstrated both nuclear and endosomal localisation, which was also observed by Graham and Zarbl, (2012), Gourronc *et al.*, (2013), and Cesur *et al.*, (2015). These were all in keeping with the literature where E6 and E7 expression is seen within the nucleus, cytoplasm, and endosomes (Lee *et al.*, 2007, Knapp *et al.*, 2009, Ganti *et al.*, 2016). However, there were limitations with these studies as Graham and Zarbl, (2012) demonstrated higher levels of aptamer expression within non-cancerous



revertant cell lines of HeLa and SiHa cells than cancerous cells, whereas Gourronc *et al.*, (2013) identified aptamers that bound to both primary HTECs and HPV-16 E6/E7 transformed HTECs. Therefore, these studies have demonstrated aptamers that would be insufficient for use within cancerous cells, unlike our aptamers which demonstrated expression within HPV-positive cell lines. These groups primarily focussed on the HPV-16 subtype only; therefore, our work would be the first to design and develop DNA aptamers against HPV-16 E2, and HPV-18 E6 and E7 proteins and test them in HNSCC cell lines which has not been discussed before.

As there are issues surrounding p16 specificity, the development of aptamers that detect HPV proteins within HNSCC and OPSCC could have a significant impact on disease stratification, prognosis, and treatment in HPV-positive patients (Ang *et al.*, 2010, Gupta *et al.*, 2018). It could also help contribute to the United Nations (UN) sustainability development goals (SDG), particularly goal three-good health and well-being (United Nations, 2015, United Nations Development Programme, 2015). The use of aptamers could widen the access to healthcare for millions of people in less-developed countries where healthcare is expensive and inaccessible as well as provide new strategies for disease detection. Unlike antibodies, aptamers are chemically synthesised from their known aptamer sequence and easily reproducible; therefore, removing the animal model and batch-to-batch variation. They can also be produced fairly quickly reducing time, cost, and labour (Zhang *et al.*, 2010, Bauer *et al.*, 2019, Zhang *et al.*, 2019, Li *et al.*, 2021). Antibodies on the other hand have a limited shelf-life and have to be kept at a suitable temperature (-20°C or -80°C) for transportation as repeated freeze/thaw cycles can make them susceptible to deterioration and irreversible denaturation (Stoltenburg *et al.*, 2007, Keefe *et al.*, 2010, Voskuil, 2014, Bauer *et al.*, 2019). Conversely, aptamers are thermally stable and have a long shelf-life, allowing them to be stored and transported easily (Sun and Zu, 2015, Zhang *et al.*, 2019, Li *et al.*, 2021). This will be advantageous particularly in warmer climates and less-developed countries where there is limited access to healthcare. Additionally, aptamers have clinical and industrial advantages over antibodies including non-immunogenicity, high penetration, and unlimited targets (Sun and Zu, 2015). In comparison to antibodies, aptamers are non-immunogenic and non-toxic and therefore do not elicit an immune response (Sun and Zu, 2015). Due to their small size, aptamers are capable of crossing the blood-brain barrier and penetrating

tissues (Keefe *et al.*, 2010, Cheng *et al.*, 2013, Sun and Zu, 2015, Li *et al.*, 2021). Therefore, aptamers could be used as an alternative to antibodies in IHC.

Since the expiration of the original SELEX patents in the early 2010s, there has been an increased academic and commercial interest in aptamers (DeRosa *et al.*, 2023). In March 2024, the aptamers market was estimated at 1.48 billion USD, which is projected to reach 2.77 billion USD by the year 2030 (Research and Markets, 2024). The increased interest in aptamers highlights their potential use for diagnostic and therapeutic approaches. In this instance, the development of aptamers against HPV proteins could potentially allow for differentiation between LR- and HR-HPV types based on changes in their protein structure and provide a more specific technique for determining HPV status.

#### **6.4 Future work**

This study has provided a basis for undertaking aptamer development of HPV proteins further, which could be used to help determine the HPV subtype within tissues. Firstly, we would need to run proof of principle testing by returning to the final positive selection pool for each HPV aptamer and performing cell-SELEX. This is similar to the SELEX process we carried out as part of this study; however, the target protein is unknown, and the selection process is carried out on live cells expressing non-specific proteins (Pleiko *et al.*, 2019). This would be run as a comparison on a non-specific cell line to help select out the non-HPV containing cell types. As we could not demonstrate HPV-16 E2 staining, it would need to be reviewed in cells with an early HPV-16 infection such as an S12 or W12 cell line, or artificially through transfection of HPV-16 E2 into a cell line such as HEK293. Ultimately, if this work was successful, the development of staining protocols could progress forward to be tested in tissues.

## CHAPTER 7: CONCLUSION

In this thesis, we described that the morphology of OPSCC does not reliably inform HPV status, if diagnosis was based solely on H&E examination. Despite the strong correlation with p16 and HPV DNA ISH positivity observed in this study, others have questioned the validity of p16 as a surrogate marker for HPV within the head and neck. Additionally, other prognostic biomarkers tested deviated from the typical tumour profiles of both HPV-positive and HPV-negative OPSCCs and would therefore be inadequate for prognosis. Together, these observations highlight the complexity of OPSCC development, and the difficulty in identifying suitable biomarkers to diagnose and stratify HPV-mediated disease. Furthermore, we found that HPV antibodies were unsuccessful within tissues and would not be adequate in determining HPV subtype, which were confirmed by molecular testing. We proposed a novel approach to targeting HPV proteins which could replace the current methodology of p16 testing for HPV status, with promising results. In conclusion we find that aptamer development could be a useful tool for determining HPV status, as well as be beneficial to less developed countries. The data we present is encouraging; therefore, further work is required to determine if aptamers can be tested and used in aptahistochemistry.

## REFERENCES

- AARTHY, M., KUMAR, D., GIRI, R. & SINGH, S. K. 2018. E7 oncoprotein of human papillomavirus: structural dynamics and inhibitor screening study. *Gene*, 658, 159-177.
- ABBATE, E. A., VOITENLEITNER, C. & BOTCHAN, M. R. 2006. Structure of the papillomavirus DNA-tethering complex E2:Brd4 and a peptide that ablates HPV chromosomal association. *Mol Cell*, 24, 6, 877-889.
- ABROI, A., ILVES, I., KIVI, S. & USTAV, M. 2004. Analysis of chromatin attachment and partitioning functions of bovine papillomavirus type 1 E2 protein. *J Virol*, 78, 4, 2100-2113.
- AI, L., STEPHENSON, K. K., LING, W., ZUO, C., MUKUNYADZI, P., SUEN, J. Y., HANNA, E. & FAN, C. Y. 2003. The p16 (CDKN2a/INK4a) tumor-suppressor gene in head and neck squamous cell carcinoma: a promoter methylation and protein expression study in 100 cases. *Mod Pathol*, 16, 9, 944-950.
- AKSOY, P., GOTTSCHALK, E. Y. & MENESES, P. I. 2017. HPV entry into cells. *Mutat Res Rev Mutat Res*, 772, 13-22.
- AMIN, M. B., EDGE, S. B., GREENE, F. L., BYRD, D. R., BROOKLAND, R. K., WASHINGTON, M. K., GERSHENWALD, J. E., COMPTON, C. C., HESS, K. R., SULLIVAN, D. C., MILBURN JESSUP, J., BRIERLY, J. D., GASPAR, L. E., SCHILSKY, R. L., BALCH, C. M., WINCHESTER, D. P., ASARE, E. A., MADERA, M., GRESS, D. M. & MEYER, L. R. 2017. *AJCC Cancer Staging Manual*, Springer International Publishing AG.
- AMOUTZIAS, G. D., BORNBER-BAUER, E., OLIVER, S. G. & ROBERTSON, D. L. 2006. Reduction/oxidation-phosphorylation control of DNA binding in the bZIP dimerization network. *BMC Genomics*, 7, 107.
- ANDROPHY, E. J., LOWY, D. R. & SCHILLER, J. T. 1987. Bovine papillomavirus E2 trans-activating gene product binds to specific sites in papillomavirus DNA. *Nature*, 325, 6099, 70-73.
- ANG, K. K., HARRIS, J., WHEELER, R., WEBER, R., ROSENTHAL, D. I., NGUYEN-TÂN, P. F., WESTRA, W. H., CHUNG, C. H., JORDAN, R. C., LU, C., KIM, H., AXELROD, R., SILVERMAN, C. C., REDMOND, K. P. & GILLISON, M. L. 2010. Human papillomavirus and survival of patients with oropharyngeal cancer. *N Engl J Med*, 363, 1, 24-35.

- ARSA, L., SIRIPOON, T., TRACHU, N., FOYHIRUN, S., PANGPUNYAKULCHAI, D., SANPAPANT, S., JINAWATH, N., PATTARANUTAPORN, P., JINAWATH, A. & NGAMPHAIBOON, N. 2021. Discrepancy in p16 expression in patients with HPV-associated head and neck squamous cell carcinoma in Thailand: clinical characteristics and survival outcomes. *BMC Cancer*, 21, 504.
- ATIPAS, K., LAOKULRATH, N., PETSUKSIRI, J., RATANAPRASERT, N. & PONGSAPICH, W. 2023. CD8+ T cells and PD-L1 expression as prognostic indicators in a low prevalence of HPV-associated oropharyngeal squamous cell carcinoma. *Curr Oncol*, 30, 2, 1450-1460.
- AUGUSTE, A., DELOUMEAUX, J., JOACHIM, C., GAETE, S., MICHINEAU, L., HERRMANN-STORCK, C., DUFLO, S. & LUCE, D. 2020. Joint effect of tobacco, alcohol, and oral HPV infection on head and neck cancer risk in the French West Indies. *Cancer Med*, 9, 18, 6854-6863.
- AUGUSTIN, J., OUTH-GAUER, S., MANDAVIT, M., GASNE, C., GRARD, O., DENIZE, T., NERVO, M., MIRGHANI, H., LACCOURREYE, O., BONFILS, P., BRUNEVAL, P., VEYER, D., PÉRE, H., TARTOUR, E. & BADOUAL, C. 2018. Evaluation of the efficacy of the 4 tests (p16 immunocytochemistry, polymerase chain reaction, DNA, and RNA in situ hybridization) to evaluate a human papillomavirus infection in head and neck cancers: a cohort of 348 French squamous cell carcinomas. *Hum Pathol*, 78, 63-71.
- AUTIERO, I., RUVO, M., IMPROTA, R. & VITAGLIANO, L. 2018. The intrinsic flexibility of the aptamer targeting the ribosomal protein S8 is a key factor for the molecular recognition. *Biochim Biophys Acta Gen Subj*, 1862, 4, 1006-1016.
- AYDIN, I., VILLALONGA-PLANELLAS, R., GREUNE, L., BRONNIMANN, M. P., CALTON, C. M., BECKER, M., LAI, K. Y., CAMPOS, S. K., SCHMIDT, M. A. & SCHELHAAS, M. 2017. A central region in the minor capsid protein facilitates viral genome tethering and membrane penetration for mitotic nuclear entry. *PLoS Pathog*, 13, 5, e1006308.
- AYDIN, I., WEBER, S., SNIJDER, B., VENTAYOL, P. S., KÜHBACHER, A., BECKER, M., DAY, P. M., SCHILLER, J. T., KANN, M., PELKMANS, L., HELENIUS, A. & SCHELHAAS, M. 2014. Large scale RNAi reveals the requirement of nuclear envelope breakdown for nuclear import of human papillomaviruses. *PLoS Pathog*, 10, 5, e1004162.

- BADOUAL, C., HANS, S., MERILLON, N., VAN RYSWICK, C., RAVEL, P., BENHAMOUDA, N., LEVIONNOIS, E., NIZARD, M., SI-MOHAMED, A., BESNIER, N., GEY, A., ROTEM-YEHUDAR, R., PERE, H., TRAN, T., GUERIN, C. L., CHAUVAT, A., DRANSART, E., ALANIO, C., ALBERT, S., BARRY, B., SANDOVAL, F., QUINTIN-COLONNA, F., BRUNEVAL, P., FRIDMAN, W. H., LEMOINE, F. M., OUDARD, S., JOHANNES, L., OLIVE, D., BRASNU, D. & TARTOUR, E. 2013. PD-1-expressing tumor-infiltrating T cells are favorable prognostic biomarker in HPV-associated head and neck cancer. *Cancer Res*, 73, 1, 128-138.
- BALOG, E. R. M., BURKE, J. R., HURA, G. L. & RUBIN, S. M. 2011. Crystal structure of the unliganded retinoblastoma protein pocket domain. *Proteins*, 79, 6, 2010-2014.
- BARBARESI, S., CORTESE, M. S., QUINN, J., ASHRAFI, G. H., GRAHAM, S. V. & CAMPO, M. S. 2010. Effects of human papillomavirus type 16 E5 deletion mutants on epithelial morphology: functional characterization of each transmembrane domain. *J Gen Virol*, 91, 2, 521-530.
- BARBOSA, M. S., LOWY, D. R. & SCHILLER, J. T. 1989. Papillomavirus polypeptides E6 and E7 are zinc-binding proteins. *J Virol*, 63, 3, 1404-1407.
- BASTIEN, N. & MCBRIDE, A. A. 2000. Interaction of the papillomavirus E2 protein with mitotic chromosomes. *Virology*, 270, 1, 124-134.
- BAUER, M., STROM, M., HAMMOND, D. S. & SHIGDAR, S. 2019. Anything you can do, I can do better: can aptamers replace antibodies in clinical diagnostic applications? *Molecules*, 24, 23, 4377.
- BECHTOLD, V., BEARD, P. & RAJ, K. 2003. Human papillomavirus type 16 E2 protein has not effect on transcription from episomal viral DNA. *J Virol*, 77, 3, 2021-2028.
- BERMAN, H. M., WESTBROOK, J., FENG, Z., GILLILAND, G., BHAT, T. N., WEISSIG, H., SHINDYALOV, I. N. & BOURNE, P. E. 2000. The Protein Data Bank. *Nucleic Acids Res*, 28, 1, 235-242. Available: <https://www.rcsb.org/>.
- BERNARD, B. A., BAILLY, C., LENOIR, M. C., DARMON, M., THIERRY, F. & YANIV, M. 1989. The human papillomavirus type 18 (HPV18) E2 gene product is a repressor of the HPV18 regulatory region in human keratinocytes. *J Virol*, 63, 10, 4317-4324.

- BERNARD, H. U., BURK, R. D., CHEN, Z., VAN DOORSLAER, K., ZUR HAUSEN, H. & DE VILLIERS, E. M. 2010. Classification of papillomaviruses (PVs) based on 189 PV types and proposal of taxonomic amendments. *Virology*, 401, **1**, 70-79.
- BERNIER, J., DOMENGE, C., OZSAHIN, M., MATSUSZEWSKA, K., LEFÈBVRE, J. L., GREINER, R. H., GIRALT, J., MAINGON, P., ROLLAND, F., BOLLA, M., COGNETTI, F., BOURHIS, J., KIRKPATRICK, A., GLABBEKE., V. & EUROPEAN ORGANISATION FOR RESEARCH AND TREATMENT OF CANCER TRIAL 22931 2004. Postoperative irradiation with or without concomitant chemotherapy for locally advanced head and neck cancer. *N Engl J Med*, 350, **19**, 1945-1952.
- BETTAMPADI, D., SIRAK, B. A., ABRAHAMSEN, M. E., REICH, R. R., VILLA, L. J., LAZCANO-PONCE, E. & GIULIANO, A. R. 2021. Factors associated with persistence and clearance of high-risk oral human papillomavirus (HPV) among participants in the HPV infection in men (HIM) study. *Clin Infect Dis*, 73, **9**, e3227-3234.
- BIENKOWSKA-HABA, M., WILLIAMS, C., KIM, S. M., GARCEA, R. L. & SAPP, M. 2012. Cyclophilins facilitate dissociation of the human papillomavirus type 16 capsid protein L1 from the L2/DNA complex following virus entry. *J Virol*, 86, **18**, 9875-9887.
- BISHOP, J. A. 2015. Histopathology of human papillomavirus-related oropharyngeal carcinoma: a review of classic and variant forms. *Diagn Histopathol*, 21, **2**, 70-76.
- BISHOP, J. A., MA, X. J., WANG, H., LUO, Y., ILLEI, P. B., BEGUM, S., TAUBE, J. M., KOCH, W. M. & WESTRA, W. H. 2012. Detection of transcriptionally active high-risk HPV in patients with head and neck squamous cell carcinoma as visualized by a novel E6/E7 mRNA in situ hybridization method. *Am J Surg Pathol*, 36, **12**, 1874-1882.
- BLIND, M. & BLANK, M. 2015. Aptamer selection technology and recent advances. *Mol Ther Nucleic Acids*, 4, **1**, e223.
- BLOT, W. J., MCLAUGHLIN, J. K., WINN, D. M., AUSTIN, D. F., GREENBERG, R. S., PRESTON-MARTIN, S., BERNSTEIN, L., SCHOENBERG, J. B., STEMHAGEN, A. & FRAUMENI, J. F. J. 1988. Smoking and drinking in relation to oral and pharyngeal cancer. *Cancer Res*, 48, **11**, 3282-3287.

- BLUMBERG, J., MONJANE, L., PRASAD, M., CARRILHO, C. & JUDSON, B. L. 2015. Investigation of the presence of HPV related oropharyngeal and oral tongue squamous cell carcinoma in Mozambique. *Cancer Epidemiol*, 39, **6**, 1000-1005.
- BOCK, L. C., GRIFFIN, L. C., LATHAM, J. A., VERMAAS, E. H. & TOOLE, J. J. 1992. Selection of single-stranded DNA molecules that bind and inhibit human thrombin. *Nature*, 355, **6360**, 564-566.
- BONNER, J. A., HARARI, P. M., GIRALT, J., COHEN, R. B., JONES, C. U., SUR, R. K., RABEN, D., BASELGA, J., SPENCER, S. A., ZHU, J., YOUSOUFIAN, H., ROWINSKY, E. K. & ANG, K. K. 2010. Radiotherapy plus cetuximab for locoregionally advanced head and neck cancer: 5-year survival data from a phase 3 randomised trial, and relation between cetuximab-induced rash and survival. *Lancet Oncol*, 11, **1**, 21-28.
- BOUVARD, V., MATLASHEWSKI, G., GU, Z. M., STOREY, A. & BANKS, L. 1994a. The human papillomavirus type 16 E5 gene cooperates with the E7 gene to stimulate proliferation of primary cells and increases viral gene expression. *Virology*, 203, **1**, 73-80.
- BOUVARD, V., STOREY, A., PIM, D. & BANKS, L. 1994b. Characterization of the human papillomavirus E2 protein: evidence of trans-activation and trans-repression in cervical keratinocytes. *EMBO J*, 13, **22**, 5451-5459.
- BRAY, F., FERLAY, J., SOERJOMATARAM, I., SIEGEL, R. L., TORRE, L. A. & JEMAL, A. 2018. Global cancer statistics 2018: GLOBOCAN estimates of incidence and mortality worldwide for 36 cancers in 185 countries. *CA Cancer J Clin*, 68, **6**, 394-424.
- BRIERLY, J. D., GOSPODAROWICZ, M. K. & WITTEKINDT, C. 2016. *TNM Classification of Malignant Tumours*, Wiley-Blackwell.
- BRISTOL, M. L., JAMES, C. D., WANG, X., FONTAN, C. T. & MORGAN, I. M. 2020. Estrogen attenuates the growth of human papillomavirus-positive epithelial cells. *mSphere*, 5, **2**, e00049-20.
- BRONIARCZYK, J., BERGANT, M., GOŹDZICKA-JÓZEFIAK, A. & BANKS, L. 2014. Human papillomavirus infection requires the TSG101 component of the ESCRT machinery. *Virology*, 460-461, 83-90.
- BROWN, D. R., KITCHIN, D., QADARI, B., NEPTUNE, N., BATTEIGER, T. & ERMEL, A. 2006. The human papillomavirus type-11 E1-E4 protein is a



- transglutaminase 3 substrate and induces abnormalities of the cornified cell envelope. *Virology*, 345, 1, 290-298.
- BRUNI, L., ALBERO, G., ROWLEY, J., ALEMANY, L., ARBYN, M., GUILIANO, A. R., MARKOWITZ, L. E., BROUTET, N. & TAYLOR, M. 2023. Global and regional estimates of genital human papillomavirus prevalence among men: a systematic review and meta-analysis. *Lancet Glob Health*, 11, 9, e1345-1362.
- BRUNI, L., SAURA-LÁZARO, A., MONTOLIU, A., BROTONS, M., ALEMANY, L., DIALLO, M. S., AFSAR, O. Z., LAMONTAGNE, D. S., MOSINA, L., CONTERAS, M., VELANDIA-GONZÁLEZ, M., PASTORE, P., GACIC-DOBO, M. & BLOEM, P. 2021. HPV vaccination introduction worldwide and WHO and UNICEF estimates of national HPV immunization coverage 2010-2019. *Prev Med*, 144, 106399.
- BRUNI, L., SERRANO, B., ROURA, E., ALEMANY, L., COWAN, M., HERRERO, R., POLIJAK, M., MURILLO, R., BROUTET, N., RILEY, L. M. & DE SANJOSÉ, S. 2022. Cervical cancer screening programmes and age-specific coverage estimates for 202 countries and territories worldwide: a review and synthetic analysis. *Lancet Glob Health*, 10, 8, e1115-1127.
- BU, J. Q., BU, X., CHEN, P., LIU, B. & CHEN, F. 2015. Differences in expression of EGFR, Ki67 and p-EPK in oral cavity squamous cell carcinoma. *Trop J Pharm Res*, 14, 12, 2213-2216.
- BUCK, C. B., CHENG, N., THOMPSON, C. D., LOWY, D. R., STEVEN, A. C., SCHILLER, J. T. & TRUS, B. L. 2008. Arrangement of L2 within the papillomavirus capsid. *J Virol*, 82, 11, 5190-5197.
- BUTLER, J. E., NI, L., NESSLER, R., JOSHI, K. S., SUTER, M., ROSENBERG, B., CHANG, J., BROWN, W. R. & CANTARERO, L. A. 1992. The physical and functional behavior of capture antibodies adsorbed on polystyrene. *J Immunol Methods*, 150, 1-2, 77-90.
- BUTZ, K., RISTRANI, T., HENGSTERMANN, A., DENK, C., SCHEFFNER, M. & HOPPE-SEYLER, F. 2003. siRNA targeting of the viral E6 oncogene efficiently kills human papillomavirus-positive cancer cells. *Oncogene*, 22, 38, 5938-5945.
- CAMPOS, S. K. & OZBUN, M. A. 2009. Two highly conserved cysteine residues in HPV16 L2 form an intramolecular disulfide bond and are critical for infectivity in human keratinocytes. *PLoS One*, 4, 2, e4463.

- CASTELLSAGUÉ, X., ALEMANY, L., QUER, M., HALEC, G., QUIRÓS, B., TOUS, S., CLAVERO, O., ALÒS, L., BIEGNER, T., SZAFAROWSKI, T., ALEJO, M., HOLZINGER, D., CADENA, E., CLAROS, E., HALL, G., LACO, J., POLJAK, M., BENEVOLO, M., KASAMATSU, E., MEHANNA, H., NDIAYE, C., GUIMERÀ, N., LLOVERAS, B., LEÓN, X., RUIZ-CABEZAS, J. C., ALVARADO-CABRERO, I., KANG, C. S., OH, J. K., GARCIA-ROJO, M., ILJAZOVIC, E., AJAYI, O. F., DUARTE, F., NESSA, A., TINOCO, L., DURAN-PADILLA, M. A., PIROG, E. C., VIARHEICHYK, H., MORALES, H., COSTES, V., FÉLIX, A., GERMAR, M. J. V., MENA, M., RUACAN, A., JAIN, A., MEHROTRA, R., GOODMAN, M. T., LOMBARDI, L. E., FERRERA, A., MALAMI, S., ALBANESI, E. I., DABED, P., MOLINA, C., LÓPEZ-REVILLA, R., MANDYS, V., GONZÁLEZ, M. E., VELASCO, J., BRAVO, I. G., QUINT, W., PAWLITA, M., MUÑOZ, N., DE SANJOSÉ, S., BOSCH, F. X. & ICO INTERNATIONAL HPV IN HEAD AND NECK CANCER STUDY GROUP 2016. HPV involvement in head and neck cancers: comprehensive assessment of biomarkers in 3680 patients. *J Natl Cancer Inst*, 108, **6**, djv403.
- CASTRO-MUÑOZ, L. J., MANZO-MERINO, J., MUÑOZ-BELOO, J. O., OLMEDO-NIEVA, L., CEDRO-TANDA, A., ALFARO-RUIZ, L. A., HIDALGO-MIRANDA, A., MADRID-MARINA, V. & LIZANO, M. 2019. The human papillomavirus (HPV) E1 protein regulates the expression of cellular genes involved in immune response. *Sci Rep*, 9, **1**, 13620.
- CERQUEIRA, C., LIU, Y., KÜHLING, L., CHAI, W., HAFEZI, W., VAN KUPPEVELT, T. H., KÜHN, J. E., FEIZI, T. & SCHELHAAS, M. 2016. Heparin increases the infectivity of human papillomavirus type 16 independent of cell surface proteoglycans and induces L1 epitope exposure. *Cell Microbiol*, 15, **11**, 1818-1836.
- CESUR, Ö., NICOL, C., GROVES, H., MANKOURI, J., BLAIR, G. E. & STONEHOUSE, N. J. 2015. The subcellular localisation of the human papillomavirus (HPV) 16 E7 protein in cervical cancer cells and its perturbation by RNA aptamers. *Viruses*, 7, **7**, 3443-3461.
- CHANG, E. T., LIU, Z., HILDESHEIM, A., LIU, Q., CAI, Y., ZHANG, Z., CHEN, G., XIE, S. H., CAO, S. M., SHAO, J. Y., JIA, W. H., ZHENG, Y., LIAO, J., CHEN, Y., LIN, L., ERNBERG, I., VAUGHAN, T. L., ADAMI, H. O., HUANG, G., ZENG, Y., ZENG, Y. X. & YE, W. 2017. Active and passive smoking and risk of

- nasopharyngeal carcinoma: a population-based case-control study in southern china. *Am J Epidemiol*, 185, **12**, 1272-1280.
- CHARBONNIER, S., NOMINÉ, Y., RAMÍREZ, J., LUCK, K., CHAPELLE, A., STOTE, R. H., TRAVÉ, G., KIEFFER, B. & ATKINSON, R. A. 2011. The structural and dynamic response of MAGI-1 PDZ1 with noncanonical domain boundaries to the binding of human papillomavirus E6. *J Mol Biol*, 406, **5**, 745-763.
- CHATURVEDI, A. K., ANDERSON, W. F., LORTET-TIEULENT, J., CURADO, M. P., FERLAY, J., FRANCESCHI, S., ROSENBERG, P. S., BRAY, F. & GILLISON, M. L. 2013. Worldwide trends in incidence rates for oral cavity and oropharyngeal cancers. *J Clin Oncol*, 31, **36**, 4550-4559.
- CHATURVEDI, A. K., ENGELS, E. A., ANDERSON, W. F. & GILLISON, M. L. 2008. Incidence trends for human papillomavirus-related and -unrelated oral squamous cell carcinomas in the United States. *J Clin Oncol*, 26, **4**, 612-619.
- CHATURVEDI, A. K., ENGELS, E. A., PFEIFFER, R. M., HERNANDEZ, B. Y., XIAO, W., KIM, E., JIANG, B., GOODMAN, M. T., SIBUG-SABER, M., COZEN, W., LIU, L., LYNCH, C. F., WENTZENSEN, N., JORDAN, R. C., ALTEKRUSE, S., ANDERSON, W. F., ROSENBERG, P. S. & GILLISON, M. L. 2011. Human papillomavirus and rising oropharyngeal cancer incidence in the United States. *J Clin Oncol*, 29, **32**, 4294-4301.
- CHATURVEDI, A. K., GRAUBARD, B. I., BROUTIAN, T., PICKARD, R. K. L., TONG, Z. Y., XIAO, W., KAHLE, L. & GILLISON, M. L. 2015. NHANES 2009-2012 findings: association of sexual behaviours with higher prevalence of oral oncogenic human papillomavirus infections in U.S. men. *Cancer Res*, 75, **12**, 2468-2477.
- CHATZKEL, J., LEWIS, J. S. J., LEY, J. C., WILDES, T. M., THORSTAD, W. L., GAY, H., DALY, M., JACKSON, R., RICH, J., PANIELLO, R., NUSSENBAUM, B., LIU, J., SIEGEL, B. A., DEHDASHTI, F. & ADKINS, D. 2017. Correlation of Ki-67 proliferative antigen expression and tumor response to induction chemotherapy containing cell cycle-specific agents in head and neck squamous cell carcinoma. *Head Neck Pathol*, 11, **3**, 338-345.
- CHELLAPPAN, S. P., HIEBERT, S., MUDRYJ, M., HOROWITZ, J. M. & NEVINS, J. R. 1991. The E2F transcription factor is a cellular target for the RB protein. *Cell*, 65, **6**, 1053-1061.

- CHEN, J. J., HONG, Y., RUSTAMZADEH, E., BALEJA, J. D. & ANDROPHY, E. J. 1998. Identification of an alpha helical motif sufficient for association with papillomavirus E6. *J Biol Chem*, 273, **22**, 13537-13544.
- CHEN, S. Y., MASSA, S., MAZUL, A. L., KALLOGJERI, D., YAEGER, L., JACKSON, R. S., ZEVALLOS, J. & PIPKORN, P. 2020. The association of smoking and outcomes in HPV-positive oropharyngeal cancer: A systematic review. *Am J Otolaryngol*, 41, **5**, 102592.
- CHEN, X. S., GARCEA, R. L., GOLDBERG, I., CASINI, G. & HARRISON, S. C. 2000. Structure of small virus-like particles assembled from the L1 protein of human papillomavirus 16. *Mol Cell*, 5, **3**, 557-567.
- CHENG, C., CHEN, Y. H., LENNOX, K. A., BEHLKE, M. A. & DAVIDSON, B. L. 2013. In vivo SELEX for identification of brain-penetrating aptamers. *Mol Ther Nucleic Acids*, 2, **1**, e67.
- CHENG, S., SCHMIDT-GRIMMINGER, D. C., MURANT, T., BROKER, T. R. & CHOW, L. T. 1995. Differentiation-dependent up-regulation of the human papillomavirus E7 gene reactivates cellular DNA replication in suprabasal differentiated keratinocytes. *Genes Dev*, 9, **19**, 2335-2349.
- CHERNOCK, R. D., EL-MOFTY, S. K., THORSTAD, W. L., PARVIN, C. A. & J.S.JR, L. 2009. HPV-related nonkeratinizing squamous cell carcinoma of the oropharynx: utility of microscopic features in predicting patient outcome. *Head Neck Pathol*, 3, **3**, 186-194.
- CHI, A. C., DAY, T. A. & NEVILLE, B. W. 2015. Oral cavity and oropharyngeal squamous cell carcinoma-an update. *CA Cancer J Clin*, 65, **5**, 401-421.
- CHIANG, C. M., USTAV, M., STENLUND, A., HO, T. F., BROKER, T. R. & CHOW, L. T. 1992. Viral E1 and E2 proteins support replication of homologous and heterologous papillomaviral origins. *Proc Natl Acad Sci USA*, 89, **13**, 5799-5803.
- CHU, P., WU, E. & WEISS, L. M. 2000. Cytokeratin 7 and cytokeratin 20 expression in epithelial neoplasms: a survey of 435 cases. *Mod Pathol*, 13, **9**, 962-972.
- CIANCHETTI, M., MANCUSO, A. A., AMDUR, R. J., WERNING, J. W., KIRWAN, J., MORRIS, C. G. & MENDENHALL, W. M. 2009. Diagnostic evaluation of squamous cell carcinoma metastatic to cervical lymph nodes from an unknown head and neck primary site. *Laryngoscope*, 119, **12**, 2348-2354.
- COHEN, E. E. W., SOULIÈRES, D., LE TOURNEAU, C., DINIS, J., LICITRA, L., AHN, M. J., SORIA, A., MACHIELS, J. P., MACH, N., MEHRA, R., BURTNESSE, B.,

- ZHANG, P., CHENG, J., SWABY, R. F., HARRINGTON, K. J. & KEYNOTE-040 INVESTIGATORS 2019. Pembrolizumab versus methotrexate, docetaxel, or cetuximab for recurrent or metastatic head-and-neck squamous cell carcinoma (KEYNOTE-040): a randomised, open-label, phase 3 study. *Lancet*, 393, **10167**, 156-167.
- CONCHA-BENAVENTE, F., SRIVASTAVA, R. M., TRIVEDI, S., LEI, Y., CHANDRAN, U., SEETHALA, R. R., FREEMAN, G. J. & FERRIS, R. L. 2016. Identification of the cell-intrinsic and extrinsic pathways downstream of EGFR and IFN $\gamma$  that induce PD-L1 expression in head and neck cancer. *Cancer Res*, 76, **5**, 1031-1043.
- COONS, A. H., CREECH, H. J. & JONES, R. N. 1941. Immunological properties of an antibody containing a fluorescent group. *Proc Soc Exp Biol Med*, 47, **2**, 200-202.
- COOPER, J. S., PAJAK, T. F., FORASTIERE, A. A., JACOBS, J., CAMPBELL, B. H., SAXMAN, S. B., KISH, J. A., KIM, H. E., CMELAK, A. J., ROTMAN, M., MACHTAY, M., ENSLEY, J. F., CHAO, K. S. C., SCHULTZ, C. J., LEE, N., FU, K. K. & 9501/INTERGROUP, R. T. O. G. 2004. Postoperative concurrent radiotherapy and chemotherapy for high-risk squamous-cell carcinoma of the head and neck. *N Engl J Med*, 350, **19**, 1937-1944.
- COUTURE, C., RAYBAUD-DIOGÈNE, H., TÊTU, B., BAIRATI, I., MURRY, D., ALLARD, J. & FORTIN, A. 2002. p53 and Ki-67 as markers of radioresistance in head and neck carcinoma. *Cancer*, 94, **3**, 713-722.
- CRAIG, S. G., ANDERSON, L. A., MORAN, M., GRAHAM, L., CURRIE, K., ROONEY, K., ROBINSON, M., BINGHAM, V., CUSCHIERI, K. S., MCQUAID, S., SCHACHE, A. G., JONES, T. M., MCCANCE, D., SALTO-TELLEZ, M., MCDADE, S. S. & JAMES, J. A. 2020. Comparison of molecular assays for HPV testing in oropharyngeal squamous cell carcinomas: a population-based study in Northern Ireland. *Cancer Epidemiol Biomarkers Prev*, 29, **1**, 31-38.
- CRAIG, S. G., ANDERSON, L. A., SCHACHE, A. G., MORAN, M., GRAHAM, L., CURRIE, K., ROONEY, K., ROBINSON, M., UPILE, N. S., BROOKER, R., MESRI, M., BINGHAM, V., MCQUAID, S., JONES, T., MCCANCE, D. J., SALTO-TELLEZ, M., MCDADE, S. S. & JAMES, S. A. 2019. Recommendations for determining HPV status in patients with oropharyngeal cancers under TNM8 guidelines: a two-tier approach. *Br J Cancer*, 120, **8**, 827-833.

- CROOK, T., TIDY, J. A. & VOUSDEN, K. H. 1991. Degradation of p53 can be targeted by HPV E6 sequences distinct from those required for p53 binding and trans-activation. *Cell*, 67, 3, 547-556.
- CULP, T. D., BUDGEON, L. R. & CHRISTENSEN, N. D. 2006. Human papillomaviruses bind a basal extracellular matrix component secreted by keratinocytes which is distinct from a membrane-associated receptor. *Virology*, 347, 1, 147-159.
- CUSCHIERI, K. S., CUBIE, H. A., WHITLEY, M. W., GILKISON, G., ARENDS, M. J., GRAHAM, C. & MCGOOGAN, E. 2005. Persistent high risk HPV infection associated with development of cervical neoplasia in a prospective population study. *J Clin Pathol*, 58, 9, 946-950.
- D'SOUZA, G., AGRAWAL, Y., HALPERN, J., BODISON, S. & GILLISON, M. L. 2009. Oral sexual behaviours associated with prevalent oral papillomavirus infection. *J Infect Dis*, 199, 9, 1263-1269.
- D'SOUZA, G., CLEMENS, G., STRICKLER, H. D., WILEY, D. J., TROY, T., STRUIJK, L., GILLISON, M. & FAKHRY, C. 2020. Long-term persistence of oral HPV over 7 years of follow-up. *JNCI Cancer Spectr*, 4, 5, pkaa047.
- D'SOUZA, G., TEWARI, S. R., TROY, T., WEBSTER-CYRIAQUE, J., WILEY, D. J., LAHIRI, C. D., PALELLA, F. J., GILLISON, M. L., STRICKLER, H. D., STRUIJK, L., WATERBOER, T., HO, K., KWAIT, J., LAZAR, J., WEBER, K. M. & FAKHRY, C. 2024. Oncogenic oral human papillomavirus clearance patterns over 10 years. *Cancer Epidemiol Biomarkers Prev*, OF1-OF9.
- DAHIYA, A., GAVIN, M. R., LUO, R. X. & DEAN, D. C. 2000. Role of the LXCXE binding site in Rb function. *Mol Cell Biol*, 20, 18, 6799-6805.
- DAVY, C., MCINTOSH, P., JACKSON, D. J., SORATHIA, R., MIELL, M., WANG, Q., KHAN, J., SONEJI, Y. & DOORBAR, J. 2009. A novel interaction between the human papillomavirus type 16-E2 and E1-E4 proteins leads to stabilization of E2. *Virology*, 394, 2, 266-275.
- DAY, P. M., BAKER, C. C., LOWY, D. R. & SCHILLER, J. T. 2004. Establishment of papillomavirus infection is enhanced by promyelocytic leukemia protein (PML) expression. *Proc Natl Acad Sci USA*, 101, 39, 14252-14257.
- DAY, P. M., THOMPSON, C. D., SCHOWALTER, R. M., LOWY, D. R. & SCHILLER, J. T. 2013. Identification of a role for the trans-Golgi network in human papillomavirus 16 pseudovirus infection. *J Virol*, 87, 7, 3862-3870.

- DE MARTEL, C., GEORGES, D., BRAY, F., FERLAY, J. & CLIFFORD, G. M. 2020. Global burden of cancer attributable to infections in 2018: a worldwide incidence analysis. *Lancet Glob health*, 8, 2, e180-190.
- DE MARTEL, C., PLUMMER, M., VIGNAT, J. & FRANCESCHI, S. 2017. Worldwide burden of cancer attributable to HPV by site, country and HPV type. *Int J Cancer*, 141, 4, 664-670.
- DE PERROT, T., LENOIR, V., DOMINGO AYLLÓN, M., DULGUEROV, N., PUSZTASZERI, M. & BECKER, M. 2017. Apparent diffusion coefficient histograms of human papillomavirus–positive and human papillomavirus–negative head and neck squamous cell carcinoma: assessment of tumor heterogeneity and comparison with histopathology. *AJNR Am J Neuroradiol*, 38, 11, 2153-2160.
- DE RODA HUSMAN, A. M., WALBOOMERS, J. M. M., VAN DEN BRULE, A. J. C., MEIJER, C. J. L. M. & SNIJDERS, P. J. F. 1995. The use of general primers GP5 and GP6 elongated at their 3' ends with adjacent highly conserved sequences improves human papillomavirus detection by PCR. *J Gen Virol*, 76, 4, 1057-1062.
- DE SANJOSÉ, S., QUINT, W. G., ALEMANY, L., GERAETS, D. T., KLAUSTERMEIER, J. E., LLOVERAS, B., TOUS, S., FELIX, A., BRAVO, L. E., SHIN, H. R., VALLEJOS, C. S., DE RUIZ, P. A., LIMA, M. A., GUIMERA, N., CLAVERO, O., ALEJO, M., LLOMBART-BOSCH, A., CHENG-YANG, C., TATTI, S. A., KASAMATSU, E., ILJAZOVIC, E., ODIDA, M., PRADO, R., SEOUD, M., GRCE, M., USUBUTUN, A., JAIN, A., SUAREZ, G. A. H., LOMBARDI, L. E., BANJO, A., MENÉNDEZ, C., DOMINGO, E. J., VELASCO, J., NESSA, A., CHICHAREON, S. C. B., QIAO, Y. L., LERMA, E., GARLAND, S. M., SASAGAWA, T., FERRERA, A., HAMMOUDA, D., MARIANI, L., PELAYO, A., STEINER, I., OLIVA, E., MEIJER, C. J., AL-JASSAR, W. F., CRUZ, E., WRIGHT, T. C., PURAS, A., LLAVE, C. L., TZARDI, M., AGORASTOS, T., GARCIA-BARRIOLA, V., CLAVEL, C., ORDI, J., ANDÚJAR, M., CASTELLSAGUÉ, X., SÁNCHEZ, G. I., NOWAKOWSKI, A. M., BORNSTEIN, J., MUÑOZ, N. & BOSCH, F. X. 2010. Human papillomavirus genotype attribution in invasive cervical cancer: a retrospective cross-sectional worldwide study. *Lancet Oncol*, 11, 11, 1048-1056.

- DE VILLIERS, E. M., FAUQUET, C., BROKER, T. R., BERNARD, H. U. & ZUR HAUSEN, H. 2004. Classification of papillomaviruses. *Virology*, 324, 1, 17-27.
- DE VINCENTE, J. C., RODRÍGUEZ-SANTAMARTA, T., RODRIGO, J. P., BLANCO-LORENZO, V., ALLONCA, E. & GARCÍA-PEDRERO, J. M. 2019. PD-L1 expression in tumor cells is an independent unfavourable prognostic factor in oral squamous cell carcinoma. *Cancer Epidemiol Biomarkers Prev*, 28, 3, 546-554.
- DEEPAK, R. N. V. K. & SANKARARAMAKRISHNAN, R. 2016. Unconventional N-H...N hydrogen bonds involving proline backbone nitrogen in protein structures. *Biophys J*, 110, 9, 1967-1979.
- DELURY, C. P., MARSH, E. K., JAMES, C. D., SHI-BOON, S., BANKS, L., KNIGHT, G. L. & ROBERTS, S. 2013. The role of protein kinase A regulation of the E6 PDZ-binding domain during the differentiation-dependent life cycle of human papillomavirus type 18. *J Virol*, 87, 17, 9463-9472.
- DEPPMANN, C. D., THORNTON, T. M., UTAMA, F. E. & TAPAROWSKY, E. J. 2003. Phosphorylation of BATF regulates DNA binding: a novel mechanism for AP-1 (activator protein-1) regulation. *Biochem J*, 374, 423-431.
- DEROSA, M. C., LIN, A., MALLIKARATCHY, P., MCCONNELL, E. M., MCKEAGUE, M., PATEL, R. & SHIGDAR, S. 2023. In vitro selection of aptamers and their applications. *Nat Rev Methods Primers*, 3, 55.
- DEUSS, E., GÖßWEIN, D., GÜL, D., ZIMMER, S., FOERSCH, S., EGER, C. S., LIMBURG, I., STAUBER, R. H. & KÜNZEL, J. 2020. Growth factor receptor expression in oropharyngeal squamous cell cancer: Her1-4 and c-Met in conjunction with the clinical features and human papillomavirus (p16) status. *Cancers (Basel)*, 12, 11, 3358.
- DEUTSCH, F., BULLEN, I. R., NGUYEN, K., TRAN, N. H., ELLIOTT, M. & TRAN, N. 2022. Current state of play for HPV-positive oropharyngeal cancers. *Cancer Treat Rev*, 110, 102439.
- DIGIUSEPPE, S., BIENKOWSKA-HABA, M., HILBIG, L. & SAPP, M. 2014. The nuclear retention of HPV16 L2 protein is essential for incoming viral genome to transverse the trans-Golgi network. *Virology*, 458-459, 93-105.
- DONG, H., ZHU, G., TAMADA, K. & CHEN, L. 1999. B7-H1, a third member of the B7 family, co-stimulates T-cell proliferation and interleukin-10 secretion. *Nat Med*, 5, 12, 1365-1369.



- DONG, Z., HU, R., DU, Y., LI, L., DU, J., BAI, L., MA, Y. & CUI, H. 2021. Immunodiagnosis and immunotherapeutics based on human papillomavirus for HPV-induced cancers. *Front Immunol*, 11, 586796.
- DOORBAR, J. 2013. The E4 protein: structure, function and patterns of expression. *Virology*, 445, 1-2, 80-98.
- DOORBAR, J., CAMPBELL, D., GRAND, R. J. & GALLIMORE, P. H. 1986. Identification of the human papilloma virus-1a E4 gene products. *EMBO J*, 5, 2, 355-362.
- DOORBAR, J., EGAWA, N., GRIFFIN, H., KRANJEC, C. & MURAKAMI, I. 2016. Human papillomavirus molecular biology and disease association. *Rev Med Virol*, 25, 2-23.
- DOORBAR, J., ELY, S., STERLING, J., MCLEAN, C. & CRAWFORD, L. 1991. Specific interaction between HPV-16 E1-E4 and cytokeratins results in collapse of the epithelial cell intermediate filament network. *Nature*, 352, 6338, 824-827.
- DOORBAR, J., FOO, C., COLEMAN, N., MEDCALF, L., HARTLEY, O., PROSPERO, T., NAPHTHINE, S., STERLING, J., WINTER, G. & GRIFFIN, H. 1997. Characterization of events during the late stages of HPV16 infection in vivo using high-affinity synthetic Fabs to E4. *Virology*, 238, 1, 40-52.
- DOWHANICK, J. J., MCBRIDE, A. A. & HOWLEY, P. M. 1995. Suppression of cellular proliferation by the papillomavirus E2 protein. *J Virol*, 69, 12, 7791-7799.
- DOWNHAM, L., JAAFAR, I., ROL, M. L., NYAGA, V. N., VALLS, J., BAENA, A., ZHANG, L., GUNTER, M. J., ARBYN, M. & ALMONTE, M. 2024. Accuracy of HPV E6/E7 oncoprotein tests to detect high-grade cervical lesions: a systematic literature review and meta-analysis. *Br J Cancer*, 130, 4, 517-525.
- DOXTADER, E. E. & KATZENSTEIN, A. L. 2012. The relationship between p16 expression and high-risk human papillomavirus infection in squamous cell carcinomas from sites other than uterine cervix: a study of 137 cases. *Hum Pathol*, 43, 3, 327-332.
- DUDÁS, B. 2023. *Human histology: a text and atlas for physicians and scientists*, London, Elsevier Science & Technology.
- DYMALLA, S., SCHEFFNER, M., WEBER, E., SEHR, P., LOHREY, C., HOPPE-SEYLER, F. & HOPPE-SEYLER, K. 2009. A novel peptide motif binding to and blocking the intracellular activity of the human papillomavirus E6 oncoprotein. *J Mol Biol (Berl)*, 87, 3, 321-331.

- DYSON, N., GUIDA, P., MÜNGER, K. & HARLOW, E. 1992. Homologous sequences in adenovirus E1A and human papillomavirus E7 proteins mediate interaction with the same set of cellular proteins. *J Virol*, 66, **12**, 6893-6902.
- DYSON, N., HOWLEY, P. M., MÜNGER, K. & HARLOW, E. 1989. The human papilloma virus-16 E7 oncoprotein is able to bind to the retinoblastoma gene product. *Science*, 243, **4893**, 934-937.
- EGAWA, N., NAKAHARA, T., OHNO, S. I., NARISAWA-SAITO, M., YUGAWA, T., FUJITA, M., YAMATO, K., NATORI, Y. & KIYONO, T. 2012. The E1 protein of human papillomavirus type 16 is dispensable for maintenance replication of the viral genome. *J Virol*, 86, **6**, 3276-3283.
- EL-MOFTY, S. K. 2014. Histopathologic risk factors in oral and oropharyngeal squamous cell carcinoma variants: An update with special reference to HPV-related carcinomas. *Med Oral Patol Oral Cir Bucal*, 19, **4**, e377-385.
- EL-MOFTY, S. K. & LU, D. W. 2003. Prevalence of human papillomavirus type 16 DNA in squamous cell carcinoma of the palatine tonsil, and not the oral cavity, in young patients: a distinct clinicopathologic and molecular disease entity. *Am J Surg Pathol*, 27, **11**, 1463-1470.
- EL-MOFTY, S. K. & PATIL, S. 2006. Human papillomavirus (HPV)-related oropharyngeal nonkeratinising squamous cell carcinoma: characterisation of a distinct phenotype. *Oral Surg Oral Med Oral Pathol Oral Radiol Endod*, 101, **3**, 339-345.
- EL-MOFTY, S. K., ZHANG, M. Q. & DAVILA, R. M. 2008. Histologic identification of human papillomavirus (HPV)-related squamous cell carcinoma in cervical lymph nodes: a reliable predictor of the site of an occult head and neck primary carcinoma. *Head Neck Pathol*, 2, **3**, 163-168.
- EL-NAGGAR, A. K. & WESTRA, W. H. 2012. p16 expression as a surrogate marker for HPV-related oropharyngeal carcinoma: a guide for interpretative relevance and consistency. *Head Neck*, 34, **4**.
- ELLINGTON, A. D. & SZOSTAK, J. W. 1990. In vitro selection of RNA molecules that bind specific ligands. *Nature*, 346, **6287**, 818-822.
- ELLINGTON, A. D. & SZOSTAK, J. W. 1992. Selection in vitro of single-stranded DNA molecules that fold into specific ligand-binding structures. *Nature*, 355, **6363**, 850-852.

- ELREFAEY, S., MASSARO, M. A., CHIOCCA, S., CHIESA, F. & ANSARIN, M. 2014. HPV in oropharyngeal cancer: the basics to know in clinical practice. *Acta Otorhinolaryngol Ital*, 34, 5, 299-309.
- ENGEL, L. W., HEILMAN, C. A. & HOWLEY, P. M. 1983. Transcriptional organisation of bovine papillomavirus type 1. *J Virol*, 47, 3, 516-528.
- EUROPEAN MEDICINES AGENCY. 2011. *Pfizer Limited withdraws its application for an extension of the indication for Macugen (pegaptanib sodium)* [Online]. EMA. Available: <https://www.ema.europa.eu/en/news/pfizer-limited-withdraws-its-application-extension-indication-macugen-pegaptanib-sodium> [Accessed 15/05/2024].
- EWEN, M. E., SLUSS, H. K., SHERR, C. J., MATSUSHIME, H., KATO, J. Y. & LIVINGSTON, D. M. 1993. Functional interactions of the retinoblastoma protein with mammalian D-type cyclins. *Cell*, 73, 3, 487-497.
- FÅHRAEUS, R., PARAMIO, J. M., BALL, K. L., LAÍN, S. & LANE, D. P. 1996. Inhibition of pRb phosphorylation and cell-cycle progression by a 20-residue peptide derived from p16CDKN2/INK4A. *Curr Biol*, 6, 1, 84-91.
- FAKHRY, C., ROSENTHAL, B. T., CLARK, D. P. & GILLISON, M. L. 2012. Associations between oral HPV16 infection and cytopathology: evaluation of an oropharyngeal "Pap-test equivalent" in high-risk populations. *Cancer Prev Res (Phila)*, 4, 9, 1378-1384.
- FARAJI, F., RETTIG, E. M., TSAI, H. L., EL ASMAR, M., FUNG, N., EISELE, D. W. & FAKHRY, C. 2019. The prevalence of human papillomavirus in oropharyngeal cancer is increasing regardless of sex or race, and the influence of sex and race on survival is modified by human papillomavirus tumor status. *Cancer*, 125, 5, 761-769.
- FATIMA, N., COHEN, C., LAWSON, D. & SIDDIQUI, M. T. 2013. Automated and manual human papilloma virus in situ hybridization and p16 immunohistochemistry: comparison in metastatic oropharyngeal carcinoma. *Acta Cytol*, 57, 6, 633-640.
- FEENEY, K. M. & PARISH, J. L. 2009. Targeting mitotic chromosomes: a conserved mechanism to ensure viral genome persistence. *Proc Biol Sci*, 276, 1662, 1535-1544.

- FEHRMANN, F., KLUMPP, D. J. & LAIMINS, L. A. 2003. Human papillomavirus type 31 E5 protein supports cell cycle progression and activates late viral functions upon epithelial differentiation. *J Virol*, 77, 5, 2819-2831.
- FENG, W., XIAO, J., ZHANG, Z., ROSEN, D. G., BROWN, R. E., LIU, J. & DUAN, X. 2007. Senescence and apoptosis in carcinogenesis of cervical squamous carcinoma. *Mod Pathol*, 20, 9, 961-966.
- FERLAY, J., ERVIK, M., LAM, F., LAVERSANNE, M., COLOMBET, M., MERY, L., PIÑEROS, M., ZNAOR, A., SOERJOMATARAM, I. & BRAY, F. 2024. *Global Cancer Observatory: Cancer Today* [Online]. Lyon, France: International Agency for Research on Cancer. Available: <https://gco.iarc.fr/> [Accessed 28/02/2024].
- FIALOVÁ, A., KOUCKÝ, V., HAJDUŠKOVÁ, M., HLADÍKOVÁ, K. & ŠPÍŠEK, R. 2020. Immunological network in head and neck squamous cell carcinoma-a prognostic tool beyond HPV status. *Front Oncol*, 10, 1701.
- FIORETTI, A. 1957. La tonsilla palatina. *Deca*.
- FLEMINGTON, E. K., SPECK, S. H. & KAELIN, W. G. J. 1993. E2F-1-mediated transactivation is inhibited by complex formation with the retinoblastoma susceptibility gene product. *Proc Natl Acad Sci USA*, 90, 15, 6914-6918.
- FLORIN, L., SAPP, C., STREECK, R. E. & SAPP, M. 2002. Assembly and translocation of papillomavirus capsid proteins. *J Virol*, 76, 19, 10009-10014.
- FONSÊCA, T. C., JURAL, L. A., MARAÑÓN-VÁSQUEZ, G. A., MAGNO, M. B., ROZA, A. L. O. C., FERREIRA, D. M. T. P., MAIA, L. C., ROMAÑACH, M. J., AGOSTINI, M. & ABRAHÃO, A. C. 2024. Global prevalence of human papillomavirus-related oral and oropharyngeal squamous cell carcinomas: a systematic review and meta-analysis. *Clin Oral Investig*, 28, 1, 62.
- FOSSUM, C. C., CHINTAKUNTLAWAR, A. V., PRICE, D. L. & GARCIA, J. J. 2017. Characterisation of the oropharynx: anatomy, histology, immunology, squamous cell carcinoma and surgical resection. *Histopathology*, 70, 1021-1029.
- FREEDMAN, N. D., SCHATZKIN, A., LEITZMANN, M. F., HOLLENBECK, A. R. & ABNET, C. C. 2007. Alcohol and head and neck cancer risk in a prospective study. *Br J Cancer*, 96, 9, 1469-1474.
- GAMBHIRA, R., JAGU, S., KARANAM, B., DAY, P. M. & RODEN, R. 2009. Role of L2 cysteines in papillomavirus infection and neutralization. *Virology*, 6, 176.

- GAMEIRO, S., GHASEMI, F., BARRETT, J. W., KOROPATNICK, J., NICHOLS, A. C., MYMRYK, J. S. & VAREKI, S. M. 2018. Treatment-naïve HPV+ head and neck cancers display a T-cell-inflamed phenotype distinct from their HPV-counterparts that has implications for immunotherapy. *Oncoimmunology*, **7**, **10**, e1498439.
- GANESAN, R., SINGH, N. & WILLIAMS, A. T. *Dataset for histopathological reporting of cervical neoplasia*. 4th. London, UK: The Royal College of Pathologists. Available: <https://www.rcpath.org/static/eb26fb88-3db6-417b-97ee6338ef54dc79/af413185-5486-40db-b703fab65f27fe63/g071cervicalneoplasia dataset for publication.pdf>
- GANTI, K., MASSIMI, P., MANZO-MERINO, J., TOMAIĆ, V., PIM, D., PLAYFORD, M. P., LIZANO, M., ROBERTS, S., KRANJEC, C., DOORBAR, J. & BANKS, L. 2016. Interaction of the human papillomavirus E6 oncoprotein with sorting nexin 27 modulates endocytic cargo transport pathways. *PLoS Pathog*, **12**, **9**, e10005854.
- GELINAS, A. D., DAVIES, D. R. & JANJIC, N. 2016. Embracing proteins: structural themes in aptamer-protein complexes. *Curr Opin Struct Biol*, **36**, 122-132.
- GENTHER, S. M., STERLING, S., DUENSING, S., MÜNGER, K., SATTLER, C. & LAMBERT, P. F. 2003. Quantitative role of the human papillomavirus type 16 E5 gene during the productive stage of the viral life cycle. *J Virol*, **77**, **5**, 2832-2842.
- GERDES, J., LEMKE, H., BAISCH, H., WACKER, H. H., SCHWAB, U. & STEIN, H. 1984. Cell cycle analysis of a cell proliferation-associated human nuclear antigen defined by the monoclonal antibody Ki-67. *J Immunol*, **133**, **4**, 1710-1715.
- GILLISON, M. L., ALEMANY, L., SNIJDERS, P. J. F., CHATURVEDI, A., STEINBERG, B. M., SCHWARTZ, S. & CASTELLSAGUÉ, X. 2012. Human papillomavirus and diseases of the upper airway: head and neck cancer and respiratory papillomatosis. *Vaccine*, **30**, F34-54.
- GILLISON, M. L., CHATURVEDI, A. K., ANDERSON, W. F. & FAKHRY, C. 2015. Epidemiology of human papillomavirus-positive head and neck squamous cell carcinoma. *J Clin Oncol*, **33**, **29**, 3235-3242.
- GILLISON, M. L., D'SOUZA, G., WESTRA, W., SUGAR, E., XIAO, W., BEGUM, S. & VISCIDI, R. 2008. Distinct risk factor profiles for human papillomavirus type 16-

- positive and human papillomavirus type 16-negative head and neck cancers. *J Natl Cancer Inst*, 100, **6**, 407-420.
- GILLISON, M. L., KOCH, W. M., CAPONE, R. B., SPAFFORD, M., WESTRA, W. H., WU, L., ZAHURAK, M. L., DANIEL, R. W., VIGLIONE, M., SYMER, D. E., SHAH, K. V. & SIDRANSKY, D. 2000. Evidence for a causal association between human papillomavirus and a subset of head and neck cancers. *J Natl Cancer Inst*, 92, **9**, 709-720.
- GIOTAKIS, A. I., RUNGE, A., DUDAS, J., GLUECKERT, R., GOTTFRIED, T., SCHARTINGER, V. H., KLARER, J., RANDHAWA, A., CAIMMI, E. & RIECHELMANN, H. 2023. Analysis of cells of epithelial, connective tissue and immune differentiation in HPV-positive-, HPV-negative oropharyngeal carcinoma and normal oropharyngeal tissue by immunofluorescence multiplex image cytometry: a preliminary report. *BMC Cancer*, 23, **1**, 1154.
- GIRI, I. & YANIV, M. 1988. Structural and mutational analysis of E2 trans-activating proteins of papillomaviruses reveals three distinct functional domains. *EMBO J*, 7, **9**, 2823-2829.
- GIROGLOU, T., FLORIN, L., SCHÄFER, F., STREECK, R. E. & SAPP, M. 2001. Human papillomavirus infection requires cell surface heparan sulfate. *J Virol*, 75, **3**, 1565-1570.
- GIULIANO, A. R., SEDJO, R. L., ROE, D. J., HARRI, R., BALDWI, S., PAPENFUSS, M. R., ABRAHAMSEN, M. & INSERRA, P. 2002. Clearance of oncogenic human papillomavirus (HPV) infection: effect of smoking (United States). *Cancer Causes Control*, 13, **9**, 839-846.
- GOLDSMITH, J. D., TROXELL, M. L., ROY-CHOWDHURI, S., COLASACCO, C. F., EDGERTON, M. E., FITZGIBBONS, P. L., FULTON, R., HAAS, T., KANDALAFT, P. L., KALICANIN, T., LACCHETTI, C., LOYKASEK, P., THOMAS, N. E., SWANSON, P. E. & BELLIZZI, A. M. 2024. Principles of analytic validation of immunohistochemical assays: guideline update. *Arch Pathol Lab Med*, 148, **6**, e111-153.
- GONDIM, D. D., HAYNES, W., WANG, X., CHERNOCK, R. D., EL-MOFTY, S. K. & LEWIS, J. S. J. 2016. Histologic typing in oropharyngeal squamous cell carcinoma: a 4-year prospective practice study with p16 and high-risk HPV mRNA testing correlation. *Am J Surg Pathol*, 40, **8**, 1117-1124.

- GOODMAN, M. T., SARAIYA, M., THOMPSON, T. D., STEINAU, M., HERNANDEZ, B. Y., LYNCH, C. F., LYU, C. W., WILKINSON, E. J., TUCKER, T., COPELAND, G., PETERS, E. S., ALTEKRUSE, S. & UNGER, E. R. 2015. Human papillomavirus genotype and oropharynx cancer survival in the United States of America. *Eur J Cancer*, 51, **18**, 2759-2767.
- GOURRONC, F. A., ROCKEY, W. M., THIEL, W. H., GIANGRANDE, P. H. & KLINGELHUTZ, A. J. 2013. Identification of RNA aptamers that internalize into HPV-16 E6/E7 transformed tonsillar epithelial cells. *Virology*, 446, **1-2**, 325-333.
- GRAGOUDAS, E. S., ADAMIS, A. P., CUNNINGHAM, E. T. J., FEINSOD, M., GUYER, D. R. & VEGF INHIBITION STUDY IN OCULAR NEOVASCULARIZATION CLINICAL TRIAL GROUP 2004. Pegaptanib for neovascular age-related macular degeneration. *N Engl J Med*, 351, **27**, 2805-2816.
- GRAHAM, J. C. & ZARBL, H. 2012. Use of cell-selex to generate DNA aptamers as molecular probes of HPV-associated cervical cancer cells. *PLoS One*, 7, **4**, e36103.
- GRAPHPAD SOFTWARE INC 10.2.1 ed. Boston, Massachusetts, USA.
- GRASSMANN, K., RAPP, B., MASCHEK, H., PETRY, K. U. & IFTNER, T. 1996. Identification of a differentiation-inducible promoter in the E7 open reading frame of human papillomavirus type 16 (HPV-16) in raft cultures of a new cell line containing high copy numbers of episomal HPV-16 DNA. *J Virol*, 70, **4**, 2339-2349.
- GRUENKE, P. R., ANEJA, R., WELBOURN, S., UKAH, O. B., SARAFIANOS, S. G., BURKE, D. H. & LANGE, M. J. 2022. Selection and identification of an RNA aptamer that specifically binds the HIV-1 capsid lattice and inhibits viral replication. *Nucleic Acids Res*, 50, **3**, 1701-1717.
- GUO, M., GONG, Y., DEAVERS, M., SILVA, E. G., JAN, Y. S., COGDELL, D. E. & LUTHRA, R. 2008. Evaluation of a commercialized in situ hybridization assay for detecting human papillomavirus DNA in tissue specimens from patients with cervical intraepithelial neoplasia and cervical carcinoma. *J Clin Microbiol*, 46, **1**, 274-280.
- GUPTA, P., MIGLIACCI, J. C., HAY, A., ROSENTHAL, M., MIMICA, X., LEE, N., WONG, R. J., SHAH, J., PATEL, S. & GANLY, I. 2018. Validation and

assessment of discordance of the 8th edition AJCC (American Joint Committee on Cancer) clinical and pathologic staging systems in patients with p16+ oropharyngeal cancer treated with surgery and adjuvant radiation at a single institution. *Oral Oncol*, 83, 140-146.

GUZMÁN-AROCHO, Y. D. & NISHINO, M. 2022. The discordant biomarker dilemma: what are the diagnostic implications of oropharyngeal squamous cell carcinomas with discrepant p16 and HPV results? *Cancer Cytopathol*, 130, 11, 844-848.

HAMMER, A., DE KONING, M. N., BLAAKAER, J., STEINICHE, T., DOORBAR, J., GRIFFIN, H., MEJLGAARD, E., SVANHOLM, H., QUINT, W. G. & GRAVITT, P. E. 2019. Whole tissue cervical mapping of HPV infection: molecular evidence for focal latent HPV infection in humans. *Papillomavirus Res*, 7, 82-87.

HARDEN, M. E. & MUNGER, K. 2017. Human papillomavirus molecular biology. *Mutat Res*, 772, 3-12.

HARRINGTON, K. J., FERRIS, R. L., BLUMENSCHNEIN, G. J., COLEVAS, A. D., FAYETTE, J., LICITRA, L., KASPER, S., EVEN, C., VOKES, E. E., WORDEN, F., SABA, N. F., KIYOTA, N., HADDAD, R., TAHARA, M., GRÜNWARD, V., SHAW, J. W., MONGA, M., LYNCH, M., TAYLOR, F., DEROSA, M., MORRISSEY, L., COCKS, K., GILLISON, M. L. & GUIGAY, J. 2017. Nivolumab versus standard, single-agent therapy of investigator's choice in recurrent or metastatic squamous cell carcinoma of the head and neck (CheckMate 141): health-related quality-of-life results from a randomised, phase 3 trial. *Lancet Oncol*, 18, 8, 1104-1115.

HARRIS, L., MCFARLANE-MAJEED, L., CAMPOS-LEÓN, K., ROBERTS, S. & PARISH, J. L. 2017. The cellular DNA helicase ChIR1 regulates chromatin and nuclear matrix attachment of the human papillomavirus 16 E2 protein and high-copy-number viral genome establishment. *J Virol*, 91, 1, e01853-16.

HASHIBE, M., BRENNAN, P., BENHAMOU, S., CASTELLSAGUÉ, X., CHEN, C., CURADO, M. P., DAL MASO, L., DAUDT, A. W., FABIANOVA, E., FERNANDEZ, L., WÜNSCH-FILHO, V., FRANCESCHI, S., HAYES, R. B., HERRERO, R., KOIFMAN, S., LA VECCHIA, C., LAZARUS, P., LEVI, F., MATES, D., MATOS, E., MENEZES, A., MUSCAT, J., ELUF-NETO, J., OLSHAN, A. F., RUDNAI, P., SCHWARTZ, S. M., SMITH, E., STURGIS, E. M., SZESZENIA-DABROWSKA, N., TALAMINI, R., WEI, Q., WINN, D. M.,



- ZARIDZE, D., ZATONSKI, W., ZHANG, Z. F., BERTHILLER, J. & BOFFETTA, P. 2007. Alcohol drinking in never users of tobacco, cigarette smoking in never drinkers, and the risk of head and neck cancer: pooled analysis in the International Head and Neck Cancer Epidemiology Consortium. *J Natl Cancer Inst*, 99, **10**, 777-789.
- HASHIBE, M., BRENNAN, P., CHUNAG, S. C., BOCCIA, S., CASTELLSAGUÉ, X., CHEN, C., CURADO, M. P., DAL MASO, L., DAUDT, A. W., FABIANOVA, E., FERNANDEZ, L., WÜNSCH-FILHO, V., FRANCESCHI, S., HAYES, R. B., HERRERO, R., KELSEY, K., KOIFMAN, S., LA VECCHIA, C., LAZARUS, P., LEVI, F., LENCE, J. J., MATES, D., MATOS, E., MENEZES, A., MCCLEAN, M. D., MUSCAT, J., ELUF-NETO, J., OLSHAN, A. F., PURDUE, M., RUDNAI, P., SCHWARTZ, S. M., SMITH, E., STURGIS, E. M., SZESZENIA-DABROWSKA, N., TALAMINI, R., WEI, Q., WINN, D. M., SHANGINA, O., PILARSKA, A., ZHANG, Z. F., FERROO, G., BERTHILLER, J. & BOFFETTA, P. 2009. Interaction between tobacco and alcohol use and the risk of head and neck cancer: pooled analysis in the INHANCE consortium. *Cancer Epidemiol Biomarkers Prev*, 18, **2**, 541-550.
- HASSIBAN, S., TAGHDISI, S. M., JAMSHIDI, Z., SAMIE, A., NAMEGHI, M. A., SHAYAN, M., FARROKHI, N., ALIBOLANDI, M., RAMEZANI, M., DEHNAVI, S. M. & ABNOUS, K. 2024. Surface modification of hollow gold nanoparticles conducted by incorporating cancer cell membrane and AS1411 aptamer, aiming to achieve a dual-targeted therapy for colorectal cancer. *Int J Pharm*, 655, 124036.
- HAYASHI, T., OSHIMA, H., MASHIMA, T., NAGATA, T., KATAHIRA, M. & KINOSHITA, M. 2014. Binding of an RNA aptamer and a partial peptide of a prion protein: crucial importance of water entropy in molecular recognition. *Nucleic Acids Res*, 42, **11**, 6861-6875.
- HE, L., YANG, B., JIAN, D., LUO, H., WANG, D. & DAI, N. 2022. Prognostic value of HPV E6 and APOBEC3B in upper urinary tract urothelial carcinoma. *Dis Markers*, 2022, 2147494.
- HECK, D. V., LEE, C. L., HOWLEY, P. M. & MÜNGER, K. 1992. Efficiency of binding the retinoblastoma protein correlates with the transforming capacity of the E7 oncoproteins of the human papillomaviruses. *Proc Natl Acad Sci USA*, 89, **10**, 4442-4446.

- HEGDE, R. S. & ANDROPHY, E. J. 1998. Crystal structure of the E2 DNA-binding domain from human papillomavirus type 16: implications for its DNA binding-site selection mechanism. *J Mol Biol*, 284, **5**, 1479-1489.
- HELIN, K., HARLOW, E. & FATTAEY, A. 1993. Inhibition of E2F-1 transactivation by direct binding of the retinoblastoma protein. *Mol Cell Biol*, 13, **10**, 6501-6508.
- HELLIWELL, T. R. & GILES, T. E. 2016. Pathological aspects of the assessment of head and neck cancers: United Kingdom National Multidisciplinary Guidelines. *JLO*, 130, S59-S65.
- HENLEY-SMITH, R., SANTAMBROGIO, A., ANDONIADOU, C. L., ODELL, E. & THAVARAJ, S. 2020. RNA in situ hybridisation for human papillomavirus testing oropharyngeal squamous cell carcinoma on a routine clinical diagnostic platform. *J Oral Pathol Med*, 50, **1**, 68-75.
- HERFS, M., YAMAMOTO, Y., LAURY, A., WANG, X., NUCCI, M. R., MCLAUGHLIN-DRUBIN, M. E., MÜNGER, K., FELDMAN, S., MCKEON, F. D., XIAN, W. & CRUM, C. P. 2012. A discrete population of squamocolumnar junction cells implicated in the pathogenesis of cervical cancer. *Proc Natl Acad Sci USA*, 109, **26**, 10516-10521.
- HERMANN, T. & PATEL, D. J. 2000. Adaptive recognition by nucleic acid aptamers. *Science*, 287, **5454**, 820-825.
- HO, G. Y. F., STUDENTSOV, Y., HALL, C. B., BIERMAN, R., BEARDSLEY, L., LEMPA, M. & BURK, R. D. 2002. Risk factors for subsequent cervicovaginal human papillomavirus (HPV) infection and the protective role of antibodies to HPV-16 virus-like particles. *J Infect Dis*, 186, **6**, 737-742.
- HOLZINGER, D., FLECHTENMACHER, C., HENFLING, N., KADEN, I., GRABE, N., LAHRMANN, B., SCHMITT, M., HESS, J., PAWLITA, M. & BOSCH, F. X. 2013. Identification of oropharyngeal squamous cell carcinomas with active HPV16 involvement by immunohistochemical analysis of the retinoblastoma protein pathway. *Int J Cancer*, 133, **6**, 1389-1399.
- HOLZINGER, D., SCHMITT, M., DYCKHOFF, G., BRENNER, A., PAWLITA, M. & BOSCH, F. X. 2012. Viral RNA patterns and high viral load reliably define oropharynx carcinomas with active HPV16 involvement. *Cancer Res*, 72, **19**, 4993-5003.

- HOMER, J. J. & WINTER, S. C. 2024. Head and Neck Cancer: United Kingdom National Multidisciplinary Guidelines, Sixth Edition. *J Laryngol Otol*, 138, S1-224.
- HONG, A., JONES, D., CHATFIELD, M., LEE, C. S., ZHANG, M., CLARK, J., ELLIOTT, M., HARNETT, G., MILROSS, C. & ROSE, B. 2013. HPV status of oropharyngeal cancer by combination HPV DNA/p16 testing: biological relevance of discordant results. *Ann Surg Oncol*, 20, S450-458.
- HOWIE, A. J. 1980. Scanning and transmission electron microscopy on the epithelium of human palatine tonsils. *J Pathol*, 130, 2, 91-98.
- HUANG, Z., CHEN, Y., CHEN, R., ZHOU, B., WANG, Y., HONG, L., WANG, Y., WANG, J., XU, X., HUANG, Z. & CHEN, W. 2023. HPV enhances HNSCC chemosensitization by inhibiting SERPINB3 expression to disrupt the Fanconi anemia pathway *Adv Sci (Weinh)*, 10, 1, 2202437.
- HUBERT, N. L., SCHILLER, J. T., LOWY, D. R. & ANDROPHY, E. J. 1988. Bovine papillomavirus virus-transformed cells contain multiple E2 proteins. *Proc Natl Acad Sci USA*, 85, 16, 5864-5868.
- HUIBREGTSE, J. M., SCHEFFNER, M. & HOWLEY, P. M. 1991. A cellular protein mediates association of p53 with the E6 oncoprotein of human papillomavirus types 16 or 18. *EMBO J*, 10, 13, 4129-4135.
- HUIBREGTSE, J. M., SCHEFFNER, M. & HOWLEY, P. M. 1993. Localisation of the E6-AP regions that direct human papillomavirus E6 binding, association with p53, and ubiquitination of associated proteins. *Mol Cell Biol*, 13, 8, 4918-4927.
- HULL, R., MBELE, M., MAKHAFOLA, T., HICKS, C., WANG, S. M., REIS, R. M., MEHROTRA, R., MKHIZE-KWITSHANA, Z., KIBIKI, G., BATES, D. O. & DLAMINI, Z. 2020. Cervical cancer in low and middle-income countries. *Oncol Lett*, 20, 3, 2058-2074.
- HUMMEL, M., HUDSON, J. B. & LAIMINS, L. A. 1992. Differentiation-induced and constitutive transcription of human papillomavirus type 31b in cell lines containing viral episomes. *J Virol*, 66, 10, 6070-6080.
- HUNTER, K., HELLIWELL, T., SANDISON, A., ROBINSON, M. & THOMAS, G. *Dataset for the histopathological reporting of carcinomas of the oropharynx and nasopharynx*. 1st London, UK: The Royal College of Pathologists. Available: <https://www.rcpath.org/static/24d6fa0d-7462-4876->

[ab5d826e8104ddee/89177e93-75c7-48c7-82595ea4c8a39f9f/G189-Oropharynx-and-nasopharynx-datasetfor-publication.pdf](https://pubmed.ncbi.nlm.nih.gov/1044412/)

- ILVES, I., KIVI, S. & USTAV, M. 1999. Long-term episomal maintenance of bovine papillomavirus type 1 plasmids is determined by attachment to host chromosomes, which is mediated by the viral E2 protein and its binding sites. *J Virol*, 73, 5, 4404-4412.
- INTERNATIONAL AGENCY FOR RESEARCH ON CANCER. 2023. *List of Classifications by cancer sites with sufficient or limited evidence in humans, Volumes 1-135. IARC Monographs On The Identification Of Carcinogenic Hazards To Humans* [Online]. IARC. Available: <https://monographs.iarc.who.int/agents-classified-by-the-iarc/> [Accessed].
- JEDDI, I. & SAIZ, L. 2017. Three-dimensional modeling of single stranded DNA hairpins for aptamer-based biosensors. *Sci Rep*, 7, 1, 1178.
- JEFFREY, G. A. 1997. *An introduction to hydrogen bonding*, Oxford University Press: New York and Oxford.
- JENISON, R. D., GILL, S. C., PARDI, A. & POLISKY, B. 1994. High-resolution molecular discrimination by RNA. *Science*, 263, 5152, 1425-1429.
- JORDAN, R. C., LINGEN, M. W., PEREZ-ORDONEZ, B., HE, X., PICKARD, R., KOLUDER, M., JIANG, B., WAKELY, P., XIAO, W. & GILLISON, M. L. 2012. Validation of methods for oropharyngeal cancer HPV status determination in US cooperative group trials. *Am J Surg Pathol*, 36, 7, 945-954.
- JOYCE, J. G., TUNG, J. S., PRZYSIECKI, C. T., COOK, J. C., LEHMAN, E. D., SANDS, J. A., JANSEN, K. U. & KELLER, P. M. 1999. The L1 major capsid protein of human papillomavirus type 11 recombinant virus-like particles interacts with heparin and cell-surface glycosaminoglycans on human keratinocytes. *J Biol Chem*, 274, 9, 5810-5822.
- KAMB, A., GRUIS, N. A., WEAVER-FELDHAUS, J., LIU, Q., HARSHMAN, K., TAVTIGIAN, S. V., STOCKERT, E., DAY, R. S. R., JOHNSON, B. E. & SKOLNICK, M. H. 1994. A cell cycle regulator potentially involved in genesis of many tumour types. *Science*, 264, 5157, 436-440.
- KÄMPER, N., DAY, P. M., NOWAK, T., SELINKA, H. C., FLORIN, L., BOLSCHER, J., HILBIG, L., SCHILLER, J. T. & SAPP, M. 2006. A membrane-destabilizing peptide in capsid protein L2 is required for egress of papillomavirus genomes from endosomes. *J Virol*, 80, 2, 759-768.

- KANDUC, D. 2002. Translational regulation of human papillomavirus type 16 E7 mRNA by the peptide SEQIKA, shared by rabbit alpha(1)-globin and human cytokeratin 7. *J Virol*, 76, **14**, 7040-7048.
- KATO, J. Y., MATSUOKA, M., POLYAK, K., MASSAGUÉ, C. & SHERR, C. J. 1994. Cyclic AMP-induced G1 phase arrest mediated by an inhibitor (p27Kip1) of cyclin-dependent kinase 4 activation. *Cell*, 79, **3**, 487-496.
- KEEFE, A. D., PAI, S. I. & ELLINGTON, A. 2010. Aptamers as therapeutics. *Nat Rev Drug Discov*, 9, **7**, 537-550.
- KERR, D. A., ARORA, K. S., MAHADEVAN, K. K., HORNICK, J. L., KRANE, J. F., RIVERA, M. N., TING, D. T., DESHPANDE, V. & FAQUIN, W. C. 2015. Performance of a branch chain RNA in situ hybridization assay for the detection of high-risk human papillomavirus in head and neck squamous cell carcinoma. *Am J Surg Pathol*, 39, **12**, 1643-1652.
- KIM, H. S., LEE, J. Y., LIM, S. H., PARK, K., SUN, J. M., KO, Y. H., BAEK, C. H., SON, Y. I., JEONG, H. S., AHN, Y. C., LEE, M. Y., HONG, M. & AHN, M. J. 2016. Association between PD-L1 and HPV status and the prognostic value of PD-L1 in oropharyngeal squamous cell carcinoma. *Cancer Res Treat*, 48, **2**, 527-536.
- KIM, S. H., KOO, B. S., KANG, S. Y. C., PARK, K., KIM, H., LEE, K. R., LEE, M. J., KIM, J. M., CHOI, E. C. & CHO, N. H. 2007. HPV integration begins in the tonsillar crypt and leads to the alteration of p16, EGFR and c-myc during tumor formation. *Int J Cancer*, 120, **7**, 1418-1425.
- KINES, R., THOMPSON, C. D., LOWY, D. R., SCHILLER, J. T. & DAY, P. M. 2009. The initial steps leading to papillomavirus infection occur on the basement membrane prior to cell surface binding. *Proc Natl Acad Sci USA*, 106, **48**, 20458-20463.
- KIRCHLER, T., BRIESEMEISTER, S., SINGER, M., SCHÜTZE, K., KEINATH, M., KOHLBACHER, O., VICENTE-CARBAJOSA, J., TEIGE, M., HARTER, K. & CHABAN, C. 2010. The role of phosphorylatable serine residues in the DNA-binding domain of Arabidopsis bZIP transcription factors. *Eur J Cell Biol*, 89, **2-3**, 175-183.
- KIRNBAUER, R., BOOY, F., CHENG, N., LOWY, D. R. & SCHILLER, J. T. 1992. Papillomavirus L1 major capsid protein self-assembles into virus-like particles that are highly immunogenic. *Proc Natl Acad Sci USA*, 89, **24**, 12180-12184.

- KLINGELHUTZ, A. J., FOSTER, S. A. & MCDUGALL, J. K. 1996. Telomerase activation by the E6 gene product of human papillomavirus type 16. *Nature*, 380, **6569**, 79-82.
- KLINGENBERG, B., HAFKAMP, H. C., HAESEVOETS, A., MANNI, J. J., SLOOTWEG, P. J., WEISSENBORN, S. J., KLUSSMAN, J. P. & SPEEL, E. J. M. 2010. p16INK4A overexpression is frequently detected in tumour-free tonsil tissue without association with HPV. *Histopathology*, 56, **7**, 957-967.
- KLUSSMAN, J. P., GÜLTEKIN, E., WEISSENBORN, S. J., WIELAND, U., DRIES, V., DIENES, H. P., ECKEL, H. E., PFISTER, H. J. & FUCHS, P. G. 2003. Expression of p16 protein identifies a distinct entity of tonsillar carcinomas associated with human papillomavirus. *Am J Pathol*, 162, **3**, 747-753.
- KNAPP, A. A., MCMANUS, P. M., BOCKSTALL, K. & MOROIANU, J. 2009. Identification of the nuclear localization and export signals of high risk HPV16 E7 oncoprotein. *Virology*, 383, **1**, 60-68.
- KOENIGS, M. B., LEFRANC-TORRES, A., BONILLA-VELEZ, J., PATEL, K. B., HAYES, N., GLOMSKI, K., BUSSE, P. M., CHAN, A. W., CLARK, J. R., DESCHLER, D. G., EMERICK, K. S., HAMMON, R. J., WIRTH, L. J., LIN, D. T., MROZ, E. A., FAQUIN, W. C. & ROCCO, J. W. 2019. Association of estrogen receptor alpha expression with survival in oropharyngeal cancer following chemoradiation therapy. *J Natl Cancer Inst*, 111, **9**, 933-942.
- KOFI, B., MOSSORO-KPINDE, C. D., BOUASSA, R. S. M., PÉRÉ, H., ROBIN, L., GRESENGUET, G. & BÉLEC, L. 2019. Infrequent detection of human papillomavirus infection in head and neck cancers in the Central African Republic: a retrospective study. *Infect Agent Cancer*, 14, 9.
- KOMAROVA, N. & KUZNETSOV, A. 2019. Inside the black box: what makes SELEX better? *Molecules*, 24, **19**, 3598.
- KONO, H. & SARAI, A. 1999. Structure-based prediction of DNA target sites by regulatory proteins. *Proteins*, 35, **1**, 114-131.
- KOSHIOL, J. E., SCHROEDER, J. C., JAMIESON, D. J., MARSHALL, S. W., DUERR, A., HEILIG, C. M., SHAH, K. V., KLEIN, R. S., CU-UVIN, S., SCHUMAN, P., CELENTANO, D. & SMITH, J. S. 2006. Time to clearance of human papillomavirus infection by type and human immunodeficiency virus status. *Int J Cancer*, 119, **7**, 1623-1629.

- KRAWCZYK, E., SUPRYNOWICZ, F. A., HEBERT, J. D., KAMONJOH, C. M. & SCHLEGEL, R. 2011. The human papillomavirus type 16 E5 oncoprotein translocates calpactin I to the perinuclear region. *J Virol*, 85, **21**, 10968-10975.
- KREIMER, A. R., CLIFFORD, G. M., BOYLE, P. & FRANCESCHI, S. 2005. Human papillomavirus types in head and neck squamous cell carcinomas worldwide: a systematic review. *Cancer Epidemiol Biomarkers Prev*, 14, **2**, 467-475.
- KREIMER, A. R., FERRARIO-IGLESIAS, A., NYGARD, M., BENDER, N., SCHROEDER, L., HILDESHEIM, A., ROBBINS, H. A., PAWLITA, M., LANGSETH, H., SCHLECHT, N. F., TINKER, L. F., AGALLIU, I., SMOLLER, S. W., NESS-JENSEN, E., HVEEM, K., D'SOUZA, G., VISVANATHAN, K., MAY, B., URSIN, G., WEIDERPASS, E., GILES, G. G., MILNE, R. L., CAI, Q., BLOT, W. J., ZHENG, W., WEINSTEIN, S. J., ALBANES, D., BRENNER, N., HOFFMAN-BOLTON, J., KAKS, R., BARRICARTE, A., TJØNNELAND, A., SACERDOTE, C., TRICHOPOULOU, A., VERMEULEN, R. C. H., HUANG, W. Y., FREEDMAN, N. D., BRENNAN, P., WATERBOER, T. & JOHANSSON, M. 2019. Timing of HPV16-E6 antibody seroconversion before OPSCC: findings from the HPVC3 consortium. *Ann Oncol*, 30, **8**, 1335-1343.
- KREIMER, A. R., PIERCE CAMPBELL, C. M., LIN, H. Y., FULP, W., PAPPENFUSS, M. R., ABRAHAMSEN, M., HILDESHEIM, A., VILLA, L. J., SALMERÓN, J. J., LAZCANO-PONCE, E. & GIULIANO, A. R. 2013. Incidence and clearance of oral human papillomavirus infection in men: the HIM cohort study. *Lancet*, 382, **9895**, 877-887.
- KROPVELD, A., SLOOTWEG, P. J., BLANKENSTEIN, M. A., TERHAARD, C. H. & HORDIJK, G. J. 1998. Ki-67 and p53 in T2 laryngeal cancer. *Laryngoscope*, 108, **10**, 1548-1552.
- KULBACHINSKIY, A. V. 2007. Methods for selection of aptamers to protein targets. *Biochemistry (Mosc)*, 72, **13**, 1505-1518.
- KUMARASAMY, G., ISMAIL, M. N., SHARIF, S. E. T., DESIRE, C., MITTAL, P., HOFFMANN, P. & KAUR, G. 2023. Protein profiling in human-papillomavirus-associated cervical carcinogenesis: cornulin as a biomarker for disease progression. *Curr Issues Mol Biol*, 45, **4**, 3603-3627.
- KURG, R., UUSEN, P., VÕSA, B. & USTAV, M. 2010. Human papillomavirus E2 protein with single activation domain initiates HPV18 genome replication, but is

- not sufficient for long-term maintenance of virus genome. *Virology*, 408, **2**, 159-166.
- KURITA, T., CHITOSE, S., SATO, K., SAKAZAKI, T., FUKAHORI, M., SUEYOSHI, S. & UMENO, H. 2019. Pathological mechanisms of laryngeal papillomatosis based on laryngeal epithelial characteristics. *Laryngoscope Investig Otolaryngol*, 4, **1**, 89-94.
- KWON, S., AHN, S. H., JEONG, W. J., JUNG, Y. H., BAE, Y. J., PAIK, J. H., CHUNG, J. H. & KIM, H. 2020. Estrogen receptor  $\alpha$  as a predictive biomarker for survival in human papillomavirus-positive oropharyngeal squamous cell carcinoma. *J Transl Med*, 18, **1**, 240.
- LAI, Y. H., SU, C. C., WU, S. Y., HSUEH, W. T., WU, Y. H., CHEN, H. H. W., HSIAO, J. R., LIU, C. H. & TSAI, Y. S. 2022. Impact of alcohol and smoking on outcomes of HPV-related oropharyngeal cancer. *J Clin Med*, 11, **21**, 6510.
- LANIOSZ, V., DABYDEEN, S. A., HAVENS, M. A. & MENESES, P. I. 2009. Human papillomavirus type 16 infection of human keratinocytes requires clathrin and caveolin-1 and is brefeldin A sensitive. *J Virol*, 83, **16**, 8221-8232.
- LAVERTU, P., ADELSTEIN, D. J., MYLES, J. & SECIC, M. 2001. P53 and Ki-67 as outcome predictors for advanced squamous cell cancers of the head and neck treated with chemoradiotherapy. *Laryngoscope*, 111, **11**, 1878-1892.
- LAWSON, J. S., GLENN, W. K., HENG, B., YE, Y., TRAN, B., LUTZE-MANN, L. & WHITAKER, N. J. 2009. Koilocytes indicate a role for human papilloma virus in breast cancer. *Br J Cancer*, 101, **8**, 1351-1356.
- LAZZARI, M. A. 2009. Developing a standard protocol for the introduction of new testing into a clinical laboratory. *Lab Med*, 40, **7**, 389-393.
- LECHNER, M., LIU, J., MASTERSON, L. & FENTON, T. R. 2022. HPV-associated oropharyngeal cancer: epidemiology, molecular biology and clinical management. *Nat Rev Clin Oncol*, 1, 1-22.
- LEE, C. & LAIMINS, L. A. 2004. Role of the PDZ domain-binding motif of the oncoprotein E6 in the pathogenesis of human papillomavirus type 31. *J Virol*, 78, **22**, 12366-12377.
- LEE, C., WOOLDRIDGE, T. R. & LAIMINS, L. A. 2007. Analysis of the roles of E6 binding to E6TP1 and nuclear localization in the human papillomavirus type 31 life cycle. *Virology*, 358, **1**, 201-210.



- LEE, H., LEE, H. & CHO, Y. K. 2017. Cytokeratin 7 and cytokeratin 19 expression in high grade cervical intraepithelial neoplasm and squamous cell carcinoma and their possible association in cervical carcinogenesis. *Diagnostic Pathol*, 12, 1, 18.
- LEE, Y. C. A., LI, S., CHEN, Y., LI, Q., CHEN, C. J., HSU, W. L., LOU, P. J., ZHU, C., PAN, J., SHEN, H., MA, H., CAI, L., HE, B., WANG, Y., ZHOU, X., JI, Q., ZHOU, B., WU, W., MA, J., BOFFETTA, P., ZHANG, Z. F., DAI, M. & HASHIBE, M. 2018. Tobacco smoking, alcohol drinking, betel quid chewing, and the risk of head and neck cancer in an East Asian population. *Head Neck*, 41, 1, 92-102.
- LEHMAN, C. W. & BOTCHAN, M. R. 1998. Segregation of viral plasmids depends on tethering to chromosomes and is regulated by phosphorylation. *Proc Natl Acad Sci USA*, 95, 8, 4338-4343.
- LEICA BIOSYSTEMS. 2024. *BOND Polymer Refine Detection* [Online]. Newcastle. Available: <https://shop.leicabiosystems.com/en-gb/ihc-ish/detection-systems/pid-bond-polymer-refine-detection> [Accessed 03/06/2024].
- LEIJA-MONTOYA, A. G., BENÍTEZ-HESS, M. L., TOSCANO-GARIBAY, J. D. & ALVAREZ-SALAS, L. M. 2014. Characterization of an RNA aptamer against HPV-16 L1 virus-like particles. *Nucleic Acid Ther*, 24, 5, 344-355.
- LEWIS, J. S. J. 2017. Morphologic diversity in human papillomavirus-related oropharyngeal squamous cell carcinoma: catch me if you can! *Mod Pathol*, 30, S44-53.
- LEWIS, J. S. J., ADELSTEIN, D. J., AGAIMY, A., CARLSON, D. L., FAQUIN, W. C., HELLIWELL, T., HILLE, J., NG, T., NICHOLLS, J. M., O'SULLIVAN, B. & THOMPSON, L. D. R. 2018a. Data set for the reporting of carcinomas of the nasopharynx and oropharynx: explanations and recommendations of the guidelines from the International Collaboration on Cancer Reporting. *Arch Pathol Lab Med*, 143, 4, 447-451.
- LEWIS, J. S. J., BEADLE, B., BISHOP, J. A., CHERNOCK, R. D., COLASACCO, C., LACCHETTI, C., MONCUR, J. T., ROCCO, J. W., SCHWARTZ, M. R., SEETHALA, R. R., THOMAS, N. E., WESTRA, W. H. & FAQUIN, W. C. 2018b. Human papillomavirus testing in head and neck carcinomas: guideline from the College of American Pathologists. *Arch Pathol Lab Med*, 142, 5, 559-597.
- LEWIS, J. S. J., CHERNOCK, R. D., MA, X. J., FLANAGAN, J. J., LUO, Y., GAO, G., WANG, X. & EL-MOFTY, S. K. 2012. Partial p16 staining in oropharyngeal

- squamous cell carcinomas: extent and pattern correlate with human papillomavirus RNA status. *Mod Pathol*, 25, **9**, 1212-1220.
- LEWIS, J. S. J., MIRABELLO, L., LIU, P., WANG, X., DUPONT, W. D., PLUMMER, W. D., PINHEIRO, M., YEAGER, M., BOLAND, J. F., CULLEN, M., STEINBERG, M., BASS, S., MEHRAD, M., O'BOYLE, C., LIN, M., FADEN, D. L. & LANG-KUHS, K. A. 2021. Oropharyngeal squamous cell carcinoma morphology and subtypes by human papillomavirus type and by 16 lineages and sublineages. *Head Neck Pathol*, 15, **4**, 1089-1098.
- LEWIS, J. S. J., THORSTAD, W. L., CHERNOCK, R. D., HAUGHEY, B. H., YIP, J. H., ZHANG, Q. & EL-MOFTY, S. K. 2010. p16 positive oropharyngeal squamous cell carcinoma: an entity with a favourable prognosis regardless of tumor HPV status. *Am J Surg Pathol*, 34, **8**, 1088-1096.
- LI, N., FRANCESCHI, S., HOWELL-JONES, R., SNIJDERS, P. J. F. & CLIFFORD, G. M. 2011. Human papillomavirus type distribution in 30,848 invasive cervical cancers worldwide: variation by geographical region, histological type and year of publication. *Int J Cancer*, 128, **4**, 927-935.
- LI, V. C. & KIRSCHNER, M. W. 2014. Molecular ties between the cell cycle and differentiation in embryonic stem cells. *Proc Natl Acad Sci USA*, 111, **26**, 9503-9508.
- LI, W., WANG, S., ZHOU, L., CHENG, Y. & FANG, J. 2019. An ssDNA aptamer selected by cell-SELEX for the targeted imaging of poorly differentiated gastric cancer tissue. *Talanta*, 199, 634-642.
- LI, X. & COFFINO, P. 1996. High-risk human papillomavirus E6 protein has two distinct binding sites within p53, of which only one determines degradation. *J Virol*, 70 **7**, 4509-4516.
- LI, Y., NICHOLS, M. A., SHAY, J. W. & XIONG, Y. 1994. Transcriptional repression of the D-type cyclin-dependent kinase inhibitor p16 by the retinoblastoma susceptibility gene product pRb. *Cancer Res*, 54, **23**, 6078-6082.
- LI, Z., FU, X., HUANG, J. W., ZENG, P., HUANG, Y., CHEN, X. & LIANG, C. 2021. Advances in screening and development of therapeutic aptamers against cancer cells. *Front Cell Dev Biol*, 9, 662791.
- LIANG, X., KUHN, H. & FRANK-KAMENETSKII, M. D. 2006. Monitoring single-stranded DNA secondary structure formation by determining the topological state of DNA catenanes. *Biophys J*, 90, **8**, 2877-2889.

- LIPOVSKY, A., POPA, A., PIMIENTA, G., WYLER, M., BHAN, A., KURUVILLA, L., GUIE, M. A., POFFENBERGER, A. C., NELSON, C. D. S., ATWOOD, W. J. & DIMAIO, D. 2013. Genome-wide siRNA screen identifies the retromer as a cellular entry factor for human papillomavirus. *Proc Natl Acad Sci USA*, 110, **18**, 7452-7457.
- LIU, C., LU, J., TIAN, J., DU, W., ZHAO, L., FENG, J., YUAN, D. & LI, Z. 2017. Increased expression of PD-L1 by the human papillomavirus 16 E7 oncoprotein inhibits anticancer immunity. *Mol Med Rep*, 15, **3**, 1063-1070.
- LIU, J., ZHANG, M., ROSE, B., VEILLARD, A. S., JONES, D., ZHANG, X., SOON LEE, C., MILROSS, C. & HONG, A. 2015. Ki67 expression has prognostic significance in relation to human papillomavirus status in oropharyngeal squamous cell carcinoma. *Ann Surg Oncol*, 22, **6**, 1893-1900.
- LIU, M., WANG, Z., TAN, T., CHEN, Z., MOU, X., YU, X., DENG, Y., LU, G. & HE, N. 2018. An aptamer-based probe for molecular subtyping of breast cancer. *Theranostics*, 8, **20**, 5772-5783.
- LIU, W. J., GISSMANN, L., SUN, X. Y., KANJANAHALUETHAI, A., MÜLLER, M., DOORBAR, J. & ZHOU, J. 1997. Sequence close to the N-terminus of L2 protein is displayed on the surface of bovine papillomavirus type 1. *Virology*, 227, **2**, 474-483.
- LIU, X., CLEMENTS, A., ZHAO, K. & MARMORSTEIN, R. 2006. Structure of the human papillomavirus E7 oncoprotein and its mechanism for inactivation of the retinoblastoma tumor suppressor. *J Biol Chem*, 281, **1**, 578-586.
- LONGWORTH, M. S. & LAIMINS, L. A. 2004. Pathogenesis of human papillomaviruses in differentiation epithelia. *Microbiol Mol Biol Rev*, 68, **2**, 362-372.
- LORENZONI, V., CHATURVEDI, A. K., VIGNAT, J., LAVERSANNE, M., BRAY, F. & VACCARELLA, S. 2022. The current burden of oropharyngeal cancer: a global assessment based on GLOBOCAN 2020. *Cancer Epidemiol Biomarkers Prev*, 31, **11**, 2054-2062.
- LOUIE, K. S., MEHANNA, H. & SASIENI, P. 2015. Trends in head and neck cancers in England from 1995 to 2011 and projections up to 2025. *Oral Oncol*, 51, **4**, 341-348.

- LUSCOMBE, N. M., LASKOWSKI, R. A. & THORNTON, J. M. 2001. Amino acid-base interactions: a three-dimensional analysis of protein-DNA interactions at an atomic level. *Nucleic Acids Res*, 29, **13**, 2860-2874.
- LYDIATT, W. M., PATEL, S. G., O'SULLIVAN, B., BRANDWEIN, M. S., RIDGE, J. A., MIGLIACCI, J. C., LOOMIS, A. M. & SHAH, J. P. 2017. Head and neck cancers-major changes in the American Joint Committee on cancer eighth edition cancer staging manual. *CA Cancer J Clin*, 67, **2**, 122-137.
- LYFORD-PIKE, S., PENG, S., YOUNG, G. D., TAUBE, J. M., WESTRA, W. H., AKPENG, B., BRUNO, T. C., RICHMON, J. D., WANG, H., BISHOP, J. A., CHEN, L., DRAKE, C. G., TOPALIAN, S. L., PARDOLL, D. M. & PAI, S. I. 2013. Evidence for a role of the PD-1:PD-L1 pathway in immune resistance of HPV-associated head and neck squamous cell carcinoma. *Cancer Res*, 73, **6**, 1733-1741.
- LYU, X., ZHANG, M., LI, G., JIANG, Y. & QIAO, Q. 2019. PD-1 and PD-L1 expression predicts radiosensitivity and clinical outcomes in head and neck cancer and is associated with HPV infection. *J Cancer*, 10, **4**, 937-948.
- MAGLENNON, G. A., MCINTOSH, P. & DOORBAR, J. 2011. Persistence of viral DNA in the epithelial basal layer suggests a model for papillomavirus latency following immune regression. *Virology*, 414, **2**, 153-163.
- MAHAL, B. A., CATALANO, P. J., HADDAD, R. I., HANNA, G. J., KASS, J. I., SCHOENFELD, J. D., TISHLER, R. B. & MARGALIT, D. N. 2019. Incidence and demographic burden of HPV-associated oropharyngeal head and neck cancers in the United States. *Cancer Epidemiol Biomarkers Prev*, 28, **10**, 1660-1667.
- MAJOR, T., SZARKA, K., SZIKLAI, I., GERGELY, L. & CZEGLÉDY, J. 2005. The characteristics of human papillomavirus DNA in head and neck cancers and papillomas. *J Clin Pathol*, 58, **1**, 51-55.
- MALM, I. J., BRUNO, T. C., FU, J., TAUBE, J. M., WESTRA, W., PARDOLL, D., DRAKE, C. G. & KIM, Y. J. 2015. Expression profile and in vitro blockade of programmed death-1 in human papillomavirus-negative head and neck squamous cell carcinoma. *Head Neck*, 37, **8**, 1088-1095.
- MANDEL-GUTFREUND, Y., SCHUELER, O. & MARGALIT, H. 1995. Comprehensive analysis of hydrogen bonds in regulatory protein DNA-complexes: in search of common principles. *J Mol Biol*, 253, **2**, 370-382.

- MARKHAM, N. R. & ZUKER, M. 2005. DINAMelt web server for nucleic acid melting prediction. *Nucleic Acids Res*, 33, **Web server issue**, W577-581. Available: <http://www.unafold.org/Dinamelt/applications/quickfold.php>.
- MAROUN, C. A., AL FEGHALI, K., TRABOULSI, H., DABBOUS, H., ABBAS, F., DUNYA, G., ZIADE, G., MAHFOUZ, R., YOUSSEF, B., TAMIM, H., GEARA, F., KHALIFEH, I. & MOUKARBEL, R. V. 2020. HPV-related oropharyngeal cancer prevalence in a middle eastern population using E6/E7 PCR. *Infect Agent Cancer*, 15, 1.
- MARSH, E. K., DELURY, C. P., DAVIES, N. J., WESTON, C. J., MIAH, M. A. L., BANKS, L., PARISH, J. L., HIGGS, M. R. & ROBERTS, S. 2017. Mitotic control of human papillomavirus genome-containing cells is regulated by the function of the PDZ-binding motif of the E6 oncoprotein. *Oncotarget*, 8, **12**, 19491-19506.
- MARTINEZ-ZAPIEN, D., RUIZ, F. X., POIRSON, J., MITSCHLER, A., RAMIREZ, J., FORSTER, A., COUSIDO-SIAH, A., MASSON, M., VANDE POL, S., PODJARNY, A., TRAVÉ, G. & ZANIER, K. 2016. Structure of the E6/E6AP/p53 complex required for HPV-mediated degradation of p53. *Nature*, 529, **7587**, 541-545.
- MAUFORT, J. P., SHAI, A., PITOT, H. C. & LAMBERT, P. F. 2010. A role for HPV16 E5 in cervical carcinogenesis. *Cancer Res*, 70, **7**, 2924-2931.
- MAYER, G. 2009. The chemical biology of aptamers. *Angew Chem Int Ed Engl*, 48, **15**, 2672-2689.
- MCBRIDE, A. A., BYRNE, J. C. & HOWLEY, P. M. 1989. E2 polypeptides encoded by bovine papillomavirus type 1 form dimers through the common carboxyl-terminal domain: transactivation is mediated by the conserved amin-terminal domain. *Proc Natl Acad Sci USA*, 86, **2**, 510-514.
- MCBRIDE, A. A., SCHLEGEL, R. & HOWLEY, P. M. 1988. The carboxy-terminal domain is shared by the bovine papillomavirus E2 transactivator and repressor proteins contains a specific DNA binding activity. *EMBO J*, 7, **2**, 533-539.
- MCILWAIN, W. R., SOOD, A. J. & NGUYEN, S. A. 2014. Initial symptoms in patients with HPV-positive and HPV-negative oropharyngeal cancer. *JAMA Otolaryngol Head Neck Surg*, 140, **5**, 441-447.
- MCINTOSH, P. B., MARTIN, S. R., JACKSON, D. J., KHAN, J., ISAACSON, E. R., CALDER, L., RAJ, K., GRIFFIN, H. M., WANG, Q., LASKEY, P., ECCLESTON,

- J. F. & DOORBAR, J. 2008. Structural analysis reveals an amyloid form of human papillomavirus type 16 E1-E4 protein and provides a molecular basis for its accumulation. *J Virol*, 82, **16**, 8196-8203.
- MCKINNEY, C. C., KIM, M. J., CHEN, D. & MCBRIDE, A. A. 2016. Brd4 activates early viral transcription upon papillomavirus 18 infection of primary keratinocytes. *mBio*, 7, **6**, e01644-16.
- MCPHILLIPS, M. G., OLIVEIRA, J. G., SPINDLER, J. E., MITRA, R. & MCBRIDE, A. A. 2006. Brd4 is required for E2-mediated transcriptional activation but not genome partitioning of all papillomaviruses. *J Virol*, 80, **19**, 9530-9543.
- MEHANNA, H., EVANS, M., BEASLEY, M., CHATTERJEE, S., DILKES, M., HOMER, J., O'HARA, J., ROBINSON, M., SHAW, R. & SLOAN, P. 2016a. Oropharyngeal cancer: United Kingdom National Multidisciplinary Guidelines. *JLO*, 130, S90-S96.
- MEHANNA, H., FRANKLIN, N., COMPTON, N., ROBINSON, M., POWELL, N., BISWAS-BALDWIN, N., PALERI, V., HARTLEY, A., FRESCO, L., AL-BOOZ, H., JUNOR, E., EL-HARIRY, I., ROBERTS, S., HARRINGTON, K., ANG, K. K., DUNN, J. & WOODMAN, C. 2016b. Geographic variation in human papillomavirus-related oropharyngeal cancer: data from 4 multinational randomized trials. *Head Neck*, 38, E1863-1869.
- MEHANNA, H., TABERNA, M., VON BUCHWALD, C., TOUS, S., BROOKS, J., MENA, M., MOREY, F., GRØNHØJ, C., RASMUSSEN, J. H., GARSET-ZAMANI, M., BRUNI, L., BATIS, N., BRAKENHOFF, R. H., LEEMANS, C. R., BAATENBURG DE JONG, R. J., KLUSSMAN, J. P., WUERDEMANN, N., WAGNER, S., DALIANIS, T., MARKLUND, L., MIRGHANI, H., SCHACHE, A., JAMES, J. A., HUANG, S. H., O'SULLIVAN, B., NANKIVELL, P., BROGLIE, M. A., HOFFMAN, M., QUABIUS, E. S., ALEMANY, L. & HNCIG-EPIC GROUP 2023. Prognostic implications of p16 and HPV discordance in oropharyngeal cancer (HNCIG-EPIC): a multicentre, multinational, individual patient data analysis. *Lancet Oncol*, 24, **3**, 239-251.
- MEHRAD, M., DUPONT, W. D., PLUMMER, W. D. J. & LEWIS, J. S. J. 2018. Expression and significance of cytokeratin 7, a squamocolumnar junction marker, in head and neck squamous cell carcinoma. *Head Neck Pathol*, 12, **4**, 448-454.

- MENA, M., FRIAS-GOMEZ, J., TABERNA, M., QUIRÓS, B., MARQUEZ, S., CLAVERO, O., BAENA, A., LLOVERAS, B., ALEJO, M., LEÓN, X., GARCÍA, J., MESÍA, R., BERMEJO, O., BONFILL, T., AGUILÀ, A., GUIX, M., HIJANO, R., PAVÓN, M. A., TORRES, M., TOUS, S., CLÈRIES, R. & ALEMANY, L. 2020. Epidemiology of human papillomavirus-related oropharyngeal cancer in a classically low-burden region of Southern Europe. *Sci Rep*, 10, 13219.
- MENA, M., WANG, X., TOUS, S., QUIRÓS, B., CLAVERO, O., ALEJO, M., MOREY, F., TABERNA, M., VINTRO, X. L., RUBIO, B. L., ALÒS, L., MEHANNA, H., QUINT, W., PAWLITA, M., TOMMASINO, M., PAVÓN, M. A., MUÑOZ, N., DE SANJOSÉ, S., BOSCH, F. X., ALEMANY, L. & ON BEHALF OF THE ICO INTERNATIONAL HPV IN HEAD AND NECK CANCER STUDY GROUP 2022. Concordance of p16INK4A and E6\*I mRNA among HPV-DNA-positive oropharyngeal, laryngeal, and oral cavity carcinomas from the ICO international study. *Cancers (Basel)*, 14, **15**, 3787.
- MENG, X. Y., ZHANG, H. X., MEZEI, M. & CUI, M. 2011. Molecular docking: a powerful approach for structure-based drug discovery. *Curr Comput Aided Drug Des*, 7, **2**, 146-157.
- MIDDLETON, K., PEH, W., SOUTHERN, S., GRIFFIN, H., SOTLAR, K., NAKAHARA, T., EL-SHERIF, A., MORRIS, L., SETH, R., HIBMA, M., JENKINS, D., LAMBERT, P., COLEMAN, N. & DOORBAR, J. 2003. Organisation of human papillomavirus productive cycle during neoplastic progression provides a basis for selection of diagnostic markers. *J Virol*, 77, **19**, 10186-10201.
- MIETZ, J. A., UNGER, T., HUIBREGTSE, J. M. & HOWLEY, P. M. 1992. The transcriptional transactivation function of wild-type p53 is inhibited by SV40 large T-antigen and by HPV-16 E6 oncoprotein. *EMBO J*, 11, **13**, 5013-5020.
- MILLER, J. A., ALLISON, D. B. & MALEKI, Z. 2017. Interpretation of HPV DNA in situ hybridization in HPV-related head and neck squamous cell carcinoma: an achievable task in cell block and small biopsy material. *J Am Soc Cytopathol*, 6, **3**, 89-95.
- MIRGHANI, H., CASIRAGHI, O., AMEN, F., HE, M., MA, X. J., SAULNIER, P., LACROIX, L., DRUSCH, F., LAKDHAR, A. B., SAINT GUILY, J. L., BADOUAL, C., SCOAZEC, J. Y. & VIELH, P. 2015. Diagnosis of HPV-driven head and neck cancer with a single test in routine clinical practice. *Mod Pathol*, 28, **12**, 1518-1527.

- MIRGHANI, H., CASIRAGHI, O., GUERLAIN, J., AMEN, F., HE, M. X., MA, X. J., LUO, Y., MOURAREAU, C., DRUSCH, F., LAKDHAR, A. B., AUPÉRIN, A., DALSTEIN, V. & VIELH, P. 2016. Diagnosis of HPV driven oropharyngeal cancers: comparing p16 based algorithms with the RNAscope HPV-test. *Oral Oncol*, 62, 101-108.
- MODIS, Y., TRUS, B. L. & HARRISON, S. C. 2002. Atomic model of the papillomavirus capsid. *EMBO J*, 21, 18, 4754-4762.
- MOHR, I. J., CLARK, R., SUN, S., ANDROPHY, E. J., MACPHERSON, P. & BOTCHAN, M. R. 1990. Targeting the E1 replication protein to the papillomavirus origin of replication by complex formation with the E2 transactivator. *Science*, 250, 4988, 1694-1699.
- MONTAG, M., BLANKENSTEIN, T. J. F., SHABANI, N., BRÜNING, A. & MYLONAS, I. 2011. Evaluation of two commercialised in situ hybridisation assays for detecting HPV-DNA in formalin-fixed, paraffin-embedded tissue. *Arch Gynecol Obstet*, 284, 4, 999-1005.
- MOORE, T. O., MOORE, A. Y., CARRASCO, D., STRATEN, M. V., ARANY, I., AU, W. & TYRING, S. K. 2001. Human papillomavirus, smoking, and cancer. *J Cutan Med Surg*, 5, 4, 323-328.
- MOOREN, J. J., GÜLTEKIN, S. E., STRAETMANS, J. M. J. A. A., HAESEVOETS, A., PEUTZ-KOOTSTRA, C. J., HUEBBERS, C. U., DIENES, H. P., WIELAND, U., RAMAEKERS, F. C. S., KREMER, B., SPEEL, E. J. M. & KLUSSMANN, J. P. 2014. p16 (INK4A) immunostaining is a strong indicator for high-risk-HPV-associated oropharyngeal carcinomas and dysplasias, but is unreliable to predict low-risk-HPV-infection in head and neck papillomas and laryngeal dysplasias. *Int J Cancer*, 134, 9, 2108-2117.
- MORBINI, P., CAPELLO, G., ALBERIZZI, P., BENAZZO, M., PAGLINO, C., COMOLI, P. & PEDRAZZOLI, P. 2015. Markers of squamocolumnar junction cells in normal tonsils and oropharyngeal cancer with and without HPV infection. *Histol Histopathol*, 30, 7, 833-839.
- MORGAN, I. M., DINARDO, L. J. & WINDLE, B. 2017. Integration of human papillomavirus genomes in head and neck cancer: is it time to consider a paradigm shift? *Viruses*, 9, 8, 208.
- MÜNGER, K., PHELPS, W. C., BUBB, V., HOWLEY, P. M. & SCHLEGEL, R. 1989a. The E6 and E7 genes of the human papillomavirus type 16 together are



- necessary and sufficient for transformation of primary human keratinocytes. *J Virol*, 63, **10**, 4417-4421.
- MÜNGER, K., WERNESS, B. A., DYSON, N., PHELPS, W. C., HARLOW, E. & HOWLEY, P. M. 1989b. Complex formation of human papillomavirus E7 proteins with the retinoblastoma tumor suppressor gene product. *EMBO J*, 8, **13**, 4099-4105.
- MUÑOZ, N., BOSCH, F. X., DE SANJOSÉ, S., HERRERO, R., CASTELLSAGUÉ, X., SHAH, K. V., SNIJDERS, P. J. F., MEIJER, C. J. L. M. & FOR THE INTERNATIONAL AGENCY FOR RESEARCH ON CANCER MULTICENTER CERVICAL CANCER STUDY GROUP 2003. Epidemiologic classification of human papillomavirus types associated with cervical cancer. *N Engl J Med*, 348, **6**, 518-527.
- MUSAFIA, B., OREN-BANAROYA, R. & NOIMAN, S. 2014. Designing anti-influenza aptamers: novel quantitative structure activity relationship approach gives insights into aptamer-virus interaction. *PLoS One*, 9, **5**, e97696.
- NABUURS, S. B., WAGENER, M. & DE VLIEG, J. 2007. A flexible approach to induced fit docking. *J. Med. Chem*, 50, **26**, 6507-6518.
- NAKAHARA, T., TANAKA, K., OHNO, S. I., EGAWA, N., YUGAWA, T. & KIYONO, T. 2015. Activation of NF- $\kappa$ B by human papillomavirus 16 E1 limits E1-dependent viral replication through degradation of E1. *J Virol*, 89, **9**, 5040-5059.
- NAKAYAMA, T., KANEKO, M., KODAMA, M. & NAGATA, C. 1985. Cigarette smoke induces DNA single-strand breaks in human cells. *Nature*, 314, **6010**, 462-464.
- NATIONAL COMPREHENSIVE CANCER NETWORK 2020. Head and Neck Cancers. *J Natl Compr Canc Netw*, 18, **7**. Available: [https://jnccn.org/configurable/content/journals\\$002fjnccn\\$002f18\\$002f7\\$002farticle-p873.xml?t%3Aac=journals%24002fjnccn%24002f18%24002f7%24002farticle-p873.xml&ArticleBodyColorStyles=inline%20pdf#](https://jnccn.org/configurable/content/journals$002fjnccn$002f18$002f7$002farticle-p873.xml?t%3Aac=journals%24002fjnccn%24002f18%24002f7%24002farticle-p873.xml&ArticleBodyColorStyles=inline%20pdf#).
- NATIONAL INSTITUTE FOR HEALTH AND CARE EXCELLENCE (NICE). 2016. *Cancer of the upper aerodigestive tract: assessment and management in people aged 16 and over* [Online]. Available: <https://www.nice.org.uk/guidance/ng36/chapter/Recommendations#hpvrelated-disease> [Accessed 01/05/2024].

- NAVE, H., GEBERT, A. & PABST, R. 2001. Morphology and immunology of the human palatine tonsil. *Anat Embryol (Berl)*, 204, **5**, 367-373.
- NAVIEN, T. N., THEVENDRAN, R., HAMDANI, H. Y., TANG, T. H. & CITARTAN, M. 2021. In silico molecular docking in DNA aptamer development. *Biochimie*, 180, 54-67.
- NDIAYE, C., ALEMANY, L., DIOP, Y., NDIAYE, N., DIÉMÉ, M. J., TOUS, S., KLAUSTERMEIER, J. E., ALEJO, M., CASTELLSAGUÉ, X., BOSCH, F. X., TROTTIER, H. & DE SANJOSÉ, S. 2013. The role of human papillomavirus in head and neck cancer in Senegal. *Infect Agent Cancer*, 8, **1**, 14.
- NDIAYE, C., MENA, M., ALEMANY, L., ARBYN, M., CASTELLSAGUÉ, X., LAPORTE, L., BOSCH, F. X., DE SANJOSÉ, S. & TROTTIER, H. 2014. HPV DNA, E6/E7 mRNA, and p16INK4A detection in head and neck cancers: a systematic review and meta-analysis. *Lancet Oncol*, 15, **12**, 1319-1331.
- NGUYEN, E. D., NORN, C., FRIMURER, T. M. & MEILER, J. 2013. Assessment and challenges of ligand docking into comparative models of G-protein coupled receptors. *PLoS One*, 8, **7**, e67302.
- NICOL, C., CESUR, Ö., FORREST, S., BELYAEVA, T. A., BUNKA, D. H. J., BLAIR, G. E. & STONEHOUSE, N. J. 2013. An RNA aptamer provides a novel approach for the induction of apoptosis by targeting the HPV16 E7 oncoprotein. *PLoS One*, 8, **5**, e64781.
- NICOLAIDES, L., DAVY, C., RAJ, K., KRANJEC, C., BANKS, L. & DOORBAR, J. 2011. Stabilization of HPV16 E6 protein by PDZ proteins, and potential implications for genome maintenance. *Virology*, 414, **2**, 137-145.
- NOBORI, T., MIURA, K., WU, D. J., LOIS, A., TAKABAYASHI, K. & CARSON, D. A. 1994. Deletions of the cyclin-dependent kinase-4 inhibitor gene in multiple human cancers. *Nature*, 368, **6473**, 753-756.
- OFFICE FOR NATIONAL STATISTICS. *Cancer Statistics Registrations, England (Series MB1)*. Available: <https://www.ons.gov.uk/peoplepopulationandcommunity/healthandsocialcare/conditionsanddiseases/datasets/cancerregistrationstatisticscancerregistrationstatisticsengland>
- OGA, E. A., SCHUMAKER, L. M., ALABI, B. S., OBASEKI, D., UMANA, A., BASSEY, I. A., EBUGHE, G., OLUWOLE, O., AKEREDOLU, T., ADEBAMOWO, S. N.,

- DAKUM, P., CULLEN, K. & ADEBAMOWO, C. A. 2016. Paucity of HPV-related head and neck cancers (HNC) in Nigeria. *PLoS One*, 11, **4**, e0152828.
- OGUEJIOFOR, K., GALLETTA-WILLIAMS, H., DOVEDI, S. J., ROBERTS, D. L., STERN, P. L. & WEST, C. M. L. 2017. Distinct patterns of infiltrating CD8+ T cells in HPV+ and CD68 macrophages in HPV-oropharyngeal squamous cell carcinomas are associated with better clinical outcome but PD-L1 expression is not prognostic. *Oncotarget*, 8, **9**, 14416-14427.
- OH, S. T., LONGWORTH, M. S. & LAIMINS, L. A. 2004. Roles of the E6 and E7 proteins in the life cycle of low-risk human papillomavirus type 11. *J Virol*, 78, **5**, 2620-2626.
- OLAH, I. 1978. *Tonsils, structure, immunology and biochemistry*, Budapest, Akadémiai Kiadó.
- OLIVA, M., SPREAFICO, A., TABERNA, M., ALEMANY, L., COBURN, B., MESIA, R. & SIU, L. L. 2019. Immune biomarkers of response to immune-checkpoint inhibitors in head and neck squamous cell carcinoma. *Ann Oncol*, 30, **1**, 57-67.
- OZBUN, M. A. 2002. Human papillomavirus type 31b infection of human keratinocytes and the onset of early transcription *J Virol*, 76, **22**, 11291-11300.
- PAAVONEN, J., JENKINS, D., BOSCH, F. X., NAUD, P., SALMERÓN, J., WHEELER, C. M., CHOW, S. N., APTER, D., KITCHENER, H. C., CASTELLSAGUÉ, X., DE CARVALHO, N. S., SKINNER, S. R., HARPER, D. M., HEDRICK, J. A., JAISAMRARN, U., LIMSON, G. A., DIONNE, M., QUINT, W., SPIESSENS, B., PEETERS, P., STRUYF, F., WIETING, S. L., LEHTINEN, M. O., DUBIN, G. & HPV PATRICIA STUDY GROUP 2007. Efficacy of a prophylactic adjuvanted bivalent L1 virus-like-particle vaccine against infection with human papillomavirus types 16 and 18 in young women: an interim analysis of a phase III double-blind, randomised controlled trial. *Lancet*, 369, **9580**, 2161-2170.
- PAI, S. I. & WESTRA, W. H. 2009. Molecular pathology of head and neck cancer: implications for diagnosis, prognosis, and treatment. *Annu Rev Pathol*, 4, 49-70.
- PALMER, E., NEWCOMBE, R. G., GREEN, A. C., KELLY, C., GILL, O. N., HALL, G., FIANDER, A. N., PIROTTE, E., HIBBITTS, S. J., HOMER, J. & POWELL, N. G. 2014. Human papillomavirus infection is rare in nonmalignant tonsil tissue in the UK: Implications for tonsil cancer precursor lesions. *Int J Cancer*, 135, **10**, 2437-2443.

- PANNONE, G., RODOLICO, V., SANTORO, A., LO MUZIO, L., FRANCO, R., BOTTI, G., AQUINO, G., PEDICILLO, M. C., CAGIANO, S., CAMPISI, G., RUBINI, C., PAPAGERAKIS, S., DE ROSA, G., TORNESELLO, M. L., BUONAGURO, F. M., STAIBANO, S. & BUFO, P. 2012. Evaluation of a combined triple method to detect causative HPV in oral and oropharyngeal squamous cell carcinomas: p16 immunohistochemistry, consensus PCR HPV-DNA, and in situ hybridization. *Infect Agent Cancer*, 7, 4.
- PARFENOV, M., PEDAMALLU, C. S., GEHLENBORG, N., FREEMAN, S. S., DANILOVA, L., BRISTOW, C. A., LEE, S., HADJIPANAYIS, A. G., IVANOVA, E. V., WILKERSON, M. D., PROTOPOPOV, A., YANG, L., SETH, S., SONG, X., TANG, J., REN, X., ZHANG, J., PANTAZI, A., SANTOSO, N., XU, A. W., MAHADESHWAR, H., WHEELER, D. A., HADDAD, R. I., JUNG, J., OJESINA, A. I., ISSAEVA, N., YARBROUGH, W. G., HAYES, D. N., GRANDIS, J. R., EL-NAGGAR, A. K., MEYERSON, M., PARK, P. J., CHIN, L., SEIDMAN, J. G., HAMMERMAN, P. S., KUCHERLAPATI, R. & CANCER GENOME ATLAS NETWORK 2014. Characterization of HPV and host genome interactions in primary head and neck cancers. *Proc Natl Acad Sci USA*, 111, **43**, 15544-15549.
- PARISH, J. L., BEAN, A. M., PARK, R. B. & ANDROPHY, E. J. 2006a. ChIR1 is required for loading papillomavirus E2 onto mitotic chromosomes and viral genome maintenance. *Mol Cell*, 24, **6**, 867-876.
- PARISH, J. L., ROSA, J., WANG, X., LAHTI, J. M., DOXSEY, S. J. & ANDROPHY, E. J. 2006b. The DNA helicase ChIR1 is required for sister chromatid cohesion in mammalian cells. *J Cell Sci*, 119, 4857-4865.
- PARK, B., KIM, H. & HAN, K. 2014. DBBP: database of binding pairs in protein-nucleic acid interactions. *BMC Bioinformatics*, 15, S5.
- PATEL, D., HUANG, S. M., BAGLIA, L. A. & MCCANCE, D. J. 1999. The E6 protein of human papillomavirus type 16 binds to and inhibits co-activation by CBP and p300. *EMBO J*, 18, **18**, 5061-5072.
- PATRICK, D. R., OLIFF, A. & HEIMBROOK, D. C. 1994. Identification of a novel retinoblastoma gene product binding site on human papillomavirus type 16 E7 protein. *J Biol Chem*, 269, **9**, 6842-6850.
- PIERCE, B. G., WIEHE, K., HWANG, H., KIM, B. H., VREVEN, T. & WENG, Z. 2014. ZDOCK server: interactive docking prediction of protein-protein complexes and

- symmetric multimers. *Bioinformatics*, 30, **12**, 1771-1773. Available: <https://zdock.umassmed.edu/>.
- PITIYAGE, G., LEI, M., URBANO, T. G., ODELL, T. & THAVARAJ, S. 2015. Biphenotypic human papillomavirus-associated head and neck squamous cell carcinoma: a report of two cases. *Diagn Histopathol*, 10, 97.
- PLATH, M., BROGLIE, M. A., FÖRBS, D., STOECKLI, S. J. & JOCHUM, W. 2018. Prognostic significance of cell cycle-associated proteins p16, pRB, cyclin D1 and p53 in resected oropharyngeal carcinoma. *J Otolaryngol Head Neck Surg*, 47, **1**, 53.
- PLEIKO, K., SAULITE, L., PARFEJEVS, V., MICULIS, K., VJATERS, E. & RIEKSTINA, U. 2019. Differential binding cell-SELEX method to identify cell-specific aptamers using high-throughput sequencing. *Sci Rep*, 9, 8142.
- PLUMMER, M., SCHIFFMAN, M., CASTLE, P. E., MAUCORT-BOULCH, D., WHEELER, C. M. & GROUP, A. 2007. A 2-year prospective study of human papillomavirus persistence among women with a cytological diagnosis of atypical squamous cells of undetermined significance or low-grade squamous intraepithelial lesion. *J Infect Dis*, 195, **11**, 1582-1589.
- POKRÝVKOVÁ, B., GREGA, M., KLOZAR, J., VENCÁLEK, O., NUNVÁŘ, J. & TACHEZY, R. 2022. PD1+CD8+ cells are an independent prognostic marker in patients with head and neck cancer. *Biomedicines*, 10, **11**, 2794.
- POPENDA, M., SZACHNIUK, M., ANTCZAK, M., PURZYCKA, K. J., KLUKASIAK, P., BARTOL, N., BLAZEWICZ, J. & ADAMIAK, R. W. 2012. Automated 3D structure composition for large RNAs. *Nucleic Acids Res*, 40, **14**, e112. Available: <http://rnacomposer.ibch.poznan.pl/>
- PRIGGE, E. S., ARBYN, M., VON KNEBEL DOEBERITZ, M. & REUSCHENNAC, M. 2017. Diagnostic accuracy of p16(INK4A) immunohistochemistry in oropharyngeal squamous cell carcinomas: a systematic review and meta-analysis. *Int J Cancer*, 140, **5**, 1186-1198.
- PYEON, D., PEARCE, S. M., LANK, S. M., AHLQUIST, P. & LAMBERT, P. F. 2009. Establishment of human papillomavirus infection requires cell cycle progression. *PLoS Pathog*, 5, **2**, e1000318.
- QUABIUS, E. S., TRIBIUS, S., HEINRICHS, A., HAASER, D., KÜHNEL, A., LAUDIEN, M., HOPPE, F., MLYNSKI, R., AMBROSCH, P. & HOFFMANN, M. 2021. HPV DNA/RNA detection in various oral and oropharyngeal biomaterials identifies

- active HPV infections also in non-neoplastic tonsils. *Transl Oncol*, 14, 2, 101002.
- RADUCANU, V. S., RASHID, F., ZAHER, M. S., LI, Y., MERZABAN, J. S. & HAMDAN, S. M. 2020. A direct fluorescent signal transducer embedded in a DNA aptamer paves the way for versatile metal-ion detection. *Sens Actuators B Chem*, 304, 127376.
- RAGIN, C., LIU, J. C., JONES, G., SHOYELE, O., SOWUNMI, B., KENNETT, R., GIBBS, D., BLACKMAN, E., ESAN, M., BRANDWEIN, M. S., DEVARAJAN, K., BUSSU, F., CHERNOCK, R., CHIEN, C. Y., COHEN, M. A., EL-MOFTY, S., SUZUKI, M., D'SOUZA, G., FUNCHAIN, P., ENG, C., GOLLIN, S. M., HONG, A., JUNG, Y. S., KRÜGER, M., LEWIS, J. J., MORBINI, P., LANDOLFO, S., RITTÀ, M., STRAETMANS, J., SZARKA, K., TACHEZY, R., WORDEN, F. P., NELSON, D., GATHERE, S. & TAIOLI, E. 2016. Prevalence of HPV infection in racial-ethnic subgroups of head and neck cancer patients. *Carcinogenesis*, 38, 2, 218-229.
- RAMOS-VARA, J. A. 2005. Technical aspects of immunohistochemistry. *Vet Pathol*, 42, 4, 405-426.
- RANDÉN-BRADY, R., CARPÉN, T., JOUHI, L., SYRJÄNEN, S., HAGLUND, C., TARKKANEN, J., REMES, S., MÄKITIE, S., MATTILA, P. S., SILÉN, S. & HAGSTRÖM, J. 2019. In situ hybridization for high-risk HPV E6/E7 mRNA is a superior method for detecting transcriptionally active HPV in oropharyngeal cancer. *Hum Pathol*, 90, 97-105.
- RAUTAVA, J. & SYRJÄNEN, S. 2012. Biology of human papillomavirus infections in head and neck carcinogenesis. *Head Neck Pathol*, 6, S3-15.
- REED, N., BALEGA, J., BARWICK, T., BUCKLEY, L., BURTON, K., EMINOWICZ, G., FORREST, J., GANESAN, R., HARRAND, R., HOLLAND, C., HOWE, T., IND, T., IYER, R., KAUSHUK, S., MUSIC, R., SADOZYE, A., SHANBHAG, S., SIDDIQUI, N., SYED, S., PERCIVAL, N., WHITHAM, N. L., NORDIN, A. & FOTOPOULOU, C. 2021. British Gynaecological Cancer Society (BGCS) cervical cancer guidelines: recommendations for practice. *Eur J Obstet Gynecol Reprod Biol*, 256, 433-465.
- REINSON, T., HENNO, L., USTAV, M. J. & USTAV, M. 2015. The cell cycle timing of human papillomavirus DNA replication. *PLoS One*, 10, 7, e0131675.

- REITER, P., PENDERGRAFT, W. F. I. & BREWER, N. T. 2010. Meta-analysis of human papillomavirus infection concordance. *Cancer Epidemiol Biomarkers Prev*, 19, 11, 2916-2931.
- RESEARCH AND MARKETS. 2024. *Global Aptamers Market by Product (Nucleotide Based, Peptide Based), Application (Diagnostics, Research & Development, Therapeutics Development), End-User - Forecast 2024-2030* [Online]. Research and Markets. [Accessed 15/05/2024].
- RETTIG, E. M., GOOI, Z., BARDIN, R., BOGALE, M., ROOPER, L., ACHA, E. & KOCH, W. M. 2019. Oral human papillomavirus infection and head and neck squamous cell carcinoma in rural northwest cameroon. *OTO Open*, 3, 1, 2473974X18818415.
- RICHARDS, R. M., LOWY, D. R., SCHILLER, J. T. & DAY, P. M. 2006. Cleavage of the papillomavirus minor capsid protein, L2, at a furin consensus site is necessary for infection. *Proc Natl Acad Sci USA*, 103, 5, 1522-1527.
- RIETBERGEN, M. M., BRAKENHOFF, R. H., BLOEMENA, E., WITTE, B. I., SNIJDERS, P. J. F., HEIDEMAN, D. A. M., BOON, D., KOLJENOVIC, S., BAATENBURG DE JONG, R. J. & LEEMANS, C. R. 2013. Human papillomavirus detection and comorbidity: critical issues in selection of patients with oropharyngeal cancer for treatment de-escalation trials. *Ann Oncol*, 24, 11, 2740-2745.
- RIETBERGEN, M. M., SNIJDERS, P. J. F., BEEKZADA, D., BRAAKHUIS, B. J. M., BRINK, A., HEIDEMAN, D. A. M., HESSELINK, A. T., WITTE, B. I., BLOEMENA, E., BAATENBURG DE JONG, R. J., LEEMANS, C. R. & BRAKENHOFF, R. H. 2014. Molecular characterisation of p16-immunopositive but HPV DNA-negative oropharyngeal carcinomas. *Int J Cancer*, 134, 10, 2366-2372.
- RISCHIN, D., YOUNG, R. J., FISHER, R., FOX, S. B., LE, Q. T., PETERS, L. J., SOLOMON, B., CHOI, J., O'SULLIVAN, B., KENNY, L. M. & MCARTHUR, G. A. 2010. Prognostic significance of p16INK4A and human papillomavirus in patients with oropharyngeal cancer treated on TROG 02.02 phase III trial. *J Clin Oncol*, 28, 27, 4142-4148.
- ROBERTS, J. N., BUCK, C. B., THOMPSON, C. D., KINES, R., BERNARDO, M., CHOYKE, P. L., LOWY, D. R. & SCHILLER, J. T. 2007. Genital transmission

- of HPV in a mouse model is potentiated by nonoxynol-9 and inhibited by carrageenan. *Nat Med*, 13, 7, 857-861.
- ROBERTS, S., EVANS, D., MEHANNA, H. & PARISH, J. L. 2019. Modelling human papillomavirus biology in oropharyngeal keratinocytes. *Philos Trans R Soc Lond B Biol Sci*, 374, **1773**, 20180289.
- ROBERTSON, D. L. & JOYCE, G. F. 1990. Selection in vitro of an RNA enzyme that specifically cleaves single-stranded DNA. *Nature*, 344, **6265**, 467-468.
- ROBINSON, M., SCHACHE, A., SLOAN, P. & THAVARAJ, S. 2012. HPV specific testing: a requirement for oropharyngeal squamous cell carcinoma patients. *Head Neck Pathol*, 6, **83-90**.
- ROCHE DIAGNOSTICS. 2024. *INFORM HPV III FAMILY 16 PROBE (B)* [Online]. Roche Diagnostics. Available: <https://elabdoc-prod.roche.com/eLD/web/gb/en/products/RTD000970?searchTerm=hpv%20inform&catalog=ProductCatalog&orderBy=Relevance&fromResults=true> [Accessed 27/05/2024].
- ROMAGOSA, C., SIMONETTI, S., LÓPEZ-VICENTE, L., MAZO, A., LLEONART, M. E., CASTELLVI, J. & RAMON Y CAJAL, S. 2011. p16(Ink4a) overexpression in cancer: a tumor suppressor gene associated with senescence and high-grade tumors. *Oncogene*, 30, **18**, 2087-2097.
- ROMANCZUK, H., THIERRY, F. & HOWLEY, P. M. 1990. Mutational analysis of cis elements involved in E2 modulation of human papillomavirus type 16 P97 and type 18 P105 promoters. *J Virol*, 64, **6**, 2849-2859.
- ROSSI, P. G., CAROZZI, F., RONCO, G., ALLIA, E., BISANZI, S., GILLIO-TOS, A., DE MARCO, L., RIZZOLO, R., GUSTINUCCI, D., DEL MISTRO, A., FRAYLE, H., CONFORTINI, M., IOSSA, A., CESARINI, E., BULLETTI, S., PASSAMONTI, B., GORI, S., TONIOLO, L., BARCA, A., BONVICINI, L., MANCUSO, P., VENTURELLI, F., BENEVOLO, M. & NEW TECHNOLOGY FOR CERVICAL CANCER 2 WORKING GROUP 2021. p16/ki67 and E6/E7 mRNA accuracy and prognostic value in triaging HPV DNA-positive women. *J Natl Cancer Inst*, 113, **3**, 292-300.
- RÖTHLISBERGER, P. & HOLLENSTEIN, M. 2018. Aptamer chemistry. *Adv Drug Deliv Rev*, 134, 3-21.
- RUCKMAN, J., GREEN, L. S., BEESON, J., WAUGH, S., GILLETTE, W. L., HENNINGER, D. D., CLAEISSON-WELSH, L. & JANJIĆ, N. 1998. 2'-



- Fluoropyrimidine RNA-based aptamers to the 165-amino acid form of vascular endothelial growth factor (VEGF165). Inhibition of receptor binding and VEGF-induced vascular permeability through interactions requiring the exon 7-encoded domain. *J Biol Chem*, 273, **32**, 20556-20567.
- RUIGROK, V. J. B., LEVISSON, M., HEKELAAR, J., SMIDT, H., DIJKSTRA, B. W. & VAN DER OOST, J. 2012. Characterization of aptamer-protein complexes by x-ray crystallography and alternative approaches. *Int J Mol Sci*, 13, **8**, 10537-10552.
- SABRI, M. Z., HAMID, A. A. A., HITAM, S. M. S. & RAHIM, M. Z. A. 2018. In-silico selection of aptamer: A review on the revolutionary approach to understand the aptamer design and interaction through computational chemistry. *Mater Today: Proc*, 19, 1572-1581.
- SABRI, M. Z., HAMID, A. A. A., HITAM, S. M. S. & RAHIM, M. Z. A. 2019. In silico screening of aptamers configuration against Hepatitis B surface antigen. *Adv Bioinformatics*, 2019, **3**, 1-12.
- SAFAEIAN, M., PORRAS, C., SCHIFFMAN, M., RODRIGUEZ, A. C., WACHOLDER, S., GONZALEZ, P., QUINT, W., VAN DOORN, L. J., SHERMAN, M. E., XHENSEVAL, V., HERRERO, R., HILDESHEIM, A. & COSTA RICAN VACCINE TRIAL GROUP 2010. Epidemiological study of anti-HPV16/18 seropositivity and subsequent risk of HPV16 and -18 infections. *J Natl Cancer Inst*, 102, **21**, 1653-1662.
- SÁNCHEZ, I. E., DELLAROLE, M., GASTON, K. & DE PRAT GAY, G. 2008. Comprehensive comparison of the interaction of the E2 master regulator with its cognate target DNA sites in 73 human papillomavirus types by sequence statistics. *Nucleic Acids Res*, 36, **3**, 756-769.
- SANDERS, C. M. & STENLUND, A. 1998. Recruitment and loading of the E1 initiator protein: an ATP-dependent process catalysed by a transcription factor. *EMBO J*, 17, **23**, 7044-7055.
- SANTALUCIA, J. J. & HICKS, D. 2004. The thermodynamics of DNA structural motifs. *Annu Rev Biophys Biomol Struct*, 33, 415-440.
- SAVORY, N., ABE, K., SODE, K. & IKEBUKURO, K. 2010. Selection of DNA aptamer against prostate specific antigen using a genetic algorithm and application to sensing. *Biosens Bioelectron*, 26, **4**, 1386-1391.

- SCARTH, J. A., PATTERSON, M. R., MORGAN, E. L. & MACDONALD, A. 2021. The human papillomavirus oncoproteins: a review of the host pathways targeted on the road to transformation. *J Gen Virol*, 102, **3**, 001540.
- SCHACHE, A. G., LILOGLOU, T., RISK, J. M., FILIA, A., JONES, T. M., SHEARD, J., WOOLGAR, J. A., HELLIWELL, T. R., TRIANTAFYLLOU, A., ROBINSON, M., SLOAN, P., HARVEY-WOODWORTH, C., SISSON, D. & SHAW, R. J. 2011. Evaluation of human papilloma virus diagnostic testing in oropharyngeal squamous cell carcinoma: sensitivity, specificity and prognostic discrimination. *Clin Cancer Res*, 17, **19**, 6262-6271.
- SCHACHE, A. G., POWELL, N. G., CUSCHIERI, K. S., ROBINSON, M., LEARY, S., MEHANNA, H., RAPOZO, D., LONG, A., CUBIE, H., JUNOR, E., MONAGHAN, H., HARRINGTON, K. J., NUTTING, C. M., SCHICK, U., LAU, A. S., UPILE, N. S., SHEARD, J., BROUGHAM, K., WEST, C. M. L., OGUEJIOFOR, K., THOMAS, S., NESS, A. R., PRING, M., THOMAS, G. J., KING, E. V., MCCANCE, D. J., JAMES, J. A., MORAN, M., SLOAN, P., SHAW, R. J., EVANS, M. & JONES, T. M. 2016. HPV-related oropharynx cancer in the United Kingdom: an evolution in the understanding of disease etiology. *Cancer Res*, 76, **22**, 6598-6606.
- SCHEFFNER, M., HUIBREGTSE, J. M., VIERSTRA, R. D. & HOWLEY, P. M. 1993. The HPV-16 E6 and E6-AP complex functions as a ubiquitin-protein ligase in the ubiquitination of p53. *Cell*, 75, **3**, 495-505.
- SCHEFFNER, M., MÜNGER, K., HUIBREGTSE, J. M. & HOWLEY, P. M. 1992. Target degradation of the retinoblastoma protein by human papillomavirus E7-E6 fusion proteins. *EMBO J*, 11, **7**, 2425-2431.
- SCHEFFNER, M., WERNESS, B. A., HUIBREGTSE, J. M., LEVINE, A. J. & HOWLEY, P. M. 1990. The E6 oncoprotein encoded by human papillomavirus types 16 and 18 promotes the degradation of p53. *Cell*, 63, **6**, 1129-1136.
- SCHELHAAS, M., EWERS, H., RAJAMÄKI, M. L., DAY, P. M., SCHILLER, J. T. & HELENIUS, A. 2008. Human papillomavirus type 16 entry: retrograde cell surface transport along actin-rich protrusions. *PLoS Pathog*, 4, **9**, e1000148.
- SCHELHAAS, M., SHAH, B., HOLZER, M., BLATTMANN, P., KÜHLING, L., DAY, P. M., SCHILLER, J. T. & HELENIUS, A. 2012. Entry of human papillomavirus type 16 by actin-dependent, clathrin- and lipid raft-independent endocytosis. *PLoS Pathog*, 8, **4**, e1002657.

- SCHIFFMAN, M., DOORBAR, J., WENTZENSEN, N., DE SANJOSÉ, S., FAKHRY, C., MONK, B. J., STANLEY, M. A. & FRANCESCHI, S. 2016. Carcinogenic human papillomavirus infection. *Nat Rev Dis Primers*, 2, 16086.
- SCHIFFMAN, M., RODRIGUEZ, A. C., CHEN, Z., WACHOLDER, S., HERRERO, R., HILDESHEIM, A., DESALLE, R., BEFANO, B., YU, K., SAFAEIAN, M., SHERMAN, M. E., MORALES, J., GUILLEN, D., ALFARO, M., HUTCHINSON, M., SOLOMON, D., CASTLE, P. E. & BURK, R. D. 2010. A population-based prospective study of carcinogenic human papillomavirus variant lineages, viral persistence, and cervical neoplasia. *Cancer Res*, 70, 8, 3159-3169.
- SCHLECHT, N. F., BRANDWEIN-GENSLER, M., NUOVO, G. J., LI, M., DUNNE, A., KAWACHI, N., SMITH, R. V., BURK, R. D. & PRYSTOWSKY, M. B. 2012. A comparison of clinically utilised human papillomavirus detection methods in head and neck cancer. *Mod Pathol*, 24, 10, 1295-1305.
- SCHMINCKE, A. 1921. *Beitr Pathol Anat*, 68, 161-170.
- SCHNEIDER-GÄDICKE, A. & SCHWARZ, E. 1986. Different human cervical carcinoma cell lines show similar transcription patterns of human papillomavirus type 18 early genes. *EMBO J*, 5, 9, 2285-2292.
- SCHNEIDER, C. A., RASBAND, W. S. & ELICEIRI, K. W. 2012. NIH Image to ImageJ: 25 years of image analysis. *Nat Methods*, 9, 7, 671-675.
- SCHRÖDINGER LLC 2015. The PyMOL Molecular Graphics System. 2.5.5 ed.
- SEDGHIZADEH, P. P., BILLINGTON, W. D., PAXTON, D., EBEED, R., MAHABADY, S., CLARK, G. T. & ENCISO, R. 2016. Is p16-positive oropharyngeal squamous cell carcinoma associated with favorable prognosis? A systematic review and meta-analysis. *Oral Oncol*, 54, 15-27.
- SERRANO, M. 1997. The tumor suppressor protein p16INK4a. *Exp Cell Res*, 237, 1, 7-13.
- SERRANO, M., HANNON, G. J. & BEACH, D. 1993. A new regulatory motif in cell-cycle control causing specific inhibition of cyclin D/CDK4. *Nature*, 366, 6456, 704-707.
- SGARAMELLA, N., COATES, P. J., STRINDLUND, K., LOLJUNG, L., COLELLA, G., LAURELL, G., ROSSIELLO, R., MUZIO, L. L., LOIZOU, C., TARTARO, G., OLOFSSON, K., DANIELSSON, K., FÅHRAEUS, R. & NYLANDER, K. 2015. Expression of p16 in squamous cell carcinoma of the mobile tongue is

- independent of HPV infection despite presence of the HPV-receptor syndecan-1. *Br J Cancer*, 113, 2, 321-326.
- SHELTON, J., PURGINA, B. M., CIPRIANI, N. A., DUPONT, W. D., PLUMMER, D. & LEWIS, J. S. J. 2017. p16 immunohistochemistry in oropharyngeal squamous cell carcinoma: a comparison of antibody clones using patient outcomes and high-risk human papillomavirus RNA status. *Mod Pathol*, 30, 9, 1194-1203.
- SHIGDAR, S., LV, L., WANG, L. & DUAN, W. 2016. Application of aptamers in histopathology. *Methods Mol Biol*, 1380, 191-196.
- SHINN, J. R., DAVIS, S. J., LANG-KUHS, K. A., ROHDE, S., WANG, X., LIU, P., DUPONT, W. D., PLUMMER, W. D. J., THORSTAD, W. L., CHERNOCK, R. D., MEHRAD, M. & LEWIS, J. S. J. 2021. Oropharyngeal squamous cell carcinoma with discordant p16 and HPV mRNA results-incidence and characterization in a large, contemporary United States cohort. *Am J Surg Pathol*, 45, 7, 951-961.
- SILVA, S. D., AGOSTINI, M., NISHIMOTO, I. N., COLETTA, R. D., ALVES, F. A., LOPES, M. A., KOWALSKI, L. P. & GRANER, E. 2004. Expression of fatty acid synthase, ErbB2 and Ki-67 in head and neck squamous cell carcinoma. A clinicopathological study. *Oral Oncol*, 40, 7, 688-696.
- SINGH, T., CHHOKAR, A., THAKUR, K., AGGARWAL, N., PRAGYA, P., YADAV, J., TRIPATHI, T., JADLI, M., BHAT, A., GUPTA, P., KHURANA, A. & BHARTI, A. C. 2021. Targeting aberrant expression of STAT3 and AP-1 oncogenic transcription factors and HPV oncoproteins in cervical cancer by Berberis aquifolium. *Front Pharmacol*, 12, 757414.
- SINGHI, A. D. & WESTRA, W. H. 2010. Comparison of human papillomavirus in situ hybridization and p16 immunohistochemistry in the detection of human papillomavirus-associated head and neck cancer based on a prospective clinical trial. *Cancer*, 116, 9, 2166-2173.
- SIVAKUMAR, N., NARWAL, A., KAMBOJ, M., DEVI, A., KUMAR, S. & BHARDWAJ, R. 2021. Molecular and immunohistochemical cognizance of HPV16 in oral leukoplakia, oral squamous cell carcinoma and oropharyngeal squamous cell carcinoma. *Head Neck Pathol*, 15, 3, 882-892.
- SKIADOPOULOS, M. H. & MCBRIDE, A. A. 1998. Bovine papillomavirus type I genomes and the E2 transactivator protein are closely associated with mitotic chromatin. *J Virol*, 72, 3, 2079-2088.

- SMEETS, S. J., HESSELINK, A. T., SPEEL, E. J. M., HAESEVOETS, A., SNIJDERS, P. J. F., PAWLITA, M., MEIJER, C. J. L. M., BRAAKHUIS, B. J. M., LEEMANS, C. R. & BRAKENHOFF, R. H. 2007. A novel algorithm for reliable detection of human papillomavirus in paraffin embedded head and neck cancer specimen. *Int J Cancer*, 121, **11**, 2465-2472.
- SMITH, E. M., RUBENSTEIN, L. M., HAUGEN, T. H., HANSIKOVA, E. & TUREK, L. P. 2010. Tobacco and alcohol use increases the risk of both HPV-associated and HPV-independent head and neck cancers. *Cancer Causes Control*, 21, **9**, 1369-1378.
- SMITH, E. M., WANG, D., KIM, Y., RUBENSTEIN, L. M., LEE, J. H., HAUGEN, T. H. & TUREK, L. P. 2008a. p16INK4A expression, human papillomavirus, and survival in head and neck cancer. *Oral Oncol*, 44, **2**, 133-142.
- SMITH, J. L., LIDKE, D. S. & OZBUN, M. A. 2008b. Virus activated filopodia promote human papillomavirus type 31 uptake from the extracellular matrix. *Virology*, 381, **1**, 16-21.
- SMITH, J. S., LINDSAY, L., HOOTS, B., KEYS, J., FRANCESCHI, S., WINER, R. & CLIFFORD, G. M. 2007. Human papillomavirus type distribution in invasive cervical cancer and high-grade cervical lesions: a meta-analysis update. *Int J Cancer*, 121, **3**, 621-632.
- SMOTKIN, D. & WETTSTEIN, F. O. 1986. Transcription of human papillomavirus type 16 early genes in a cervical cancer and a cancer-derived cell line and identification of the E7 protein *Proc Natl Acad Sci USA*, 83, **13**, 4680-4684.
- SOLARES, M. J., JONAI, G. M., LUQU, W. Y., BERRY, S., KHADELA, J., LIANG, Y., EVANS, M. C., PRIDHAM, K. J., DEARNALEY, W. J., SHENG, Z. & KELLY, D. F. 2022. High-resolution imaging of human cancer proteins using microprocessor materials. *ChemBiochem*, 23, **17**, e202200310.
- SPODEN, G., FREITAG, K., HUSMANN, M., BOLLER, K., SAPP, M., LAMBERT, C. & FLORIN, L. 2008. Clathrin- and caveolin-independent entry of human papillomavirus type 16-involvement of tetraspanin-enriched microdomains (TEMs). *PLoS One*, 3, **10**, e3313.
- STEUER, C. E., GRIFFITH, C. C., NANNAPANENI, S., PATEL, M. R., LIU, Y., MAGLIOCCA, K. R., EL-DEIRY, M. W., COHEN, C., OWONIKOKO, T. K., SHIN, D. M., CHEN, Z. G. & SABA, N. F. 2018. A correlative analysis of PD-

- L1, PD-1, PD-L2, EGFR, HER2, and HER3 expression in oropharyngeal squamous cell carcinoma. *Mol Cancer Ther*, 17, 3, 710-716.
- STIASNY, A., KUHN, C., MAYR, D., ALEXIOU, C., JANKO, C., WIEST, I., JESCHKE, U. & KOST, B. 2016. Immunohistochemical evaluation of E6/E7 HPV oncoproteins staining in cervical cancer. *Anticancer Res*, 36, 6, 3195-3198.
- STÖHR, P. 1882. *Biolog Zentralbl*, 368-370.
- STOLTENBURG, R., REINEMANN, C. & STREHLITZ, B. 2007. SELEX-a (r)evolutionary method to generate high-affinity nucleic acid ligands. *Biomol ENg*, 24, 4, 381-403.
- STRAUB, E., FERTEY, J., DREER, M., IFTNER, T. & STUBENRAUCH, F. 2015. Characterization of the human papillomavirus 16 E8 promoter. *J Virol*, 89, 14, 7304-7313.
- STURGEON, C., HILL, R., HORTIN, G. L. & THOMPSON, D. 2010. Taking a new biomarker into routine use-a perspective from the routine clinical biochemistry laboratory. *Proteomics Clin Appl*, 4, 12, 892-903.
- SU, C. H., TSAI, M. H., LIN, C. Y., MA, Y. D., WANG, C. H., CHUNG, Y. D. & LEE, G. B. 2020. Dual aptamer assay for detection of *Acinetobacter baumannii* on an electromagnetically-driven microfluidic platform. *Biosens Bioelectron*, 159, 112148.
- SUAREZ, I. P., BONHOURE, A., COUSIDO-SIAH, A., CHEBARO, Y., KOSTMANN, C., EBERLING, P., ALTSCHUH, D., MITSCHLER, A., PODJARNY, A. & TRAVÉ, G. Unpublished.
- SUCCARIA, F., KVISTBORG, P., STEIN, J. E., ENGLE, E. L., MCMILLER, T. L., ROOPER, L. M., THOMPSON, E., BERGER, A. E., VAN DEN BREKEL, M., ZUUR, C. L., HAANEN, J., TOPALIAN, S. L. & TAUBE, J. M. 2021. Characterization of the tumor immune microenvironment in human papillomavirus-positive and -negative head and neck squamous cell carcinomas. *Cancer Immunol Immunother*, 70, 5, 1227-1237.
- SUN, H. & ZU, Y. 2015. A highlight of recent advances in aptamer technology and its application. *Molecules*, 20, 7, 11959-11980.
- SUN, T. T., EICHNER, R., SCHERMER, A., COOPER, D., NELSON, W. G. & WEISS, R. A. 1984. *Classification, expression and possible mechanisms of evolution of mammalian epithelial keratins: a unifying model*, New York: Cold Spring Harbour Laboratory.

- SURESH, K., SHAH, P. V., COATES, S., ALEXIEV, B. A. & SAMANT, S. 2021. In situ hybridization for high risk HPV E6/E7 mRNA in oropharyngeal squamous cell carcinoma. *Am J Otolaryngol*, 41, 1, 102782.
- SYRJÄNEN, K., SYRJÄNEN, S., LAMBERG, M., PYRHÖNEN, S. & NUUTINEN, J. 1983. Morphological and immunohistochemical evidence suggesting human papillomavirus (HPV) involvement in oral squamous cell carcinogenesis. *Int J Oral Surg*, 12, 418-424.
- SYRJÄNEN, S. 2018. Oral manifestations of human papillomavirus infections. *Eur J Oral Sci*, 126, 49-66.
- TABERNA, M., TORRES, M., ALEJO, M., MENA, M., TOUS, S., MARQUEZ, S., PAVÓN, M. A., LEÓN, X., GARCÍA, J., GUIX, M., HIJANO, R., BONFILL, T., AGUILÀ, A., LOZANO, A., MESÍA, R., ALEMANY, L. & BRAVO, I. G. 2018. The use of HPV16-E5, EGFR, and pEGFR as prognostic biomarkers for oropharyngeal cancer patients. *Front Oncol*, 8, 589.
- TAMÁS, L., SZENTKÚTI, G., ERŐS, M., DÁNOS, K., BRAUSWETTER, D., SZENDE, B., ZSÁKOVICS, I. & KRENÁCS, T. 2011. Differential biomarker expression in head and neck cancer correlates with anatomical localization. *Pathol Oncol Res*, 17, 3, 721-727.
- TAN, W. C. C., NERURKAR, S. N., CAI, H. Y., NG, H. H. M., WU, D., WEE, Y. T. F., LIM, J. C. T., YEONG, J. & LIM, T. K. H. 2020. Overview of multiplex immunohistochemistry/immunofluorescence techniques in the era of cancer immunotherapy. *Cancer Commun (Lond)*, 40, 4, 135-153.
- THAM, T., AHN, S., FRANK, D., KRAUS, D. & COSTANTINO, P. 2020. Anatomical subsite modifies survival in oropharyngeal squamous cell carcinoma: National Cancer Database study. *Head Neck*, 42, 3, 434-445.
- THAVARAJ, S., STOKES, A., GUERRA, E., BIBLE, J., HALLIGAN, E., LONG, A., OKPOKAM, A., SLOAN, P., ODELL, E. & ROBINSON, M. 2011. Evaluation of human papillomavirus testing for squamous cell carcinoma of the tonsil in clinical practice. *J Clin Pathol*, 64, 4, 308-312.
- THE CANCER GENOME ATLAS NETWORK 2015. Comprehensive genomic characterization of head and neck squamous cell carcinomas. *Nature*, 517, 7536, 576-582.
- THE UNIPROT CONSORTIUM 2022. UniProt: the Universal Protein Knowledgebase in 2023. *Nucleic Acids Research*, 51, D1, D523-D531.

- THIEL, W. H. & GIANGRANDE, P. H. 2016. AFBI assay-aptamer fluorescence binding and internalisation assay for cultured adherent cells. *Methods*, 103, 180-187.
- THIERRY, F., HEARD, J. M., DARTMANN, K. & YANIV, M. 1987. Characterization of a transcriptional promoter of human papillomavirus 18 and modulation of its expression by simian virus 40 and adenovirus early antigens. *J Virol*, 61, 1, 134-142.
- THIERRY, F. & HOWLEY, P. M. 1991. Functional analysis of E2-mediated repression of the HPV18 P105 promoter. *New Biol*, 3, 1, 90-100.
- THOMAS, J. T., HUBERT, W. G., RUESCH, M. N. & LAIMINS, L. A. 1999. Human papillomavirus type 31 oncoproteins E6 and E7 are required for the maintenance of episomes during the viral life cycle in normal human keratinocytes. *Proc Natl Acad Sci USA*, 96, 15, 8449-8454.
- THOMAS, M., DASGUPTA, J., ZHANG, Y., CHEN, X. & BANKS, L. 2008. Analysis of specificity determinants in the interactions of different HPV E6 proteins with their PDZ domain-containing substrates. *Virology*, 376, 2, 371-378.
- TIMBANG, M. R., SIM, M. W., BEWLEY, A. F., FARWELL, D. G., MANTRAVADI, A. & MOORE, M. G. 2019. HPV-related oropharyngeal cancer: a review on burden of the disease and opportunities for prevention and early detection. *Hum Vaccin Immunother*, 15, 7-8, 1920-1928.
- TORRE, V., BUCOLO, S., GIORDANO, C., CICCARELLO, R., CAVALLARI, V., GAROFALO, L. & BEATRICE, F. 2005. Palatine tonsils in smoker and non-smoker patients: a pilot clinicopathological and ultrastructural study. *J Oral Pathol Med*, 34, 7, 390-396.
- TOSCANO-GARIBAY, J. D., BENÍTEZ-HESS, M. L. & ALVAREZ-SALAS, L. M. 2011. Isolation and characterization of an RNA aptamer for the HPV-16 E7 oncoprotein. *Arch Med Res*, 42, 2, 88-96.
- TOSCANO-GARIBAY, J. D., BENÍTEZ-HESS, M. L. & ALVAREZ-SALAS, L. M. 2015. Targeting of the HPV-16 E7 protein by RNA aptamers. *Methods Mol Biol*, 1249, 221-239.
- TOTA, J. E., BEST, A. F., ZUMSTEG, Z. S., GILLISON, M. L., ROSENBERG, P. S. & CHATURVEDI, A. K. 2019. Evolution of the oropharynx cancer epidemic in the United States: moderation of increasing incidence in younger individuals and shift in the burden to older individuals. *J Clin Oncol*, 37, 18, 1538-1546.



- TRAUSCH, J. J., SHANK-RETZLAFF, M. & VERCH, T. 2017. Development and characterization of an HPV type-16 specific modified DNA aptamer for the improvement of potency assays. *Anal Chem*, 89, **6**, 3554-3561.
- TSENG, S. C., JARVINEN, M. J., NELSON, W. G., HUANG, J. W., WOODCOCK-MITCHELL, J. & SUN, T. T. 1982. Correlation of specific keratins with different types of epithelial differentiation: monoclonal antibody studies. *Cell*, 30, **2**, 361-372.
- TSUCHIDA, K., SUGAI, T., UESUGI, N., ISHIDA, K., MATSUURA, K., SATO, I., SHIGA, K. & SATO, H. 2017. Expression of cell cycle-related proteins in oropharyngeal squamous carcinoma based on human papilloma virus status. *Oncol Rep*, 38, **2**, 908-916.
- TUERK, C. & GOLD, L. 1990. Systematic evolution of ligands by exponential enrichment: RNA ligands to bacteriophage T4 DNA polymerase. *Science*, 249, **4968**, 505-510.
- U.S. FOOD AND DRUGS ADMINISTRATION. 2011. *Drugs@FDA: FDA-Approved Drugs* [Online]. FDA. Available: <https://www.accessdata.fda.gov/scripts/cder/daf/index.cfm?event=BasicSearch.process> [Accessed 15/05/2024].
- UK NATIONAL SCREENING COMMITTEE. 2022. *Criteria for a population screening programme* [Online]. UK: UK National Screening Committee. Available: <https://www.gov.uk/guidance/screening-programmes-across-the-uk> [Accessed].
- UKPO, O. C., FLANAGAN, J. J., MA, X. J., LUO, Y., THORSTAD, W. L. & LEWIS, J. S. J. 2011. High-risk human papillomavirus E6/E7 mRNA detection by a novel in situ hybridization assay strongly correlates with p16 expression and patient outcomes in oropharyngeal squamous cell carcinoma. *Am J Surg Pathol*, 35, **9**, 1343-50.
- UNITED NATIONS. 2015. *Transforming our world: the 2030 agenda for sustainable development* [Online]. United Nations. Available: <https://sdgs.un.org/sites/default/files/publications/21252030%20Agenda%20for%20Sustainable%20Development%20web.pdf> [Accessed 05/06/2024].
- UNITED NATIONS DEVELOPMENT PROGRAMME. 2015. *Sustainable Development Goals* [Online]. United Nations. Available: <https://www.undp.org/sustainable-development-goals> [Accessed 05/05/2024].

- VALENCIA-RESÉNDIZ, D. G., PALOMINO-VIZCAINO, G., TAPIA-VIEYRA, J. V., BENÍTEZ-HESS, M. L., LEIJA-MONTOYA, A. G. & ALVAREZ-SALAS, L. M. 2018. Inhibition of Human Papillomavirus Type 16 Infection Using an RNA Aptamer. *Nucleic Acid Ther*, 28, 2, 97-105.
- VALLE, G. F. & BANKS, L. 1995. The human papillomavirus (HPV)-6 and HPV-16 E5 proteins co-operate with HPV-16 E7 in the transformation of primary rodent cells. *J Gen Virol*, 76, 5, 1239-1245.
- VAN DOORSLAER, K. & BURK, R. D. 2012. Association between hTERT activation by HPV E6 proteins and oncogenic risk. *Virology*, 433, 1, 216-219.
- VAN DOORSLAER, K., LI, Z., XIRASAGAR, S., MAES, P., KAMINSKY, D., LIOU, D., SUN, Q., KAUR, R., HUYEN, Y. & MCBRIDE, A. A. 2016. The Papillomavirus Episteme: a major update to the papillomavirus sequence database. *Nucleic Acids Research*, 45, D1, D499-D506. Available: <https://pave.niaid.nih.gov/>.
- VEGF INHIBITION STUDY IN OCULAR NEOVASCULARIZATION (V.I.S.I.O.N.) CLINICAL TRIAL GROUP 2006. Year 2 efficacy results of 2 randomized controlled clinical trials of pegaptanib for neovascular age-related macular degeneration. *Ophthalmology*, 113, 9, 1508.e1-25.
- VELDMAN, T., HORIKAWA, I., BARRETT, J. C. & SCHLEGEL, R. 2001. Transcriptional activation of the telomerase hTERT gene by human papillomavirus type 16 E6 oncoprotein. *J Virol*, 75, 9, 4467-4472.
- VERMORKEN, J. B., MESIA, R., RIVERA, F., REMENAR, E., KAWECKI, A., ROTTEY, S., ERFAN, J., ZABOLOTNY, D., KIENZER, H. R., CUISSOL, D., PEYRADE, F., BENASSO, M., VYNNYCHENKO, I., DE RAUCOURT, D., BOKEMEYER, C., SCHUELER, A., AMELLAL, N. & HITT, R. 2008. Platinum-based chemotherapy plus cetuximab in head and neck cancer. *N Engl J Med*, 359, 11, 1116-1127.
- VINOKUROVA, S., WENTZENSEN, N., KRAUS, I., KLAES, R., DRIESCH, C., MELSHEIMER, P., KISSELJOV, F., DÜRST, M., SCHNEIDER, A. & VON KNEBEL DOEBERITZ, M. 2008. Type-dependent integration frequency of human papillomavirus genomes in cervical lesions. *Cancer Res*, 68, 1, 307-313.
- VOSKUIL, J. L. A. 2014. Commercial antibodies and their validation. *F1000Res*, 3, 232.

- WAGNER, S., PRIGGE, E. S., WUERDEMANN, N., REDER, H., BUSHNAK, A., SHARMA, S. J., OBERMUELLER, T., VON KNEBEL DOEBERITZ, M., DREYER, T., GATTENLÖHNER, S., WOLF, G., PONS-KÜHNEMANN, J., WITTEKINDT, C. & KLUSSMAN, J. P. 2021. Evaluation of p16INK4A expression as a single marker to select patients with HPV-driven oropharyngeal cancers for treatment de-escalation. *Br J Cancer*, 125, **2**, 307.
- WALBOOMERS, J. M. M., JACOBS, M. V., MANOS, M. M., BOSCH, F. X., KUMMER, J. A., SHAH, K. V., SNIJDERS, P. J., PETO, J., MEIJER, C. J. & MUÑOZ, N. 1999. Human papillomavirus is a necessary cause of invasive cervical cancer worldwide. *J Pathol*, 189, **1**, 12-19.
- WALDEYER, W. 1884. *Dtsch Med Wochenschr*, 10, 313.
- WANG, J., GAO, T., LUO, Y., WANG, Z., ZHANG, Y., ZHANG, Y., ZHANG, Y. & PEI, R. 2019a. In vitro selection of a DNA aptamer by cell-SELEX as a molecular probe for cervical cancer recognition and imaging. *J Mol Evol*, 87, **2-3**, 72-82.
- WANG, L. & BROWN, S. J. 2006. BindN: a web-based tool for efficient prediction of DNA and RNA binding sites in amino acid sequences. *Nucleic Acids Res*, 34, **2**, W243-248.
- WANG, Q., GRIFFIN, H., SOUTHERN, S., JACKSON, D., MARTIN, A., MCINTOSH, P., DAVY, C., MASTERSON, P. J., WALKER, P. A., LASKEY, P., OMARY, M. B. & DOORBAR, J. 2004. Functional analysis of the human papillomavirus type-16 E1-E4 protein provides a mechanism for in vivo and in vitro keratin filament reorganization. *J Virol*, 78, **2**, 821-833.
- WANG, Q. L., CUI, H. F., DU, J. F., LV, Q. Y. & SONG, X. 2019b. In silico post-SELEX screening and experimental characterisations for acquisition of high affinity DNA aptamers against carcinoembryonic antigen. *RSC Adv*, 9, **11**, 6328-6334.
- WANG, X., HELFER, C. M., PANCHOLI, N., BRADNER, J. E. & YOU, J. 2013. Recruitment of Brd4 to the human papillomavirus type 16 DNA replication complex is essential for replication of viral DNA. *J Virol*, 87, **7**, 3871-3884.
- WANG, X., MEYERS, C., WANG, H. K., CHOW, L. T. & ZHENG, Z. M. 2011. Construction of a full transcription map of human papillomavirus type 18 during productive viral infection. *J Virol*, 85, **16**, 8080-8092.
- WARNER, K. D., CHEN, M. C., SONG, W., STRACK, R. L., THORN, A., JAFFREY, S. R. & FERRÉ-D'AMARÉ, A. R. 2014. Structural basis for activity of highly

- efficient RNA mimics of green fluorescent protein. *Nat Struct Mol Biol*, 21, **8**, 658-663.
- WASSON, C. W., MORGAN, E. L., MÜLLER, M., ROSS, R. L., HARTLEY, M., ROBERTS, S. & MACDONALD, A. 2017. Human papillomavirus type 18 E5 oncogene supports cell cycle progression and impairs epithelial differentiation by modulating growth factor receptor signalling during the virus life cycle. *Oncotarget*, 8, **61**, 103581-103600.
- WEI, L., GRAVITT, P. E., SONG, H., MALDONADO, A. M. & OZBUN, M. A. 2009. Nitric oxide induces early viral transcription coincident with increased DNA damage and mutation rates in human papillomavirus-infected cells. *Cancer Res*, 69, **11**, 4878-4884.
- WHITEMAN, D. C. & WILSON, L. F. 2016. The fractions of cancer attributable to modifiable factors: A global review. *Cancer Epidemiol*, 44, 203-221.
- WHITTON, A. F., KNIGHT, G. L. & MARSH, E. K. 2024. Risk factors associated with oral human papillomavirus (HPV) prevalence within a young adult population. *BMC Public Health*, 24.
- WILSON, C., TELLEZ, F., C.M., AWAN, K. H., AJDAHARIAN, J., GEILER, J. & THIRUCENTHILVELAN, P. 2022. Adverse effects of E-cigarettes on head, neck, and oral cells: A systematic review. *J Oral Pathol Med*, 51, **2**, 113-125.
- WILSON, L. F., PAWLITA, M., CASTLE, P. E., WATERBOER, T., SAHASRABUDDHE, V., GRAVITT, P. E., SCHIFFMAN, M. & WENTZENSEN, N. 2014. Seroprevalence of 8 oncogenic human papillomavirus genotypes and acquired immunity against reinfection. *J Infect Dis*, 210, **3**, 448-455.
- WINDON, M. J., D'SOUZA, G., RETTIG, E. M., WESTRA, W. H., VAN ZANTE, A., WANG, S. J., RYAN, W. R., MYDLARZ, W. K., HA, P. K., MILES, B. A., KOCH, W. M., GOURIN, C., EISELE, D. W. & FAKHRY, C. 2018. Increasing prevalence of human papillomavirus-positive oropharyngeal cancers among older adults. *Cancer*, 124, **14**, 2993-2999.
- WINDON, M. J., WATERBOER, T., HILLEL, A. T., CHIEN, W., BEST, S., STEWART, C., AKST, L., TROY, T., BENDER, N., MILES, B. A., RYAN, W. R., MANDAL, R., PITMAN, K., EISELE, D. W., FAKHRY, C. & D'SOUZA, G. 2019. Sex differences in HPV immunity among adults without cancer. *Hum Vaccin Immunother*, 15, **7-8**, 1935-1941.

- WITT, B. L., ALBERTSON, D. J., COPPIN, M. G., HORROCKS, C. F., POST, M. & GULBAHCE, H. E. 2014. Use of in situ hybridization for HPV in head and neck tumors: experience from a national reference laboratory. *Head Neck Pathol*, 9, 1, 60-64.
- WOLF, M., GARCEA, R. L., GRIGORIEFF, N. & HARRISON, S. C. 2010. Subunit interactions in bovine papillomavirus. *Proc Natl Acad Sci USA*, 107, 14, 6298-6303.
- WOOD, Z. C., BAIN, C. J., SMITH, D. D., WHITEMAN, D. C. & ANTONSSON, A. 2017. Oral human papillomavirus infection incidence and clearance: a systematic review of the literature. *J Gen Virol*, 98, 4, 519-526.
- WOODCOCK-MITCHELL, J., EICHNER, R., NELSON, W. G. & SUN, T. T. 1982. Immunolocalization of keratin polypeptides in human epidermis using monoclonal antibodies. *J Cell Biol*, 95, 2, 580-588.
- WOODS, R. S. R., CALLANAN, D., JAWAD, H., MOLONY, P., WERNER, R., HEFFRON, C., FEELEY, L. & SHEAHAN, P. 2022. Cytokeratin 7 and 19 expression in oropharyngeal and oral squamous cell carcinoma. *Eur Arch Otorhinolaryngol*, 279, 3, 1435-1443.
- WOODS, R. S. R., KEEGAN, H., WHITE, C., TEWARI, P., TONER, M., KENNEDY, S., O'REGAN, E. M., MARTIN, C. M., TIMON, C. V. I. & O'LEARY, J. J. 2017. Cytokeratin 7 in oropharyngeal squamous cell carcinoma: a junctional biomarker for human papillomavirus-related tumors. *Cancer Epidemiol Biomarkers Prev*, 26, 5, 702-710.
- WORLD HEALTH ORGANISATION 2004. *ICD-10: International statistical classification of diseases and related health problems*, Geneva.
- WORLD HEALTH ORGANISATION 2019/2021. *ICD-11: International Classification of Diseases*, Geneva.
- WORLD HEALTH ORGANISATION. 2022. *A short guide to cancer screening: increase effectiveness, maximize benefits and minimize harm* [Online]. Copenhagen: WHO Regional Office for Europe. [Accessed].
- WORLD HEALTH ORGANISATION 2024. *WHO Classification of Tumours: Head and Neck Tumours*, Lyon, France, IARC Press.
- WORLD HEALTH ORGANISATION 2021. WHO global report on trends in prevalence of tobacco use 2000-2025. 4th ed. Geneva.

- XI, L. F., KOUTSKY, L. A., CASTLE, P. E., EDELSTEIN, Z. R., MEYERS, C., HO, J. & SCHIFFMAN, M. 2009. Relationship between cigarette smoking and human papilloma virus types 16 and 18 DNA load. *Cancer Epidemiol Biomarkers Prev*, 18, 12, 3490-3496.
- XUE, Y., BELLANGER, S., ZHANG, W., LIM, D., LOW, J., LUNNY, D. & THIERRY, F. 2010. HPV16 E2 is an immediate early marker of viral infection, preceding E7 expression in precursor structures of cervical carcinoma. *Cancer Res*, 70, 13, 5316-5325.
- YADAV, P., MALIK, R., BALANI, S., NIGAM, R. K., JAIN, P. & TANDON, P. 2019. Expression of p-16, Ki-67 and p-53 markers in dysplastic and malignant lesions of the oral cavity and oropharynx. *J Oral Maxillofac Pathol*, 23, 2, 224-230.
- YAMADA, T., SAITO, T., HILL, Y., SHIMIZU, Y., TSUKAKOSHI, K., MIZUNO, H., HAYASHI, H., IKEBUKURO, K., TOYO'OKA, T. & TODOROKI, K. 2019. High-throughput bioanalysis of bevacizumab in human plasma based on enzyme-linked aptamer assay using anti-idiotypic DNA aptamer. *Anal Chem*, 91, 4, 3125-3130.
- YANG, G., LI, W., ZHANG, S., HU, B. & HUANG, Z. 2024. Highly-efficient selection of aptamers for detecting various HPV subtypes in clinical samples. *Talanta*, 266, 125039.
- YARIZADEH, K., BEHBAHANI, M., MOHABATKAR, H. & NOORBAKHS, A. 2019. Computational analysis and optimisation of carcinoembryonic antigen aptamers and experimental evaluation. *J Biotechnol*, 306, 1-8.
- YASUGI, T., BENSON, J. D., SAKAI, H., VIDAL, M. & HOWLEY, P. M. 1997. Mapping and characterization of the interaction domains of human papillomavirus type 16 E1 and E2 proteins. *J Virol*, 71, 2, 891-899.
- YOU, J., CROYLE, J. L., NISHIMURA, A., OZATO, K. & HOWLEY, P. M. 2004. Interaction of the bovine papillomavirus E2 protein with Brd4 tethers the viral DNA to host mitotic chromosomes. *Cell*, 117, 3, 349-360.
- YU, L., MAJERCIK, V. & ZHENG, Z. M. 2022. HPV16 and HPV18 genome structure, expression, and post-transcriptional regulation. *Int J Mol Sci*, 23, 9, 4943.
- YUN, H. Y., KIM, M. W., LEE, H. S., KIM, W., SHIN, J. H., KIM, H., SHIN, H. C., PARK, H., OH, B. H., KON, W. K., BAE, K. H., LEE, S. C., LEE, E. W., KU, B. & KIM, S. J. 2019. Structural basis for recognition of the tumor suppressor protein

- PTPN14 by the oncoprotein E7 of the human papillomavirus. *PLoS Biol*, 17, 7, e3000367.
- ZAMAY, G. S., IVANCHENKO, T. I., ZAMAY, T. N., GRIGORIEVA, V. L., GLAZYRIN, Y. E., KOLOVSKAYA, O. S., GARANZHA, I. V., BARINOV, A. A., KRAT, A. V., MIRONOV, G. G., GARGAUN, A., VEPRINTSEV, D. V., BEKUZAROV, S. S., KIRICHENKO, A. K., ZUKOV, R. A., PETROVA, M. M., MODESTOV, A. A., BEREZOVSKI, M. V. & ZAMAY, A. S. 2017. DNA aptamers for the characterization of histological structure of lung adenocarcinoma. *Mol Ther Nucleic Acids*, 6, 150-162.
- ZANIER, K., CHARBONNIER, S., SIDI, A. O. M. O., MCEWEN, A. G., FERRARIO, M. G., POUSSIN, P., CURA, V., BRIMER, N., BABAH, K. O., ANSARI, T., MULLER, I., STOTE, R. H., CAVARELLI, J., VANDE POL, S. & TRAVÉ, G. 2013. Structural basis for hijacking of cellular LxxLL motifs by papillomavirus E6 proteins. *Science*, 339, 6120, 694-698.
- ZANIER, K., SIDI, A. O. M. O., BOULADE-LADAME, C., RYBIN, V., CHAPPELLE, A., ATKINSON, A., KIEFFER, B. & TRAVÉ, G. 2012. Solution structure analysis of the HPV16 E6 oncoprotein reveals a self-association mechanism required for E6-mediated degradation of p53. *Structure*, 20, 4, 604-617.
- ZENG, Z., ZHANG, P., ZHAO, N., SHEEHAN, A. M., TUNG, C. H., CHANG, C. C. & ZU, Y. 2010. Using oligonucleotide aptamer probes for immunostaining of formalin-fixed and paraffin-embedded tissues. *Mod Pathol*, 23, 12, 1553-1558.
- ZHANG, B., CHEN, W. & ROMAN, A. 2006. The E7 proteins of low- and high-risk human papillomaviruses share the ability to target the pRB family member p130 for degradation. *Proc Natl Acad Sci USA*, 103, 2, 437-442.
- ZHANG, E., ZHOU, R., YANG, Y., PENG, S., XIAO, D., KONG, T., CAI, X. & ZHU, B. 2021. Aptamer-mediated synthesis of multifunctional nano-hydroxyapatite for active tumour bioimaging and treatment. *Cell Prolif*, 54, 9, e13105.
- ZHANG, L. W., LI, J., CONG, X., HU, X. S., LI, D., WU, L. L., HUA, H., YU, G. Y. & KERR, A. R. 2018. Incidence and mortality trends in oral and oropharyngeal cancers in China, 2005-2013. *Cancer Epidemiol*, 57, 120-126.
- ZHANG, P., ZHAO, N., ZENG, Z., CHANG, C. C. & ZU, Y. 2010. Combination of an aptamer probe to CD4 and antibodies for multicolored cell phenotyping. *Am J Clin Pathol*, 134, 4, 586-593.

- ZHANG, S., WANG, H., LIU, J., TAO, T., ZENG, Z. & WANG, M. 2022a. RGS1 and related genes as potential targets for immunotherapy in cervical cancer: computational biology and experimental validation. *J Transl Med*, 20, **1**, 334.
- ZHANG, S., WANG, H., LIU, Y., TAO, T., ZENG, Z., ZHOU, Y. & WANG, M. 2022b. *Nocardia rubra* cell-wall skeleton influences the development of cervical carcinoma by promoting the antitumour effect of macrophages and dendritic cells. *Cancer Med*, 11, **5**, 1249-1268.
- ZHANG, Y., DASGUPTA, J., MA, R., BANKS, L., THOMAS, M. & CHEN, X. S. 2007. Structures of a human papillomavirus (HPV) E6 polypeptide bound to MAGUK proteins: mechanisms of targeting tumor suppressors by a high-risk HPV oncoprotein. *J Virol*, 81, **7**, 3618-3626.
- ZHANG, Y., LAI, B. S. & JUHAS, M. 2019. Recent advances in aptamer discovery and applications. *Molecules*, 24, **5**, 941.
- ZHANG, Z., TIAN, Y., HUANG, P. & WU, F. Y. 2020. Using target-specific aptamers to enhance the peroxidase-like activity of gold nanoclusters for colorimetric detection of tetracycline antibiotics. *Talanta*, 208, 120342.
- ZHENG, Z. M. & BAKER, C. C. 2006. Papillomavirus genome structure, expression, and post-transcriptional regulation. *Front Biosci*, 11, 2286-2302.
- ZHENG, Z. M., TAO, M., YAMANEGI, K., BODAGHI, S. & XIAO, W. 2004. Splicing of a cap-proximal human papillomavirus 16 E6E7 intron promotes E7 expression, but can be restrained by distance of the intro from its RNA 5' cap. *J Mol Biol*, 337, **5**, 1091-1108.
- ZHU, Q., LIU, G. & KAI, M. 2015. DNA aptamers in the diagnosis and treatment of human diseases. *Molecules*, 20, **12**, 20979-20997.
- ZHU, Q., SHIBATA, T., KABASHIMA, T. & KAI, M. 2012. Inhibition of HIV-1 protease expression in T cells owing to DNA aptamer-mediated specific delivery of siRNA. *Eur J Med Chem*, 56, 396-399.
- ZIMMERMAN, H., DEGENKOLBE, R., BERNARD, H. U. & O'CONNOR, M. J. 1999. The human papillomavirus type 16 E6 oncoprotein can down-regulate p53 activity by targeting the transcriptional coactivator CBP/p300. *J Virol*, 73, **8**, 6209-6219.
- ZUKER, M. 2003. Mfold web server for nucleic acid folding and hybridization prediction. *Nucleic Acids Res*, 31, **13**, 3406-3415.



- ZUMSTEG, Z. S., COOK-WIENS, G., YOSHIDA, E., SHIAO, S. L., LEE, N. Y., MITA, A., JEON, C., GOODMAN, M. T. & HO, A. S. 2016. Incidence of oropharyngeal cancer among elderly patients in the United States. *JAMA Oncol*, 2, **12**, 1617-1623.
- ZUR HAUSEN, H., DÜRST, M., GISSMANN, L. & IKENBERG, H. 1983. A papillomavirus DNA from a cervical carcinoma and its prevalence in cancer biopsy samples from different geographic regions. *Proc Natl Acad Sci USA*, 80, 3812-3815.

## APPENDICES

### Appendix 1: Ethical approval ETH2021-3493

*Content removed for data protection purposes*

*Content removed for data protection purposes*

*Content removed for data protection purposes*

*Content removed for data protection purposes*

*Content removed for data protection purposes*

*Content removed for data protection purposes*

*Content removed for data protection purposes*



*Content removed for data protection purposes*

*Content removed for data protection purposes*

*Content removed for data protection purposes*

*Content removed for data protection purposes*

*Content removed for data protection purposes*

*Content removed for data protection purposes*

*Content removed for data protection purposes*

*Content removed for data protection purposes*



*Content removed for data protection purposes*

*Content removed for data protection purposes*

*Content removed for data protection purposes*

*Content removed for data protection purposes*

*Content removed for data protection purposes*

*Content removed for data protection purposes*

*Content removed for data protection purposes*

## Appendix 6: BOND™ RX IHC protocol F-standard



Full name: \*IHC Protocol F

ID: L.242

Type: IHC staining

Created by: Leica

Creation time: 7/13/2023 2:55:22 AM

Facility: Histologix

Staining method: Single

### Protocol: \*IHC F

#### BOND RX

<b>Step Reagent</b>				<i>Supplier: Leica Microsystems</i>
1 *Peroxide Block				
Step type: Reagent	Inc. (min): 5:00	Temperature: Ambient	Dispense type: 150 µL	
<b>Step Reagent</b>				<i>Supplier: Leica Microsystems</i>
2 *Bond Wash Solution				
Step type: Wash	Inc. (min): 0:00	Temperature: Ambient	Dispense type: 150 µL	
<b>Step Reagent</b>				<i>Supplier: Leica Microsystems</i>
3 *Bond Wash Solution				
Step type: Wash	Inc. (min): 0:00	Temperature: Ambient	Dispense type: Open	
<b>Step Reagent</b>				<i>Supplier: Leica Microsystems</i>
4 *Bond Wash Solution				
Step type: Wash	Inc. (min): 0:00	Temperature: Ambient	Dispense type: 150 µL	
<b>Step Reagent</b>				<i>Supplier: Not applicable</i>
5 Primary				
Step type: Reagent	Inc. (min): 15:00	Temperature: Ambient	Dispense type: 150 µL	
<b>Step Reagent</b>				<i>Supplier: Leica Microsystems</i>
6 *Bond Wash Solution				
Step type: Wash	Inc. (min): 0:00	Temperature: Ambient	Dispense type: 150 µL	
<b>Step Reagent</b>				<i>Supplier: Leica Microsystems</i>
7 *Bond Wash Solution				
Step type: Wash	Inc. (min): 0:00	Temperature: Ambient	Dispense type: 150 µL	
<b>Step Reagent</b>				<i>Supplier: Leica Microsystems</i>
8 *Bond Wash Solution				
Step type: Wash	Inc. (min): 0:00	Temperature: Ambient	Dispense type: 150 µL	





Full name: \*IHC Protocol F

ID: L.242

Type: IHC staining

Created by: Leica

Creation time: 7/13/2023 2:55:22 AM

Facility: Histologix

Staining method: Single

**Protocol: \*IHC F**

<b>Step Reagent</b>		<i>Supplier: Leica Microsystems</i>	
9 *Post Primary			
Step type: Reagent	Inc. (min): 8:00	Temperature: Ambient	Dispense type: 150 µL
<b>Step Reagent</b>		<i>Supplier: Leica Microsystems</i>	
10 *Bond Wash Solution			
Step type: Wash	Inc. (min): 2:00	Temperature: Ambient	Dispense type: 150 µL
<b>Step Reagent</b>		<i>Supplier: Leica Microsystems</i>	
11 *Bond Wash Solution			
Step type: Wash	Inc. (min): 2:00	Temperature: Ambient	Dispense type: 150 µL
<b>Step Reagent</b>		<i>Supplier: Leica Microsystems</i>	
12 *Bond Wash Solution			
Step type: Wash	Inc. (min): 2:00	Temperature: Ambient	Dispense type: 150 µL
<b>Step Reagent</b>		<i>Supplier: Leica Microsystems</i>	
13 *Polymer			
Step type: Reagent	Inc. (min): 8:00	Temperature: Ambient	Dispense type: 150 µL
<b>Step Reagent</b>		<i>Supplier: Leica Microsystems</i>	
14 *Bond Wash Solution			
Step type: Wash	Inc. (min): 2:00	Temperature: Ambient	Dispense type: 150 µL
<b>Step Reagent</b>		<i>Supplier: Leica Microsystems</i>	
15 *Bond Wash Solution			
Step type: Wash	Inc. (min): 2:00	Temperature: Ambient	Dispense type: 150 µL
<b>Step Reagent</b>		<i>Supplier: Not applicable</i>	
16 *Deionized Water			
Step type: Wash	Inc. (min): 0:00	Temperature: Ambient	Dispense type: 150 µL

1/31/2024 9:12 AM

**BOND RX**  
For research use only. Not for use in clinical procedures.

2/4



Full name: \*IHC Protocol F

ID: L.242

Type: IHC staining

Created by: Leica

Creation time: 7/13/2023 2:55:22 AM

Facility: Histologix

Staining method: Single

**Protocol: \*IHC F**

<b>Step Reagent</b>	<i>Supplier: Leica Microsystems</i>		
17 *Mixed DAB Refine			
Step type: Reagent	Inc. (min): 0:00	Temperature: Ambient	Dispense type: 150 µL
<b>Step Reagent</b>	<i>Supplier: Leica Microsystems</i>		
18 *Mixed DAB Refine			
Step type: Reagent	Inc. (min): 10:00	Temperature: Ambient	Dispense type: 150 µL
<b>Step Reagent</b>	<i>Supplier: Not applicable</i>		
19 *Deionized Water			
Step type: Wash	Inc. (min): 0:00	Temperature: Ambient	Dispense type: 150 µL
<b>Step Reagent</b>	<i>Supplier: Not applicable</i>		
20 *Deionized Water			
Step type: Wash	Inc. (min): 0:00	Temperature: Ambient	Dispense type: 150 µL
<b>Step Reagent</b>	<i>Supplier: Not applicable</i>		
21 *Deionized Water			
Step type: Wash	Inc. (min): 0:00	Temperature: Ambient	Dispense type: 150 µL
<b>Step Reagent</b>	<i>Supplier: Leica Microsystems</i>		
22 *Hematoxylin			
Step type: Reagent	Inc. (min): 5:00	Temperature: Ambient	Dispense type: 150 µL
<b>Step Reagent</b>	<i>Supplier: Not applicable</i>		
23 *Deionized Water			
Step type: Wash	Inc. (min): 0:00	Temperature: Ambient	Dispense type: 150 µL
<b>Step Reagent</b>	<i>Supplier: Leica Microsystems</i>		
24 *Bond Wash Solution			
Step type: Wash	Inc. (min): 0:00	Temperature: Ambient	Dispense type: 150 µL



Full name: \*IHC Protocol F

ID: L.242

Type: IHC staining

Created by: Leica

Creation time: 7/13/2023 2:55:22 AM

Facility: Histologix

Staining method: Single

**Protocol: \*IHC F**

---

**Step Reagent**

*Supplier: Not applicable*

25 \*Deionized Water

Step type: Wash

Inc. (min): 0:00

Temperature: Ambient

Dispense type: 150  $\mu$ L

## Appendix 7: BOND™ RX IHC protocol F 30 min primary antibody incubation



### Protocol: IHCF 30

**Full name:** IHC Protocol F 30 min  
**ID:** U.165  
**Type:** IHC staining  
**Created by:** rebecca  
**Creation time:** 5/20/2022 11:16:42 AM  
**Facility:** Histologix  
**Staining method:** Single

### BOND RX

<b>Step Reagent</b>				<i>Supplier: Leica Microsystems</i>
1 *Peroxide Block				
Step type: Reagent	Inc. (min): 5:00	Temperature: Ambient	Dispense type: 150 µL	
<b>Step Reagent</b>				<i>Supplier: Leica Microsystems</i>
2 *Bond Wash Solution				
Step type: Wash	Inc. (min): 0:00	Temperature: Ambient	Dispense type: 150 µL	
<b>Step Reagent</b>				<i>Supplier: Leica Microsystems</i>
3 *Bond Wash Solution				
Step type: Wash	Inc. (min): 0:00	Temperature: Ambient	Dispense type: Open	
<b>Step Reagent</b>				<i>Supplier: Leica Microsystems</i>
4 *Bond Wash Solution				
Step type: Wash	Inc. (min): 0:00	Temperature: Ambient	Dispense type: 150 µL	
<b>Step Reagent</b>				<i>Supplier: Not applicable</i>
5 Primary				
Step type: Reagent	Inc. (min): 30:00	Temperature: Ambient	Dispense type: 150 µL	
<b>Step Reagent</b>				<i>Supplier: Leica Microsystems</i>
6 *Bond Wash Solution				
Step type: Wash	Inc. (min): 0:00	Temperature: Ambient	Dispense type: 150 µL	
<b>Step Reagent</b>				<i>Supplier: Leica Microsystems</i>
7 *Bond Wash Solution				
Step type: Wash	Inc. (min): 0:00	Temperature: Ambient	Dispense type: 150 µL	
<b>Step Reagent</b>				<i>Supplier: Leica Microsystems</i>
8 *Bond Wash Solution				
Step type: Wash	Inc. (min): 0:00	Temperature: Ambient	Dispense type: 150 µL	



**Full name:** IHC Protocol F 30 min

**ID:** U.165

**Type:** IHC staining

**Created by:** rebecca

**Creation time:** 5/20/2022 11:16:42 AM

**Facility:** Histologix

**Staining method:** Single

## Protocol: IHCF 30

<b>Step Reagent</b>	<i>Supplier: Leica Microsystems</i>		
9 *Post Primary			
Step type: Reagent	Inc. (min): 8:00	Temperature: Ambient	Dispense type: 150 µL
<b>Step Reagent</b>	<i>Supplier: Leica Microsystems</i>		
10 *Bond Wash Solution			
Step type: Wash	Inc. (min): 2:00	Temperature: Ambient	Dispense type: 150 µL
<b>Step Reagent</b>	<i>Supplier: Leica Microsystems</i>		
11 *Bond Wash Solution			
Step type: Wash	Inc. (min): 2:00	Temperature: Ambient	Dispense type: 150 µL
<b>Step Reagent</b>	<i>Supplier: Leica Microsystems</i>		
12 *Bond Wash Solution			
Step type: Wash	Inc. (min): 2:00	Temperature: Ambient	Dispense type: 150 µL
<b>Step Reagent</b>	<i>Supplier: Leica Microsystems</i>		
13 *Polymer			
Step type: Reagent	Inc. (min): 8:00	Temperature: Ambient	Dispense type: 150 µL
<b>Step Reagent</b>	<i>Supplier: Leica Microsystems</i>		
14 *Bond Wash Solution			
Step type: Wash	Inc. (min): 2:00	Temperature: Ambient	Dispense type: 150 µL
<b>Step Reagent</b>	<i>Supplier: Leica Microsystems</i>		
15 *Bond Wash Solution			
Step type: Wash	Inc. (min): 2:00	Temperature: Ambient	Dispense type: 150 µL
<b>Step Reagent</b>	<i>Supplier: Not applicable</i>		
16 *Deionized Water			
Step type: Wash	Inc. (min): 0:00	Temperature: Ambient	Dispense type: 150 µL



Full name: IHC Protocol F 30 min

ID: U.165

Type: IHC staining

Created by: rebecca

Creation time: 5/20/2022 11:16:42 AM

Facility: Histologix

Staining method: Single

## Protocol: IHCF 30

Step	Reagent	Supplier
17	*Mixed DAB Refine	Leica Microsystems
Step type:	Reagent	Inc. (min): 0:00 Temperature: Ambient Dispense type: 150 µL
18	*Mixed DAB Refine	Leica Microsystems
Step type:	Reagent	Inc. (min): 10:00 Temperature: Ambient Dispense type: 150 µL
19	*Deionized Water	Not applicable
Step type:	Wash	Inc. (min): 0:00 Temperature: Ambient Dispense type: 150 µL
20	*Deionized Water	Not applicable
Step type:	Wash	Inc. (min): 0:00 Temperature: Ambient Dispense type: 150 µL
21	*Deionized Water	Not applicable
Step type:	Wash	Inc. (min): 0:00 Temperature: Ambient Dispense type: 150 µL
22	*Hematoxylin	Leica Microsystems
Step type:	Reagent	Inc. (min): 5:00 Temperature: Ambient Dispense type: 150 µL
23	*Deionized Water	Not applicable
Step type:	Wash	Inc. (min): 0:00 Temperature: Ambient Dispense type: 150 µL
24	*Bond Wash Solution	Leica Microsystems
Step type:	Wash	Inc. (min): 0:00 Temperature: Ambient Dispense type: 150 µL



## Protocol: IHCF 30

**Full name:** IHC Protocol F 30 min

**ID:** U.165

**Type:** IHC staining

**Created by:** rebecca

**Creation time:** 5/20/2022 11:16:42 AM

**Facility:** Histologix

**Staining method:** Single

---

**Step Reagent**

*Supplier: Not applicable*

25 \*Deionized Water

Step type: Wash

Inc. (min): 0:00

Temperature: Ambient

Dispense type: 150 µL

## Appendix 8: BOND™ RX IHC protocol F 60 min primary antibody incubation



**Full name:** IHC Protocol F 60 min

**ID:** U.151

**Type:** IHC staining

**Created by:** rebecca

**Creation time:** 12/6/2021 10:05:24 AM

**Facility:** Histologix

**Staining method:** Single

### Protocol: IHCF 60

#### BOND RX

<b>Step Reagent</b>			<i>Supplier: Leica Microsystems</i>
1 *Peroxide Block			
Step type: Reagent	Inc. (min): 5:00	Temperature: Ambient	Dispense type: 150 µL
<b>Step Reagent</b>			<i>Supplier: Leica Microsystems</i>
2 *Bond Wash Solution			
Step type: Wash	Inc. (min): 0:00	Temperature: Ambient	Dispense type: 150 µL
<b>Step Reagent</b>			<i>Supplier: Leica Microsystems</i>
3 *Bond Wash Solution			
Step type: Wash	Inc. (min): 0:00	Temperature: Ambient	Dispense type: Open
<b>Step Reagent</b>			<i>Supplier: Leica Microsystems</i>
4 *Bond Wash Solution			
Step type: Wash	Inc. (min): 0:00	Temperature: Ambient	Dispense type: 150 µL
<b>Step Reagent</b>			<i>Supplier: Not applicable</i>
5 Primary			
Step type: Reagent	Inc. (min): 60:00	Temperature: Ambient	Dispense type: 150 µL
<b>Step Reagent</b>			<i>Supplier: Leica Microsystems</i>
6 *Bond Wash Solution			
Step type: Wash	Inc. (min): 0:00	Temperature: Ambient	Dispense type: 150 µL
<b>Step Reagent</b>			<i>Supplier: Leica Microsystems</i>
7 *Bond Wash Solution			
Step type: Wash	Inc. (min): 0:00	Temperature: Ambient	Dispense type: 150 µL
<b>Step Reagent</b>			<i>Supplier: Leica Microsystems</i>
8 *Bond Wash Solution			
Step type: Wash	Inc. (min): 0:00	Temperature: Ambient	Dispense type: 150 µL

1/31/2024 9:14 AM

**BOND RX**  
For research use only. Not for use in clinical procedures.

1/4





Full name: IHC Protocol F 60 min

ID: U.151

Type: IHC staining

Created by: rebecca

Creation time: 12/6/2021 10:05:24 AM

Facility: Histologix

Staining method: Single

## Protocol: IHCF 60

<b>Step Reagent</b>				<i>Supplier: Leica Microsystems</i>
9 *Post Primary				
Step type: Reagent	Inc. (min): 8:00	Temperature: Ambient	Dispense type: 150 µL	
<b>Step Reagent</b>				<i>Supplier: Leica Microsystems</i>
10 *Bond Wash Solution				
Step type: Wash	Inc. (min): 2:00	Temperature: Ambient	Dispense type: 150 µL	
<b>Step Reagent</b>				<i>Supplier: Leica Microsystems</i>
11 *Bond Wash Solution				
Step type: Wash	Inc. (min): 2:00	Temperature: Ambient	Dispense type: 150 µL	
<b>Step Reagent</b>				<i>Supplier: Leica Microsystems</i>
12 *Bond Wash Solution				
Step type: Wash	Inc. (min): 2:00	Temperature: Ambient	Dispense type: 150 µL	
<b>Step Reagent</b>				<i>Supplier: Leica Microsystems</i>
13 *Polymer				
Step type: Reagent	Inc. (min): 8:00	Temperature: Ambient	Dispense type: 150 µL	
<b>Step Reagent</b>				<i>Supplier: Leica Microsystems</i>
14 *Bond Wash Solution				
Step type: Wash	Inc. (min): 2:00	Temperature: Ambient	Dispense type: 150 µL	
<b>Step Reagent</b>				<i>Supplier: Leica Microsystems</i>
15 *Bond Wash Solution				
Step type: Wash	Inc. (min): 2:00	Temperature: Ambient	Dispense type: 150 µL	
<b>Step Reagent</b>				<i>Supplier: Not applicable</i>
16 *Deionized Water				
Step type: Wash	Inc. (min): 0:00	Temperature: Ambient	Dispense type: 150 µL	



Full name: IHC Protocol F 60 min

ID: U.151

Type: IHC staining

Created by: rebecca

Creation time: 12/6/2021 10:05:24 AM

Facility: Histologix

Staining method: Single

## Protocol: IHCF 60

<b>Step Reagent</b>			<i>Supplier: Leica Microsystems</i>
17 *Mixed DAB Refine			
Step type: Reagent	Inc. (min): 0:00	Temperature: Ambient	Dispense type: 150 µL
<b>Step Reagent</b>			<i>Supplier: Leica Microsystems</i>
18 *Mixed DAB Refine			
Step type: Reagent	Inc. (min): 10:00	Temperature: Ambient	Dispense type: 150 µL
<b>Step Reagent</b>			<i>Supplier: Not applicable</i>
19 *Deionized Water			
Step type: Wash	Inc. (min): 0:00	Temperature: Ambient	Dispense type: 150 µL
<b>Step Reagent</b>			<i>Supplier: Not applicable</i>
20 *Deionized Water			
Step type: Wash	Inc. (min): 0:00	Temperature: Ambient	Dispense type: 150 µL
<b>Step Reagent</b>			<i>Supplier: Not applicable</i>
21 *Deionized Water			
Step type: Wash	Inc. (min): 0:00	Temperature: Ambient	Dispense type: 150 µL
<b>Step Reagent</b>			<i>Supplier: Leica Microsystems</i>
22 *Hematoxylin			
Step type: Reagent	Inc. (min): 5:00	Temperature: Ambient	Dispense type: 150 µL
<b>Step Reagent</b>			<i>Supplier: Not applicable</i>
23 *Deionized Water			
Step type: Wash	Inc. (min): 0:00	Temperature: Ambient	Dispense type: 150 µL
<b>Step Reagent</b>			<i>Supplier: Leica Microsystems</i>
24 *Bond Wash Solution			
Step type: Wash	Inc. (min): 0:00	Temperature: Ambient	Dispense type: 150 µL



**Full name:** IHC Protocol F 60 min

**ID:** U.151

**Type:** IHC staining

**Created by:** rebecca

**Creation time:** 12/6/2021 10:05:24 AM

**Facility:** Histologix

**Staining method:** Single

## Protocol: IHCF 60

---

### Step Reagent

*Supplier: Not applicable*

25 \*Deionized Water

Step type: Wash

Inc. (min): 0:00

Temperature: Ambient

Dispense type: 150 µL

## Appendix 9: VENTANA DISCOVERY ULTRA RUO universal protocol: mouse and mouse first and second primary antibodies

**Protocol # 519 : 2x TSA Ms Ms 1Ab 60m (31/01/2024)**

**Version: 6**

**Validated: No**

**Active: Yes**

**Procedure: RUO DISCOVERY Universal ( v0.00.0408 )**

DISCOVERY ULTRA

Histologix Ltd

Step No	Procedure Step
1	[ version 20 ]
2	[ For Research Use Only. Not intended for diagnostic purposes. ]
3	Enable Mixers
4	Warmup Slide to 37 Deg C
5	[ Delay refers to a time delayed start: Select time until run start ]
6	Disable Mixers
7	[ 72°C is the standard temperature ]
8	Warmup Slide to [72 Deg C] from Medium Temperatures ( Deparaffinization )
9	Incubate for 4 Minutes
10	Apply EZPrep Volume Adjust
11	Rinse Slide With EZ Prep
12	Apply EZPrep Volume Adjust
13	Apply Coverslip
14	Rinse Slide With EZ Prep
15	Apply EZPrep Volume Adjust
16	Apply Coverslip
17	Enable Mixers
18	Apply EZPrep Volume Adjust
19	Rinse Slide With EZ Prep
20	Apply Coverslip
21	Apply EZPrep Volume Adjust
22	Rinse Slide With EZ Prep
23	Apply Coverslip
24	Apply EZPrep Volume Adjust
25	Rinse Slide With EZ Prep
26	Apply Depar Volume Adjust
27	Apply Coverslip
28	Warmup Slide to 37 Deg C
29	Rinse Slide With EZ Prep
30	Apply Long Cell Conditioner #2
31	Apply CC Coverslip Long
32	[ 91°C is the standard temperature ]
33	Warmup Slide to [93 Deg C], and Incubate for 4 Minutes ( Cell Conditioner #2 )
34	Incubate for 4 Minutes
35	Incubate for 8 Minutes
36	Apply Cell Conditioner #2
37	Apply CC Medium Coverslip No BB
38	Incubate for 8 Minutes
39	Incubate for 8 Minutes
40	Apply Cell Conditioner #2
41	Apply CC Medium Coverslip No BB
42	Incubate for 8 Minutes
43	Incubate for 8 Minutes
44	Apply Cell Conditioner #2

\* one drop is one reagent dispense

Histologix Ltd  
VSS v12.5.4 Build 20234.1

Printed 31/01/2024 10:58:55

Page 1 of 7

**Protocol # 519 : 2x TSA Ms Ms 1Ab 60m (31/01/2024)**

**Version: 6**

**Validated: No**

**Active: Yes**

**Procedure: RUO DISCOVERY Universal ( v0.00.0408 )**

**DISCOVERY ULTRA**

**Histologix Ltd**

Step No	Procedure Step
45	Apply CC Medium Coverslip No BB
46	Incubate for 8 Minutes
47	Incubate for 8 Minutes
48	Apply Cell Conditioner #2
49	Apply CC Medium Coverslip No BB
50	Incubate for 8 Minutes
51	Incubate for 8 Minutes
52	Apply Cell Conditioner #2
53	Apply CC Medium Coverslip No BB
54	Apply Cell Conditioner #2
55	Apply CC Medium Coverslip No BB
56	Apply Cell Conditioner #2
57	Apply CC Medium Coverslip No BB
58	Apply Cell Conditioner #2
59	Apply CC Medium Coverslip No BB
60	Disable Slide Heater
61	Apply Cell Conditioner #2
62	Apply CC Medium Coverslip No BB
63	Warmup Slide to 37 Deg C
64	Rinse Slide With Reaction Buffer
65	Adjust Slide Volume With Reaction Buffer
66	Apply Coverslip
67	[ Inhibitor Solution will not be applied ]
68	Rinse Slide With Reaction Buffer
69	Adjust Slide Volume With Reaction Buffer
70	Apply Coverslip
71	Rinse Slide With Reaction Buffer
72	Adjust Slide Volume With Reaction Buffer
73	Apply Coverslip
74	Incubate for 4 Minutes
75	Disable Slide Heater
76	Apply One Drop of [ANTIBODY 15] ( Antibody ), and Incubate for [0 Hr 16 Min]
77	Rinse Slide With Reaction Buffer
78	Adjust Slide Volume With Reaction Buffer
79	Apply Coverslip
80	[ Inhibitor Solution will not be applied after the primary ]
81	Disable Slide Heater
82	Warmup Slide to 37 Deg C
83	Disable Slide Heater
84	Warmup Slide to 37 Deg C
85	[ DISC Inhibitor will not be applied ]
86	Rinse Slide With Reaction Buffer
87	Adjust Slide Volume With Reaction Buffer
88	Apply Coverslip

\* one drop is one reagent dispense

Histologix Ltd

VSS v12.5.4 Build 20234.1

Printed 31/01/2024 10:58:55

Page 2 of 7

**Protocol # 519 : 2x TSA Ms Ms 1Ab 60m (31/01/2024)**

**Version: 6**

**Validated: No**

**Active: Yes**

**Procedure: RUO DISCOVERY Universal ( v0.00.0408 )**

**DISCOVERY ULTRA**

**Histologix Ltd**

Step No	Procedure Step
89	Rinse Slide With Reaction Buffer
90	Adjust Slide Volume With Reaction Buffer
91	Apply Coverslip
92	Disable Slide Heater
93	Apply One Drop of [ANTIBODY 60] ( DS Antibody ), and Incubate for [0 Hr 28 Min]
94	Rinse Slide With Reaction Buffer
95	Adjust Slide Volume With Reaction Buffer
96	Apply Coverslip
97	Disable Slide Heater
98	Warmup Slide to 37 Deg C
99	Disable Slide Heater
100	Warmup Slide to 37 Deg C
101	[ DISC Inhibitor will not be applied ]
102	Rinse Slide With Reaction Buffer
103	Adjust Slide Volume With Reaction Buffer
104	Apply Coverslip
105	Disable Slide Heater
106	Disable Mixers
107	Wait For Button ( DS Primary Antibody )
108	Enable Mixers
109	Warmup Slide to 37 Deg C
110	Rinse Slide With Reaction Buffer
111	Adjust Slide Volume With Reaction Buffer
112	Apply Coverslip
113	Warmup Slide to [37 Deg C] from Very Low Temperatures ( TS Primary Antibody )
114	Hand Apply ( TS Primary Antibody ), and Incubate for [60 Minutes]
115	Rinse Slide With Reaction Buffer
116	Adjust Slide Volume With Reaction Buffer
117	Apply Coverslip
118	Disable Slide Heater
119	Warmup Slide to 37 Deg C
120	Disable Slide Heater
121	Warmup Slide to 37 Deg C
122	[ DISC Inhibitor will not be applied ]
123	Rinse Slide With Reaction Buffer
124	Adjust Slide Volume With Reaction Buffer
125	Apply Coverslip
126	Rinse Slide With Reaction Buffer
127	Adjust Slide Volume With Reaction Buffer
128	Apply Coverslip
129	Disable Slide Heater
130	Apply One Drop of [ANTIBODY 75] ( QuS Antibody ), and Incubate for [0 Hr 32 Min]
131	Rinse Slide With Reaction Buffer
132	Adjust Slide Volume With Reaction Buffer

\* one drop is one reagent dispense

Histologix Ltd  
VSS v12.5.4 Build 20234.1

Printed 31/01/2024 10:58:55

Page 3 of 7

## Protocol # 519 : 2x TSA Ms Ms 1Ab 60m (31/01/2024)

Version: 6

Validated: No

Active: Yes

Procedure: RUO DISCOVERY Universal ( v0.00.0408 )

DISCOVERY ULTRA

Histologix Ltd

Step No	Procedure Step
133	Apply Coverslip
134	Disable Slide Heater
135	Warmup Slide to 37 Deg C
136	[ Requires DETECTION dispensers ]
137	Rinse Slide With Reaction Buffer
138	Adjust Slide Volume With Reaction Buffer
139	Apply Coverslip
140	Rinse Slide With Reaction Buffer
141	Adjust Slide Volume With Reaction Buffer
142	Apply Coverslip
143	Rinse Slide With Reaction Buffer
144	Adjust Slide Volume With Reaction Buffer
145	Apply Coverslip
146	Incubate for 4 Minutes
147	Disable Slide Heater
148	Disable Mixers
149	Wait For Button ( QuS 2nd Antibody )
150	Enable Mixers
151	Rinse Slide With Reaction Buffer
152	Adjust Slide Volume With Reaction Buffer
153	Apply Coverslip
154	Hand Apply ( QuS 2nd Antibody ), and Incubate for [0 Hr 8 Min]
155	Rinse Slide With Reaction Buffer
156	Adjust Slide Volume With Reaction Buffer
157	Apply Coverslip
158	Rinse Slide With Reaction Buffer
159	Adjust Slide Volume With Reaction Buffer
160	Apply Coverslip
161	Rinse Slide With Reaction Buffer
162	Adjust Slide Volume With Reaction Buffer
163	Apply Coverslip
164	Incubate for 4 Minutes
165	Disable Slide Heater
166	Disable Mixers
167	Wait For Button ( QuS 3rd Antibody )
168	Enable Mixers
169	Rinse Slide With Reaction Buffer
170	Adjust Slide Volume With Reaction Buffer
171	Apply Coverslip
172	Hand Apply ( QuS 3rd Antibody ), and Incubate for [0 Hr 8 Min]
173	Rinse Slide With Reaction Buffer
174	Adjust Slide Volume With Reaction Buffer
175	Apply Coverslip
176	Disable Slide Heater

\* one drop is one reagent dispense

Histologix Ltd

VSS v12.5.4 Build 20234.1

Printed 31/01/2024 10:58:55

Page 4 of 7

**Protocol # 519 : 2x TSA Ms Ms 1Ab 60m (31/01/2024)**

**Version: 6**

**Validated: No**

**Active: Yes**

**Procedure: RUO DISCOVERY Universal ( v0.00.0408 )**

**DISCOVERY ULTRA**

**Histologix Ltd**

Step No	Procedure Step
177	Warmup Slide to 37 Deg C
178	Warmup Slide to [60 Deg C], and Incubate for [32 Minutes] ( Denaturation #5 )
179	Warmup Slide to 37 Deg C
180	[ DISC Inhibitor will not be applied ]
181	Rinse Slide With Reaction Buffer
182	Adjust Slide Volume With Reaction Buffer
183	Apply Coverslip
184	Rinse Slide With Reaction Buffer
185	Adjust Slide Volume With Reaction Buffer
186	Apply Coverslip
187	Disable Slide Heater
188	Apply One Drop of [ANTIBODY 15] ( QnS Antibody ), and Incubate for [0 Hr 16 Min]
189	Rinse Slide With Reaction Buffer
190	Adjust Slide Volume With Reaction Buffer
191	Apply Coverslip
192	Disable Slide Heater
193	Warmup Slide to 37 Deg C
194	Disable Slide Heater
195	Warmup Slide to 37 Deg C
196	[ DISC Inhibitor will not be applied ]
197	Rinse Slide With Reaction Buffer
198	Adjust Slide Volume With Reaction Buffer
199	Apply Coverslip
200	Rinse Slide With Reaction Buffer
201	Adjust Slide Volume With Reaction Buffer
202	Apply Coverslip
203	Disable Slide Heater
204	Apply One Drop of [ANTIBODY 60] ( SxS Antibody ), and Incubate for [0 Hr 28 Min]
205	Rinse Slide With Reaction Buffer
206	Adjust Slide Volume With Reaction Buffer
207	Apply Coverslip
208	Disable Slide Heater
209	Warmup Slide to 37 Deg C
210	[ Requires DETECTION dispensers ]
211	Rinse Slide With Reaction Buffer
212	Adjust Slide Volume With Reaction Buffer
213	Apply Coverslip
214	Rinse Slide With Reaction Buffer
215	Adjust Slide Volume With Reaction Buffer
216	Apply Coverslip
217	Disable Slide Heater
218	Disable Mixers
219	Wait For Button ( SxS 2nd Antibody )
220	Enable Mixers

\* one drop is one reagent dispense

Histologix Ltd  
VSS v12.5.4 Build 20234.1

Printed 31/01/2024 10:58:55

Page 5 of 7



## Protocol # 519 : 2x TSA Ms Ms 1Ab 60m (31/01/2024)

Version: 6

Validated: No

Active: Yes

Procedure: RUO DISCOVERY Universal ( v0.00.0408 )

DISCOVERY ULTRA

Histologix Ltd

Step No	Procedure Step
221	Rinse Slide With Reaction Buffer
222	Adjust Slide Volume With Reaction Buffer
223	Apply Coverslip
224	Warmup Slide to [37 Deg C] from Very Low Temperatures ( SxS 2nd Antibody )
225	Hand Apply ( SxS 2nd Antibody ), and Incubate for [1 Hour]
226	Rinse Slide With Reaction Buffer
227	Adjust Slide Volume With Reaction Buffer
228	Apply Coverslip
229	Disable Slide Heater
230	Warmup Slide to 37 Deg C
231	[ DISC Inhibitor will not be applied ]
232	Rinse Slide With Reaction Buffer
233	Adjust Slide Volume With Reaction Buffer
234	Apply Coverslip
235	Rinse Slide With Reaction Buffer
236	Adjust Slide Volume With Reaction Buffer
237	Apply Coverslip
238	Disable Slide Heater
239	Apply One Drop of [ANTIBODY 75] ( SpS Antibody ), and Incubate for [0 Hr 32 Min]
240	Rinse Slide With Reaction Buffer
241	Adjust Slide Volume With Reaction Buffer
242	Apply Coverslip
243	Disable Slide Heater
244	Warmup Slide to 37 Deg C
245	[ Requires DETECTION dispensers ]
246	Rinse Slide With Reaction Buffer
247	Adjust Slide Volume With Reaction Buffer
248	Apply Coverslip
249	Rinse Slide With Reaction Buffer
250	Adjust Slide Volume With Reaction Buffer
251	Apply Coverslip
252	Disable Slide Heater
253	Disable Mixers
254	Wait For Button ( SpS 2nd Antibody )
255	Enable Mixers
256	Rinse Slide With Reaction Buffer
257	Adjust Slide Volume With Reaction Buffer
258	Apply Coverslip
259	Hand Apply ( SpS 2nd Antibody ), and Incubate for [0 Hr 8 Min]
260	Rinse Slide With Reaction Buffer
261	Adjust Slide Volume With Reaction Buffer
262	Apply Coverslip
263	Rinse Slide With Reaction Buffer
264	Adjust Slide Volume With Reaction Buffer

\* one drop is one reagent dispense

Histologix Ltd  
VSS v12.5.4 Build 20234.1

Printed 31/01/2024 10:58:55

Page 6 of 7

**Protocol # 519 : 2x TSA Ms Ms 1Ab 60m (31/01/2024)**

**Version: 6**

**Validated: No**

**Active: Yes**

**Procedure: RUO DISCOVERY Universal ( v0.00.0408 )**

**DISCOVERY ULTRA**

**Histologix Ltd**

Step No	Procedure Step
265	Apply Coverslip
266	Disable Slide Heater
267	Disable Mixers
268	Wait For Button ( SpS 3rd Antibody )
269	Enable Mixers
270	Rinse Slide With Reaction Buffer
271	Adjust Slide Volume With Reaction Buffer
272	Apply Coverslip
273	Hand Apply ( SpS 3rd Antibody ), and Incubate for [0 Hr 8 Min]
274	Rinse Slide With Reaction Buffer
275	Adjust Slide Volume With Reaction Buffer
276	Apply Coverslip
277	Disable Slide Heater
278	Warmup Slide to 37 Deg C
279	Warmup Slide to [60 Deg C], and Incubate for [32 Minutes] ( Denaturation 8 )
280	Warmup Slide to 37 Deg C
281	[ DISC Inhibitor will not be applied ]
282	Disable Slide Heater
283	Disable Slide Heater
284	Warmup Slide to 37 Deg C

# Appendix 10: VENTANA DISCOVERY ULTRA RUO universal protocol: rabbit and rabbit first and second primary antibodies

## Protocol # 520 : 2x TSA Rb Rb 1Ab 60m (31/01/2024)

Version: 4                                      Validated: No                                      Active: Yes

Procedure: RUO DISCOVERY Universal ( v0.00.0408 )

DISCOVERY ULTRA

Histologix Ltd

Step No	Procedure Step
1	[ version 20 ]
2	[ For Research Use Only. Not intended for diagnostic purposes. ]
3	Enable Mixers
4	Warmup Slide to 37 Deg C
5	[ Delay refers to a time delayed start: Select time until run start ]
6	Disable Mixers
7	[ 72°C is the standard temperature ]
8	Warmup Slide to [72 Deg C] from Medium Temperatures ( Deparaffinization )
9	Incubate for 4 Minutes
10	Apply EZPrep Volume Adjust
11	Rinse Slide With EZ Prep
12	Apply EZPrep Volume Adjust
13	Apply Coverslip
14	Rinse Slide With EZ Prep
15	Apply EZPrep Volume Adjust
16	Apply Coverslip
17	Enable Mixers
18	Apply EZPrep Volume Adjust
19	Rinse Slide With EZ Prep
20	Apply Coverslip
21	Apply EZPrep Volume Adjust
22	Rinse Slide With EZ Prep
23	Apply Coverslip
24	Apply EZPrep Volume Adjust
25	Rinse Slide With EZ Prep
26	Apply Depar Volume Adjust
27	Apply Coverslip
28	Warmup Slide to 37 Deg C
29	Rinse Slide With EZ Prep
30	Apply Long Cell Conditioner #2
31	Apply CC Coverslip Long
32	[ 91°C is the standard temperature ]
33	Warmup Slide to [93 Deg C], and Incubate for 4 Minutes ( Cell Conditioner #2 )
34	Incubate for 4 Minutes
35	Incubate for 8 Minutes
36	Apply Cell Conditioner #2
37	Apply CC Medium Coverslip No BB
38	Incubate for 8 Minutes
39	Incubate for 8 Minutes
40	Apply Cell Conditioner #2
41	Apply CC Medium Coverslip No BB
42	Incubate for 8 Minutes
43	Incubate for 8 Minutes
44	Apply Cell Conditioner #2

\* one drop is one reagent dispense  
Histologix Ltd  
VSS v12.5.4 Build 20234.1

Printed 31/01/2024 10:59:17  
Page 1 of 7

**Protocol # 520 : 2x TSA Rb Rb 1Ab 60m (31/01/2024)**

**Version: 4**

**Validated: No**

**Active: Yes**

**Procedure: RUO DISCOVERY Universal ( v0.00.0408 )**

**DISCOVERY ULTRA**

**Histologix Ltd**

Step No	Procedure Step
45	Apply CC Medium Coverslip No BB
46	Incubate for 8 Minutes
47	Incubate for 8 Minutes
48	Apply Cell Conditioner #2
49	Apply CC Medium Coverslip No BB
50	Incubate for 8 Minutes
51	Incubate for 8 Minutes
52	Apply Cell Conditioner #2
53	Apply CC Medium Coverslip No BB
54	Apply Cell Conditioner #2
55	Apply CC Medium Coverslip No BB
56	Apply Cell Conditioner #2
57	Apply CC Medium Coverslip No BB
58	Apply Cell Conditioner #2
59	Apply CC Medium Coverslip No BB
60	Disable Slide Heater
61	Apply Cell Conditioner #2
62	Apply CC Medium Coverslip No BB
63	Warmup Slide to 37 Deg C
64	Rinse Slide With Reaction Buffer
65	Adjust Slide Volume With Reaction Buffer
66	Apply Coverslip
67	[ Inhibitor Solution will not be applied ]
68	Rinse Slide With Reaction Buffer
69	Adjust Slide Volume With Reaction Buffer
70	Apply Coverslip
71	Rinse Slide With Reaction Buffer
72	Adjust Slide Volume With Reaction Buffer
73	Apply Coverslip
74	Incubate for 4 Minutes
75	Disable Slide Heater
76	Apply One Drop of [ANTIBODY 15] ( Antibody ), and Incubate for [0 Hr 16 Min]
77	Rinse Slide With Reaction Buffer
78	Adjust Slide Volume With Reaction Buffer
79	Apply Coverslip
80	[ Inhibitor Solution will not be applied after the primary ]
81	Disable Slide Heater
82	Warmup Slide to 37 Deg C
83	Disable Slide Heater
84	Warmup Slide to 37 Deg C
85	[ DISC Inhibitor will not be applied ]
86	Rinse Slide With Reaction Buffer
87	Adjust Slide Volume With Reaction Buffer
88	Apply Coverslip

\* one drop is one reagent dispense

Histologix Ltd  
VSS v12.5.4 Build 20234.1

Printed 31/01/2024 10:59:17

Page 2 of 7

**Protocol # 520 : 2x TSA Rb Rb 1Ab 60m (31/01/2024)**

**Version: 4**

**Validated: No**

**Active: Yes**

**Procedure: RUO DISCOVERY Universal ( v0.00.0408 )**

**DISCOVERY ULTRA**

**Histologix Ltd**

Step No	Procedure Step
89	Rinse Slide With Reaction Buffer
90	Adjust Slide Volume With Reaction Buffer
91	Apply Coverslip
92	Disable Slide Heater
93	Apply One Drop of [ANTIBODY 60] ( DS Antibody ), and Incubate for [0 Hr 28 Min]
94	Rinse Slide With Reaction Buffer
95	Adjust Slide Volume With Reaction Buffer
96	Apply Coverslip
97	Disable Slide Heater
98	Warmup Slide to 37 Deg C
99	Disable Slide Heater
100	Warmup Slide to 37 Deg C
101	[ DISC Inhibitor will not be applied ]
102	Rinse Slide With Reaction Buffer
103	Adjust Slide Volume With Reaction Buffer
104	Apply Coverslip
105	Disable Slide Heater
106	Disable Mixers
107	Wait For Button ( DS Primary Antibody )
108	Enable Mixers
109	Warmup Slide to 37 Deg C
110	Rinse Slide With Reaction Buffer
111	Adjust Slide Volume With Reaction Buffer
112	Apply Coverslip
113	Warmup Slide to [37 Deg C] from Very Low Temperatures ( TS Primary Antibody )
114	Hand Apply ( TS Primary Antibody ), and Incubate for [60 Minutes]
115	Rinse Slide With Reaction Buffer
116	Adjust Slide Volume With Reaction Buffer
117	Apply Coverslip
118	Disable Slide Heater
119	Warmup Slide to 37 Deg C
120	Disable Slide Heater
121	Warmup Slide to 37 Deg C
122	[ DISC Inhibitor will not be applied ]
123	Rinse Slide With Reaction Buffer
124	Adjust Slide Volume With Reaction Buffer
125	Apply Coverslip
126	Rinse Slide With Reaction Buffer
127	Adjust Slide Volume With Reaction Buffer
128	Apply Coverslip
129	Disable Slide Heater
130	Apply One Drop of [ANTIBODY 70] ( QuS Antibody ), and Incubate for [0 Hr 32 Min]
131	Rinse Slide With Reaction Buffer
132	Adjust Slide Volume With Reaction Buffer

\* one drop is one reagent dispense

Histologix Ltd  
VSS v12.5.4 Build 20234.1

Printed 31/01/2024 10:59:17

Page 3 of 7

## Protocol # 520 : 2x TSA Rb Rb 1Ab 60m (31/01/2024)

Version: 4

Validated: No

Active: Yes

Procedure: RUO DISCOVERY Universal ( v0.00.0408 )

DISCOVERY ULTRA

Histologix Ltd

Step No	Procedure Step
133	Apply Coverslip
134	Disable Slide Heater
135	Warmup Slide to 37 Deg C
136	[ Requires DETECTION dispensers ]
137	Rinse Slide With Reaction Buffer
138	Adjust Slide Volume With Reaction Buffer
139	Apply Coverslip
140	Rinse Slide With Reaction Buffer
141	Adjust Slide Volume With Reaction Buffer
142	Apply Coverslip
143	Rinse Slide With Reaction Buffer
144	Adjust Slide Volume With Reaction Buffer
145	Apply Coverslip
146	Incubate for 4 Minutes
147	Disable Slide Heater
148	Disable Mixers
149	Wait For Button ( QuS 2nd Antibody )
150	Enable Mixers
151	Rinse Slide With Reaction Buffer
152	Adjust Slide Volume With Reaction Buffer
153	Apply Coverslip
154	Hand Apply ( QuS 2nd Antibody ), and Incubate for [0 Hr 8 Min]
155	Rinse Slide With Reaction Buffer
156	Adjust Slide Volume With Reaction Buffer
157	Apply Coverslip
158	Rinse Slide With Reaction Buffer
159	Adjust Slide Volume With Reaction Buffer
160	Apply Coverslip
161	Rinse Slide With Reaction Buffer
162	Adjust Slide Volume With Reaction Buffer
163	Apply Coverslip
164	Incubate for 4 Minutes
165	Disable Slide Heater
166	Disable Mixers
167	Wait For Button ( QuS 3rd Antibody )
168	Enable Mixers
169	Rinse Slide With Reaction Buffer
170	Adjust Slide Volume With Reaction Buffer
171	Apply Coverslip
172	Hand Apply ( QuS 3rd Antibody ), and Incubate for [0 Hr 8 Min]
173	Rinse Slide With Reaction Buffer
174	Adjust Slide Volume With Reaction Buffer
175	Apply Coverslip
176	Disable Slide Heater

\* one drop is one reagent dispense

Histologix Ltd

VSS v12.5.4 Build 20234.1

Printed 31/01/2024 10:59:17

Page 4 of 7

**Protocol # 520 : 2x TSA Rb Rb 1Ab 60m (31/01/2024)**

**Version: 4**

**Validated: No**

**Active: Yes**

**Procedure: RUO DISCOVERY Universal ( v0.00.0408 )**

**DISCOVERY ULTRA**

**Histologix Ltd**

Step No	Procedure Step
177	Warmup Slide to 37 Deg C
178	Warmup Slide to [60 Deg C], and Incubate for [32 Minutes] ( Denaturation #5 )
179	Warmup Slide to 37 Deg C
180	[ DISC Inhibitor will not be applied ]
181	Rinse Slide With Reaction Buffer
182	Adjust Slide Volume With Reaction Buffer
183	Apply Coverslip
184	Rinse Slide With Reaction Buffer
185	Adjust Slide Volume With Reaction Buffer
186	Apply Coverslip
187	Disable Slide Heater
188	Apply One Drop of [ANTIBODY 15] ( QnS Antibody ), and Incubate for [0 Hr 16 Min]
189	Rinse Slide With Reaction Buffer
190	Adjust Slide Volume With Reaction Buffer
191	Apply Coverslip
192	Disable Slide Heater
193	Warmup Slide to 37 Deg C
194	Disable Slide Heater
195	Warmup Slide to 37 Deg C
196	[ DISC Inhibitor will not be applied ]
197	Rinse Slide With Reaction Buffer
198	Adjust Slide Volume With Reaction Buffer
199	Apply Coverslip
200	Rinse Slide With Reaction Buffer
201	Adjust Slide Volume With Reaction Buffer
202	Apply Coverslip
203	Disable Slide Heater
204	Apply One Drop of [ANTIBODY 60] ( SxS Antibody ), and Incubate for [0 Hr 28 Min]
205	Rinse Slide With Reaction Buffer
206	Adjust Slide Volume With Reaction Buffer
207	Apply Coverslip
208	Disable Slide Heater
209	Warmup Slide to 37 Deg C
210	[ Requires DETECTION dispensers ]
211	Rinse Slide With Reaction Buffer
212	Adjust Slide Volume With Reaction Buffer
213	Apply Coverslip
214	Rinse Slide With Reaction Buffer
215	Adjust Slide Volume With Reaction Buffer
216	Apply Coverslip
217	Disable Slide Heater
218	Disable Mixers
219	Wait For Button ( SxS 2nd Antibody )
220	Enable Mixers

\* one drop is one reagent dispense  
Histologix Ltd  
VSS v12.5.4 Build 20234.1

Printed 31/01/2024 10:59:17  
Page 5 of 7

## Protocol # 520 : 2x TSA Rb Rb 1Ab 60m (31/01/2024)

Version: 4

Validated: No

Active: Yes

Procedure: RUO DISCOVERY Universal ( v0.00.0408 )

DISCOVERY ULTRA

Histologix Ltd

Step No	Procedure Step
221	Rinse Slide With Reaction Buffer
222	Adjust Slide Volume With Reaction Buffer
223	Apply Coverslip
224	Warmup Slide to [37 Deg C] from Very Low Temperatures ( SxS 2nd Antibody )
225	Hand Apply ( SxS 2nd Antibody ), and Incubate for [1 Hour]
226	Rinse Slide With Reaction Buffer
227	Adjust Slide Volume With Reaction Buffer
228	Apply Coverslip
229	Disable Slide Heater
230	Warmup Slide to 37 Deg C
231	[ DISC Inhibitor will not be applied ]
232	Rinse Slide With Reaction Buffer
233	Adjust Slide Volume With Reaction Buffer
234	Apply Coverslip
235	Rinse Slide With Reaction Buffer
236	Adjust Slide Volume With Reaction Buffer
237	Apply Coverslip
238	Disable Slide Heater
239	Apply One Drop of [ANTIBODY 70] ( SpS Antibody ), and Incubate for [0 Hr 32 Min]
240	Rinse Slide With Reaction Buffer
241	Adjust Slide Volume With Reaction Buffer
242	Apply Coverslip
243	Disable Slide Heater
244	Warmup Slide to 37 Deg C
245	[ Requires DETECTION dispensers ]
246	Rinse Slide With Reaction Buffer
247	Adjust Slide Volume With Reaction Buffer
248	Apply Coverslip
249	Rinse Slide With Reaction Buffer
250	Adjust Slide Volume With Reaction Buffer
251	Apply Coverslip
252	Disable Slide Heater
253	Disable Mixers
254	Wait For Button ( SpS 2nd Antibody )
255	Enable Mixers
256	Rinse Slide With Reaction Buffer
257	Adjust Slide Volume With Reaction Buffer
258	Apply Coverslip
259	Hand Apply ( SpS 2nd Antibody ), and Incubate for [0 Hr 8 Min]
260	Rinse Slide With Reaction Buffer
261	Adjust Slide Volume With Reaction Buffer
262	Apply Coverslip
263	Rinse Slide With Reaction Buffer
264	Adjust Slide Volume With Reaction Buffer

\* one drop is one reagent dispense

Histologix Ltd

VSS v12.5.4 Build 20234.1

Printed 31/01/2024 10:59:17

Page 6 of 7



**Protocol # 520 : 2x TSA Rb Rb 1Ab 60m (31/01/2024)**

**Version: 4**

**Validated: No**

**Active: Yes**

**Procedure: RUO DISCOVERY Universal ( v0.00.0408 )**

**DISCOVERY ULTRA**

**Histologix Ltd**

Step No	Procedure Step
265	Apply Coverslip
266	Disable Slide Heater
267	Disable Mixers
268	Wait For Button ( SpS 3rd Antibody )
269	Enable Mixers
270	Rinse Slide With Reaction Buffer
271	Adjust Slide Volume With Reaction Buffer
272	Apply Coverslip
273	Hand Apply ( SpS 3rd Antibody ), and Incubate for [0 Hr 8 Min]
274	Rinse Slide With Reaction Buffer
275	Adjust Slide Volume With Reaction Buffer
276	Apply Coverslip
277	Disable Slide Heater
278	Warmup Slide to 37 Deg C
279	Warmup Slide to [60 Deg C], and Incubate for [32 Minutes] ( Denaturation 8 )
280	Warmup Slide to 37 Deg C
281	[ DISC Inhibitor will not be applied ]
282	Disable Slide Heater
283	Disable Slide Heater
284	Warmup Slide to 37 Deg C

## Appendix 11: VENTANA DISCOVERY ULTRA RUO universal protocol: mouse and rabbit first and second primary antibodies

**Protocol # 521 : 2x TSA Ms Rb 1Ab 60m (31/01/2024)**

**Version: 2                      Validated: No                      Active: Yes**

**Procedure: RUO DISCOVERY Universal ( v0.00.0408 )**

DISCOVERY ULTRA

Histologix Ltd

Step No	Procedure Step
1	[ version 20 ]
2	[ For Research Use Only. Not intended for diagnostic purposes. ]
3	Enable Mixers
4	Warmup Slide to 37 Deg C
5	[ Delay refers to a time delayed start: Select time until run start ]
6	Disable Mixers
7	[ 72°C is the standard temperature ]
8	Warmup Slide to [72 Deg C] from Medium Temperatures ( Deparaffinization )
9	Incubate for 4 Minutes
10	Apply EZPrep Volume Adjust
11	Rinse Slide With EZ Prep
12	Apply EZPrep Volume Adjust
13	Apply Coverslip
14	Rinse Slide With EZ Prep
15	Apply EZPrep Volume Adjust
16	Apply Coverslip
17	Enable Mixers
18	Apply EZPrep Volume Adjust
19	Rinse Slide With EZ Prep
20	Apply Coverslip
21	Apply EZPrep Volume Adjust
22	Rinse Slide With EZ Prep
23	Apply Coverslip
24	Apply EZPrep Volume Adjust
25	Rinse Slide With EZ Prep
26	Apply Depar Volume Adjust
27	Apply Coverslip
28	Warmup Slide to 37 Deg C
29	Rinse Slide With EZ Prep
30	Apply Long Cell Conditioner #2
31	Apply CC Coverslip Long
32	[ 91°C is the standard temperature ]
33	Warmup Slide to [93 Deg C], and Incubate for 4 Minutes ( Cell Conditioner #2 )
34	Incubate for 4 Minutes
35	Incubate for 8 Minutes
36	Apply Cell Conditioner #2
37	Apply CC Medium Coverslip No BB
38	Incubate for 8 Minutes
39	Incubate for 8 Minutes
40	Apply Cell Conditioner #2
41	Apply CC Medium Coverslip No BB
42	Incubate for 8 Minutes
43	Incubate for 8 Minutes
44	Apply Cell Conditioner #2

\* one drop is one reagent dispense  
Histologix Ltd  
VSS v12.5.4 Build 20234.1

Printed 31/01/2024 10:58:43  
Page 1 of 7

**Protocol # 521 : 2x TSA Ms Rb 1Ab 60m (31/01/2024)**

**Version: 2**

**Validated: No**

**Active: Yes**

**Procedure: RUO DISCOVERY Universal ( v0.00.0408 )**

**DISCOVERY ULTRA**

**Histologix Ltd**

Step No	Procedure Step
45	Apply CC Medium Coverslip No BB
46	Incubate for 8 Minutes
47	Incubate for 8 Minutes
48	Apply Cell Conditioner #2
49	Apply CC Medium Coverslip No BB
50	Incubate for 8 Minutes
51	Incubate for 8 Minutes
52	Apply Cell Conditioner #2
53	Apply CC Medium Coverslip No BB
54	Apply Cell Conditioner #2
55	Apply CC Medium Coverslip No BB
56	Apply Cell Conditioner #2
57	Apply CC Medium Coverslip No BB
58	Apply Cell Conditioner #2
59	Apply CC Medium Coverslip No BB
60	Disable Slide Heater
61	Apply Cell Conditioner #2
62	Apply CC Medium Coverslip No BB
63	Warmup Slide to 37 Deg C
64	Rinse Slide With Reaction Buffer
65	Adjust Slide Volume With Reaction Buffer
66	Apply Coverslip
67	[ Inhibitor Solution will not be applied ]
68	Rinse Slide With Reaction Buffer
69	Adjust Slide Volume With Reaction Buffer
70	Apply Coverslip
71	Rinse Slide With Reaction Buffer
72	Adjust Slide Volume With Reaction Buffer
73	Apply Coverslip
74	Incubate for 4 Minutes
75	Disable Slide Heater
76	Apply One Drop of [ANTIBODY 15] ( Antibody ), and Incubate for [0 Hr 16 Min]
77	Rinse Slide With Reaction Buffer
78	Adjust Slide Volume With Reaction Buffer
79	Apply Coverslip
80	[ Inhibitor Solution will not be applied after the primary ]
81	Disable Slide Heater
82	Warmup Slide to 37 Deg C
83	Disable Slide Heater
84	Warmup Slide to 37 Deg C
85	[ DISC Inhibitor will not be applied ]
86	Rinse Slide With Reaction Buffer
87	Adjust Slide Volume With Reaction Buffer
88	Apply Coverslip

\* one drop is one reagent dispense

Histologix Ltd

VSS v12.5.4 Build 20234.1

Printed 31/01/2024 10:59:43

Page 2 of 7

**Protocol # 521 : 2x TSA Ms Rb 1Ab 60m (31/01/2024)**

**Version: 2**

**Validated: No**

**Active: Yes**

**Procedure: RUO DISCOVERY Universal ( v0.00.0408 )**

**DISCOVERY ULTRA**

**Histologix Ltd**

Step No	Procedure Step
89	Rinse Slide With Reaction Buffer
90	Adjust Slide Volume With Reaction Buffer
91	Apply Coverslip
92	Disable Slide Heater
93	Apply One Drop of [ANTIBODY 60] ( DS Antibody ), and Incubate for [0 Hr 28 Min]
94	Rinse Slide With Reaction Buffer
95	Adjust Slide Volume With Reaction Buffer
96	Apply Coverslip
97	Disable Slide Heater
98	Warmup Slide to 37 Deg C
99	Disable Slide Heater
100	Warmup Slide to 37 Deg C
101	[ DISC Inhibitor will not be applied ]
102	Rinse Slide With Reaction Buffer
103	Adjust Slide Volume With Reaction Buffer
104	Apply Coverslip
105	Disable Slide Heater
106	Disable Mixers
107	Wait For Button ( DS Primary Antibody )
108	Enable Mixers
109	Warmup Slide to 37 Deg C
110	Rinse Slide With Reaction Buffer
111	Adjust Slide Volume With Reaction Buffer
112	Apply Coverslip
113	Warmup Slide to [37 Deg C] from Very Low Temperatures ( TS Primary Antibody )
114	Hand Apply ( TS Primary Antibody ), and Incubate for [60 Minutes]
115	Rinse Slide With Reaction Buffer
116	Adjust Slide Volume With Reaction Buffer
117	Apply Coverslip
118	Disable Slide Heater
119	Warmup Slide to 37 Deg C
120	Disable Slide Heater
121	Warmup Slide to 37 Deg C
122	[ DISC Inhibitor will not be applied ]
123	Rinse Slide With Reaction Buffer
124	Adjust Slide Volume With Reaction Buffer
125	Apply Coverslip
126	Rinse Slide With Reaction Buffer
127	Adjust Slide Volume With Reaction Buffer
128	Apply Coverslip
129	Disable Slide Heater
130	Apply One Drop of [ANTIBODY 75] ( QuS Antibody ), and Incubate for [0 Hr 32 Min]
131	Rinse Slide With Reaction Buffer
132	Adjust Slide Volume With Reaction Buffer

\* one drop is one reagent dispense

Histologix Ltd  
VSS v12.5.4 Build 20234.1

Printed 31/01/2024 10:59:43

Page 3 of 7

**Protocol # 521 : 2x TSA Ms Rb 1Ab 60m (31/01/2024)**

**Version: 2**

**Validated: No**

**Active: Yes**

**Procedure: RUO DISCOVERY Universal ( v0.00.0408 )**

**DISCOVERY ULTRA**

**Histologix Ltd**

Step No	Procedure Step
133	Apply Coverslip
134	Disable Slide Heater
135	Warmup Slide to 37 Deg C
136	[ Requires DETECTION dispensers ]
137	Rinse Slide With Reaction Buffer
138	Adjust Slide Volume With Reaction Buffer
139	Apply Coverslip
140	Rinse Slide With Reaction Buffer
141	Adjust Slide Volume With Reaction Buffer
142	Apply Coverslip
143	Rinse Slide With Reaction Buffer
144	Adjust Slide Volume With Reaction Buffer
145	Apply Coverslip
146	Incubate for 4 Minutes
147	Disable Slide Heater
148	Disable Mixers
149	Wait For Button ( QuS 2nd Antibody )
150	Enable Mixers
151	Rinse Slide With Reaction Buffer
152	Adjust Slide Volume With Reaction Buffer
153	Apply Coverslip
154	Hand Apply ( QuS 2nd Antibody ), and Incubate for [0 Hr 8 Min]
155	Rinse Slide With Reaction Buffer
156	Adjust Slide Volume With Reaction Buffer
157	Apply Coverslip
158	Rinse Slide With Reaction Buffer
159	Adjust Slide Volume With Reaction Buffer
160	Apply Coverslip
161	Rinse Slide With Reaction Buffer
162	Adjust Slide Volume With Reaction Buffer
163	Apply Coverslip
164	Incubate for 4 Minutes
165	Disable Slide Heater
166	Disable Mixers
167	Wait For Button ( QuS 3rd Antibody )
168	Enable Mixers
169	Rinse Slide With Reaction Buffer
170	Adjust Slide Volume With Reaction Buffer
171	Apply Coverslip
172	Hand Apply ( QuS 3rd Antibody ), and Incubate for [0 Hr 8 Min]
173	Rinse Slide With Reaction Buffer
174	Adjust Slide Volume With Reaction Buffer
175	Apply Coverslip
176	Disable Slide Heater

\* one drop is one reagent dispense  
Histologix Ltd  
VSS v12.5.4 Build 20234.1

Printed 31/01/2024 10:59:43  
Page 4 of 7

**Protocol # 521 : 2x TSA Ms Rb 1Ab 60m (31/01/2024)**

**Version: 2**

**Validated: No**

**Active: Yes**

**Procedure: RUO DISCOVERY Universal ( v0.00.0408 )**

**DISCOVERY ULTRA**

**Histologix Ltd**

Step No	Procedure Step
221	Rinse Slide With Reaction Buffer
222	Adjust Slide Volume With Reaction Buffer
223	Apply Coverslip
224	Warmup Slide to [37 Deg C] from Very Low Temperatures ( SxS 2nd Antibody )
225	Hand Apply ( SxS 2nd Antibody ), and Incubate for [1 Hour]
226	Rinse Slide With Reaction Buffer
227	Adjust Slide Volume With Reaction Buffer
228	Apply Coverslip
229	Disable Slide Heater
230	Warmup Slide to 37 Deg C
231	[ DISC Inhibitor will not be applied ]
232	Rinse Slide With Reaction Buffer
233	Adjust Slide Volume With Reaction Buffer
234	Apply Coverslip
235	Rinse Slide With Reaction Buffer
236	Adjust Slide Volume With Reaction Buffer
237	Apply Coverslip
238	Disable Slide Heater
239	Apply One Drop of [ANTIBODY 70] ( SpS Antibody ), and Incubate for [0 Hr 32 Min]
240	Rinse Slide With Reaction Buffer
241	Adjust Slide Volume With Reaction Buffer
242	Apply Coverslip
243	Disable Slide Heater
244	Warmup Slide to 37 Deg C
245	[ Requires DETECTION dispensers ]
246	Rinse Slide With Reaction Buffer
247	Adjust Slide Volume With Reaction Buffer
248	Apply Coverslip
249	Rinse Slide With Reaction Buffer
250	Adjust Slide Volume With Reaction Buffer
251	Apply Coverslip
252	Disable Slide Heater
253	Disable Mixers
254	Wait For Button ( SpS 2nd Antibody )
255	Enable Mixers
256	Rinse Slide With Reaction Buffer
257	Adjust Slide Volume With Reaction Buffer
258	Apply Coverslip
259	Hand Apply ( SpS 2nd Antibody ), and Incubate for [0 Hr 8 Min]
260	Rinse Slide With Reaction Buffer
261	Adjust Slide Volume With Reaction Buffer
262	Apply Coverslip
263	Rinse Slide With Reaction Buffer
264	Adjust Slide Volume With Reaction Buffer

\* one drop is one reagent dispense

Histologix Ltd  
VSS v12.5.4 Build 20234.1

Printed 31/01/2024 10:59:43

Page 6 of 7

**Protocol # 521 : 2x TSA Ms Rb 1Ab 60m (31/01/2024)**

**Version: 2**

**Validated: No**

**Active: Yes**

**Procedure: RUO DISCOVERY Universal ( v0.00.0408 )**

**DISCOVERY ULTRA**

**Histologix Ltd**

Step No	Procedure Step
265	Apply Coverslip
266	Disable Slide Heater
267	Disable Mixers
268	Wait For Button ( SpS 3rd Antibody )
269	Enable Mixers
270	Rinse Slide With Reaction Buffer
271	Adjust Slide Volume With Reaction Buffer
272	Apply Coverslip
273	Hand Apply ( SpS 3rd Antibody ), and Incubate for [0 Hr 8 Min]
274	Rinse Slide With Reaction Buffer
275	Adjust Slide Volume With Reaction Buffer
276	Apply Coverslip
277	Disable Slide Heater
278	Warmup Slide to 37 Deg C
279	Warmup Slide to [60 Deg C], and Incubate for [32 Minutes] ( Denaturation 8 )
280	Warmup Slide to 37 Deg C
281	[ DISC Inhibitor will not be applied ]
282	Disable Slide Heater
283	Disable Slide Heater
284	Warmup Slide to 37 Deg C

## Appendix 12: VENTANA DISCOVERY ULTRA RUO universal protocol: rabbit third primary antibody and DAPI

**Protocol # 522 : 1x TSA Rb 1Ab 60m + DAPI (31/01/2024)**

**Version: 3**

**Validated: No**

**Active: Yes**

**Procedure: RUO DISCOVERY Universal ( v0.00.0408 )**

DISCOVERY ULTRA

Histologix Ltd

Step No	Procedure Step
1	[ version 20 ]
2	[ For Research Use Only. Not intended for diagnostic purposes. ]
3	Enable Mixers
4	Warmup Slide to 37 Deg C
5	[ Delay refers to a time delayed start: Select time until run start ]
6	[ Inhibitor Solution will not be applied ]
7	Rinse Slide With Reaction Buffer
8	Adjust Slide Volume With Reaction Buffer
9	Apply Coverslip
10	Rinse Slide With Reaction Buffer
11	Adjust Slide Volume With Reaction Buffer
12	Apply Coverslip
13	Incubate for 4 Minutes
14	Disable Slide Heater
15	Apply One Drop of [ANTIBODY 15] ( Antibody ), and Incubate for [0 Hr 18 Min]
16	Rinse Slide With Reaction Buffer
17	Adjust Slide Volume With Reaction Buffer
18	Apply Coverslip
19	[ Inhibitor Solution will not be applied after the primary ]
20	Disable Slide Heater
21	Warmup Slide to 37 Deg C
22	Disable Slide Heater
23	Warmup Slide to 37 Deg C
24	[ DISC Inhibitor will not be applied ]
25	Rinse Slide With Reaction Buffer
26	Adjust Slide Volume With Reaction Buffer
27	Apply Coverslip
28	Rinse Slide With Reaction Buffer
29	Adjust Slide Volume With Reaction Buffer
30	Apply Coverslip
31	Disable Slide Heater
32	Apply One Drop of [ANTIBODY 60] ( DS Antibody ), and Incubate for [0 Hr 28 Min]
33	Rinse Slide With Reaction Buffer
34	Adjust Slide Volume With Reaction Buffer
35	Apply Coverslip
36	Disable Slide Heater
37	Warmup Slide to 37 Deg C
38	Disable Slide Heater
39	Warmup Slide to 37 Deg C
40	[ DISC Inhibitor will not be applied ]
41	Rinse Slide With Reaction Buffer
42	Adjust Slide Volume With Reaction Buffer
43	Apply Coverslip
44	Disable Slide Heater

\* one drop is one reagent dispense  
Histologix Ltd  
VSS v12.5.4 Build 20234.1

Printed 31/01/2024 11:00:03  
Page 1 of 4



**Protocol # 522 : 1x TSA Rb 1Ab 60m + DAPI (31/01/2024)**

**Version: 3**

**Validated: No**

**Active: Yes**

**Procedure: RUO DISCOVERY Universal ( v0.00.0408 )**

**DISCOVERY ULTRA**

**Histologix Ltd**

Step No	Procedure Step
45	Disable Mixers
46	Wait For Button ( DS Primary Antibody )
47	Enable Mixers
48	Warmup Slide to 37 Deg C
49	Rinse Slide With Reaction Buffer
50	Adjust Slide Volume With Reaction Buffer
51	Apply Coverslip
52	Warmup Slide to [37 Deg C] from Very Low Temperatures ( TS Primary Antibody )
53	Hand Apply ( TS Primary Antibody ), and Incubate for [60 Minutes]
54	Rinse Slide With Reaction Buffer
55	Adjust Slide Volume With Reaction Buffer
56	Apply Coverslip
57	Disable Slide Heater
58	Warmup Slide to 37 Deg C
59	Disable Slide Heater
60	Warmup Slide to 37 Deg C
61	[ DISC Inhibitor will not be applied ]
62	Rinse Slide With Reaction Buffer
63	Adjust Slide Volume With Reaction Buffer
64	Apply Coverslip
65	Rinse Slide With Reaction Buffer
66	Adjust Slide Volume With Reaction Buffer
67	Apply Coverslip
68	Disable Slide Heater
69	Apply One Drop of [ANTIBODY 70] ( QuS Antibody ), and Incubate for [0 Hr 32 Min]
70	Rinse Slide With Reaction Buffer
71	Adjust Slide Volume With Reaction Buffer
72	Apply Coverslip
73	Disable Slide Heater
74	Warmup Slide to 37 Deg C
75	[ Requires DETECTION dispensers ]
76	Rinse Slide With Reaction Buffer
77	Adjust Slide Volume With Reaction Buffer
78	Apply Coverslip
79	Rinse Slide With Reaction Buffer
80	Adjust Slide Volume With Reaction Buffer
81	Apply Coverslip
82	Rinse Slide With Reaction Buffer
83	Adjust Slide Volume With Reaction Buffer
84	Apply Coverslip
85	Incubate for 4 Minutes
86	Disable Slide Heater
87	Disable Mixers
88	Wait For Button ( QuS 2nd Antibody )

\* one drop is one reagent dispense

Histologix Ltd

VSS v12.5.4 Build 20234.1

Printed 31/01/2024 11:00:03

Page 2 of 4

**Protocol # 522 : 1x TSA Rb 1Ab 60m + DAPI (31/01/2024)**

**Version: 3**

**Validated: No**

**Active: Yes**

**Procedure: RUO DISCOVERY Universal ( v0.00.0408 )**

**DISCOVERY ULTRA**

**Histologix Ltd**

Step No	Procedure Step
89	Enable Mixers
90	Rinse Slide With Reaction Buffer
91	Adjust Slide Volume With Reaction Buffer
92	Apply Coverslip
93	Hand Apply ( QuS 2nd Antibody ), and Incubate for [0 Hr 8 Min]
94	Rinse Slide With Reaction Buffer
95	Adjust Slide Volume With Reaction Buffer
96	Apply Coverslip
97	Rinse Slide With Reaction Buffer
98	Adjust Slide Volume With Reaction Buffer
99	Apply Coverslip
100	Rinse Slide With Reaction Buffer
101	Adjust Slide Volume With Reaction Buffer
102	Apply Coverslip
103	Incubate for 4 Minutes
104	Disable Slide Heater
105	Disable Mixers
106	Wait For Button ( QuS 3rd Antibody )
107	Enable Mixers
108	Rinse Slide With Reaction Buffer
109	Adjust Slide Volume With Reaction Buffer
110	Apply Coverslip
111	Hand Apply ( QuS 3rd Antibody ), and Incubate for [0 Hr 8 Min]
112	Rinse Slide With Reaction Buffer
113	Adjust Slide Volume With Reaction Buffer
114	Apply Coverslip
115	Disable Slide Heater
116	Warmup Slide to 37 Deg C
117	[ DISC Inhibitor will not be applied ]
118	Rinse Slide With Reaction Buffer
119	Adjust Slide Volume With Reaction Buffer
120	Apply Coverslip
121	Rinse Slide With Reaction Buffer
122	Adjust Slide Volume With Reaction Buffer
123	Apply Coverslip
124	Warmup Slide to [37 Deg C] from Very Low Temperatures ( QnS Primary Antibody )
125	Apply One Drop of [ANTIBODY 80] ( QnS Antibody ), and Incubate for [32 Minutes]
126	Rinse Slide With Reaction Buffer
127	Adjust Slide Volume With Reaction Buffer
128	Apply Coverslip
129	Disable Slide Heater
130	Warmup Slide to 37 Deg C
131	Disable Slide Heater
132	Warmup Slide to 37 Deg C

\* one drop is one reagent dispense  
Histologix Ltd  
VSS v12.5.4 Build 20234.1

Printed 31/01/2024 11:00:03  
Page 3 of 4

**Protocol # 522 : 1x TSA Rb 1Ab 60m + DAPI (31/01/2024)**

**Version: 3**

**Validated: No**

**Active: Yes**

**Procedure: RUO DISCOVERY Universal ( v0.00.0408 )**

**DISCOVERY ULTRA**

**Histologix Ltd**

Step No	Procedure Step
133	Rinse Slide With Reaction Buffer
134	Rinse Slide With Reaction Buffer

## Appendix 13: VENTANA DISCOVERY ULTRA RUO universal protocol: mouse third primary antibody and DAPI

**Protocol # 523 : 1x TSA Ms 1Ab 60m + DAPI (31/01/2024)**

**Version: 6**

**Validated: No**

**Active: Yes**

**Procedure: RUO DISCOVERY Universal ( v0.00.0408 )**

DISCOVERY ULTRA

Histologix Ltd

Step No	Procedure Step
1	[ version 20 ]
2	[ For Research Use Only. Not intended for diagnostic purposes. ]
3	Enable Mixers
4	Warmup Slide to 37 Deg C
5	[ Delay refers to a time delayed start: Select time until run start ]
6	[ Inhibitor Solution will not be applied ]
7	Rinse Slide With Reaction Buffer
8	Adjust Slide Volume With Reaction Buffer
9	Apply Coverslip
10	Rinse Slide With Reaction Buffer
11	Adjust Slide Volume With Reaction Buffer
12	Apply Coverslip
13	Incubate for 4 Minutes
14	Disable Slide Heater
15	Apply One Drop of [ANTIBODY 15] ( Antibody ), and Incubate for [0 Hr 16 Min]
16	Rinse Slide With Reaction Buffer
17	Adjust Slide Volume With Reaction Buffer
18	Apply Coverslip
19	[ Inhibitor Solution will not be applied after the primary ]
20	Disable Slide Heater
21	Warmup Slide to 37 Deg C
22	Disable Slide Heater
23	Warmup Slide to 37 Deg C
24	[ DISC Inhibitor will not be applied ]
25	Rinse Slide With Reaction Buffer
26	Adjust Slide Volume With Reaction Buffer
27	Apply Coverslip
28	Rinse Slide With Reaction Buffer
29	Adjust Slide Volume With Reaction Buffer
30	Apply Coverslip
31	Disable Slide Heater
32	Apply One Drop of [ANTIBODY 60] ( DS Antibody ), and Incubate for [0 Hr 28 Min]
33	Rinse Slide With Reaction Buffer
34	Adjust Slide Volume With Reaction Buffer
35	Apply Coverslip
36	Disable Slide Heater
37	Warmup Slide to 37 Deg C
38	Disable Slide Heater
39	Warmup Slide to 37 Deg C
40	[ DISC Inhibitor will not be applied ]
41	Rinse Slide With Reaction Buffer
42	Adjust Slide Volume With Reaction Buffer
43	Apply Coverslip
44	Disable Slide Heater

\* one drop is one reagent dispense  
Histologix Ltd  
VSS v12.5.4 Build 20234.1

Printed 31/01/2024 11:00:33  
Page 1 of 4

## Protocol # 523 : 1x TSA Ms 1Ab 60m + DAPI (31/01/2024)

Version: 6

Validated: No

Active: Yes

Procedure: RUO DISCOVERY Universal ( v0.00.0408 )

DISCOVERY ULTRA

Histologix Ltd

Step No	Procedure Step
45	Disable Mixers
46	Wait For Button ( DS Primary Antibody )
47	Enable Mixers
48	Warmup Slide to 37 Deg C
49	Rinse Slide With Reaction Buffer
50	Adjust Slide Volume With Reaction Buffer
51	Apply Coverslip
52	Warmup Slide to [37 Deg C] from Very Low Temperatures ( TS Primary Antibody )
53	Hand Apply ( TS Primary Antibody ), and Incubate for [60 Minutes]
54	Rinse Slide With Reaction Buffer
55	Adjust Slide Volume With Reaction Buffer
56	Apply Coverslip
57	Disable Slide Heater
58	Warmup Slide to 37 Deg C
59	Disable Slide Heater
60	Warmup Slide to 37 Deg C
61	[ DISC Inhibitor will not be applied ]
62	Rinse Slide With Reaction Buffer
63	Adjust Slide Volume With Reaction Buffer
64	Apply Coverslip
65	Rinse Slide With Reaction Buffer
66	Adjust Slide Volume With Reaction Buffer
67	Apply Coverslip
68	Disable Slide Heater
69	Apply One Drop of [ANTIBODY 75] ( QuS Antibody ), and Incubate for [0 Hr 32 Min]
70	Rinse Slide With Reaction Buffer
71	Adjust Slide Volume With Reaction Buffer
72	Apply Coverslip
73	Disable Slide Heater
74	Warmup Slide to 37 Deg C
75	[ Requires DETECTION dispensers ]
76	Rinse Slide With Reaction Buffer
77	Adjust Slide Volume With Reaction Buffer
78	Apply Coverslip
79	Rinse Slide With Reaction Buffer
80	Adjust Slide Volume With Reaction Buffer
81	Apply Coverslip
82	Rinse Slide With Reaction Buffer
83	Adjust Slide Volume With Reaction Buffer
84	Apply Coverslip
85	Incubate for 4 Minutes
86	Disable Slide Heater
87	Disable Mixers
88	Wait For Button ( QuS 2nd Antibody )

\* one drop is one reagent dispense

Histologix Ltd  
VSS v12.5.4 Build 20234.1

Printed 31/01/2024 11:00:33

Page 2 of 4

## Protocol # 523 : 1x TSA Ms 1Ab 60m + DAPI (31/01/2024)

Version: 6

Validated: No

Active: Yes

Procedure: RUO DISCOVERY Universal ( v0.00.0408 )

DISCOVERY ULTRA

Histologix Ltd

Step No	Procedure Step
89	Enable Mixers
90	Rinse Slide With Reaction Buffer
91	Adjust Slide Volume With Reaction Buffer
92	Apply Coverslip
93	Hand Apply ( QuS 2nd Antibody ), and Incubate for [0 Hr 8 Min]
94	Rinse Slide With Reaction Buffer
95	Adjust Slide Volume With Reaction Buffer
96	Apply Coverslip
97	Rinse Slide With Reaction Buffer
98	Adjust Slide Volume With Reaction Buffer
99	Apply Coverslip
100	Rinse Slide With Reaction Buffer
101	Adjust Slide Volume With Reaction Buffer
102	Apply Coverslip
103	Incubate for 4 Minutes
104	Disable Slide Heater
105	Disable Mixers
106	Wait For Button ( QuS 3rd Antibody )
107	Enable Mixers
108	Rinse Slide With Reaction Buffer
109	Adjust Slide Volume With Reaction Buffer
110	Apply Coverslip
111	Hand Apply ( QuS 3rd Antibody ), and Incubate for [0 Hr 8 Min]
112	Rinse Slide With Reaction Buffer
113	Adjust Slide Volume With Reaction Buffer
114	Apply Coverslip
115	Disable Slide Heater
116	Warmup Slide to 37 Deg C
117	[ DISC Inhibitor will not be applied ]
118	Rinse Slide With Reaction Buffer
119	Adjust Slide Volume With Reaction Buffer
120	Apply Coverslip
121	Rinse Slide With Reaction Buffer
122	Adjust Slide Volume With Reaction Buffer
123	Apply Coverslip
124	Warmup Slide to [37 Deg C] from Very Low Temperatures ( QnS Primary Antibody )
125	Apply One Drop of [ANTIBODY 80] ( QnS Antibody ), and Incubate for [32 Minutes]
126	Rinse Slide With Reaction Buffer
127	Adjust Slide Volume With Reaction Buffer
128	Apply Coverslip
129	Disable Slide Heater
130	Warmup Slide to 37 Deg C
131	Disable Slide Heater
132	Warmup Slide to 37 Deg C

\* one drop is one reagent dispense

Histologix Ltd

VSS v12.5.4 Build 20234.1

Printed 31/01/2024 11:00:33

Page 3 of 4

**Protocol # 523 : 1x TSA Ms 1Ab 60m + DAPI (31/01/2024)**

**Version: 6**

**Validated: No**

**Active: Yes**

**Procedure: RUO DISCOVERY Universal ( v0.00.0408 )**

**DISCOVERY ULTRA**

**Histologix Ltd**

Step No	Procedure Step
133	Rinse Slide With Reaction Buffer
134	Rinse Slide With Reaction Buffer

## Appendix 14: Non-specific staining retesting and discontinuation emails

**Subject** HPV 16 E6 + HPV 18 E6 antibody (C1P5) ab70

**Our reply By E-mail** Tuesday, Oct 25, 2022 - 14:56

Hello Rebecca,


Thank you for your patience with this inquiry.

Our lab informed me that we also found positive signals in non-specific and negative control samples when retesting the Anti-HPV16 E6 + HPV18 E6 antibody [C1P5] ([ab70](#)).

I apologise for the inconvenience caused. Feel free to get in touch if you have any questions.

Thank you!  
Kind regards,  
Azme

Azme Aneez  
Scientific Support Specialist  
[www.abcam.com](http://www.abcam.com)

 +44(0)1223 696000

We are contacting you because we have very recently reviewed our information on Anti-HPV16 E6 + HPV18 E6 antibody [C1P5] (ab70) which you had previously purchased from us.

Recent retests of ab70 in western blot has shown this antibody detects multiple bands, even in negative controls. Due to the high background obtained, we have decided to remove ab70 from our catalogue since does not meet our quality criteria.

We realize your experiments may have been affected, and we sincerely apologize for the inconvenience. If you have had difficulty with this antibody, please contact me and I will arrange an immediate refund or credit note. Alternatively, we can offer you a replacement with a different antibody against HPV16 like Mouse monoclonal [HPV16L1/1058] to HPV16 - BSA and Azide free ([www.abcam.com/ab234030](http://www.abcam.com/ab234030)). Please let me know if this product is suitable for your experiments.

The quality of our antibodies is very important to us, and so we appreciate any feedback or data customers provide to us regarding their usage of our products. Therefore, please do not hesitate to share with us your own experience with this product by replying to this e-mail, contacting us at [technical@abcam.com](mailto:technical@abcam.com) or by using the "contact us" information on our homepage.

I look forward to hearing from you which resolution you would prefer and any suggestions you might have.

Kind regards,  
Andrea

**Andrea Gonzalez, PhD**

**Senior Scientific Support Specialist**



**Appendix 15: mFold secondary structures for other aptamer candidate sequences for each HPV protein target**



**Figure 56: Secondary DNA structures of seven aptamer candidates chosen from the top ten sequence candidates based on  $\Delta G$  predicted by mFold for HPV-16 E2**

*Content removed for copyright purposes*

**Figure 57: Secondary DNA structures of seven aptamer candidates chosen from the top ten sequence candidates based on  $\Delta G$  predicted by mFold for HPV-16 E7-E6**

*Content removed for copyright purposes*

**Figure 58: Secondary DNA structures of seven aptamer candidates chosen from the top ten sequence candidates based on  $\Delta G$  predicted by mFold for HPV-18 E6**

*Content removed for copyright purposes*

**Figure 59: Secondary DNA structures of seven aptamer candidates chosen from the top ten sequence candidates based on  $\Delta G$  predicted by mFold for HPV-18 E7**

**Appendix 16: ZDOCK scores and polar contacts between HPV-16 E2 and the control ligand 4TS2, natural ligand BRD4, and HPV-16 E2 aptamer candidates**

**Table 12: ZDOCK score, and polar contacts between HPV-16 E2 protein and the control ligand 4TS2**

Complex	Amino acid residue	Actual amino acid residue	Nucleotide	Polar contact length and average (Å)		ZDOCK score	Polar contact information
1	His288	His290	C34	2.8	2.88	1435.638	O2' (C2 OH) within sugar group and NE2 (+NH2) of His228 side chain
	Ser315	Ser317	C34	3.5			OP1 (P=O) within phosphate backbone and OG (OH) of Ser315 side chain
	Trp319	Trp321	A69	3.1			O2' (C2 OH) within sugar group and O (C=O) of Trp319 side chain
	Thr332	Thr334	C34	2.7			O3' (C3 OH) within sugar group within phosphodiester bond between A35 (O-) and OG1 (OH) of Thr332 side chain
	Phe360	Phe362	G63	2.4			OP2 (O-) within phosphate backbone and N within peptide bond between Gly359 (COO-) and Phe360 (+NH3)
	Ser362	Ser364	G60	2.8			O2' (C2 OH) within sugar group and N within peptide bond between Met361 (COO-) and Ser362 (+NH3)

**Table 13: ZDOCK score, and polar contacts between HPV-16 E2 protein and the natural ligand Brd4**

Complex	Protein amino acid residue	Actual amino acid residue	Ligand amino acid residue	Polar contact length and average (Å)		ZDOCK score	Polar contact information
1	Lys290	Lys292	Ile1345	2.7	2.95	1127.953	NZ (+NH3) of Lys290 side chain and O (C=O) of Ile1345 carboxyl group
	Trp319	Trp321	Asn1348	3.2			NE1 (NH) of Trp319 side chain and O (C=O) of Asn1348 side chain

**Table 14: ZDOCK scores, and polar contacts between HPV-16 E2 protein and HPV-16 E2 sequence 4995 aptamer candidate-experiment one**

Complex	Amino acid residue	Actual amino acid residue	Nucleotide	Polar contact length and average (Å)		ZDOCK score	Polar contact information
1	His288	His290	G34	2.4	2.70	1348.197	N2 (NH2) of nucleotide base and ND1 (NH) of His288 side chain
	Thr334	Thr336	C37	3.5			OP1 (P=O) within phosphate backbone and OG1 (OH) of Thr334 side chain
	Phe360	Phe362	T6	2.2			O2 (C2 C=O) of nucleotide base and N within peptide bond between Gly359 (COO-) and Phe360 (+NH3)
2	Thr320	Thr322	G31	2.6	2.75	1347.188	N3 (N) of nucleotide base and N within peptide bond between Trp319 (COO-) and Thr320 (+NH3)
	Thr332	Thr334	T33	2.9			O3' (C3 OH) within sugar group within phosphodiester bond between G34 (O-) and OG1 (OH) of Thr330 side chain
3	Ser362	Ser364	G63	3.3	-	1340.671	O4' (O between C1' and C4') within sugar group and N within peptide bond between Met361 (COO-) and Ser362 (+NH3)

**Table 15: ZDOCK scores, and polar contacts between HPV-16 E2 protein and HPV-16 E2 sequence 4995 aptamer candidate-experiment two**

Complex	Amino acid residue	Actual amino acid residue	Nucleotide	Polar contact length and average (Å)		ZDOCK score	Polar contact information
1	His288	His290	G34	2.4	2.7	1348.197	Polar contact between N2 (NH2) of nucleotide base and ND1 (NH) of His288 side chain
	Thr334	Thr336	C37	3.5			Polar contact between OP1 (P=O) within phosphate backbone and OG1 (OH) of Thr334 side chain
	Phe360	Phe362	T6	2.2			Polar contact between O2 (C2 C=O) of nucleotide base and N within peptide bond between Gly359 (COO-) and Phe360 (+NH3)
2	Ser362	Ser364	G63	3.3	-	1340.671	Polar contact between O4' (O between C1' and C4') within sugar group and N within peptide bond between Met361 (COO-) and Ser362 (+NH3)
3	His318	His320	T6	3.2	3.15	1337.086	Polar contact between N3 (N) of nucleotide base and O (C=O) of His318 carboxyl group
	Thr332	Thr334	C8	3.1			Polar contact between O2 (C2 C=O) of nucleotide base and OG1 (OH) of Thr332 side chain
	Thr332	Thr334	G34	3.3			Polar contact between N2 (C2 NH2) of nucleotide base and OG1 (OH) of Thr332 side chain
	Thr334	Thr336	A9	3.0			Polar contact between O3' (C3 OH) within sugar group within phosphodiester bond between G10 (O-) and OG1 (OH) of Thr334 side chain

**Table 16: ZDOCK scores, and polar contacts between HPV-16 E2 protein and HPV-16 E2 sequence 324 aptamer candidate-experiment one**

Complex	Amino acid residue	Actual amino acid residue	Nucleotide	Polar contact length and average (Å)	ZDOCK score	Polar contact information
1	Tyr301	Tyr303	A24	2.3	1577.154	N3 (N) of nucleotide base and OH (OH) of Tyr301 side chain
	Tyr301	Tyr303	G25	2.4		O4' (O between C1' and C4') within sugar group and OH (OH) of Tyr301 side chain
	Tyr310	Tyr312	G55	2.2		O3' (C3 OH) within sugar group within phosphodiester bond between G56 (O-) and OH (OH) of Tyr310 side chain
	Ser314	Ser316	C8	3.4		O3' (C3 OH) within sugar group within phosphodiester bond between A9 (O-) and OG (OH) of Ser314 side chain
	Trp317	Trp319	C8	2.9		O3' (C3 OH) within sugar group within phosphodiester bond between A9 (O-) and NE1 (NH) of Trp317 side chain
	Thr332	Thr334	C8	2.4		O3' (C3 OH) within sugar group within phosphodiester bond between A9 (O-) and OG1 (OH) of Thr332 side chain
	Thr334	Thr336	G10	2.9		OP1 (P=O) within sugar group and OG1 (OH) of Thr334 side chain
	Ser362	Ser364	G10	3.1		N2 (C2 NH2) of nucleotide base and O (C=O) of Ser362 carboxyl group
2	Ser357	Ser359	T60	-	1431.306	OP1 (P=O) within nucleotide base and OG (OH) of Ser357 side chain
3	Val313	Val315	C20	2.8	1426.811	N4 (C4 NH2) of nucleotide base and O (C=O) of Val313 carboxyl group
	Thr332	Thr334	G48	3.4		O3' (C3 OH) within sugar group within phosphodiester bond between C49 (O-) and OG1 (OH) of Thr332 side chain
	Phe360	Phe362	T31	3.3		O2 (C2 C=O) of nucleotide base and N within peptide bond between Gly359 (COO-) and Phe360 (+NH3)
	Phe360	Phe362	T31	3.6		N3 (N) of nucleotide base and O (C=O) of Phe360 carboxyl group

**Table 17: ZDOCK scores, and polar contacts between HPV-16 E2 protein and HPV-16 E2 sequence 324 aptamer candidate-experiment two**

Complex	Amino acid residue	Actual amino acid residue	Nucleotide	Polar contact length and average (Å)		ZDOCK score	Polar contact information
1	Ser357	Ser359	T60	3.5	-	1431.307	OP1 (P=O) within phosphate backbone and OG (OH) of Ser357 side chain
2	Tyr301	Tyr303	G25	3.3	3.13	1413.374	O3' (C3 OH) within sugar group within phosphodiester bond between G26 (O-) and OH (OH) of Tyr301 side chain
	Thr308	Thr310	A54	3.3			OP1 (P=O) within phosphate backbone and OG1 (OH) of Thr313 side chain
	Val313	Val315	A57	2.9			OP2 (O-) within phosphate backbone and N within peptide bond between Ala312 (COO-) and Val313 (+NH3)
	Thr320	Thr322	T6	3.0			O2 (C2 C=O) of nucleotide base and N within peptide bond between Trp319 (COO-) and Thr320 (+NH3)
	Thr332	Thr334	C8	2.9			O3' (C3 OH) within sugar group between A9 (O-) and OG1 (OH) of Thr332 side chain
	Ser362	Ser364	A62	3.4			N1 (N) of nucleotide base and N within peptide bond between Met361 (COO-) and Ser362 (+NH3)
3	Ser314	Ser316	C8	3.3	3.16	1375.259	O3' (C3 OH) within sugar group within phosphodiester bond between A9 (O-) and OG (OH) of Ser314 side chain
	Ser315	Ser317	A9	3.5			O3' (C3 OH) within sugar group within phosphodiester bond between G10 (O-) and OG (OH) of Ser315 side chain
	Ser315	Ser317	A9	3.2			O4' (O between C1 and C4) within sugar group and N within peptide bond between Ser314 (COO-) and Ser315 (+NH3)
	His318	His320	A11	3.5			OP1 (P=O) within phosphate backbone and NE2 (+NH) of His318 side chain
	Trp319	Trp321	G56	3.4			OP2 (O-) within phosphate backbone and N within peptide bond between His318 (COO-) and Trp319 (+NH3)
	Trp319	Trp321	G56	2.3			O5' (O) within phosphate backbone and NE1 (NH) of Trp319 side chain
	Trp319	Trp321	A57	2.9			OP2 (O-) within phosphate backbone and NE1 (NH) of Trp319 side chain



**Table 18: ZDOCK scores, and polar contacts between HPV-16 E2 protein and HPV-16 E2 sequence 5709 aptamer candidate-experiment one**

Complex	Amino acid residue	Actual amino acid residue	Nucleotide	Polar contact length and average (Å)	ZDOCK score	Polar contact information
1	Arg341	Arg343	C20	2.8	1378.542	OP1 (P=O) within phosphate backbone and NH2 (NH2) of Arg341 side chain
	Arg341	Arg343	C20	2.7		O3' (C3 OH) within sugar group within phosphodiester bond between A21 (O-) and NH1 (+NH2) of Arg341 side chain
	Arg341	Arg343	A21	3.4		OP1 (P=O) within phosphate backbone and NH1 (+NH2) of Arg341 side chain
	Thr358	Thr360	A21	3.3		OP2 (O-) within phosphate backbone and OG1 (OH) of Thr358 side chain
2	Glu338	Glu340	A21	2.8	1360.132	OP2 (O-) within phosphate backbone and N within peptide bond between Ser337 (COO-) and Glu338 (+NH3)
	Trp339	Trp341	A21	2.5		OP2 (O-) within phosphate backbone and N within peptide bond between Glu338 (COO-) and Trp339 (+NH3)
	Gln340	Gln342	C20	2.9		OP2 (O-) within phosphate backbone and NE2 (NH2) of Gln340 side chain
	Thr358	Thr360	G45	2.5		N2 (C2 NH2) of nucleotide base and O (C=O) of Thr358 carboxyl group
	Thr358	Thr360	G45	2.8		N2 (C2 NH2) of nucleotide base and OG1 (OH) of Thr358 side chain
	Thr358	Thr360	G45	3.3		N3 (N) of nucleotide base and OG1 (OH) of Thr358 side chain
	Thr358	Thr360	G46	1.9		O4' (O between C1' and C4') within sugar group and OG1 (OH) of Thr358 side chain
	Phe360	Phe362	G34	2.2		O4' (O between C1 and C4) within sugar group and N within peptide bond between Gly359 (COO-) and Phe360 (+NH3)
	Ser362	Ser364	G34	3.1		O3' (C3 OH) within sugar group within phosphodiester bond between C35 (O-) and N within peptide bond between Met361 (COO-) and Ser362 (+NH3)
Ser362	Ser364	C35	3.0	O5' (O) within phosphate backbone and N within peptide bond between Met361 (COO-) and Ser362 (+NH3)		
3	Lys290	Lys292	G10	2.1	1347.031	O3' (C3 OH) within sugar group within phosphodiester bond between A11 (O-) and NZ (+NH3) of Lys290 side chain
	Thr320	Thr322	G58	3.4		OP2 (O-) within phosphate backbone and N within peptide bond between Trp319 (COO-) and Thr320 (+NH3)

**Table 19: ZDOCK scores, and polar contacts between HPV-16 E2 protein and HPV-16 E2 sequence 5709 aptamer candidate-experiment two**

Complex	Amino acid residue	Actual amino acid residue	Nucleotide	Polar contact length and average (Å)	ZDOCK score	Polar contact information	
1	Glu338	Glu340	A21	2.8	2.79	1360.133	OP2 (O-) within phosphate backbone and N within peptide bond between Ser337 (COO-) and Glu338 (+NH3)
	Trp339	Trp341	A21	2.5			OP2 (O-) within phosphate backbone and N within peptide bond between Glu338 (COO-) and Trp339 (+NH3)
	Gln340	Gln342	C20	2.9			OP2 (O-) within phosphate backbone and NE2 (NH2) of Gln340 R group
	Thr358	Thr360	G45	2.5			N2 (C2 NH2) of nucleotide base and O (C=O) of Thr358 carboxyl group
	Thr358	Thr360	G45	2.8			N2 (C2 NH2) of nucleotide base and OG1 (OH) of Thr358 side chain
	Thr358	Thr360	G45	3.3			N3 (N) of nucleotide base and OG1 (OH) of Thr358 side chain
	Thr358	Thr360	G46	1.9			O4' (O between C1' and C4') within sugar group and OG1 (OH) of Thr358 side chain
	Phe360	Phe362	G34	2.2			O4' (O between C1' and C4') within sugar group and N within peptide bond between Gly359 (COO-) and Phe360 (+NH3)
	Ser362	Ser364	G34	3.1			O3' (C3 OH) within sugar group within phosphodiester bond between C35 (O-) and N within peptide bond between Met361 (COO-) and Ser362 (+NH3)
Ser362	Ser364	C35	3.0	O5' (O) within phosphate backbone and N within peptide bond between Met361 (COO-) and Ser362 (+NH3)			
2	Lys290	Lys292	G10	2.1	2.75	1347.032	O3' (C3 OH) within sugar group within phosphodiester bond between A11 (O-) and NZ (+NH3) of Lys290 side chain
	Thr320	Thr322	G58	3.4			OP2 (O-) within phosphate backbone and N within peptide bond between Trp319 (COO-) and Thr320 (+NH3)
3	Ser357	Ser359	T14	3.1	3.00	1320.256	O3' (C3 OH) within sugar group within phosphodiester bond between C15 (O-) and OG (OH) of Ser357 side chain
	Phe360	Phe362	C13	2.9			O4' (O between C1' and C4') within sugar group and N within peptide bond between Gly359 (COO-) and Phe360 (+NH3)
	Ser362	Ser364	T12	3.0			O2 (C2 C=O) of nucleotide base and N within peptide bond between Met361 (COO-) and Ser362 (+NH3)

**Appendix 17: ZDOCK scores and polar contacts between HPV-16 E6 and the control ligand 4TS2, natural ligand p53, and HPV-16 E7-E6 aptamer candidates**

**Table 20: ZDOCK score, and polar contacts between HPV-16 E6 protein and the control ligand 4TS2**

Complex	Amino acid residue	Actual amino acid residue	Nucleotide	Polar contact length and average (Å)	ZDOCK score	Polar contact information
1	Arg10	Arg17	G70	2.4	2.99	OP2 (O-) within phosphate backbone and NH2 (NH2) of Arg10 side chain
	Tyr79	Tyr86	A83	3.5		OP1 (P=O) within phosphate backbone and OH (OH) of Tyr79 side chain
	Ser80	Ser87	U82	3.2		O2' (C2 OH) within sugar group and O (C=O) of Ser80 carboxyl group
	Ser80	Ser87	G19	3.0		O2' (C2 OH) within sugar group and OG (OH) of Ser80 side chain
	Tyr81	Tyr88	G19	2.0		N3 (N) of nucleotide base and OH (OH) of Tyr81 side chain
	Tyr81	Tyr88	G19	2.8		N2 (C2 NH2) of nucleotide base and OH (OH) of Tyr81 side chain
	Gln91	Gln98	C80	2.7		O2' (C2 OH) within sugar group and OE1 (C=O) of Gln91 side chain
	Gln91	Gln98	C80	3.0		O2 (C2 C=O) of nucleotide base and NE2 (NH2) of Gln91 side chain
	Gln91	Gln98	U21	2.9		O2' (C2 OH) within sugar group and O (C=O) of Gln91 carboxyl group
	Gln91	Gln98	G20	2.9		N3 (N) of nucleotide base and NE2 (NH2) of Gln91 side chain
	Gln91	Gln98	G20	3.3		O2 (C2 OH) (bound to Tyr 92) within sugar group and NE2 (NH2) of Gln91 side chain
	Tyr92	Tyr99	U21	3.1		O2' (C2 OH) within sugar group and O (C=O) of Tyr92 carboxyl group
	Lys94	Lys101	G22	3.3		OP1 (P=O) within phosphate backbone and NZ (+NH3) of Lys94 side chain
	Asn127	Asn134	G20	3.6		O4' (O between C1' and C4') within sugar group and ND2 (NH2) of Asn127 side chain
	Gly130	Gly137	G19	2.3		O3' (C3 OH) within phosphate backbone between G20 (O-) and N within peptide bond between Arg129 (COO-) and Gly130 (+NH3)
	Gly130	Gly137	G19	2.8		O3' (C3 OH) within phosphate backbone between G20 (O-) in phosphate backbone and CA (central C) of Gly130
	Trp132	Trp139	G20	3.4		O2' (C2 OH) (bound to Tyr 92) within sugar group and NE1 (NH1) of Trp132 side chain
	Arg146	Arg153	A83	2.3		O2' (C2 OH) within sugar group and NH2 (NH2) of Arg146 side chain
	Arg146	Arg153	A83	2.5		O2' (C2 OH) within sugar group and NE (NH) of Arg146 side chain
	Arg146	Arg153	A83	2.0		N3 (N) of nucleotide base and NH2 (NH2) of Arg146 side chain
Arg146	Arg153	A83	2.9	N3 (N) of nucleotide base and NH1 (+NH2) of Arg146 side chain		
Arg146	Arg153	A84	3.5	O4' (O between C1' and C4') within sugar group and NH2 (NH2) of Arg146 side chain		
Arg147	Arg154	A84	3.4	OP1 (P=O) within phosphate backbone and NH2 (NH2) of Arg147 side chain		

**Table 21: ZDOCK score, and polar contacts between HPV-16 E6 protein and the natural ligand p53**

Complex	Protein amino acid residue	Actual amino acid residue	Ligand amino acid residue	Polar contact length and average (Å)	ZDOCK score	Polar contact information
1	Tyr81	Tyr88	Ser99	2.1	1127.953	OH (OH) of Tyr81 side chain and N within peptide bond between Pro98 (COO-) and Ser99 (+NH3)
	Ser82	Ser89	Tyr103	1.9		OH (OH) of Tyr103 side chain and O (C=O) of Ser82 carboxyl group
	Ser82	Ser89	Tyr103	2.9		OH (OH) of Tyr103 side chain and N within peptide bond between Tyr81 (COO-) and Ser82 (+NH3)
	Gln91	Gln98	Val97	2.8		NE2 (H2N) of Gln91 side chain and O (C=O) of Val97 carboxyl group
	Tyr92	Tyr99	Val97	3.0		OH (OH) of Tyr92 side chain and O (C=O) of Val97 carboxyl group
	Gly130	Gly137	Ser94	2.9		O (C=O) of Gly130 carboxyl group and N within peptide bond between Leu93 (COO-) and Ser94 (+NH3)
	Glu148	Glu155	Lys370	2.5		OE1 (C=O) of Glu148 side chain and NZ (+NH3) of Lys370 side chain

**Table 22: ZDOCK scores, and polar contacts between HPV-16 E6 protein and HPV-16 E7-E6 sequence 6045 aptamer candidate-experiment one**

Complex	Amino acid residue	Actual amino acid residue	Nucleotide	Polar contact length and average (Å)	ZDOCK score	Polar contact information	
1	Tyr76	Tyr83	G64	2.4	2.84	1381.706	O3' (C3 OH) within sugar group within phosphodiester bond between A65 (O-) and OH (OH) of Tyr76 side chain
	Arg77	Arg84	C68	3.1			OP1 (P=O) within phosphate backbone and NE (NH) of Arg77 side chain
	Ser80	Ser87	G19	3.3			N2 (C2 NH2) of nucleotide base and O (C=O) of Ser80 carboxyl group
	Tyr81	Tyr88	A21	3.2			O4' (O between C1 and C4) within sugar group and OH (OH) of Tyr81 side chain
	Tyr81	Tyr88	A21	2.5			O5' (O) within phosphate backbone and OH (OH) of Tyr81 side chain
	Tyr81	Tyr88	C20	2.7			O4' (O between C1 and C4) within sugar group and OH (OH) of Tyr81 side chain
	Tyr92	Tyr99	A21	2.3			OP1 (P=O) within phosphate backbone and OH (OH) of Tyr92 side chain
	Asn127	Asn134	G19	2.5			O3' (C3 OH) within sugar group within phosphodiester bond between C20 (O-) and ND2 (NH2) of Asn127 side chain
	Arg129	Arg136	G19	3.1			O4' (O between C1' and C4') within sugar group and N within peptide bond between Ile128 (COO-) and Arg129 (+NH3)
	Arg129	Arg136	G70	2.2			OP1 (P=O) within phosphate backbone and NH2 (NH2) of Arg129 side chain
	Arg129	Arg136	G70	2.9			OP2 (O-) within phosphate backbone and NH2 (NH2) of Arg129 side chain
	Arg129	Arg136	G70	3.2			OP2 (O-) within phosphate backbone and NH1 (+NH2) of Arg129 side chain
	Arg146	Arg153	G64	3.4			O4' (O between C1' and C4') within sugar group and NH1 (+NH2) of Arg146 side chain
	Arg146	Arg153	G63	3.0			N3 (N) of nucleotide base and NH2 (NH2) of Arg146 side chain
Arg147	Arg154	G63	2.0	OP1 (P=O) within phosphate backbone and NH2 (NH2) of Arg147 side chain			
2	Ser80	Ser87	G25	3.1	2.98	1349.532	O3' (C3 OH) within sugar group within phosphodiester bond between A65 (O-) and OH (OH) of Tyr76 side chain
	Tyr81	Tyr88	G56	2.0			OP1 (P=O) within phosphate backbone and NE (NH) of Arg77 side chain
	Tyr81	Tyr88	C27	3.3			N2 (C2 NH2) of nucleotide base and O (C=O) of Ser80 carboxyl group
	Tyr84	Tyr91	C17	3.1			O4' (O between C1 and C4) within sugar group and OH (OH) of Tyr81 side chain
	Tyr84	Tyr91	C16	3.5			O5' (O) within phosphate backbone and OH (OH) of Tyr81 side chain
	Gln91	Gln98	C27	2.4			O4' (O between C1 and C4) within sugar group and OH (OH) of Tyr81 side chain
	Gln91	Gln98	G56	3.1			OP1 (P=O) within phosphate backbone and OH (OH) of Tyr92 side chain
	Tyr92	Tyr99	C27	3.0			O3' (C3 OH) within sugar group within phosphodiester bond between C20 (O-) and ND2 (NH2) of Asn127 side chain
	Arg124	Arg131	C16	3.1			O4' (O between C1' and C4') within sugar group and N within peptide bond between Ile128 (COO-) and Arg129 (+NH3)
	Arg124	Arg131	C17	3.4			OP1 (P=O) within phosphate backbone and NH2 (NH2) of Arg129 side chain
	Asn127	Asn134	C27	2.9			OP2 (O-) within phosphate backbone and NH2 (NH2) of Arg129 side chain
	Arg146	Arg153	T14	2.6			OP2 (O-) within phosphate backbone and NH1 (+NH2) of Arg129 side chain
	Arg146	Arg153	T14	2.2			O4' (O between C1' and C4') within sugar group and NH1 (+NH2) of Arg146 side chain
	Arg146	Arg153	C15	1.9			N3 (N) of nucleotide base and NH2 (NH2) of Arg146 side chain
3	Tyr81	Tyr88	G53	2.5	2.83	1346.698	OP1 (P=O) within phosphate backbone and NH2 (NH2) of Arg147 side chain
	Tyr81	Tyr88	C52	2.8			O3' (C3 OH) within sugar group within phosphodiester bond between A65 (O-) and OH (OH) of Tyr76 side chain
	Gln91	Gln98	G53	2.7			OP1 (P=O) within phosphate backbone and NE (NH) of Arg77 side chain
	Arg124	Arg131	A31	3.5			N2 (C2 NH2) of nucleotide base and O (C=O) of Ser80 carboxyl group
	Arg124	Arg131	G32	2.4			O4' (O between C1 and C4) within sugar group and OH (OH) of Tyr81 side chain
	Arg147	Arg154	G34	3.1			O5' (O) within phosphate backbone and OH (OH) of Tyr81 side chain

**Table 23: ZDOCK scores, and polar contacts between HPV-16 E6 protein and HPV-16 E7-E6 sequence 6045 aptamer candidate-experiment two**

Complex	Amino acid residue	Actual amino acid residue	Nucleotide	Polar contact length and average (Å)	ZDOCK score	Polar contact information
1	Tyr76	Tyr83	G64	2.4	1381.706	O3' (C3 OH) within sugar group within phosphodiester bond between A65 (O-) and OH (OH) of Tyr76 side chain
	Arg77	Arg84	C68	3.1		OP1 (P=O) within phosphate backbone and NE (NH) of Arg77 side chain
	Ser80	Ser87	G19	3.3		N2 (C2 NH2) of nucleotide base and O (C=O) of Ser80 carboxyl group
	Tyr81	Tyr88	A21	3.2		O4' (O between C1 and C4) within sugar group and OH (OH) of Tyr81 side chain
	Tyr81	Tyr88	A21	2.5		O5' (O) within phosphate backbone and OH (OH) of Tyr81 side chain
	Tyr81	Tyr88	C20	2.7		O4' (O between C1 and C4) within sugar group and OH (OH) of Tyr81 side chain
	Tyr92	Tyr99	A21	2.3		OP1 (P=O) within phosphate backbone and OH (OH) of Tyr92 side chain
	Asn127	Asn134	G19	2.5		O3' (C3 OH) within sugar group within phosphodiester bond between C20 (O-) and ND2 (NH2) of Asn127 side chain
	Arg129	Arg136	G19	3.1		O4' (O between C1' and C4') within sugar group and N within peptide bond between Ile128 (COO-) and Arg129 (+NH3)
	Arg129	Arg136	G70	2.2		OP1 (P=O) within phosphate backbone and NH2 (NH2) of Arg129 side chain
	Arg129	Arg136	G70	2.9		OP2 (O-) within phosphate backbone and NH2 (NH2) of Arg129 side chain
	Arg129	Arg136	G70	3.2		OP2 (O-) within phosphate backbone and NH1 (+NH2) of Arg129 side chain
	Arg146	Arg153	G64	3.4		O4' (O between C1' and C4') within sugar group and NH1 (+NH2) of Arg146 side chain
	Arg146	Arg153	G63	3.0		N3 (N) of nucleotide base and NH2 (NH2) of Arg146 side chain
Arg147	Arg154	G63	2.0	OP1 (P=O) within phosphate backbone and NH2 (NH2) of Arg147 side chain		
2	Ser80	Ser87	G25	3.1	1349.532	O3' (C3 OH) within sugar group within phosphodiester bond between A65 (O-) and OH (OH) of Tyr76 side chain
	Tyr81	Tyr88	G56	2.0		OP1 (P=O) within phosphate backbone and NE (NH) of Arg77 side chain
	Tyr81	Tyr88	C27	3.3		N2 (C2 NH2) of nucleotide base and O (C=O) of Ser80 carboxyl group
	Tyr84	Tyr91	C17	3.1		O4' (O between C1 and C4) within sugar group and OH (OH) of Tyr81 side chain
	Tyr84	Tyr91	C16	3.5		O5' (O) within phosphate backbone and OH (OH) of Tyr81 side chain
	Gln91	Gln98	C27	2.4		O4' (O between C1 and C4) within sugar group and OH (OH) of Tyr81 side chain
	Gln91	Gln98	G56	3.1		OP1 (P=O) within phosphate backbone and OH (OH) of Tyr92 side chain
	Tyr92	Tyr99	C27	3.0		O3' (C3 OH) within sugar group within phosphodiester bond between C20 (O-) and ND2 (NH2) of Asn127 side chain
	Arg124	Arg131	C16	3.1		O4' (O between C1' and C4') within sugar group and N within peptide bond between Ile128 (COO-) and Arg129 (+NH3)
	Arg124	Arg131	C17	3.4		OP1 (P=O) within phosphate backbone and NH2 (NH2) of Arg129 side chain
	Asn127	Asn134	C27	2.9		OP2 (O-) within phosphate backbone and NH2 (NH2) of Arg129 side chain
	Arg146	Arg153	T14	2.6		OP2 (O-) within phosphate backbone and NH1 (+NH2) of Arg129 side chain
	Arg146	Arg153	T14	2.2		O4' (O between C1' and C4') within sugar group and NH1 (+NH2) of Arg146 side chain
	Arg146	Arg153	C15	1.9		N3 (N) of nucleotide base and NH2 (NH2) of Arg146 side chain
3	Tyr81	Tyr88	G53	2.5	1346.698	OP1 (P=O) within phosphate backbone and NH2 (NH2) of Arg147 side chain
	Tyr81	Tyr88	C52	2.8		O3' (C3 OH) within sugar group within phosphodiester bond between A65 (O-) and OH (OH) of Tyr76 side chain
	Gln91	Gln98	G53	2.7		OP1 (P=O) within phosphate backbone and NE (NH) of Arg77 side chain
	Arg124	Arg131	A31	3.5		N2 (C2 NH2) of nucleotide base and O (C=O) of Ser80 carboxyl group
	Arg124	Arg131	G32	2.4		O4' (O between C1 and C4) within sugar group and OH (OH) of Tyr81 side chain
	Arg147	Arg154	G34	3.1		O5' (O) within phosphate backbone and OH (OH) of Tyr81 side chain

**Table 24: ZDOCK scores, and polar contacts between HPV-16 E6 protein and HPV-16 E7-E6 sequence 6362 aptamer candidate-experiment one**

Complex	Amino acid residue	Actual amino acid residue	Nucleotide	Polar contact length and average (Å)	ZDOCK score	Polar contact information	
1	Tyr 79	Tyr86	C50	3.5	1426.703	O3' (C3 OH) within sugar group within phosphodiester bond between T51 (O-) and OH (OH) of Tyr79 side chain	
	Tyr 81	Tyr88	G31	2.7		3.04	N3 (N) of nucleotide base and OH (OH) of Tyr81 side chain
	Tyr 81	Tyr88	G31	3.0			N2 (C2 NH2) of nucleotide base and OH (OH) of Tyr81 side chain
	Tyr92	Tyr99	T32	2.5			OP1 (P=O) within phosphate backbone and OH (OH) of Tyr92 side chain
	Tyr92	Tyr99	T32	3.0			OP2 (O-) within phosphate backbone and OH (OH) of Tyr92 side chain
	Asn127	Asn134	G31	3.2			O3' (C3 OH) within sugar group within phosphodiester bond T31 (O-) and ND2 (NH2) of Asn117 side chain
	Asn127	Asn134	T32	3.4			OP2 (O-) within phosphate backbone and ND2 (NH2) of Asn117 side chain
	2	Tyr70	Tyr77	G44			3.1
Tyr70		Tyr77	C45	3.3	OP2 (O-) within phosphate backbone and OH (OH) of Tyr70 side chain		
Tyr76		Tyr83	A54	3.0	N3 (N) of nucleotide base and OH (OH) of Tyr76 side chain		
Tyr76		Tyr83	G55	2.0	O4' (O between C1' and C4') within sugar group and OH (OH) of Tyr76 side chain		
Arg77		Arg84	A28	3.1	O3' (C3 OH) within sugar group within phosphodiester bond between A28 and G29 and NH1 (+NH2) of Arg77 side chain		
Arg77		Arg84	G29	2.8	O4' (O between C1' and C4') within sugar group and NH2 (NH2) of Arg77 side chain		
Arg147		Arg154	G56	3.3	O5' (O) within phosphate backbone and NH1 (+NH2) of Arg147 side chain		
3	Tyr81	Tyr88	G31	2.4	1387.724	N3 (N) of nucleotide base and OH (OH) of Tyr81 side chain	
	Tyr81	Tyr88	G31	3.2		N2 (C2 NH2) of nucleotide base and OH (OH) of Tyr81 side chain	
	Tyr92	Tyr99	T33	2.4		O4' (O between C1' and C4') within sugar group and OH (OH) of Tyr81 side chain	
	Tyr92	Tyr99	T32	3.2		OP1 (P=O) within phosphate backbone and OH (OH) of Tyr92 side chain	
	Arg124	Arg131	T51	2.2		OP1 (P=O) within phosphate backbone and NH1 (+NH2) of Arg124 side chain	
	Arg124	Arg131	C50	2.8		O3' (C3 OH) within sugar group within phosphodiester bond between C50 and T51 and NH1 (+NH2) of Arg124 side chain	
	Asn127	Arg131	G31	2.6		O3' (C3 OH) within sugar group within phosphodiester bond between G31 and T32 and ND2 (NH2) of Asn127 side chain	
	Asn127	Arg131	T32	2.5		OP2 (O-) within phosphate backbone and ND2 (NH2) of Asn127 side chain	

**Table 25: ZDOCK scores, and polar contacts between HPV-16 E6 protein and HPV-16 E7-E6 sequence 6362 aptamer candidate-experiment two**

Complex	Amino acid residue	Actual amino acid residue	Nucleotide	Polar contact length and average (Å)		ZDOCK score	Polar contact information
1	Tyr79	Tyr86	C50	3.5	3.04	1426.701	O3' (C3 OH) within sugar group within phosphodiester bond between T51 (O-) and OH (OH) of Tyr79 side chain
	Tyr81	Tyr88	G31	2.7			N3 (N) of nucleotide base and OH (OH) of Tyr81 side chain
	Tyr81	Tyr88	G31	3.0			N2 (C2 NH2) of nucleotide base and OH (OH) of Tyr81 side chain
	Tyr92	Tyr99	T32	2.5			OP1 (P=O) within phosphate backbone and OH (OH) of Tyr92 side chain
	Tyr92	Tyr99	T32	3.0			OP2 (O-) within phosphate backbone and OH (OH) of Tyr92 side chain
	Asn127	Asn134	G31	3.2			O3' (C3 OH) within sugar group within phosphodiester bond T32 (O-) and ND2 (NH2) of Asn117 side chain
	Asn127	Asn134	T32	3.4			OP2 (O-) within phosphate backbone and ND2 (NH2) of Asn117 side chain
2	Tyr81	Tyr88	G31	2.4	2.66	1387.723	N3 (N) of nucleotide base and OH (OH) of Tyr81 side chain
	Tyr81	Tyr88	G31	3.2			N2 (C2 NH2) of nucleotide base and OH (OH) of Tyr81 side chain
	Tyr92	Tyr99	T33	2.4			O4' (O between C1' and C4') within sugar group and OH (OH) of Tyr92 side chain
	Tyr92	Tyr99	T32	3.2			OP1 (P=O) within phosphate backbone and OH (OH) of Tyr92 side chain
	Arg124	Arg131	T51	2.2			OP1 (P=O) within phosphate backbone and NH1 (+NH2) of Arg124 side chain
	Arg124	Arg131	C50	2.8			O3' (C3 OH) within sugar group within phosphodiester bond between T51 (O-) and NH1 (+NH2) of Arg124 side chain
	Asn127	Asn134	G31	2.6			O3' (C3 OH) within sugar group within phosphodiester bond between T32 (O-) and ND2 (NH2) of Asn127 side chain
3	Asn127	Asn134	T32	2.5	3.03	1383.313	OP2 (O-) within phosphate backbone and ND2 (NH2) of Asn127 side chain
	Ser80	Ser87	G19	2.9			O4' (O between C1' and C4') within sugar group and OG (OH) of Ser80 side chain
	Tyr81	Tyr88	G19	2.9			N3 (N) of nucleotide base and OH (OH) of Tyr81 side chain
	Tyr81	Tyr88	G19	2.8			N2 (C2 NH2) of nucleotide base and OH (OH) of Tyr81 side chain
	Gln91	Gln98	A21	2.7			O4' (O between C1' and C4') within sugar group and NE2 (NH2) of Gln91 side chain
	Arg146	Arg153	G64	3.1			O3' (C3 OH) within sugar group within phosphodiester bond between A65 (O-) and NH2 (NH2) of Arg146 side chain
	Arg147	Arg154	A65	3.3			OP1 (P=O) within phosphate backbone and NH1 (+NH2) of Arg147 side chain
Arg147	Arg154	A65	3.5	OP2 (O-) within phosphate backbone and NH2 (NH2) of Arg147 side chain			



**Table 26: ZDOCK scores, and polar contacts between HPV-16 E6 protein and HPV-16 E7-E6 sequence 3271 aptamer candidate-experiment one**

Complex	Amino acid residue	Actual amino acid residue	Nucleotide	Polar contact length and average (Å)	ZDOCK score	Polar contact information
1	Gln6	Gln13	T48	3.4	1398.289	O2 (C2 C=O) of nucleotide base and NE2 (NH2) of Gln6 side chain
	Gln6	Gln13	A54	3.4		N3 (N) of nucleotide base and NE2 (NH2) of Gln6 side chain
	Ser80	Ser87	C8	2.9		C2 (C2 C=O) of nucleotide base and OG (OH) of Ser80 side chain
	Tyr81	Tyr88	A9	2.5		N1 (N) of nucleotide base and OH (OH) of Tyr81 side chain
	Tyr84	Tyr91	G3	2.4		OP2 (O-) within phosphate backbone and OH (OH) of Tyr84 side chain
	Tyr84	Tyr91	G2	2.5		O5' (O) within phosphate backbone and OH (OH) of Tyr84 side chain
	Tyr92	Tyr99	G10	2.0		N3 (N) of nucleotide base and OH (OH) of Tyr92 side chain
	Asn93	Asn100	T12	2.5		O3' (C3 OH) within sugar group and ND2 (NH2) of Asn93 side chain
	Lys94	Lys101	A11	3.3		O3' (C3 OH) within sugar group within phosphodiester bond between A11 and T12 and NZ (+NH3) of Lys94 side chain
	Arg124	Arg131	G2	2.9		O6 (C6 C=O) of nucleotide base and NH2 (NH2) of Arg124 side chain
	Arg124	Arg131	G2	3.1		OP2 (O-) within phosphate backbone and N within peptide bond between Gln 123 (COO-) and Arg124 (+NH3)
	Asn127	Asn134	A9	3.4		N3 (N) of nucleotide base and ND2 (NH2) of Asn127 side chain
	Glu148	Glu155	G3	2.2		N1 (NH) of nucleotide base and OE1 (C=O) of Glu148 side chain
	Glu148	Glu155	A4	3.0		N6 (C6 NH2) of nucleotide base and OE1 (C=O) of Glu148 side chain
Glu148	Glu155	A4	3.3	N6 (C6 NH2) of nucleotide base and OE2 (O-) of Glu148 side chain		
2	Gln35	Gln42	T25	3.2	1333.033	O4 (C4 C=O) of nucleotide base and NE2 (NH2) of Gln35 side chain
	Arg55	Arg62	C23	3.3		OP1 (P=O) within phosphate backbone and NE (NH) of Arg55 side chain
	Tyr70	Tyr77	G22	2.7		OP2 (O-) within phosphate backbone and OH (OH) of Tyr70 side chain
	Tyr70	Tyr77	A21	3.2		O5' (O) within phosphate backbone and OH (OH) of Tyr70 side chain
	Arg77	Arg84	G43	3.0		N2 (C2 NH2) of nucleotide backbone and O (C=O) of Arg77 carboxyl group
	Tyr79	Tyr86	G58	2.4		N2 (C2 NH2) of nucleotide backbone and O (C=O) of Tyr79 carboxyl group
	Ser80	Ser87	T45	2.8		O4' (O between C1' and C4') within sugar group and OG (OH) of Ser80 side chain
	Arg129	Arg136	C44	2.9		O3' (C3 OH) within sugar group within phosphodiester bond between C44 and T45 and NE (NH) of Arg129 side chain
	Arg129	Arg136	T45	2.8		OP1 (P=O) within phosphate backbone and NE (NH) of Arg129 side chain
	Arg129	Arg136	T45	3.0		OP1 (P=O) within phosphate backbone and NH2 (NH2) of Arg129 side chain
	Thr145	Thr152	A62	2.8		N6 (C6 NH2) of nucleotide base and O (C=O) of Thr145 carboxyl group
	Arg146	Arg153	C59	2.9		O2 (C2 C=O) of nucleotide base and NH1 (+NH2) of Arg146 side chain
	Arg147	Arg154	T60	2.1		OP1 (P=O) within phosphate backbone and NH1 (+NH2) of Arg147 side chain
	Arg147	Arg154	C59	3.2		O3' (C3 OH) within sugar group within phosphodiester bond between C59 and T60 and NH1 (+NH2) of Arg147 side chain
Arg147	Arg154	T60	3.1	OP2 (O-) within phosphate backbone and NH1 (+NH2) of Arg147 side chain		
Arg147	Arg154	C59	3.3	OP1 (P=O) within phosphate backbone and NH2 (NH2) of Arg147 side chain		
3	Tyr81	Tyr88	C15	2.5	1331.377	O2 (C2 C=O) of nucleotide base and OH (OH) of Tyr81 side chain
	Tyr92	Tyr99	C15	2.1		O4' (O between C1' and C4') within sugar group and OH (OH) of Tyr92 side chain
	Tyr92	Tyr99	T14	3.4		O3' (C3 OH) within sugar group within phosphodiester bond between T15 and C15 and OH (OH) of Tyr92 side chain
	Asn127	Asn134	T14	3.0		O4' (O between C1' and C4') within sugar group and ND2 (NH2) of Asn127 side chain
	Asn127	Asn134	T14	3.0		O2 (C2 C=O) of nucleotide base and ND2 (NH2) of Asn127 side chain
	Ser143	Ser150	A4	3.1		OP2 (O-) within phosphate backbone and OG (OH) of Ser143 side chain
	Ser143	Ser150	G3	3.0		O5' (O) within phosphate backbone and OG (OH) of Ser143 side chain

	Ser143	Ser150	G3	3.3			OP2 (O-) within phosphate backbone and OG (OH) of Ser143 side chain
	Arg144	Arg151	G3	2.5			OP2 (O-) within phosphate backbone and N within peptide bond between Ser133 (COO-) and Arg144 (+NH3)
	Arg147	Arg154	T7	3.1			O4 (C4 C=O) of nucleotide base and NH2 (NH2) of Arg147 side chain

**Table 27: ZDOCK scores, and polar contacts between HPV-16 E6 protein and HPV-16 E7-E6 sequence 3271 aptamer candidate-experiment two**

Complex	Amino acid residue	Actual amino acid residue	Nucleotide	Polar contact length and average (Å)	ZDOCK score	Polar contact information
1	Gln6	Gln13	T48	3.4	1398.288	O2 (C2 C=O) of nucleotide base and NE2 (NH2) of Gln6 side chain
	Gln6	Gln13	A54	3.4		N3 (N) of nucleotide base and NE2 (NH2) of Gln6 side chain
	Ser80	Ser87	C8	2.9		C2 (C2 C=O) of nucleotide base and OG (OH) of Ser80 side chain
	Tyr81	Tyr88	A9	2.5		N1 (N) of nucleotide base and OH (OH) of Tyr81 side chain
	Tyr84	Tyr91	G3	2.4		OP2 (O-) within phosphate backbone and OH (OH) of Tyr84 side chain
	Tyr84	Tyr91	G2	2.5		O5' (O) within phosphate backbone and OH (OH) of Tyr84 side chain
	Tyr92	Tyr99	G10	2.0		N3 (N) of nucleotide base and OH (OH) of Tyr92 side chain
	Asn93	Asn100	T12	2.5		O3' (C3 OH) within sugar group and ND2 (NH2) of Asn93 side chain
	Lys94	Lys101	A11	3.3		O3' (C3 OH) within sugar group with phosphodiester bond between A11 and T12 and NZ (+NH3) of Lys94 side chain
	Arg124	Arg131	G2	2.9		O6 (C6 C=O) of nucleotide base and NH2 (NH2) of Arg124 side chain
	Arg124	Arg131	G2	3.1		OP2 (O-) within phosphate backbone and N within peptide bond between Gln123 (COO-) and Arg124 (+NH3)
	Asn127	Asn134	A9	3.4		N3 (N) of nucleotide base and ND2 (NH2) of Asn127 side chain
	Glu148	Glu155	G3	2.2		N1 (NH) of nucleotide base and OE1 (C=O) of Glu148 side chain
	Glu148	Glu155	A4	3.0		N6 (C6 NH2) of nucleotide base and OE1 (C=O) of Glu148 side chain
Glu148	Glu155	A4	3.3	N6 (C6 NH2) of nucleotide base and OE2 (O-) of Glu148 side chain		
2	Tyr81	Tyr88	C15	2.5	1331.378	O2 (C2 C=O) of nucleotide base and OH (OH) of Tyr81 side chain
	Tyr92	Tyr99	C15	2.1		O4' (O between C1' and C4') within sugar group and OH (OH) of Tyr92 side chain
	Tyr92	Tyr99	T14	3.4		O3' (C3 OH) within sugar group within phosphodiester between C15 (O-) and OH (OH) of Tyr92 side chain
	Asn127	Asn134	T14	3.0		O2 (C2 C=O) of nucleotide base and ND2 (NH2) of Asn127 side chain
	Asn127	Asn134	T14	3.0		O4' (O between C1' and C4') within sugar group and ND2 (NH2) of Asn127 side chain
	Ser143	Ser150	G3	3.3		OP2 (O-) within phosphate backbone and OG (OH) of Ser143 side chain
	Ser143	Ser150	G3	3.0		O5' (O) within phosphate backbone and OG (OH) of Ser143 side chain
	Ser143	Ser150	A4	3.1		OP2 (O-) within phosphate backbone and OG (OH) of Ser143 side chain
Arg144	Arg151	G3	2.5	OP2 (O-) within phosphate backbone and N within peptide bond between Ser143 (COO-) and Arg144 (+NH3)		
3	Ser80	Ser87	T7	2.5	1329.755	O2 (C2 C=O) of nucleotide base and OG (OH) of Ser80 side chain
	Ser80	Ser87	T7	3.1		O4' (O between C1' and C4') within sugar group and OG (OH) of Ser80 side chain
	Ser82	Ser89	A4	2.8		N6 (C6 NH2) of nucleotide base and O (C=O) of Ser82 carboxyl group
	Gln91	Gln98	G10	1.9		N2 (C2 NH2) of nucleotide base and O (C=O) of Gln91 carboxyl group
	Gln91	Gln98	A9	3.3		N1 (N) of nucleotide base and NE2 (NH2) of Gln91 side chain
	Tyr92	Tyr99	A9	2.2		N3 (N) of nucleotide base and OH (OH) of Tyr92 side chain
	Arg124	Arg131	G2	2.2		O6 (C6 C=O) of nucleotide base and NH1 (+NH2) of Arg124 side chain
	Arg124	Arg131	G3	2.4		O6 (C6 C=O) of nucleotide base and NH1 (+NH2) of Arg124 side chain
	Asn127	Arg154	C8	2.6		O2 (C2 C=O) of nucleotide base and ND2 (H2N) of Asn127 side chain
Glu148	Glu155	G3	3.1	N2 (C2 NH2) of nucleotide base and OE1 (O-) of Glu148 side chain		

## Appendix 18: ZDOCK outputs and polar contacts between HPV-18 E6 and the control ligand 4TS2, natural ligand p53, and HPV-18 E6 aptamer candidates

**Table 28: ZDOCK score, and polar contacts between HPV-18 E6 protein and the control ligand 4TS2**

Complex	Amino acid residue	Actual amino acid residue	Nucleotide	Polar contact length and average (Å)	ZDOCK score	Polar contact information
1	Ser1024	Ser24	C79	2.2	1298.337	O2' (C2' OH) of sugar group and OG (OH) of Ser1024 side chain
	Ser1024	Ser24	C79	3.2		O3' (C3' OH) of sugar group within phosphodiester bond between C80 (O-) and N within peptide bond between Thr1023 (COO-) and Ser1024 (+NH3)
	Ala1048	Ala48	A23	3.2		O2' (C2' OH) of sugar group and O (C=O) of Ala1048 carboxyl group
	Arg1049	Arg49	A23	3.1		OP1 (P=O) of phosphate backbone and NH1 (+NH2) of Arg1049 side chain
	Tyr1099	Tyr99	G25	3.3		O2' (C2' OH) of sugar group and OH (OH) of Tyr1099 side chain
	Tyr1099	Tyr99	U62	3.1		OP2 (O-) of phosphate backbone and N within peptide bond between Leu1098 (COO-) and Tyr1099 (+NH3)
	Asn1100	Asn100	U62	2.8		OP2 (O-) of phosphate backbone and N within peptide bond between Tyr1099 (COO-) and Asn1100 (+NH3)
	Asn1100	Asn100	A27	3.5		OP1 (P=O) of phosphate backbone and ND2 (NH2) of Asn1100 side chain
	Asn1113	Asn113	G65	3.3		O3' (C3' OH) of sugar group within phosphodiester bond between U66 (O-) and ND2 (NH2) of Asn1113 side chain
His1139	His139	A67	2.6	N6 (C6 NH2) of nucleotide base and ND1 (NH1) of His1139 side chain		

**Table 29: ZDOCK score, and polar contacts between HPV-18 E6 protein and the natural ligand p53**

Complex	Protein amino acid residue	Actual amino acid residue	Ligand amino acid residue	Polar contact length and average (Å)	ZDOCK score	Polar contact information
1	Pro1007	Pro7	Thr329	2.6	1324.301	O (C=O) of Pro1007 carboxyl group and OG (OH) of Thr329 side chain
	Pro1007	Pro7	Thr329	3.0		O (C=O) of Pro1007 carboxyl group and N within peptide bond between Phe328 (COO-) and Thr329 (+NH3)
	Tyr1012	Tyr12	Thr329	3.5		OH (OH) of Tyr1012 side chain and N within peptide bond between Phe328 (COO-) and Thr329 (+NH3)
	Lys1092	Lys92	Val147	2.8		NZ (+NH3) of Lys1091 side chain and O (C=O) of Val147 carboxyl group
	Leu1098	Leu98	Asp228	3.2		N within peptide bond of Gly1097 (COO-) and Leu1098 (+NH3) and OD2 (O-) of Asp228 side chain
	Gly1132	Gly132	Arg363	2.6		O (C=O) of Gly1132 carboxyl group and NH1 (+NH2) of Arg363 side chain

**Table 30: ZDOCK scores, and polar contacts between HPV-18 E6 protein and HPV-18 E6 sequence 12797 aptamer candidate-experiment one**

Complex	Amino acid residue	Actual amino acid residue	Nucleotide	Polar contact length and average (Å)	ZDOCK score	Polar contact information
1	Asp1016	Asp16	G39	2.6	1389.297	N2 (C2 NH2) of the nucleotide base and OD1 (C=O) of Asp1016 side chain
	Ser1024	Ser24	A57	3.5		OP1 (P=O) within the phosphate backbone and N within peptide bond between Thr1023 (COO-) and Ser1024 (+NH3)
	Gln1026	Gln26	G55	3.3		N2 (C2 NH2) of the nucleotide base and OE1 (C=O) of Gln1026 side chain
	Arg1049	Arg49	C8	3.0		OP1 (P=O) within the phosphate backbone and NH2 (NH2) of Arg1049 side chain
	Asp1051	Asp51	G19	3.1		N2 (C2 NH2) of the nucleotide base and OD1 (C=O) of Asp1051 side chain
	His1066	His66	T7	3.2		OP1 (P=O) within the phosphate backbone and NE2 (NH2) of His1066 side chain
	His1066	His66	T6	3.2		O3' (O-) within the sugar group within phosphodiester bond between T7 (O-) and NE2 (NH2) of His1066 side chain
	Tyr1099	Tyr99	C16	2.5		O2 (C2 C=O) of the nucleotide base and OH (OH) of Tyr1099 side chain
2	Gln1026	Gln26	A5	3.0	1378.423	OP2 (O-) within the phosphate backbone and NE2 (NH2) of Gln1026 side chain
	Gln1026	Gln26	T6	3.1		OP2 (O-) within the phosphate backbone and NE2 (NH2) of Gln1026 side chain
	Arg1049	Arg49	T7	3.3		OP1 (P=O) within the phosphate backbone and NH1 (+NH2) of Arg1049 side chain
	Arg1049	Arg49	T7	3.8		O3' (C3 OH) within the sugar group within phosphodiester bond between C8 (O-) and NH1 (+NH2) of Arg1049 side chain
	Tyr1072	Tyr72	A21	2.7		OP2 (O-) within the phosphate backbone and OH of Tyr1072 side chain
	Tyr1072	Tyr72	A21	3.0		O5' (O) within the phosphate backbone and OH of Tyr1072 side chain
	Arg1074	Arg74	C40	3.0		O4' (O between C1' and C4') within the sugar group and NH1 (+NH2) of Arg1074 side chain
	Arg1079	Arg79	C23	2.7		OP1 (P=O) within the phosphate backbone and NH2 (NH2) of Arg1079 side chain
	Tyr1086	Tyr86	C59	2.8		OP1 (P=O) within the phosphate backbone and OH (OH) of Tyr1086 side chain
	Arg1119	Arg119	C69	2.6		OP2 (O-) within the phosphate backbone and NH2 (NH2) of Arg1119 side chain
	Arg1119	Arg119	C68	3.4		O5' (O) within the phosphate backbone and NH2 (NH2) of Arg1119 side chain
	Glu1123	Glu123	G56	2.3		N2 (C2 NH2) of the nucleotide base and OE1 (C=O) of Glu1123 side chain
	Glu1123	Glu123	G56	2.7		N2 (C2 NH2) of the nucleotide base and OE2 (O-) of Glu1123 side chain
	Lys1124	Lys124	G63	3.1		O5' (O) within the phosphate backbone and NZ (+NH3) of Lys1124 side chain
	Arg1126	Arg126	C59	3.2		OP2 (O-) within the phosphate backbone and NH1 (+NH2) of Arg1126 side chain
	Arg1126	Arg126	G58	3.5		OP1 (C=O) within the phosphate backbone and NH1 (+NH2) of Arg1126 side chain
	Gln1137	Gln137	A57	3.4		O3' (C3 OH) within the sugar group within phosphodiester bond between G58 (O-) and NE2 (NH2) of Gln1137 side chain
	Asn1143	Asn143	C69	2.2		O2 (C2 OH) of the nucleotide base and ND2 (NH2) of Asn1143 side chain
3	Ser1024	Ser24	T6	2.8	1359.978	O4' (O between C1' and C4') within the sugar group and OG (OH) of Ser1024 side chain
	Tyr1099	Tyr99	G39	2.4		N3 (N) of nucleotide base and OH (OH) of Tyr1099 side chain
	Leu1102	Leu102	A57	2.4		OP1 (P=O) within the phosphate backbone and N within peptide bond between Leu1101 (COO-) and Leu1102 (H3N+)
	Asn1129	Asn129	C59	2.0		OP1 (P=O) within the phosphate backbone and ND2 (NH2) of Asn1129 side chain
	Tyr1134	Tyr134	G58	3.0		OP1 (P=O) within the phosphate backbone and N within peptide bond between His1133 (COO-) and Tyr1134 (H3N+)

**Table 31: ZDOCK scores, and polar contacts between HPV-18 E6 protein and HPV-18 E6 sequence 12797 aptamer candidate-experiment two**

Complex	Amino acid residue	Actual amino acid residue	Nucleotide	Polar contact length and average (Å)	ZDOCK score	Polar contact information
1	Asp1006	Asp6	A1	3.6	1355.813	N6 (C6 NH2) of nucleotide base and OD2 (O-) of Asp1006 side chain
	Thr1008	Thr8	A1	2.3		N6 (C6 NH2) of nucleotide base and OG1 (OH) of Thr1008 side chain
	Thr1008	Thr8	G2	2.6		N1 (NH) of nucleotide base and O (C=O) of Thr1008 carboxyl group
	Arg1009	Arg9	G3	2.5		N2 (C2 NH2) of nucleotide base and O (C=O) of Arg1009 carboxyl group
	Arg1010	Arg10	G3	3.6		N2 (C2 NH2) of nucleotide base and O (C=O) of Arg1010 carboxyl group
	Thr1089	Thr89	G56	2.9		O3' (C3 OH) within sugar group within phosphodiester bond between A57 (O-) and OG1 (OH) of Thr1089 side chain
	Thr1096	Thr96	A9	3.0		OP1 (P=O) within phosphate backbone and OG1 (HO) of Thr1096 side chain
	Thr1096	Thr96	A9	3.0		OP2 (O-) within phosphate backbone and OG1 (HO) of Thr1096 side chain
	Leu1098	Leu98	A41	2.6		OP1 (P=O) within phosphate backbone and N within peptide bond of Gly1097 (COO-) and Leu1098 (+NH3)
	Asn1100	Asn100	A42	2.6		O3' (C3 OH) within sugar group within phosphodiester bond between G43 (O-) and ND2 (NH2) of Asn1100 side chain
2	Asn1100	Asn100	G43	3.1	1332.657	OP1 (P=O) within phosphate backbone and ND2 (NH2) of Asn1100 side chain
	Thr1094	Thr94	C67	3.3		N4 (C4 NH2) of nucleotide base and O (C=O) of Thr1094 carboxyl group
	Asn1095	Asn95	G51	3.4		O6 (C6 C=O) of nucleotide base and ND2 (NH2) of Asn1095 side chain
	Asn1095	Asn95	C68	3.2		N4 (C4 NH2) of nucleotide base and O (C=O) of Asn1095 carboxyl group
	Asn1095	Asn95	C67	2.6		N4 (C4 NH2) of nucleotide base and O (C=O) of Asn1095 carboxyl group
	Thr1096	Thr96	C67	3.6		N4 (C4 NH2) of nucleotide base and OG1 (OH) of Thr1096 side chain
	Thr1096	Thr96	G56	2.6		O6 (C6 C=O) of nucleotide base and OG1 (OH) of Thr1096 side chain
	Thr1096	Thr96	A57	2.5		N6 (C6 NH2) of nucleotide base and OG1 (OH) of Thr1096 side chain
	Thr1096	Thr96	T66	3.0		O4 (C4 C=O) of nucleotide base and OG1 (OH) of Thr1096 side chain
	Asn1100	Asn100	G56	3.4		O5' (O) within phosphate backbone and ND2 (NH2) of Asn1100 side chain
	Asn1100	Asn100	A57	2.1		OP2 (O-) within phosphate backbone and ND2 (NH2) of Asn1100 side chain
	Asn1100	Asn100	C59	3.5		N4 (C4 NH2) of nucleotide base and O (C=O) of Asn1100 carboxyl group
	3	Arg1003	Arg3	A33		3.1
Thr1008		Thr8	C56	3.2	OP2 (O-) within phosphate backbone and OG1 (OH) of Thr1008 side chain	
Arg1009		Arg9	G35	2.9	N7 (N) of nucleotide base and NH2 (NH2) of Arg1009 side chain	
Arg1009		Arg9	G35	2.6	OP2 (O-) within phosphate backbone and NH1 (+NH2) of Arg1009 side chain	
Arg1009		Arg9	G35	3.2	O5' (O) within phosphate backbone and NH1 (+NH2) of Arg1009 side chain	
Asn1095		Asn95	G10	2.1	OP2 (O-) within phosphate backbone and ND2 (NH2) of Asn1095 side chain	

**Table 32: ZDOCK scores, and polar contacts between HPV-18 E6 protein and HPV-18 E6 sequence 2720 aptamer candidate-experiment one**

Complex	Amino acid residue	Actual amino acid residue	Nucleotide	Polar contact length and average (Å)	ZDOCK score	Polar contact information
1	Tyr1012	Tyr12	C69	3.4	1389.297	O3' (C3 OH) within sugar group within phosphodiester bond between G70 (O-) and OH (OH) of Tyr1012 side chain
	Ser1082	Ser82	T31	3.1		OP2 (O-) within phosphate backbone and OG (OH) of Ser1082 side chain
	Thr1096	Thr96	A65	3.3		O3' (C3 OH) within sugar group within phosphodiester bond between T66 (O-), and OG1 (OH) of Thr1096 side chain
	Thr1096	Thr96	T66	2.7		OP1 (P=O) within phosphate backbone and OG1 (OH) of Thr1096 side chain
	Asn1100	Asn100	G63	2.8		N2 (C2 NH2) of nucleotide base and OD1 (C=O) of Asn1100 side chain
	Leu1102	Leu102	T66	2.5		O4' (O between C1 and C4) within sugar group and N within peptide bond between Leu1101 (COO-) and Leu1102 (+NH3)
	Lys1110	Lys110	A44	2.7		OP1 (P=O) within phosphate backbone and NZ (+NH3) of Lys1110 side chain
	Tyr1134	Tyr134	T31	3.4		OP1 (P=O) within phosphate backbone and OH (OH) of Tyr1134 side chain
2	Thr1008	Thr8	G36	3.5	1378.423	N2 (C2 NH2) of nucleotide base and OG1 (OH) of Thr1008 side chain
	Ser1024	Ser24	T14	2.9		OP1 (P=O) within phosphate backbone and OG (OH) of Ser1024 side chain
	Leu1093	Leu93	G63	3.5		N2 (C2 NH2) of nucleotide base and O (C=O) of Leu1093 carboxyl group
	Asn1095	Asn95	A43	3.2		O4' (O between C1 and C4) within sugar group and N within peptide bond between Thr1094 (COO-) and Asn1095 (+NH3)
	Tyr1099	Tyr99	T30	3.1		O3' (O) within phosphate backbone within phosphodiester bond between T31 (O-) and OH (OH) of Tyr1099 side chain
	Tyr1099	Tyr99	T31	1.9		OP2 (O-) within phosphate backbone and OH (OH) of Tyr1099 side chain
	Tyr1099	Tyr99	T31	2.8		O5' (O-) within phosphate backbone and OH (OH) of Tyr1099 side chain
	Lys1117	Lys117	T32	3.0		OP2 (O-) within phosphate backbone and NZ (+NH3) of Lys1117 side chain
3	Phe1071	Phe71	C20	2.7	1359.978	O3' (C3' OH) within sugar group within phosphodiester bond between A21 (O-) and N of Phe1071 amine group
	Tyr1072	Tyr72	C20	2.2		N3 (N) of nucleotide base and OH (OH) of Tyr1072 side chain
	Tyr1072	Tyr72	C20	2.5		N4 (C4 NH2) of nucleotide base and OH (OH) of Tyr1072 side chain
	Arg1074	Arg74	A21	3.3		OP1 (P=O) within phosphate backbone and NE (NH) of Arg1074 side chain
	Arg1079	Arg79	T14	2.7		O4 (C4 C=O) of nucleotide base and NH1 (+NH2) of Arg1079 side chain
	His1080	His80	T14	3.1		OP1 (P=O) within phosphate backbone and NE2 (+NH) of His1080 side chain
	Tyr1081	Tyr81	C13	3.0		OP1 (P=O) within phosphate backbone and N within peptide bond between His1080 (COO-) and Tyr1081 (+NH3)
	Arg1107	Arg107	A35	2.3		N1 (N) of nucleotide base and NH2 (NH2) of Arg1107 side chain
	Arg1107	Arg107	A35	2.9		N3 (N) of nucleotide base and NH1 (+NH2) of Arg1107 side chain
	Cys1141	Cys141	G36	3.2		N2 (C2 NH2) of nucleotide base and O (C=O) of Cys1141 carboxyl group
	Asn1143	Asn143	G36	2.2		N2 (C2 NH2) of nucleotide base and O (C=O) of Asn1143 carboxyl group

**Table 33: ZDOCK scores, and polar contacts between HPV-18 E6 protein and HPV-18 E6 sequence 2720 aptamer candidate-experiment two**

Complex	Amino acid residue	Actual amino acid residue	Nucleotide	Polar contact length and average (Å)	ZDOCK score	Polar contact information
1	Thr1008	Thr8	G36	3.5	1425.395	N2 (C2 NH2) of nucleotide base and OG1 (OH) of Thr1008 side chain
	Ser1024	Ser24	T14	2.9		OP1 (P=O) within phosphate backbone and OG (OH) of Ser1024 side chain
	Leu1093	Leu93	G63	3.5		N2 (C2 NH2) of nucleotide base and O (C=O) of Leu1093 carboxyl group
	Asn1095	Asn95	A43	3.2		O4' (O between C1 and C4) within sugar group and N within peptide bond between Thr1094 (COO-) and Asn1095 (+NH3)
	Tyr1099	Tyr99	T30	3.1		O3' (C3 OH) within sugar group within phosphodiester bond between T31 (O-) and OH (OH) of Tyr1099 side chain
	Tyr1099	Tyr99	T31	1.9		OP2 (O-) within phosphate backbone and OH (OH) of Tyr1099 side chain
	Tyr1099	Tyr99	T31	2.8		O5' (O) within phosphate backbone and OH (OH) of Tyr1099 side chain
2	Lys1117	Lys117	T32	3.0	1332.035	OP2 (O-) within phosphate backbone and NZ (+NH3) of Tyr1117 side chain
	Val1054	Val54	G19	1.9		N2 (C2 NH2) of nucleotide base and O (C=O) of Val1054 carboxyl group
	Asn1095	Asn95	G10	2.9		OP1 (P=O) within phosphate backbone and N within peptide bond between Thr1094 (COO-) and Asn1095 (+NH3)
	Asn1100	Asn100	A35	3.1		N6 (C6 NH2) of nucleotide base and OD1 (C=O) of Asn1100 carboxyl group
3	His1133	His133	G23	3.5	1173.236	O4' (O between C1 and C4) within sugar group and NE2 (+NH) of His133 side chain
	Lys1013	Lys13	C61	3.5		O3' (C3 OH) within sugar group within phosphodiester bond between A62 (O-) and NZ (+NH3) of Lys1013 side chain
	Lys1013	Lys13	A62	2.4		OP1 (P=O) within phosphate backbone and NZ (+NH3) of Lys1013 side chain
	Asp1016	Asp16	T60	2.6		N3 (N) of nucleotide base and OD2 (O-) of Asp1016 side chain
	Thr1096	Thr96	A45	3.4		O3' (C3 OH) within sugar group within phosphodiester bond between C46 (O-) and OG1 (OH) of Thr1096 side chain
	Asn1113	Asn113	G64	2.9	O6 (C6 C=O) of nucleotide base and ND2 (NH2) of Asn1113 side chain	



**Table 34: ZDOCK scores, and polar contacts between HPV-18 E6 protein and HPV-18 E6 sequence 10017 aptamer candidate-experiment one**

Complex	Amino acid residue	Actual amino acid residue	Nucleotide	Polar contact length and average (Å)	ZDOCK score	Polar contact information	
1	Pro1007	Pro7	C52	2.9	1446.35	N4 (C4 NH2) of nucleotide base and O (C=O) of Pro1007 carboxyl group	
	Lys1013	Lys13	G56	2.8		N3 (N) of nucleotide base and NZ (+NH3) of Lys1013 side chain	
	Ser1024	Ser24	A34	3.3		N6 (C6 NH2) of nucleotide base and OG (OH) of Ser1024 side chain	
	Asp1051	Asp51	G56	2.1		N2 (C2 NH2) of nucleotide base and OD2 (O-) of Asp1051 side chain	
	Thr1096	Thr96	C48	3.1		OP2 (O-) within phosphate backbone and OG1 (OH) of Thr1096 side chain	
	Thr1096	Thr96	T47	3.5		O3' (C3 OH) within sugar group within phosphodiester bond between C48 (O-) and OG1 (OH) of Thr1096 side chain	
	Tyr1099	Tyr99	T60	3.1		O4' (O between C1 and C4) within sugar group and OH (OH) of Tyr1099 side chain	
	Tyr1099	Tyr99	C59	3.5		O3' (C3 OH) within sugar group within phosphodiester bond between T60 (O-) and OH (OH) of Tyr1099 side chain	
	Asn1100	Asn100	G58	2.4		N2 (C2 NH2) of nucleotide base and OD1 (C=O) of Asn1100 side chain	
	Leu1102	Leu102	C48	2.5		O4' (O between C1 and C4) within sugar group and N within peptide bond between Leu1101 (COO-) and Leu1102 (+NH3)	
Leu1102	Leu102	C48	3.5	O5' (O) within phosphate backbone and N within peptide bond between Leu1101 (COO-) and Leu1102 (+NH3)			
Asn1113	Asn113	C59	3.1	OP1 (P=O) within phosphate backbone and ND2 (NH2) of Asn1113 side chain			
2	Tyr1012	Tyr12	A62	2.9	1407.050	OP1 (P=O) within phosphate backbone and N within peptide bond between Pro1011 (COO-) and Leu1012 (+NH3)	
	Tyr1099	Tyr99	A65	2.6		O3' (C3 OH) within sugar group within phosphodiester bond between T66 (O-) and OH (OH) of Tyr1099 side chain	
	Asn1100	Asn100	T35	2.3		O4' (O between C1 and C4) within sugar group and ND2 (NH2) of Asn1100 side chain	
3	Asp1016	Asp16	G29	3.2	-	1358.217	N2 (C2 NH2) and OD2 (O-) of Asp1016 side chain

**Table 35: ZDOCK scores, and polar contacts between HPV-18 E6 protein and HPV-18 E6 sequence 10017 aptamer candidate-experiment two**

Complex	Amino acid residue	Actual amino acid residue	Nucleotide	Polar contact length and average (Å)		ZDOCK score	Polar contact information
1	Lys1013	Lys13	C41	3.1	3.00	1293.622	O3' (C3 OH) within sugar group within phosphodiester bond between T42 (O-) and NZ (+NH3) of Lys1013 side chain
	Asn1095	Asn95	C48	3.0			O3' (C3 OH) within sugar group within phosphodiester bond between C49 (O-) and ND2 (NH2) of Asn1095 side chain
	Tyr1099	Tyr99	T38	1.9			O2 (C2 C=O) of nucleotide base and OH (OH) of Tyr1099 side chain
	Asn1100	Asn100	G58	2.7			OP1 (P=O) within phosphate backbone and ND2 (NH2) of Asn1100 side chain
	Ile1103	Ile103	G40	3.2			OP2 (O-) within phosphate backbone and N within peptide bond between Leu1102 (COO-) and Ile1103 (+NH3)
	Pro1111	Pro111	A34	3.2			N6 (C6 NH2) of nucleotide base and O (C=O) of Pro1111 carboxyl group
	Ala1131	Ala131	A54	2.6			N6 (C6 NH2) of nucleotide base and O (C=O) of Ala1131 carboxyl group
	Ala1131	Ala131	G53	3.2			N2 (C2 NH2) of nucleotide base and O (C=O) of Ala1131 carboxyl group
2	Lys1013	Lys13	G63	3.0	2.94	1281.251	OP1 (P=O) within phosphate backbone and NZ (+NH3) of Lys1013 side chain
	Ser1024	Ser24	C8	3.4			N3 (N) of nucleotide base and OG (OH) of Ser1024 side chain
	Ser1024	Ser24	C8	2.7			N4 (C4 NH2) of nucleotide base and OG (OH) of Ser1024 side chain
	Ser1024	Ser24	T7	3.2			O4 (C4 C=O) of nucleotide base and OG (OH) of Ser1024 side chain
	Gln1026	Gln26	C8	3.3			N4 (C4 NH2) of nucleotide base and OE1 (C=O) of Gln1026 side chain
	Tyr1099	Tyr99	C67	2.7			O2 (C2 C=O) of nucleotide base and OH (OH) of Tyr1099 side chain
	Asn1100	Asn100	T35	2.3			O4' (O between C1 and C4) within sugar group and ND2 (NH2) of Asn1100 side chain
	His1133	His133	G43	1.9			O4' (O between C1 and C4) within sugar group and NE (+NH) of His1133 side chain
3	Arg1003	Arg3	T18	3.0	2.97	1083.764	OP1 (P=O) within phosphate backbone and NH2 (NH2) of Arg1003 side chain
	Tyr1012	Tyr12	C69	3.3			OP2 (P=O) within phosphate backbone and OH (OH) of Tyr1012 side chain
	Asp1016	Asp16	C67	2.2			N4 (C4 NH2) of nucleotide base and OD2 (O-) of Asp1016 side chain
	Asp1016	Asp16	T33	3.2			N3 (N) of nucleotide base and OD1 (C=O) of Asp1016 side chain
	Ser1059	Ser59	G70	3.4			N1 (NH) of nucleotide base and OG (OH) of Ser1059 side chain
	Asn1095	Asn95	G10	2.1			N2 (C2 NH2) of nucleotide base and O (C=O) of Asn1095 carboxyl group
	Thr1096	Thr96	G10	3.2			N2 (C2 NH2) of nucleotide base and OG1 (OH) of Thr1096 side chain
	Thr1096	Thr96	A11	1.9			O4' (O between C1' and C4') within sugar group and OG1 (OH) of Thr1096 side chain
	Tyr1099	Tyr99	G64	3.2			O6 (C6 C=O) of nucleotide base and OH (OH) of Tyr1099 side chain
	Tyr1099	Tyr99	G63	2.2			N7 (N) of nucleotide base and OH (OH) of Tyr1099 side chain
	Leu1102	Leu102	A11	3.0			OP1 (P=O) within phosphate backbone and N within peptide bond between Leu1101 (COO-) and Leu1102 (+NH3)
	Lys1117	Lys117	G64	1.9			OP2 (O-) within phosphate backbone and NZ (+NH3) of Lys1117 side chain

**Appendix 19: ZDOCK outputs and polar contacts between HPV-18 E7 and the control ligand 4TS2, natural ligand pRb, and HPV-18 E7 aptamer candidates**

**Table 36: ZDOCK score, and polar contacts between HPV-18 E7 protein and the control ligand 4TS2**

Complex	Amino acid residue	Nucleotide	Polar contact length and average (Å)		ZDOCK score	Polar contact information
1	Glu55	U59	3.3	3.08	1344.035	O2' (C2 OH) within sugar group and OE2 (O-) of Glu55 side chain
	Arg58	U59	3.5			OP2 (O-) within phosphate backbone and NH2 (NH2) of Arg58 side chain
	Lys67	A16	3.5			O2' (C2 OH) within sugar group and O (C=O) of Lys67 carboxyl group
	Thr93	G76	3.2			O3' (C3 OH) within sugar group within phosphodiester bond between C77 and OG1 (OH) of Thr93 side chain
	Ser95	A75	2.1			O2' (C2 OH) within sugar group and N within peptide bond between Leu94 (COO-) and Ser95 (+NH3)
	Ser95	A75	2.6			O2' (C2 OH) within sugar group and O (C=O) of Ser95 carboxyl group
	Val97	G74	2.1			O2' (C2 OH) within sugar group and N within peptide bond between Phe96 (COO-) and Val97 (+NH3)
	Val97	G74	2.4			O2' (C2 OH) within sugar group and O (C=O) of Val97 carboxyl group

**Table 37: ZDOCK score, and polar contacts between HPV-18 E7 protein and the natural ligand pRb**

Complex	Amino acid residue	Ligand amino acid residue	Polar contact length and average (Å)		ZDOCK score	Polar contact information
1	Ser95	Gln444	3.0	3.07	1073.481	O (C=O) of Ser95 carboxyl group and NE2 (NH2) of Gln444 side chain
	Trp100	Thr502	3.3			NE1 (NH) of Trp100 side chain and OG1 (OH) of Thr502 side chain
	Ser102	Tyr498	2.9			OG (OH) of Ser102 side chain and O (C=O) of Tyr498 carboxyl group

**Table 38: ZDOCK scores, and polar contacts between HPV-18 E7 protein and HPV-18 E7 sequence 820 aptamer candidate-experiment one**

Complex	Amino acid residue	Nucleotide	Polar contact length and average (Å)	ZDOCK score	Polar contact information	
1	Lys67	T28	2.9	1399.341	O4' (O between C1' and C4') and NZ (+NH3) of Lys67 side chain	
	Arg71	C69	3.3		O4' (O between C1' and C4') and NH2 (NH2) of Arg71 side chain	
	Arg84	A65	2.9		N3 (N) of nucleotide base and NH2 (NH2) of Arg84 side chain	
	Arg84	G45	2.2		N3 (N) of nucleotide base and NH2 (NH2) of Arg84 side chain	
	Gln87	T44	3.1		O2 (C2 C=O) of nucleotide base and NE2 (NH2) of Gln87 side chain	
	Gln87	T66	3.1		O2 (C2 C=O) of nucleotide base and NE2 (NH2) of Gln87 side chain	
	Thr93	A11	3.0		N3 (N) of nucleotide base and OG1 (OH) of Thr93 side chain	
2	Arg58	G58	2.7	1379.164	OP1 (P=O) within phosphate backbone and N within peptide bond between Gln57 (COO-) and Arg58 (+NH3)	
	Arg58	G58	3.3		OP2 (O-) within phosphate backbone and NH2 (NH2) of Arg58 side chain	
	Ser78	G43	3.0		OP1 (P=O) within phosphate backbone and OG (OH) of Ser78 side chain	
	Thr93	C69	2.1		O3' (C3 OH) within sugar group within phosphodiester bond between G70 (O-) and OG1 (OH) of Thr93 side chain	
	Ser95	C68	3.4		O3' (C3 OH) within sugar group within phosphodiester bond between C69 (O-) and N within peptide bond between Leu94 (COO-) and Ser95 (+NH3)	
	Trp100	A11	3.2		N6 (C6 NH2) of nucleotide base and O (C=O) of Trp100 carboxyl group	
3	Glu77	G63	3.2	-	1335.645	OP1 (P=O) within phosphate backbone and N within peptide bond between Val76 (COO-) and Glu77 (+NH3)

**Table 39: ZDOCK scores, and polar contacts between HPV-18 E7 protein and HPV-18 E7 sequence 820 aptamer candidate-experiment two**

Complex	Amino acid residue	Nucleotide	Polar contact length and average (Å)	ZDOCK score	Polar contact information	
1	Lys67	T28	2.9	1399.341	O4' (O between C1' and C4') and NZ (+NH3) of Lys67 side chain	
	Arg71	C69	3.3		O4' (O between C1' and C4') and NH2 (NH2) of Arg71 side chain	
	Arg84	A65	2.9		N3 (N) of nucleotide base and NH2 (NH2) of Arg84 side chain	
	Arg84	G45	2.2		N3 (N) of nucleotide base and NH2 (NH2) of Arg84 side chain	
	Gln87	T44	3.1		O2 (C2 C=O) of nucleotide base and NE2 (NH2) of Gln87 side chain	
	Gln87	T66	3.1		O2 (C2 C=O) of nucleotide base and NE2 (NH2) of Gln87 side chain	
	Thr93	A11	3.0		N3 (N) of nucleotide base and OG1 (OH) of Thr93 side chain	
2	Arg58	G58	2.7	1379.164	OP1 (P=O) within phosphate backbone and N within peptide bond between Gln57 (COO-) and Arg58 (+NH3)	
	Arg58	G58	3.3		OP2 (O-) within phosphate backbone and NH2 (NH2) of Arg58 side chain	
	Ser78	G43	3.0		OP1 (P=O) within phosphate backbone and OG (OH) of Ser78 side chain	
	Thr93	C69	2.1		O3' (C3 OH) within sugar group within phosphodiester bond between G70 (O-) and OG1 (OH) of Thr93 side chain	
	Ser95	C68	3.4		O3' (C3 OH) within sugar group within phosphodiester bond between C69 (O-) and N within peptide bond between Leu94 (COO-) and Ser95 (+NH3)	
	Trp100	A11	3.2		N6 (C6 NH2) of nucleotide base and O (C=O) of Trp100 carboxyl group	
3	Glu77	G63	3.2	-	1335.645	OP1 (P=O) within phosphate backbone and N within peptide bond between Val76 (COO-) and Glu77 (+NH3)

**Table 40: ZDOCK scores, and polar contacts between HPV-18 E7 protein and HPV-18 E7 sequence 392 aptamer candidate-experiment one**

Complex	Amino acid residue	Nucleotide	Polar contact length and average (Å)	ZDOCK score	Polar contact information
1	Met64	A9	3.4	1634.326	O4' (O between C1' and C4') within sugar group and N within peptide bond between Cys63 (COO-) and Met64 (+NH3)
	Gln87	C8	3.2		OP2 (O-) within phosphate backbone and NE2 (NH2) of Gln87 side chain
	Cys101	G44	3.3		N2 (C2 NH2) of nucleotide base and O (C=O) of Cys101 carboxyl group
2	Arg58	A11	3.1	1542.659	OP2 (O-) within phosphate backbone and NH2 (NH2) of Arg58 side chain
	Arg58	A9	3.5		N6 (C6 NH2) of nucleotide base and O (C=O) of Arg58 carboxyl group
	Arg58	A9	3.8		N6 (C6 NH2) of nucleotide base and C (C=O) within peptide bond of Arg58 (COO-) and His59 (+NH3)
	Thr60	A9	3.0		N1 (N) of nucleotide base and OG1 (OH) of Thr60 side chain
	Thr60	A9	3.2		N6 (C6 NH2) of nucleotide base and OG1 (OH) of Thr60 side chain
	Thr60	G64	3.1		O4' (O between C1' and C4') within sugar group and OG1 (OH) of Thr60 side chain
	Leu62	G64	2.6		OP1 (P=O) within phosphate backbone and N within peptide bond between Met61 (COO-) and Leu62 (+NH3)
	Arg71	A57	3.4		N1 (N) of nucleotide base and N within peptide bond between Ala70 (COO-) and Arg71 (+NH3)
	Arg71	C59	3.4		O2 (C2 C=O) of nucleotide base and NH1 (+NH2) of Arg71 side chain
	Val75	G33	3.2		OP1 (P=O) within phosphate backbone and N within peptide bond between Leu74 (COO-) and Val75 (+NH3)
	Gln87	G63	2.2		OP1 (P=O) within phosphate backbone and NE2 (NH2) of Gln87 side chain
3	Lys67	G10	2.5	1465.278	N7 (N) of nucleotide base and NZ (+NH3) of Lys67 side chain
	Lys67	G64	3.4		N2 (C2 NH2) of nucleotide base and O (C=O) Lys67 carboxyl group
	Val75	C46	2.5		N4 (C4 NH2) of nucleotide base and O (C=O) of Val75 carboxyl group
	Ser95	G10	3.3		O4' (O between C1 and C4) within sugar group and OG (OH) of Ser95 side chain
	Pro99	G47	2.0		N1 (NH2) of nucleotide base and O (C=O) of Pro99 side chain

**Table 41: ZDOCK scores, and polar contacts between HPV-18 E7 protein and HPV-18 E7 sequence 392 aptamer candidate-experiment two**

Complex	Amino acid residue	Nucleotide	Polar contact length and average (Å)		ZDOCK score	Polar contact information
1	Met64	A9	3.4	3.30	1634.325	O4' (O between C1' and C4') within sugar group and N within peptide bond between Cys63 (COO-) and Met64 (+NH3)
	Gln87	C8	3.2			OP2 (O-) within phosphate backbone and NE2 (NH2) of Gln87 side chain
	Cys101	G44	3.3			N2 (C2 NH2) of nucleotide base and O (C=O) of Cys101 carboxyl group
2	Lys67	G10	2.5	2.93	1465.278	N7 (N) of nucleotide base and NZ (+NH3) of Lys67 side chain
	Lys67	G64	3.4			N2 (C2 NH2) of nucleotide base and O (C=O) of Lys67 carboxyl group
	Val75	C46	2.5			N4 (C4 NH2) of nucleotide base and O (C=O) of Val75 carboxyl group
	Ser95	G10	3.3			O4' (O between C1' and C4') within sugar group and OG (OH) of Ser95 side chain
	Pro99	G47	2.0			N1 (HN) of nucleotide base and O (C=O) of Pro99 carboxyl group
3	Leu62	G64	3.1	3.23	1411.166	N2 (C2 NH2) of nucleotide base and O (C=O) of Leu62 carboxyl group
	Met64	A9	3.5			O4' (O between C1' and C4') within sugar group and N within peptide bond between Cys63 (COO-) and Met64 (+NH3)
	Glu69	G10	3.5			N1 (NH) of nucleotide base and OE2 (O-) of Glu69 side chain
	Gln87	T7	2.0			OP1 (P=O) within phosphate backbone and NE2 (NH2) of Gln87 side chain
	Gln87	T7	3.4			O3' (C3 OH) within sugar group within phosphodiester bond between C8 (O-) and NE2 (NH2) of Gln87 side chain
	Cys101	G44	3.6			N2 (C2 NH2) of nucleotide base and O (C=O) of Cys101 carboxyl group
	Ser103	G44	2.3			N2 (C2 NH2) of nucleotide base and O (C=O) of Ser103 carboxyl group

**Table 42: ZDOCK scores, and polar contacts between HPV-18 E7 protein and HPV-18 E7 sequence 5772 aptamer candidate-experiment one**

Complex	Amino acid residue	Nucleotide	Polar contact length and average (Å)	ZDOCK score	Polar contact information	
1	Lys67	G40	3.4	2.87	1436.474	O5' (O) within phosphate backbone and NZ (+NH3) of Lys67 side chain
	Glu69	G39	2.8			OP2 (O-) within phosphate backbone and N within peptide bond between Cys68 (COO-) and Glu69 (+NH3)
	Arg71	G37	2.1			OP2 (O-) within phosphate backbone and NH1 (+NH2) of Arg71 side chain
	Arg71	A36	2.2			O3' (C3 OH) within sugar group within phosphodiester bond between G37 (O-) and NH1 (+NH2) of Arg71 side chain
	Thr93	C69	2.7			OP2 (O-) within phosphate backbone and OG1 (OH) of Thr93 side chain
	Thr93	C68	3.1			N4 (C4 NH2) of nucleotide base and O (C=O) of Thr93 carboxyl group
	Ser95	C69	3.0			N4 (C4 NH2) of nucleotide base and OG (OH) of Ser95 side chain
	Ser95	T38	3.1			O4 (C4 C=O) of nucleotide base and OG (OH) of Ser95 side chain
	Ser95	G39	2.1			O6 (C6 C=O) of nucleotide base and OG (OH) of Ser95 side chain
	Ser95	C66	3.1			N4 (C4 NH2) of nucleotide base and O (C=O) of Ser95 carboxyl group
	Ser95	C67	2.4			N4 (C4 NH2) of nucleotide base and O (C=O) of Ser95 carboxyl group
	Val97	T66	2.7			O4 (C4 C=O) of nucleotide base and N within peptide bond between Phe96 (COO-) and Val97 (+NH3)
	Trp100	G63	3.2			OP2 (O-) within phosphate backbone and N within peptide bond between Pro99 (COO-) and Trp100 (+NH3)
	Trp100	C61	3.3			O5' (O) within phosphate backbone and NE1 (NH) of Trp100 side chain
	Ala102	C44	2.5			N4 (C4 NH2) of nucleotide base and O (C=O) of Ala102 carboxyl group
2	Ser103	A62	2.6	2.82	1302.250	N6 (C6 NH2) of nucleotide base and OG (OH) of Ser103 side chain
	Ser103	A62	3.0			N7 (N) of nucleotide group and OG (OH) of Ser103 side chain
	Arg58	C68	3.3			OP2 (O-) within phosphate backbone and NH2 (NH2) of Arg58 side chain
	Leu62	G64	2.7			OP2 (O-) within phosphate backbone and N within peptide bond between Met61 (COO-) and Leu62 (+NH3)
	Arg71	A62	2.2			N7 (N) of nucleotide base and NH1 (+NH2) of Arg71 side chain
3	Arg71	A62	3.3	3.18	1291.008	N7 (N) of nucleotide base and NH2 (NH2) of Arg71 side chain
	Glu73	A41	2.6			N6 (C6 NH2) of nucleotide base and OE2 (O-) of Glu73 side chain
	Leu62	G58	3.5			N7 (N) of nucleotide base and N within peptide bond between Met61 (COO-) and Leu62 (+NH3)
	Met64	A57	3.0			OP2 (O-) within phosphate backbone and N within peptide bond between Cys63 (COO-) and Met64 (+NH3)
3	Val75	C44	3.4	3.18	1291.008	N4 (C4 NH2) of nucleotide base and O (C=O) of Val75 carboxyl group
	Gln87	G58	2.8			O3' (C3 OH) within sugar group within phosphodiester bond C59 (O-) and NE2 (NH2) of Gln87 side chain

**Table 43: ZDOCK scores, and polar contacts between HPV-18 E7 protein and HPV-18 E7 sequence 5772 aptamer candidate-experiment two**

Complex	Amino acid residue	Nucleotide	Polar contact length and average (Å)	ZDOCK score	Polar contact information	
1	Lys67	G40	3.4	2.87	1436.474	OP1 (P=O) within phosphate backbone and N within peptide bond between Ser78 (COO-) and Ser79 (+NH3)
	Glu69	G39	2.8			O3' (C3 OH) within sugar group within phosphodiester bond between T25 (O-) and N within peptide bond between Phe96 (COO-) and Val97 (+NH3)
	Arg71	A36	2.2			OP2 (O-) within phosphate backbone and N within peptide bond between Pro99 (COO-) and Trp100 (+NH3)
	Arg71	G37	2.1			N6 (C6 NH2) of nucleotide base and OG (OH) of Ser103 side chain
	Thr93	C69	2.7			O6 (C6 C=O) of nucleotide base and OG (OH) of Ser103 side chain
	Thr93	C68	3.1			OP1 (P=O) within phosphate backbone and N within peptide bond between Ser78 (COO-) and Ser79 (+NH3)
	Ser95	T38	3.1			O3' (C3 OH) within sugar group within phosphodiester bond between T25 (O-) and N within peptide bond between Phe96 (COO-) and Val97 (+NH3)
	Ser95	C69	3.0			OP2 (O-) within phosphate backbone and N within peptide bond between Pro99 (COO-) and Trp100 (+NH3)
	Ser95	G39	2.1			N6 (C6 NH2) of nucleotide base and OG (OH) of Ser103 side chain
	Ser95	C68	3.1			O6 (C6 C=O) of nucleotide base and OG (OH) of Ser103 side chain
	Ser95	C67	2.4			OP1 (P=O) within phosphate backbone and N within peptide bond between Ser78 (COO-) and Ser79 (+NH3)
	Val97	T66	2.7			O3' (C3 OH) within sugar group within phosphodiester bond between T25 (O-) and N within peptide bond between Phe96 (COO-) and Val97 (+NH3)
	Trp100	C61	3.3			OP2 (O-) within phosphate backbone and N within peptide bond between Pro99 (COO-) and Trp100 (+NH3)
	Trp100	G63	3.2			N6 (C6 NH2) of nucleotide base and OG (OH) of Ser103 side chain
	Ala102	C44	2.5			O6 (C6 C=O) of nucleotide base and OG (OH) of Ser103 side chain
	2	Ser79	C15			3.4
Val97		C24	2.6	O3' (C3 OH) within sugar group within phosphodiester bond between T25 (O-) and N within peptide bond between Phe96 (COO-) and Val97 (+NH3)		
Trp100		G3	3.2	OP2 (O-) within phosphate backbone and N within peptide bond between Pro99 (COO-) and Trp100 (+NH3)		
Ser103		A4	2.3	N6 (C6 NH2) of nucleotide base and OG (OH) of Ser103 side chain		
Ser103		G3	3.4	O6 (C6 C=O) of nucleotide base and OG (OH) of Ser103 side chain		
3	Val75	A21	3.3	3.25	1281.106	OP1 (P=O) within phosphate backbone and N within peptide bond between Ser78 (COO-) and Ser79 (+NH3)
	Glu77	A5	3.2			O3' (C3 OH) within sugar group within phosphodiester bond between G22 (O-) and N within peptide bond between Leu74 (COO-) and Val75 (+NH3)
						OP1 (P=O) within phosphate group and N within peptide bond between Val76 (COO-) and Glu77 (+NH3)



## Appendix 20: Final HPV aptamer candidates and observed polar contacts

**Table 44: ZDOCK scores, and observed polar contacts between HPV-16 E2 protein and HPV-16 E2 sequence 324 aptamer candidate**

Complex	Amino acid residue	Actual amino acid residue	Nucleotide	Polar contact length and average (Å)	ZDOCK score	Polar contact information	Additional information	
<b>1</b>	Tyr301	Tyr303	A24	2.3	<b>2.70</b> 1577.154	N3 (N) of nucleotide base and OH (OH) of Tyr301 side chain	Protein side-chain-DNA base edge interaction. A N3 acts as H-bond acceptor and Tyr OH acts as H-bond donor. O-H...N H-bond	
	Tyr301	Tyr303	G25	2.4		O4' (O between C1' and C4') within sugar group and OH (OH) of Tyr301 side chain	Protein side chain-DNA backbone interaction. G O4' acts as H-bond acceptor and Tyr OH acts as H-bond donor. G O4' has lone electron pair that can form a H-bond. O-H...O H-bond	
	Tyr310	Tyr312	G55	2.2		O3' (C3' OH) within sugar group within phosphodiester bond between G56 (O-) and OH (OH) of Tyr310 side chain	Protein side chain-DNA backbone interaction. G O3' acts as H-bond acceptor and Tyr OH acts as H-bond donor. O-H...O H-bond	
	Ser314	Ser316	C8	3.4		O3' (C3' OH) within sugar group within phosphodiester bond between A9 (O-) and OG (OH) of Ser314 side chain	Protein side chain-DNA backbone interaction. C O3' acts as H-bond acceptor and Ser OH acts as H-bond donor. O-H...O H-bond	
	Trp317	Trp319	C8	2.9		O3' (C3 OH) within sugar group within phosphodiester bond between A9 (O-) and NE1 (NH) of Trp317 side chain	Protein side chain-DNA backbone interaction. C O3' acts as H-bond acceptor and Trp NE1 acts as H-bond donor. N-H...O H-bond	
	Thr332	Thr334	C8	2.4		O3' (C3' OH) within sugar group within phosphodiester bond between A9 (O-) and OG1 (OH) of Thr332 side chain	Protein side chain-DNA backbone interaction. C O3' acts as H-bond acceptor and Thr OG1 acts as H-bond donor. O-H...O H-bond	
	Thr334	Thr336	G10	2.9		OP1 (P=O) within phosphate backbone and OG1 (OH) of Thr334 side chain	Protein side chain-DNA backbone interaction. G OP1 acts as H-bond acceptor and Thr OG1 acts as H-bond donor. O-H...O H-bond	
	Ser362	Ser364	G10	3.1		(C2 NH2) of nucleotide base and O (C=O) of Ser362 carboxyl group	Protein backbone-DNA base edge interaction. G N2 acts as H-bond donor and backbone O of Ser carboxyl group acts as H-bond acceptor. Also, G N2 acts as H-bond donor as seen in Watson-Crick base pairing, with C=O as H-bond acceptor. N-H...O H-bond	
<b>2</b>	Ser357	Ser359	T60	3.5	-	<b>1431.306</b>	OP1 (P=O) within phosphate backbone and OG (OH) of Ser357 side chain	Protein side chain-DNA backbone interaction. T OP1 acts as H-bond acceptor and Ser OG1 act as H-bond donor. O-H...O H-bond
<b>3</b>	Val313	Val315	C20	2.8	<b>3.28</b>	<b>1426.811</b>	N4 (C4 NH2) of nucleotide base and O (C=O) of Val313 carboxyl group	Protein backbone-DNA base edge interaction. C N4 acts as H-bond donor and backbone O of Val carboxyl group acts as H-bond acceptor. Also, C N4 acts as H-bond donor as seen in Watson-Crick base pairing, with C=O as H-bond acceptor. Val can only participate in H-bonds only through backbone atoms. N-H...O H-bond

	Thr332	Thr334	G48	3.4		O3' (C3' OH) within sugar group within phosphodiester bond between C49 (O-) and OG1 (OH) of Thr332 side chain	Protein side chain-DNA backbone interaction. G O3' acts as H-bond acceptor and Thr OG1 acts as H-bond donor. O-H...O H-bond
	Phe360	Phe362	T31	3.3		O2 (C2 C=O) of nucleotide base and N within peptide bond between Gly359 (COO-) and Phe360 (+NH3)	Protein backbone-DNA base edge interaction. T O2 acts as H-bond acceptor and backbone N of Phe amide group acts as H-bond donor. N-H...O H-bond
	Phe360	Phe362	T31	3.6		N3 (NH) of nucleotide base and O (C=O) of Phe360 carboxyl group	Protein backbone-DNA base edge interaction. T N3 acts as H-bond donor as seen in Watson-Crick base pairing with backbone O of Phe carboxyl group as H-bond acceptor. N-H...O H-bond

**Table 45: ZDOCK scores, and observed polar contacts between HPV-16 E6 protein and HPV-16 E7-E6 sequence 3271 aptamer candidate**

Complex	Amino acid residue	Actual amino acid residue	Nucleotide	Polar contact length and average (Å)	ZDOCK score	Polar contact information	Additional information
1	Gln6	Gln13	T48	3.4	2.9	O2 (C2 C=O) of nucleotide base and NE2 (NH2) of Gln6 side chain	Protein side-chain-DNA base edge interaction. T O2 acts as H-bond acceptor and Gln NE2 acts as H-bond donor. N-H...O H-bond
	Gln6	Gln13	A54	3.4		N3 (N) of nucleotide base and NE2 (NH2) of Gln6 side chain	Protein side-chain-DNA base edge interaction. A N3 acts as H-bond acceptor and Gln NE2 acts as H-bond donor. N-H...N H-bond
	Ser80	Ser87	C8	2.9		O2 (C2 C=O) of nucleotide base and OG (OH) of Ser80 side chain	Protein side-chain-DNA base edge interaction. C O2 acts as H-bond acceptor and Ser OG acts as H-bond donor. O-H...O H-bond
	Tyr81	Tyr88	A9	2.5		N1 (N) of nucleotide base and OH (OH) of Tyr81 side chain	Protein side-chain-DNA base edge interaction. A N1 acts as H-bond acceptor as seen in Watson-Crick base pairing, with Tyr OH as H-bond donor. O-H...N H-bond
	Tyr84	Tyr91	G3	2.4		OP2 (O-) within phosphate backbone and OH (OH) of Tyr84 side chain	Protein side chain-DNA backbone interaction. G OP2 acts as H-bond acceptor and Tyr OH acts as H-bond donor. O-H...O H-bond
	Tyr84	Tyr91	G2	2.5		O5' (O) within phosphate backbone and OH (OH) of Tyr84 side chain	Protein side chain-DNA backbone interaction. G O5' acts as H-bond acceptor and Tyr OH acts as H-bond donor. O-H...O H-bond
	Tyr92	Tyr99	G10	2.0		N3 (N) of nucleotide base and OH (OH) of Tyr92 side chain	Protein side-chain-DNA base edge interaction. G N3 acts as H-bond acceptor and Tyr OH acts as H-bond donor. O-H...N H-bond
	Asn93	Asn100	T12	2.5		O3' (C3' OH) within sugar group within phosphodiester bond between C13 (O-) and ND2 (NH2) of Asn93 side chain	Protein side chain-DNA backbone interaction. T O3' acts as H-bond acceptor and Asn ND2 acts as H-bond donor. N-H...O H-bond
	Lys94	Lys101	A11	3.3		O3' (C3' OH) within sugar group within phosphodiester bond between T12 (O-) and NZ (+NH3) of Lys94 side chain	Protein side chain-DNA backbone interaction. A O3' acts as H-bond acceptor and Lys NZ acts as H-bond donor. N-H...O H-bond
	Arg124	Arg131	G2	2.9		O6 (C6 C=O) of nucleotide base and NH2 (NH2) of Arg124 side chain	Protein side-chain-DNA base edge interaction. G O6 acts as H-bond acceptor and Arg NH2 acts as H-bond donor. Also, G O6 acts as H-bond acceptor as seen in Watson-Crick base pairing, with NH2 as H-bond donor. N-H...O H-bond. Arg contains multiple NH groups that have the potential of forming H-bonds
	Arg124	Arg131	G2	3.1		OP2 (O-) within phosphate backbone and N within peptide bond between Gln123 (COO-) and Arg124 (+NH3)	Protein backbone-DNA backbone interaction. G OP2 acts as H-bond acceptor and backbone N of Arg amide group acts as H-bond donor. N-H...O H-bond
Asn127	Asn134	A9	3.4	N3 (N) of nucleotide base and ND2 (NH2) of Asn127 side chain	Protein side-chain-DNA base edge interaction. A N3 acts as H-bond acceptor and Asn ND2 acts as H-bond donor. N-H...N H-bond		

	Glu148	Glu155	G3	2.2			N1 (NH) of nucleotide base and OE1 (C=O) of Glu148 side chain	Protein side-chain-DNA base edge interaction. A N1 acts as H-bond donor as seen in Watson-Crick base pairing, with backbone O of Glu carboxyl group as H-bond acceptor. N-H...O H-bond
	Glu148	Glu155	A4	3.0			N6 (C6 NH2) of nucleotide base and OE1 (C=O) of Glu148 side chain	Protein side-chain-DNA base edge interaction. A N6 acts as H-bond donor and Glu OE1 acts as H-bond acceptor. Also, A N6 acts as H-bond donor as seen in Watson-Crick base pairing, with C=O as H-bond acceptor. N-H...O H-bond
	Glu148	Glu155	A4	3.3			N6 (C6 NH2) of nucleotide base and OE2 (O-) of Glu148 side chain	Protein side-chain-DNA base edge interaction. A N6 acts as H-bond donor and Glu OE2 acts as H-bond acceptor. N-H...O H-bond
2	Gln35	Gln42	T25	3.2	2.97	1333.033	O4 (C4 C=O) of nucleotide base and NE2 (NH2) of Gln35 side chain	Protein side-chain-DNA base edge interaction. T O4 acts as H-bond acceptor and Gln NE2 acts as H-bond donor. Also, T O4 acts as H-bond acceptor as seen in Watson-Crick base pairing, with H2N as H-bond donor. N-H...O H-bond
	Arg55	Arg62	C23	3.3			OP1 (P=O) within phosphate backbone and NE (NH) of Arg55 side chain	Protein side chain-DNA backbone interaction. C OP1 acts as H-bond acceptor and Arg NE acts as H-bond donor. Arg contains multiple NH groups that have the potential of forming hydrogen bonds. N-H...O H-bond.
	Tyr70	Tyr77	G22	2.7			OP2 (O-) within phosphate backbone and OH (OH) of Tyr70 side chain	Protein side chain-DNA backbone interaction. G OP2 acts as H-bond acceptor and Tyr OH acts as H-bond donor. O-H...O H-bond
	Tyr70	Tyr77	A21	3.2			O5' (O) within phosphate backbone and OH (OH) of Tyr70 side chain	Protein side chain-DNA backbone interaction. A O5' acts as H-bond acceptor and Tyr OH acts as H-bond donor. O-H...O H-bond
	Arg77	Arg84	G43	3.0			N2 (C2 NH2) of nucleotide base and O (C=O) of Arg77 carboxyl group	Protein backbone-DNA base edge interaction. G N2 acts as H-bond donor and backbone O of Arg carboxyl group acts as H-bond acceptor. Also, G N2 acts as H-bond donor as seen in Watson-Crick base pairing, with C=O as H-bond acceptor. N-H...O H-bond
	Tyr79	Tyr86	G58	2.4			N2 (C2 NH2) of nucleotide base and O (C=O) of Tyr79 carboxyl group	Protein backbone-DNA base edge interaction. G N2 acts as H-bond donor and backbone O of Tyr carboxyl group acts as H-bond acceptor. Also, G N2 acts as H-bond donor as seen in Watson-Crick base pairing, with C=O as H-bond acceptor. N-H...O H-bond
	Ser80	Ser87	T45	2.8			O4' (O between C1' and C4') within sugar group and OG (OH) of Ser80 side chain	Protein side chain-DNA backbone interaction. T O4' acts as H-bond acceptor and Ser OG acts as H-bond donor. O4' has a lone electron pair that can form a H-bond. O-H...O H-bond
	Arg129	Arg136	C44	2.9			O3' (C3' OH) within sugar group within phosphodiester bond between T45 (O-) and NE (NH) of Arg129 side chain	Protein side chain-DNA backbone interaction. C O3' acts as H-bond acceptor and Arg NE acts as H-bond donor. Arg contains multiple NH groups that have the potential of forming hydrogen bonds. N-H...O H-bond
	Arg129	Arg136	T45	2.8			OP1 (P=O) within phosphate backbone and NE (NH) of Arg129 side chain	Protein side chain-DNA backbone interaction. T OP1 acts as H-bond acceptor and Arg NE acts as H-bond donor.

								Arg contains multiple NH groups that have the potential of forming hydrogen bonds. N-H...O H-bond
	Arg129	Arg136	T45	3.0			OP1 (P=O) within phosphate backbone and NH2 (NH2) of Arg129 side chain	Protein side chain-DNA backbone interaction. T OP1 acts as H-bond acceptor and Arg NH2 acts as H-bond donor. Arg contains multiple NH groups that have the potential of forming hydrogen bonds. N-H...O H-bond
	Thr145	Thr152	A62	2.8			N6 (C6 NH2) of nucleotide base and O (C=O) of Thr145 carboxyl group	Protein backbone-DNA base edge interaction. A N6 acts as H-bond donor and backbone O of Thr carboxyl group acts as H-bond acceptor. Also, A N6 acts as H-bond donor as seen in Watson-Crick base pairing, with C=O as H-bond acceptor. N-H...O H-bond
	Arg146	Arg153	C59	2.9			O2 (C2 C=O) of nucleotide base and NH1 (+NH2) of Arg146 side chain	Protein side-chain-DNA base edge interaction. C O2 acts as H-bond acceptor and Arg NH1 acts as H-bond donor. Arg contains multiple NH groups that have the potential of forming hydrogen bonds. N-H...O H-bond
	Arg147	Arg154	T60	2.1			OP1 (P=O) within phosphate backbone and NH1 (+NH2) of Arg147 side chain	Protein side chain-DNA backbone interaction. T OP1 acts as H-bond acceptor and Arg NH1 acts as H-bond donor. Arg contains multiple NH groups that have the potential of forming hydrogen bonds. N-H...O H-bond
	Arg147	Arg154	C59	3.2			O3' (C3' OH) within sugar group within phosphodiester bond between T60 (O-) and NH1 (+NH2) of Arg147 side chain	Protein side chain-DNA backbone interaction. C O3' acts as H-bond acceptor and Arg NH1 acts as H-bond donor. Arg contains multiple NH groups that have the potential of forming hydrogen bonds. N-H...O H-bond
	Arg147	Arg154	T60	3.1			OP2 (O-) within phosphate backbone and NH1 (+NH2) of Arg147 side chain	Protein side chain-DNA backbone interaction. T OP2 acts as H-bond acceptor and Arg NH1 acts as H-bond donor. Arg contains multiple NH groups that have the potential of forming hydrogen bonds. N-H...O H-bond
	Arg147	Arg154	C59	3.3			OP1 (P=O) within phosphate backbone and NH2 (NH2) of Arg147 side chain	Protein side chain-DNA backbone interaction. C OP1 acts as H-bond acceptor and Arg NH2 acts as H-bond donor. Arg contains multiple NH groups that have the potential of forming hydrogen bonds. N-H...O H-bond
<b>3</b>	Tyr81	Tyr88	C15	2.5	<b>2.99</b>	1331.377	O2 (C2 C=O) of nucleotide base and OH (OH) of Tyr81 side chain	Protein side-chain-DNA base edge interaction. C O2 acts as H-bond acceptor and Tyr OH acts as H-bond donor. O-H...O H-bond
	Tyr92	Tyr99	C15	2.1			O4' (O between C1' and C4') within sugar group and OH (OH) Tyr92 side chain	Protein side chain-DNA backbone interaction. C O4' acts as H-bond acceptor and Tyr OH acts as H-bond donor. O4' has a lone electron pair that can form a H-bond. O-H...O H-bond
	Tyr92	Tyr99	T14	3.4			O3' (C3 OH) within sugar group within phosphodiester bond between C15 (O-) and OH (OH) of Tyr92 side chain	Protein side chain-DNA backbone interaction. T O3' acts as H-bond acceptor and Tyr OH acts as H-bond donor. O-H...O H-bond
	Asn127	Asn134	T14	3.0			O4' (O between C1' and C4') within sugar group and ND2 (NH2) of Asn127 side chain	Protein side chain-DNA backbone interaction. T O4' acts as H-bond acceptor and Asn ND2 acts as H-bond donor. O4' has a lone electron pair that can form a H-bond. N-H...O H-bond
	Asn127	Asn134	T14	3.0			O2 (C2 C=O) of nucleotide base and ND2 (NH2) of Asn127 side chain	Protein side-chain-DNA base edge interaction. T O2 acts as H-bond acceptor and Asn ND2 acts as H-bond donor. N-H...O H-bond

	Ser143	Ser150	A4	3.1		OP2 (O-) within phosphate backbone and OG (OH) of Ser143 side chain	Protein side chain-DNA backbone interaction. A OP2 acts as H-bond acceptor and Ser OG acts as H-bond donor. O-H...O H-bond
	Ser143	Ser150	G3	3.0		O5' (O) within phosphate backbone and OG (OH) of Ser143 side chain	Protein side chain-DNA backbone interaction. G O5' acts as H-bond acceptor and Ser OG acts as H-bond donor. O-H...O H-bond
	Ser143	Ser150	G3	3.3		OP2 (O-) within phosphate backbone and OG (OH) of Ser143 side chain	Protein side chain-DNA backbone interaction. G OP2 acts as H-bond acceptor and Ser OG acts as H-bond donor. O-H...O H-bond
	Arg144	Arg151	G3	2.5		OP2 (O-) within phosphate backbone and N within peptide bond between Ser133 (COO-) and Arg144 (+NH3)	Protein backbone-DNA backbone interaction. G OP2 acts as H-bond acceptor and backbone N of Arg amide group acts as H-bond donor. Arg contains multiple NH groups that have the potential of forming hydrogen bonds. N-H...O H-bond
	Arg147	Arg154	T7	3.1		O4 (C4 C=O) of nucleotide base and NH2 (NH2) of Arg147 side chain	Protein side-chain-DNA base edge interaction. T O4 acts as H-bond acceptor and Arg NH2 acts as H-bond donor. Also, T O4 acts as H-bond acceptor as seen in Watson-Crick pairing, with NH2 as H-bond donor. N-H...O H-bond. Arg contains multiple NH groups that have the potential of forming hydrogen bonds

**Table 46: ZDOCK scores, and observed polar contacts between HPV-18 E6 protein and HPV-18 E6 sequence 2720 aptamer candidate**

Complex	Amino acid residue	Actual amino acid residue	Nucleotide	Polar contact length and average (Å)	ZDOCK score	Polar contact information	Additional information
1	Tyr1012	Tyr12	C69	3.4	2.99 1389.297	O3' (C3 OH) within sugar group within phosphodiester bond between G70 (O-) and OH (OH) of Tyr1012 side chain	Protein side chain-DNA backbone interaction. C O3' acts as H-bond acceptor and Tyr OH acts as H-bond donor. O-H...O H-bond
	Ser1082	Ser82	T31	3.1		OP2 (O-) within phosphate backbone and OG (OH) of Ser1082 side chain	Protein side chain-DNA backbone interaction. T OP2 acts as H-bond acceptor and Ser OG acts as H-bond donor. O-H...O H-bond
	Thr1096	Thr96	A65	3.3		O3' (C3 OH) within sugar group within phosphodiester bond between T66 (O-) and OG1 (OH) of Thr1096 side chain	Protein side chain-DNA backbone interaction. A O3' acts as H-bond acceptor and Thr OG1 acts as H-bond donor. O-H...O H-bond
	Thr1096	Thr96	T66	2.7		OP1 (P=O) within phosphate backbone and OG1 (OH) of Thr1096 side chain	Protein side chain-DNA backbone interaction. T OP1 acts as H-bond acceptor and Thr OG1 acts as H-bond donor. O-H...O H-bond
	Asn1100	Asn100	G63	2.8		N2 (C2 NH2) of nucleotide base and OD1 (C=O) of Asn1100 side chain	Protein backbone-DNA base edge interaction. G N2 acts as H-bond donor and backbone O of Asn acts as H-bond acceptor. Also, G N2 acts as H-bond donor as seen in Watson-Crick base pairing, with backbone O of Asn carboxyl group as H-bond acceptor. N-H...O H-bond
	Leu1102	Leu102	T66	2.5		O4' (O between C1 and C4) within sugar group and N within peptide bond between Leu1101 (COO-) and Leu1102 (+NH3)	Protein backbone-DNA backbone interaction. T O4' acts as H-bond acceptor and backbone N of Leu amide group acts as H-bond donor. O4' has a lone electron pair that can form a H-bond. N-H...O H-bond
	Lys1110	Lys110	A44	2.7		OP1 (P=O) within phosphate backbone and NZ (+NH3) of Lys1110 side chain	Protein side chain-DNA backbone interaction. A OP1 acts as H-bond acceptor and Lys NZ acts as H-bond donor. N-H...O H-bond
	Tyr1134	Tyr134	T31	3.4		OP1 (P=O) within phosphate backbone and OH (OH) of Tyr1134 R side chain	Protein side chain-DNA backbone interaction. T OP1 acts as H-bond acceptor and Tyr OH acts as H-bond donor. O-H...O H-bond
2	Thr1008	Thr8	G36	3.5	3.14 1378.423	N2 (C2 NH2) of nucleotide base and OG1 (OH) of Thr1008 side chain	Protein side-chain-DNA base edge interaction. G N2 acts as H-bond donor and Thr OG1 acts as H-bond acceptor. N-H...O H-bond
	Ser1024	Ser24	T14	2.9		OP1 (P=O) within phosphate backbone and OG (OH) of Ser1024 side chain	Protein side chain-DNA backbone interaction. T OP1 acts as H-bond acceptor and Ser OG acts as H-bond donor. O-H...O H-bond
	Leu1093	Leu93	G63	3.5		N2 (C2 NH2) of nucleotide base and O (C=O) of Leu1093 carboxyl group	Protein backbone-DNA base edge interaction. G N2 acts as H-bond donor and backbone O of Leu carboxyl group acts as H-bond acceptor. Also, G N2 acts as H-bond donor as seen in Watson-Crick base pairing, with backbone O of Leu carboxyl group as H-bond acceptor. N-H...O H-bond

	Asn1095	Asn95	A43	3.2			O4' (O between C1' and C4') within sugar group and N within peptide bond between Thr1094 (COO-) and Asn1095 (+NH3)	Protein backbone-DNA backbone interaction. A O4' acts as H-bond acceptor and backbone N of Asn amide group acts as H-bond donor. O4' has a lone electron pair that can form a H-bond. N-H...O H-bond
	Tyr1099	Tyr99	T30	3.1			O3' (C3 OH) within phosphate backbone within phosphodiester bond between T31 (O-) and OH (OH) of Tyr1099 side chain	Protein side chain-DNA backbone interaction. T O3' acts as H-bond acceptor and Tyr OH acts as H-bond donor. O-H...O H-bond
	Tyr1099	Tyr99	T31	1.9			OP2 (O-) within phosphate backbone and OH (OH) of Tyr1099 side chain	Protein side chain-DNA backbone interaction. T OP2 acts as H-bond acceptor and Tyr OH acts as H-bond donor. O-H...O H-bond
	Tyr1099	Tyr99	T31	2.8			O5' (O-) within phosphate backbone and OH (OH) of Tyr1099 side chain	Protein side chain-DNA backbone interaction. T O5' acts as H-bond acceptor and Tyr OH acts as H-bond donor. O-H...O H-bond
	Lys1117	Lys117	T32	3.0			OP2 (O-) within phosphate backbone and NZ (+NH3) of Lys1117 side chain	Protein side chain-DNA backbone interaction. T OP2 acts as H-bond acceptor and Lys NZ acts as H-bond donor. N-H...O H-bond
3	Phe 1071	Phe 71	C20	2.7	2.74	1359.978	O3' (C3' OH) within sugar group within phosphodiester bond between A21 (O-) and N within peptide bond between Asp1070 (COO-) and Phe1071 (+NH3)	Protein side chain-DNA backbone interaction. C O3' acts as H-bond acceptor and backbone N of Phe amide group acts as H-bond donor. N-H...O H-bond
	Tyr 1072	Tyr 72	C20	2.2			N3 (N) of nucleotide base and OH (OH) of Tyr1072 side chain	Protein side-chain-DNA base edge interaction. C N3 acts as H-bond acceptor as seen in Watson-Crick base pairing. Tyr OH acts as H-bond donor. O-H...N H-bond
	Tyr 1072	Tyr 72	C20	2.5			N4 (C4 NH2) of nucleotide base and OH (OH) of Tyr1072 side chain	Protein side-chain-DNA base edge interaction. C N4 acts as H-bond donor and Tyr OH acts as H-bond acceptor. N-H...O H-bond
	Arg 1074	Arg 74	A21	3.3			OP1 (P=O) within phosphate backbone and NE (NH) of Arg1074 side chain	Protein side chain-DNA backbone interaction. A OP1 acts as H-bond acceptor and Arg NE acts as H-bond donor. Arg contains multiple NH groups that have the potential of forming hydrogen bonds. N-H...O H-bond.
	Arg 1079	Arg 79	T14	2.7			O4 (C4 C=O) of nucleotide base and NH1 (+NH2) of Arg1079 side chain	Protein side-chain-DNA base edge interaction. T O4 acts as H-bond acceptor and Arg NH1 acts as H-bond donor. Arg contains multiple NH groups that have the potential of forming hydrogen bonds. N-H...O H-bond
	His 1080	His 80	T14	3.1			OP1 (P=O) within phosphate backbone and NE2 (+NH) of His1080 side chain	Protein side chain-DNA backbone interaction. T OP1 acts as H-bond acceptor and His NE2 acts as H-bond donor. His R group has a positive charge, allowing it to form electrostatic interactions with the phosphate group of the nucleotide. Also contains multiple N atoms that are involved in hydrogen bonds. N-H...O H-bond
	Tyr 1081	Tyr 81	C13	3.0			OP1 (P=O) within phosphate backbone and N within peptide bond between His1080 (COO-) and Tyr1081 (+NH3)	Protein backbone-DNA backbone interaction. C OP1 acts as H-bond acceptor and backbone N of Tyr amide group acts as H-bond donor. N-H...O H-bond
	Arg 1107	Arg 107	A35	2.3			N1 (N) of nucleotide base and NH2 (NH2) of Arg1107 side chain	Protein side-chain-DNA base edge interaction. A N1 acts as H-bond acceptor as seen in Watson-Crick base pairing. Arg NH2 acts as H-bond donor. Arg contains multiple NH groups that have the potential of forming hydrogen bonds. N-H...N H-bond



	Arg 1107	Arg 107	A35	2.9		N3 (N) of nucleotide base and NH1 (+NH2) of Arg1107 side chain	Protein side-chain-DNA base edge interaction. A N3 acts as H-bond acceptor and Arg NH1 acts as H-bond donor. Arg contains multiple NH groups that have the potential of forming hydrogen bonds. N-H...N H-bond
	Cys 1141	Cys 141	G36	3.2		N2 (C2 NH2) of nucleotide base and O (C=O) of Cys1141 carboxyl group	Protein backbone-DNA base edge interaction. G N2 acts as H-bond donor and backbone O of Cys carboxyl group acts as H-bond acceptor. Also, G N2 acts as H-bond donor as seen in Watson-Crick base pairing, with backbone O of Cys carboxyl group as H-bond acceptor. N-H...O H-bond
	Asn 1143	Asn 143	G36	2.2		N2 (C2 NH2) of nucleotide base and O (C=O) of Asn1143 carboxyl group	Protein backbone-DNA base edge interaction. G N2 acts as H-bond donor and backbone O of Asn carboxyl group acts as H-bond acceptor. Also, G N2 acts as H-bond donor as seen in Watson-Crick base pairing, with backbone O of Asn carboxyl group as H-bond acceptor. N-H...O H-bond

**Table 47: ZDOCK scores, and observed polar contacts between HPV-18 E7 protein and HPV-18 E7 sequence 5772 aptamer candidate**

Complex	Amino acid residue	Nucleotide	Polar contact length and average (Å)	ZDOCK score	Polar contact information	Additional information	
1	Lys67	G40	3.4	2.87	1436.474	O5' (O) within phosphate backbone and NZ (+NH3) of Lys67 side chain	Protein side chain-DNA backbone interaction. G O5' acts as H-bond acceptor and Lys NZ acts as H-bond donor. N-H...O H-bond
	Glu69	G39	2.8			OP2 (O-) within phosphate backbone and N within peptide bond between Cys68 (COO-) and Glu69 (H3N+)	Protein backbone-DNA backbone interaction. G OP2 acts as H-bond acceptor and backbone N of Glu amide group acts as H-bond donor. N-H...O H-bond
	Arg71	G37	2.1			OP2 (O-) within phosphate backbone and NH1 (+NH2) of Arg71 side chain	Protein side chain-DNA backbone interaction. G OP2 acts as H-bond acceptor and Arg NH1 acts as H-bond donor. Arg contains multiple NH groups that have the potential of forming hydrogen bonds. N-H...O H-bond
	Arg71	A36	2.2			O3' (C3' OH) within sugar group within phosphodiester bond between G37 (O-) and NH1 (+NH2) of Arg71 side chain	Protein side chain-DNA backbone interaction. A O3' acts as H-bond acceptor and Arg NH1 acts as H-bond donor. Arg contains multiple NH groups that have the potential of forming hydrogen bonds. N-H...O H-bond
	Thr93	C69	2.7			OP2 (O-) within phosphate backbone and OG1 (OH) of Thr93 side chain	Protein side chain-DNA backbone interaction. G OP2 acts as H-bond acceptor and Thr OH acts as H-bond donor. O-H...O H-bond
	Thr93	C68	3.1			N4 (C4 NH2) of nucleotide base and O (C=O) of Thr93 carboxyl group	Protein backbone-DNA base edge interaction. C N4 acts as H-bond donor and backbone O of Thr carboxyl group acts as H-bond acceptor. Also, C N4 acts as H-bond donor as seen in Watson-Crick base pairing, with backbone O of Thr carboxyl group as H-bond acceptor. N-H...O H-bond
	Ser95	C69	3.0			N4 (C4 NH2) of nucleotide base and OG (OH) of Ser95 side chain	Protein side-chain-DNA base edge interaction. C N4 acts as H-bond donor and Ser OG acts as H-bond acceptor. N-H...O H-bond
	Ser95	T38	3.1			O4 (C4 C=O) of nucleotide base and OG (OH) of Ser95 side chain	Protein side-chain-DNA base edge interaction. T O4 acts as H-bond acceptor and Ser OG acts as H-bond donor. O-H...O H-bond
	Ser95	G39	2.1			O6 (C6 C=O) of nucleotide base and OG (OH) of Ser95 side chain	Protein side-chain-DNA base edge interaction. G O6 acts as H-bond acceptor and Ser OG acts as H-bond donor. O-H...O H-bond
	Ser95	C66	3.1			N4 (C4 NH2) of nucleotide base and O (C=O) of Ser95 carboxyl group	Protein backbone-DNA base edge interaction. C N4 acts as H-bond donor and backbone O of Ser carboxyl group acts as H-bond acceptor. Also, C N4 acts as H-bond donor as seen in Watson-Crick base pairing, with backbone O of Ser carboxyl group as H-bond acceptor. N-H...O H-bond
Ser95	C67	2.4	N4 (C4 NH2) of nucleotide base and O (C=O) of Ser95 carboxyl group	Protein backbone-DNA base edge interaction. C N4 acts as H-bond donor and backbone O of Ser carboxyl group acts as H-bond acceptor. Also, C N4 acts as H-bond donor as seen in Watson-Crick base pairing, with backbone O of Ser carboxyl group as H-bond acceptor. N-H...O H-bond			

	Val97	T66	2.7			O4 (C4 C=O) of nucleotide base and N within peptide bond between Phe96 (COO-) and Val97 (+NH3)	Protein backbone-DNA base edge interaction. T O4 acts as H-bond acceptor and backbone N of Val amide group acts as H-bond donor. Val can only participate in H-bonds only through backbone atoms. N-H...O H-bond
	Trp100	G63	3.2			OP2 (O-) within phosphate backbone and N within peptide bond between Pro99 (COO-) and Trp100 (+NH3)	Protein backbone-DNA backbone interaction. G OP2 acts as H-bond acceptor and backbone N of Trp amide group acts as H-bond donor. N-H...O H-bond
	Trp100	C61	3.3			O5' (O) within phosphate backbone and NE1 (NH) of Trp100 side chain	Protein side chain-DNA backbone interaction. C O5' acts as H-bond acceptor and Trp NE1 acts as H-bond donor. N-H...O H-bond
	Ala102	C44	2.5			N4 (C4 NH2) of nucleotide base and O (C=O) of Ala102 carboxyl group	Protein backbone-DNA base edge interaction. C N4 acts as H-bond donor and backbone O of Ala carboxyl group acts as H-bond acceptor. Also, C N4 acts as H-bond donor as seen in Watson-Crick base pairing, with backbone O of Ala carboxyl group as H-bond acceptor. Ala can only participate in H-bonds only through backbone atoms. N-H...O H-bond
	Ser103	A62	2.6			N6 (C6 NH2) of nucleotide base and OG (OH) of Ser103 side chain	Protein side-chain-DNA base edge interaction. A N6 acts as H-bond donor and Ser OG acts as H-bond acceptor. N-H...O H-bond
	Ser103	A62	3.0			N7 (N) of nucleotide base and OG (OH) of Ser103 side chain	Protein side-chain-DNA base edge interaction. A N7 acts as H-bond acceptor and Ser OG acts as H-bond donor. O-H...N H-bond
<b>2</b>	Arg58	C68	3.3	<b>2.82</b>	1302.250	OP2 (O-) within phosphate backbone and NH2 (NH2) of Arg58 side chain	Protein side chain-DNA backbone interaction. C OP2 acts as H-bond acceptor and Arg NH2 acts as H-bond donor. Arg contains multiple NH groups that have the potential of forming hydrogen bonds. N-H...O H-bond
	Leu62	G64	2.7			OP2 (O-) within phosphate backbone and N within peptide bond between Met61 (COO-) and Leu62 (+NH3)	Protein backbone-DNA backbone interaction. G OP2 acts as H-bond acceptor and backbone N of Leu amide group acts as H-bond donor. N-H...O H-bond
	Arg71	A62	2.2			N7 (N) of nucleotide base and NH1 (+NH2) of Arg71 side chain	Protein side-chain-DNA base edge interaction. A N7 acts as H-bond acceptor and Arg NH1 acts as H-bond donor. Arg contains multiple NH groups that have the potential of forming hydrogen bonds. N-H...N H-bond
	Arg71	A62	3.3			N7 (N) of nucleotide base and NH2 (NH2) of Arg71 side chain	Protein side-chain-DNA base edge interaction. A N7 acts as H-bond acceptor and Arg NH2 acts as H-bond donor. Arg contains multiple NH groups that have the potential of forming hydrogen bonds. N-H...N H-bond
	Glu73	A41	2.6			N6 (C6 NH2) of nucleotide base and OE2 (O-) of Glu73 side chain	Protein side-chain-DNA base edge interaction. A N6 acts as H-bond donor and Glu OE2 acts as H-bond acceptor. N-H...O H-bond
<b>3</b>	Leu62	G58	3.5	<b>3.18</b>	1291.008	N7 (N) of nucleotide base and N within peptide bond between Met61 (COO-) and Leu62 (+NH3)	Protein backbone-DNA base edge interaction. G N7 acts as H-bond acceptor and backbone N of Leu amide group acts as H-bond donor. N-H...N H-bond
	Met64	A57	3.0			OP2 (O-) within phosphate backbone and N within peptide bond between Cys63 (COO-) and Met64 (+NH3)	Protein backbone-DNA backbone interaction. A OP2 acts as H-bond acceptor and backbone N of Met amide group acts as H-bond donor. N-H...N H-bond
	Val75	C44	3.4			N4 (C4 NH2) of nucleotide base and O (C=O) of Val75 carboxyl group	Protein backbone-DNA base edge interaction. C N4 acts as H-bond donor and backbone O of Val carboxyl group acts as

							H-bond acceptor. Also, C N4 acts as H-bond donor as seen in Watson-Crick base pairing, with backbone O of Val carboxyl group as H-bond acceptor. Val can only participate in H-bonds only through backbone atoms. N-H...O H-bond
	Gln87	G58	2.8			O3' (C3' OH) within sugar group within phosphodiester bond C59 (O-) and NE2 (NH2) of Gln87 side chain	Protein side chain-DNA backbone interaction. G O3' acts as H-bond acceptor and Gln NE2 acts as H-bond donor. N-H...O H-bond